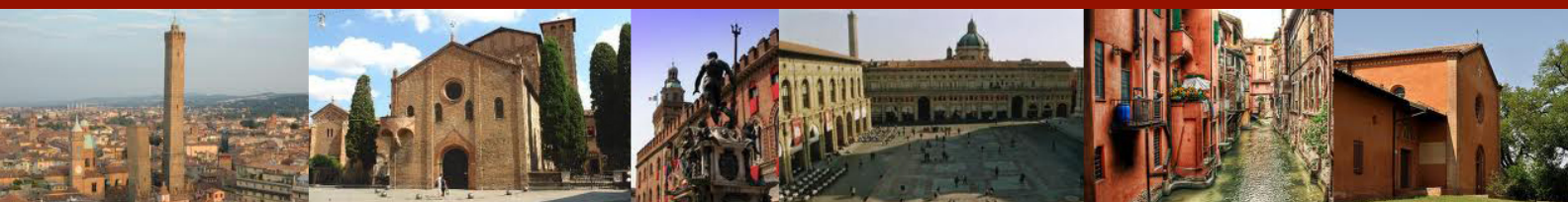# XII International Symposium on 3D Analysis of Human Movement

Technology & Treatment

Bologna (Italy), 18-20 July 2012

www.3DAHM2012.com

Book of Abstracts

Proceedings of the XII International Symposium on 3D Analysis of Human Movement

Symposium President

Alberto Leardini (IOR)

Board of Directors

Vincenzo Parenti-Castelli (DIEM)
Ugo Della Croce (UniSS)
Rita Stagni (DEIS)
Andrea G. Cutti (INAIL)

Editors

Alberto Leardini
Rita Stagni

	Wed - July 18th 2012		Wed - July 18th 2012		Thu - July 19th 2012		Fri - July 20th 2012
		8.00-8.45	Registration	8.00-8.30	Secretary open	8.00-8.30	Secretary open
		8.45-9.15	Keynote Lecture #1:	8.30-9.00	Keynote Lecture #3:	8.30-9.00	Keynote Lecture #6:
		9.15-10.45	Podium #1	9.00-10.30	Podium #3	9.00-10.30	Podium #5
		10.45-11.15	Coffee Break	10.30-11.00	Coffee Break	10.30-11.00	Coffee Break
		11.15-12.45	Industry #1	11.00-11.30	Keynote Lecture #4:	11.00-11.30	Keynote Lecture #7:
				11.30-12.00	Industry #2	11.30-13.00	Podium #6
				12.00-12.45	General Assembly		
		12.45-14.00	Lunch	12.45-14.00	Lunch	13.00	Close Day #3
		14.00-15.30	Poster #1	14.00-15.30	Poster #2		
		15.30-16.00	Coffee Break	15.30-16.00	Coffee Break		
		16.00-16.30	Keynote Lecture #2:	16.00-16.30	Keynote Lecture #5:		
		16.30-18.00	Podium #2	16.30-18.00	Podium #4		
18.00	Welcome	18.00	Close Day #1	18.00	Close Day #2		
				20.00	Gala dinner		

Wed – July 18th 2012

Chairmen: **Lorenzo Chiari (DEIS, University of Bologna, Italy)**
Kamiar Aminian (Ecole Polytechnique Fédérale de Lausanne,

Switzerland)

Keynote lecture: *"Human motion analysis using body worn sensors: technical issues for*
8.45 : 9.15   *outcome evaluation in medicine and sport"*
               Kamiar Aminian

Podium session #1: "Outdoor measurements, inertial and wearable devices"
9.15 : 10.45

9.15	Kinematics of a musculoskeletal model using inertial and magnetic measurement units	Koning B.H.W., Van der Krogt M.M., Baten C.T.M., Koopman H.F.J.M.
9.30	Development of independent walking and gait stability in infants using inertial sensors	Bisi M.C., Riva F., Stagni R.
9.45	Arm velocity distribution during daily activity: objective outcome evaluation after shoulder surgery	Duc C., Pichonnaz C., Bassin J.P., Farron A., Aminian K.
10.00	Ambulatory assessment of hand kinematics using an instrumented glove.	Kortier H.G., Schepers H.M., Sluiter V.I., Veltink P.H.
10.15	Characterisation of input parameter influence on dynamic orbital stability of walking	Riva F., Bisi M.C., Stagni R.
10.30	Concurrent validity of three measurement systems for the evaluation of cervical spine mobility: a wearable inertial sensor system, an optoelectronic system and a 6 dof electrogoniometer	Lubansu A., Duc C., Lebaillif N., Aminian K., Feipel V., Salvia P.

!

Keynote lecture

!

Human motion analysis using body worn sensors: technical issues for outcome evaluation in medicine and sport

Kamiar Aminian

Ecole Polytechnique Fédérale de Lausanne, Switzerland

With the progress of microtechnology is late 20 century, miniature body fixed inertial sensors were proposed for healthcare applications. These sensors can be used in real world conditions offering new possibilities in clinical practice for diagnosis and objective outcomes evaluation. More recently due to mobile communication a significant advance in inertial sensors was performed making this technology very promising for 3D movement analysis. This talk reviews some issues with regard to wearable technology and particularly those related to sensors configuration, kinematics and kinetics evaluation and environment conditions. The possibilities to estimate joint orientation, 3D segment translation and joint moment are introduced through several clinical applications. We show how joint orientation measurement based on body fixed sensors can be used for outcome evaluation after knee ligament rupture. The possibility to estimate ground reaction force, ankle force and moment based on inertial sensors and pressure insoles are also described in patients with ankle arthritis. 3D gait analysis in clinical environment is shown through foot worn inertial sensors in two cohorts of elderly subjects (more than 1500 subjects). Finally, we consider the application of inertial suit in snow sports and swimming as examples of restraining conditions where standard video based motion capture are difficult or impossible to use.

Kinematics of a musculoskeletal model using inertial and magnetic measurement units

Koning B.H.W. [1,2], Van der Krogt M.M. [1,3], Baten C.T.M. [2], Koopman H.F.J.M. [1]

[1] Laboratory of Biomechanical Engineering, University of Twente, Enschede, The Netherlands

[2] Roessingh Research and Development, Enschede, The Netherlands

[3] Dept. of Rehabilitation Medicine, Research Institute MOVE, VU University Medical Center, Amsterdam, The Netherlands

Inertial and magnetic measurement units; global optimization; joint constraints; kinematic driver

1. INTRODUCTION

Inertial and magnetic measurement units (IMMUs, [1]) are becoming a serious candidate for human movement analysis in clinical settings or sports [2, 3]. They are (relatively) cheap, quick and not bothered by typical drawbacks of optical motion capturing devices, such as occlusion of markers and restriction to a lab environment. Combined with instrumented force shoes [4], it enables musculoskeletal modelling based on ambulatory measurements. However, currently available commercial musculoskeletal modelling programs, such as the AnyBody Modeling System (AMS, [5]), only provide integrated routines to drive these models using measured optical markers. We therefore developed a new IMMU driver for the AMS, which we validated against default marker drivers. For this purpose we compared the right hip kinematics of three simulations where we used marker drivers, IMMU drivers and a combination of both. We also compared simulated right thigh IMMU sensor signals (accelerometer and gyroscope) of each simulation to those measured by the real sensor. The results show to be promising and sensor signals can be reproduced accurately. However, before application of the new IMMU drivers important issues regarding sensor to segment calibration, appropriate joint constraints and handling of soft tissue artefacts (STAs) need to be solved.

2. METHODS

Definition of the IMMU driver

The IMMU driver is included in the AnyBody model in a way similar to the currently available marker drivers, by defining each IMMU twice (Figure 1). First, a *model IMMU* segment is rigidly attached to a default position on the model, with its orientation with respect to segment determined by functional calibration [2]. Secondly, a *real IMMU* segment is linked to the model IMMU using a hinge joint. Its orientation in global space is determined by fusion of the sensor signals outside the AMS [1]. Next, a three dimensional variable is used to define the rotation between the model and real IMMU using the attitude 'vector' defined by Woltring, [6];
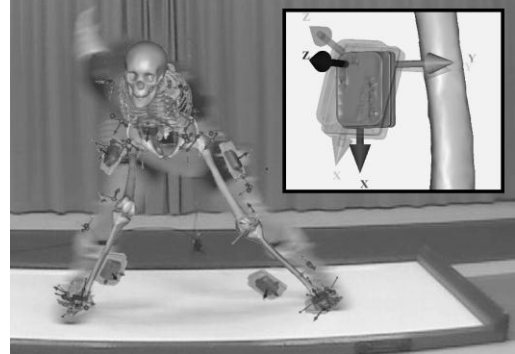
$$AV = \alpha u. \tag{1}$$

Figure 1 Screen capture of the slideboard experiment with an overlay of the AnyBody model. Top right shows the real (transparent) and model IMMU on the right thigh segment, including the local reference frames. Note the rotation around the sensor Y-axis.

Where u defines the instantaneous axis of rotation in the model IMMU frame (direction cosines) and α the angle of rotation around this axis (helical angle).

Global optimization and sensor signal reproduction

The variables are implemented as soft constraints, which results in an over-determinate (bio)mechanical system. The motion of the complete model in terms of the time-dependent generalised coordinates $q(t)$ is determined by minimization of these soft constrains, $\Psi(q, t)$, whilst fulfilling the hard constraints defined by joint constraints in the biomechanical model, $\Phi(q, t)$ [5].

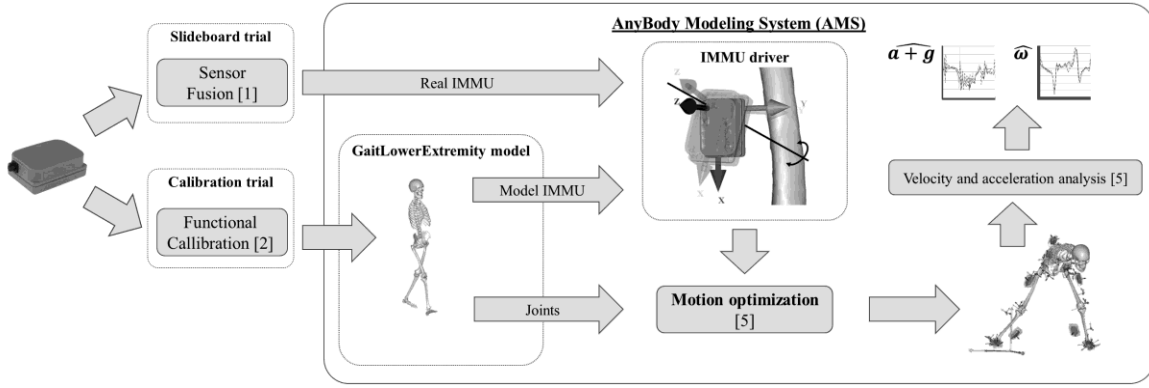$$\min_q G(\Psi(q, t))$$
$$\text{s. t. } \Phi(q, t). \tag{2}$$

Figure 2 Optimization scheme for the new IMMU driver. Segment calibration determines the orientation of each model IMMU with respect to its segment of the GaitLowerExtremity model and fusion of the sensor signals during the slideboard experiment determines the orientation of the real IMMU in global space. The difference in orientation between the model and real IMMUs are minimized for each time step during the motion optimization, whilst completely fulfilling the joint constraints. After solving the optimization for the complete trial, model IMMU accelerometer ($\widehat{a+g}$) and gyroscope signals ($\widehat{\omega}$) are calculating using the Karush-Kuhn-Tucker conditions.

Once the generalised coordinates are known for the complete trial, the Karush-Kuhn-Tucker (KKT) are applied to calculate the model IMMU sensor signals [5]. The whole optimization scheme and reconstruction of the IMMU sensor signals is illustrated in Figure 2.

Weight functions

The objective function is a weighted least-square, with a constant weight.

$$G\big(\Psi(q,t)\big) = \Psi(q,t)^T\, W\, \Psi(q,t) \tag{3}$$

In this abstract the weight of the IMMU sensors was based on setting a constraint violation of 3 degrees equal to a 0.5 cm marker constraint violation, resulting in an IMMU weight of 0.095 m/rad. For the simulation without using IMMU drivers, the weight function was set to zero, so the IMMU driver constraint violations and sensor signals could still be determined for the marker driven model.

Experiments

Kinematics were obtained using synchronized measurements with IMMUs (Xsens Technologies, Enschede, The Netherlands) and optical markers (Vicon, Oxford, United Kingdom) of a subject using a slideboard, which is a land training setup for speed skating. The IMMU to segment calibration was performed using the direction of the accelerometer signal during a neutral upright pose to define the vertical segment axis and the gyroscope signal (angular velocities) during a sagittal plane squat to determine the mediolateral segment axis. For the simulations we used a slightly adapted version of the GaitLowerExtremity model from the AnyBody Modeling System repository (AnyBody Technology A/S, Aalborg, Denmark), having 15 joint constraints; Pelvis/Trunk (ball), Hip (ball), Knee (hinge), Ankle (hinge) and Subtalar (hinge). Three simulation were performed; one using marker drivers, one using the new IMMU drivers and one using both drivers simultaneously. The pelvis was fixed to the global reference frame when using IMMU drivers, due to the lack of position information.

3. RESULTS

Figure 3 shows the right hip kinematics of one motion cycle (3.68s) for the three simulations. Hip flexion angles showed an offset between simulations that included IMMU drivers and the one without, and also the hip external rotation angles were more similar for simulation including the IMMU drivers. The hip abduction angles showed opposite results; these were more similar for simulations including marker drivers.

Figure 4 shows the simulated and measured sensor signals around (gyroscope) and in the direction of (accelerometer) the right thigh sensor Z-axis. This axis happened to be approximately aligned with the segment's mediolateral segment axis (see Figure 1), i.e. the main direction of the sideways slideboard movement and the segment rotation axis associated with hip flexion. All simulated gyroscope signals (Figure 4, left) represented the measured gyroscope signals well, except where the simulated signals using marker drivers deviate from the measured signals (0 to10% and 52 to 70%). The accelerometer signals (Figure 4, right) simulated using IMMU drivers showed the biggest deviations from the measured signal and also a more high frequent behaviour. Which in some cases showed great resemblance to the measured accelerometer signal (0-5% and 30-35%). Best correspondence with the measured accelerometer signals was achieved for simulations that included both drivers.

Hip flexion (deg)

Hip abduction (deg)

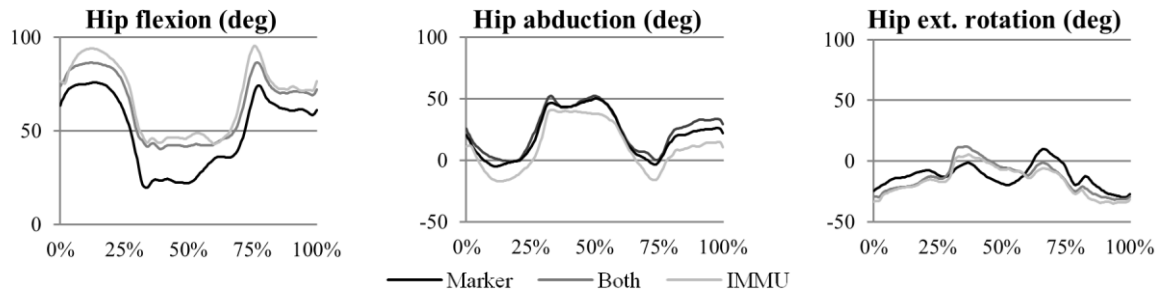## Hip ext. rotation (deg)

—— Marker —— Both —— IMMU

Figure 3 Simulated hip, knee and ankle flexion angles using marker, IMMU and both drivers. The cycle started with the moment where the right foot hit the side of the slideboard (0%). The subject prepared for push-off by flexing the right leg, followed by the actual push-off from 20 to 31%. The right leg was nearly extended while the subject slid to the left and was being pulled in after the left foot hit the board (52%). During the left leg push-off (starting at 70%) the right leg was pushed forward and lateral, and finally placed back on the slideboard (82%). After which it slid to the right, without fully extending the leg, until it hit the board again (100%).

ω around sensor Z-axis (deg/s)

a+g in sensor Z-direction (m/s2)

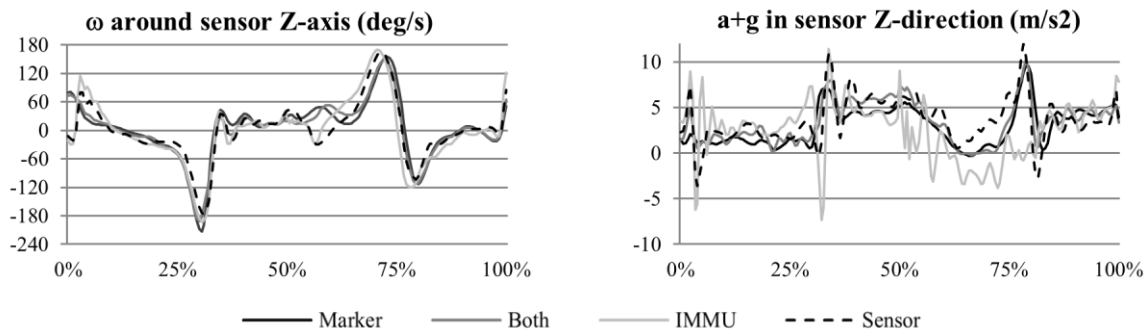—— Marker —— Both —— IMMU - - - - Sensor

Figure 4 Simulated right thigh sensor kinematics for simulations using marker, IMMU and both drivers, compared to the measured sensor signals (Real). LEFT: gyroscope signals, RIGHT: accelerometer signals.

4. DISCUSSION

The great similarities between the right hip flexion and external rotation angles for simulations that included IMMU drivers and abduction angles for simulations that included marker drivers (Figure 3) were caused by two effects. The first was a methodological difference between the IMMU and marker drivers; for marker drivers a rotation around the segment long axis, compared to a similar rotation around one of the other axes, results in a smaller marker constraint violation due to the short distance of the markers to the segment long axis. There is no such direction dependency in the IMMU driver, implicitly making the IMMU driver more dominant for rotations along the long axes and small segments such as the feet.

The second and more important cause was a difference in segment calibration, which for the marker driven model was implicitly defined by the model marker placement. Figure 5 shows the soft constraint violations of the right thigh IMMU driver during the calibration trial. The offsets around the sensors local X and Z-axis (Mx, My), and thus the helical angle (Mα), when using marker drivers illustrated the difference between the model IMMU functional calibration and implicit marker calibration in the neutral position (10 to 12.5s).

However, it lowered during the squat movement which is a more relevant pose for the slideboard trial. Optimization of both model marker and IMMU placement on the biomechanical model could reduce this calibration offset.

When using the IMMU drivers the constraint violation logically started at zero, as this was the starting pose for the functional calibration. But the constraint violation increased during the squat by rotating along the Y-axis (Iy), which was approximately aligned with the segment's frontal axis. This was caused by motion artefacts during the squat and the model's joint constraints in the knee. The latter actually prevented the squat movement to be simulated completely in the sagittal plane, which was the assumption for the used segment calibration procedure, unless the model's anatomical knee axis was normal to this plane. This illustrates the incorrectness of the used knee joint constraints.

IMMU driver
Attitude Vector Z (deg)

- · - · Mx - - - My ······ Mz —— Mα
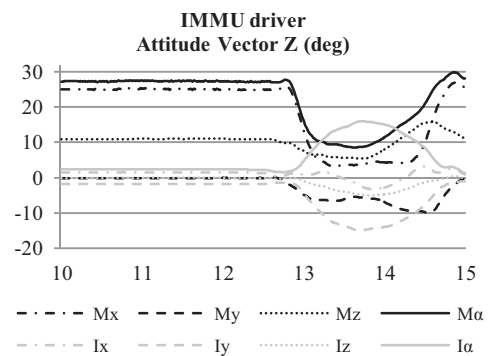- · - · Ix - - - Iy ······ Iz —— Iα

Figure 5 Values of the right thigh IMMU driver soft constraint violations for the marker (M) and IMMU driven (I) simulation of the calibration trial; a neutral upright body position, followed by a squat. It shows the x/y/z attitude vector elements and helical angle, α, of (1).

The early peaks (0-5%) in both measured sensor signals of Figure 4 were the result of soft tissue artefacts (STAs) caused by hitting the side of the board, from which it can be concluded that the IMMU driver is more sensitive to STAs. One reason is the limited amount of IMMU drivers, compared to the marker drivers. So the degree of model over-determinacy is much bigger when using marker drivers, effectively filtering the simulation output. This also explains some the higher frequency content of the simulated accelerometer signals when using only IMMU drivers. However, this hypothesis needs validation.
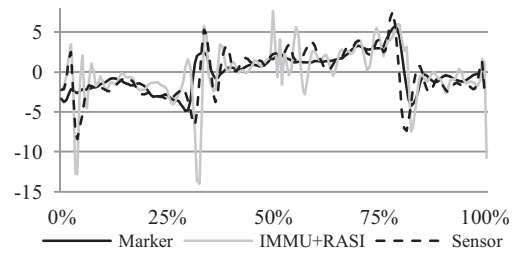
a in sensor Z-direction (m/s²)

Figure 6 Simulated right thigh sensor net accelerations by subtracting the gravity component in the model IMMU frame for simulations using marker drivers and the IMMU drivers with one marker placed at the right anterior superior iliac spine (RASI) instead of pelvic fixation. The real IMMU net acceleration (Sensor) is calculated by subtracting gravity in the real IMMU frame.

The greater similarity between the simulated and measured gyroscope signals for the simulation using IMMU drivers was expected, as the real IMMU orientation was based on integration of the gyroscopic signal and the only deviation between the real and model IMMU was caused by the joint constraints. Direct comparison of the accelerometer signals was limited by the difference in segment calibration, inducing a different gravitational component, and also because pelvic fixation when using IMMU drivers eliminated an important component of the linear acceleration. Both causes for accelerometer signal difference were eliminated by removing the model estimate of the gravitational component and including one marker driver at the pelvis in the simulation using IMMU drivers (Figure 6). The resulting net linear acceleration estimates showed no further offset. So it can be concluded that the possible bias caused by the (a priori) estimated position of the model IMMU on the segment, and its effect on the net acceleration ($a = \omega^2 r$), was negligible.

In conclusion, we have developed a new kinematic driver for the AnyBody Modeling System that uses the orientation estimate obtained from sensor fusion of 3D accelerometers, gyroscopes and magnetometers. After the motion optimization, model sensor signals were calculated and compared to the measured sensor signals. It was even possible to further investigate the individual sensor signals by decomposition of the accelerometer signal. Results showed promising, but also illustrated the need for a more accurate sensor to segment calibration using a more task and pose specific method or minimization of the difference between simulated and measured sensor signals. Additionally, negative effects of the joint constraints and STAs on the resulting motion should be evaluated. Some effects of STAs could be reduced by using multiple sensors for each segment or by lowering the sensor weight functions for segments and directions where STAs are expected. To enable analysis of the accelerometer signals and improve the model's global accelerations (and thus inertial forces) global position constraints are necessary, such as GPS or UWB measurements, estimates of the centre of mass [4] or by implementing boundary conditions during contact with the environment.

5. ACKNOWLEDGMENTS

6. REFERENCES

[1] D. Roetenberg, 2006. "Inertial and magnetic sensing of human motion", PhD Thesis, University of Twente, Enschede.

[2] A. Cutti, A. Ferrari, P. Garofalo, M. Raggi, A. Cappello, and A. Ferrari, 2010. 'Outwalk': a protocol for clinical gait analysis based on inertial and magnetic sensors. Medical and Biological Engineering and Computing, vol. 48, pp. 17-25.

[3] J. Chardonnens, J. Favre, B. Le Callennec, F. Cuendet, G. Gremion, and K. Aminian, 2011. Automatic measurement of key ski jumping phases and temporal events with a wearable system. Journal of Sports Sciences, vol. 30, pp. 53-61.

[4] H. M. Schepers, E. van Asseldonk, J. H. Buurke, and P. H. Veltink, 2009. Ambulatory Estimation of Center of Mass Displacement During Walking. Biomedical Engineering, IEEE Transactions on, vol. 56, p. 1189.

[5] M. S. Andersen, M. Damsgaard, and J. Rasmussen, 2009. Kinematic analysis of over-determinate biomechanical systems. Computer Methods in Biomechanics and Biomedical Engineering, vol. 12, pp. 371-384.

[6] H. J. Woltring, 1994. 3-D attitude representation of human joints: A standardization proposal. Journal of Biomechanics, vol. 27, pp. 1399-1414.

Development of independent walking and gait stability in infants using inertial sensors

(A longitudinal study to evaluate the development of different strategies, coordination and stability in new walkers: preliminary results)

Bisi M.C. [1], Riva F. [1], Stagni R. [1]

[1] Department of Electronic Computer Science and Systems, University of Bologna, Bologna, Italy

Despite the number of studies that analyzed the development of independent walking in literature, the number of infants included was always small and only few studies performed longitudinal observations. The aim of the present study was to collect longitudinally data from a large group of infants (>20) using inertial sensors over a 6-months period after the onset of independent walking. This database will allow evaluating the changes in gait temporal parameters, stability and coordination at the beginning of independent walking. Moreover, it will permit to observe when and how the development of pendulum mechanism occurs. Since there is not a commonly accepted way to define or quantify locomotor stability, the collected data will permit also to apply and evaluate the stability indexes proposed in literature, looking for the index that better describes infant locomotor stability and its relation to infant risk of falls.

New walkers; Gait stability; development of independent walking.

1. INTRODUCTION

Many studies have been observing infants at the onset of walking in order to evaluate the development of different strategies and coordination [1,2,3]. These studies regard most of the times small groups (<10) and only few studies observed longitudinally the evolution of independent walking (on 2 or 5 subjects) [4,5].

An important aspect of the development of independent walking is how gait stability is gained by toddlers during the first months of walking experience, which is directly related to a decreasing risk of falling. Despite its importance, this aspect has not been studied yet, probably because there is not a commonly accepted way to define or quantify locomotor stability [6]. Many stability indexes have been proposed in literature for clinical application, including methods coming from dynamical systems analysis. The problem in validating these methods is the necessity to identify a-priori instable individuals. Given that infants at the onset of independent walking can be assumed a-priori unstable and that with months of experience their gait will tend to be more and more stable, the application of these methods could lead to i) the evaluation of which of the proposed indexes is the best estimator of gait stability and to ii) the identification of how infant locomotor stability changes with months of walking experience and relates with daily falls.

To the authors' knowledge, the development of infant independent walking was always assessed using optoelectronic or video-based data. The use of wireless inertial sensors is more practical when aiming at the measurements of large populations. Moreover inertial sensors can be worn under the clothes facilitating the experiments with infants who are not distracted by markers and can freely walk and move in any environment.

The aims of the present study were

i)   to observe longitudinally a large group of infants (>20) using inertial sensors over a 6-months period after the onset of independent walking (period in which the most dramatic changes of maturation of many gait parameters occurs [7]). This database will allow evaluating the changes in gait temporal parameters, stability and coordination at the beginning of independent walking. Moreover it will permit to evaluate when and how the development of pendulum mechanism occurs.

ii) to apply and evaluate the stability indexes proposed in literature (variability, local stability and orbital stability), looking for the index that better describes infant locomotor stability and its relation to infant risk of falls.

Up to now only seven infants were tested and only some tests for each one, thus, the presented results are only preliminary.

2. MATERIALS AND METHODS

Seven healthy infants (77±2cm, 9.3±0.8kg, 13±1months at the time of the first test) were included in the study. The tests were scheduled ones a month after the onset of independent walking for three months and one after six months. When possible a test during the very first week of independent walking was performed. The

onset of independent walking was defined as the child's ability to perform 5 consecutive steps without help. The schedule of the tests performed up to now is shown in Table 1.

Table 1. Timesheet of the performed tests.

sbj n°	1 week	1 month	2 months	3 months	6months
1	x	x			
2	x	x			
3		x			
4		x			
5		x	x	x	
6	x	x	x		
7	x				

All of the infants were full-term at birth and had no known developmental delays.

The participants were asked to walk at self-selected speed. Two tri-axial wireless inertial sensors (OPALS, Apdm, USA) were used to measure accelerations and angular velocity of body segments.

The test was repeated twice, changing the position of one inertial sensor:

1) Test 1: the inertial sensors were mounted respectively on the lower back and on the right lower leg. Measures of accelerations and angular velocity of the trunk and of the right leg were recorded.
2) Test 2: the inertial sensors were mounted on the lower legs. Measures of accelerations and angular velocity of the two legs were recorded.

Right heel strike (HS) and toe off (TO) instants were estimated from the mediolateral angular velocity of the lower limb, looking at the sharp negative peaks involving medium and relative high frequencies just before (TO) and after (HS) the swing phase [8]. For all the participants 10 consecutive strides were analyzed: 10 was the maximum number of strides obtained in the less experienced infant.

Analyzed gait parameters

a) Temporal parameters:
    Mean stride (stride), swing (swing), stance (stance) and double support (DST) times were calculated.
b) Regularity:
    Step-, stride- regularity were evaluated using trunk vertical acceleration [9].
c) Variability:
    Strides were time-normalized and at each percentage of the stride cycle mean standard deviation between strides was calculated for the trunk kinematics in the medio-lateral plane, both in acceleration (SDa) and in angular velocity (SDv). Subsequently, these estimates were averaged over the normalized stride cycle resulting in variability measures.

Measures of gait stability

d) Variability.
    As calculated for the gait parameters.
e) Local stability
    State spaces were created using the linear acceleration of the trunk in all three directions. Local stability was estimated by calculating short-term and long-term Lyapunov exponents (sLE and LE) on three delay embedded state spaces (v-vertical (v), medio-lateral (ml) and antero-posterior (ap)).
f) Orbital stability
    Orbital stability was calculated via maximum Floquet multipliers (FM) on a state space composed by trunk acceleration data in the three directions.

3.   RESULTS

The results of two infants on which three tests were performed are shown in Fig. 1a, 1b, 2a, 2b, 3a, 3b.

Gait temporal parameters showed that the infants increased the swing phase while reducing DST, and stance. The coordination indexes were always below 0.5 with opposite trend between the two infants (one showed growing and the other decreasing indexes).

Short Lyapunov exponent decreased with months of experience while long Lyapunov exponents and Floquet Multipliers were almost constant. Variability increased with walking experience starting from the first month of independent walking.
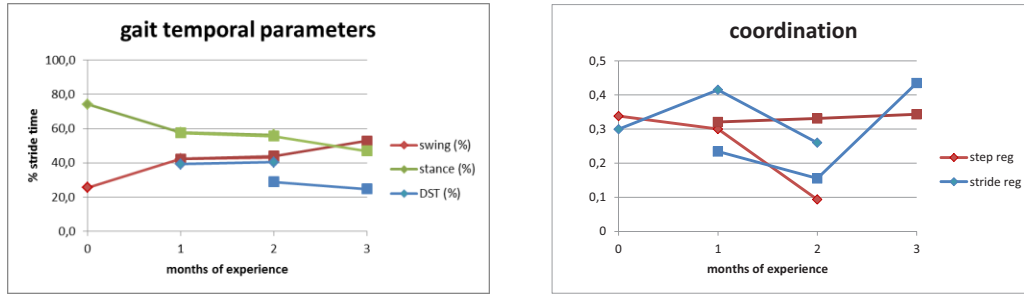
Figure 1 a) Swing (red), stance (green) and DST (blue) expressed as percentage of mean stride time at different months of walking experience. b) Step regularity (red) and stride regularity (blue) at different months of walking experience. Squares and diamonds represent the two different subjects.
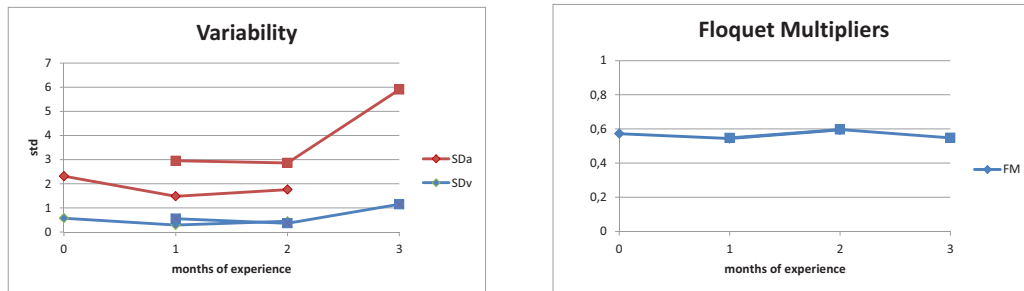

Figure 2 a) variability of trunk mediolateral acceleration, SDa (red), and of angular velocity, SDv (blue) at different months of walking experience. b) Floquet multipliers at different months of walking experience. Squares and diamonds represent respectively the two subjects.
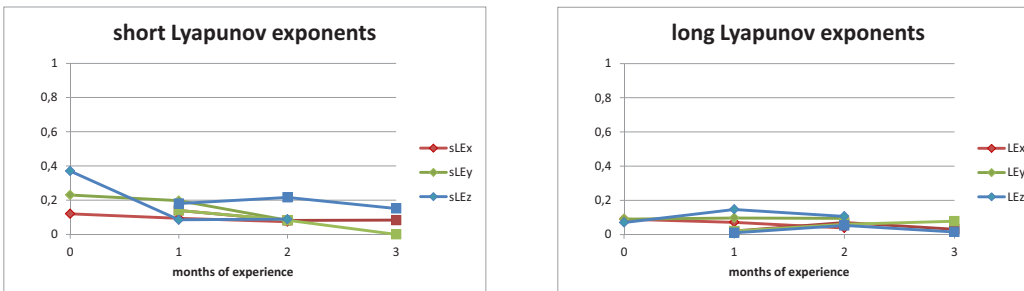

Figure 3 a) Short Lyapunov exponents calculated with the three linear accelerations (vertical (red), mediolateral (green) and anteroposterior (blue)) at different months of walking experience. b) Long Lyapunov exponents calculated with the three linear accelerations (vertical (red), mediolateral (green) and anteroposterior (blue)) at different months of walking experience. Squares and diamonds represent respectively the two subjects.

4. DISCUSSION

The discussed results refer only to two infants since they were the only two who participated to the test more than twice. Therefore these conclusions are not generalizable and have to be further discussed when the data of the other infants will be available.

Gait parameters
Gait temporal parameters showed that the infants increased the swing phase while reducing DST and stance phases with experience, evidencing the fear of falling at the onset of walking.
Gait regularity was low in all the tests, as expected. The trends were opposite for the two infants (one showed increasing and the other decreasing indexes): more data will show if this trends are significant or not.
Variability measures showed a slight decrease from the first week to the first month of walking experience and then increased with months: this preliminary results suggest that during the first month of independent

walking the infants consolidate the first gait pattern they learnt, reducing variability and then, from month 1 to 3, infants looked for different strategies being more stable and conscious of their capabilities.

Measures of gait stability

Short Lyapunov exponents decreased with months of experience while long Lyapunov exponents and Floquet Multipliers were almost constant. Variability measures increased with month indicating theoretically a less stable gait. From these results it appears that only Short Lyapunov exponents can distinguish the variations in stability of the infant indicating correctly that the infant is going toward a more a priori stable gait pattern, that is toward a minor risk of falling.

5.   ACKNOWLEDGMENT

6.   REFERENCES

[1] Kubo, M, Ulrich B.D., 2006. Early stage of walking: development of control in mediolateral and anteroposterior directions. J Mot Behav 38(3), 229-237

[2] Roncesvalles MN, Woollacott MH, Jensen JL., 2000, the development of compensatory stepping skills in children. J Mot Behav. 32(1):100-11

[3] Ivanenko YP, Dominici N, Cappellini G, Lacquaniti F., 2005, Kinematics in newly walking toddlers does not depend upon postural stability. J Neurophysiol. 94(1):754-63

[4] Bril, B, Breniere, Y., 1992, Postural requirements and progression velocity in young walkers. J Mot Behav. 24(1):105-16

[5] Ivanenko YP, Dominici N, Cappellini G, Dan B, Cheron G, Lacquaniti F., 2004, Development of pendulum mechanism and kinematic coordination from the first unsupported steps in toddlers. J Exp Biol. 207(Pt 21):3797-810

[6] Dingwell, J.B., Kang, H.G., 2007. Differences between local and orbital dynamic stability during human walking. Journal of Biomechanical Engineering 129(4), 586-593.

[7] Ivanenko YP, Dominici N, Lacquaniti F., 2007, Development of independent walking in toddlers. Exerc Sport Sci Rev. 35(2):67-73

[8] Aminian K, Najafi B, Büla C, Leyvraz PF, Robert P., Spatio-temporal parameters of gait measured by an ambulatory system using miniature gyroscopes. J Biomech 35(5): 689-99

[9] Moe-Niellsen, R, Helbostad, J.L., 2004. Estimation of gait cycle characteristics by trunk accelerometry. J Biomech 37(1): 121-6

Arm velocity distribution during daily activity: objective outcome evaluation after shoulder surgery

Duc C.[1], Pichonnaz C.[2], Bassin J.P.[2], Farron A.[3], Aminian K.[1]

[1] LMAM, Ecole Polytechnique Fédérale (EPFL), Lausanne, Switzerland, cyntia.duc@epfl.ch
[2] Physiotherapy, Haute Ecole de Santé Vaud (HECVSanté), Lausanne, Switzerland
[3] Orthopedic Surgery and Traumatology, Centre Hospitalier Universitaire (CHUV), Lausanne, Switzerland

This study proposed a new metric to assess the arm mobility based on the monitoring of daily activity using inertial sensors. Forty-one healthy participants and 21 patients suffering from rotator cuff tear disease were evaluated using a clinical questionnaire and one day measurement of the arm kinematics. Arm movements were detected from inertial data, and characterized by their velocity. Cumulative distribution of the velocities of each patient was compared to the reference distribution of controls, using the Kolmogorov-Smirnov distance. This distance was significantly correlated to clinical score. Moreover, it was used to compute the probability of "healthiness of arm movement" for each patient. The approach, based on the mobility of daily activity, offers an effective way to quantify the deviation of one patient from the group of controls.

Arm usage; daily activity; inertial sensors

1. INTRODUCTION

Patients with shoulder disorders are restricted in their arm function [1]. Assessment of arm movements during daily life conditions is thus essential for the evaluation of upper limb function and of the surgery outcome. Wearable measurement systems are useful tools to monitor upper limb movements in real-life condition. Such systems have been used to classify upper limb usage and non-usage [2] or to report the frequency of movement [3]. Even if those quantifications of movements are important, there is also a need to evaluate the quality of the movement. Previous studies showed that parameters related to velocity and acceleration are relevant metrics in order to evaluate the effect of pathology and pain on the mobility, and to estimate the difference between patient and healthy groups [4]. Therefore the first goal of this study was to propose a new metric for the assessment of the 3D arm velocity during the day based on body worn sensors. The second aim was to evaluate the sensitivity of this metric to discriminate healthy and painful shoulders.

2. MATERIAL AND METHODS

Patients and Measurements

Forty-one control subjects (34 ± 9 year old) and twenty-one patients (53 ± 9 years old) with rotator cuff disease were enrolled. Patients were assessed before surgery (baseline) and after surgery (at 3, 6 and 12 months). Participants completed the Constant score [5], a clinical evaluation containing measurement of range of motion and force as well as subjective items evaluated by the patient, scored up to 100 points. The participants were then monitored during 7 hours in real world conditions and during their usual activity. Inertial modules with miniature three-dimensional gyroscope and accelerometer were fixed on each humerus and on the sternum (Fig. 1). The inertial modules were linked to an embedded datalogger (Physilog®, CH) worn at the waist and recording the data at 200 Hz.

Data Analysis

The movements of the humerus during daily activity were detected using the angular velocity of the arm and thorax [6]. Walking episodes were identified using the inertial signal of the trunk [7]. For each detected movement in non-walking periods, the mean arm velocity was extracted according to the angular velocity norms. The empirical cumulative distribution function (CDF) of the arm velocity was then estimated for the whole day, with the hypothesis that painful arms would present a function shifted to the low velocities compared to healthy arms. First, all detected movements of the dominant and non-dominant arms of the control group were used to define a reference CDF for dominant, respectively non-dominant sides. Then, the CDF of each painful side was compared to the dominant, respectively non-dominant reference depending on the side of the pathology, using the Kolmogorov-Smirnov distance (KS) [8], a non-parametric statistical distance. A typical painful arm of a patient affected on the dominant side is compared to the reference in Fig. 2.

Figure 1. Measurement system: A) Inertial modules attached to the dorsal part of humerus and to the sternum; B) Detail of an inertial module with tri-axial gyroscope and accelerometer.
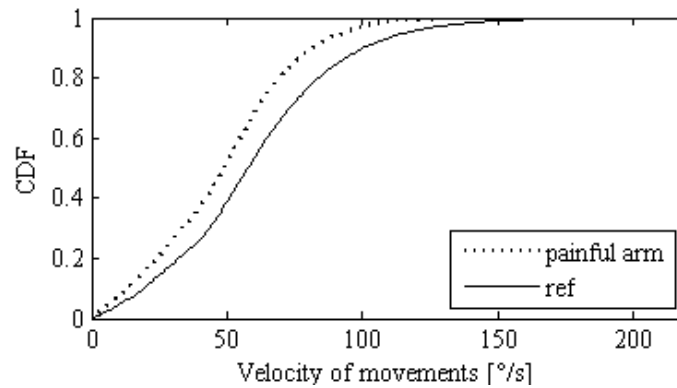

Figure 2. A typical cumulative distribution function (CDF) for the painful dominant side of one patient before surgery (in dashed line) and for the reference for dominant side. It can be observed that the painful arm presents higher probabilities for low arm velocity, leading to a KS distance of +0.15.

The KS distance for the controls and the patients at baseline and follows-up were computed. After verifying the normality assumption with Shapiro-Wilk test for each group, differences between groups were evaluated by a t-test. Then, the KS distance of each patient was compared to the values of the control group using the z-score and the corresponding probability to be similar to the control group, called $pr_{healthy}$, the probability of "healthiness of arm movement". Finally, multiple regression analysis was used to estimate the relationship between the KS distance and the clinical score within patients.

3.   RESULTS

The reference CDF for dominant and non-dominant sides were built based on data of the control group. The KS distance between each arm and its reference are reported in Table 1. These values were normally distributed for all groups. $pr_{healthy}$ was computed for each patient and summarized in Table 2. Finally the relationship between the KS distance and the Constant score within patients, illustrated on Fig. 3, was evaluated using a regression on the Constant score with KS distance and time of evaluation as fixed factors and the subject as a random factor. The effect of the KS distance was significant (F = 73.9, p < 0.0001), and it corresponds to a coefficient of determination reaching 0.55 (r = 0.74).

Table 1. Means and standard deviations of the KS distance for the controls and for the painful and healthy sides of patients. Significant differences with the control group (p < 0.01) are indicated with *.

	Baseline	3 months	6 months	12 months
Painful sides	0.15 ± 0.11 *	0.16 ± 0.13 *	0.09 ± 0.11 *	0.08 ± 0.11 *
Healthy sides	0.03 ± 0.10	0.01 ± 0.09	0.02 ± 0.09	0.00 ± 0.10
Controls	0.00 ± 0.10			

Table 2. Number of patients according to the value of the probability of "healthiness of arm movement", $pr_{healthy}$.

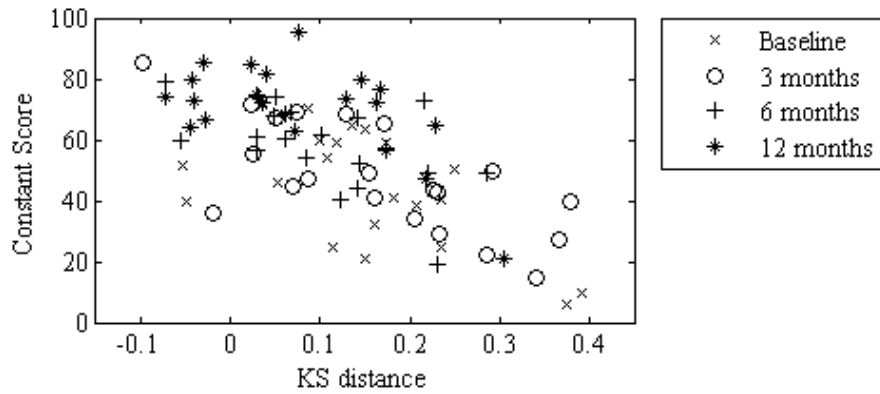|	Baseline	3 months	6 months	12 months
$pr_{healthy} < 0.25$	15	13	9	8
$0.25 < pr_{healthy} < 0.5$	2	3	4	2
$0.5 < pr_{healthy} < 0.75$	2	3	5	4
$pr_{healthy} > 0.75$	2	2	3	7

Figure 3. Values of the Constant score relative to the KS distance for the painful arms at baseline and 3, 6 and 12 months after surgery ($R^2 = 0.55$).

4. DISCUSSION

The analysis of the distribution of the arm velocity during non-walking episodes highlighted differences between pathological arms of patients and a reference based on typical healthy participants. Indeed, KS distance showed that the painful arms are significantly different from the controls at each stage of evaluation, and that this distance started to decrease at 6 months after surgery. At 12 months follow-up, the patient group still presented a difference in the distribution of the arm velocity, meaning that, in average, the patients were not able to perform arm movements with velocities comparable to healthy subjects.

The multiple regression analysis showed a significant relationship between the KS distance and the Constant score. The KS distance explained 55% of the variance of the clinical score. The unexplained part can at least partially come from the additional information provided by the measurement of velocity ability during usual daily activity.

The proposed approach allowed defining a new metric for the "healthiness of arm movement", $pr_{healthy}$, based on the 3D components of arm angular velocity of the movements performed during a day. In this way, each patient was evaluated individually: seven patients appeared to have recovered a normal arm velocity as they had a $pr_{healthy}$ of at least 0.75 at 12 months after surgery. On the opposite, ten patients still presented a $pr_{healthy}$ lower than 0.50. Through them, five patients had a Constant score higher than 72 points, which is in the range of the values for healthy subjects [9]. Even though the clinical evaluation was good, the assessment based on arm velocity showed a lack of mobility. The analysis of arm velocities in daily environment provides thus an objective assessment of the upper limb mobility, which is complementary to the evaluation given by the Constant clinical score.

5. REFERENCES

[1] Bunker, T. 2002. Rotator cuff disease. Curr Orthopaed 16(3), 223-233.
[2] Schasfoort, F.C., Bussmann, J.B., Stam, H.J., 2002. Ambulatory measurement of upper limb usage and mobility-related activities during normal daily life with an upper limb-activity monitor: a feasibility study. Med Biol Eng Comput 40(2), 173-182.
[3] Coley, B., Jolles, B.M., Farron, A., Aminian, K., 2009. Detection of the movement of the humerus during daily activity. Med Biol Eng Comput 47(5), 467-474.
[4] Jolles, B.M., Duc, C., Coley, B., Aminian, K., Pichonnaz, C., Bassin, J.P., et al., 2011. Objective evaluation of shoulder function using body-fixed sensors: a new way to detect early treatment failures? J Shoulder Elbow Surg 20(7), 1074-1081.
[5] Constant, C.R., Murley, A.H., 1987. A clinical method of functional assessment of the shoulder. Clin Orthop Relat Res 214, 160-164.
[6] Duc, C., Pichonnaz, C. Bassin, J.P., Jolles, B.M., Djahangiri, A., Farron, A., Aminian, K., 2011. New method for detection of shoulder movement during daily activity, Proceedings of the 20th Annual Meeting of ESMAC, p. 6.
[7] Najafi, B., Aminian, K., Paraschiv-Ionescu, A., Loew, F., Bula, C.J., Robert, P., 2003. Ambulatory system for human motion analysis using a kinematic sensor: monitoring of daily physical activity in the elderly. IEEE Trans Biomed Eng 50(6), 711-723.
[8] Massey, F.J., 1951. The Kolmogorov-Smirnov Test for Goodness of Fit. J Am Stat Assoc 46(253), 68-78.
[9] Constant, C.R., Gerber, C., Emery, R.J., Sojbjerg, J.O., Gohlke, F., Boileau, P., 2008. A review of the Constant score: modifications and guidelines for its use. J Shoulder Elbow Surg 17(2), 355-361.

Ambulatory Assesment of Hand Kinematics

using an instrumented glove

Kortier H.G.[1], Schepers H.M.[2], Sluiter V.I.[1], Veltink P.H.[1]

[1] Biomedical Signals and Systems, MIRA Institute, University of Twente, Enschede, The Netherlands
[2] Xsens Technologies B.V., Enschede, the Netherlands
First author email: h.g.kortier@utwente.nl

Inertial and magnetic sensors, attached to various segments of the human hand, can be used to measure movements of the hand. This paper proposes a new method to assess hand kinematics by applying an Extended Kalman Filter in which prior information of the hand is fused with actual measurements obtained from various sensors.

Keywords - hand kinematics, inertial movement sensing, instrumented glove, sensor fusion

1. INTRODUCTION

Analysis of hand kinematics is important in several application areas, such as rehabilitation, sports and ergonomics. In particular, ambulatory tracking of the whole hand configuration is valuable for kinematic assessment under daily life conditions. Current instrumented glove systems primary use resistive, magnetic or optical sensing methods [1]. A common drawback of these systems is that the sensing elements are mounted across the phalangeal joints, which requires an accurate alignment of body and sensor axes. Moreover, sensors that measure joints with multiple degrees of freedom (DoF) are difficult to calibrate because they often suffer from crosstalk due to misalignments. Finally, current instrumented gloves do not measure the translational and rotational movements of the complete hand, which is important when assessing the functionality of hand movements.

Inertial sensors combined with magnetic sensors have proven to be accurate in estimating orientations without the need for external actuators or cameras [2]. The development of MEMS technology resulted in tiny and low-cost Inertial Measurement Units (IMU's) that could be implemented in textile clothing easily without impairing the freedom of movement and tactile sensations.

It is the objective within the PowerSensor project [3,4] to assess the kinematics of the hand using 3D inertial and magnetic sensors, which are attached to the various segments of the hand. To minimize hardware needs, our current version only allows for tracking of the thumb and index finger with 3D accelerometer and magnetometer pairs, and in addition to, tracking of the hand with a full IMU. However, the described algorithm can handle all fingers and thumb in parallel, so as to capture the movement of all degrees of freedom of the hand.

2. METHODS

Theory

The human hand is a highly articulated system but one that is also highly constrained. It's skeleton can be modeled with 21 internal DoF (Fig 1). The distal interphalangeal (DIP) joints and proximal interphalangeal (PIP) joints of each finger have one DoF each, while the metacarpophalangeal (MCP) joints have two DoF. Unlike the fingers, the thumb has five DoF. There are two at the trapeziometacarpal (TM) joint, two DoF at the metacarpophalangeal (MCP) joint and the remaining DoF is located at the interphalangeal (IP) joint [1].
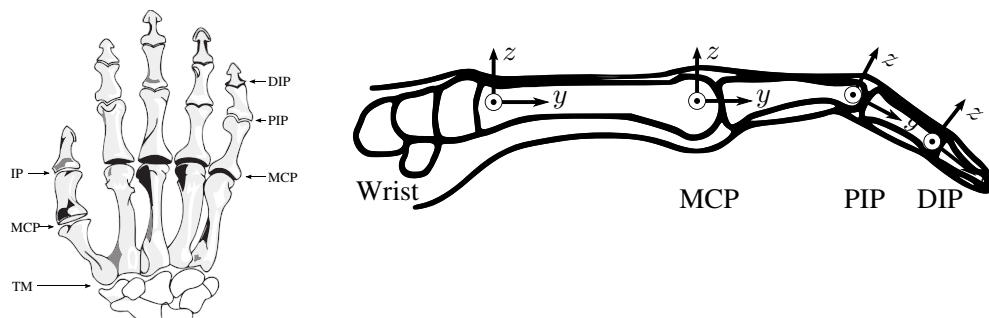

Figure 1. (Left) Capital bones of the human hand. Joints are indicated with their abbreviations. (Right) Defined coordinate frames within the various bones of the index finger.

Estimation of kinematics at any one time is calculated using an Extended Kalman Filter (EKF). The Kalman filter requires a model that describes the evolution of the process and the relation between the measurements taken and the current states, which are the relative segment orientations. The articulated finger and thumb were modeled as two kinematic chains originating from the hand coordinate frame (Ψ_H). This frame is defined by the y-axis pointing to the MCP joint, the z-axis pointing outwards with respect to the dorsal side of the palm and the x-axis is defined according the right-handed coordinate frame (Fig. 1). The position of the fingertip ($\mathbf{p}_E^G$) in global frame (Ψ_G) is obtained after transformation of the fingertip expressed in the distal segment ($\mathbf{p}_E^D$), which can be described by multiplication of subsequent transformation matrices (H) (Fig. 2):

$$\begin{bmatrix} \mathbf{p}_E^G \\ 1 \end{bmatrix} = \mathrm{H}^{GH}\mathrm{H}^{HM}\mathrm{H}^{MP}\mathrm{H}^{PD} \begin{bmatrix} \mathbf{p}_E^D \\ 1 \end{bmatrix} = \mathrm{H}^{GD} \begin{bmatrix} \mathbf{p}_E^D \\ 1 \end{bmatrix} \qquad \text{with:} \qquad \mathrm{H}^{GD} = \begin{bmatrix} \mathrm{R}(q^{GD}) & \mathbf{p}_D^G \\ \mathbf{0}_3^T & 1 \end{bmatrix} \qquad (1)$$

This net transformation H^{GD} contains a rotational part $\mathrm{R}(q^{GD})$, which is the orientation matrix as function of the net quaternion, and a translational part $\mathbf{p}_D^G$, which is the distal segment expressed in global frame. The former is estimated using the Kalman filter whereas the latter is measured in advance. In addition, the orientation of the sensors with respect to the particular segment is obtained during a calibration measurement.

Relative orientation estimates between two linked segments are used for the Kalman's filter input. To estimate the orientation we use a 3D accelerometer as an inclination estimate and a 3D magnetometer to estimate the heading. Now, solving the following cost function result in the optimal orientation estimate (q^{HM}) between two linked segments, for example the hand (H) and the proximal phalanx (M) [5]:

$$L(\mathrm{R}(q^{HM})) := \frac{1}{2} \sum_i^N \left(\boldsymbol{s}^H - \mathrm{R}(q^{HM})\boldsymbol{s}^M \right)^2 \qquad (2)$$

The optimal orientation (q^{HM}) transforms the set of independent vectors measured at the proximal phalanx into a second set of independent vectors, measured at the hand.

Next, during a measurement update the Kalman filter applies dimensionality constraints of the particular joint using a virtual measurement. The angle around the constrained axis of rotation, for example endo-exoration of the MCP joint, should be zero in the optimal case [2]. In case of the MCP joint this can be measured using the dot product of the hand's x-axis ($\mathbf{x}_H$) and the z-axis of the proximal finger segment after transformation to the hand's coordinate frame ($\mathrm{R}(q^{HM})\mathbf{z}_M$).
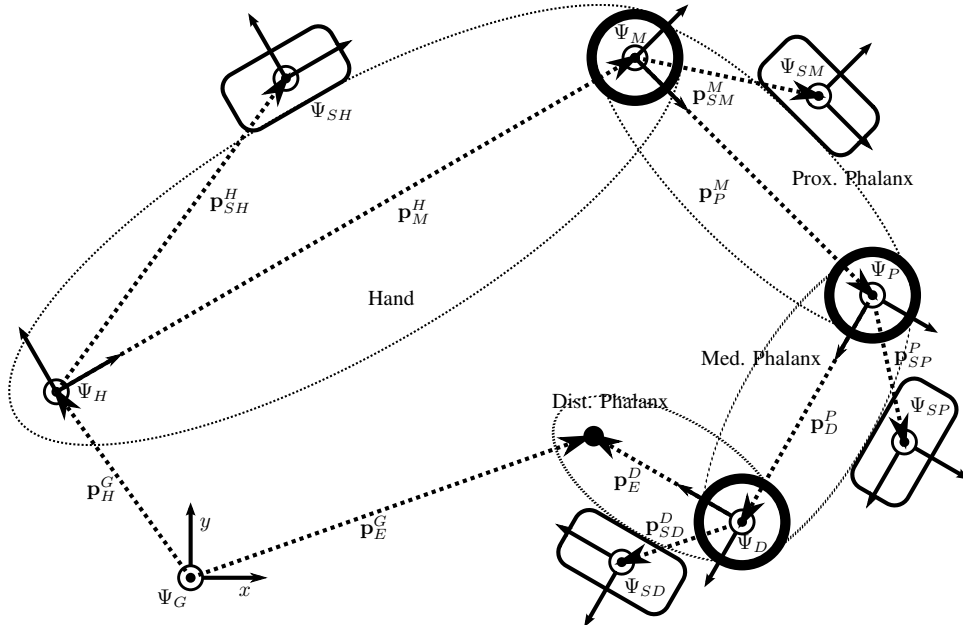

Figure 2. Modeled kinematic chain of four rigid bodies illustrating the hand with one finger. To all segments an accelerometer plus magnetometer pair was attached. Given are the vectors describing the position of both the joint and the IMU to its prior coordinate frame.

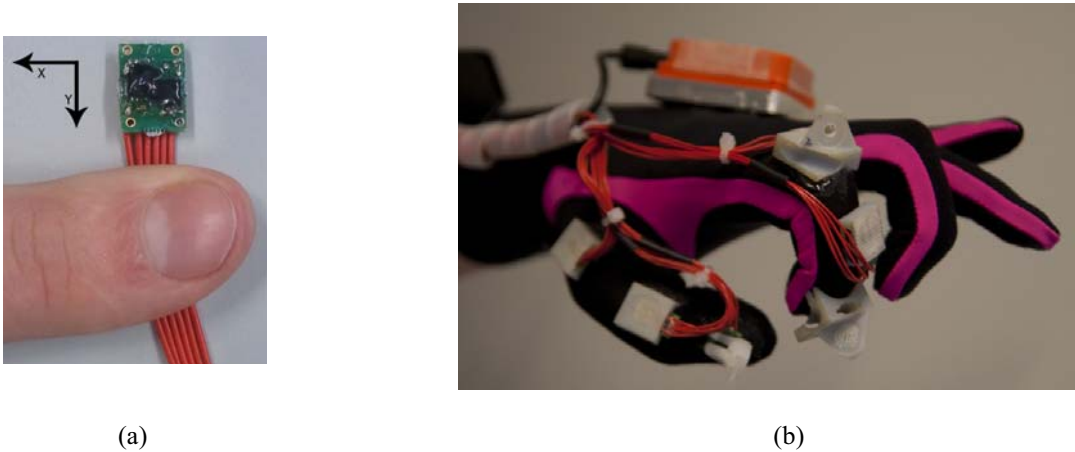(a)   (b)

Figure 3. (a) Single sensor PCB containing a 3D accelerometer and 3D magnetometer (b) Instrumented glove. The PCB's are mounted in a synthetic housing (white). These sensor housings can be expanded with markers for optical measurements. In addition a full 3D IMU (orange, back of the hand is visible. The subject repeatedly made contact with the tips of index finger and thumb (pinch task).

Experimental methods
Multiple, custom made, printed circuit boards (PCB's) equipped with a 3D accelerometer and magnetometer pair have been developed (Fig. 3a). They were mounted to the proximal and medial digits of both the index finger and the thumb. In addition a commercial IMU (Xsens technologies), containing a 3D rate gyroscope, 3D magnetometer and 3D accelerometer) was attached to the back of the hand (Fig. 3b). Sensor data is captured by a microcontroller and subsequently transmitted via USB to a computer where it has been processed offline in Matlab.

3.   RESULTS

As an example trial, one subject performed a pinching task, i.e. the thumb and index finger start completely extended and are subsequently brought in contact by flexing the particular joints (Fig. 3b and 4).
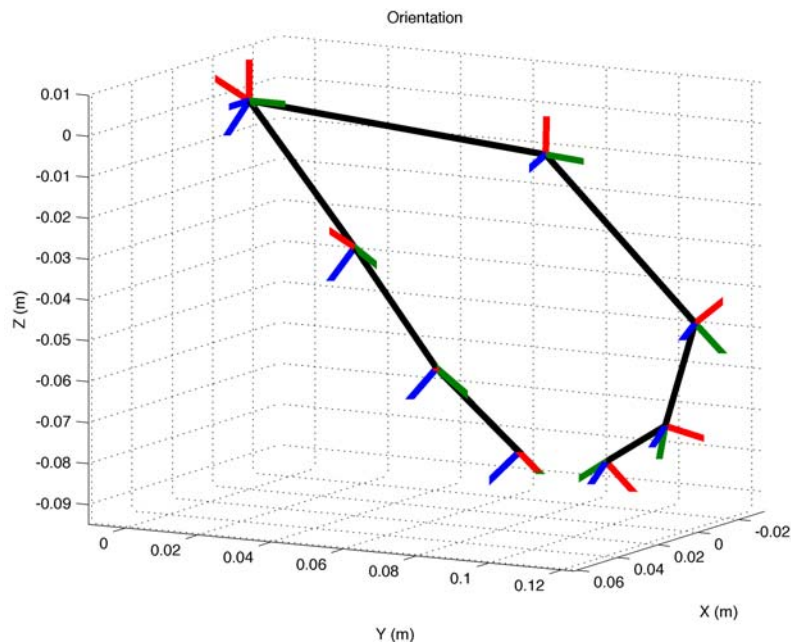

Figure 4. Pose estimate of the hand, index finger and thumb during a pinch task (Fig. 3b). Both index and thumb chains originate from the wrist. The axes of joint coordinate frames and end-effectors of both thumb and finger chains are indicated (x is blue, y is green and z is red)

4. DISCUSSION

The accuracy of the system is currently being evaluated using an optical reference system (PTI VisualEyez 4000).

It should be noted that an inaccurate calibration of sensor to segment orientation causes incorrect orientation updates. We are currently working on a sophisticated calibration method that should result in a more accurate calibration.

The current method determines the relative orientation using 3D accelerometer and magnetometer pair outputs. It is assumed that the difference in inertial acceleration between two subsequent segments is zero or at least small compared to the gravitational acceleration. Hence, during tasks with large finger accelerations (dynamic tasks like piano playing) the error of estimated orientation will be significant. Moreover, it is assumed that both magnetometers are exposed to the same magnetic fields. Local field disturbances to either of both sensors will also result in incorrect orientation estimates.

Therefore a new glove system is currently under development where, in addition to the current sensory, 3D rate gyroscopes will be applied to estimate the orientation under conditions with large inertial acceleration and disturbed magnetic fields.

5. ACKNOWLEDGMENT

6. REFERENCES

[1] L. Dipietro, A. Sabatini, and P. Dario, "A survey of glove-based systems and their applications," *Systems, Man, and Cybernetics, Part C: Applications and Reviews, IEEE Transactions on*, vol. 38, no. 4, pp. 461–482, 2008.

[2] H. Luinge, P. Veltink, and C. Baten, "Ambulatory measurement of arm orientation," *Journal of Biomechanics*, vol. 40, no. 1, pp. 78–85, 2007.

[3] H. G. Kortier and P. H. Veltink, "Load identification during object handling," in *Engineering in Medicine and Biology Society, EMBC, 2011 Annual International Conference of the IEEE*, 2011, pp. 3500–3502.

[4] P. Veltink, H. Kortier, and H. Schepers, "Sensing Power Transfer Between the Human Body and the Environment," *Biomedical Engineering, IEEE Transactions on*, vol. 56, no. 6, pp. 1711–1718, 2009.

[5] F. Markley and D. Mortari, "Quaternion attitude estimation using vector observations.," *Journal of the Astronautical Sciences*, vol. 48, no. 2, pp. 359–380, 2000.

Characterisation of input parameter influence on dynamic orbital stability of walking

(An in-silico and experimental analysis on the effects on maximum Floquet multipliers of implementations of orbital stability technique and of experimental noise)

Riva F. [1], Bisi M.C. [1], Stagni R. [1]

[1] DEIS, [1]Department of Electronics, Computer Sciences and Systems, University of Bologna, Bologna, Italy

Still in literature there is no consensus on how to define or quantify locomotor stability. Nevertheless, locomotor stability represents an important issue in clinical assessment procedures. Orbital stability analysis applied to biomechanics (and in particular to walking) can help reaching such definition, but still this technique is deemed to be controversial, possibly because of the lack of a standard implementation. The aim of this study was to analyse the influence of the number of analysed gait cycles and of the experimental measurement noise on the orbital stability analysis outcomes (maximum Floquet multipliers). In-silico and experimental analysis were conducted on acceleration data. The number of cycles included in the analysis strongly influenced the stability result, while simulated experimental noise did not affect maximum Floquet multipliers. Experimental analysis generally confirmed these results, showing similar trends.

Orbital stability; Walking; Fall risk; Floquet multipliers; Elderly

1. INTRODUCTION

Falls in elderly represent a major community and public health problem, with large clinical and economic consequences [1,2]. The identification of individual chronic characteristics associated with falling is of fundamental importance for the clinicians [3]. In particular, a better understanding of locomotor stability is a critical issue in clinical assessment procedures [4]. Many stability indices have been proposed for clinical application [5–9], but still there is no commonly accepted way to define or quantify locomotor stability [10]. The application of stability analysis of nonlinear dynamic systems to biomechanics can lead to a comprehensive definition of locomotor stability.

Many human tasks are structurally cyclic, and show a periodic-like behaviour. With this assumption, a motor task can be treated as a nonlinear dynamic system: biomechanical variables (e.g. joint angles, accelerations) vary during the temporal evolution of the task, defining a system that continuously changes over time. Techniques of nonlinear stability analysis basically consist in the quantification of the tendency of an orbit (defined by the temporal evolution of a set of variables called *state space*) to diverge or converge to the previous one or to an attracting limit cycle. Two main approaches for nonlinear stability analysis in biomechanics are present in literature: local and orbital stability analysis [10]. In particular, orbital stability analysis seems a promising approach for the definition of a reliable motor stability index [11–13]. This approach can be applied to periodic systems with a limit cycle behaviour; it has been extensively used in the study of passive dynamic walking robots [14], and in the last years it has been applied also to biomechanics [4]. Fundamental indicators of orbital stability are maximum Floquet multipliers (maxFM) quantifying, discretely from one cycle to the next, the tendency of the system's states to return to the periodic limit cycle orbit after small perturbations [10].

Despite the good premises, the use of maxFM in the assessment of fall risk has been deemed controversial [9]. A possible cause of this controversy lies in the lack of a "standard" implementation of this technique, being the technique relatively novel in biomechanics. When dealing with biomechanical time series, orbital stability implementation is not straightforward; for example, the minimum and optimum number of task cycles to include in the analysis to obtain reliable stability results is not defined. Moreover, it is yet not clear how the experimental noise can affect maxFM calculation.

The aim of the present study was to analyse the influence on the final results of orbital stability analysis, applied to walking, of the number of analysed cycles and of the experimental measurement noise. First an in-silico analysis was implemented on a 5-link walking model [15], which provided walking patterns of known

stability with a more physiological characterization of walking pattern than previous studies performed on 2-link models [16,17]. Then, results of in-silico analysis were verified experimentally on 10 subjects performing long overground walks.

2.   MATERIALS AND METHODS

An in-silico orbital stability analysis of a 5-link stable walking model [15] was performed. The analysis was performed for increasing number of cycles (from 10 to 300) on two acceleration based state spaces (one composed by noise free acceleration signals and one composed by signals affected by simulated experimental noise). Experimental analysis was then performed to reproduce the conditions implemented in the model. Orbital stability was calculated using an established technique [13]. If maxFM have magnitude < 1, perturbations tend to shrink by the next repetition, and the system remains stable.

In-silico data

The 2-dimensional, five-link biped walking model analysed [15] consisted in one trunk, two thigh and two shank segments. Model orientation was described by stance and swing knee angles, stance and swing hip angles and upper body angle ($\phi_{k,sw}$, $\phi_{k,st}$, $\phi_{h,st}$, $\phi_{h,sw}$, ϕ_{ub}, all with respect to gravity). The model was adapted to perform 300 consecutive steps. Accelerations of the trunk segment at the level of the fifth lumbar vertebra (l5) were calculated. Realistic instrumentation noise was added to acceleration signals of the trunk segment at the level of l5. The aim was to simulate signals that could be obtained from an inertial sensor located in that area. White noise with an SNR of 10 dB and alignment error with a normal distribution and a standard deviation of 0.1 degrees were added.

Experimental data

10 healthy young subjects [age 28 ± 3 years, height 174 ± 11 cm, weight 67 ± 13 kg] were involved in the study. Subjects gave informed consent before participating. Two synchronized triaxial inertial sensors (Opal, APDM, Portland, OR, USA) were placed on the subjects at the level of l5 and of the right shank. Sampling rate was 128 Hz. The subjects were instructed to walk normally at their preferred speed on a 250 m long road.

Data processing

For both model and experimental data, stride cycles were considered as the time between each right heel strike and resampled to be 100 samples long. For experimental data, right heel strike instants were estimated from the angular velocity of the lower limb with a method based on wavelet analysis [18].,Angular velocity of the lower limb was measured with the inertial sensor placed on the right shank. Both for model and experimental data, orbital stability analysis was performed on a state space composed by the accelerations in the anterior-posterior (AP) and vertical (V) direction of the trunk at the level of l5 (Eq. 1).

$$SS(t) = \left[a_{l5,vt}(t), a_{l5,ap}(t) \right] \in \Re^2 \qquad (1)$$

Mean values of maximum Floquet multipliers across the gait cycle were calculated upon increasing number of strides (from 10 to 300 for model data, from 10 to 160 for experimental data).

3.   RESULTS

MaxFM calculated on in-silico data showed a different behavior with respect of the number of gait cycles (Figure 1a); for less than 30 cycles, values of maxFM gradually decrease, starting from values near (or above) one, indicating very poor stability. Nevertheless, the model is known to be stable, so these values are incoherent with the model and not believed to be reliable. From about 30 cycles on, values of maxFM stabilize around 0.34, with a standard deviation of about 0.09. Results coming from analysis of noisy accelerations signals are very similar to the ones obtained from noise-free signals; the value of maxFM tend to stabilize around 0.34 from about 30 cycles on. MaxFM calculated on experimental data showed decreasing value for increasing number of cycles analysed (Figure 1b), reaching values close to 0.4 for 80 cycles on, with a standard deviation of about 0.1.
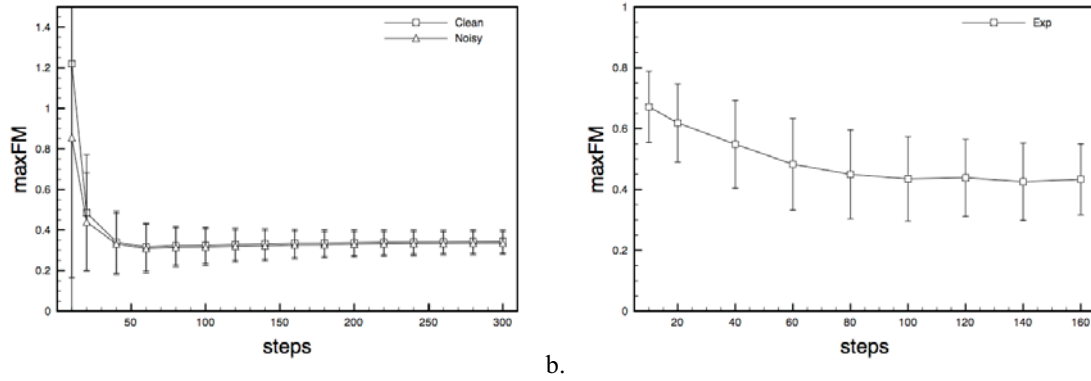
a.   b.

Figure 1. a) Mean maxFM values across the step cycle calculated on state spaces composed by vertical and anterior-posterior l5 accelerations (noisy and clean) coming from the model for increasing number of step cycles used in the calculations. b) Mean maxFM values across the step cycle calculated on state spaces composed by vertical and anterior-posterior l5 accelerations coming from experimental trials for increasing number of step cycles used in the calculations.

4.   DISCUSSION

In this explorative study orbital stability analysis have been applied to 5-link stable walking model, with the aim to better understand the influence of number of analysed cycles and experimental noise on the stability results. Simulated experimental noise were also generated and added to the signals coming from the model, in order to reproduce experimental conditions. Results were then compared to experimental results obtained from a sample of 10 young subjects walking at their preferred speed.

The number of cycles included in the analysis strongly influenced the stability result; it seems to play a fundamental role when trying to obtain a reliable orbital stability measure. Orbital stability analysis conducted on "clean" acceleration signals coming from the stable walking model resulted in maxFM values that tend to the value of 0.34, with a strong dependance from the number of cycles considered; at least 30 cycles are needed to reach this value analysing a state space containing vertical and anterior-posterior accelerations of l5. Analysis of noisy accelerations of l5 led basically to the same results obtained for clean signals; simulated inertial sensor experimental noise did not influence the maximum Floquet multiplier result and its dependance upon the number of analysed cycles. This leads to the conclusion that orbital stability analysis performed on state spaces composed by accelerations coming from inertial sensors is noise robust.

Experimental trials results on the accelerations-based state space showed a similar trend with respect to the ones obtained from the analysis of the same variables derived from the model; nevertheless, the value of maxFM obtained was slightly higher, and so the standard deviation. A limitation of this experimental session was the relatively short length of the walks (160 steps) with respect to the model data.

The exploration of the influence of experimental input parameters in orbital stability analysis led to interesting results. The number of analysed cycles plays a critical role in maxFM calculation; when dealing with acceleration data of the trunk at the level of l5, at least 30 cycles are needed to obtain a reliable value for the maxFM from model analysis. Preliminary experimental results show a similar trend of maxFM values for increasing number of cycles, but the final value for the maxFM is slightly different (0.4 instead 0.34), obtained from 80 cycles on. These results seem to confirm that orbital stability analysis of acceleration data coming from a single inertial sensor could significantly contribute to define a reliable locomotor stability index, but an appropriate number of gait cycles must be analysed. The possibility to obtain reliable orbital stability measures with a single inertial sensor could lead to advantages in the development of a simple and fast data acquisition protocol.

5.   ACKNOWLEDGMENT

The authors gratefully thank Dr. Martijn Wisse for its contribution in the implementation of the model.

6.   REFERENCES

[1]   Fuller G. F., 2000. Falls in the elderly. Am Fam Physician, 61(7) 2159-2168, 2173-2174.
[2]   Heinrich S., Rapp K., Rissmann U., Becker C., König H.-H., 2009. Cost of falls in old age: a systematic review. Osteoporosis International, 21, 891-902.
[3]   Tinetti M. E., Williams T. F., Mayewski R., 1986. Fall risk index for elderly patients based on number of chronic disabilities. Am. J. Med, 80(3), 429-434.
[4]   Hurmuzlu Y., Basdogan C., 1994. On the measurement of dynamic stability of human locomotio. J Biomech Eng, 116(1), 30-36.

[5] Hausdorff J. M., Rios D. A., Edelberg H. K., 2001. Gait variability and fall risk in community-living older adults: a 1-year prospective study. Arch Phys Med Rehabil, 82(8), 1050-1056.

[6] Hof A. L., Gazendam M. G. J., Sinke W. E., 2005. The condition for dynamic stability. Journal of Biomechanics, 38(1), 1-8.

[7] Holt K. J., Jeng S. F., RR R. R., Hamill J., 1995. Energetic Cost and Stability During Human Walking at the Preferred Stride Velocity. J Mot Behav, 27(2), 164-178.

[8] Karcnik T., 2004. Stability in legged locomotion. Biological Cybernetics, 90(1), 51-58.

[9] Hamacher D., Singh N. B., Van Dieën J. H., Heller M. O., Taylor W. R., 2011. Kinematic measures for assessing gait stability in elderly individuals: a systematic review. Journal of The Royal Society Interface, 8(65), 1682 -1698.

[10] Dingwell J. B., Kang H. G., 2007. Differences between local and orbital dynamic stability during human walking. J Biomech Eng, 129(4), 586-593.

[11] Dingwell J. B., Kang H. G., Marin L. C., 2006. The effects of walking speed on orbital stability of human walking. Journal of Biomechanics, 39(Supplement 1), pag. S114.

[12] Dingwell J. B., Robb R. T., Troy K. L., Grabiner M. D., 2008. Effects of an attention demanding task on dynamic stability during treadmill walking. J Neuroeng Rehabil, 5, pag. 12.

[13] Hurmuzlu Y., Basdogan C., Stoianovici D., 1996. Kinematics and dynamic stability of the locomotion of post-polio patients. J Biomech Eng, 118(3), 405-411.

[14] McGeer T., 1990. Passive Dynamic Walking. The International Journal of Robotics Research, 9(2), 62-82.

[15] Solomon J. H., Wisse M., Hartmann M. J., 2010. Fully interconnected, linear control for limit cycle walking. Adaptive Behavior, 18(6), 492 -506.

[16] Su J. L.-S., Dingwell J. B., 2007. Dynamic stability of passive dynamic walking on an irregular surface. J Biomech Eng, 129(6), 802-810.

[17] Roos P. E., Dingwell J. B., 2011. Influence of simulated neuromuscular noise on the dynamic stability and fall risk of a 3D dynamic walking model. Journal of Biomechanics, 44(8), 1514-1520.

[18] Aminian K., Najafi B., Büla C., Leyvraz P.-F., Robert P., 2002. Spatio-temporal parameters of gait measured by an ambulatory system using miniature gyroscopes. Journal of Biomechanics, 35(5), 689-699.

Wed – July 18th 2012

Chairmen: **Nicola Sancisi (DIEM, University of Bologna, Italy)**
            Alberto Leardini (Istituto Ortopedico Rizzoli, Italy)

Industry #1 and Projects session:
11.15 : 12.50

11.15	Charnwood Dynamics Ltd. / Codamotion
11.25	Motion Analysis Corporation
11.35	Xsens Technologies B.V.
11.50	Ergonomics in Ducati motorcycles, Simone Di Piazza (Vehicle Design and R&D services Manager, Ducati Bologna)
12.05	Motor Science Research Center, Università degli Studi di Torino, Donato Formicola
12.20	"Acceleromics: the art to use mobile accelerometry to improve human health", Martin Daumer *(*The Human Motion Institute, Trium Analysis Online GmbH, Germany*)*
12.35	"Closed-loop system for personalized and at-home rehabilitation of people with Parkinson's Disease – The CuPiD research project", Laura Rocchi (DEIS, University of Bologna, Italy)

!

Motor Science Research Center

<u>Presenter:</u> Donato Formicola

Motor Science Research Center, School of Exercise and Sport Sciences, Università degli Studi di Torino, Italy

The Motor Science Research Center (MSRC) of the University of Turin is an International Italian research center where the motor activity (MA) is studied under the behavioral and neuromechanical points of view.

MA modeling is pivotal to describe the dynamic of human motions and it needs the application of bioengineering procedures. Using such an approach we could define the aim of MSRC as to study the transfer function which link the electrical activity of the muscles with the equation of the motions calculated by the biomechanics analysis of the MA. For this reason, surface electromyography, force plates, qualitative electroencephalography, and three-dimensional motion capture systems are the tools adopted to "sense" the real world trying to model the MA. At the MSRC very comfortable biosensors were used to allow MA without MA without constraints. To date, an innovative markerless motion capture system was designed to the evaluation of sport performances and it is under modification to be adopted in the evaluation of daily life activities. A multidisciplinary and kinesiological approach is used to disentangle the outcomes from MA models.

From the analysis of the sport techniques to the effectiveness of the daily life activities, MSRC is prone to evaluate MA in a range of situations: both in pathological and healthy conditions. The results can be used to help sport preparations and rehabilitation treatments, to improve the ergonomic of the workplaces, to prevent the onset of the injuries, and to counteract aging effects.

Project

!

Acceleromics: the art to use mobile accelerometry to improve human health

Presenter: Dr. Martin Daumer

Director SLC e.V. - The Human Motion Institute (www.thehumanmotioninstitute.org) , Managing Director Trium Analysis Online GmbH (www.trium.de)

We report about the outcomes of several European and national project related to capturing and analysing human motion data with mobile accelerometry,

comprising an accelerometry data warehouse of more the 100.000 hours of high quality recordings of human motion. A focus will be on the question if

the public funding has helped to bring scientific results and technological developments to the market.

1. VPHOP - The osteoporotic virtual physiological human (EU FP7 - http://www.vphop.eu/)

2. NETSIM - "Acceleromics and genomics" for cardiovascualr diseases - (EU-FP7 - https://haemgen.haem.cam.ac.uk/netsim/)

3. IPAT - An integrated platform for measureing physical activity as outcome and treatment option in Multiple Sclerosis (BMBF)

4. ABMA - Advanced body motion analysis - wireless communication and sport science (BWiMi)

We describe the technology platform "actibelt" (www.actibelt.com) and the corresponding algorithms and their validation, inparticular fall detection, rapid tests for fall risk assessment,

innovative measurements of real life walking speed and the use for exercise therapy. Clinical applications of this nice field of "computational medicine" including business models are highlighted.

Project

!

Closed-loop system for personalized and at-home rehabilitation of people with Parkinson's Disease – The CuPiD research project

Presenter: Laura Rocchi

Department of Electronics, Computer Science and Systems, University of Bologna, Italy

People with Parkinson's disease (PD) suffer from motor and cognitive impairments that severely impact mobility, fall risk, and multiple key aspects of functional independence. Until recently, treatment goals focused almost exclusively on symptom relief, but exciting recent works have demonstrated that motor learning and rehabilitation principles can be effective even in the presence of PD.

 Optimal rehabilitation of such a neurodegenerative disease requires personalized training paradigms that patients can integrate into their everyday routine. Ongoing, long-term treatment in a clinical setting is not feasible, cost effective, or likely something that patients can comply with year after year.

CuPiD is designed to meet this challenge by means of ICT-enabled solutions and on-board intelligence, to target in particular mobility, cognitive function and debilitating PD symptoms such as freezing of gait.

Key components of the CuPiD solution are: - a home-based rehabilitation system (based on unobtrusive wearable sensors, on-board intelligence for real-time biofeedback, virtual reality, and modular restitution interfaces); - an intelligent telemedicine infrastructure for remote monitoring and supervision of the rehabilitation program by a clinician.

Two main application scenarios are present in the CuPiD framework: - a first set of motor learning exercises using a virtual reality/gaming approach; - an outdoor scenario mainly to rehabilitate gait which will integrate wearable sensors to detect gait phases and real time feedback returned to the user via a portable computation unit. The motor learning exercises are designed to be subject-specific and tuned, in real time, to the subject's daily condition.

While pilot experiments are still running, an extended validation of the CuPiD system on more than 40 subjects with PD is planned for the second half of the project's life.

www.cupid-project.eu

Wed – July 18th 2012

__Chairmen:__   **Georgios Stylianides (Towson University, USA)**
Andrea G. Cutti (INAIL, Italy)

__Poster session #1__: *"Outdoor measurements, inertial and wearable devices*
14.00 : 15.30   *& Video-based motion tracking"*

P01	Estimation of spatial-temporal gait parameters and pelvis kinematics in level walking based on a single inertial sensor	Bugané F., Benedetti M.G., Casadio G., Leardini A.
P02	Towards an integrated 3D accelerometry platform to assess the risk of falling: a feasibility study Logistic. Data management and data extraction in an European multi-center setting	Soaz C., Daumer M.
P03	INTERACTION - Training and monitoring of daily-life physical interaction with the environment after stroke	Veltink P.H., van Meulen F.B., van Beijnum B.J.F., Hermens H.J., De Rossi D., Lorussi F., Tognetti A., Buurke J.H., Reenalda J., Baten C.T.M., Simons C.D.M., Luft A.R. Schepers H.M., Luinge H.J., Paradiso R., Orselli R.
P04	PowerGlove - Concepts and current results	Veltink P.H., Kortier H.G., Schepers H.M., Sluiter V.I., Brookhuis R.A., Lammerink T.S.J., Wiegerink R.J.
P05	Improving inertial sensor measurement of the relative orientation between trunk and pelvis using a potentiometer	Larue C., Plamondon A., Desjardins P., Salazar E., Mecheri H., Sirard C.
P06	Motion sensors for measurement of gait modifications in knee osteoarthritis	Wrigley T.V., Lai D.T.H., Shilton A.
P08	Performance analysis of an automatic tracking software in underwater exercises	Magalhães F. A., Sawacha Z., Di Michele R., Cortesi M., Gatta G., Fantozzi S.
P09	Passive drag and body position of swimmers wearing a rubber full-body swimsuit	Cortesi M., Di Michele R., Fantozzi S., Zamparo P., Gatta G.
P10	Underwater Gait Analysis: A Markerless Approach	Mantoan A., Sawacha Z., Fantozzi S., Cortesi M., Rigato A., Gatta G., Cobelli C.
P11	In-vivo vs. in-vitro kinematics of the proximal inter-phalangeal joint in the finger	Caravaggi P., Chen L., Uko L., Shamian B., Capo J.T.
P13	Do people follow the principle of end-state comfort in a rotation task?	Lardy J., Beurier G., Wang X.
P14	Biomechanical analysis of self-selected upper limb posture for grasping and holding	Zhou W., Armstrong T., Wegner D., Reed M.
P15	A 3D model of reach limitations for workstation design	Rempel D., Barr A., Baum D., Camilleri M., Duarte R., Janowitz I., Woo J.
P16	Effects of high-heeled shoes on the control of the body's center of mass motion in relation to center of pressure during gait	Chien H.L., Lu T.W., Liu M.W.
P17	Influence of speed of progression on the gait of young children	Van Hamme A., Samson W., Dohin B., Dumas R., Chèze L.
P18	Effect of high-heeled shoes on three-dimensional body center of mass displacement during walking	Sidequersky F.V., Annoni I., Mapelli A., Lenci B., Colangelo V., Sforza C.
P19	Performance of the stabilizing system of the lumbar spine during a functional task	Preuss R., Al Zoubi F., Pakzad M.

Estimation of spatial-temporal gait parameters and pelvis kinematics in level walking based on a single inertial sensor
Validation on normal subjects by standard gait analysis

Bugané F.[1], Benedetti M.G.[3], Casadio G.[1], Leardini A.[2]

[1] LorAn Engineering Srl, Castel Maggiore, Bologna, Italy
[2] Movement Analysis Laboratory, Istituto Ortopedico Rizzoli, Bologna, Italy
[3] Functional Recovery and Rehabilitation, Istituto Ortopedico Rizzoli, Bologna, Italy

Lower trunk acceleration, walking, inertial sensing, validation, pelvis kinematics.

1. INTRODUCTION

Human mobility is a fundamental requirement for a satisfactory quality of life. Level walking is a basic requirement for many daily activities, therefore modern gait analysis provides essential information on the functional capabilities of subjects [1,2]. This is obtained by measuring the kinematics and kinetics of the main body segments and joints using stereophotogrammetry and dynamometry in well-instrumented and specifically-designed laboratories. Wireless inertial sensing devices are being developed recently also for the assessment of spatial-temporal parameters in unobstructed environment outdoors, thus overcoming the typical limitations of measurements in indoor laboratory settings [3-5]. The specific scope of the present study was to assess the relevant performance of a novel technique based on a single wireless inertial sensing device, Free4Act (F4A - LorAn Engineering, Bologna, Italy), in particular to validate the estimation of the traditional spatial-temporal parameters once this is located on the lower trunk. The measurements obtained with this device and relevant original algorithms were compared with corresponding ones obtained by state-of-the-art gait analysis (GA). Furthermore the present study was aimed at investigating whether the same single sensor on the same location can provide reliably also kinematics of the pelvis during level walking.

2. MATERIAL AND METHODS

The new portable F4A consists of a wireless network of inertial sensors for human movement analysis. The sensors are controlled by a data logger unit (up to 16 elements) by a ZigBee radio type communication. Each sensor is sized 62x36x16 mm, has a weight of 60 g, and is composed of a 3-axis accelerometer (max range ± 6·g), a 3-axis gyroscope (full scale ± 300 deg/s) and a 3-axis magnetometer (full scale ± 6 gauss). This sensing device is calibrated with the gravitational acceleration immediately after manufacturing. The F4A sensor is attached to the subject's waist with a semi-elastic belt, covering the L4-L5 inter-vertebral space. Ten women and twelve men volunteered for the first series of the validation experiments, those for spatial-temporal parameters estimation. The subjects were recruited among students of the University of Bologna and none had a previous history of muscle-skeletal, neurological, or generic gait disorders. Their age ranged from 20 to 35 years (mean and standard deviation - SD - of age for women: 24.1 years SD 1.29; for men: 27.4 years SD 3.77), their body mass ranged from 51 to 95 kg (for women: 55.8 kg SD 5.07; for men: 79.4 kg SD 8.42) and their height ranged from 160 to 187 cm (for women: 166.8 cm SD 4.92; for men: 176.8 cm SD 6.20). Each subject was fitted with the relevant reflective markers and the F4A sensor. This motion analysis was performed with a sensitivity for the F4A accelerometer of 6G and a sampling frequency of 50 Hz. The subjects were asked to stand up and remain in the up-right posture for a few seconds, and then to walk barefoot along a 10-m pathway, at a self-selected speed. This entailed 8 to 12 steps, according to the subject's natural cadence; the central three, for the right and left full gait cycles, were analyzed also by the GA system. This exercise was repeated 5 times for each participant. To test the right and left step identification procedure, the subjects were asked to start walking always with the right foot. In a few subjects, at the beginning of the study, two additional F4A sensors were placed on the dorsal aspect of the forefeet. From the collected acceleration signals, the typical spatial-temporal gait parameters [6] are then obtained. The validation of this system was performed by using a GA system, which included a stereophotogrammetric unit with eight M2-cameras (Vicon 612, Vicon Motion Capture, Oxford, UK) and two dynamometric platforms (Kistler Instruments, Einterthur, Switzerland). For marker positioning and lower limb 3-D kinematics, a recently established protocol for clinical analysis was used [6,7]. All relevant raw data were first filtered by a first-

order Butterworth low-pass filter with a cut off frequency of 2 Hz. To estimate the spatial-temporal parameters, the anterior-posterior (z-axis) accelerometer signal of F4A was found to be the most revealing, while to discriminate automatically between left and right steps, the medial-lateral (y-axis) acceleration was analyzed.

Five healthy adult male volunteers were recruited for the second part of this study in which the gyroscopic signals were analyzed in order to describe the kinematics of the pelvis in the sagittal, frontal and transverse planes. Their age ranged from 34 to 44 years (mean and standard deviation - SD - of age: 38.4 years SD 3.78), their body mass ranged from 71 to 84 kg (76.8 kg SD 5.07) and their height ranged from 172 to 180 cm (175.4 cm SD 3.13). The subjects were asked to perform the same exercises described in the validation experiments here above. The F4A gyroscope sensitivity was set at 300 deg/s and the sampling frequency at 100 Hz. Two different experiments were performed to assess variability of the measurements obtained. First intra-subject repeatability was assessed by analyzing 5 repetitions of walking exercise performed by each of the 5 subjects wearing own shoes. Similarly, inter-subject variability was assessed by analyzing one repetition from each of the 5 subjects within the same gait conditions, i.e. a single subject walked barefoot to avoid irregular pelvic kinematic patterns due to wearing different types of shoes. To describe kinematics of the pelvis all the three gyroscopic signals were elaborated, in order to obtain the tilt rotation with positive angular values for forward bending (gyroscope x-axis), the obliquity rotation with positive angular values for bending to the left side (gyroscope z-axis) and the axial rotation with positive angular values for rotation to the left side (gyroscope y-axis).

3. RESULTS

Antero-posterior acceleration at L5 (Figure 1) was found cyclic, with two close positive peaks and a single negative peak. Corresponding signals from the sensors on the forefeet and the preliminary comparison with GA data suggested associating the second positive peak to heel strike. Each step was identified between two consecutive of these peaks, and right/left discrimination was obtained successfully for each trial. The good intra- and inter-subject consistency among the subjects of the parameter estimations was also supported by the direct observation of the anterior-posterior acceleration patterns (Figure 2); the thin standard deviation band demonstrates the small intra-subject variability. The curve shows a maximum peak precisely at 50% of the cycle, in correspondence of the heel contact of the contralateral, i.e. left, foot. Minimum peaks are at about 10% and 60%, in correspondence of the toe-off events, respectively of the left and right feet. The three positive and the two negative peaks of acceleration have a very similar timing and value over the subjects. Based on this identification, the spatial-temporal parameters were determined; for one of these parameters, values obtained from all subjects are provided (Table 1). The values obtained were consistent over subjects, in the range of physiological gait, and in particular these compared well with corresponding values from GA-based measurements. Less reliable results were obtained for the identification of the phases within the gait cycles, where significant differences were found for some subjects. In this table, most t-test values of the two comparisons with the GA, i.e. the gold standard, appeared to be smaller when all cycles were included, showing that the two cycles exactly corresponding to those from GA compared better than all possible cycles all together.
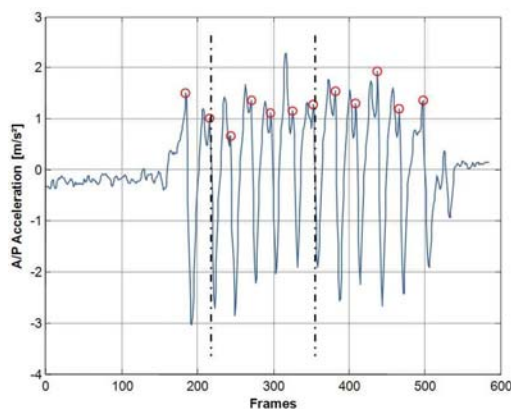

Figure 1. Antero-posterior acceleration signal from the F4A sensor in a representative subject (#2) during the full exercise of standing and walking, after Butterworth low-pass filtering. The period when the GA system collects data is shown between vertical lines (dash-dot). Peaks for heel-strike are pointed out (red circles).
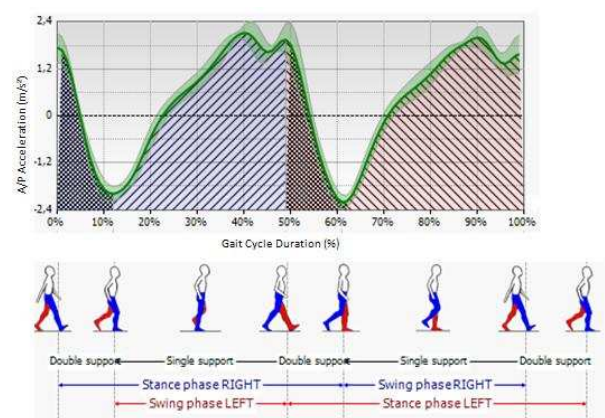

Figure 2. Anterior-posterior acceleration over the normalized cycle (0 - 100%) of the right leg; the cycle taken was the one observed also by GA. Mean (solid curve) and one standard deviation (grey band) are shown as calculated over 5 repetitions of subject #2.

Table 1. Left Step Duration as calculated with GA and estimated with the F4A system for each subject.

Subjects	GA data		GA-cycle F4A data		t-test	All cycles F4A data		t-test
	Mean	SD	Mean	SD		Mean	SD	
#1	0.50	0.01	0.48	0.01	0.086	0.48	0.02	0.105
#2	0.54	0.02	0.55	0.03	0.603	0.55	0.02	0.338
#3	0.54	0.01	0.54	0.02	0.783	0.56	0.02	0.110
#4	0.55	0.01	0.58	0.03	0.197	0.58	0.03	0.209
#5	0.53	0.01	0.55	0.03	0.262	0.56	0.03	0.066
#6	0.54	0.01	0.53	0.02	0.065	0.54	0.02	0.623
#7	0.56	0.01	0.56	0.03	0.639	0.56	0.02	0.886
#8	0.59	0.01	0.60	0.04	0.312	0.60	0.03	0.719
#9	0.54	0.01	0.54	0.02	0.589	0.55	0.02	0.356
#10	0.47	0.01	0.50	0.03	0.164	0.48	0.03	0.381
#11	0.54	0.02	0.56	0.06	0.841	0.57	0.03	0.203
#12	0.51	0.02	0.47	0.02	0.093	0.48	0.02	0.100
#13	0.53	0.01	0.49	0.03	0.094	0.50	0.03	0.220
#14	0.52	0.01	0.53	0.02	0.912	0.53	0.01	0.630
#15	0.54	0.02	0.55	0.01	0.333	0.56	0.01	0.359
#16	0.48	0.01	0.47	0.01	0.185	0.49	0.02	0.278
#17	0.53	0.02	0.54	0.02	0.551	0.55	0.01	0.206
#18	0.58	0.02	0.62	0.05	0.206	0.63	0.01	0.067
#19	0.52	0.02	0.49	0.03	0.077	0.50	0.01	0.080
#20	0.56	0.02	0.56	0.02	0.573	0.56	0.02	0.907
#21	0.54	0.03	0.56	0.05	0.296	0.77	0.45	0.302
#22	0.61	0.03	0.61	0.02	0.955	0.81	0.45	0.397
Mean	0.54	0.02	0.54	0.03	-	0.57	0.06	-

Table 2. Average value and standard deviation over the walking cycle for the three pelvis rotations in space obtained on 5 trials of a single subject (#5b).

Intra-subject repeatability [deg]						
Subject #5b	Avg RoM	SD RoM	Avg Max	SD Max	Avg Min	SD Min
Pelvic tilt [deg]	4.64	0.38	2.66	0.35	-2.02	0.39
Pelvic obliquity [deg]	8.1	0.22	3.42	0.11	-4.7	0.17
Pelvic rotation [deg]	11.04	1.09	5.8	0.84	-5.26	0.43

Table 3. Maximum and minimum angular values and relative range of motion over the walking cycle for pelvis rotations as measured on one repetition over the group of 5 subjects walking barefoot.

Inter-subject variability [deg]									
Subjects	Tilt [deg]			Obliquity [deg]			Rotation [deg]		
	Max	Min	RoM	Max	Min	RoM	Max	Min	RoM
#1b	2.6	-0.9	3.4	2.4	-2.8	5.2	3.7	-0.9	4.5
#2b	0.8	-1.6	2.5	4.1	-3.5	7.6	7.2	-5.1	12.2
#3b	1.3	-1.9	3.1	2.8	-3.4	6.2	5.7	-4.2	9.8
#4b	3.2	-0.7	3.9	5.2	-6.5	11.7	2.6	-3.6	6.2
#5b	1.7	-1.5	3.2	2.6	-3.6	6.2	5.7	-4.1	9.8
Mean	1.92	-1.32	3.22	3.42	-3.96	7.38	4.98	-3.58	8.5
SD	0.97	0.50	0.51	1.20	1.45	2.56	1.82	1.59	3.10

After the gyroscopic signal elaboration, the main pelvis motion patterns in the three anatomical planes were also obtained. In order to verify the good intra- and inter-subject consistency of the estimated parameters, the maximum and minimum angular values and the relevant range of motion (RoM) were reported (Tables 2 and 3). Intra-subject repeatability was high for all the measurements (Table 2). SD of RoM was less than 1.1° for

all three pelvis rotations. The most repeatable rotation within the same subject was pelvic obliquity (0.22°) and the least was pelvic rotation (1.09°). Inter-subject variability was moderately small (Table 3). The most repeatable inter-subject motion was pelvic tilt (0.51°) and the least was pelvic rotation (3.1°).

4. DISCUSSION

The present values of spatial-temporal parameters compare well with corresponding reference data reported in the literature [4,8,9] from large populations of healthy subjects and by a variety of comprehensive instruments. Furthermore, the present results are in agreement also with those reported in previous works where lower trunk accelerometer signals were analyzed [10-12]. However, there are a few previous studies reporting these parameters for the gait cycle phases [12]. For these phases, the calculation of the parameters is critical, due to a difficult timing identification for the gait cycle events. This problem might be limited by increasing the present acquisition frequency, for which the typical two-peak curve can no longer be flattened. Furthermore, since the GA system uses a semiautomatic procedure for calculating the gait cycle phases, it might be valuable in the future to compare these parameters given by the F4A system with those obtained by a mat of electronic sensors, acquiring simultaneously the walking performance by the two measurement systems. Finally, the statistically significant difference observed for a number of these measurements does not diminish the overall value of the present novel technique; all spatial-temporal parameters including the various phases within the gait cycle can be obtained reliably despite the simple and cheap instrumentation. Regarding kinematics of the pelvis this study shows, though preliminarily, that also these measurements can be obtained reliably by a single inertial sensor. This would allow that such measurements can be taken routinely also in standard clinical settings, though relevant further validation work should be performed. In the near future, some of the algorithms devised for the present system will be investigated for possible further improvements. However, the results obtained for the gait parameters estimation and for the pelvis kinematics are very encouraging, therefore the applicability of present system can be exploited in various fields of human movement. In the analysis of the physiology of gait, a much larger normal population size can be analyzed, and the effect of gender, age, weight etc. on gait performance can be addressed quantitatively. The system also has the potential to be of value for future quantitative assessments within routine clinical analyses of pathologies affecting locomotion. In particular, the quality of level walking before and after relevant treatments, as well as over the recommended rehabilitation program, can be monitored with these measurements, which do not require expensive instrumentation, large and special rooms, long patient preparation, and challenging clinical interpretation.

5. ACKNOWLEDGMENTS

6. REFERENCES

[1] J. Dicharry, Kinematics and kinetics of gait: from lab to clinic, Clin Sports Med. 29 (3),2010, 347-364.

[2] T.A.L. Wren, G.E. Gorton III, S. Ounpuu, C. A. Tucker, Efficacy of clinical gait analysis: A systematic review, Gait & Posture 34, 2011, 149-153.

[3] J. Rueterbories, E.G. Spaich, B. Larsen, O.K. Andersen, Methods for gait event detection and analysis in ambulatory systems, Medical Engineering & Physics, 32 (6) (2010) 545-552.

[4] R. Schwesig, S. Leuchte, D. Fischer, R. Ullmann, A. Kluttig, Inertial sensor based reference gait data for healthy subjects, Gait Posture (2011) [Epub ahead of print].

[5] A. Godfrey, R. Conway, D. Meagher, G. O'Laighin, Direct measurement of human movement by accelerometry, Medical Engineering & Physics 30 (2008) 1364-1386

[6] A. Leardini, Z. Sawacha, G. Paolini, S. Ingrosso, R. Nativo, MG. Benedetti, A new anatomically based protocol for gait analysis in children, Gait Posture. 26 (4), 2007, 560-71.

[7] M. Manca, A. Leardini, S. Cavazza, G. Ferraresi, P. Marchi, E. Zanaga, MG. Benedetti, Repeatability of a new protocol for gait analysis in adult subjects, Gait Posture 32 (2), 2010, 282-4.

[8] R. Senden, B. Grimm, I.C. Heyligers, H.H.C.M. Savelberg, K. Meijer, Acceleration-based gait test for healthy subjects: reliability and reference data, Gait Posture 30 (2), 2009, 192-196.

[9] V. Macellari, C. Giacomozzi, R. Saggini, Spatial-temporal parameters of gait: reference data and a statistical method for normality assessment, Gait Posture 10 (2), 1999, 171-181.

[10] W. Zijlstra, Assessment of spatio-temporal gait parameters during unconstrained walking, Eur. J. Appl. Physiol. 92 (1-2), 2004, 39-44.

[11] H. B. Menz, S. R. Lord, R. C. Fitzpatrick, Acceleration patterns of the head and pelvis when walking on level and irregular surface, Gait Posture 18 (1), 2003, 35-46.

[12] B. Auvinet, G. Berrut, C. Touzard, L. Muotel, N. Collet, D. Chaleil, E. Barrey, Reference data for normal subjects obtained with an accelerometric device, Gait Posture 16 (2), 2002, 124-134.

Towards an integrated 3D accelerometry platform to assess the risk of falling: a feasibility study

Logistic data management and data extraction in an European multi-center setting.

Soaz C. [1,2], Daumer M. [1,2,3] for the VPHOP Consortium

[1] SLCMSR-The Human Motion Institute, Munich, Germany, gonzalez@slcmsr.org
[2] Institute for Real-Time Computer Systems, TUM, Munich, Germany, gonzalez@rcs.ei.tum.de
[3] Trium Analysis Online, Munich, Germany, daumer@slcmsr.org

Keywords; accelerometry , risk of falling, osteoporosis

1. INTRODUCTION

Many of the devices currently used for the clinical assessment of balance and gait quality are cumbersome, can only be used in a gait laboratory and the cost can be prohibitive. However, recent developments in micro-technology make it possible to measure activity with miniaturized and relatively inexpensive mobile accelerometers. We aimed to develop a set of standardized tests enriched by parallel use of accelerometry that a) are known and may be used in a wide range of diseases and/or b) that are associated with fall risk.

2. METHODS

In our study we used a custom-built 3D accelerometer with a sample frequency of 100 Hz, the actibelt® [1-3]. The device is integrated in a belt buckle and placed near the center of mass of the human body (Fig. 1). We also developed an acquisition protocol to perform a set of clinical test in such a way that we could subsequently identify them in the whole sequence. Test are performed in a row and separated by tapping on the belt at the beginning and end of the tests. A peak detection algorithm based on the "DMW"- algorithm [4] was improved to detect the peaks originated by the tap in the acceleration signal and allow the automatic extraction of each individual test.

The sequence of tests was developed in the context of a European project (VPHOP) to assess functional mobility in osteoporotic elderly females. The battery of tests was agreed upon by an interdisciplinary panel of clinicians and consists of a series of 11 rapid functional tests specially selected to assess risk of falling. The battery consists of the following test: normal walking (repeated twice), normal walking with cognitive task, tandem walk along a line, Timed Up and Go test (TUG), chair rise test, Romberg stance (quiet-standing), semi-tandem stance, tandem stance and one-legged stance (on right and left leg).

Four European centers are involved in the data collection: Charité (Berlin), Istituto Ortopedico Rizzoli (Italy), INSERM (France), University of Geneve (Switzerland). After the collection the data is uploaded into a webplatform were is safely stored together with clinical patient data.

The analysis output includes, for example, number of steps, estimated step length, asymmetry index, mean speed and acceleration stabilograms (Fig.2).

Additionally, 7-days continuous actibelt® measurements were recorded to explore possible relationships with the physical activity levels of the patients.

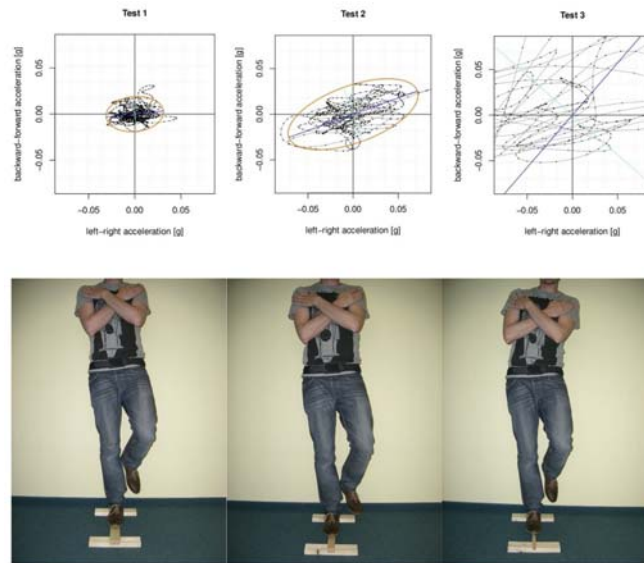Figure 1. Photos of the actibelt® accelerometer used for the data acquisition.

Figure 1. Example of acceleration stabilogram captured with the actibelt® while performing the single leg balance test with 3 difficulty levels.

3. RESULTS

Our algorithms extracted automatically gait and postural stability parameters from high quality 3D accelerometry data corresponding to 495 rapid clinical tests recorded at the Charité clinic in Berlin, Germany (database freeze in 30-11-2010). The peak detection algorithm used to identify each single measurement was tested obtaining the following results: precision=99.59%, recall=86.96%, F-measure=95%.
Patients (45 female; mean age 69.4 +/- 4.6 years old) were divided in three cohorts: "healthy control", "risk for falling" and "recent fracture". Exploratory analysis of these rapid test measurements suggests that the less stable tests (i.e. one legged stance) are more capable of differentiating between cohorts of subjects than the more stable activities (e.g. walking, quiet standing)
The deviation between subjects in many of the tests is large, indicating that individuals within the groups may vary considerably across a "stability" spectrum. This suggests that although many tests here show little or no significance between cohorts, the tests themselves may be capable of detecting changes within individuals with lower stability.

4. DISCUSSION

Exploratory analysis reveals the ability of some test to differentiate between cohorts but due to the small amount of sample size not significant results were expected. The current study shows that is possible to introduce accelerometry into the clinical practice in the context of a standardized fall risk assessment in an European multi-center setting. The positive outcome of the feasibility study let to the decision to expand the number of European centers to collect data. The ability of these tests will therefore only be fully elucidated in the context of the clinical follow-up data. These acceleration data will need to be linked with the data from the other parts of the multi-scale program to allow the exploration of novel combined biomarkers and their additional predictive value for fall risk and bone fracture risk.

We see the potential that these "rapid clinical tests" could become a standard in the clinical assessment of fall risk which may be important to design fall prevention programs.

5. REFERENCES

[1] Daumer M, Thaler K, Kruis E, Feneberg W, Staude G, Scholz M. Steps towards a miniaturized, robust and autonomous measurement device for the long-term monitoring of the activity of patients – ActiBelt. Biomedizinische Technik/Biomedical Engineering. 2007; 52: 149–155.
[2] Schimpl M, Lederer C, Daumer M, 2011 Development and Validation of a New Method to Measure Walking Speed in Free-Living Environments Using the Actibelt® Platform. PLoS ONE 6(8): e23080. doi:10.1371/journal.pone.0023080
[3] Schimpl M, Moore C, Lederer C, Neuhaus A, Sambrook J, et al. 2011 Association between Walking Speed and Age in Healthy, Free-Living Individuals Using Mobile Accelerometry—A Cross-Sectional

Study. PLoS ONE 6(8): e23299. doi:10.1371/journal.pone.0023299

[4]   Daumer, M. and Neiss, A. A new adaptive algorithm to detect shifts, drifts and outliers in biomedical time series. Mathematical Statistics with Applications in Biometry, Josef Eul, Lohmar, 2001. pp. 201-204.

INTERACTION

Training and monitoring of daily-life physical interaction with the environment after stroke

Veltink P.H.[1], van Meulen F.B.[1], van Beijnum B.J.F. [1], Hermens H.J. [1,3], De Rossi D. [2], Lorussi F. [2], Tognetti A. [2], Buurke J.H. [3], Reenalda J. [3], Baten C.T.M. [3], Simons C.D.M.[3], Luft A.R. [4] Schepers H.M.[5], Luinge H.J.[5], Paradiso R.[6], Orselli R.[6]

[1] Biomedical Signals and Systems, MIRA Institute, University of Twente, Enschede, the Netherlands, [2]Research Centre "Enrico Piaggio", University of Pisa, Pisa, Italy; [3]Roessingh Research and Development, Enschede, the Netherlands; [4]Neurology Department, University of Zurich, Zurich, Switzerland [5]Xsens Technologies B.V., Enschede, the Netherlands; [6]Smartex s.r.l., Pisa, Italy
First author e-mail address: P.H.Veltink@utwente.nl

The objective of the recently started EU project INTERACTION is to develop an unobtrusive and modular system for monitoring the quality of daily-life activities of stroke subjects involving the upper and lower limbs.

Keywords – Daily-life activity, stroke survivors, rehabilitation, ambulatory monitoring, unobtrusive monitoring, textile-based and micromechanical integrated sensing, distributed sensing, telemonitoring, on-body feedback.

1.   INTRODUCTION

Persons who suffered a stroke are trained to improve adequate control over their movements with the objective to optimize their daily-life functional performance. Critical is how good they are able to interact physically with the daily-life environment, including handling objects, controlling body balance during functional ambulation and while interacting with the environment.

Continuous daily-life monitoring of the functional activities of stroke survivors, in their physical interaction with the environment, is essential for optimal guidance of rehabilitation therapy by medical professionals and coaching of the patient. Such information cannot be obtained with present monitoring systems.

It is the objective of the INTERACTION project to develop and validate an unobtrusive and modular system that enables monitoring the quality of daily-life activities and physical interactions with the environment (Fig. 1). Data can be used to guide specific training interventions to regain upper and lower limb motor function after stroke.
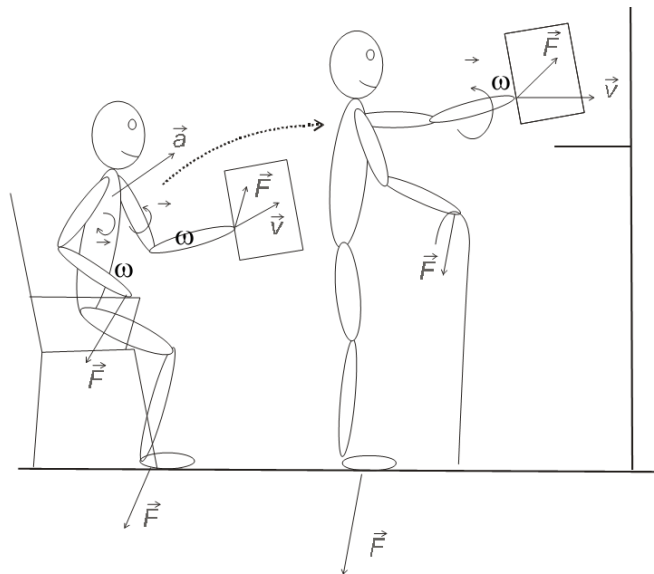

Figure 1. The INTERACTION concept: monitoring the quality of daily-life physical interaction with the environment for control of body balance and upper-extremity function during daily life. The interaction quality is derived from muscle activation (EMG), and movement and interaction force sensed at the interface with the environment.

2. METHODS

In order to realise the INTERACTION concept, the following methods are used:

- Instrumented textiles (shoes, trousers, shirt and gloves) with integrated textile-based and micromechanical sensors, to unobtrusively sense muscle activation (EMG), interaction forces and body movements
- Methods for qualitative and quantitative assessment of the dynamic interaction of a person with the environment, identifying activity tasks during daily-life and evaluating the quality of performance of these tasks, applying task-dependent performance criteria
- Telesupervision and intelligent on-body feedback, well integrated in clinical training concepts

The INTERACTION system will be evaluated in an experimental clinical setting, simulating daily-life conditions and demonstrated under daily-life conditions in stroke survivors.

3. PAST RESULTS

The project builds on the results of former research [1]:

- Instrumented textiles developed at the University of Pisa [2,5] (Fig. 2)
- Method to assess human body balance using instrumented shoes, measuring foot movement and ground reaction forces [3] (Fig. 3)
- Method to assess power exchange with the environment from inertial movement sensing and interaction forces [4]
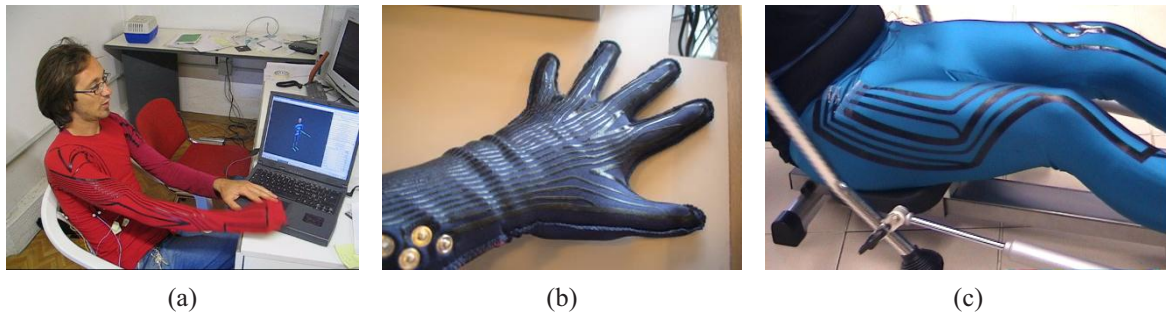

(a) (b) (c)

Figure 2. Fabric-based human motion monitoring devices using screen printed piezoresistive rubber sensors and sensor track (black stripes in the garments), developed by the University of Pisa and Smartex [5]: a) upper-limb monitoring device developed for post stroke telerehabilitation. b) instrumented glove. c) fabric-based motion classification garments for monitoring leg kinematics.
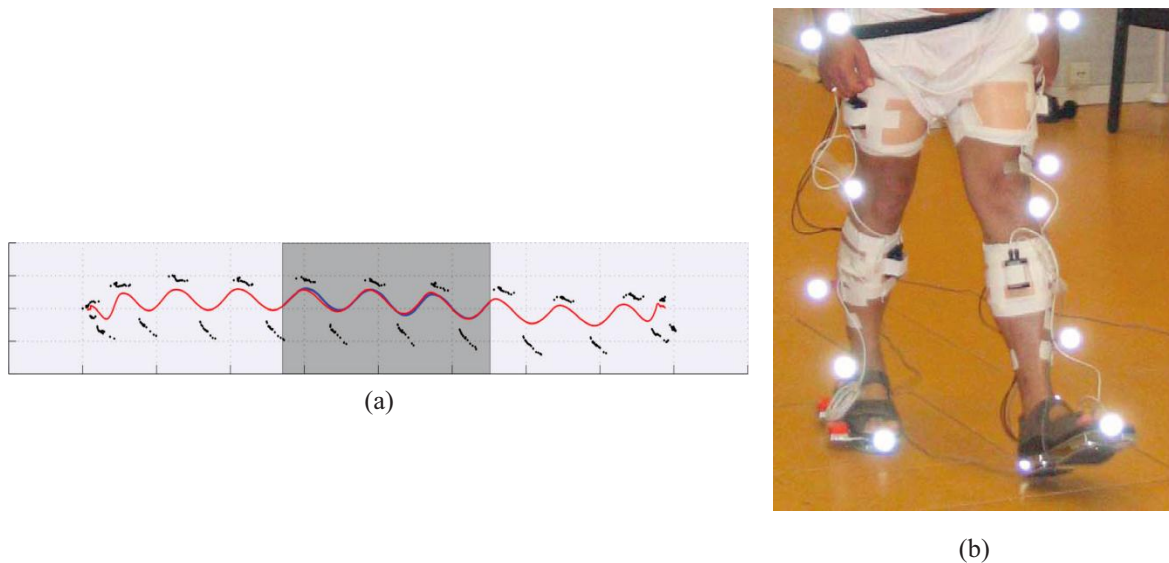

(a)

(b)

Figure 3. Assessment of human balance performance by estimating body center of mass movement relative to foot placement (a) from instrumented shoes (b) as developed and evaluated by the University of Twente, Xsens and Roessingh Research and Development [3].

REFERENCES

[1]   De Rossi D., Veltink P.H., Wearable technology for biomechanics: e-textile or micromechanical sensors?, IEEE Engineering in Medicine and Biology Magazine, vol. 29, issue 3, 2010, pp. 37-43.

[2]   Lorussi F., Rocchia W., Scilingo E.P., Tognetti A., De Rossi D., Wearable, Redundant Fabric-Based Sensor Arrays for Reconstruction of Body Segment Posture, IEEE Sensors Journal, vol.4, no. 6, 2004 pp.807-818.

[3]   Schepers H.M., van Asseldonk E.H.F., Buurke J.H., Veltink P.H., Ambulatory Estimation of Center of Mass Displacement during Walking, IEEE transactions on Biomedical Engineering, vol. 56, 2009, pp. 1189-1195.

[4]   Veltink P.H., Kortier H.G., Schepers H.M., Sensing power transfer between the human body and the environment, IEEE Transactions on Biomedical Engineering, vol. 56, 2009, pp. 1711-1718.

[5]   Pacelli M., Loriga G., Taccini N., Paradiso R., Sensing Fabrics for Monitoring Physiological and Biomechanical Variables: e-textile solutions, Proceedings of the 3rd Summer School and Symposium on Medical Devices and Biosensors, MIT, Boston, USA. Sept. 4-6, 2006.

PowerGlove

Concepts and current results

Veltink P.H. [1], Kortier H.G. [1], Schepers H.M. [3], Sluiter V.I. [1],
Brookhuis R.A. [2], Lammerink T.S.J. [2], Wiegerink R.J. [2]

[1] Biomedical Signals and Systems, MIRA Institute; [2] Transducer Science and Technology, MESA+ Institute,
University of Twente, Enschede, the Netherlands,
[3] Xsens Technologies B.V., Enschede, the Netherlands
First author e-mail: p.h.veltink@utwente.nl

Dynamic interaction between the human body and the environment can be assessed by measuring force and estimating velocity at their interface. A sensorized glove with movement and force sensing is developed in which this principles is applied.

Keywords – inertial movement sensing, six degree-of-freedom force / moment sensing, power sensing, load identification, dynamic interaction.

1. INTRODUCTION

Measuring the physical interaction between the human body and the environment is important in medicine, ergonomics and sports. Potential applications include the assessment of motor performance in rehabilitation, measuring whether the human body is loaded within safe limits in ergonomics and training for optimal performance of motor activities in sports.

The physical interaction between the human body and the environment can be assessed by measuring force and velocity at their interface (Fig 1a). Power transfer can be derived from the inner product of force and velocity [1,2], the dynamics of environment can be derived by relating movement to force under conditions in which the human body is the actor and the environment behaves passively and does not change in certain time periods [1,3].

It is the objective of our current PowerSensor project to demonstrate these principles and to develop a sensorized glove that is able to measure hand and finger movements as well as interface forces. The sensor system that is to be applied on the finger tips and selected finger and hand segments will include inertial and magnetic sensors for movement and an accurate 3D force sensor for interface forces (Fig. 1b). Optionally, the 3D force sensor may be extended by 3D moment sensing. This paper provides an overview of our current research achievements in this area, with reference to papers that provide more detail.
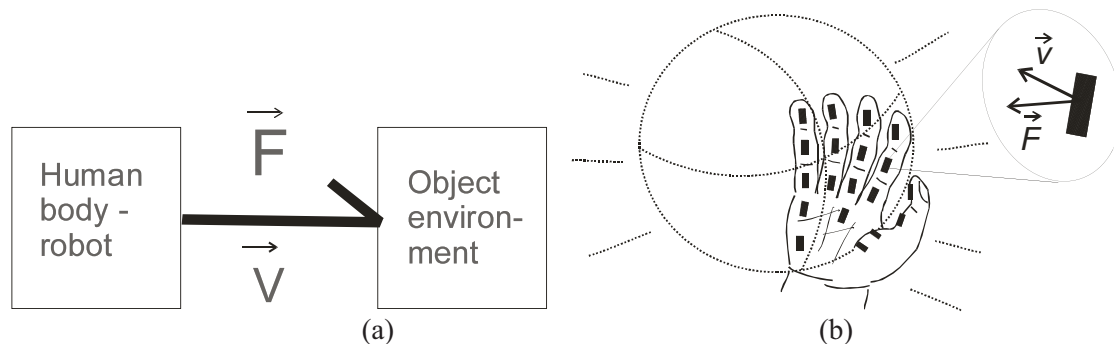

Figure 1. The PowerGlove concept [1]. (a) Dynamic interaction between the human body and the environment can be assessed by measuring force and estimating velocity at the interface, (b) a sensorized glove with movement and force sensing is developed in which these principles are applied.
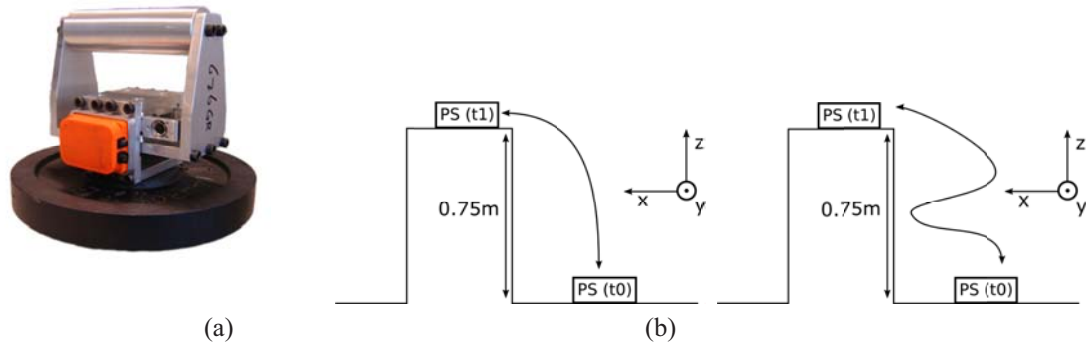
(a)　　　　　　　　　　　　　　　　(b)

Figure 2. Feasibility demonstration of power sensing and load identification. A mass was moved from the ground to a table following arbitrary trajectories (b) using a sensorized handle with an Xsens inertial sensing unit and an ATI-mini45 6 DoF force/moment sensor (a). Work performed and mass were estimated from measured movement and force information and compared to changes of potential energy and actual value of the mass. Similar tests were performed using spring loads [2,3].

2. MATERIALS AND METHODS

Feasibility demonstration of concepts

We propose two concepts concerning the assessment of the dynamic interaction between the human body and the environment, being the estimation of power transferred and dynamics of the environment.

Concept 1: Sensing power transfer between the body and the environment

The power transfer between the body and the environment was estimated for the displacement of an unknown load. First, relevant movement quantities were estimated: the sensor orientation was estimated at any moment by integrating the signals of the 3D angular velocity sensors and correcting the resulting estimate for drift, applying known orientations at the start and end of the movement. The 3D acceleration was transferred to global coordinates using the estimated orientation at any moment. Subsequently, the gravitational acceleration was subtracted and the resulting acceleration integrated to velocity, and velocity subsequently to change of position. Integration drift was reduced by applying known zero velocity at the start and end of the movement, information about change of height was not used. Power transfer was estimated at each moment in time by multiplying force and velocity, multiplying moment and angular velocity and adding both components of power transfer. Performed work was estimated by integrating power transfer over time [2].

Concept 2: Identifying load dynamics

A second order load model, including mass, damping and stiffness parameters, was identified by relating estimated acceleration, velocity and displacement to measured force as function of time using least squares estimation [3]. These movement quantities were derived as described above.

Experimental methods applied in the feasibility demonstration

Work performed and load dynamics were estimated from inertial movement sensing and force/moment sensing at the interface between a handle and the load, while displacing the load. The estimated work performed was compared to the change of potential energy and the load dynamics with the known characteristics of the load (Fig. 2).

Development of the PowerGlove

In addition to demonstrating the principles of dynamic interaction assessment, we are developing a prototype of the sensorized glove, including movement and force sensing.

Inertial sensing of hand and finger movements

Hand and finger movements are estimated by fusing inertial and magnetic movement sensing on the segments of the fingers and the back of the hand with a kinematic anatomical model of the hand. The applied optimal estimation method was initially developed using a model that generates sensor signals when performing certain hand and finger movements. It is now evaluated using a complete inertial/magnetic sensor module on the back of the hand and 3D accelerometers and magnetometers on the segments of index finger and thumb [4]. A more extensive distributed movement sensing system, including 3D gyroscopes is currently being developed.
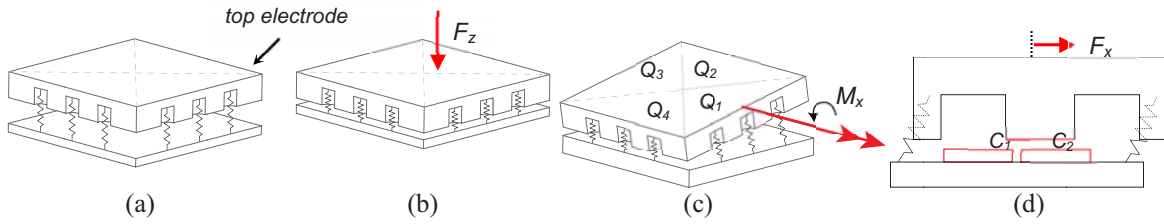
Figure 3. Working principle of the six degree-of-freedom force/moment sensor [5] (a,b) normal force sensing, (c) moment sensing, (d) shear force sensing

<u>Six degree-of-freedom fingertip force/moment sensor</u>

The six degree-of-freedom fingertip force/moment sensor consists of a silicon top electrode which is supported by many thin silicon pillars. These pillars are the spring elements of the force sensor for all degrees of freedom. An applied load to the sensor results in a small displacement of the top electrode relative to the bottom part. Capacitive read-out is used to detect this displacement, determining all axial force components and all torque components simultaneously. For determining forces/moments which cause out of plane displacement of the top part, four triangular electrodes are realized in the bottom wafer (Fig. 3a,b,c). Each force component is determined by measuring the change in capacitance between these electrodes and the top wafer. For measuring shear forces and a moment around the normal axes, comb-shaped electrodes are realized in the top and bottom part. An applied shear force causes a differential change in capacitance with respect to the top wafer (Fig. 3d) [5].

3.   RESULTS

Feasibility demonstration of concepts

The estimated work performed on a 9.4 kg mass and a spring with a spring constant of 88 N/m appeared to be accurate within 4 % for varying movements with durations between 3 and 5 s [2].

The mass parameter of the mass load was identified within 5 % error, with negligible forces due to stiffness and damping. The stiffness parameter of the spring load was identified within 3 % error with negligible forces due to mass and damping. Variances accounted for were above 99 %.

Development of the PowerGlove

<u>Inertial sensing of hand and finger movements</u>

The first version of the inertial and magnetic movement sensing system, including a complete Xsens movement sensing module on the back of the hand and small distributed PCBs with 3D accelerometers and magnetometers on the segments of the index finger and the thumb, is illustrated in figure 4. Further descriptions of the sensor fusion algorithms, this movement sensing system and the initial evaluation of measuring hand and finger movements are provided in another paper in this proceedings [4].

Figure 4. (a) first version of a movement sensor PCB with 3D accelerometer and magnetometer, (b) the first prototype kinematic glove with partial instrumentation of index finger and thumb [4]
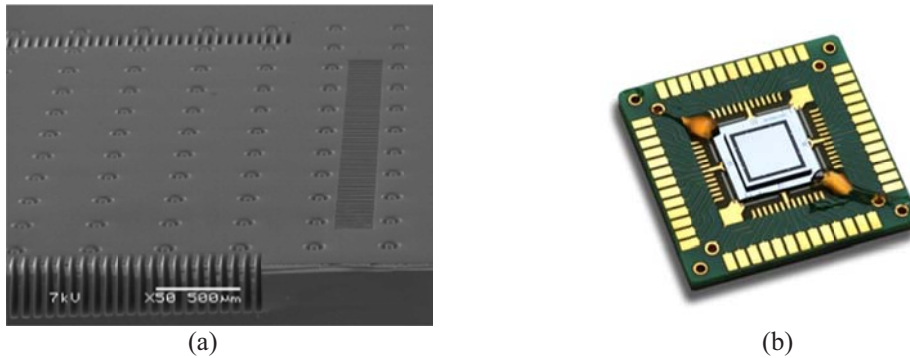
(a)	(b)

Figure 5. (a) SEM picture showing the top electrode with the silicon pillars and the comb-structure for measuring forces and moments, (b) Six degrees of freedom force-moment sensor mounted on a test PCB [5]

Six degree-of-freedom fingertip force/moment sensor
The six degree-of-freedom force-moment sensor has been realized and tested [5] (Fig. 5). The force range is up to 50 N in normal direction and 10 N in shear direction, the moment range is between 0 and 25 N·mm around each axis. Force measurements showed a full scale error of 0.9 % in normal and of 0.4% in shear directions, moments showed a full scale error of 2.8% around the normal and 1.1 % around the other axes.

4. DISCUSSION

It should be noted that load identification was performed under the condition that the human body is actively perturbing a constant passive load. When the load is varying and/or generates forces on the human body, the estimated dynamics are the combined effective dynamics of both human body and load, since measurements are performed in a closed dynamic loop. It is, therefore, important to assess the measurement condition in daily-life situations, possibly by identifying the performed activity. This is to be further investigated.

In the coming period, we plan to combine inertial and force sensors in the prototype sensorized glove and demonstrate the power sensing and load identification principles when interacting with the environment using the glove.

In addition to assessing the dynamic interaction between the human body and the environment, the sensorized glove is expected to be useful in biomechanical analysis of hand function and assessment of human motor control, as well as in animation and serious gaming.

5. ACKNOWLEDGMENT

6. REFERENCES

[1] P.H. Veltink, Device and method for measuring the dynamic interaction between bodies, US Patent Application 20090056445, March 5, 2009.

[2] P.H. Veltink, H.G. Kortier, H.M. Schepers, Sensing power transfer between the human body and the environment, IEEE Transactions on Biomedical Engineering, vol. 56, 2009, pp. 1711-1718.

[3] H.G. Kortier, P.H. Veltink, Load identification during object handling, Proceedings of the 33rd Annual International Conference of the IEEE Engineering in Medicine and Biology Society, Boston MA USA, 30 August – 3 September 2011, 3 pp.

[4] H.G. Kortier, H.M. Schepers, P.H. Veltink, inertial sensing of hand and finger movements, Proceedings of the XII International Symposium on 3D Analysis of Human Movement, Bologna I, 18-20 July 2012, this proceedings.

[5] R.A. Brookhuis, R.J. Wiegerink, T.S.J. Lammerink, M.J. de Boer, K. Ma, M.C. Elwenspoek, Scalable six-axis force-torque sensor with a large range for biomechanical applications, The 25th international Conference on Micro Mechanical Systems, MEMS 2012, Paris F, 29 January – 2 February 2012, accepted.

Improving inertial sensor measurement of the relative orientation between trunk and pelvis using a potentiometer

Larue C. [1], Plamondon A. [1], Desjardins P. [1,2], Salazar E. [1], Mecheri H. [1], Sirard C. [1]

[1] Institut de recherche Robert-Sauvé en santé et en sécurité du travail (IRSST), Montréal, Québec, Canada
[2] Centre de recherche interdisciplinaire en réadaptation du Montréal métropolitain, Montréal, Québec, Canada

An inertial measurement unit (IMU) was used to measure the orientation of the trunk relative to the pelvis in material handling workers. The potentiometer was incorporated between two IMUs to improve the level of accuracy in the presence of local magnetic perturbations. The prototype was tested on six subjects in the laboratory simulating manual material handling loads. Grood and Suntay angles were computed from the quaternion provided from the Kalman filter (Xsens) and from a complementary filter and were compared to those obtained from a 3D optoelectronic system. The results showed that the potentiometer proved to be an essential addition, particularly when the magnetometer signals were corrupted or when the gyroscopes drifted.

Keywords- component; Inertial tracking device; accelerometers; gyroscope; magnetometer; potentiometer

1. INTRODUCTION

Inertial measurement units, or IMUs, are used to measure the orientation of the trunk relative to the pelvis. These units combine triads of accelerometers, magnetometers and gyroscopes, but magnetometers are particularly sensitive to local magnetic fields and are sometimes inaccurate. To overcome this problem, our group incorporated a potentiometer between two IMUs to improve the level of accuracy in the presence of local magnetic perturbations [3]. The mechanism linking the potentiometer to the IMUs does not perturb the magnetic field, and transmits the relative rotation between the units to a potentiometer along their longitudinal axes [1]. Integration of the potentiometer data into a fusion algorithm has already been presented but the prototype used has been improved and tested on six subjects in the laboratory [1][2][3]. The purpose of this paper is to present the new development associated with our system comprised of two IMUs and one potentiometer. Five sequences of movements of different duration were performed by six subjects, including a task that lasted around 10 minutes of simulated manual material load handling. A workplace environment was recreated in the laboratory where some ferromagnetic perturbations were imposed.

2. MATERIAL AND METHODS

The system is based on two Xsens ® Motion Tracker sensors connected to their Xbus Master unit. The raw data and the orientation in quaternion from their Kalman filter are collected on a PDA (Personal Digital Assistant) via a CSharp application. A potentiometer is fixed by a flexible shaft between a thorax IMU and a pelvis IMU (Fig. 1).
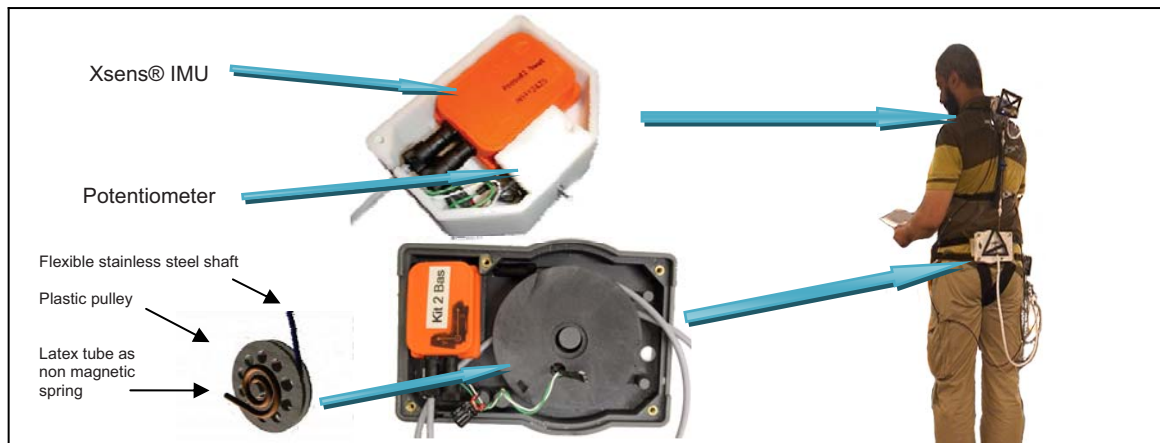

Figure 1.   Illustration of the inertial measurement system.

The potentiometer measures the torsion along the flexible shaft. The shaft's flexibility gives the possibilities of flexion/extension movement without perturbing the potentiometer's rotary reading. The angle between the two IMUs measured by the potentiometer is the one around an axis that can be calculated by the Crawford approach (1) [5] (Fig. 3). For example, vector $\vec{i}$ in Fig. 2a represents the vertical orientation of the trunk sensor, and $\vec{i}\,'$ that of the pelvis. For pure flexion/extension, the angle is represented by ϕ when $\theta = 0$ (Fig. 2b). Lateral flexion is defined by a non null ϕ and θ angles as seen in Fig. 3.
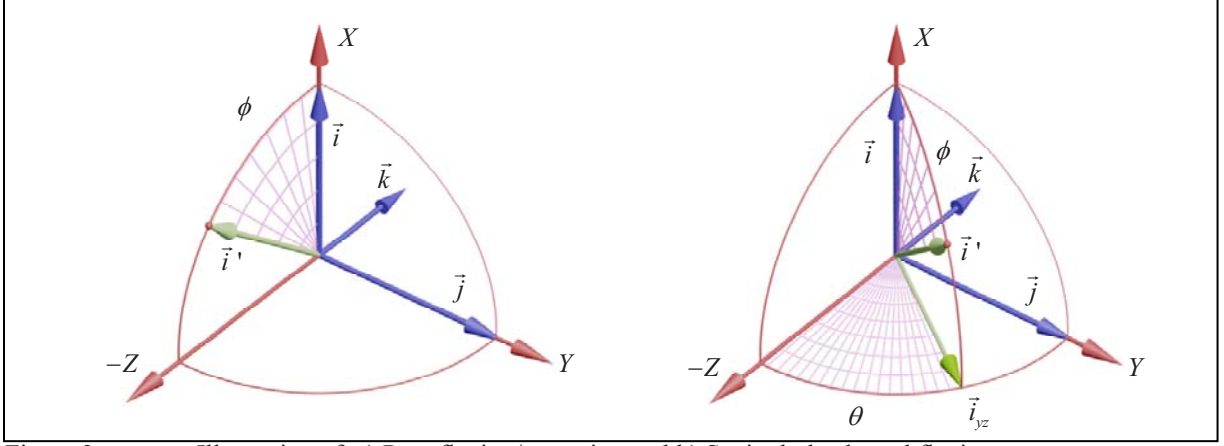

Figure 2.   Illustration of a) Pure flexion/extension and b) Sagittal plus lateral flexion

From these two angles, we can define the $\vec{i}\,_{1/2}$ axis as in (1)(Fig. 3).

$$\vec{i}_{1/2} = \begin{bmatrix} \cos\left(\dfrac{\varphi}{2}\right) \\ \sin\left(\dfrac{\varphi}{2}\right)\sin(\theta) \\ -\sin\left(\dfrac{\varphi}{2}\right)\cos(\theta) \end{bmatrix} \qquad (1)$$

An angle τ measured around this axis between $\vec{h}_0$ and $\vec{h}'$ on Fig. 3, corresponds to the angle measured by the potentiometer on the flexible shaft between the trunk and the pelvis.

$$h_0 = i_{1/2} \times j \qquad (2) \qquad\qquad h' = i_{1/2} \times j' \qquad (3)$$

Once calibrated, the measured voltage between potentiometer's leads gives us the angle that should correspond to τ computed with the estimated orientation from the IMUs. The sensors' output, i.e., their absolute orientation in an Earth coordinate system, is in quaternion form. Once the output has been estimated for each sensor, the relative orientation between the pelvis and the thorax is calculated; it is then possible to estimate the torsion angle τ using Crawford's method.
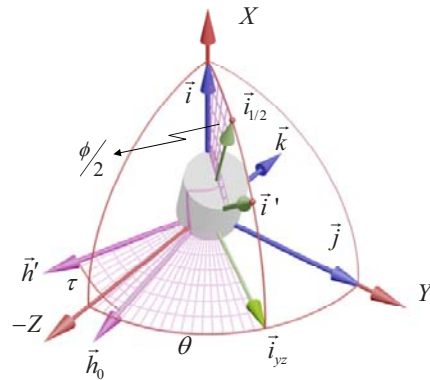

Figure 3.   Rotation angle description

The quaternion form of the outputs is difficult to interpret and is therefore transformed into direction cosines where the three angles of Grood and Suntay are found [4]: flexion-extension (angle alpha), lateral bending (angle beta) and axial rotation (angle gamma). The angle most sensitive to magnetic field disturbance is the gamma angle. Comparing the two torsion angles, the one from the IMUs and the one from the potentiometer allow a correction to gamma.

Two fusion algorithms were used to estimate the quaternions, a Kalman filter (K) and a complementary filter (C). Once the quaternions and the Grood and Suntay angles were calculated with both fusion algorithms, the errors about the gamma angle (relative angle) were evaluated. Four types of gamma errors were computed: 1) the error from the Kalman filter (RK); 2) the error from the Kalman filter corrected by the potentiometer (RCorK); 3) the error from the complementary filter (RC); 4) the error from the complementary filter corrected by the potentiometer (RCorC), where R symbolize relative.

3. RESULTS

Fig. 4 shows RMS errors on the Grood & Suntay gamma angle (torsion) for the sequence of movements 4 and 5 (the longest ones) performed by the 6 subjects. All represent the errors in the Grood & Suntay gamma computed from the relative quaternion. Note that the results presented in sequence 5 are the most important ones because they represent the longer task simulating manual handling. In Table 1, gamma's errors for all sequences are given. As an example, RMS errors reach 66 degrees in sequence 5 for computed results from the Kalman filter. This error is due to a drift in gamma as can be seen in Fig. 5. For that data set, the correction induced in gamma by the potentiometer substantially reduces the error.
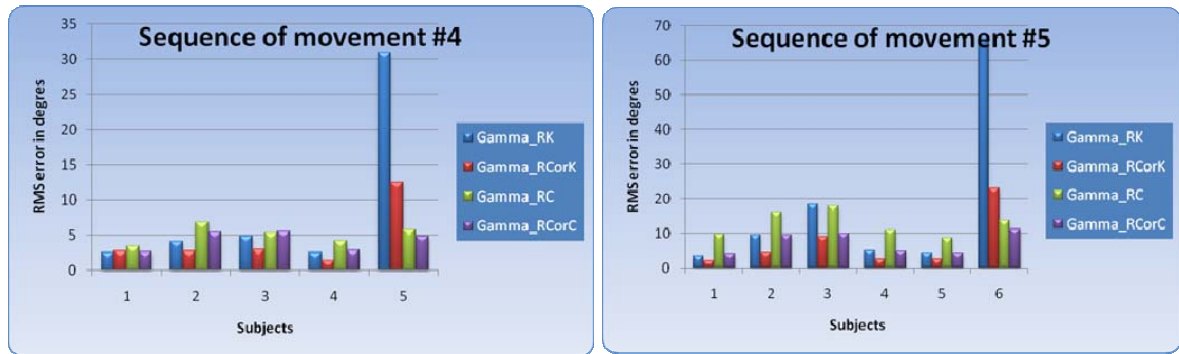

Figure 4.   RMS errors in degrees for the six subjects, sequences 4 and 5

Table 1. RMS gamma errors estimated under different experimental conditions. Sequences 1, 2 and 3 last less than 2 minutes, sequence 4 approximately 6 minutes, and sequence 5 more than 10 minutes.

Subject	Sequence	Gamma_RK	Gamma_RCorK	Correction	Gamma_RC	Gamma_RCorC	Correction	Significant drift
1	1	2	2	0	1	2	-2	no drift
1	2	2	1	1	3	1	2	no drift
1	3	1	2	-1	6	2	4	no drift
1	4	3	3	0	3	3	1	no drift
1	5	3	2	1	10	4	6	no drift
2	1	1	1	0	1	1	0	no drift
2	2	2	2	0	6	5	0	no drift
2	3	2	2	0	4	2	1	no drift
2	4	4	3	1	7	5	1	no drift
2	5	9	4	5	16	9	7	no drift
3	1	3	3	0	2	2	0	no drift
3	3	1	2	-1	5	2	3	no drift
3	4	5	3	2	5	6	0	no drift
3	5	18	9	9	18	10	8	no drift
4	1	2	1	1	1	1	0	no drift
4	2	2	2	-1	4	4	0	no drift
4	3	2	1	1	4	2	2	no drift
4	4	2	1	1	4	3	1	no drift
4	5	5	3	3	11	5	6	no drift
5	1	8	3	5	1	1	0	drift
5	2	32	4	27	5	4	0	drift
5	3	57	2	55	5	3	2	drift
5	4	31	13	18	6	5	1	drift
5	5	4	2	2	8	4	4	no drift
6	1	8	2	6	1	4	-3	drift
6	2	29	5	24	4	2	2	drift
6	3	60	1	58	5	2	3	drift
6	5	66	23	43	14	11	2	drift

Note: There is no subject 3 for the movement 2 sequence and no subject 6 for sequence 4.

4. DISCUSSION

The results show that the potentiometer used in combination with the Kalman and the complementary filters reduced the errors in the "torsion" axis. The Kalman filter seems to give better results than our complementary filter for most of the cases. The poor performance of the Kalman filter for subjects 5 and 6 is related to a drift in the output data. This drift appears to be a problem and limits the accuracy of the results. Fig. 5 shows the plot of alpha, beta and gamma from the 3D optoelectronic system and the Kalman filter for subject 6 in sequence 5. The drift in gamma can be seen, as well as the gamma corrected by the potentiometer. Comparison of the τ computed from Crawford with the one measured with the potentiometer is a good way of determining whether there is a drift in gamma.
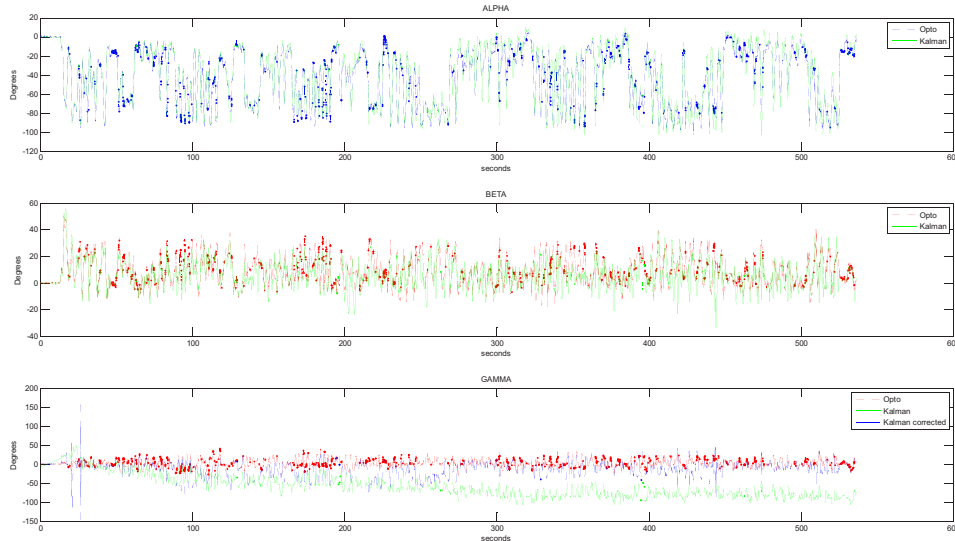

Figure 5.   ALPHA, BETA and GAMMA between Optotrak and Kalman, Subject 6 sequence 5

5. REFERENCES

[1]   Larue, C. Desjardins, P. Plamondon, A. Delisle, A.2009 Mechanism to link two inertial measurement units to a potentiometer: improvements of measurements between pelvis and trunk motion. XXII Congress of the International Society of Biomechanics, (22nd : July 5-9, 2009 : Cape Town, South Africa).

[2]   Plamondon, A. Delisle, A. Larue, C. McFadden, D. Desjardins, P. 2008 The use of a potentiometer as a complement to inertial sensors in the measurement of trunk posture in motion in International Symposium of 3D analysis of Human Movement. (10th : October, 28-31 : Snatpoort/Amsterdam, The Netherlands), 2008, p. 30.

[3]   Plamondon, A., Delisle, A., Larue, C., Brouillette, D.,McFadden, D., Desjardins, P., Lariviere, C., 2007. Evaluation of a hybrid system for three-dimensional measurement of trunk posture in motion. Applied Ergonomics 38, 697-712.

[4]   Grood, E.S., Suntay, W.J., 1983. A joint coordinate system for the clinical description of three-imensional motions: application of the knee. J. Biomech. Eng. 105, 136–144.

[5]   Crawford, N.R., Yamaguchi, G.T., Dickman, C.A., 1999. A new technique for determining 3-D joint ngles: the tilt/twist method. Clin. Biomech. (Bristol, Avon.) 14, 153–165.

Motion sensors for measurement of gait modifications in knee osteoarthritis

Tim V. Wrigley [1], Daniel T.H. Lai [2], Alistair Shilton [1]

[1] Department of Physiotherapy, University of Melbourne, Melbourne Australia, timw@unimelb.edu.au
[2] School of Engineering and Science, Victoria University, Melbourne, Australia

Keywords; inertial sensors; knee joint; osteoarthritis; smartphones; telehealth; Android

1. INTRODUCTION

While there has been considerable work on inertial sensors for human movement measurement over the last decade, considerable difficulties remain. As such, practical applications of these sensors are still limited, both within and outside the research domain. Accurate body *position* measurement by such sensors, commensurate with that achievable by laboratory-based optical motion capture systems, and over anything more that short periods of time, remains a somewhat elusive prospect. Conversely, accurate measurement of body segment *orientation* is more feasible. The best prospects for practical and useful application of motion sensors in research and clinical contexts are therefore most logically where there is a 'nexus' between a demonstrated, validated need, and the specific capabilities and limitations of the sensors. The prospects for successful implementation are heightened where the need cannot be met effectively in other ways. An application that can be achieved with a minimal number of sensors is more likely to be successful than one which requires many sensors. One particular area in which motion sensors are needed - and where inertial sensors may be the most practical option - is for portable, field-based (clinic, home, and outdoors) movement sensing for the assessment and conservative management of osteoarthritis.

Osteoarthritis (OA) is a chronic condition affecting up to a third of older adults. The major symptom of OA is pain. There is no cure, and OA greatly affects quality of life and leads to high medical costs. OA is particularly common in the medial tibiofemoral joint, where joint loading is closely related to disease progression [1]. Conservative strategies are needed to slow disease progression in osteoarthritis, reduce pain, improve function, and enhance quality of life. Joint load reduction has been the focus of attempts to identify effective strategies. Knee joint loading can be affected by specific variations in the kinematics of walking by people with OA [2]. Indeed patients with painful OA *naturally* adopt ways of walking that may reduce knee joint pain, such as lateral trunk lean [3], and such natural strategies are also associated with reduced loading on the knee joint [4].

Furthermore, OA patients can be trained to walk in these ways that reduce knee loading [5]. Because of the quite precise nature of the kinematic gait modifications required to achieve optimal joint load reduction [5], real-time movement biofeedback can facilitate adoption of the specific gait changes by providing patients with simple but accurate information as they walk during the training phase, regarding the magnitude of the modification desired and their success in achieving it. In some cases, modifications will be difficult to teach patients without such feedback. While real-time movement biofeedback systems built on top of complex 3D motion capture systems have been shown to aid instruction for knee load reduction in OA [5, 6], deployment of these effective strategies outside the laboratory will require a less expensive and complex approach. Fortunately, modifications such as lateral trunk lean require only body segment orientation measurement, and at only one segment; thus their measurement is potentially feasible with inertial sensors.

While there is a growing understanding of the relative efficacy of various gait modifications for reducing knee load in OA, the understanding of what OA patients *naturally* do to reduce load is incomplete. In particular, how patients ambulate in more realistic environments than 3D gait labs - as they go about their activities of daily living – still requires study. Therefore, in addition to the need for a motion sensor system that could be deployed to clinics, there is also a need for 'remote monitoring', to understand movement of OA patients in more realistic environments away from the lab or clinic.

This paper describes the development of two systems based on inertial sensors, one suitable for use in a fixed environment such as a clinic, and another for remote motion monitoring of OA patients. Both systems utilize similar sensors, but use different strategies for data transmission. Given the need for specialized data fusion algorithms to derive final measures from the raw inertial sensor data, it is also important to evaluate the accuracy of these devices for the specific intended application before using them with OA patients.

2. MATERIAL AND METHODS

System one

The first system, for monitoring in a fixed environment such as a clinic, is based on the x-IMU sensor (x-io Technologies, UK), which includes a triaxial accelerometer (± 8g), gyroscope (± 2000 deg/s), and magnetometer (although we do not currently utilize the magnetometer, because of the well-known problems of magnetic distortion), integrated with an IMU-3000 motion processor (InvenSense). Device orientation is estimated from the former two sensors via a complementary filter, quaternion-based algorithm [7]. It communicates with the data acquisition computer via Bluetooth or direct USB connection. The encoded real-time serial data stream is decoded in our custom Matlab software to yield device orientation angles.

System two

The inertial sensor is similar to that used in the first system, but was custom-constructed from different components: a triaxial accelerometer (± 5g) and gyroscope (± 1200 deg/s), connected to a microcontroller (Freescale Coldfire), and Bluetooth transceiver (Parani ESD 200). Calibration is according to [8], and orientation is calculated using the same above-mentioned algorithm [7]. In contrast to system one, this sensor device transmits movement data to an Android smartphone. A custom application running on the smartphone then transmits the data to a remote server via wireless internet or 3G mobile phone networks. Therefore, the system can be used either when in range of a wireless internet network (eg in the home), or anywhere via the 3G phone network (eg outside the home). At the server end, data can be observed and recorded in real-time. Data is also recorded on the phone, and data files can also be transmitted transparently to the server after data collection in a non-real-time, 'store-and-forward' scheme, again via available wireless or 3G networks. The Android application also samples data from the phone's onboard accelerometer and the Android 'location service' (GPS- and phone network tower-based location tracking) for monitoring overall body movement.

Common evaluation methods

As the measurement aims of these systems are similar, they were evaluated at the same time using similar methods. The accuracy of the devices for measuring lateral trunk lean was assessed against a Vicon MX optical motion capture system (Oxford, UK). Training a patient to employ a gait modification strategy typically involves an initial phase where the patient performs the modification while standing in place. Thus the first evaluation test simulated 'standing' lateral trunk lean of a 'trunk' base plate, to which a triad of three reflective markers and the sensor device under test were attached. This rig was suspended, aligned with the laboratory frontal plane, and physically oscillated to simulate side-to-side lateral trunk lean. A second evaluation test then utilized the same rig attached to the thorax of a subject walking along the laboratory walkway, using somewhat exaggerated lateral trunk lean. The location of the marker triad on the trunk rig was reconstructed in Vicon Nexus software. Trunk lean angle was determined by a custom Vicon Body Builder model that calculated lean of the rig coordinate system in relation to the laboratory frontal plane as the first angle in a Cardan angle sequence, in the same way we have previously used in an OA context [5, 9, 10]. This angle was initially compared to the equivalent quaternion-derived Cardan angle from the x-IMU device (system one). The same tests were repeated with the remote sensor system (system two), using data transmission via Bluetooth, Android smartphone, and wireless internet.

3. RESULTS

System one

The 'standing' test showed a very close match between the trunk lean Cardan angle calculated from the Vicon marker triad and the x-IMU sensor; the walking test also showed a close match between the two angles (Fig. 1).

System two

Similar to system one, the tests of system two showed a good match between the trunk lean Cardan angle calculated from the Vicon marker triad and the custom IMU sensor (Fig. 2).
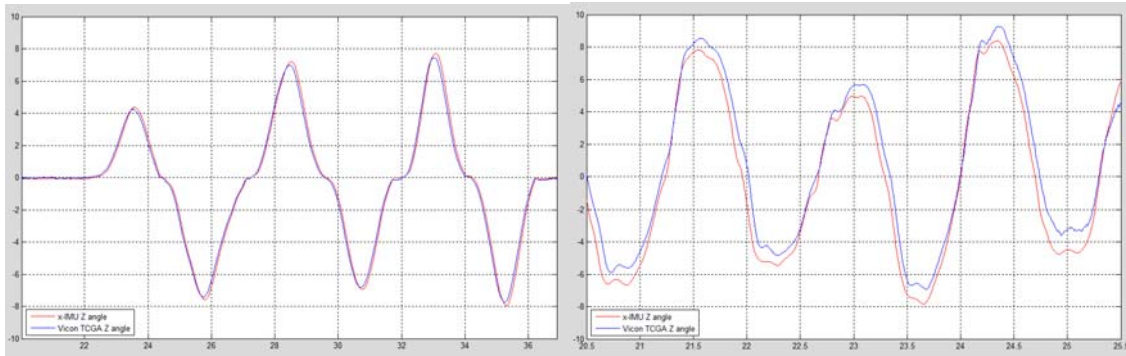
Figure 1. Trunk lean Cardan angle calculated by Vicon (-) and inertial sensor system one (-) during 'standing' (left) and walking (right) tests.
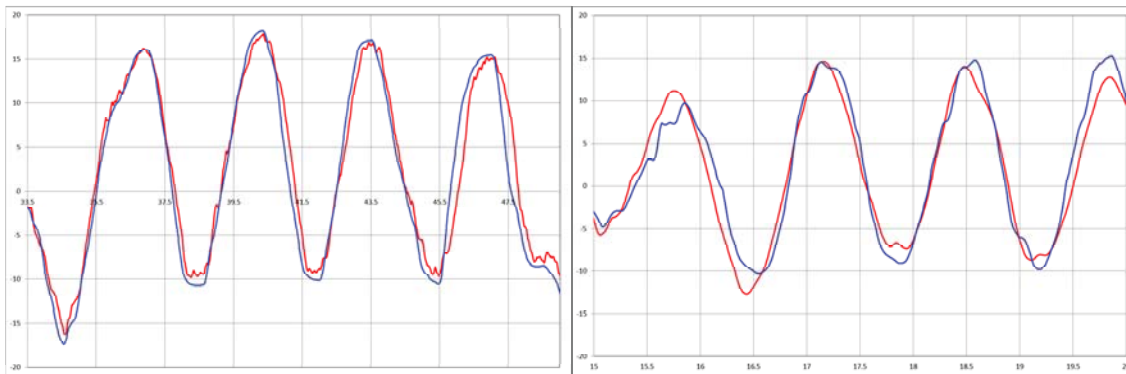

Figure 2. Trunk lean Cardan angle calculated by Vicon (-) and inertial sensor system two (-) during 'standing' (left) and walking (right) tests.

4. DISCUSSION

The two sensor systems were capable of measuring lateral trunk lean angles similar to those measured by a lab-based, 3D optical motion analysis system (Vicon MX). As such, they appear suitable for monitoring trunk lean angle in knee OA patients outside the 3D gait laboratory. The results for system one are also consistent with the more general accuracy testing for this device in [7].

There is a 'dose-response' relationship for gait modifications in OA – the extent of the load reduction is closely related to the magnitude of the gait modification [5]. Relatively small variations in the magnitude of modifications can affect the reduction in knee loading. Therefore, good system precision is important in this context. This poses a considerable challenge for the measurement of gait modification strategies outside the laboratory. However, the results suggest that a sufficient level of accuracy is achievable with the tested sensor systems.

In considering what measurements can realistically be moved out of the gait lab for use in more 'portable' biofeedback systems, one is still faced with certain limitations in current sensor technology and processing. Although data fusion algorithms for derivation of device orientation from accelerometers and gyroscopes - such as that used here - are not trivial, the conservative aspirations for the two systems for viable, single-device trunk lean measurement were met. More complex measures may not be as readily achieved. Knee loading in OA is generally assessed in the lab by measurement of the external knee adduction moment (KAM), requiring both body position and ground reaction force measurement. Despite the development of force-instrumented and position-sensing shoes [11, 12], the immediate prospects for knee load measures to be made widely, cost-effectively, and unobtrusively in the field in free-moving conditions are not as yet encouraging [13]. We have taken the approach in the gait lab, and now potentially outside it, to generate biofeedback of the *kinematic* gait changes that lead to KAM reduction, not feedback of the KAM itself. We have used this approach successfully with OA patients to achieve acute load reduction [5], and we and others have used similar feedback systems with healthy subjects [10, 14-16]. The results presented here suggest that the inertial sensor systems can perform similarly as a basis for this feedback as the lab-based systems, when measuring the orientation of the trunk.

The impetus for the development of the *remote* monitoring system was not only the need for understanding gait modifications in knee OA, but also the increasing general interest in remote health monitoring. In Australia, the imminent rollout of the "National Broadband Network" (NBN) promises a higher bandwidth network,

potentially scalable to accommodate 'dense' data transmitted from many patients. The increasing prevalence of higher-bandwidth consumer networks around the world raises the prospect of wider motion monitoring for research, clinical, and general health applications.

5. ACKNOWLEDGMENTS

6. REFERENCES

[1] Miyazaki T, Wada M, Kawahara H, Sato M, Baba H, Shimada S., 2002. Dynamic load atbaseline can predict radiographic disease progression in medial compartment knee osteoarthritis. Ann Rheum Dis. 61, 617-22.

[2] Simic M, Hinman RS, Wrigley TV, Bennell KL, Hunt MA, 2011. Gait modification strategies for altering medial knee joint load: A systematic review. Arthritis Care Res, 63, 405-426.

[3] van der Esch M, Steultjens MP, Harlaar J, van den Noort JC, Knol DL, Dekker J., 2011. Lateral trunk motion and knee pain in osteoarthritis of the knee: a cross-sectional study. BMC Musculoskeletal Disorders, 12, 141.

[4] Hunt MA, Birmingham TB, Bryant D, Jones I, Giffin JR, Jenkyn TR, Vandervoort AA, 2008. Lateral trunk lean explains variation in dynamic knee joint load in patients with medial compartment knee osteoarthritis. Osteoarthritis Cartilage, 16, 591-9.

[5] Simic M, 2012. Gait modification strategies for people with medial knee osteoarthritis. Unpublished PhD thesis, Department of Physiotherapy, University of Melbourne.

[6] Wrigley TV, Simic M, Hunt MA, Hinman RS, Bennell KL, 2009. Real-time movement biofeedback for walking gait modification in knee osteoarthritis. In: Virtual Rehabilitation 2009 International Conference. Haifa, Israel. June 29 - July 2, 2009. Cobb, S, ed. pp 132-135. Piscataway, New Jersey: IEEE.

[7] Madgwick, S.O.H. Harrison, A.J.L.Vaidyanathan, R. Estimation of IMU and MARG orientation using a gradient descent algorithm. 2011 IEEE International Conference on Rehabilitation Robotics (ICORR), June 29-July 1, 2011. Zurich, Switzerland. pp 1-7.

[8] Ferraris F, Grimaldi U, Parvis M, 1995. Procedure for effortless in-field calibration of three-axis rate gyros and accelerometers. Sensors and Materials, 7, 311-330.

[9] Hunt MA, Wrigley TV, Hinman RS, Bennell KL, 2010. Individuals with severe knee osteoarthritis (OA) exhibit altered proximal walking mechanics compared with individuals with less severe OA and those without knee pain. Arthritis Care Res., 62, 1426-32.

[10] Hunt MA, Simic M, Hinman RS, Bennell KL, Wrigley TV, 2011. Feasibility of a gait retraining strategy for reducing knee joint loading: increased trunk lean guided by real-time biofeedback. J Biomechanics, 44, 943-7.

[11] Liu T; Inoue Y, Shibata K; Shiojima K; 2010. Design and characterization of a mobile force plate and three-dimensional motion analysis System. IEEE SENSORS 2010 Conference. Kona, Hawai. pp. 557-561.

[12] van den Noort JC, van der Esch M, Steultjens MP, Dekker J, Schepers HM, Veltink PH, Harlaar J, 2012. The knee adduction moment measured with an instrumented force shoe in patients with knee osteoarthritis. J Biomech., 45, 281-8

[13] Wrigley TV, 2011. "Motion sensors in osteoarthritis – prospects and issues", in Healthcare Sensor Networks: Challenges Toward Practical Implementation. D. Lai, R. Begg, M. Palaniswami, Eds. Boca Raton, Fla.: Taylor and Francis, pp. 183-220.

[14] Barrios JA, Crossley KM, Davis IS, 2010. Gait retraining to reduce the knee adduction moment through real-time visual feedback of dynamic knee alignment. J Biomech., 43, 2208-13.

[15] Shull PB, Lurie KL, Cutkosky MR, Besier TF, 2011. Training multi-parameter gaits to reduce the knee adduction moment with data-driven models and haptic feedback. J Biomech. 44, 1605-9.

[16] Wheeler JW, Shull PB, Besier TF, 2011. Real-time knee adduction moment feedback for gait retraining through visual and tactile displays. J Biomech Eng. 133, 041007.

[17] Wrigley TV, 2008. Flexible real-time movement biofeedback. An approach using Vicon optical motion capture and Matlab. 3DMA-08 - 10th International Symposium on 3D Analysis of Human Movement. Santpoort, Netherlands, October 28-31.

Performance analysis of an automatic tracking software in underwater exercises

(Automatic tracking in underwater exercises)

Magalhães, F. A.[1], Sawacha, Z.[3], Di Michele, R.[2], Cortesi, M.[2], Gatta, G.[2], Fantozzi, S.[1,2]

[1] Department of Electronics, Computer Sciences and Systems, University of Bologna, Bologna, Italy

[2] Faculty of Exercise and Sport Sciences, University of Bologna, Bologna, Italy

[3] Department of Information Engineering, University of Padua, Padua, Italy

The aim of this study was to test the performance of an automatic tracking software of features, FeatureTracker, developed for underwater motion analysis, and to compare it with another commercially available software, SIMI Motion System. Samples of 19 video recordings of different aquatic exercises (n=2340 frames) were manually tracked using the SIMI software in order to determine the markers center coordinates. Then they were automatically tracked using both the FeatureTracker and the SIMI software as follows: an operator stopped the automatic procedure in case the distance between the calculated marker and the reference one was higher than 4 pixels and then the action proceeded with a manual intervention in order to correct the cursor position. In all exercise modes, the manual intervention was required the 12% of the complete tracking procedure for the FeatureTracker and the 28% for the SIMI one, thus demonstrating the optimal automatic tracking performance of FeatureTracker. Therefore, the FeatureTracker software can be considered a valid tool for underwater motion analysis.

Keywords-automatic tracking; passive markers; sport; swimming

1. INTRODUCTION

Different computer software are used to track markers attached or fixed to the human body in order to measure the variables related to swimming performance. Markers' tracking has been considered as a gold standard procedure because of its high accuracy. Furthermore, such a procedure allows to present intuitively and informatively some relevant data for coaches and swimmers [1]. Manual tracking, however, requires an extensive amount of time and it is operator dependent, thus resulting unreliable because the margin of human error is high [2, 3]. Therefore, different software were developed with the aim of automatically tracking the markers in human motion analysis. This automation achieves good precision and requires little time to analyze the data [4], though at the cost of being expensive, complex and bulky [2]. Taken for itself, tracking is a solved problem, but it's not easy to select features that can be tracked properly and that correspond to physical points in the world [5]. The different techniques for automatic tracking of objects which have been proposed in the literature can be divided into "point tracking" and "kernel tracking" approaches [6]. The "point tracking" approach is based on the detection of points that represents objects in consecutive frames. Commonly used point detectors include the Harris corner detector and Difference-of-Gaussians, Fast Hessian and Center-Surround Extrema detectors [7]. On the other hand, the "kernel tracking" methods represent the objects as primitive shapes, and compute their motion from frame to frame. The simplest approach is represented by the *template matching,* in which a similarity measure, e.g. cross correlation, is used to search the object template in each image. Alternatively, the motion in a region can be computed exploiting optical flow methods, assuming small displacements and brightness constancy, as in the Kanade-Lucas-Tomasi (KLT) feature tracker [8, 9]. In this contest, a software for automatic tracking of user-defined features has been developed starting from a freely available, open-source implementation of the KLT feature tracker [8]. The performance of this software in underwater motion analysis was tested and compared with that of another commercially available software.

2. MATERIAL AND METHODS

Algorithm theoretical background

The used feature-tracking algorithm aims to individuate the displacement of small patches between two consecutive images. Under the assumption of brightness constancy, changes in the image intensity are only due to motion: the intensity of a patch $I(x)$, where x are the coordinates of its centroid, should correspond to the intensity of patch $J(x) = I(x - d)$ in the following image, being d the displacement that has occurred on the image plane. The value of d is calculated by minimizing the residual error:

$$\left(J(x) - I(x-d)\right)^2 \qquad (1)$$

over all the pixels that compose the patch W:

$$d \int_W \left(J(x) - I(x-d)\right)^2 dA \qquad (2)$$

For small displacements, the intensity function can be approximated by its Taylor series expansion truncated to the linear term:

$$l(x-d) = l(x) - g \cdot d \qquad (3)$$

where g is the spatial gradient of the first image around x. This yields to a closed form solution of the minimization problem, as the residual becomes a quadratic function of the displacement d:

$$\left(\int_W (gg^T) dA\right) d = \int_W (J(x) - I(x)) g \, dA \qquad (4)$$

The first-order approximation however is likely to determine inaccurate determinations of d, especially at high-curvature points in the image intensity function, and for finite displacements (not approaching zero). Therefore, the minimization step is repeated iteratively in a Newton-Raphson style, upon registration of the image patches according to the current solution.

Experimental analysis

Sample of 19 AVI video files (720 x 572 pixels, 50 frames/second) was used to perform the manual and automatic tracking. Color analog cameras (TS-6021PSC, Tracer Technology Co. Ltd) were used to collect videos, connected to a computer through an Analog to Digital Video Converter (Canopus ADVC55, Grass Valley, USA, LLC). The cameras were automatically synchronized with an ad-hoc software application [10]. Three passive markers were positioned on key anatomical landmarks of exercising subjects, according to the activity performed. Black on white and white on black contrasts between the markers and relevant background were used. The examined videos were divided into five sets, according to the underwater activity performed: 1) two videos of walking on a water treadmill; 2) two videos of running simulation on a water elliptical machine; 3) six videos of passive-towing swimming in a prone position, using a full body swimsuit (n= 3 videos) or a traditional brief swimsuit (n=3 videos); 4) three videos of flutter kick; 5) six videos of front crawl swimming, recorded using six cameras positioned in order to maximize the visualization of the right upper limb. Each video was tracked manually by an experienced operator using the manual-tracking mode of the SIMI software (SIMI Reality Motion Systems GmbH, version 7.5.288), with the aim to determine a gold standard for the 2D coordinates of the center of the markers. Then, the 19 videos were tracked automatically by using both the SIMI and the FeatureTracker software. SIMI is one of the most popular software in human movement research, whereas FeatureTracker is a software specifically developed to perform the automatic tracking of passive markers, providing a simple user interface to Birchfield's implementation of the KLT tracker [11]. For both software, an operator stopped the automatic tracking procedure and performed a manual intervention to correct the software's cursor position in the case that, for at least one marker, the distance between the calculated center of the marker and the reference one (i.e., that determined using the manual tracking) was higher than 4 pixels. A 4-pixel threshold was used as corresponding to the radius of markers. Given the multidirectional movements of the limbs and trunk during the performed activities, some markers were not visible in some frames. In such cases, the frame was excluded from calculation, i.e., the manual and automatic tracking were performed only on visible markers (n=2340). In order to analyze the software's automatic tracking performance, the proportion of manual interventions was compared using odds ratios, both in the single exercise modes and in the whole sample of frames.

3. RESULTS

The number of frames requiring or not the manual interventions for the SIMI and the FeatureTracker software are shown in Table 1. In all sets of videos, an OR lower than 1 was found demonstrating that the averaged proportion of the manual interventions in SIMI (28%) and FeatureTracker (12%) was different (p <0.05). The only exception was the "Towed swimming" exercise mode, in which both the software required almost no manual interventions.

Table 1. The automatic tracking performance of the SIMI and the FeatureTracker software

Exercise	Software	Automatic [a]	Manual [b]	% [c]	OR [d]	95% CI for OR [e]
Front Crawl	SIMI	432	219	51	0.34	026 – 0.44
	FeatureTracker	556	95	17		
Running	SIMI	158	136	86	0.24	0.16 – 0.35
	FeatureTracker	244	50	21		
Towed	SIMI	496	0	0	∞	1 – ∞
	FeatureTracker	492	4	1		
Flutter kick	SIMI	310	79	26	0.67	0.46 – 0.98
	FeatureTracker	332	57	17		
Walking	SIMI	440	70	16	0.55	0.37 – 0.83
	FeatureTracker	469	41	9		
Total	SIMI	1836	504	28	0.43	0.36 – 0.51
	FeatureTracker	2093	247	12		

a. Automatic tracking; b. Manual intervention; c. %: Percentage of manual intervention;
d. OR: Odds Ratio; e. CI: Confidence Interval

4. DISCUSSION

The aim of this study was to analyze the automatic tracking performance of two software: the FeatureTracker, a software specifically designed to automatically track passive markers in the aquatic environment, and the SIMI, a software often used in biomechanics laboratories for the kinematic analysis of sport gestures. It is important to have an automatic tracking system that works with minimal necessity of manual correction and non-operator dependent in order to save time. To this purpose, the amount of manual interventions during the automatic tracking procedure was assessed. The manual intervention percentage for the various sets of videos ranged from 0% to 86% for SIMI and 1% to 21% for FeatureTracker. The odds ratios computed by the number of frames automatically tracked and those that required a manual intervention was less than 1 showing that the automatic tracking performance of FeatureTracker in all sets of videos, with exception of "Towed swimming" exercise mode, was different to that of SIMI ($p < 0,05$).

The automatic tracking of markers in aquatic environment requires special attention from the video recording procedure until the tracking itself. First, hindrances that may hinder the clear identification of markers by the underwater cameras must be avoided. Bubbles, visibility of the marker in a particular frame and water transparency are examples of possible obstacles that may limit the visualization of markers during underwater activities. Another factor that influences a correct identification of markers is the inadequate video quality due to a low contrast between "marker – anatomical landmark – background". In the sets of videos in which a higher proportion of manual interventions was necessary, some of the factors previously mentioned were actually present. For example, in "Front Crawl Swimming", the multidirectional movements of the upper limbs that continuously alternated between shoulder internal-external rotation, elbow flexion-extension and forearm pronation-supination, did not allow an optimal markers' visualization in all frames. In addition, it was not possible to record the markers placed on the hand and elbow by the underwater cameras when they lifted water during the aerial phase in the front crawl stroke. In "Running", the contrast between "marker – anatomical landmark – background" was not high enough to allow the correct identification of the markers in certain frames by both the software, whereas in "Flutter Kick swimming" the rapid movements of the lower limbs produced bubbles that obscured the identification of the marker located in the ankle. On the other hand, the "towed swimming" was characterized by all the needed conditions for a proper identification of markers. Even at the highest speeds of movement, there were no bubbles and the contrast between "marker – anatomical landmark – background" was good, allowing a correct automatic tracking to both the software.

Another issue to be pointed out concerns the link between the automatic tracking performance and the type of marker used, because the software's algorithms are situation-specific. Reflective passive markers are the most used in the analysis of human movement, but it is known they are not suitable for underwater motion analysis. There are some passive underwater marker consisting of a spherical body covered in a retro-reflective tape that is designed to work underwater, as those from Qualiysis Motion Sytem Analysis [12], but they may be uncomfortable for swimmers and can increase the drag effect. A viable solution is the use of markers drawn on the skin or on the swimsuit. Thus, in this study, three types of markers were used: full black circles on the light skin, partial black circles (two empty quarters and two full quarters) on the light skin, and full white circles on the dark swimsuit. As the sets of videos and the criterion used by the operator to identify the markers were the same, one probable reason for the difference of the automatic tracking performance between both software is related to the calculation method used to automatically identify the markers. The method used by FeatureTracker is an open-source implementation of the KLT feature tracker described by Lucas and

Kanade (1981), whilst the automatic tracking method used by SIMI is a closed-source, i.e., not available for consulting. Moreover, an out-of-date SIMI version was used, so perhaps another result can be obtained using the newest release of the SIMI software. Hence, the FeatureTracker can be used in researches approaching automatic tracking of passive markers during underwater motion analysis because of its optimal performance.

5. REFERENCES

[1] A. J. Callaway, J. E. Cobb, and I. Jones, "A comparison of video and accelerometer based approaches applied to performance monitoring in swimming," *Int J Sports Sci & Coaching,* vol. 4, pp. 139-153, 2009.

[2] S. Daukantas, V. Marozas, and A. Lukosevicius, "Inertial sensor for objective evaluation of swimmer performance," in *11th International Biennial Baltic*, 2008, pp. 321-324.

[3] S. E. Slawson, P. P. Conway, L. M. Justham, and A. A. West, "The development of an inexpensive passive marker system for the analysis of starts and turns in swimming," in *8th Conference of the International Sports Engineering Association (ISEA)*, 2010, pp. 2727-2733.

[4] S. Ma, Z. Liu, B. Yang, and J. Wang, "Moving target detection and labeling in video sequence based on spatial-temporal information fusion," in *Bio-Inspired Computational Intelligence and Applications*. vol. 4688, K. Li, M. Fei, G. Irwin, and S. Ma, Eds., ed: Springer Berlin / Heidelberg, 2007, pp. 795-802.

[5] J. Shi and C. Tomasi, "Good features to track," *IEEE Conference on Computer Vision and Pattern Recognition,* pp. 593-600, 1994.

[6] A. Yilmaz, O. Javed, and M. Shah, "Object tracking: A survey," *ACM Comput.Surv.,* vol. 38, p. Article 13, 2006.

[7] S. Gauglitz, T. Höllerer, and M. Turk, "Evaluation of interest point detectors and feature descriptors for visual tracking," *Int J Comput Vis,* pp. 335-360, 2011.

[8] B. D. Lucas and T. Kanade, "An Interative Image Registration Technique with an Application to Stereo," *International Joint Conference on Artificial Intelligence,* pp. 674-679, 1981.

[9] C. Tomasi and T. Kanade, "Detection and tracking of point features," *Carnegie Mellon University Technical Report CMU-CS,* pp. 91-132, 1991.

[10] E. Ceseracciu, Z. Sawacha, S. Fantozzi, M. Cortesi, G. Gatta, S. Corazza, and C. Cobelli, "Markerless analysis of front crawl swimming," *J Biomech,* vol. 44, pp. 2236-42, Aug 11 2011.

[11] S. Birchfield. (1997). *Derivation of Kanade-Lucas-Tomasi tracking equation*. Available: http://www.ces.clemson.edu/~stb/klt/birchfield-klt-derivation.pdf

[12] *Qualiysis Motion Sytem Analysis.* Available: http://www.qualisys.com/products/accessories/passive-markers/underwater/

Passive drag and body position of swimmers wearing a rubber full-body swimsuit

Cortesi M. [1], Di Michele R. [1], Fantozzi S. [1,2], Zamparo P. [3], Gatta G. [1,4]

[1] Department of Histology, Embryology and Applied Biology, University of Bologna, Italy
[2] Department of Electronics, Computer Sciences and Systems, University of Bologna, Italy
[3] Department of Neurological, Neuropsychological, Morphological and Movement Sciences,
Faculty of Exercise and Sport Sciences, University of Verona, Italy
[4] Faculty of Exercise and Sport Science, University of Bologna, Italy

The introduction of rubber suits abruptly improved the swimming performance. However, it is not still clear how this kind of suit affects the drag of swimmers. The purpose of the present study was to analyze how the trunk and lower limbs hydrodynamic position, induced by wearing a rubber swimsuit, affects the Dp in front crawl swimming. Fourteen male high-level swimmers performed six 20-m trials of passive swimming at increasing velocities (1.0, 1.2, 1.4, 1.6, 1.8 and 2.0 m/s). The whole protocol was repeated in random order wearing a brief-traditional suit and a full-body synthetic rubber swimsuit. The present data showed that the synthetic rubber swimsuit induced an increase of the legs inclination with a raising effect similar to that involved by a pull-buoy. As the drag is reduced by changing the body position during gliding, a modified position of the lower limbs may be a further factor contributing to the passive drag reduction observed when using a full-body swimsuit.

Glide swimming; passive drag; performance; technology (key words)

INTRODUCTION

The slowing down action (drag) due to the water's viscosity is the reason for the reduction of displacement velocity in the water with respect to the air [1]. The swimmer's drag, due in its majority (>50%) to the shape of the body (pressure drag) and for a lower proportion to characteristics of the boundary layer around the body (friction drag) and to wave formation (wave drag), [2] is then the variable that most affects the swimming performance. Full-body swimsuits, initially manufactured using a textile material, are known to considerably reduce the active drag of a swimmer [3] as well as the passive drag (Dp), i.e. that measured when towing the swimmer in the best glide position [4; 5]. The horizontal position assumed by a gliding swimmer allows to reduce the frontal cross-section of the body and the pressure drag [6], being actually a performing position. A reduction of the energy cost of swimming is obtained when contrasting the lower limbs sinking [7]. The trunk inclination determined by the legs sinking affects the swimmer's drag due to a higher body cross-section [8]. In 2008, some manufacturers, exploiting the fact that technical rules were not yet well defined at that time, put some rubber parts on textile suits, and then produced the first full-body synthetic rubber (polyurethane or neoprene) swimsuits. The introduction of rubber suits abruptly improved the swimming performances [9]. However, it is not still clear how this kind of suit affects the drag of swimmers [10]. Some authors postulated that such a swimsuit may have some kind of biomechanical effects as those determined by rubberized panels put in parts of the body in which the water collides with the highest pressure [11], or the high mechanical compression and the subsequent energetic benefits [12]. To our knowledge, however, no study has explained the actual reasons for which the swimming velocity increase when using a rubber swimsuit, or how this kind of swimsuit may affect the swimmer's position. Therefore, the purpose of the present study was to analyze how the trunk and lower limbs hydrodynamic position, induced by wearing a rubber swimsuit, affects the Dp in front crawl swimming.

MATERIAL AND METHODS

Fourteen male high-level swimmers (age 24 ± 4 years, body length 180 ± 4 cm and body mass 73.5 ± 3.9 kg) were involved. The swimmers performed six 20-m trials of passive swimming: from the best glide position (i.e. a prone position with hand between arms), they were towed at the surface by means of an electromechanical motor (Ben-Hur, ApLap Roma) (Zamparo, 2009) at increasing velocities (1.0, 1.2, 1.4, 1.6, 1.8 and 2.0 m/s). The whole protocol was repeated in random order two times, namely when wearing a brief-traditional suit (TS, Sali, Arena, Italy) and a full-body (shoulder to ankle) synthetic rubber swimsuit (RS, X-glide Power-skin, Arena, Italy). The force needed to tow a swimmers at a given velocity equalled to the Dp for that swimmer at that velocity, and was recorded using a specific software (ApLap, Sport DAQ, Italy). Furthermore, the swimmers were filmed at a sampling rate of 50 Hz with an underwater camera (Sony Hyper Had, TS-6021PSC, Japan) placed perpendicular to the their displacement direction on a sagittal view. The

number of frames elaborated were from a minimum of 30 to a maximum of 60 depending on the towing velocity. Anatomical landmarks were drawn on the inferior angle of scapula, greater trochanter, and head of the fibula (Fig. 1). The markers on the skin were visible through the full body suit, thus it was possible to verify the correspondence between the markers in the two conditions. The digitalization of the positions of features on each video sequence, namely tracking, was automatically performed by an ad-hoc software based on [13]. Then, the following angles were computed: TI, between the horizontal and the trunk segment (angle of scapula - greater trochanter); LI, between the horizontal and the lower limbs segment (greater Trochanter - head of the Fibula). In order to roughly have an accuracy index, the distance between greater trochanter and the head of the fibula was estimated for all frames of a subject at all towing velocities, the standard deviation value was 0.8 cm. Paired Student's t-tests were used to assess the differences between the mean values of dependent variables (TI, LI and Dp) as assessed respectively in the two considered swimsuit conditions. Significance was set at $\alpha = 0.05$.
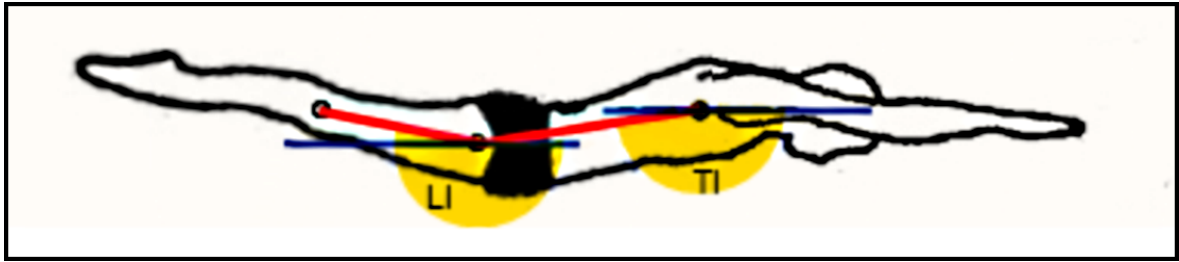

Figure 1. Swimmer in the best glide position.

RESULTS

When pooling together the data of all the velocities, the mean ($\pm$ SD) TI angle was of 172.8 ± 3.3 degrees for S and of 171.6 ± 4.0 degrees for RS ($p>0.05$), whereas the mean LI angle was significantly larger in RS (188.4 ± 3.9) compared to S (185.5 ± 3.7). Figure 2 displays the mean TI and LI values recorded in S and RS at each of the six considered towing velocities. Concerning TI values, no significant differences were found between S and RS, with the exception of the 1.6 m/s, showing a higher trunk incline in the traditional suit ($p=0.043$). Conversely, the mean LI angle was significantly larger when the swimmers wore the rubbers swimsuit at all the considered velocities. The mean ($\pm$ SD) Dp values were similar between the two conditions at the lowest velocities (< 1.6 m/s), whereas Dp was significantly lower in RS at the highest velocities (1.6 to 2.0 m/s) (Table 1).
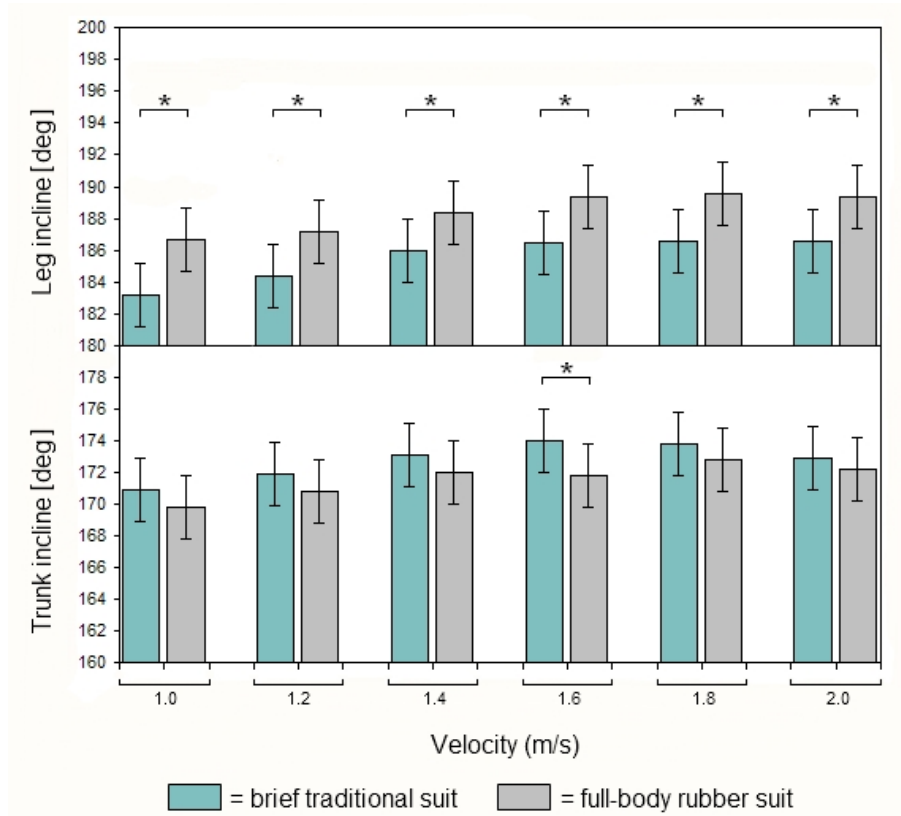
Figure 2.   Mean and SD of trunk and legs incline at the examined towing velocities (✷ p<0.05).

Table 1. Mean ± SD passive drag values at the examined towing velocities for the traditional swimsuit (S) and the rubber full-body swimsuit (RS)

Passive drag	Towing velocity (m/s)					
	1.0	*1.2*	*1.4*	*1.6*	*1.8*	*2.0*
Pd in S (N)	29.3 ± 4.7	42.2 ± 9.5	56.7 ± 6.4	71.8 ± 10.0	90.0 ± 11.6	120.3 ± 15.1
Pd in Rs (N)	28.8 ± 4.9	41.4 ± 6.8	54.0 ± 9.5	65.8 ± 9.2 [a]	77.9 ± 9.6 [a]	102.7 ± 13.8 [a]

a.   Significantly different in S vs. Rs; p < 0.05

DISCUSSION

An unprecedented increase of swimming performances has been determined in last years by the introduction of rubber full-body swimsuits [9]. This study aimed to analyze the changes in the body position of a gliding swimmer induced by wearing such a kind of swimsuit. This aspect is of great interest for the analysis of the swimming performance, as the body position may affect the hydrodynamic resistances and thus the swimming velocity [14]. An horizontal body position involves a limited frontal impact area [6]. In fact, the effective frontal impact area of a swimmer is determined as the product between the frontal impact section, a variable independent from the used swimsuit, and the inclination of the swimmer's body with respect to the displacement direction [1]. The present results confirms the argument that the trunk position during passive gliding is not substantially affected by the swimsuit [15] as TI showed no relevant differences between R and RS. Therefore, the effective impact area does not change when using a rubber full-body suit. Conversely, at all the velocities, LI was significantly higher in RS vs. S, actually affecting the swimmers' position. The rubber full-body suit showed lower Dp values at the highest towing velocities (1.6 to 2.0 m/s). These data are in agreement with previous observations concerning a textile full-body suit [4; 5]. The characteristics of the super-hydrophobic material of which the rubber suit is made could explain the Dp reduction, as a drag reduction was shown under condition of laminar flow [16], and, up to 50%, in turbulent flows [17]. The present data showed that the RS induced an increase of the legs inclination with a raising effect similar to that involved by a pull-buoy. As the drag is reduced by changing the body position during gliding [14], a modified position of the lower limbs may be a further factor contributing to the Dp reduction observed when using a full-body swimsuit Future investigations will aim to assess the effects of the specific fabric composition of the full-body suit on

hydrodynamic resistances, in order to further improve the understanding of the relevant effects on swimming performance.

REFERENCES

[1] Mollendorf, J.C., Termin, A.C., Oppenheim, E., Pendergast, D.R., 2004. Effect of swim suit design on passive drag. Med Sci Sports Exerc 36(6), 1029-35.

[2] Pendergast, D. et al., 2005. The influence of drag on human locomotion in water. Undersea Hyperbar M 32, 45-57.

[3] Toussaint, H.M., et al., 2002. Effect of a Fast-skin "body" suit on drag during front crawl swimming. Sport Biomech 1(1), 1-10.

[4] Benjanuvatra, N., Dawson, G., Blanksby, B.A., Elliott, B.C., 2002. Comparison of buoyancy, passive and net active drag forces between Fastskin and standard swimsuits. J Sci Med Sport 5(2), 115-23.

[5] Smith, J., Joseph, M., Pascoe, D., 2007. The influence of a compressive laminar flow body suit for use in competitive swimming. The Journal of Swimming Research 17, 10-16.

[6] Clarys, J.P., Human morphology and hydrodynamics. In: Terauds, J., Bedingfield EW (eds) Swimming III. University Park Press, Baltimore, 1979, pp 3–41.

[7] Pendergast, D.R., di Prampero, P.E., Craig, A.B. Jr., Wilson, D.R., Rennie, D.W. 1977. Quantitative analysis of the front crawl in men and women. J Appl Physiol 43, 475–479.

[8] Zamparo, P., Gatta, G., Capelli, C., Pendergast, D.R., 2009. Active and passive drag: the role of trunk incline. Eur J Appl Physiol 106,195–205.

[9] O'Connor, L., Vozenilek, J., Is It the Athlete or the Equipment? An analysis of the top swim performances from 1990-2010. J Strength Cond Res (in press).

[10] Toussaint, H.M., 2011. Measurement of drag to assess the effect of swim suits. Rev Port Cien Desp 11(3), 77-80.

[11] Bixler, B., Pease, D., Fairhurst, F., 2007. The accuracy of computational fluid dynamics analysis of the passive drag of a male swimmer. Sport Biomech 6(1), 81-98.

[12] Kainuma, E., et al., 2009. Proposal of alternative mechanism responsible for the function of high-speed swimsuits. Biomed Res 30(1), 69-70.

[13] Lucas, B.D., Kanade, T., 1981. An iterative image registration technique with an application to stereo vision. Intl Joint Conference on Artificial Intelligence 16(3), 674-679.

[14] Pendergast, D.R., Mollendorf, J.C., Cuviello, R., Termin, II., 2006. Application of teoretical principles to swimsuit drag reduction. Sports Eng 9, 65-76.

[15] Roberts, B.S., Kamel, K.S., Hedrick, C., McLean, S.P., Sharp, R.L., 2003. Effect of a FastSkin suit on submaximal freestyle swimming. Med Sci Sports Exerc 35(3), 519-24.

[16] Gogte, S., et al., 2005. Effective slip on textured superhydrophobic surfaces. Phys Fluids 17, 051701.

[17] Daniello, R., Waterhouse, N.E., Rothstein, J.P., 2009. Turbulent drag reduction using superhydrophobic surfaces. Phys Fluids 21. 085103.

Underwater Gait Analysis:

A Markerless Approach

Mantoan A.[1], Sawacha Z.[1], Fantozzi S.[2,3], Cortesi M.[3], Rigato A.[1], Gatta G.[3], Cobelli C.[1]

[1] *Department of Information Engineering, University of Padova, Padova, Italy*
[2] *DEIS, University of Bologna, Bologna, Italy*
[3] *Faculty of Exercise and Sport Sciences, University of Bologna, Bologna, Italy*

A fundamental need for modern biomechanical and clinical application is the ability to accurately capture normal and pathologic human movement. In this contest, nowadays, the aquatic environment is gaining an even important role within the rehabilitation world, thanks to water physical properties. Walking is one of the most common motor tasks in water-based exercise programs and it may be considered a major underwater rehabilitative tool. However state of the art marker based gait analysis cannot be performed in water environment, where the attachment of skin surface markers is not easy. A markerless approach, based only on synchronized video sequences, has been proposed as a potential solution for underwater (UW) applications. In the present work, an automatic markerless motion capture system has been investigated and its accuracy in UW three-dimensional (3D) lower limbs joint kinematics reconstruction has been tested. The results demonstrate the feasibility of calculating meaningful joint kinematics from subjects walking underwater without any markers attached to the limb. Thus, a markerless approach seems to offer the promise of expanding the applicability of human motion capture in an aquatic environment.

markerless gait analysis, underwater, biomechanics, 3D joint kinematics

1. INTRODUCTION

Nowadays, the aquatic environment is gaining an even important role within the rehabilitation world, thanks to water physical properties. A variety of physical activities different from swimming can be proposed in water to take advantages of its unique characteristics. Walking is one of the most common motor tasks in water-based exercise programs and it may be considered a major underwater rehabilitative tool [1]. Nevertheless, at present, few empirical data have been collected in order to quantitatively assess its effectiveness [2]. A biomechanics characterization of normal and pathologic walking in water could be useful to contribute to a more appropriate prescription of walking in water as part of training and alternative water-based rehabilitation programs. However, the measurement of common biomechanical parameters during water locomotion is more complicated than in laboratory conditions, since most instruments are not suitable for operating in a water environment. Therefore, new technologies, which allow evaluating and quantifying the progression of an aquatic therapy, may be extremely useful, and give an important incentive to the development of even better rehabilitative programmes. The aim of this work is to test the applicability of a markerless approach for underwater gait analysis. In this context, a three-dimensional underwater markerless approach is investigated in order to estimate lower limb (LL) joints kinematics during gait. Underwater gait analysis of three healthy subjects were performed and LL joint angles evaluated. The approach proposed in Corazza et al. [3] and Mundermann et al. [4], that relies on video sequences of the subjects to automatically estimate their kinematics, was taken as starting point for the development of a novel underwater markerless motion capture system. This approach indeed has been successfully adopted in the clinical field [3]. In order to take into account the presence of water, the modified version of this algorithm presented in Ceseracciu et al. [5] has been adopted. The accuracy of the proposed technique has been evaluated with respect to a commercial video-based motion analysis system that requires manual digitization of points.

2. MATERIAL AND METHODS

Data acquisition
Three healthy male subjects were recruited (mean age and BMI were respectively 33.3±15.7 and 24.1±3.2). Six walking trials at a self-selected speed have been acquired with six subaqueous video cameras (TS-6021PSC, Tracer Technology Co. Ltd) in a swimming pool with water at 1.20 m. Each camera was connected to a FireWire (IEEE 1934a)-equipped notebook through an Analog to Digital Video Converter (Canopus ADVC55; output DV video, PAL interlaced, 25 frames/second). A total of 5 notebooks were involved: one of them was equipped with a PCMCIA IEEE 1394a card, which enable it to be connected to two cameras. Although in theory two cameras could be connected to the same FireWire controller, provided that multiple input ports are available, this solution has proved to be experimentally unreliable. All notebooks were linked to a hub through

Ethernet cables. A custom-made software that could allow to acquire data simultaneously from different A/D converters has been adopted in order to synchronize the acquisition from all cameras [5].

A two steps calibration algorithm has been adopted [7], performed using the Camera Calibration Toolbox for Matlab by Jean-Yves Bouguet (http://www.vision.caltech.edu/bouguetj/calib_doc/). Intrinsic parameters were calculated from a series of images of a wooden panel with checkerboard-pattern drawn on it (13 x 9 black and white squares, side 42 millimeters), acquired from different angulations in space. Since calibration of intrinsic parameters has been performed out of water, they need to be corrected for use in the underwater environment. The change in refractive index from air to water must be taken into account. Following the work of Lavest et al. [8], the focal length has to be multiplied by n = 1.333. Extrinsic (or external) parameters were instead obtained capturing a calibration grid of known geometry (sized 2.07 x 1.07 x 1.40 meters). 24 control points were identified on it, and their position relative to an embedded system of reference were known [5].

Data Analysis

The method proposed by Corazza et al. [3] was applied. In order to consider the water environment the background subtraction algorithm was modified according to Ceseracciu et al. [5]. Pearson's correlation analysis was used to aid in selecting which of each subject's representative walking trials were to be included in the computation of the mean; thus the correlation coefficient was calculated for each subject's kinematic parameter. Walking trials with a correlation coefficient lower than 0.75 (75%) were excluded from the statistical analysis [6]. For each subject, representative bands (mean $\pm$ 1 standard deviation (SD)) of the correlated results were thus obtained (Figure 1).
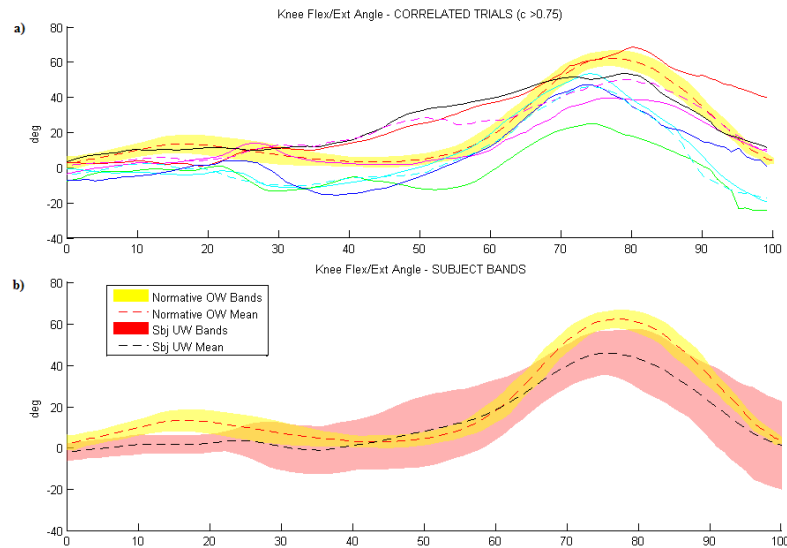

Figure 1: Example from subject 1: (a) all correlated trials used to compute the mean patterns, (b) subject specific band for the knee.

The same methodology has been adopted considering altogether the three control subjects' joints angles: correlation has been assessed combining each subject correlated trails together. Inter-subjects mean and standard deviation has been calculated and thus UW Markerless Bands have been obtained (mean $\pm$ 1SD, see Figure 1). In order to compare UW data with the state of the art, UW Bands have been compared with Normative Out of Water (OW) Bands obtained with the data of 10 healthy subjects in laboratory condition in Sawacha et. al [6].

Accuracy and reliability of the proposed technique were evaluated by means of comparison with traditional manual digitization (MAN) using a dedicated software (SIMI Reality Motion Systems GmbH). In order to compare the two techniques, knee joint planar angles were evaluated and root mean square distance (RMSD) values between angles estimated (Matlab R2011a).

3.   RESULTS

Mean and SD of the angles for the hip, knee and ankle joints (considering the data of the three subjects) are reported in Table 1, while mean and SD values for the corresponding ranges of motion (ROM) are shown in Table 2.

Table 1: Mean and SD of hip, knee and ankle joint angles.

	Hip	Knee		Ankle
flexion-extension [deg]	-14.1±13.5	14.8 ±13.8	flexion-extension [deg]	-1.4±6.0
abduction-adduction [deg]	3.4±3.0	-	inversion-eversion [deg]	-1.7±3.0
internal-external rotation [deg]	1.4±5.4	-	internal-external rotation [deg]	-0.6±3.2

Table 2: Mean and SD of hip, knee and ankle joint ranges of motion (ROM).

	Hip	Knee		Ankle
flexion-extension [deg]	61.8±19.9	50.1 ±11.8	flexion-extension [deg]	37.0±15.9
abduction-adduction [deg]	20.0±3.4	-	inversion-eversion [deg]	7.6±4.0
internal-external rotation [deg]	15.6±1.9	-	internal-external rotation [deg]	11.1±3.7

Resulting UW Bands for the knee flexion-extension angle from the three control subjects over the Normative OW Bands [3] were displayed in Fig. 2, as an example.
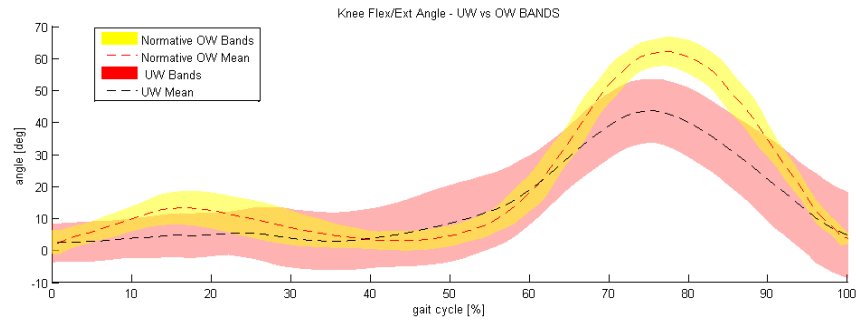

Figure 2: Normative OW vs UW bands for the knee joint flexion-extension angle.

RMSD mean value between knee planar angles evaluated with MAN and markerless techniques is estimated and found equal to 8.1°.
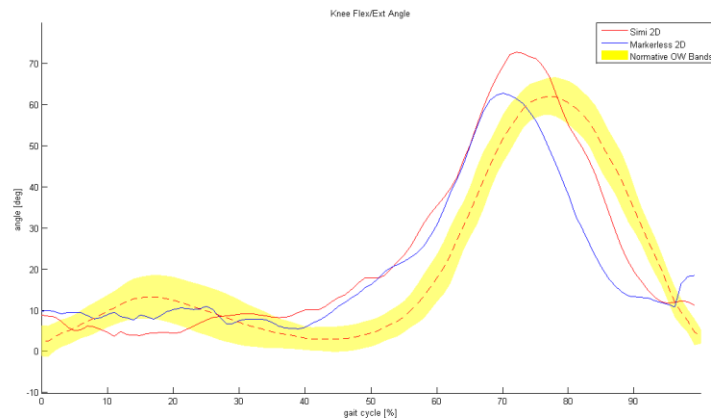An example of the knee flexion-extension angle patterns evaluated with both techniques is shown in Fig.3.

Figure 3: Knee flex/ext angles: comparison between planar angle evaluated with MAN and markerless technique.

4. DISCUSSION

Results show the feasibility of the present approach with respect to the sagittal plane and are in agreement with what reported in Barela et al. [2]. Even though 3D joint angles were estimated for hip, knee and ankle joints, results concerning knee abduction-adduction and internal-external rotation were not considered reliable. This finds agreement with the state of the art of marker based motion analysis [9] apart when multiple calibration technique is applied [10], and should not be considered a limitation of this specific approach. Unfortunately

also in the case of hip and ankle joints the estimated abduction-adduction and internal-external rotation angles were not find reliable due to the presence of reflexes in the water which altered the visual hull reconstruction. Nevertheless, an important limitation of the study is that the comparison with state of the art techniques for UW gait analysis was possible only by computing 2D angles. Even though markerless technique has been conceived aiming at 3D analysis [3], in this context, planar angles evaluation is required for the comparison with SIMI software. Differences between the two methodologies, however are due to the fact that SIMI planar angles estimation relies on anatomical landmarks (AL) identification on each video sequence by manual digitization, meanwhile the markerless approach is based on automatic reconstruction of joint center positions. The comparison between 3 dimensional joint angles estimated with the 2 different techniques (MAN and markerless) necessarily would be the next step to evaluate accuracy of the proposed technique [5]. When considering joint angles estimation the reconstruction of knee joint angle comes out to be the most reliable. Common drawbacks have been found handling underwater data with a markerless approach [5]. Background subtraction step is the most sensitive to the unusual aquatic environment. The presence of water causes continuous variation of the scene and makes necessary the adoption of an adaptive background model. The main problem within underwater images is represented by reflexes, which are identified as part of the foreground object and, consequently, extracted from the background. The moving subject shadow on the pool pavement is in some cases recognized as a foreground element too. To avoid its detection, more strict parameters can be imposed, at the expense of a loss in feet details. This may affects estimation of ankle joint angular patterns. A next critical step is the matching process. Since the subjects walked with the head out of water, the reconstructed visual hulls appear without heads, while the model has been still automatically generated including all body parts [3]. This also may affect the tracking procedure. Future development will include a modification in the model kinematic chain without accounting for the head.

A significant difference comparing the obtained UW bands with the out of water ones stands in the greater standard deviations (Fig. 2). Future developments will be the extension of this study to a larger sample of subjects in order to be able to analyze also inter-subject variations. The recruitment of a larger number of subjects could be useful and relevant either to establish control subjects Underwater Bands, or to be able to assess more general differences in the strategy of walking in UW conditions. Future developments should concentrate also on enhancing the background subtraction step, as well as the matching process.

Even if additional evaluations of the system are still needed, the results demonstrate the feasibility of calculating meaningful joint kinematics from subjects walking without any markers attached to the limb. The markerless framework introduced in this work should be taken as just a starting point for developing a broader application of markerless motion capture. Each of the modules should be independently considered and improved as newer methods become available, thus making markerless tracking a feasible and practical alternative to marker based systems. A markerless approach offers the promise of expanding the applicability of human motion capture, since the implementation of this new technology will allow for simple, time-efficient, and potentially more meaningful assessments of gait in research and clinical practice.

5.   REFERENCES

[1] R.A. Harrison, M. Hilman, and S. Bulstrode. Loading of the lower limb when walking partially immersed: Implications for clinical practice. Physioteraphy., 78:164, 1992.

[2] A.M. Barela, S.F. Stolf, and M. Duarte. Biomechanical characteristics of aldults walking in shallow water and on land. J ElectromyogrKinesiol., 16(3):250-6, Jun 2006

[3] S. Corazza, L. Mundermann, A.M. Chaudhari, C. Cobelli, and T.P. Andriacchi. A markerless motion capture system to study musculoskeletal biomechanics: Visual hull and simulated annealing approach. Annals of Biomedical Engineering, 34(6):1019-1029, 2006.

[4] L. Mundermann, S. Corazza, and T.P. Andriacchi. The evolution methods for the capture of human movement leading to markerless motion capture for biomechanical application. Journal of Neuroengineering and Rehabilitation, 3, 2006.

[5] Ceseracciu et al. Markerless analysis of front crawl swimming. J. of Biomechanics, 2011.

[6] Sawacha et al. Clinical Biomechanics, 24(9):722-728, 2009.

[7] Z. Zhang and O.M. Way. Flexible camera calibration by viewing a plane from unknown orientations. Proceedings of the Seventh IEEE International Conference on Computer Vision, 1:666-673, 1999.

[8] J.M. Lavest and G. Rives. Dry camera calibration for underwater applications. Machine Vision and Applications, 13:245-253, Mar. 2003.

[9] Della Croce, U., Leardini, A., Chiari, L., Cappozzo, A. Human movement analysis using stereophotogrammetry: Part 4: assessment of anatomical landmark misplacement and its effects on joint kinematics. Gait Posture 21 (2), 226–237, 2005.

[10] Cappello et al. Multiple anatomical landmark calibration for optimal bone pose estimation. Human Movement Science, Volume 16, Issues 2–3, April 1997, Pages 259–27, 3-D Analysis of Human Movement – II

In-vivo vs. in-vitro kinematics of the proximal interphalangeal joint in the finger
(A pilot study performed at UMDNJ)

Caravaggi P., Chen L., Uko L., Shamian B., Capo J.

[1] Dept. of orthopedics, University of Medicine and Dentistry of New Jersey, Newark, US

Kinematics; Proximal Interphalangeal Joint; ROM; In-vivo; In-vitro

1. INTRODUCTION

Human dexterity, which is in fact a trait of all primates, is based on the grasping capabilities and fine control provided by the joints in the hand. Intrinsic and extrinsic muscles coordinate the movement of the fingers allowing firm grip or precise handling of objects according to the task to be achieved [1-2]. While the thumb is articulated to a highly movable metacarpal bone that allows opposition movement, the other digits show mobility mainly in the sagittal plane, with some degree of adduction/abduction at the metacarpophalangeal joint. It is commonly assumed that the joints in the finger, i.e. the proximal interphalangeal (PIP) and the distal interphalangeal joints, work as simple hinge joints that allow flexion/extension of the phalanges. Only a few in-vitro studies have attempted to estimate the triplanar rotations occurring at the interphalangeal (IP) joints [3-4] and most of our current understanding of finger kinematics is based on in-vivo measurement of the sagittal-plane rotations using skin markers [5-7].

The kinematics and dynamics of the PIP joint are particularly critical as the distal phalanges provide long levers that can result in large bending moments being applied on relatively small joint surface areas. The latter, together with two collateral ligaments and the volar plate, help maintain stability at the joint which shows the largest range of motion in the hand [8]. Its morphology, which resembles the bicondylar knee joint, suggests that a more complex pattern of rotation may occur between proximal and middle phalanx during the full range of motion [9].

The aim of this study was to provide a more detailed description of the kinematics in the PIP joint during free flexion/extension movement of the fingers. Stereophotogrammetry was employed to estimate PIP joint rotations and translations: 1) in-vitro, using intracortical pins in a cadaver model and, 2) in–vivo, by employing clusters of active sensors to track the motion of the proximal and middle phalanx of the second (index finger), third (middle finger) and fourth digit (ring finger) in 10 subjects.

2. MATERIALS AND METHODS

In-vivo experiment
Ten male subjects (age 27±5 yrs; height 1.8±0.1 m; weight 83±16 kg) volunteered and their informed consent was obtained for the study performed in accordance with the ethical policies for research of the University of Medicine and Dentistry of New Jersey.

The centro-dorsal portion of each proximal and middle phalanx of the tested finger was instrumented with a cluster of four infrared light-emitting diodes, which was attached to the skin using a 19 mm round double-adhesive tape (Fig. 1, left). An Optotrak motion capture system (Optotrak Certus, Northern Digital Inc, Waterloo, Ontario, Canada) was used to track the sensors while the subject performed a full flexion/extension movement of the PIP joint of the instrumented finger. Five trials were performed for the second, third and fourth digit of the left and right hand of each subject, for a total of 50 samples recorded for each digit.

In-vitro experiment
Six fresh-frozen hands (2 left, 4 right) from six cadavers (77±15 yrs) were defrosted, and ten digits (5 second, 5 fourth) from these hands were used in the study. X-ray imaging was obtained to exclude those specimens showing severe arthritic joints.

For each tested digit, in order to allow for load application, the proximal end of the tendons of the two main flexor muscles (i.e. the flexor digitorum sublimis and the flexor digitorum profundus) were each sutured and attached to a metal wire. Similarly, metal wires were sutured to the tendon of the extensor digitorum communis, and to the tendon of the indicis proprius when testing the second digit.
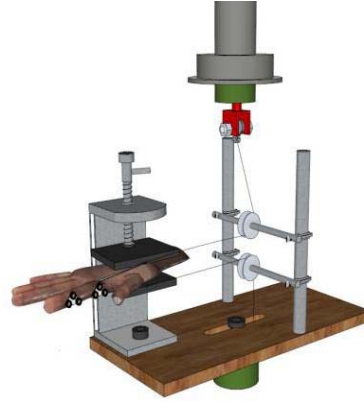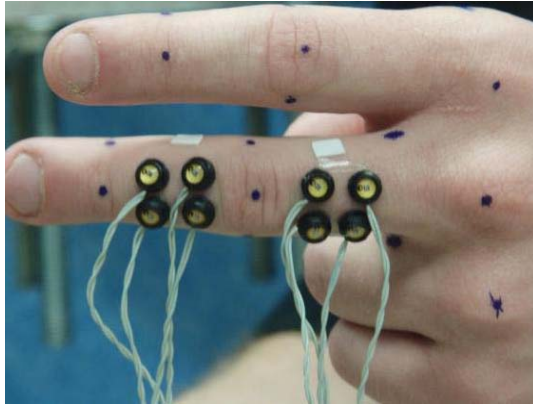
Figure 1. Left: the two four-sensor clusters attached to the proximal and middle phalanx of the middle finger of one of the subjects who participated in the in-vivo study. The black marks are the locations of the digitized points that were used to establish the local reference frames. Right: a 3-D rendering of the setup employed in the in-vitro experiment. Motion at the PIP joint was simulated by pulling the tendons of the extrinsic flexor and extensor muscles. Intracortical pins allowed for rigid fixation of the motion sensors to the proximal and middle phalanx of the tested finger.

Each hand was firmly clamped on a custom jig and the actuator of a MTS servohydraulic testing machine (MTS 851, MTS Corporation, Minneapolis, MN) was employed to apply tension to the extensor tendon(s) in order to simulate extension at the PIP joint (Fig. 1, right). The actuator of the MTS was set to move in displacement control at 0.5 mm/s until maximum extension of the PIP joint was achieved. A load cell in line with the actuator was set to stop, hold for three seconds, and invert the motion of the actuator when the tension in the wire reached the desired threshold. The latter was determined for each specimen before testing and ranged between 15 N to 30 N. Full flexion was achieved by gradual release of the tension in the extensor tendons and by gravity pull of two 5 N passive weights attached to the wires of the flexor tendons.

A rigid plate, fitted with three infra-red sensors, was bone-pinned onto the centro-lateral side of the shaft of each proximal and middle phalanx of the tested digit. The Optotrak motion capture system recorded the motion of the sensors during a full extension/flexion cycle of the PIP joint.

Kinematic protocol

A similar kinematic protocol was employed for the in-vivo and in-vitro experiment. The Optotrak digitizing probe was employed to associate the location of three anatomical landmarks, on the proximal and on the middle phalanx, to the relative cluster of sensors. The digitized points helped to establish local reference frames on the two phalanges, following recommendations by Wu et al. [10]. Rotations and translations at the PIP joint were calculated according to the joint coordinate system [11]. Neutral position of the PIP joint (0º of rotations; 0 mm of translations) was defined to be that of maximum extension of the finger.

3. RESULTS

In-vivo experiment

In all digits, the profiles of the triplanar rotations and translations at the PIP joint showed good consistency inter-subject, and inter-side within the same subject. Exemplary temporal profiles of the triplanar rotations at the PIP joint of the second digit in the left hand are shown in Fig. 2. Across all subjects, and for each anatomical plane, there was no statistical difference in the rotation ROM between left and right side and inter-digit on the same side ($p > 0.05$). The mean ($\pm$SD) rotation ROMs of the PIP joint in the index finger across all subjects (50 samples) were: 106º$\pm$8º; 10º$\pm$7º, and 11º$\pm$5º in the sagittal, frontal and transverse planes, respectively. In general large flexion angles (greater than 60º) were associated with volar displacement (Fig. 3, left) and distraction at the PIP joint.

In-vitro experiment

Flexion/extension at the PIP joint was associated with some degrees of rotation in the other two anatomical planes across all specimens. The interspecimen mean ($\pm$SD) rotation ROMs were: 84º$\pm$18º; 5º$\pm$2º, and 7º$\pm$4º in the sagittal, frontal and transverse planes, respectively. A trend for ulnar deviation and radial rotation (pronation) in the five second-digit specimens, and for radial deviation and ulnar rotation (supination) in the five fourth-digit specimens, was observed. The mean ($\pm$SD) of the translation ROMs in the three anatomical planes were: 0.4$\pm$0.2 mm (radial/ulnar), 1.7$\pm$0.9 mm (dorsal/volar), and 1.2$\pm$0.6 mm (compression/distraction). All but one specimen showed volar displacement (Fig. 3, right) and compression with flexion of the PIP joint.
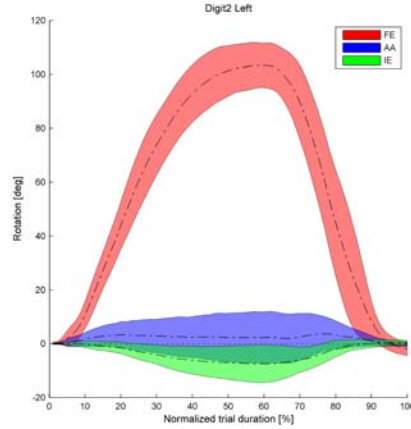
Figure 2. Intersubject mean (±SD) of the triplanar rotations at the PIP joint measured in-vivo during a full flexion/extension of the index finger in the left hand. The mean rotation angles were determined across 5 flexion/extension trials for each of the 10 subjects, for a total of 50 samples. Positive rotation angles are flexion (FE), ulnar deviation (AA) and radial rotation (IE).

4. DISCUSSION

Understanding the normal ROM of the joints in the human body is critical in the clinical evaluation of joint pathologies/abnormalities and in designing better implants for arthroplasty. While several in-vivo studies have reported ROM and correlation between sagittal plane rotations of the joints in the finger during flexion/extension [12], only few in-vitro investigations have tried to describe the IP motion in the three anatomical planes [4]. Herein we have presented a pilot study, based on in-vitro and in-vivo measurements of joint kinematics, which helped to reach a better insight in the extent of rotations and translations of the middle phalanx relative to the proximal phalanx in the finger during free flexion/extension.

Although the smaller interspecimen range of motion achieved in the in-vitro study did not allow for quantitative comparison with the motion recorded in-vivo, the kinematics from two experiments revealed some common trends. Good agreement was found between translations at the PIP joint measured in-vivo and in-vitro, however attention should be paid in the clinical interpretation of the data. In fact, the amount of measured displacement is affected by the distance of the chosen origins - of each local reference frame - to the axis of rotation [10]. The fourth digit showed some degrees of ulnar rotation whereas the second digit showed radial rotation – however, in-vivo this was most evident for the right second digit. Moreover, in the cadaver experiment, all second digits showed ulnar deviation whereas all fourth digits showed radial deviation – i.e. both digits points towards the middle finger during flexion. In-vivo, a similar trend was detected mainly in the fourth digit. The morphology of the joint surfaces could account for some of the digit-specific kinematic patterns that have been inferred in this study [9].
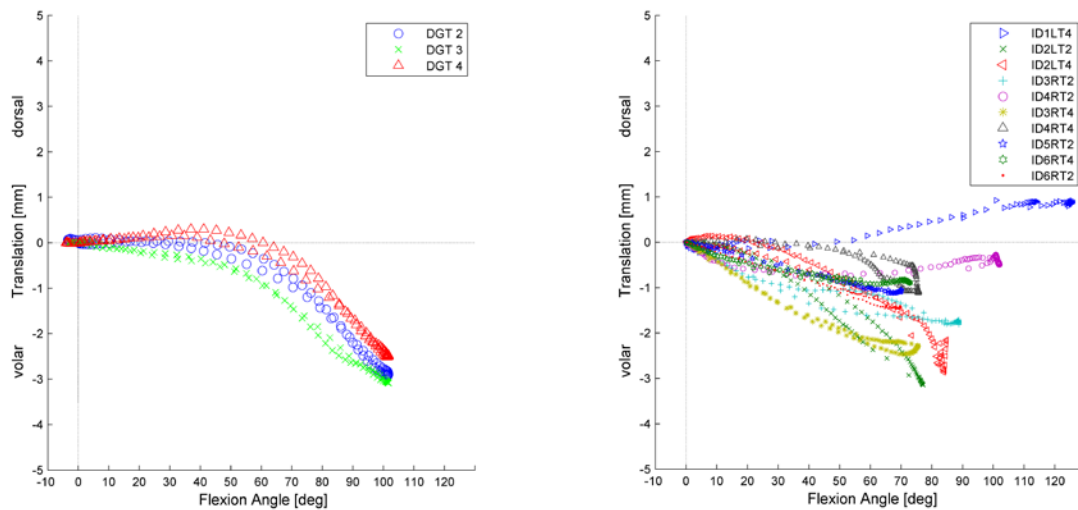

Figure 3. Left: in-vivo intersubject mean of the dorsal/volar translation at the PIP joint during flexion/extension of the middle phalanx of the second (DGT2), third (DGT3) and fourth digit (DGT4) in the right hand. The mean curves have been determined over 50 flexion/extension trials – 5 trials for each digit in 10 subjects. Right: in-vitro mean dorsal/volar translation at the PIP joint during flexion/extension of the middle phalanx for each of the 10 specimens. The mean curves have been determined over 5 flexion/extension trials recorded for each specimen.

Both experiments had some limitations. The in-vitro protocol was designed to ensure that the maximum ROM at the PIP joint could be achieved for each specimen. Variability was detected in the tension required to produce maximum flexion/extension across the specimens, however the maximum force employed was found to be consistent with in-vivo data on tension in the extrinsic muscles during free flexion/extension [13-14]. Furthermore the setup did not allow simulation of the forces exerted by the intrinsic muscles. While EMG studies have shown that these muscles seem to be inactive during free flexion of the finger [1-2], their contribution to IP joint during extension has been reported [2, 15]. In the in-vivo experiment, a double-adhesive round tape was employed to group the sensors. Clusters of markers have been previously used to measure bone segment kinematics, however they are normally fitted on rigid plates. A flexible media was preferred because of the small space available and to limit the impediment caused to the fingers during full flexion. Further investigations should be performed to assess the bias from soft tissue artifacts when employing clusters of skin markers to measure the motion of the phalanges.

It seems plausible that the limitations mentioned above, together with physiologic intersubject variability, prevented the identification of a clear pattern for rotation especially in the frontal plane. Nevertheless, within each subject and for each digit, a good inter-side consistency in the profile and ROM of the rotations was detected. This seems to support the validity of the proposed in-vivo protocol and its potential in measuring subject-specific kinematics in the joints of the fingers.

5. REFERENCES

[1] Long, C., 2nd, Conrad, P. W., Hall, E. A., and Furler, S. L., 1970, "Intrinsic-extrinsic muscle control of the hand in power grip and precision handling. An electromyographic study," J Bone Joint Surg Am, 52(5), pp. 853-867.

[2] Long, C., 2nd, 1968, "Intrinsic-extrinsic muscle control of the fingers. Electromyographic studies," J Bone Joint Surg Am, 50(5), pp. 973-984.

[3] Uchiyama, S., Cooney, W. P., 3rd, Linscheid, R. L., Niebur, G., and An, K. N., 2000, "Kinematics of the proximal interphalangeal joint of the finger after surface replacement," J Hand Surg Am, 25(2), pp. 305-312.

[4] Minamikawa, Y., Horii, E., Amadio, P. C., Cooney, W. P., Linscheid, R. L., and An, K. N., 1993, "Stability and constraint of the proximal interphalangeal joint," The Journal of Hand Surgery, 18(2), pp. 198-204.

[5] Metcalf, C. D., Notley, S. V., Chappell, P. H., Burridge, J. H., and Yule, V. T., 2008, "Validation and Application of a Computational Model for Wrist and Hand Movements Using Surface Markers," Biomedical Engineering, IEEE transactions, 55(3), pp. 1199 - 1210.

[6] Zhang, X., Lee, S. W., and Braido, P., 2003, "Determining finger segmental centers of rotation in flexion-extension based on surface marker measurement," J Biomech, 36(8), pp. 1097-1102.

[7] Chiu, H.-Y., Lin, S.-C., Su, F. C., Wang, S.-T., and Hsu, H.-Y., 2000, "The Use of the Motion Analysis System for Evaluation of Loss of Movement in the Finger," Journal of Hand Surgery (British and European Volume), 25(2), pp. 195-199.

[8] Chiu, H. Y., Su, F. C., Wang, S. T., and Hsu, H. Y., 1998, "The motion analysis system and goniometry of the finger joints," J Hand Surg Br, 23(6), pp. 788-791.

[9] Dumont, C., Albus, G., Kubein-Meesenburg, D., Fanghanel, J., Sturmer, K. M., and Nagerl, H., 2008, "Morphology of the interphalangeal joint surface and its functional relevance," J Hand Surg Am, 33(1), pp. 9-18.

[10] Wu, G., van der Helm, F. C., Veeger, H. E., Makhsous, M., Van Roy, P., Anglin, C., Nagels, J., Karduna, A. R., McQuade, K., Wang, X., Werner, F. W., and Buchholz, B., 2005, "ISB recommendation on definitions of joint coordinate systems of various joints for the reporting of human joint motion--Part II: shoulder, elbow, wrist and hand," J Biomech, 38(5), pp. 981-992.

[11] Grood, E. S., and Suntay, W. J., 1983, "A joint coordinate system for the clinical description of three-dimensional motions: application to the knee," J Biomech Eng, 105(2), pp. 136-144.

[12] Hahn, P., Krimmer, H., Hradetzky, A., and Lanz, U., 1995, "Quantitative analysis of the linkage between the interphalangeal joints of the index finger: An in vivo study," The Journal of Hand Surgery: Journal of the British Society for Surgery of the Hand, 20(5), pp. 696-699.

[13] Nikanjam, M., Kursa, K., Lehman, S., Lattanza, L., Diao, E., and Rempel, D., 2007, "Finger flexor motor control patterns during active flexion: An in vivo tendon force study," Human Movement Science, 26(1), pp. 1-10.

[14] Kursa, K., Lattanza, L., Diao, E., and Rempel, D., 2006, "In vivo flexor tendon forces increase with finger and wrist flexion during active finger flexion and extension," Journal of Orthopaedic Research, 24(4), pp. 763-769.

[15] Srinivasan, H., 1977, "Movement patterns of intrinsic minus fingers. Role of intrinsic and extrinsic muscles in finger posture control," Ann R Coll Surg Engl, 59(1), pp. 33-38.

Do people follow the principle of end-state comfort in a rotation task?

Lardy J. [1], Beurier G. [1], Wang X. [1*]

[1] Université de Lyon, F-69622, Lyon, France;
IFSTTAR, UMR_T9406, LBMC, Bron;
Université Lyon 1, Villeurbanne, France
* Corresponding author's email: xuguang.wang@ifsttar.fr

Arm rotation; end-state comfort; joint limits; motion simulation

1. INTRODUCTION

Simulation of arm movement when manipulating an object requires defining a starting posture, a final one and a transition strategy. However, there is no unique solution due to kinematic redundancy of human body. In case of a 7-DOF arm model (3 for the shoulder, 2 for the elbow and 2 for the wrist), the arm pivoting angle along the shoulder-wrist axis is undetermined for a given hand position and orientation [1]. For an object rotation task, several studies [2, 3, 4] observed that different starting postures were adopted depending rotation amplitude. One of the explanations was that people follow the principle of end-state comfort initially proposed by Rosenbaum [5]. This hypothesis states that the movement is selected to ensure a comfortable final posture. In case of an arm rotational task described by van der Vaart [2], this hypothesis implies that one would prefer to adopt an arm posture further away from joint limits at the end of a motion than at the beginning whenever possible. Another implication would be that one prefers an elbow position close to the body due to gravitation at the end.

Therefore, the purpose of this paper is to investigate whether the principle of end-state comfort applies to arm movements when rotating an object . For this, data from a previous study [6], representing arm movements for rotating a sphere with a large range of rotation amplitude, is to be used.

2. MATERIAL AND METHODS

Experimental data

Twelve right-handed subjects (age = 27.8 ± 5.3 years; size = 170.1 ± 9.4 cm) participated in the experiment. From an initial posture (see Figure 1), they were asked to reach, grasp and rotate a sphere without changing their grip. The object was located in front of their right shoulder, at a distance of about 3/5 of their arm length and its axis of rotation was orthogonal to the frontal plane of the subject. Amplitudes of rotation were ranged from -360° (counter clockwise: CCW) to +360° (clockwise: CW), by increments of 45°, and presented in a randomized way. A Vicon system was used to measure the 3D trajectories of a set of 28 markers located on the torso, upper limb, hand and object.
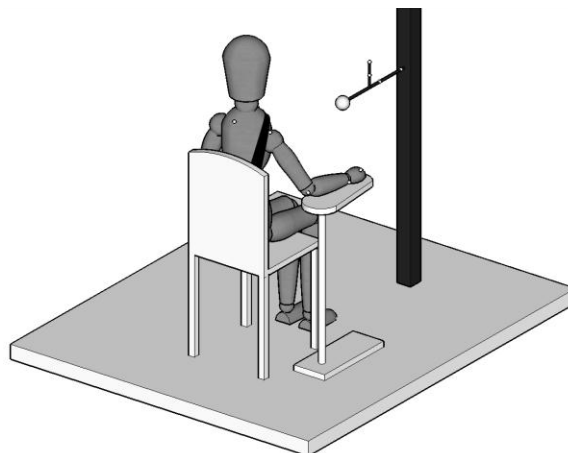

Figure 1. Experimental set-up showing the subject in the rest position. The main markers in white are also illustrated. A belt was used to limit the torso movement when manipulating the object. A very light resistance for each increment of 45° was used to indicate rotation amplitude
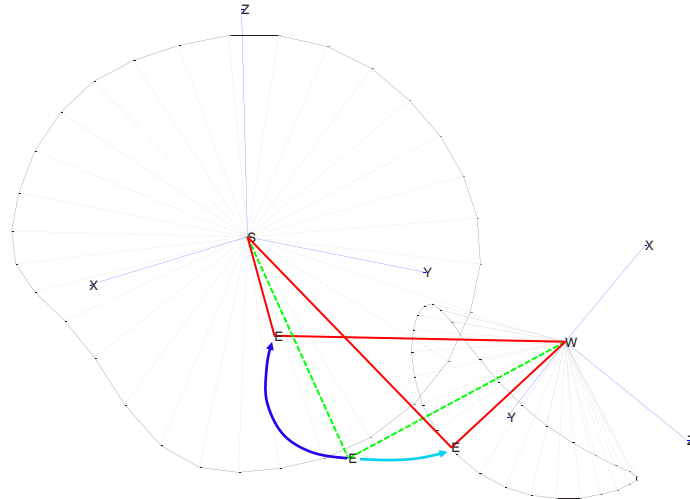
Figure 2. Example of two extreme arm postures (in red) allowed by joint limits for a given arm posture (in green) obtained experimentally. Joint limits are defined in [8]. The global torso-fixed coordinate system is centered at the shoulder S, with X, Y and Z being defined, respectively, aligned to the medial-lateral (M-L), posterior-anterior (P-A) and inferior-superior (I-S) anatomical directions.

Method for determining two extreme arm postures allowed by joint limits for a given hand attitude

In an earlier work by Wang [1], a geometric inverse kinematics algorithm for a 7-DOF arm model was proposed taking into account nonlinear joint limits, especial those of the shoulder [7]. For a given hand attitude including its position and orientation, two extreme arm postures allowed by joint limits can be estimated (see Figure 2 for an example).

Data processing

The shoulder, elbow and wrist angles were calculated using a simplified 7-DOF arm model thanks to recorded markers positions. The beginning and the end of the manipulation phase were determined according to the angular velocity of the objet (5% of the peak). Then postures at two instants were used as inputs for determining the two extreme arm postures allowed by joint limits. Due to loss of markers in some trials (either at the beginning or the end of manipulation), we were able to simulate here a total of 130 motions at the beginning, and 149 motions at the end of the manipulation.

Analyzed variables

Only shoulder pivoting angle remains undetermined for an imposed hand position and orientation. From a known arm posture, two extreme postures allowed by joint limits were simulated at the beginning and at the end of manipulation. Two shoulder pivoting margins are defined: a positive margin "M+" between the original position of the elbow and its maximal position when rotating along the shoulder-wrist axis, a negative margin "M-" when rotating negatively along the shoulder-wrist axis. The total margin "M" is the sum of "M+" and "M-".

3.   RESULTS

Figure 3 shows the total margin of the shoulder pivoting at the beginning and at the end of the object rotation. As expected, the margin decreased with the increase of rotation amplitude in both directions. Statistical analysis shows significant differences in the total margin M between the beginning and end of object rotation for the rotation amplitudes from -225° to 90° (with an exception for -45°).

Figure 4 represents the negative margin ("M-" in dark blue) and the positive margin ("M+" in light blue) at the beginning of the rotation. No significant difference was observed between "M+" and "M-" for CCW rotations (from -315° to -45°), implying that the subjects were in the middle of the available range of motion when grasping the object. For CW rotations, negative margin "M-" seemed to be higher than M+ especially for small amplitudes (45° and 90°). It means that lower elbow position was preferred with respect to what is allowed by joint limits.

Figure 5 shows the negative and positive margins ("M+" and "M-") at the end of the rotation. Higher values of negative margin "M-" were observed especially for the tasks from -135° to +90°, meaning that subjects preferred a low elbow position.
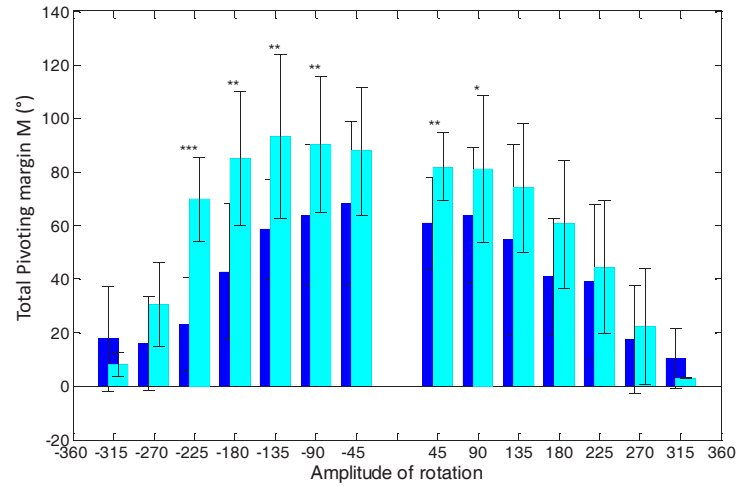
Figure 3. Comparison of the total pivoting margins at the beginning (dark blue) and end (light blue) of rotation.. For each amplitude, significant difference between initial and final "M" is shown: *p<0.05; **p<0.01; ***p<0.001.
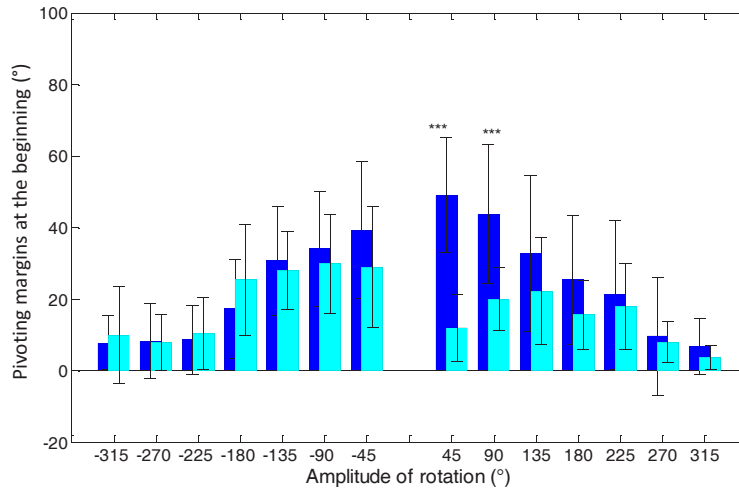

Figure 4. Negative ("M-": dark blue) and positive ("M+": light blue) margins for shoulder pivoting angle at the beginning of object rotation. For each amplitude, significant difference between "M+" and "M-" is shown: *p<0.05; **p<0.01; ***p<0.001.

4. DISCUSSION

In this paper, the end-state comfort hypothesis was investigated with arm movements when rotating an object with high amplitudes. Our results tend to confirm this idea. Indeed, we observed a higher margin of shoulder pivoting at the end of rotation than at the beginning. When looking at the negative and positive pivoting margins, higher negative margins were generally observed at the beginning of rotation for CW tasks and at the end of rotation for CCW tasks. This means that subjects preferred keeping a low elbow position at the beginning when rotating in CW direction and at the end when rotating in CCW direction. Clearly, keeping an elbow position close to the body applied to both the beginning and end of rotation. This observation seems to suggest that movements are not only controlled so as to achieve an end-state comfort, but the comfort of beginning state is also considered. In addition, keeping a low elbow position also reduces shoulder pivoting. This goes with the principle of minimum work [9].

In conclusion, our results confirm the end-state comfort hypothesis. But the end-state comfort hypothesis alone could not explain all observations. Starting state comfort and principle of minimum work should also be considered. These observations will allow us to definea simulation algorithm that could give natural-looking motions.
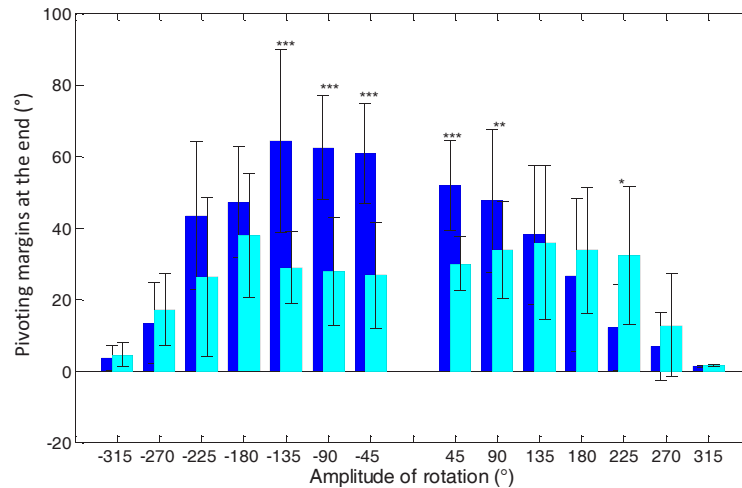
Figure 5. Final negative margin ("M-": dark blue) and positive margin ("M+": light blue) for pivoting angle. Values are absolute ones and represent the amplitude of movement available in both directions when grasping the object before the rotation. For each amplitude, significant difference between "M+" and "M-" is shown: *p<0.05; **p<0.01; ***p<0.001.

5. REFERENCES

[1] Wang, X., 1999. Three-dimensional kinematic analysis of influence of hand orientation and joint limits on the control of arm postures and movements. Biol. Cybern. 80, 449-463.

[2] Van der Vaart, A.J.M., 1995. Arm movement in operating rotary controls. Delft University of Technology.

[3] Robert, T., Beurier, G. and Wang, X., 2009. Arm postural anticipation for rotating a spherical object. Comput. Methods Biomech. Biomed. Engin 12(S1), 217-218.

[4] Herbort, O. and Butz, M.V., 2010. Planning and control of hand orientation in grasping movement. Exp. Brain Res. 202, 867-878.

[5] Rosenbaum, D.A.., Marchak, F., Barnes, H.J., Vaughan, J., Slotta, J.D. and Jorgensen, M.J., 1990. Constraints for action selection: Overhand versus underhand grips. Attention and Performance XIII, 321-342.

[6] Lardy, J., Wang, X., Beurier, G. and Robert, T., 2010. Arm movement coordination when rotating a spherical object. Comput. Methods Biomech. Biomed. Engin 13(S1), 83-85.

[7] Wang, X., Maurin, M., Mazet, F., De Castro Maia, N., Voinot, K., Verriest, J.-P. and Fayet, M., 1998. Three-dimensional modelling of the motion range of axial rotation of the upper arm. J. Biomech. 31, 899-908.

[8] Wang, X., 1996. Construction of arm kinematic linkage from external surface markers. 4th International Symposium on 3D Analysis of Human Movement.

[9] Soechting, J., Buneo, C., Herrmann, U. and Flanders, M., 1995. Moving effortlessly in three dimensions: Does Donder's law apply to arm movement? J. Neurosci. 15, 6271-6280.

Biomechanical Analysis of Self-selected Upper Limb Posture for Grasping and Holding

Zhou W. [1], Armstrong T. [1], Wegner D. [2], Reed M. [1]

[1] University of Michigan, Ann Arbor, MI, USA
[2] General Motors, Warren, MI, USA

Key words: Biomechanics; Work; Design

1. INTRODUCTION

This work aims to collect new information for quantitative modeling of the posture and movement behavior used to grasp, hold and place work objects. This information is needed for designing work equipment and methods that provide workers with sufficient control over objects in object transfer tasks. Previous studies show that postures are affected by comfort or effort [1-3]. It can be shown that perceived effort is related to biomechanical factors, such as external joint load moments [4-5]. Computation of moment requires knowledge of the spatial relationship between the location of load with respect to the joints. 3D motion tracking is ideal for tracking the object and joint locations and can be used to compute joint moments for developing models. This paper describes the use of 3D motion tracking to collect data and develop models for predicting upper limb posture probabilities for given loads.

2. METHODS

We used 3D motion tracking to determine the spatial relationship between the major joints of the upper limb and a work object as 10 healthy female college age subjects reached for, grasped, held and finally placed a work object at an arbitrary location on the work surface from which they started. Moment arms and quasi-static load moments were estimated for the wrist, elbow and shoulder for the grasp and hold postures and used to compute relative load moments based on corresponding subject strengths for each posture. Models were then proposed that described the probability of a given posture for given relative load moments. All subjects gave written informed consent in accordance with our University IRB regulations. The hand lengths ranged from 1st percentile to 72th percentile based on the population data from Garrett [6]. The dependent variable was upper limb posture. The independent variable was object weight. Cylindrical objects were 25.5 cm in length and 7 cm in diameter with four different weights (0.3, 2.0, 3.7, and 5.4 kg). The object was supported on each end at elbow height with adequate horizontal and vertical finger clearance. The object height was adjusted to elbow height for each subject. Subjects stood one horizontal forearm length from the grip object with long axis of the object perpendicular to the sagittal plane of the body. Starting with their hand at the side of their body, subjects reach for, grasped and held the object for approximately 8s as though they were carrying it until they were told to put it down at a self-selected, arbitrary location and orientation. Trials were blocked on object weight, with the weight order randomly selected for each subject. Three trials were performed for each condition following several practice trials to familiarize the subjects with each condition. There were at least two minute breaks between trials, except for the lightest object.

An eight-camera Qualisys motion tracking system (Qualisys Inc., Sweden) was used to record the upper body kinematics. Retro-reflective markers were attached to the dorsal side of middle metacarpophalangeal (MCP) joint of the right hand, the radial and ulnar sides of the wrist, lateral and medial epicondyles, and the acromion of the right arm. The position of the cylindrical object (handle) was tracked using two markers placed on the centers of the two ends of the object. The Qualisys system was sampled at 60 Hz. All trials were also videotaped using a camcorder.

The motion data were filtered using a bidirectional second order Butterworth filter with a cut-off frequency of 6 Hz. The frames for grasping, holding, and placing were estimated manually based on the video analysis and then refined by searching the nearest 30 frames of estimated frames using a threshold of 20 cm/s of the velocity of object center displacement. The object center position was assumed to be the average of the positions of the two object markers. The wrist joint center was assumed to be the average of the positions of the lateral and medial wrist markers. The shoulder joint center was assumed to be 10% of the upper arm length inferior to the acromion marker in laboratory coordinate system [7]. The elbow joint center was assumed to be the average of the positions of lateral and medial epicondyle markers. In the case that the medial epicondyle marker data was missing, the elbow joint center was calculated by offsetting the lateral

epicondyle marker position by half the distance between the medial and lateral epicondyles in the direction of the vector that is the cross product of the vector from lateral epicondyle to shoulder joint and the vector from lateral epicondyle to wrist joint [8]. The load moment arms were calculated from the object center to joint centers in x-y plane of the laboratory coordinate system. Relative moment was computed as the joint load moment divided by respective joint strength for that posture. Functional strength tests were conducted to quantify joint strengths for given posture for each subject.

3. RESULTS

Subjects demonstrated three basic behaviors for this task (Fig. 1). In Case A (Fig. 1A), a subject grasped a 0.3 kg cylinder using an overhand grip at elbow height, held it at elbow height using a semi-pronated posture, then placed it back onto the wood stand using an overhand posture. In Case B (Fig. 1B), a subject grasped a 2.0 kg cylinder using an overhand grip, moved the object to thigh height and held it using a hook grip, then placed it back onto the wood stand using an overhand posture. In Case C (Fig. 1C), a subject grasped a 3.7 kg cylinder using an underhand grip, moved the object to shoulder height and held it using a palm grip, then placed it back onto the wood stand using an underhand posture.

The frequencies of observed postures as a function of object weight are shown in Fig. 2. During grasping, subjects used either an overhand or an underhand posture. During holding, as weight increases, the frequencies of at shoulder or thigh height posture increase, while the ones for at elbow height postures (semi-pronated grip or underhand grip) decrease. Likelihood ratio test for holding posture by object weight was significant with $p<0.001$.

Table 1 shows the moment arms from the load to the wrist, elbow, and shoulder for grasping and for holding the object at elbow height, at shoulder height and thigh height. The shoulder height and thigh height are similar and pooled. When holding at elbow height, subjects extended their shoulder, which reduced the moment arm for the shoulder about 25%, but did not affect the moment arms of the elbow and wrist. When holding at shoulder or thigh height, the wrist, elbow, and shoulder moment arms were reduced 62%, 72%, and 70% respectively.

Predicted probability from logistic regression of selecting holding posture at elbow height, or at shoulder or thigh height is shown in Fig. 3 as function of the relative moment (%strength) of wrist, elbow, or shoulder at the time the weight of the object is transferred to the hand. For low load, about 20% of the subjects maintained the same arm posture in which they first gained control of the object, while 80% selected an at thigh or shoulder height posture. As the relative load moment on the wrist, elbow, and shoulder increased to 30% of maximum, approximately 90% assumed at shoulder or thigh height posture and as the load increased to 90% nearly every one chose the at shoulder or thigh height posture.

4. DISCUSSION

These data show that the postures selected to grasp, hold and place work objects are influenced by the relative load moments on wrist, elbow, and shoulder at the time when the hand gains control over the work object. For this case with the horizontal forearm and elbow and shoulder aligned vertically, the load moment is quite low for the wrist and they are approximately equal for the elbow and shoulder. Subjects reduced shoulder moment by extending shoulder for holding, which may suggest shoulder is more sensitive than the elbow. Further studies can now be conducted to determine if selection of at shoulder or thigh height holding posture is more sensitive to determine the relative sensitivity of wrist, elbow, or shoulder. This study was performed on a sample of ten females. Because the load moments were normalized with respect to maximum strength, we believe that these results should apply to males as well, but this should be verified in future studies.

5. CONCLUSION

Three-dimensional motion tracking was used to show that the postures selected to hold objects with the hand are influenced by relative wrist, elbow, and shoulder load moments. It appears that the wrist, elbow, and shoulder exert approximately the same effect on hold posture. This observation can be confirmed in future studies using a an experimental protocol that produces different load moments simultaneously to the wrist, elbow, and shoulder. This study was based on a sample of females. Future studies should verify that there is not a gender effect on posture beyond that of relative joint moments. Three-dimensional motion tracking is an important tool for understandng and modeling work behavior.
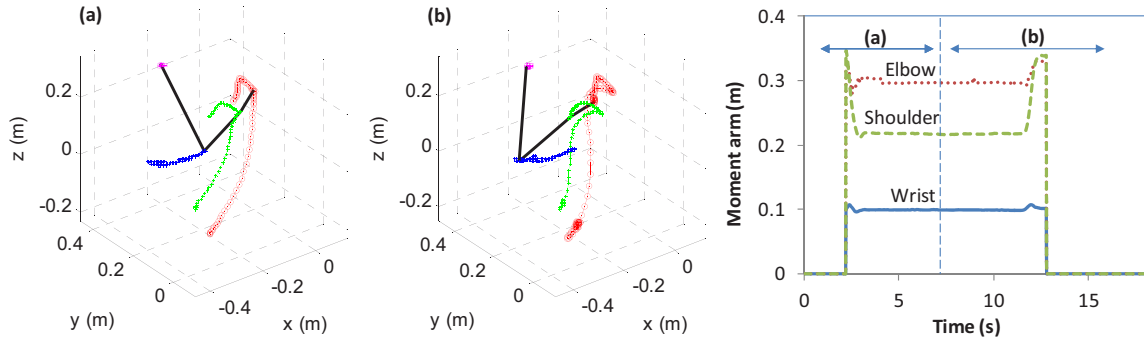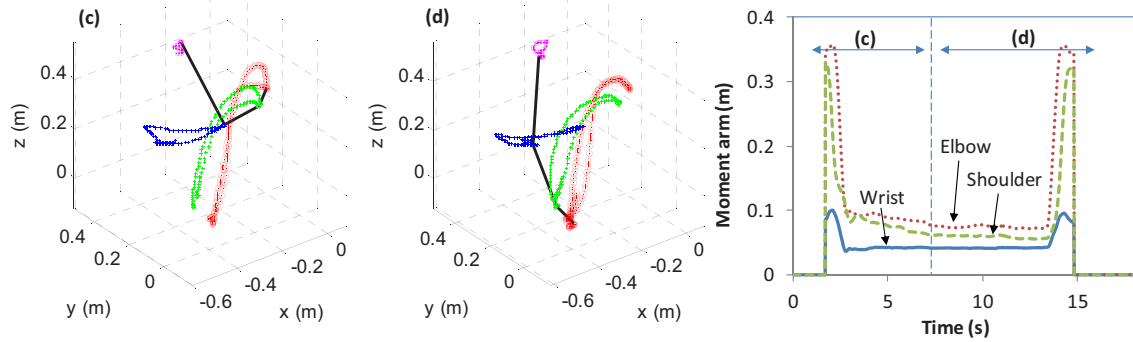
6. ACKNOWLEDGMENT

(A) Reach grasp a 0.3 kg cylinder using overhand posture, hold it using semi-pronated posture at elbow height, then place it down

(B) Reach grasp a 2.0 kg cylinder using overhand posture, hold it using hookgrip posture at thigh height, then place it down

(C) Reach grasp a 3.7 kg cylinder using underhand posture, hold it using palm grip at shoulder height, then place it down
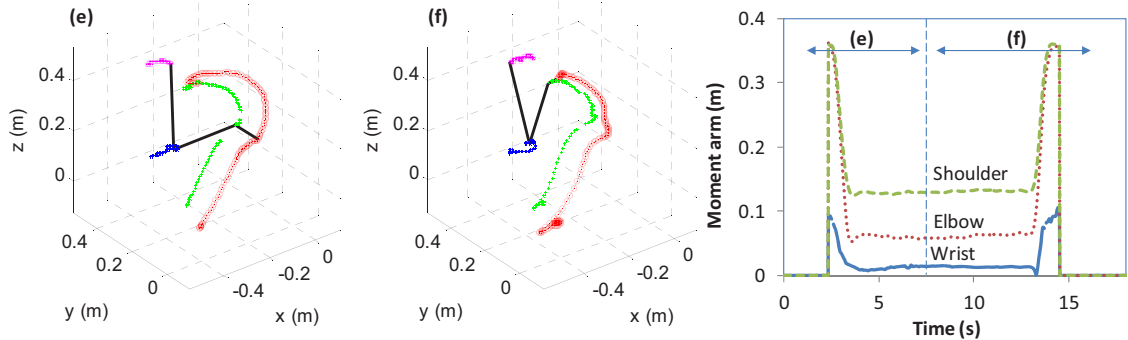
Figure 1. Trajectories of the right hand middle MCP joint marker, wrist, elbow, and shoulder joint centers in three representative trials in laboratory coordinate system. The moments of wrist, elbow, and shoulder as function of time are also shown.
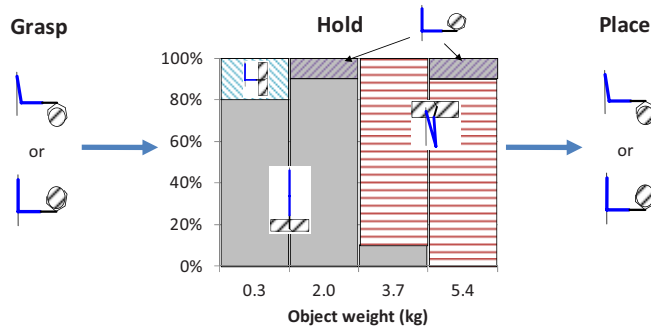
Figure 2. Frequencies of observed postures as a function of object weight (pooled for all subjects).

Table 1. Moment arms from the load to wrist, elbow, and shoulder joints for grasping and holding postures (cm, mean ± SD)

Posture	Wrist (cm)	Elbow (cm)	Shoulder (cm)
Grasp	9.7 ± 1.6	32.7 ± 2.5	30.7 ± 4.5
Hold at elbow height	9.6 ± 1.5	31.7 ± 1.7	23.1 ± 3.1
Hold at shoulder or thigh height	3.7 ± 1.7	9.2 ± 2.8	9.2 ± 2.5

Figure 3. Predicted probability from logistic regression of selecting holding posture at elbow height, or at shoulder or thigh height as function of the relative moment (%strength) of wrist, elbow, or shoulder at the time the weight of the object is transferred to the hand.

7. REFERENCES

[1] Zhou, W., Armstrong, T., Wegner, D.M., and Reed, M.P. Influence of object weight and terminal orientation on upper limb postures during grasping, holding, and placing cylindrical object. in Proceedings of Human Factors and Ergonomics Society Annual Meeting. 2011.
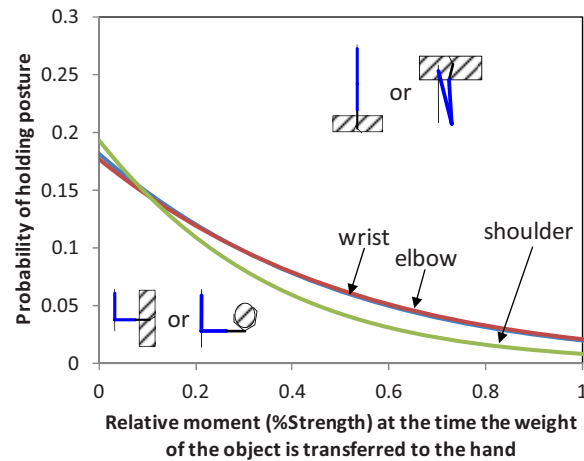
[2] Rosenbaum, D.A., van Heugten, C.M., and Caldwell, G.E., From cognition to biomechanics and back: The end-state comfort effect and the middle-is-faster effect. Acta psychologica 94(1), pp. 59-85, 1996.

[3] Rosenbaum, D.A., Marchak, F., Barnes, H.J., Vaughan, J., Slotta, J.D., and Jorgensen, M.J., Constraints for action selection: Overhand versus underhand grips, in Motor representation and control, attention and performance xiii, M. Jeannerod, Editor. 1990, Erlbaum: Hillsdale. pp. 321-342.

[4] Dickerson, C.R., Martin, B.J., and Chaffin, D.B., Predictors of perceived effort in the shoulder during load transfer tasks. Ergonomics 50(7), pp. 1004 - 1016, 2007.

[5] Carey, E. and Gallwey, T., Effects of wrist posture, pace and exertion on discomfort. International Journal of Industrial Ergonomics 29(2), pp. 85-94, 2002.

[6] Garrett, J.W., The adult human hand: Some anthropometric and biomechanical considerations. Human Factors 13(2), pp. 117-31, 1971.

[7] De Leva, P., Joint center longitudinal positions computed from a selected subset of chandler's data. Journal of Biomechanics 29(9), pp. 1231-1233, 1996.

[8] Reed, M.P., Manary, M.A., and Schneider, L.W., Methods for measuring and representing automobile occupant posture. SAE Transactions: Journal of Passenger Cars 108, 1999.

A 3D Model of Reach Limitations for Workstation Design

Rempel D. [1], Barr A. [1], Baum D. [2], Camilleri M. [1], Duarte R. [2], Janowitz I. [3], Woo J. [2]

[1] Department of Bioengineering, University of California, Berkeley, USA
[2] Department of Engineering, Lawrence Berkeley National Laboratory, Berkeley, USA,
[3] Department of Health and Safety, Lawrence Berkeley National Laboratory, Berkeley, USA,

The purpose of this project is to present the development plan for a reach model for workstation design that incorporates shoulder moment, shoulder posture, anthropometry, task duration, and duty cycle. Phase I of the project identifies existing software and literature with which to estimate shoulder strength and reach envelope. Phase II integrates task duration with shoulder strength to define volumes in the reach envelope in which a task can be performed continuously for 2 hours (green), performed for 2 minutes or less every 10 minutes (red), and performed for intermediate durations (yellow). Ultimately, the model will be incorporated into CAD design software, via mannequins of different anthropometry and gender, to allow workstation designers to consider human capabilities in order to reduce pain and fatigue and increase the work quality in the design process.

Keywords: shoulder, workplace, design, ergonomics, reach, fatigue

1. INTRODUCTION

Repeated or sustained reach during assembly, maintenance or production work is associated with shoulder pain and injury (e.g., pipetting, dental hygiene, etc.). The primary risk factors are shoulder moment, shoulder posture, and duration of exertion or duty cycle. Some CAD design packages (e.g. Creo Mannikin, *PTC*; 3D-Mannequin, *Ergo-Link*) include mannequins that can be manipulated for design work, but provide only simple reach envelopes defined with the arms fully extended, and do not consider biomechanical loads or muscle fatigue of the shoulder which will vary with posture and anthropometry. Most work tasks are not performed at the limits of reach (i.e. arms fully extended), but are performed well within the reach envelope. Additionally, many work activities place the employee in awkward upper body postures for extended periods of time, for example, pipetting in biosafety cabinets, glove-box work, dental hygiene, and construction (Fig. 1). Although CAD design software can be used to lay out the work area, these CAD applications do not provide assistance with proactively identifying workstation layouts that may compromise quality of work or productivity by causing shoulder fatigue or increasing the risk of shoulder pain and injury.

A current design model for evaluating the limitations of reach at work (3DSSPP, U Michigan, Ann Arbor, MI, USA) provides output on the percent of maximum voluntary contraction (MVC) and percent population capable of applying a given force at any point within the reach envelope, but the model does not account for reduction in shoulder strength with shoulder flexion or abduction and does not consider duration of activity and shoulder fatigue. The design model is also not readily integrated with CAD applications.

Figure 1. Examples of work activities that involve sustained reach: glovebox and clean room work.

The purpose of this project is to develop a CAD integratable model for identifying 3 dimensional risk/duration zones that consider shoulder moment and population strength capabilities, anthropometry, fatigue, shoulder posture and strength capabilities, and task duration.

2. METHODS

Phase I

The basic 3D reach model is based on anthropometry, posture prediction, and stress estimates from the 3DSSPP model (U Michigan, Ann Arbor, MI, USA). The model output has been compared to empirical results from the literature and areas of model refinement have been identified. With increasing flexion and abduction, from 0 (upper arm vertical) to 90 degrees (upper arm horizontal), there is a decline in shoulder strength by 20% to 30% [1, 2]. This decrement in strength will be incorporated into the model to better estimate shoulder strength at postures *within* the reach envelope and *between* the cardinal planes.

Phase II

Shoulder muscle fatigue will be incorporated into the model using data from nine psychophysical studies of repetitive hand activities recently summarized in a review article by Potvin [3]. The equation linking percent strength to duty cycle is modified from Potvin,

$$\%MVC = -0.139 \ln(DC) + 0.0783. \quad (1)$$

Where %MVC (range 0-1) is the reduction in shoulder strength due to duty cycle (DC, range: 0 to 1). Duty cycle is considered the cumulative percentage of time during a 2-hour work period that the shoulder is exerting more than five percent of strength. This decrement in strength will be incorporated into the model to define the boundaries of the reach zones.

3. RESULTS

An example of the reach zones is presented in Fig. 2. In this example, the hand is modeled statically holding a 1kg object for the 50th percentile male with 50th percentile strength. Regions within the reach envelope, in the sagittal plane through the shoulder, are identified in colors based on percent shoulder strength. The blue/green zone is that region where the mean percent strength is below 10% and corresponds to work that can be performed continuously for 2 hours. The red zone is that region where the mean strength is above 20% and corresponds to work that can be performed for 2 minutes or less every 10 minutes. The yellow/orange zone is that region where the mean strength is between 10 and 20% of strength and corresponds to work that can be performed continuously for intermediate durations.
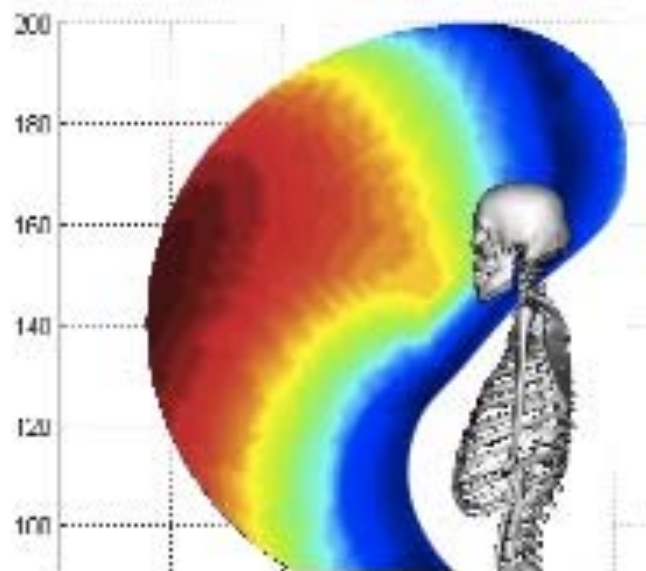
Figure 2. Risk/Duration Zones. Example of reach zones in the sagittal plane through the right shoulder of a 50th percentile male. Three zones will be identified that indicate reach areas of low (blue/green), moderate (yellow/orange), and high (red) risk for developing work-related fatigue and discomfort. Alternatively, the zones can be used to define acceptable hand locations for long durations (blue/green), moderate durations (yellow/orange), and short durations (red).

4. DISCUSSION

Work is ongoing to compute the 3 dimensional zones for both male and female populations, as a function of stature, fitness, and hand-dominance. The zones and related models, essentially point clouds of 3D data, will integrated into existing CAD software to define 3D surfaces that separate the three risk/duration zones.

The models may be used for both specific and general worksites. As an example, consider a general work station that must accommodate an extreme stature-range of users (Fig. 3). While the reach envelopes may vary considerable in area/volume, the risk/duration zones scale nearly linearly; the greater strength of tall men is offset by their greater segment masses and moment arms about the shoulder. During the design phase, CAD interventions such as adjustable console/seat height and desk depth can be included to optimize the usability across the extremes of stature.

As another example, consider a specific workstation that must accommodate both male and female users of a specific stature (Fig. 4). While the envelopes are similar in size, perhaps suggesting a similar layout between the genders, the risk/duration zones demonstrate that females should bring the hands closer to the torso. Again, during the design phase, CAD interventions such as an adjustable workstation may be considered. If workstation constraints preclude adjustability, then the workstation may be laid out to distribute the load appropriately between males and females.
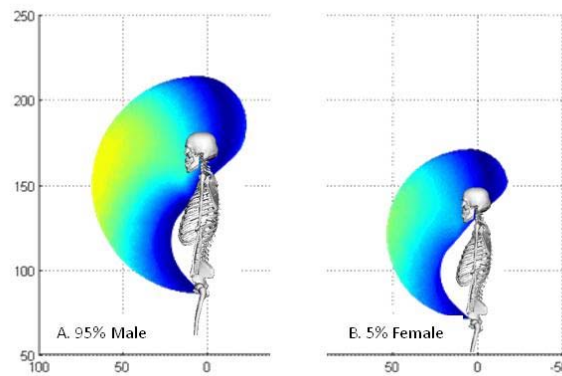
Figure 3: Reach Envelopes and Risk/Duration Zones in the Sagittal Plane for the Tall Male and Short Female. The risk/duration zones are similar but the envelopes vary considerably in size.
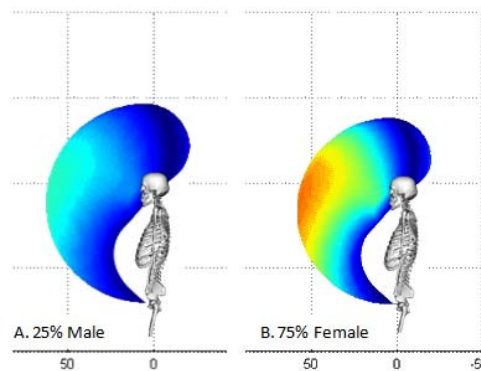
Figure 4: Reach Envelopes and Risk/Duration Zones in the Sagittal Plane for Similar Stature Males and Females. The envelopes have similar size but the risk/duration zones vary considerably.

The completed model, incorporating risk/duration zones for the shoulder as well as the neck and eyes, would provide a valuable tool for engineers and workstation designers to optimize workstation design *in-silico*, prior to deployment. Such a proactive approach could decrease the cost and increase the speed of the design phase of workstations.

5.   REFERENCES

[1]   Hughes R.E., Johnson M.E., O'Driscoll S.W. , and An K. Age-Related Changes in Normal Isometric Shoulder Strength. The American Journal of Sports Medicine, 27 (5) 651-657.

[2]   Otis JC, Warren RF, Backus SI, Santner TJ, Mabrey JD. Torque production in the shoulder of the normal young adult male. The interaction of function, dominance, joint angle, and angular velocity. The American Journal of Sports Medicine, 18(2) 119-123.

[3]   Potvin, J. 2012. Predicting maximun acceptable efforts for repetitive tasks: An equation based on duty cycle. Human Factors (in press).

Effects of High-Heeled Shoes on the Control of the Body's Center of Mass Motion in Relation to Center of Pressure During Gait

Hui-Lien Chien [1], Tung-Wu Lu [2], Ming-Wei Liu [3]

[1] Institute of Biomedical Engineering, National Taiwan University, Taiwan, R.O.C., d95548006@ntu.edu.tw
[2] Institute of Biomedical Engineering, National Taiwan University, Taiwan, R.O.C., twlu@ntu.edu.tw
[3] Department of Surgery, Tai-An Adventist Hospital, Taiwan, R.O.C., drliumw@yahoo.com.tw

Keywords-gait; high heels; center of mass; center of pressure; balance

1. INTRODUCTION

Surveys on shoe use show that 37% to 69% of women wear high-heeled shoes on a daily basis [1-3]. High-heeled shoes have been shown to be responsible for instability and falling, leading to injuries [Add Citation]. Most studies have investigated the kinematic and kinetic changes of the lower-extremity when wearing high-heeled shoes [1, 4-6], but few have studied balance control of the whole body during dynamic activities, such as gait [7-8]. COM-COP inclination angles (CCIA) have been used to describe the body's dynamic control during locomotion without the influence of stature differences among subjects [9]. Apart from CCIA, COM-COP inclination angular velocities (CCIV) were also useful for assessing one's ability to control the body's COM during functional activities [9]. Quantifying of the variables associated with body balance control in women who wear high-heeled shoes may offer insights into clinically preventable musculoskeletal problems and provide a basis for designs that minimize adverse effects. The purposes of this study were to investigate the influence of the heel base and height of shoes on the COM motion in terms of CCIA and CCIV during normal walking.

2. MATERIAL AND METHODS

Fifteen female adults (age: 24.4±3.4 years; height: 158.9±5.7 cm; weight: 49.2±5.1 kg) who were regular wearers of shoes with heels of more than 3 cm in height participated in the current study. In a gait laboratory, each subject walked at a self-selected pace under each of the following conditions: (a) barefoot, (b) low-heeled shoes (3.9 cm), (c) medium-heeled shoes (6.3 cm), and (d) high-heeled shoes (7.3 cm). Thirty-nine retro-reflective markers were used to track the motion of the body segments. Three-dimensional (3D) marker trajectory data were measured using a 7-camera motion analysis system (Vicon512, Oxford Metrics Group, U.K.). Ground reaction forces were simultaneously measured by two forceplates (Advanced Mechanical Technology Inc., U.S.A.). A 13-body-segment model of the whole body modeled as rigid bodies was used for the analysis of the body's COM motion. The CCIA in the sagittal plane (α; A/P inclination angle) and frontal plane (β; M/L inclination angle) were then calculated using the method reported by Hsu, et. al. [10]. With the current forceplate setup, α and β were calculated during the period from the beginning of the single leg stance (SLS) to the subsequent heel-strike. CCIA of α and β were also calculated by smoothing and differentiating their trajectories using the generalized cross-validatory spline method. The average, critical points and peaks of CCIA and CCIV were tested using repeated ANOVA (α=0.05). The independent t-test with Bonferroni correction (α=0.05/6=0.0082) was used for between-conditions comparisons.

3. RESULTS

After normalizing the gait speeds, stride lengths and step widths were significantly decreased for all heel heights when compared to barefoot walking (p<0.0001). No significant differences were found between heel heights in any temporal-spatial variable. All variables related to frontal CCIA were reduced in all shoe conditions when compared to barefoot walking, but no differences were found between heel heights. The ensemble-averaged curves of the CCIV showed double-peak patterns during DLS (Fig. 1 and Fig. 2). At the first peak during DLS, narrow-heeled shoes showed smaller lateral CCIV than barefoot (p<0.0001), while high-heeled shoes had smaller lateral CCIV than low-heeled shoes (p<0.0001). In the sagittal plane, high-heeled and medium-heeled shoes showed smaller posterior CCIV than barefoot, and those for high-heeled shoes were smaller than those for low-heeled shoes. For the second peak, no significant differences were

found in the frontal plane, while statistically smaller values in the sagittal plane for barefoot and low-heeled shoes were found compared to those for middle-heeled and high-heeled shoes (p<0.0001).

4. DISCUSSION

The reduced base of the heels was found to be the primary factor for the reduced walking speed, as well as the reduced CCIA in the frontal plane throughout the gait cycle. This was achieved mainly through the control of the CCIV during DLS. The observed CCIV changes in the frontal plane appeared to be related to the narrow heels of the shoes, especially those of the contralateral limb around its heelstrike. The significantly reduced CCIV at contralateral heelstrike indicated the need for a better control of the transfer of the body weight to the relatively reduced base of suport of the contralateral limb. The reduced step width also contributed to this requirement. A similar strategy of CCIV control was also found in the sagittal plane, except during the second half of the DLS. The sagittal CCIV was increased during the second half to maintain the continuing progression of the body's COM. The height of the heels affected mainly the peak CCIV during DLS, which were not big enough to affect the CCIA. These results suggest a conservative strategy for dynamic balance control during narrow-heeled gait. The current results will serve as baseline data for future evaluation of patients and/or older adults during narrow-heeled gait aiming at reducing risks of falls.

5. REFERENCES

[1] Esenyel M., Walsh K., Walden J.G. and Gitter A., 2003. Kinetics of high-heeled gait. J. Am. Podiatr. Med. Assoc. 9, 27-32.

[2] Frey C., Thompson F., Smith J., Sanders M. and Horstman H., 1993. American Orthopaedic Foot and Ankle Society women's shoe survey. Foot Ankle 14, 78-81.

[3] The Gallup Organization Inc., 1986. Women's Attitudes and Usage of High Heel Shoes, Surrey, England.

[4] Lee C.M., Jeong E.H. and Freivalds A., 2001. Biomechanical effects of wearing high-heeled shoes. Int. J. Ind. Ergon. 28, 321-326.

[5] Opila-Correia K.A., 1990. Kinematics of high-heeled gait. Arch. Phys. Med. Rehabil. 71, 304-309

[6] Opila-Correia K.A., 1990. Kinematics of high-heeled gait with consideration for age and experience of wearers. Arch. Phys Med. Rehabil. 71, 905-909.

[7] Lord S.R. and Bashford G.M., 1996. Shoe characteristics and balance in older women. J. Am. Geriat.r Soc. 44, 429-433.

[8] Menant J.C., Perry S.D., Steele J.R., Menz H.B., Munro B.J. and Lord S.R., 2008. Effects of shoe characteristics on dynamic stability when walking on even and uneven surfaces in young and older people. Arch. Phys Med. Rehabil. 89, 1970-1976.

[9] Huang S.C., Lu T.W., Chen H.L., Wang T.M. and Chou L.S., 2008. Age and height effects on the center of mass and center of pressure inclination angles during obstacle-crossing. Med. Eng. Phys. 30, 968-975.

[10] Hsu W.C., Wang T.M., Liu M.W., Chang C.F., Chen H.L. and Lu T.W., 2010. Control of body's center of mass motion during level walking and obstacle-crossing in older patients with knee osteoarthritis. J. Mech. 26, 229-237.
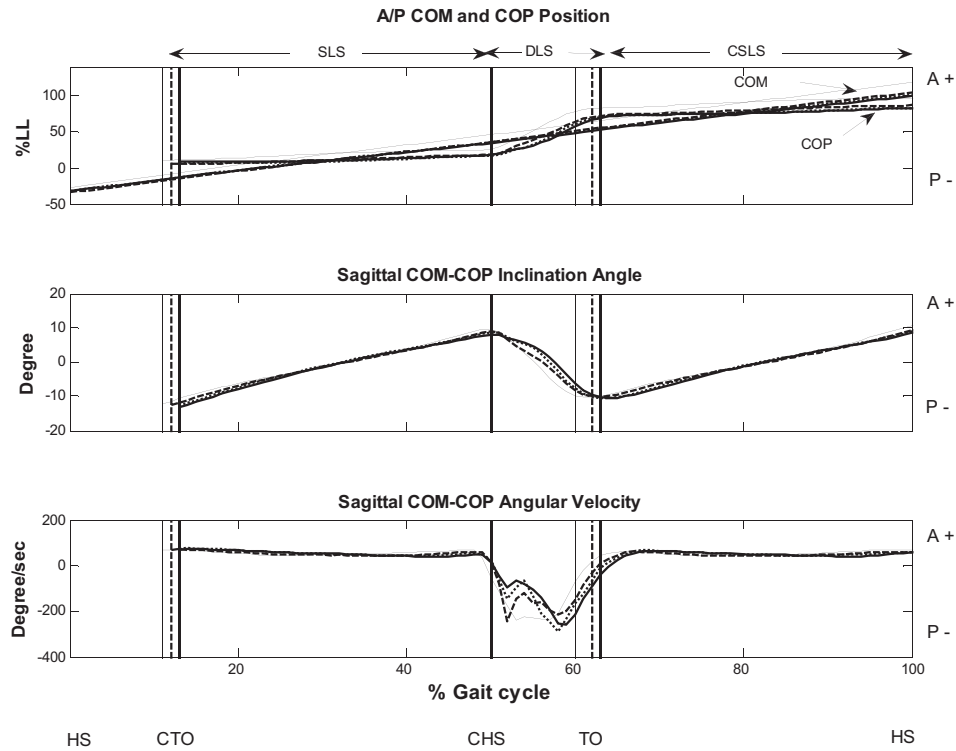
A/P COM and COP Position

Sagittal COM-COP Inclination Angle

Sagittal COM-COP Angular Velocity

HS   CTO   CHS   TO   HS

Figure 1. Ensemble-averaged COP and COM positions, COM-COP inclination angle, and COM-COP inclination angular velocity in the sagittal plane when barefoot (thin curves, solid) and narrow-heeled walking (thick curves) with low heel height (dashed), medium heel height (dotted) and high heel height (solid). Vertical lines indicate the critical times (HS: heel-strike; CTO: toe-off of the contralateral leg; CHS: heel-strike of the contralateral leg; TO: toe-off).

M/L COM and COP Position

Frontal COM-COP Inclination Angle

Frontal COM-COP Angular Velocity

HS   CTO   CHS   TO   HS
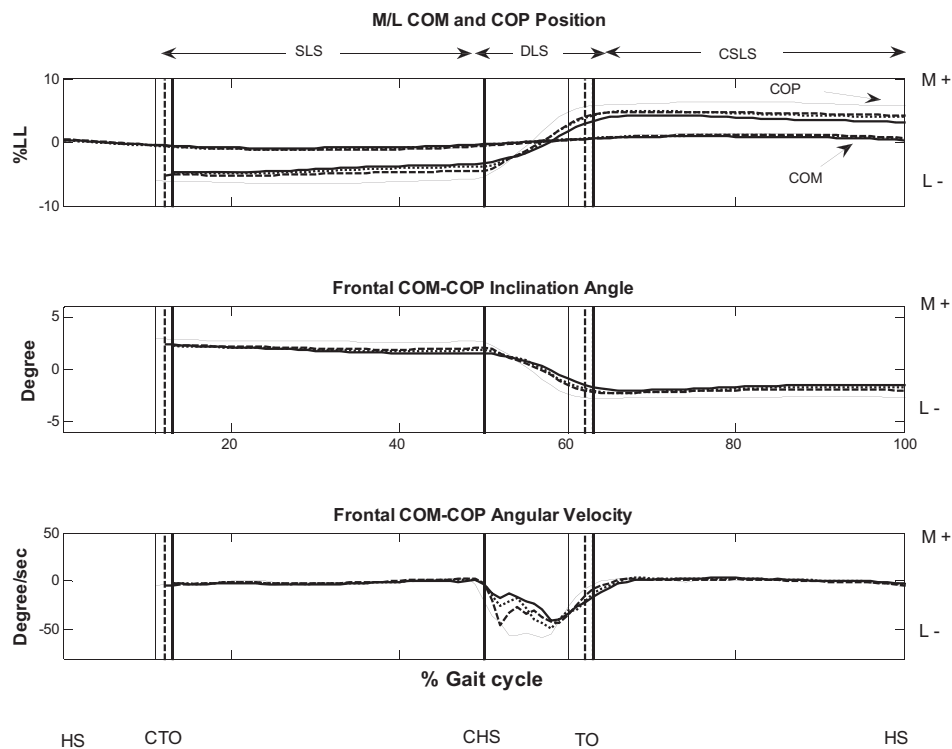
Figure 2. Ensemble-averaged COP and COM positions, COM-COP inclination angle, and COM-COP inclination angular velocity in the frontal plane when barefoot (thin curves, solid) and narrow-heeled walking (thick curves) with low heel height (dashed), medium heel height (dotted) and high heel height (solid).

Vertical lines indicate the critical times (HS: heel-strike; CTO: toe-off of the contralateral leg; CHS: heel-strike of the contralateral leg; TO: toe-off).

Influence of speed of progression on the gait of young children

Van Hamme A.[1,2], Samson W.[3,4], Dohin B.[5], Dumas R.[1], Chèze L.[1]

[1] Laboratoire de Biomécanique et Mécanique des Chocs (UMR_T 9406), Université Lyon 1/IFSTTAR, Villeurbanne, France, avanhamme@ctcgroupe.com

[2] CTC, Lyon, France

[3] Lion Systems S.A, Foetz, Luxembourg

[4] Laboratory of Functional Anatomy (CP 619), Université Libre de Bruxelles, Brussels, Belgium

[5] Hôpital Nord CHU, Université Claude Monnet, Saint-Etienne, France

675 gait trials are considered to characterize the influence of speed progression on the gait of young children (under 6 years old). Trials are distributed in 5 speed groups (with the same average age of 3 years old) in order to underline the effect of speed of progression on kinematics and kinetics. The speed effect is notable on gait parameters (especially in sagittal plane) and therefore has to be considered for gait children comparison.

Keywords : children; gait; speed of progression; kinematics; kinetics

1. INTRODUCTION

Children gait changes during the first years of independent walking [1] and persists to be different from adult gait up to 10 years old [2]. Many studies deal with the influence of speed of progression on gait parameters and recommend considering this influence for results interpretation [3-4]. Some authors examine the effect of speed of progression for children and conclusions are similar to adults: speed of progression has an influence on children gait parameters [5-7]. Nevertheless, these studies evaluate children with an average age around 10 years old. The influence of speed progression on gait parameters has not been studied on a large population of young children (under 6 years old) to our knowledge. Gait maturation is important in young children. Then, it seems to be useful to examine the influence of speed of progression on gait parameters.

2. MATERIALS AND METHODS

Participants

Sixty-four healthy children (31 girls and 33 boys) are included in the study. A total of 675 gait trials were collected. These trials are divided in 5 speed of progression groups (groups' characteristics in Table 1). Independent walking was acquired between 10 and 17 months of age and medical examination did not revealed any orthopedic or neurological disorder. Parents gave their informed consent for their child to participate in the study which was approved by the local ethics committee.

Experimental set-up

Thirty-two retro-reflective markers were fixed on classical anatomical landmarks of pelvis and lower limbs. Children walked at self-selected speed, exceptionally with a parent or experimenter assistance for the toddlers. Fifteen to twenty gait trials were measured for each subject using a Motion Analysis® system with 8 Eagle® cameras (Santa Rosa, USA) and one Bertec® force platform (Colombus, USA), synchronized to a sampling frequency of 100 Hz.

Data processing

After signal processing (fourth-order butterworth filter, 6Hz cutoff frequency), all markers' trajectories were obtained in an Inertial Coordinate System (ICS) via Cortex ® software and then, enabled the construction of each Segment Coordinate System. The hip joint center coordinates were calculated using regression equations of Harrington et al [8] considering only the healthy children's data. The inertial parameters were estimated from scaling equations [9]. The joint forces and moments were computed in the ICS by bottom-up inverse dynamics and the joint angular velocity was computed using the quaternion algebra [10]. The 3D joint power is calculated as the dot product of joint moment and angular velocity. The parameters are normalized following the recommendations of Hof [11].

Statistical analysis

A statistical analysis is realized on the peaks of the average curve of each group of speed. Due to the non-normal distribution of the values (Shapiro-Wilk test, $p<0.05$), a Kruskal-Wallis test ($p<0.05$) is used to determine if speed

of progression has a significant influence for the considered peak. When significant, a Mann-Withney test ($p<0.05$) is realized to compare the significance 2-to-2 between the 5 speed groups.

3. RESULTS

3D joint angles, moments and power [12] for ankle, knee and hip, and Ground Reaction Force (GRF) on sagittal, coronal and frontal axes are processed. Considering all of these curves a total of 67 peak values are identified. For kinematics, all peak values on joint flexion/extension angles show more than 4 significant differences. In abduction/adduction and internal/external rotation angles, there are fewer differences. For dynamics, the peak values of GRF present more than 6 significant differences on the 3 axes. The hip flexion/extension moment is the curve showing the most significant differences (8 for the maximum extension at the beginning of stance phase, 10 for the maximum flexion and 10 for the maximum extension at the end of the swing phase). Also, knee flexion/extension moments peak values present more than 8 significant differences. For the other moments, there are less significant differences (7 for the maximum plantar flexion and less than 7 for the other peak values). For 3D powers, there are more than 6 significant differences for ankle and knee peak values, except for the maximum knee power at 50% of gait cycle (no significant difference). For 3D hip power, all differences between each speed group are significant. It can also be noticed that almost all peaks have an ordered evolution with speed of progression.

4. DISCUSSION

The aim of this study was to explore the influence of speed of progression on the gait parameters in a specific population: children under 6 years old. The effect of speed progression on gait parameters for young children is obvious like it was already observed for older children, especially in the sagittal plane [5]. For kinematics, it has been noticed more significant differences than in [5] for hip and knee flexion/extension (Fig. 1a-b). Results for the ankle kinematics are similar to those of Stansfield (Fig. 1c). Some differences are observed for the vertical GRF, especially for the vertical component. Significant differences are notably noticed at the beginning of stance phase (Fig. 2): these differences are less important in older children [6]. For joint moments, significant differences are higher on peaks for hip, knee and ankle flexion/extension moments than in Stansfield's study (Fig. 1d-f). The difference of hip 3D power with regards to Stansfield's results is probably due to the definition of the hip center (Fig. 1g). Knee 3D power patterns are different from Stansfield's ones (Fig. 1h) while in the present study, 3D powers are processed whereas Stansfield's results are 2D powers. Maximum ankle 3D power is non-ordered with speed progression, contrarily to the results published by Stansfield and all differences are not significant (Fig. 1i). These observations lead to assume that speed of progression effect is present for young children and maybe is more important than for older children.

A limitation of this study concerns the subject ages. The groups have the same age on average (around 3 years old) but it will be necessary to compare the influence of speed of progression and the influence of age to quantify the relative contribution of each factor on gait parameters.

Table 1. Subject's groups characteristics

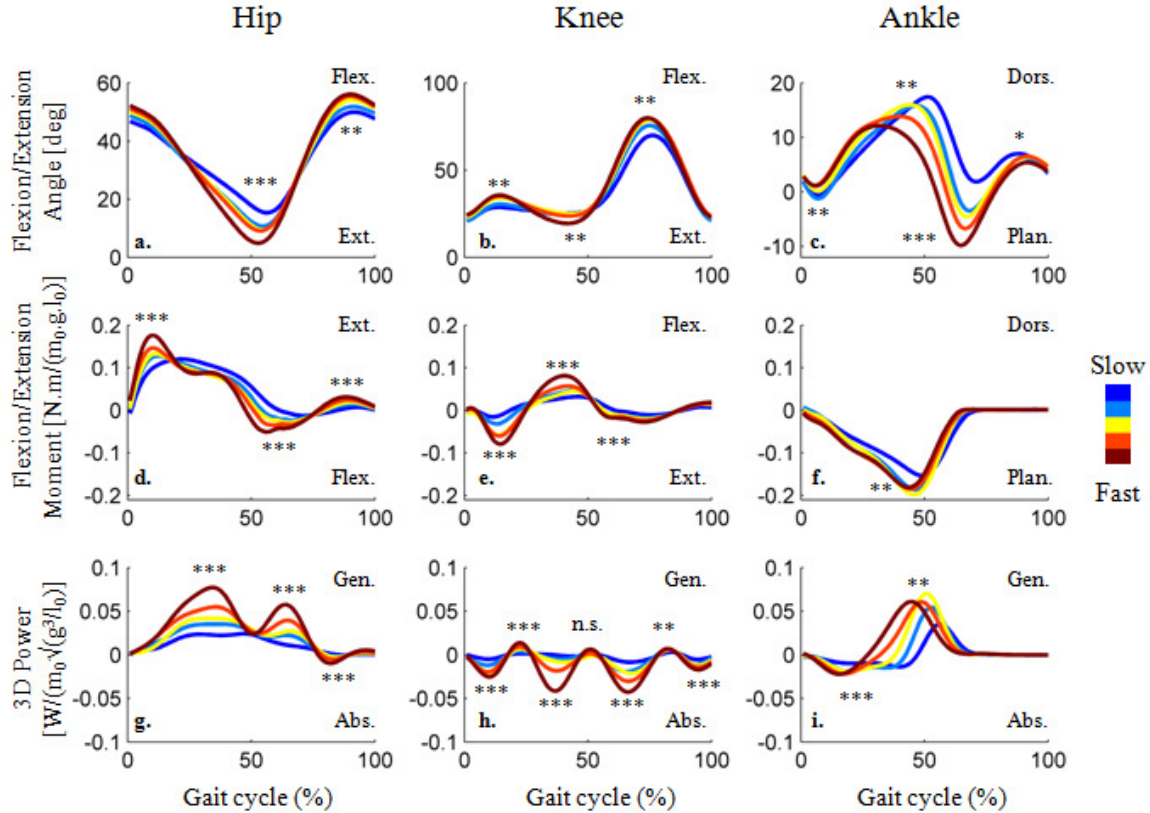|	Group 1	Group 2	Group 3	Group 4	Group 5
Color Code					
Number of processed kinematic gait trials					
	135	135	135	135	135
Number of processed dynamic gait trials					
	126	100	107	117	94
Age [years]					
average	3.06	3.43	3.39	3.47	3.38
SD	1.10	1.42	1.23	1.49	1.46
Normalized speed of progression [m.s^{-1}/($\sqrt{gl_0}$)]					
average	0.25	0.36	0.42	0.48	0.58
SD	0.05	0.02	0.01	0.02	0.05

Figure 1. Biomechanical parameters variations during gait cycle. Each column represents respectively hip, knee and ankle joint. a-c: Flexion/Extension angle ; d-f : Flexion/Extension moment ; g-i: 3D power. Each speed of progression group is represented with one color from dark blue for slowest speed to dark red for fastest. The number of significant differences on peak values are represented : n.s : no significant difference, *:1 to 4 significant differences, ** : 5 to 7 significant differences, *** : 8 to 10 significant differences. (m_0: mass; l_0:leg length g: acceleration of gravity)

5. CONCLUSION

Speed of progression has an effect on the gait parameters for young children (under 6 years old). The influence of speed of progression on young children gait parameters is often similar to those observed in previous studies considering older children. Nevertheless, some specific differences (e.g. hip and knee flexion/extension angle) observed in the present study let thinking that the speed influence seems to be different depending on age. Studies considering both age and speed of progression effects are necessary to better characterize the evolution of young children gait.

6. REFERENCES

[1] Samson W, Dohin B, Desroches G, Chaverot JL, Dumas R, Chèze L. The foot mechanics during the first six years of independent walking. Journal of Biomechanics, 44, 1321-1327, 2011.

[2] Oeffinger D, Augsburger S, Cupp T. Pediatric kinetics : Age related changes in able-bodied populations. Gait and Posture 5, 155-156, 1997.

[3] Lelas J, Merriman G, Riley P, Kerrigan C. Predicting peak kinematic and kinetic parameters from gait speed. Gait and Posture 17, 106-112, 2002.

[4] Kirtley C, Whittle MW, Jefferson RJ. Influence of walking speed on gait parameters. Journal of Biomedical Engineering 7, 4, 282-288, 1987.

[5] Stansfield BW, Hillman SJ, Hazlewood ME, Lawson AA, Mann AM, Loudon IR et al. Sagittal joint kinematics, moments, and powers are predominantly characterized by speed of progression, not age, in normal children. Journal of Pediatric Orthopaedics 21, 403-411, 2001.

[6] van der Linden ML, Kerr AM, Hazlewood ME, Hillman SJ, Robb JE. Kinematic and kinetic gait characteristics of normal children walking at a range of clinically relevant speeds. Journal of Pediatric Orthopaedics 22, 800-806, 2002.

[7] Schwartz MH, Rozumalski A, Trost JP. The effect of walking speed on the gait of typically developing children. Journal of Biomechanics, 41, 1639-1650, 2008.

[8] Harrington ME, Zavatsky AB, Lawson SEM, Yuan Z, Theologis TN. Prediction of the hip joint centre in adults, children, and patients with cerebral palsy based on magnetic resonance imaging. Journal of Biomechanics, 40, 595-602, 2007.

[9]   Jensen RK. Changes in segment inertia proportions between 4 and 20 years. Journal of Biomechanics. 22, 529-536, 1989.

[10] Dumas R, Aissaoui R, de Guise JA. A 3D generic inverse dynamic method using wrench notation and quaternion algebra. Computer Methods in Biomechanics and Biomedical Engineering, 7, 159-166, 2004.

[11] Hof AL. Scaling gait data to body size. Gait and Posture, 4, 222-223, 1996.

[12] Dumas R, Chèze L. Hip and knee joints are more stabilized than driven during the stance phase of gait: An analysis of the 3D angle between joint moment and joint angular velocity. Gait and Posture, 28, 243-250, 2008.

Effect of high-heeled shoes on three-dimensional body Center of Mass displacement during walking

Sidequersky F.V. [1], Annoni I. [1], Mapelli A. [1], Lenci B. [1], Colangelo V. [1,2], Sforza C. [1]

[1] Dipartimento di Morfologia Umana e Scienze Biomediche "Città Studi", Università degli Studi di Milano, Milano, Italy.

[2] Dipartimento di Bioingegneria, Politecnico di Milano, Milano, Italy.

Human body; center of mass; heeled shoes

1. INTRODUCTION

Although millions of women daily wear high-heeled shoes, the potential detrimental effects of high-heeled shoes on the development of degenerative joint disease are well known [1, 2, 3]. Anyway, there is not yet a complete knowledge of the changes of the body center of mass (CoM) position due to heel height. The purpose of the study was to quantitatively compare the 3D displacement of the CoM [4], also focusing on its upper and lower components, during flat-heeled and high-heeled gait.

2. MATERIAL AND METHODS

Eleven volunteer women (mean age, 24 years) without gait dysfunction participated in the study performing two sets of ten trials of comfortable walking, wearing their own high-heeled shoes (heel, at least 8 cm high) and flat-heeled shoes (heel, at most 1 cm high). On each subject, the 3D coordinates of reflective markers (diameter, 1.5 cm), firmly attached to the skin by means of plastic supports and double-sided adhesive tape, were non-invasively recorded by an optoelectronic motion analyzer (BTS S.p.a, Garbagnate Milanese, Italy) [5, 6]. Nine infrared TV-cameras, with a sampling frequency of 60 Hz, were positioned beyond the perimeter of a working volume of 520 (length) x 210 (height) x 180 (depth) cm. After the system calibration, the 3D marker coordinates were reconstructed with an average error of 0.63 mm (SD, 0.7 mm) on a reference distance of 40 cm. Fourteen body landmarks (left and right tragion, acromion, olecranum, ulna styloid process, great trochanter, femur lateral epicondyle, lateral malleolus) allowed the body segmentation in 10 independent masses [7]: a head, a torso, two upper arms and two lower arms constituted the upper body; two upper legs and two lower legs constituted the lower body (Fig. 1).
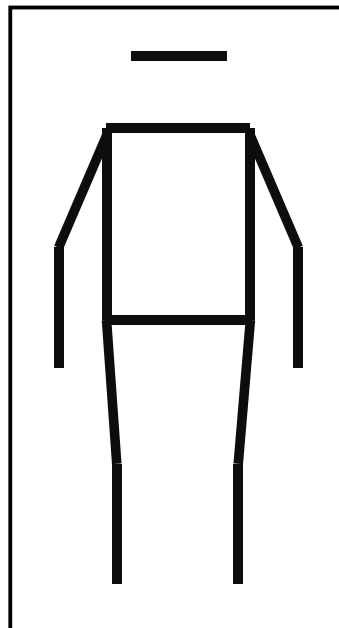

Figure 1. Segmental model of the human body.

Using mean anthropometric data previously collected [8], including the mass distribution within the segments and the locations of their centers of mass, the whole body CoM was computed by means of weighted average. The body CoM was separately evaluated in its anterior-posterior, vertical and medio-lateral displacements in each normalized stride cycle (from right heel strike to right heel strike, one for each trial). In particular, for both flat-heeled and high-heeled gait: CoM anterior-posterior coordinate was related to the simultaneous position of the center of pelvis; its vertical component, normalized to leg length, started from the plane passing across the malleoli when soles were in full contact with the ground; CoM medio-lateral coordinate was related to the gait direction. Each subject's mean and standard deviation (SD) of the three CoM coordinates were extracted in three standardized gait events (right (R) heel strike, left (L) heel strike, right toe off) for both flat-heeled trials and high-heeled trials. Additionally, all these computations were separately applied to the upper (uCoM) and lower (lCoM) components of the whole body CoM. Wilcoxon signed rank test was used to test differences of CoM displacement between flat-heeled and high-heeled gaits, whereas two-way ANOVA for repeated measures was used to test differences of CoM position variability between the two gait modalities and among the three gait events.

3. RESULTS

High-heeled gait, compared to flat-heeled gait, was kinematically characterized by a significantly lower CoM at R heel strike (p=0.024, median difference: 0.6%) and L heel strike (p=0.030, median difference: 1.1%). The same findings were also observed for uCoM (p=0.042, p=0.038 respectively) and lCoM (p=0.004, p=0.005 respectively) (Fig. 2). No significant differences were found at R toe off. In addition, a significant forward displacement of the lCoM in high-heeled gait was observed at each of the three stages (R heel strike, p=0.017, median difference: 6 mm; L heel strike, p=0.034, median difference: 9 mm; R toe off, p=0.003, median difference: 15 mm). Similar results were found for the whole CoM (p=0.024, p=0.038, p=0.004 respectively). The uCoM in high-heeled gait, instead, was significantly more anterior than in flat-heeled gait only at R toe off (p=0.024, median difference: 6 mm) (Fig. 3). On average, intra-individual variability of CoM coordinates did not change significantly in none of the three gait events, nor between the two gait modalities (p>0.05): the median of the 11 subjects' SDs ranged between 3 and 4 mm in the anterior-posterior direction, between 0.3 and 0.5% in vertical direction, between 16 and 18 mm in medio-lateral direction.
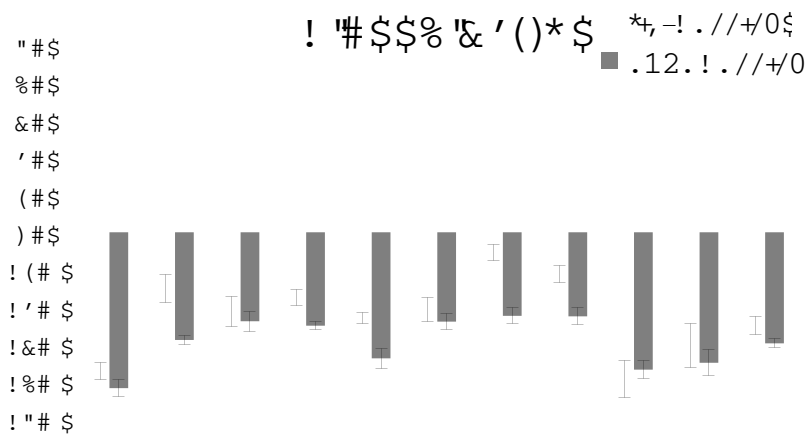

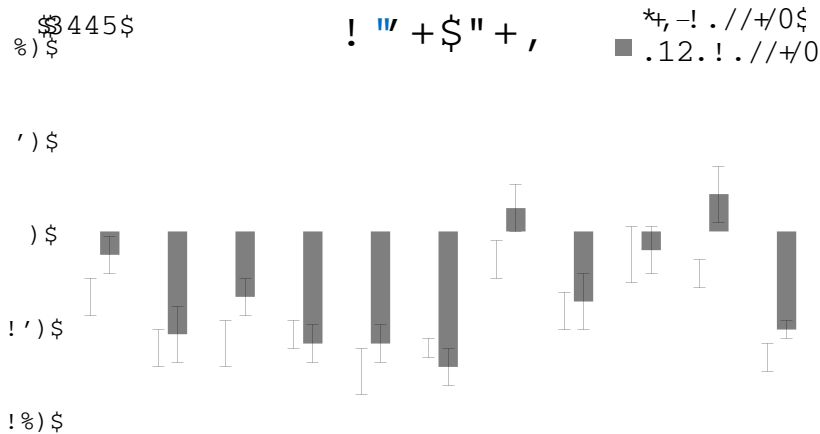Figure 2. Mean±SD of the lower CoM vertical displacement in the 11 recorded women at right heel strike. W-test: p<0.05.

Figure 3. Mean±SD of the upper CoM anterior-posterior displacement in the 11 recorded women at right toe off. W-test: p<0.05.

4. DISCUSSION

Our findings confirm that wearing high-heeled shoes significantly alters the normal displacement of the human CoM (both its components). In particular, the lower and more anterior CoM position, respectively referenced to the plane of malleoli and the pelvis center, during high-heeled gait could be seen as the biomechanical adaptation of the body posture in order to maintain a dynamic balance and avoid falls. In the future, these data will be integrated with inter-segmental angular relationships, and used to estimate the metabolic cost of high-heeled gait.

5. REFERENCES

[1] Kerrigan, DC, Todd, MK, Riley, PO. Knee osteoarthritis and high-heeled shoes. Lancet 351(9113), 1399-1401, 1998.

[2] Gefen, A, Megido-Ravid, M, Itzchak, Y, Arcan, M. Analysis of muscular fatigue and foot stability during high-heeled gait. Gait Posture 15(1), 56-63, 2002.

[3] Yung-Hui, L, Wei-Hsien, H. Effects of shoe inserts and heel height on foot pressure, impact force, and perceived comfort during walking. Appl. Ergon. 36(3), 355-362, 2005.

[4] Tesio, L, Rota, V, Chessa, C, Perucca, L. The 3D path of body centre of mass during adult human walking on force treadmill. J. Biomech. 43(5), 938-944, 2010.

[5] Sforza, C, Ugolini, A, Sozzi, D, Galante, D, Mapelli, A, Bozzetti, A. Three-dimensional mandibular motion after closed and open reduction of unilateral mandibular condylar process fractures. J. Craniomaxillofac. Surg. 39(4), 249-255, 2011.

[6] Sforza, C, Mapelli, A, Galante, G, Moriconi, S, Ibba, TM, Ferrario, L, Ferrario, VF. The effect of age and sex on facial mimicry: a three-dimensional study in healthy adults. Int. J. Oral Maxillofac. Surg. 39(10), 990-999, 2010.

[7] Fusini, L, Shirai, YF, Mapelli, A, Galante, D, Sforza, C. Balance control during the execution of traditional karate technique. Proc. ISPGR XIX Satellite Pre-Conference, Pavia, p. 23-24, 2009.

[8] D.A. Winter, Biomechanics and motor control of human movement, 2nd ed., Toronto: John Wiley and Sons, Inc., 1990.

Performance of the stabilizing system of the lumbar spine during a functional task

Preuss R.[1,2], Al Zoubi F.[1,2], Pakzad M.[1,2]

[1] School of Physical and Occupational Therapy, McGill University, Montreal, Canada.
[2] Constance-Lethbridge Rehabilitation Centre site of the CRIR, Montreal, Canada.

Keywords - Lumbar spine; dynamic stability; matrix factorization

1. INTRODUCTION

To date, most studies of lumbar spine stability have focused on the response to perturbation under static conditions [1–3]. Dynamic stability, however, is equally important. Under controlled, dynamic conditions, the performance of the system may be examined by assessing the displacement from a planned movement trajectory that occurs following a perturbation [4]. In the absence of an external perturbation, however, the performance of the system is also reflected in the variability of its movement trajectory with repeated execution of a given task. Examining the variability of spine movement during repeated execution of a functional task, therefore, may provide insight into the performance of the stabilizing system of the spine. Less variability would be reflective of improved performance, as it relates to the dynamic stability of the system, and would be achievable either through increased energy expenditure [4] or more accurate and precise control [5].

The sit-to-stand movement is a proven measure of functional performance in individuals with low back pain (LBP) [6], and as such may be an ideal means by which to study the performance of the spine stabilizing system. Previous studies have shown that individuals with LBP tend to reduce the amplitude of spine motion during the sit-to-stand task [7], which likely reflects a strategy to prioritize spine stability by making the system more robust (increasing the margin for movement error). If this strategy is executed through isometric muscle contractions, however, rather than through more precise control of the movement, it is likely to result in a reduction in movement amplitude without a change in the underlying coordinative structure of the movement pattern. Matrix factorization provides an approach to studying the coordinative structure of a data set [8,9], while at the same time removing the effects of movement amplitude by appropriately normalizing the data [10].

The objective of this study is to describe an approach to assess the performance of the stabilizing system of the lumbar spine, using matrix factorization, during repeated trials of the sit-to-stand movement task.

2. MATERIAL AND METHODS

2.1. SUBJECT

The subject for this study was a 29-year old male with a history of recurrent low back pain, who was asymptomatic at the time of testing.

2.2. TASK

For the sit-to-stand task, the subject was asked to rise from, and return to, sitting, as rapidly as possible, without the use of his arms. Eight repetitions of the task were performed.

2.3. DATA ACQUISITION

Segmental motion (position and orientation) was acquired, in three dimensions, using a TrakSTAR electromagnetic motion capture system (Ascension Technology, Milton, VT), sampled at 200Hz. Sensors (model 800; 8x8x20mm) were mounted over the lateral side of the legs and thighs (bilaterally), the base of the sacrum, and the spinous process of the fourth lumbar, second lumbar, and twelfth thoracic vertebrae using custom molded urethane clips and double-sided tape. These data were then low-pass filtered, with a cut-off frequency of 10Hz, using a 4th order, zero phase-lag Butterworth filter, and re-sampled at 1000Hz using a cubic spline interpolation. Joint angles for the hips, knees and spine were determined by multiplying the 4x4 rotation-translation matrix for one segment by the inverse of the rotation-translation matrix for the adjacent segment, using custom software written in Matlab (each rotation matrix having been derived from the position and orientation data of the sensors in the transmitter-embedded reference frame).
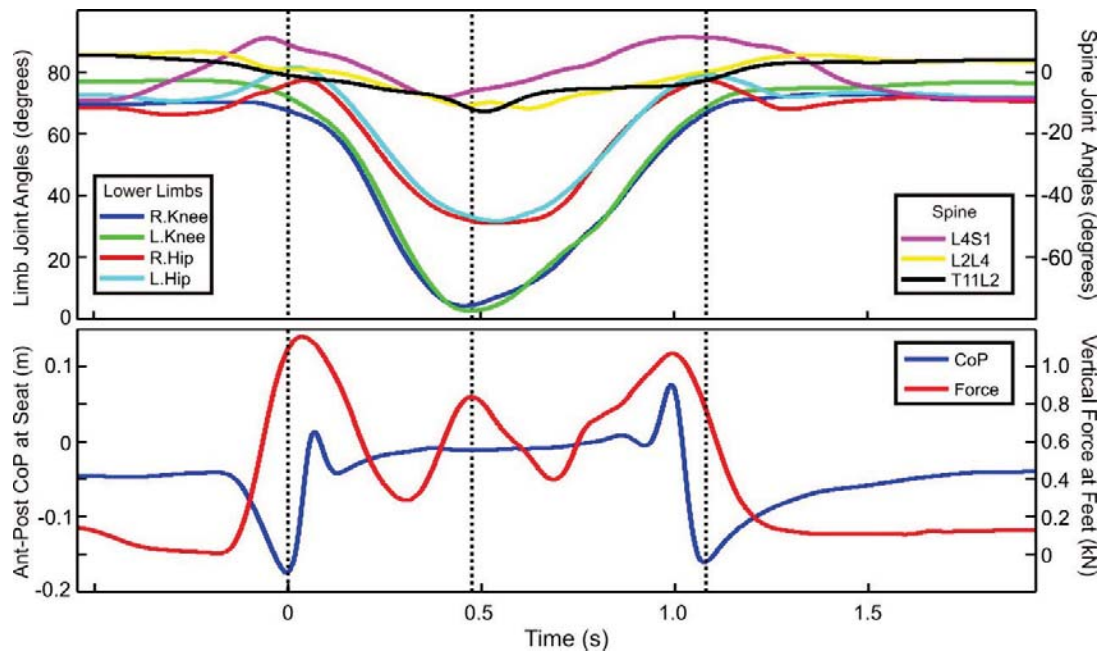
Figure 1. Sagittal plane joint angles (top: positive = flexion) and support surface reaction data (bottom) from a single sit-to-stand trial.

Contact forces at the seat and under both feet were recorded simultaneously using three BP400600 NC force plates (AMTI, Watertown, MA), sampled at 2000Hz. These data were then low-pass filtered and re-sampled as described above. The anterior-posterior position of the centre of pressure at the surface of the seat (CoP), and the net vertical ground reaction force under the feet (Fz), were used to divide the kinematic data into the "up" (sit-to-stand) and "down" (stand-to-sit) phases of the movement.

Fig. 1 illustrates one repetition of the sit-to-stand motion. The "up" phase of the movement was taken to begin at the first point of greatest posterior motion of the CoP, reflecting the counter motion used to initiate standing, and end at the first local maximum in Fz following the initial unloading resulting from the upward acceleration of the body. The "down" phase was taken to beging from this same local maximum in Fz, and end at the second point of greatest posterior motion of the CoP, reflecting the peak horizontal deceleration of the body's mass upon return to sitting.

2.4. MATRIX FACTORIZATION ANALYSIS

For trials 2 to 8, the mean duration of the "up" and "down" phases of the sit-to-stand task was 0.492s (+/-0.025s) and 0.615s (+/-0.076s) respectively (the first trial was excluded, as the duration of these phases was notably longer: 0.739s and 1.254s for the "up" and "down" phases respectively). Based these durations, the "up" and "down" phases of the spine joint angle data, for each trial, were re-sampled to 500 and 600 frames respectively. Data for each trial were then compiled into [1100 x 9] matrices (1100 frames per trial x 3 rotation axes from the 3 joints).

An expanding-window singular value decomposition (SVD) was used for matrix factorization, with the eigenvalues for each resulting eigenvector reflecting the variance in the original data set explained by that eigenvector [11]. Analysis began with data from a single trial. The expanding-window approach began with the first 100 data points, and then increased the number of points by 10 for each subsequent analysis. This analysis was then repeated 6 additional times, with the data matrix expanded at each step to include data from one additional trial (i.e. a total of 7 data sets, with data from 1 to 7 trials). Prior to each matrix SVD, the data to be analyzed was normalized by dividing each variable by its amplitude range, and then again by its standard deviation, giving each variable unit variance [10]. In this manner, the amplitude of movement at any given joint did not disproportionately affect the variance contained within the data set.

For each step in the expanding-window analysis, the effect of adding data from an additional trial was assessed by comparing the cumulative variance explained by each eigenvector across the 7 data sets (e.g. variance explained by one eigenvector for data containing 2 trials vs. 1 trial).
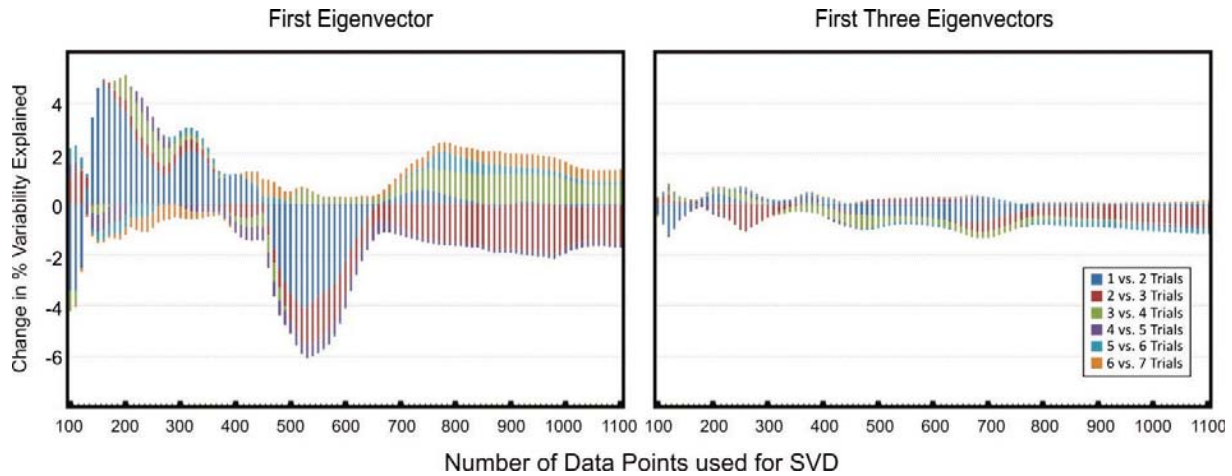
Figure 2. Change in the percentage of variance explained in the original data for each additional trial.

3. RESULTS

Fig.2 illustrates the change in the variance explained by the first eigenvector (left), and the first three eigenvectors (right), at each step in the expanding-window analysis, as data for each subsequent trial was included in the analysis. More than 99% of the variance in each data set, at each step in the analysis, was explained by 3 eigenvectors. This is reflected by the minimal changes seen on the right of Fig.2. The variance explained by the first eigenvector, however, differed substantially as data for additional trials was added to the analysis. One notable change, for example, was the general drop in the variance explained by the first eigenvector between frames 450 and 650. This is reflective of an increase in the between-trial variability of the joint movement patterns at the transition from the "up" to the "down" phase of the movement.

4. DISCUSSION

This study describes an approach to assess the performance of the stabilizing system of the lumbar spine, using matrix factorization, during repeated trials of the sit-to-stand movement task. On repeated trials of a movement, if all joint trajectories are perfectly repeated, adding data from multiple trials would cause no change in the coordinative structure of the data (i.e. perfect performance in relation to the stability of the movement trajectories). The eigenvectors derived from matrix factorization, therefore, would not change, nor would the proportion of the variability in the original data set explained by those eigenvectors. A change in the joint trajectories between trials, however, would lead to changes in those eigenvectors, and in the proportion of variability explained by each.

For the sit-to-stand task assessed in the current study, SVD was used to assess spine joint angle data taken from the lumbo-sacral, mid-lumbar and thoraco-lumbar levels. More than 99% of the variance in the data could be explained by only 3 eigenvectors, regardless of the number of trials included in the analysis. This reflects a tight coordinative structure in the joint trajectories of the lumbar spine. The variance explained by the first eigenvector, however, changed over the progression of the movement, as additional trials were included the analysis (Fig.2). This indicates a change in the performance of the spine stabilizing system at different phases of this functional task, suggesting that the challenge to spine stability differs over the course of this functional movement pattern.

5. ACKNOWLEDGMENTS

6. REFERENCES

[1] Bergmark A (1989) Stability of the lumbar spine: a study in mechanical engineering. Acta Orthop Scand Suppl 230: 1-54.

[2] Cholewicki J, VanVliet J (2002) Relative contribution of trunk muscles to the stability of the lumbar spine during isometric exertions. Clin Biomech 17: 99-105.

[3] Granata K, Orishimo K (2001) Response of trunk muscle coactivation to changes in spinal stability. J Biomech 34: 1117-1123.

[4] Reeves N, Narendra K, Cholewicki J (2007) Spine stability: the six blind men and the elephant. Clin Biomech 22: 266-274.

[5] Kording K, Wolpert D (2004) Bayesian integration in sensorimotor learning. Nature 427: 244-247.

[6] Andersson E, Lin C, Smeets R (2010) Performance tests in people with chronic low back pain: responsiveness and minimal clinically important change. Spine 35: E1559-E1563.

[7] Shum G, Crosbie J, Lee R (2005) Effect of low back pain on the kinematics and joint coordination of the lumbar spine and hip during sit-to-stand and stand-to-sit. Spine 30: 1998-2004.

[8] Daffertshofer A, Lamoth C, Meijer O, Beek P (2004) PCA in studying coordination and variability: a tutorial. Clin Biomech 19: 415-428.

[9] Tresch M, Cheung V, d'Avella A (2006) Matrix factorization algorithms for the identification of muscle synergies: evaluation on simulated and experimental data sets. J Neurophysiol 95: 2199-2212.

[10] Torres-Oviedo G, Ting L (2007) Muscle synergies characterizing human postural responses. J Neurophysiol 98: 2144-2156.

[11] Jolliffe, I. (1986) Principal Component Analysis. New York: Springer-Verlag.

Wed – July 18th 2012

Chairmen: **Silvia Fantozzi (DEIS, University of Bologna, Italy)**
Tung Wu Lu (National Taiwan University, Taiwan)

Keynote lecture: *"Image-based analyses of natural and replaced human joints*
16.00 : 16.30   *during activities"*
Tung Wu Lu

Podium session #2: "Video-based motion tracking – I"
16.30 : 18.00

16.30	Assessment of lower limb joint kinematics using a 2-D hybrid markerless approach applied to a video camcorder acquisition	Surer E., Cereatti A., Della Croce U.
16.45	Characterization of 3D Fluoroscopy calibration: joint kinematics quantification sensitivity to calibration errors	Tersi L., Fantozzi S., Stagni R.
17.00	Accuracy assessment of scapular motion estimation using acromion marker cluster	Cereatti A., Rosso C., Nazarian A., Della Croce U.
17.15	Comparison of three different methods for hand segment coordinate system definition.	Goislard de Monsabert B., Visser J.M.A., Veeger H.E.J., van der Helm F.C.T.
17.30	Effect of markers attachment on soft tissue artifact and knee kinematics during gait	Barré A., Thiran J.P., Jolles B.M., Theumann N., Aminian K.
17.45	Improved 3-D spine & human skeleton model for posture and movement analysis	D'Amico M., Roncoletta P., Iodice P., Di Pancrazio L., Bellomo R.G., Saggini R.

!

Keynote lecture

Image-Based Analyses of Natural and Replaced Human Joints During Activities

Tung Wu Lu

Institute of Biomedical Engineering, National Taiwan University, Taiwan

The mobility and stability of human joints are controlled by a complex interaction between the articular surfaces and the surrounding connective tissues, including ligaments and muscles. Study of the kinematic and force interactions between these force-bearing structures during multi-joint functional tasks is helpful for a better understanding of the etiology of relevant diseases, and for planning and evaluating subsequent treatments such as ligament reconstruction, total joint replacements and rehabilitation. Skin marker-based stereophotogrammetry has been widely used to measure inter-segmental motions of human movement, both for research and clinical purposes. However, the detailed motions of the articular surfaces and the surrounding connective tissues cannot be measured. In order to bridge the gap, there has been a growing interest in developing medical image-based approaches for measuring the kinematics of the joints during activities. In this presentation, a brief review of these developments will be given. In particular, the development of a digitally reconstructed radiograph (DRR)-based 3D fluoroscopy method and its application to the study of a series of natural and replaced human joints will be described. The 3D fluoroscopy method has also been integrated with a skin marker-based motion capture system and forceplates for the simultaneous measurement of the detailed motion of the knee joint and its coordination with other joints within the limb during multi-joint weight-bearing tasks. With 3D mathematical and finite element modeling, the accurate *in vivo* skeletal motion data of the knee provide a good opportunity for a more comprehensive subject-specific analysis of the articular contacts and ligaments of the joint during functional activities. Because of the hazards of ionizing radiation involved in fluoroscopy-based methods, the development of a new slice-to-volume registration method using FLASH MRI for the real-time measurement of joint kinematics *in vivo* will also be described.

Assessment of Lower Limb Joint Kinematics using a 2-D Hybrid Markerless Approach applied to a Video Camcorder Acquisition

Surer E. [1], Cereatti A. [1], Della Croce U. [1]

[1] Information Technology and Social Sciences Department, University of Sassari, Sassari, Italy

In this study, a 2-D hybrid markerless technique is proposed to estimate the lower limb joint kinematics from data recorded using a video camcorder. The presented markerless methodology is defined as hybrid because garments like high-cut underwear and ankle socks were used as "segmental markers". High-cut underwear contributed in defining the pelvis segment and ankle socks are used for the definition of the foot segment. The method was applied to a video sequence acquired with a video camcorder. The method was validated by using a stereophotogrammetric marker-based system. Correlation and Root Mean Square Deviation (RMSD) of the joint kinematics estimates obtained with the two techniques were found to be similar. The proposed hybrid technique can be considered as an easy-to-configure and affordable alternative to marker-based photogrammetric systems for the estimation of the lower limb joint kinematics.

Keywords: markerless; 2-D joint kinematics; lower limbs

1. INTRODUCTION

Lower limb joint kinematics during walking is commonly estimated using marker-based techniques. Markers attached to the skin may cause uneasiness, may interfere with normal walking and need an extended set-up time. To overcome these limitations, we present a 2D hybrid approach (*Hyb*) based on markerless methodologies in which underwear and socks worn by subjects are used as "segmental markers". The proposed study is an enhancement to our previous study [1] which used the sagittal images recorded by a modified infrared camera synchronized with a stereophotogrammetric system. Aim of this preliminary study was to test the performance of the previous approach using a low-cost commercial camcorder in a simpler setup. The results provided by the proposed *Hyb* approach were compared with those obtained using a marker-based approach.

2. MATERIAL AND METHODS

One healthy subject (female, age = 29 yrs) walked at self-paced speed and one trial was recorded. During the acquisition, the subject wore white high-cut underwear and white ankle socks. Marker-based (*Mb*) data were acquired using a 10-camera stereophotogrammetric system (BTS® SMART-D, 640x480 pixels, frame rate: 60Hz). Lower limb kinematics was estimated according to BTS Simple Davis protocol. An AMTI force platform was used to detect heel strikes and toe offs.

Anthropometric Measurements

To extract additional information for the use of high-cut underwear and ankle socks as "segmental markers", the following anthropometric measurements were acquired before the acquisitions:
m1: distance between the high-cut of the underwear (hip) and the femoral condyle;
m2: distance between the femoral condyle and the edge of the ankle sock (ankle);
m3: foot length
The camera was positioned laterally and the m3 was used to map the pixel-lengths of m1 and m2 on the images.

Video Acquisition and Video Editing

Sagittal view images of the lower limbs of the subject were acquired with a hard disk camcorder (JVC GZ-MG77E, 720x576 pixels, frame rate: 25 Hz). Since the JVC camcorder stored the video acquisitions in .MOD format, a video editing tool (Virtualdub-MPEG2 1.6.19 build 24586) was used to open and edit the acquired video.

De-interlacing

Most of the digital camcorders working at 25 fps record at 50 fps and mix every two consecutive pictures with half the height (i.e. fields) into one frame (interlacing). Since the interlaced video output contains two fields of a video frame recorded at different times, visual defects called "interlace artifacts" or "combing" occur with moving objects in the image. To overcome these defects, de-interlacing techniques are used. De-interlacing techniques can be classified into three different groups. The first group is called "field combination de-interlacers" since they take the even and odd fields and combine them into one frame. The second group is called "field extension de-interlacers" where each field (with only half the lines) is extended to the entire screen to compose a frame. The third type uses a combination of both and is called "motion compensation" [2]. In this study, we used a motion compensation-based de-interlacing technique. First, we wrote an AVISynth script (AVISynth software, version 2.5.8) to separate the consecutive fields in VirtualDub and then used VirtualDub's smooth de-interlacer filter [3]. This filter de-interlaces the frames only where it's needed by simply looking for interlace lines in each frame individually. In non-interlaced areas (in static frames) two fields are combined to give a full resolution frame while in interlaced areas the current field is interpolated up to full frame size. The output of this filter was a 50 fps de-interlaced video. The outputs of an interlaced frame, de-interlaced frame and grayscale output of the de-interlaced frame are presented in figure 1a, 1b and 1c, respectively.

Segmentation

After editing the acquired video, segmentation of the lower limbs was performed in order to subtract the static background from the moving foreground. To this purpose, the Mixture of Gaussians (MoG) method was used. MoG uses statistical models while calculating the foreground and the pixels are modelled as a combination of Gaussian distributions instead of a single Gaussian [4]. MoG was preferred in this study since it handles illumination changes and deals with moving objects. An example of the output of the segmentation procedure is reported in figure 2a.

Skeletonization

Medial Axis Transform (MAT) was applied in order to "skeletonize" the segmentation outputs of the lower limbs. MAT is an iterative thinning operation where the pixels are eroded from the boundary until a skeleton is formed. The skeleton can be considered as the loci of the centers of the bi-tangent circles fit into the region [5].The skeleton of the segmented frame is shown in figure 2b.

Thresholding

To distinguish the high-cut underwear and the ankle socks, intensity values of the garments were used in thresholding. Thresholded garments can be seen in figure 2c.

Edge Detection and Extracting Body Segments

Following the thresholding, Robert's edge operator [6] was applied to the distinctive garments in order to find the edges. The outputs of the edge detection were overlapped with the skeletonization outputs so that the intersection points, which were used to define hip and ankle joint centers, were identified. Edged garments and intersection points can be seen in figure 3a and 3b, respectively.
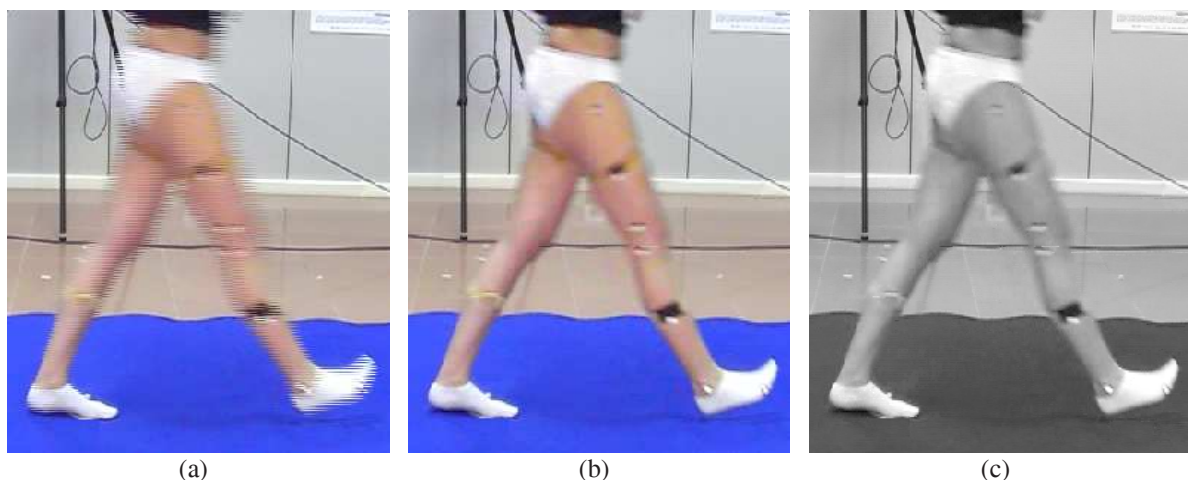

| (a) | (b) | (c) |

Figure 1. (a) Interlaced image. (b) De-interlaced image. (c) De-interlaced image converted to grayscale.
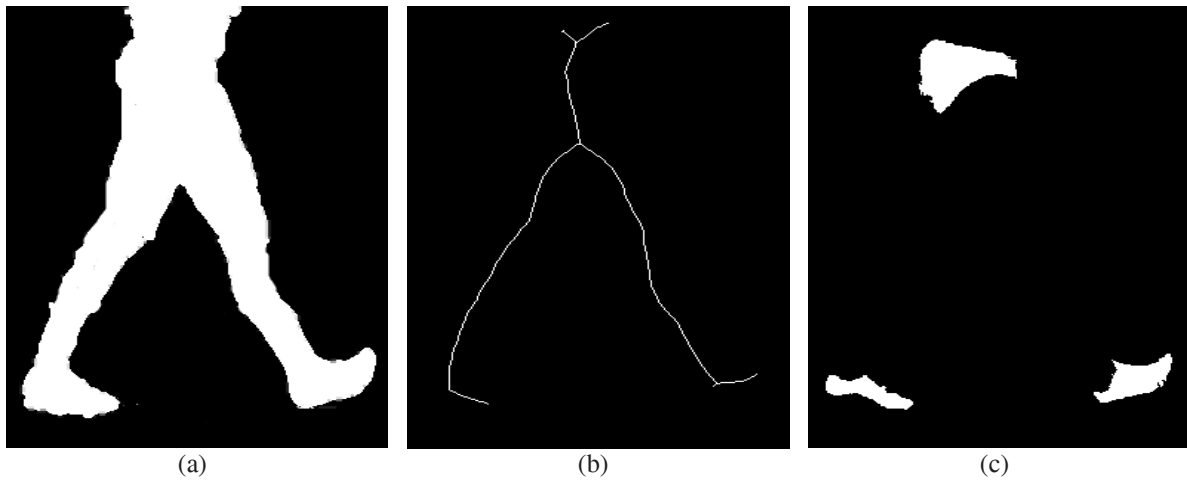
Figure 2. (a).Segmented frame. (b) Skeletonized frame. (c) Thresholded garments.
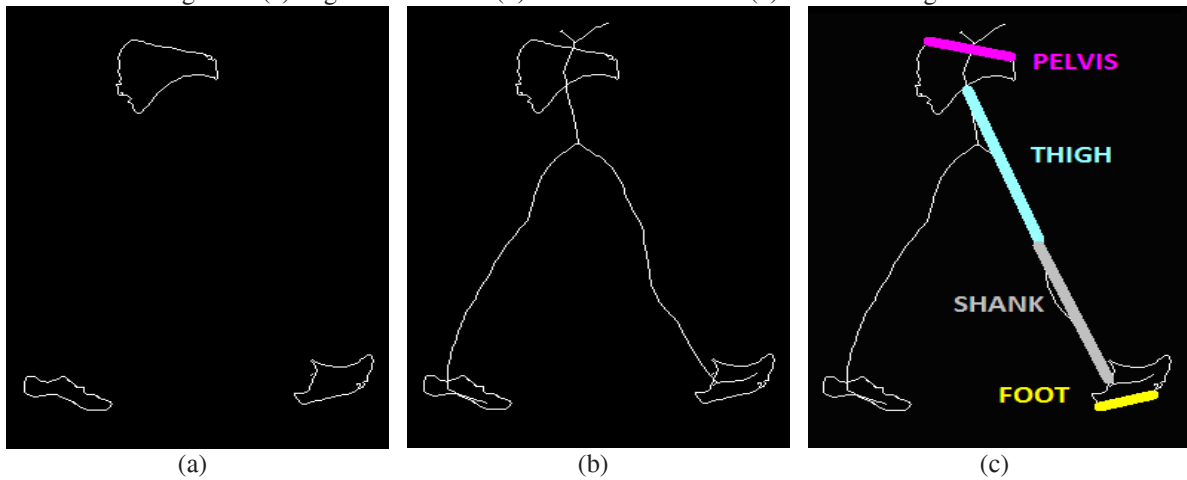

Figure 3. (a) Edged garments. (b) Intersection points. (c) The four reference axes fitted on the skeleton.

To define the thigh segment, a line was drawn from the hip joint center to the intersection of the circle of m1 radius and the skeletonized line of the leg. Similarly, to locate the shank, a line was drawn from the ankle joint center to the intersection of the circle of m2 radius with the skeletonized leg (figure 3c).

The pelvis reference axis was extracted by fitting a line to the upper edge of the underwear. The foot reference axis was extracted by fitting a line to the rear part of the lower edge of the sock. The four segment axes can be seen in figure 3c.

3.   RESULTS

Figures 4a, 4b and 4c show the resulting ankle plantar/dorsi-flexion (α), knee flexion/extension (β) and hip flexion/extension (γ). The blue lines represent the joint kinematics obtained using the *Hyb* technique while red lines represent the joint kinematics obtained using the *Mb* technique. The kinematic curves obtained using the *Hyb* and the *Mb* techniques were compared by computing the correlation and RMSD. Table 1 shows the values of RMSD relative to the lower limbs sagittal kinematics and correlation between the two techniques.

4.   DISCUSSION

The proposed hybrid method aims at providing clinicians with a practical, low-cost system for sagittal gait analysis.

The lower limb kinematics estimated with the *Hyb* and *Mb* techniques showed similar results throughout the gait cycle. While the knee and hip kinematics show similar patterns and high correlation, ankle kinematics has a lower correlation value (86%) which may stem from the less rigid structure of the foot and its reduced size.

In this study, the hybrid method was tested with a common video camcorder and the problems stemming from the de-interlacing and low frame rate have been dealt with. The study represents an important step towards the use of a common video camcorder as an alternative to a more expensive photogrammetric system. The proposed method has some limitations such as processing time. By using parallel processing, this limitation co uld be overcome.

(a)

(b)

(c)
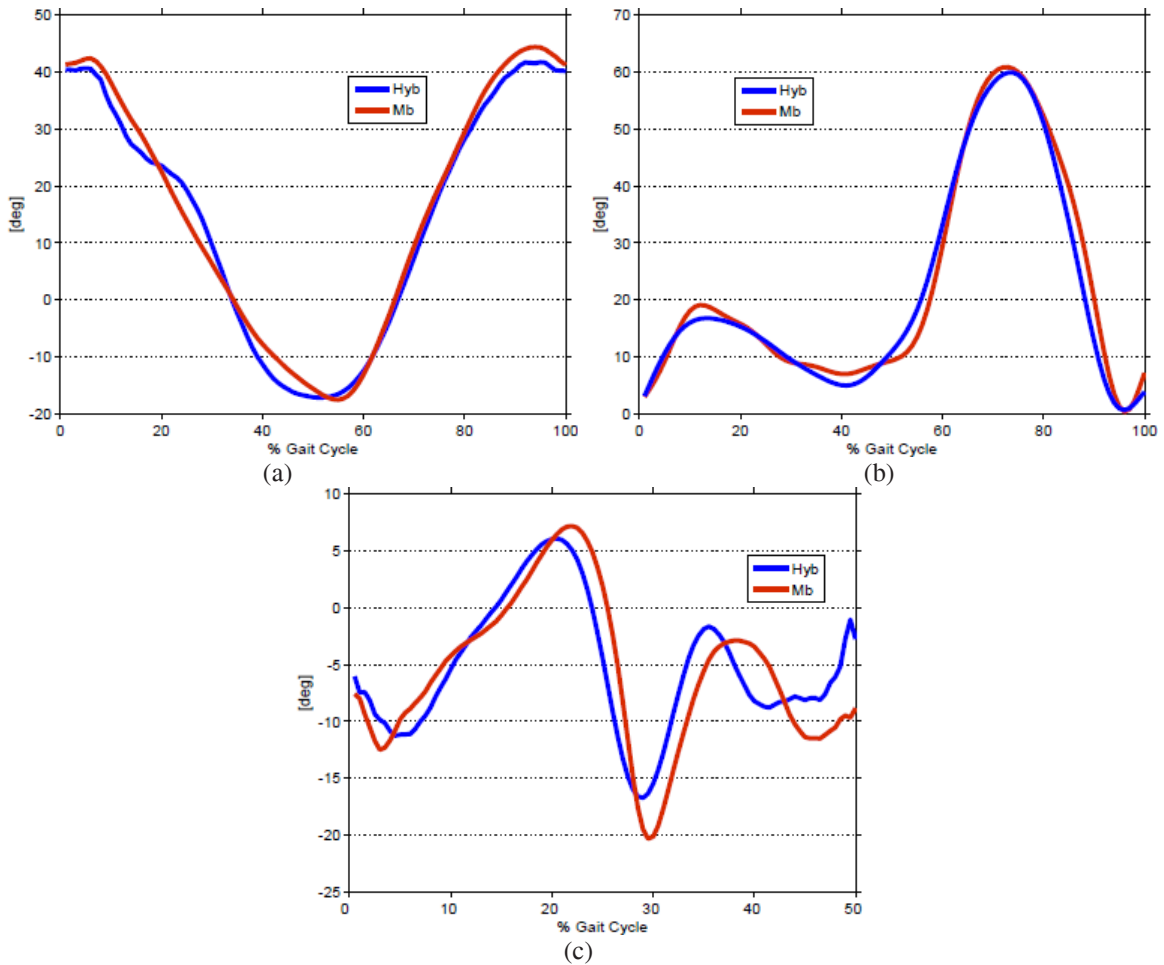
Figure 4. (a) Hip Flexion/Extension. (b) Knee Flexion/Extension. (c) Ankle Plantar/Dorsi-Flexion.

Table 1. RMSD and correlation values of the subject for the ankle plantar/dorsi-flexion (α), knee flexion/extension (β) and hip flexion/extension (γ) and the relevant correlation values.

	α	β	γ
RMSD	3.3	2.8	2.6
Correlation	0.86	0.98	0.98

5.   REFERENCES

[1] Surer, E, Kasi, P, Cereatti, A, Bonato, P, Della Croce, U, 2011. A hybrid markerless approach for 2D gait analysis: application to gait of children with cerebral palsy, 23rd Congress of International Society of Biomechanics (ISB'11), Brussels, Belgium.

[2] De Haan, G, Bellers, EB, 1998. Deinterlacing – an Overview, Proceedings of the IEEE, 86:9:1839-1857.

[3] Spot G, 2011. Deinterlace-smooth [Computer software], Available from: http://www.guthspot.se/video/index.htm#deinterlacesmooth

[4] Stauffer, C, Grimson, WEL, 1999. Adaptive background mixture models for realtime tracking. In: Proceedings of IEEE Conference on Computer Vision and Pattern Recognition, Ft. Collins, CO, USA, 2246-2252, 1999.

[5] Lam, L., Lee, S.W., Suen, C.Y, 1997. Thinning methodologies: a comprehensive survey. IEEE Transactions on Pattern Analysis and Machine Intelligence, 27:5:553-568, 1997.

[6] Roberts, L, 1965. Machine Perception of 3-D Solids, Optical and Electro-optical Information Processing, MIT Press, 1965.

Characterization of 3D Fluoroscopy calibration

Joint kinematics quantification sensitivity to calibration errors

Tersi L. [1], Fantozzi S. [1,2], Stagni R. [1,2]

[1] Health Sciences and Technologies - Interdepartmental Center for Industrial Research (HST – ICIR), University of Bologna, Bologna, Italy

[2] Department of Electronics, Computer Science, and Systems (DEIS), University of Bologna, Bologna, Italy

Model based 3D fluoroscopy can quantify joint kinematics with a mm/deg accuracy level. A calibration based on the acquisition of specific devices is usually applied to size the system. This study aimed at the characterization of the sensitivity of the pose estimation accuracy to errors in the calibration process, in order to evaluate a possible simplification of the calibration procedure. In-silico simulations were performed to analyze a data-set obtained adding controlled perturbation in the calibration process. The estimation of the rotations was scarcely influenced by calibration errors, while a linear trend was highlighted for translations with a sensitivity of 20% correspondent to approximately a 1 mm error for realistic calibration errors. This error is compensated when computing relative kinematics between two joint segments.

Human joint kinematics; 3D Fluoroscopy; Calibration; Computer simulation

1. INTRODUCTION

Several clinical [1–3], and methodological [4] applications are based on the accurate knowledge of in-vivo kinematics of intact and replaced joints. 3D fluoroscopy (3DF) is a technique that allows to accurately reconstruct joint kinematics, combining series of 2D X-ray fluoroscopic projections, and the knowledge of 3D geometric models of relevant bony segments or prosthetic components [5]. 3D models can be acquired using intact joints CT or MRI datasets, or prostheses CAD; 2D projections are typically gathered using clinical fluoroscopes and C-arms. C-arms, however, are designed to be easily moved inside the operating room for qualitative real-time imaging of internal body moving structures, and they are not meant for quantitative studies: the X-ray image intensifier is typically used to convert X-ray to visible images, but it is affected by sigmoidal and pincushion distortion, and the accuracy, with which the X-ray focus position is operatively set, is affected by the physical deformation of the C-arm [6] and dependent by the specific acquisition setup.

To step from qualitative to quantitative analysis, algorithms are applied to properly size a virtual model of the fluoroscope, to correct for image geometrical distortion, and to calibrate the position of the X-ray focus. The calibration is carried out with the acquisition of known geometry devices such as 2D calibration grid and 3D calibration cage. Once the calibration is performed, for each video frame of the acquisition, the 6 degrees of freedom (DOFs) absolute pose (3 translations and 3 rotations) of bony segments or prostheses is quantified moving the 3D model until it is best aligned to the relevant 2D image. This automatic procedure is carried out by means of optimization algorithms (e.g. Levenberg-Marquardt [7], genetic algorithm [8]) that optimize a metric quantifying the entity of the matching such as: (a) the euclidean distance between the contour of the virtual projection of the model and the contour extracted from the fluoroscopic image [9]; (b) the root mean square distance (RMSD) between the projection lines and the model surface [1]; and (c) similarity measures between the fluoroscopic image and digitally reconstructed radiographies (DRRs) [8].

3DF theoretically permits to achieve a millimeter/degree accuracy level in joint motion analysis (for the intact knee joint: 0.2 mm for translation, 1.2 deg for rotation with bi-planar fluoroscopy [10]; and 0.4 mm for in-plane and 5.6 mm for out-of-plane translations, 1.3 deg for rotation for mono-planar fluoroscopy [11]). Several sources of error contribute to this accuracy and were previously characterized: local optima of the metric [12], segmentation inaccuracies [14], symmetries of the models [12], geometrical distortions [15]. Conversely, the extent to which X-ray focus calibration affects the reliability of the measurements has not been clarified yet. Some authors proposed to assume the X-ray focus centered in the image plane and to consider valid the focus distance provided by the fluoroscope [16]. This assumption may be useful to simplify the 3DF setup and analysis, especially for clinical applications, but neglecting the calibration may lead to a further loss of accuracy of the measurements.

The present work is aimed at the in-silico characterization of the calibration, specifically investigating the sensitivity of the accuracy of 3DF to X-ray focus calibration error.

2. MATERIAL & METHODS

In order to quantify the sensitivity of the 6 DOFs estimation to focus calibration error, a synthetic data-set of reference images was created with 3D models and focus in known position. A controlled calibration error for the focus was simulated and the model pose was estimated. Discrepancies between the known and estimated poses were quantified and related to the imposed calibration error.

Data-set

The acquisition system was outlined defining a global reference frame with x and y axes parallel, z-axis perpendicular to the image plane, and with the origin in the center of the image plane. The X-ray source was virtually placed in:

$$F_{ref} = (F_x, F_y, F_z) = (0, 0, 1000) \text{ mm} \qquad (1)$$

representing a typical distance of a standard fluoroscope, and pixel spacing was fixed at 0.3 mm, as for 315x315 mm FOV, and 1024x1024 pixel image. No geometrical distortion was considered as already successfully investigated in a previous study [15].

High resolution models of humerus, ulna, and radius were downloaded from the official site of the European project VAKHUM (contract #IST-1999-10954 [17]) and used to generate the controlled fluoroscopic dataset. An anatomical reference frame was associated to each bone model according to the ISB recommendations [18], and the Euler zxy convention was adopted for rotations. Each model was placed in 3 reference random poses:

$$P_{ref} = [T_x, T_y, T_z, O_x, O_y, O_z]_{ref} \qquad (2)$$

and flat shaded projections were generated.

Pose estimation algorithm

The implemented alignment algorithm was based on 3D surface models and adaptive distance maps (DM) with a resolution of 0.5 mm [12]. The pose was estimated minimizing with a memetic algorithm [13] the euclidean root mean square distance (RMSD) between the surface model and the beam of lines connecting the X-ray source focus and the edge of the bone, extracted in the projected image. The memetic algorithm considered a 18 bits Gray binary code for each DOF, 100 individuals, a mutation weight of 5%, an ageing factor of 2%, a total multi-point crossover, a local learning simulated with the Levenberg-Marquardt algorithm applied to the 5% of the population, and a stop criterion of 15 generations without reduction of the cost function. The reliability of the pose estimation algorithm was previously evaluated in [13].

Data analysis

For each 3D model, 375 alignments were carried out to estimate the pose:

$$P_{est} = [T_x, T_y, T_z, O_x, O_y, O_z]_{est} \qquad (3)$$

considering the perturbed focus position in the permutation:

$$F_{per} = F_{ref} + \Delta F \qquad (4)$$

with:

$$\Delta F_x = [-5, -1, 0, 1, 5] \text{ mm} \qquad (5)$$

$$\Delta F_y = [-5, -1, 0, 1, 5] \text{ mm} \qquad (6)$$

$$\Delta F_z = [-10, -2, 0, 2, 10] \text{ mm} \qquad (7)$$

representing ranges of typical calibration errors, and using the contour extracted from the flat shaded reference images.

The deviation between estimated and reference pose was quantified as:

$$\Delta P = P_{est} - P_{ref} \qquad (8)$$

The n-way ANOVA ($\alpha = 0.01$) was used to assess significant effects of bone model, reference pose, and focus

Table 1. Sensitivity as the slope (S) of the linear regression of the estimation error ΔP of the humerus bone model against the imposed calibration uncertainty ΔF, and relevant coefficient of determination (R^2).

DOF	F_x			F_y			F_z		
	S	R^2		S	R^2		S	R^2	
T_x [mm/mm]	0.20	0.90	*	0.00	0.00	*	0.00	0.00	*
T_y [mm/mm]	0.00	0.00		0.20	0.98	*	0.00	0.00	
T_z [mm/mm]	0.01	0.00		0.05	0.00	*	0.21	0.09	*
O_x [deg/mm]	0.00	0.00		-0.05	0.29	*	0.00	0.00	*
O_y [deg/mm]	0.06	0.88	*	0.00	0.00	*	0.00	0.00	*
O_z [deg/mm]	0.00	0.00		0.00	0.00	*	0.00	0.00	

*ANOVA P-value<0.01

calibration error on the pose estimation error for each DOF. To quantify the entity of the effect, the sensitivity of the estimation of each DOF was determined as the slope ($S=\Delta P/\Delta F$) of the fitting linear regression of data. The coefficient of determination (R^2) was also reported.

3. RESULTS

A statistically significant effect (P<0.01) of the three random reference poses on the estimation error of each DOF was highlighted: the pose with the smaller portion of visible bone in the FOV produced larger errors. ANOVA highlighted also that a significant effect of the bone model: the radius showed a largest bias and dispersion of P_{est} (best case scenario 0±0.2deg for O_z, worst case scenario 6±5mm for T_z).

The perturbation ΔF_y (y axis nearly parallel with the bone longitudinal axis) had a significant effect on all the DOF estimations, while ΔF_x affected T_x and O_y, and ΔF_z influenced T_x, T_z, O_x, O_y and O_z. Notwithstanding these statistically significant differences, only in few cases a correlation trend was found in the data. In particular, any calibration error in one direction is reflected in a concordant error in the estimation of the translation in the same direction approximately equal to the 20% of the calibration error. The coefficient of determination R^2 is larger than 0.90 for T_x and T_y, but equal to 0.09 for T_z. The rotation around the projection axis O_z is not linearly dependent on ΔF but a small correlation is found between O_y and ΔF_x and between O_x and ΔF_y. Table 1 resumes the results for the humerus bone model.

4. DISCUSSION

The effect of 3DF calibration error on the pose estimation accuracy was evaluated considering in-silico simulations. A robust memetic algorithm was used for the optimization in order to reduce the effects of uncertainties related to local minima in the metric.

The reference pose, and bone model had a significant effect on the results due to the intrinsic symmetries of the reference model and of the generated contours. The simulated calibration errors (ΔF) significantly affected the estimation of several degree of freedom, but only in few cases a correlation pattern was highlighted. A linear correlation with a sensitivity of approximately 20% was found between the calibration error in one direction and the estimation of the concordant translation. However, the coefficient of determination R^2 was small for T_z due to the intrinsic variability of the estimation of the translation along the projection axis z [12]. A linear correlation was found also between ΔF_x and O_y but with low sensitivity (0.06 deg/mm) and thus with a small impact in pose estimation accuracy.

Concluding, calibration errors mainly affected the estimation of the translations: typical calibration error of 5 mm in x, and y directions, are reflected in a pose estimation error of 1 mm in the same directions. When relative kinematics is computed, the effect of the calibration error on the two joint segments is expected to be compensated due to the linearity of the relation. The effect on the rotations is statistically significant but of low intensity. Calibration errors affect 3DF accuracy, but it might be disregarded when sub-millimeter accuracy is not needed, as for potential clinical application.

6.   REFERENCES

[1]   S. Zuffi, A. Leardini, F. Catani, S. Fantozzi, and A. Cappello, "A model-based method for the reconstruction of total knee replacement kinematics," *Medical Imaging, IEEE Transactions on*, vol. 18, no. 10, pp. 981-991, 1999.

[2]   S. Hirokawa, M. Abrar Hossain, Y. Kihara, and S. Ariyoshi, "A 3D kinematic estimation of knee prosthesis using X-ray projection images: clinical assessment of the improved algorithm for fluoroscopy images," *Medical and Biological Engineering and Computing*, vol. 46, no. 12, pp. 1253-1262, Dicembre 2008.

[3]   P. M. Ludewig and J. E. Reynolds, "The association of scapular kinematics and glenohumeral joint pathologies," *The Journal of Orthopaedic and Sports Physical Therapy*, vol. 39, no. 2, pp. 90-104, Feb. 2009.

[4]   R. Stagni, S. Fantozzi, and A. Cappello, "Double calibration vs. global optimisation: Performance and effectiveness for clinical application," *Gait & Posture*, vol. 29, no. 1, pp. 119-122, Gennaio 2009.

[5]   S. A. Banks and W. A. Hodge, "Accurate measurement of three-dimensional knee replacement kinematics using single-plane fluoroscopy," *IEEE Transactions on Bio-Medical Engineering*, vol. 43, no. 6, pp. 638-49, Jun. 1996.

[6]   L. P. Nolte et al., "A new approach to computer-aided spine surgery: fluoroscopy-based surgical navigation," *European Spine Journal: Official Publication of the European Spine Society, the European Spinal Deformity Society, and the European Section of the Cervical Spine Research Society*, vol. 9 Suppl 1, pp. S78-88, Feb. 2000.

[7]   D. W. Marquardt, "An Algorithm for Least-Squares Estimation of Nonlinear Parameters," *Journal of the Society for Industrial and Applied Mathematics*, vol. 11, no. 2, pp. 431-441, Jun. 1963.

[8]   T.-Y. Tsai, T.-W. Lu, C.-M. Chen, M.-Y. Kuo, and H.-C. Hsu, "A volumetric model-based 2D to 3D registration method for measuring kinematics of natural knees with single-plane fluoroscopy," *Medical Physics*, vol. 37, no. 3, pp. 1273-1284, Mar. 2010.

[9]   W. A. Hoff, R. D. Komistek, D. A. Dennis, S. M. Gabriel, and S. A. Walker, "Three-dimensional determination of femoral-tibial contact positions under in vivo conditions using fluoroscopy," *Clinical Biomechanics*, vol. 13, no. 7, pp. 455-472, Ottobre 1998.

[10]   B.-M. You, P. Siy, W. Anderst, and S. Tashman, "In vivo measurement of 3-D skeletal kinematics from sequences of biplane radiographs: Application to knee kinematics," *Medical Imaging, IEEE Transactions on*, vol. 20, no. 6, pp. 514-525, 2001.

[11]   B. J. Fregly, H. A. Rahman, and S. A. Banks, "Theoretical Accuracy of Model-Based Shape Matching for Measuring Natural Knee Kinematics with Single-Plane Fluoroscopy," *Journal of biomechanical engineering*, vol. 127, no. 4, pp. 692–699, Aug. 2005.

[12]   L. Tersi, S. Fantozzi, and R. Stagni, "3D elbow kinematics with mono-planar fluoroscopy: in-silico evaluation," *EURASIP Journal on Advances in Signal Processing*, vol. 2010, 2010.

[13]   L. Tersi, R. Stagni, S. Fantozzi, and A. Cappello, "Genetic Algorithm as a robust method for the joint kinematics estimation with mono-planar 3D fluoroscopy," presented at the XVII ESB Conference, Edinburgh, Scotland UK, 2010.

[14]   M. R. Mahfouz, W. A. Hoff, R. D. Komistek, and D. A. Dennis, "Effect of segmentation errors on 3D-to-2D registration of implant models in X-ray images," *Journal of Biomechanics*, vol. 38, no. 2, pp. 229-239, Feb. 2005.

[15]   E. Gronenschild, "The accuracy and reproducibility of a global method to correct for geometric image distortion in the x-ray imaging chain," *Medical Physics*, vol. 24, no. 12, pp. 1875-1888, Dec. 1997.

[16]   M. S. Zihlmann, H. Gerber, A. Stacoff, K. Burckhardt, G. Székely, and E. Stüssi, "Three-dimensional kinematics and kinetics of total knee arthroplasty during level walking using single plane video-fluoroscopy and force plates: A pilot study," *Gait & Posture*, vol. 24, no. 4, pp. 475-481, Dec. 2006.

[17]   "Virtual Animation of the Kinematics of the Human for Industrial, Educational and Research Purposes." [Online]. Available: http://www.ulb.ac.be/project/vakhum/public_dataset/public-data.htm. [Accessed: 03-Aug-2009].

[18]   G. Wu et al., "ISB recommendation on definitions of joint coordinate systems of various joints for the reporting of human joint motion--Part II: shoulder, elbow, wrist and hand," *Journal of Biomechanics*, vol. 38, no. 5, pp. 981-992, Maggio 2005.

Accuracy assesment of scapular motion estimation using acromion marker cluster

Cereatti A.[1], Rosso C.[2], Nazarian A.[3], Della Croce U.[1]

[1] Department of Information Technology and Social Sciences, University of Sassari, Sassari, Italy
[2] Orthopaedic Department, University Hospital Basel, University of Basel, Switzerland
[3] Center for Advanced Orthopaedic Studies, Beth Israel Deaconess Medical Center and Harvard Medical School, Boston, MA, USA

Scapula tracking is critical due to the detrimental effect of soft tissue artifacts. Recently, a non-invasive method for the estimate of the scapula kinematics, based on the use of an acromion skin marker cluster (ASC), was proposed. The aim of the present study was to quantify the accuracy of the ASC method by using intra-cortical pins in ex vivo experiments as a gold standard. Scapula motion was analyzed while a robotic system elevated the humerus of one specimen both in the sagittal and frontal planes. In every trial, the scapular motion resulted consistently overestimated. For arm elevations up to 90 deg errors were acceptable (<7 deg), while they increased dramatically, when the humerus elevation reached 145 deg (up to 46 deg error). Therefore, the use of the ASC provides reliable results only for a reduced shoulder range of motion.

Keywords: *3D kinematics; Scapula; Acromion; Accuracy validation*

1. INTRODUCTION

Non invasive methods for the measurement of the absolute or relative motion of the scapula are required for a large variety of clinical and sport applications [1] for which a three-dimensional kinematics, along with a high level of accuracy, is required. A commonly used technique for recording scapular motion is to rely on surface-mounted electromagnetic motion sensors [2,3]. However, the presence of soft tissue artefact limits the ability of the latter non invasive approaches in the accurate description of the scapula motion [4], especially for a reduced range of gleno-humeral joint motions and multi-joints movements such as pitching [5]. Recently, to minimize the influence of soft tissue artifacts, van Andel and colleagues [6] have proposed the use of a special acromion skin marker cluster (ASC) which can be placed to the flat part of the acromion. The accuracy of the scapular kinematics estimated using the ASC was assessed using the scapula locator as gold standard [7,8]. However, since the three dimensional scapula kinematics estimated using the scapula locator is also prone to error, a more reliable gold standard is needed for an accurate quantification of the errors associated to the ASC method [6,9]. The aim of the present study was to quantify the ASC method accuracy in estimating the scapula kinematics for different types of shoulder movements using intra-cortical pins in ex vivo experiments as gold standard.

2. MATERIAL AND METHODS

Specimen

Experiments were carried out on a single fresh frozen specimen, acquired from Medcure Anatomical Tissue Bank (Orlando, FL, USA), which included trunk and arms. No detectable degenerative damages to the shoulder complex were present. The cadaver height and weight were 1.83 m and 95 kg, respectively.

Experimental set-up

The shoulder complex movement was generated using a robotic system consisting in a fixed and a moving metal frame. The moving frame can translate and rotate along the X, Y and Z directions. Its motion is driven by actuators activated via a programmable central controller. The torso was mounted onto a rod fixture and held in place with volume expanding foam to provide a support construct. The rod fixture was attached to the fixed frame. The moving frame was secured to the radius and the ulna using a Schanz pin. Two pins (transosseous bi-cortical) were implanted into the humeral diaphysis, and into the sternum. Each steel pin (6mm in diameter) was equipped with a four marker cluster. The minimal distance between two markers of the same cluster was 50 mm. Prior to inserting the pins into the bones, cruciform incisions were made through the skin and soft tissue to reduce forces applied to the pins. For the scapula, two different acromion marker clusters were used: an acromion bone marker cluster (ABC) and an ASC. Both ABC and ASC were made of a light carbonium

frame and were equipped with a four marker cluster. The minimal distance between two markers of the same cluster was 70 mm. The frame was attached to a triangular base specifically shaped to be attached to the flat part of the acromion (triangle dimensions: 32 mm x 25 mm x17 mm). The base of the ASC was made of deformable plastic and was attached using adhesive tape. The total weight of the ASC was 5.7 g. The base of the ABC was made in alloy and was attached to the acromion using three wood screws (4x10 mm). The instantaneous position in a global frame of the markers was reconstructed using a 5-camera stereo-photogrammetric system (Qualisys ProReflex) acquiring at 120 Hz. The measurement volume was a 1.5-m-sided cube. Thorax, humerus and scapula anatomical landmarks were calibrated using a pointer equipped with a cluster of four markers and anatomical system of references were defined according to the ISB suggestion [10,11] while the humerus of the cadaver was elevated in the sagittal plane of 20 deg. The glenohumeral center was determined according to the regressive equation proposed by Meskers and colleagues [12].

Types of motion

The following types of motions were investigated:

- Humerus elevation in the sagittal plane from 50 deg to 145 deg (HES) with the elbow in full extension;

- Humerus elevation in the frontal plane from 90 deg to 145 deg (HEF) with the elbow in full extension.

For each type of movement, two trials were recorded using the ABC and ASC, respectively.

Data analysis

To describe the angular kinematics between the scapula-thorax and humerus-thorax joints motion, the attitude vector notation ($\theta = \theta\mathbf{n}$) was used [13]. The scapula-thorax angular components were derived by projecting $\theta_{s\text{-}t}$ along the thorax axes and were represented as a function of the humerus-thorax scalar rotation $\theta_{h\text{-}t}$. The scapula kinematics estimated using the ABC, which was not affected by soft tissue artifacts, was used as gold standard to assess the errors associated to the scapula movement estimated using the ASC.

For each movement, the error associated to the ASC estimates were computed as:

$$\mathbf{e}(\theta_{h-t}) = \begin{pmatrix} e_1(\theta_{h-t}) \\ e_2(\theta_{h-t}) \\ e_3(\theta_{h-t}) \end{pmatrix} = \begin{pmatrix} \theta_{1\_s-t}^{ABC}(\theta_{h-t}) - \theta_{1\_s-t}^{ASC}(\theta_{h-t}) \\ \theta_{2\_s-t}^{ABC}(\theta_{h-t}) - \theta_{2\_s-t}^{ASC}(\theta_{h-t}) \\ \theta_{3\_s-t}^{ABC}(\theta_{h-t}) - \theta_{3\_s-t}^{ASC}(\theta_{h-t}) \end{pmatrix} \qquad (1)$$

where θ_{1_s-t}, θ_{2_s-t}, θ_{3_s-t} represent the components of the attitude vector $\theta_{s\text{-}t}$ with respect to the antero-posterior, the vertical and medio-lateral axes of the thorax system of reference, respectively.

The repeatability and reliability of the scapula movements generated by the robotic system were assessed by comparing the scapula kinematics between the two trials recorded using the ABC and the two trials recorded using the ASC.

3. RESULTS

When using the ABC, the mean absolute differences of the three angular components ($\theta_{1\_s-t}^{ABC}$, $\theta_{2\_s-t}^{ABC}$, $\theta_{3\_s-t}^{ABC}$) between two recorded trials were 0.3 deg, 0.2 deg, 0.1 deg, respectively, for the HES and 0.4 deg, 0.3 deg, 0.3 deg, respectively, for the HEF. When using ASC, the mean of the absolute difference of the three angular components of the scapula-thorax kinematics were 0.4 deg, 0.1 deg, 0.2 deg respectively, for the HES and 3.3 deg, 2.1 deg, 1.3 deg, respectively, for the HEF. The scapula-thorax angular components estimated using ASC and ABC are depicted for the HES and HEF motion in Fig. 1. Overall, motions, errors $\mathbf{e}(\theta_{h-t})$ increased as the humerus elevation angle increased.
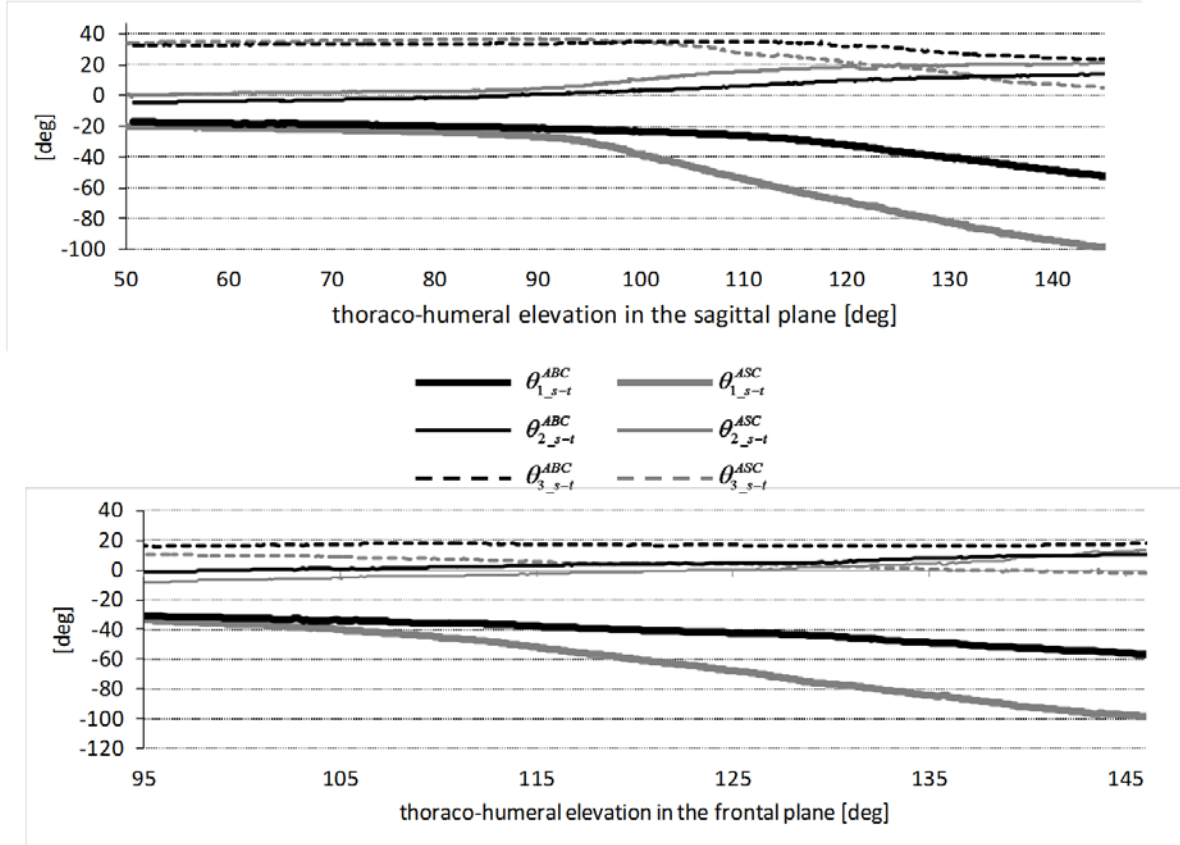
Figure 1. The scapula-thorax angular components estimated using ASC (gray lines) and ABC (black lines) expressed as function of the humerus-thorax scalar rotation for the HES and HES motions.

At the beginning and at the end of the HES motion (50 deg $< \theta_{h-t} <$ 145 deg), the errors were -2.9 deg and -46.6 deg for e_1, -2.0 deg and -18.8 deg for e_2, 4.7 deg and 7.3 deg for e_3, respectively. During the HES motion, for all angular components, error magnitudes were small and almost constant for $\theta_{h-t} <$ 90 deg. The highest errors were observed in correspondence of θ_{1_s-t}. At the beginning and at the end of the HFS motion (90 deg $< \theta_{h-t} <$ 145 deg), the errors were equal to -3.6 deg and -41.7 deg for e_1, -3.2 deg and -20.7 deg for e_2, -7.0 deg and 2.5 deg for e_3, respectively. The highest errors were observed in correspondence of θ_{1_s-t}.

4.   DISCUSSION

The estimate of scapular motion using skin markers is heavily affected by the presence of soft tissue artifacts due to the sliding of the scapula under the skin and muscles especially when the shoulder full range of motion is explored [6,9]. In the present paper, for the first time, the accuracy of the scapula kinematic obtained using a recently developed acromion tracker [6] was assessed during a continuous shoulder complex motion. The movement of the shoulder complex was generated using a robotic system which allowed to repeat selected types of motion in different experimental conditions [14]. The effectiveness of the robotic system was demonstrated by the negligible differences observed in scapula motion between trials. When the scapula motion was tracked using the bone cluster (ABC), mean angular differences between movement repetitions were less than 0.4 deg. During humerus elevation in the sagittal and frontal plane, errors were 7 deg or lower when humeral elevation did not exceed 90 deg. These findings were consistent with those reported in previous studies [3,6,15]. Conversely, errors dramatically increased when more extreme shoulder range of motion were tested. The largest errors, up to 47 deg, were found in the estimates of the upward and downward rotations, followed by errors in the scapular winging estimates up to -21 deg. Scapular movements estimated using the acromion skin cluster were consistently overestimated. Especially above 90 deg of humerus elevation, muscles and skin stretching lead to a loss of contact between the ASC and the acromion thus causing an extra undesired movement of the ASC with respect to the underlying scapula bone. These latter observation partially contradicts the conclusion reported by Van Andel and colleagues [6]. It is important to stress that the magnitude of the angular errors, computed as difference between the scapula kinematics estimated using the

ABC and ASC, depends on the shoulder kinematic configuration during which the anatomical calibration was performed [9]. In conclusion, the use of the ASC provides reliable results only for humeral elevation below 90 deg. When the humeral elevation exceed 90 deg, the effect of the soft tissue artifacts are overwhelming and countermeasures, such as double calibration techniques, should be applied [9]. For the sake of a thorough validation of the ASC method, a higher number of specimens and different types of motions will be acquired in the future.

5. REFERENCES

[1] B. Forthomme, J.M. Crielaard, J.L. Croisier, 2008. Scapular positioning in athlete's shoulder: particularities, clinical measurements and implications. Sports Medicine 38(5), 369-86.

[2] K.N. An, A.O. Browne, S. Korinek, S. Tanaka, B. F Morrey, 1991. Three-Dimensional Kinematics of Glenohumeral Elevation. J. Orthop. Res. 91, 143–149.

[3] A.R. Karduna, P.W. McClure, L.A. Michener, B. Sennett, 2001. Dynamic measurements of three-dimensional scapular kinematics: a validation study. J Biomech. Eng. 123(2), 184–90.

[4] M.J Bey, R. Zauel, S.K. Brock, S. Tashman, 2006. Validation of a new model-based tracking technique for measuring three-dimensional, in vivo glenohumeral joint kinematics. J Biomech. Eng. 128(4), 604–9.

[5] J.B. Myers, K.G. Laudner, M.R. Pasquale, J.P. Bradley, S.M. Lephart, 2005. Scapular position and orientation in throwing athletes. Am. J. Sports Med. 33(2), 263-71.

[6] C. van Andel, K. van Hutten, M. Eversdijk, D. Veeger, J. Harlaar, 2009. Recording scapular motion using an acromion marker cluster. Gait and Posture 29 (1), 123–128.

[7] G.R. Johnson, P.R. Stuart, S. Mitchell, 1993. A method for the measurement of 3-dimensional scapular movement. Clin. Biomech. 8(5), 269–73.

[8] N.D. Barnett, R.D. Duncan, G.R. Johnson, 1999. The measurement of three dimensional scapulohumeral kinematics—a study of reliability. Clin. Biomech. 14(4), 287–90.

[9] S. Brochard, M. Lempereur, O. Rémy-Néris, 2011. Double calibration: An accurate, reliable and easy-to-use method for 3D scapular motion analysis. J. Biomechanics 44(4), 751-4.

[10] A. Cappozzo, F. Catani, U. Della Croce, A. Leardini, 1995. Position and orientation of bones during movement: anatomical frame definition and determination. Clin. Biomech. 10, 171–8.

[11] G. Wu, F.C. van der Helm, H.E. Veeger, M. Makhsous, P. Van Roy, C. Anglin, et al., 2005. ISB recommendation on definitions of joint coordinate systems of various joints for the reporting of human joint motion–Part II: shoulder, elbow, wrist and hand. J. Biomech. 38 (5), 981–992.

[12] C.G. Meskers, H.M. Vermeulen, J.H. de Groot, F.C. van Der Helm, P.M. Rozing, 1998. 3D shoulder position measurements using a six-degree-of-freedom electromagnetic tracking device. Clin. Biomech. 13 , 280–292.

[13] H.J. Woltring, 1994. 3-D attitude representation of human joints: a standardization proposal. J. Biomechanics 27(12), 1399-414.

[14] V. Entezari, A. Nazarian, C. Rosso, V. Entezari, U. Della Croce, A. Cereatti et al., 2012. Design and Manufacture of A Novel System to Simulate the Real Time Biomechanics of Basic and Pitching Shoulder Motion using a Cadaveric Model. Unpublished.

[15] C.G. Meskers, M.A. van de Sande, J.H. de Groot, 2007. Comparison between tripod and skin-fixed recording of scapular motion. J. Biomechanics 40 (4), 941–946.

Comparison of three different methods for hand segment coordinate system definition.

Goislard de Monsabert B. [1,2], Visser J.M.A. [2], Veeger H.E.J. [2,3], van der Helm F.C.T. [2]

[1] Institute of Movement Sciences, Aix-Marseille Univ, Marseille, France, benjamin.demonsabert@gmail.com
[2] Department of BioMechanical Engineering, Delft University of Technology, Delft, The Netherlands
[3] Research Institute MOVE, VU Amsterdam, Amsterdam, The Netherlands

The present study is working toward an extension to the ISB segmental definitions for the hand. Three options for the calculation of Segment Coordinate Systems will be compared. The Reference method is only aligning segments with the global coordinate system. The Bony Landmarks method is based on the position of bony landmarks. The Helical Axis method is computing flexion-extension axes from instantaneous helical axes. SCS orientations from the Bony Landmarks and Reference methods were similar and output joint angles showed comparable patterns and ranges of motions. The Helical Axis method resulted also in similar joint angle evolutions for the flexion-extension but showed the smallest ranges of motion on secondary and tertiary rotation components. In conclusion, all three methods provide a good estimation of large amplitude motions for one degree of freedom, but the Helical Axis method is the best choice to study all three joint rotations at the same time.

Segment coordinate system (SCS); Euler angles; helical axis; joint angles; 3D kinematics.

1. INTRODUCTION

Assessment of finger and wrist joint angles is important for several domains like hand rehabilitation medicine [1], biomechanical modeling [2] or handle ergonomics [3]. Because the hand is a complex system with small segments, measuring its kinematics is difficult. Even for a simple daily task such as grasping a door handle, more than fifteen joints are involved for the motion of the five fingers and the wrist.

In the literature, the simplest methods for the computation of finger joint angles use spatial projections with vectors and planes defined by landmarks [4], [5] whereas in the most complicated cases, optimization procedures were used to assess center or axes of rotation [6], [7]. Wu et al. [8] provided a set of segment coordinate system (SCS) for hand and wrist joints kinematic analysis but the definitions concerning the finger segments were not complete. The present study is working toward an extension to the segmental definition proposed by Wu et al. [8]. For this purpose, three SCS computation methods will be compared on the occurrence of secondary and tertiary rotations for a single degree of freedom (DoF) motion.

2. MATERIAL AND METHOD

Subject, apparatus and tasks

One subject (Gender: female, age: 31 yrs, height: 1.79m) with no history of trauma or pathologies to the right upper limb participated in this experiment. Kinematic data of the forearm and the thumb, index and middle fingers was recorded at a sampling rate of 50 Hz using three Optotrak (Northern Digital Inc., Canada, nominal accuracy 0.3 mm) camera sets and 33 active markers (Fig. 1). First, the subject was asked to take a neutral posture with the forearm and hand on a surface, defined as the X-Y plane (i.e. Z is vertically up). As defined in [8], for the wrist, the third metacarpal was aligned with the long axis of the forearm, for the middle and index fingers, all phalanges were aligned with each others and also with the long axis of the forearm. For the thumb, all phalanges were aligned with each other and oriented at 35° of abduction of the third metacarpal [9]. Then, 19 bony landmarks (BLM) on hand and forearm segments were palpated using a six-marker pointer.

After that, calibration motions were performed by the subject for determination of helical flexion-extension (F-E) axes of the middle finger metacarpophalangeal (MCP3), proximal interphalangeal (PIP3) and distal interphalangeal (DIP3) joints. Finally, the subject executed one test motion that consisted in a repetitive back-and-forth motion between maximal flexion and maximal extension of all metacarpophalangeal joints at the same time. Other joints were kept straight.

Data processing

For all three methods, general SCS orientations were defined as follows: X was the flexion-extension (F-E) axis and was radially oriented, Y was the pronation-supination (P-S) axis and was proximally oriented and Z was the abduction-adduction (A-A) axis and was dorsally oriented. In that way, flexion, abduction and pronation corresponded to positive joint angles.

Figure 1. Marker set used to record kinematic data of the forearm and the thumb, index and middle fingers.

Three different methods were used for axes definitions:

- The "Reference" method consisted in aligning the forearm and hand SCSs with the global coordinate system defined during calibration of Optotrak cameras. In that way, in the initial neutral posture all joint angles were set to 0°.
- The "BLM" method was based on the study of Wu et al. [8]. Two dorsal bony landmarks corresponding to proximal and distal segment extremities were used to compute the Y axis and a local sagittal plane was defined using the global Z.
- Finally, the "Helical Axis" method consisted in finding the F-E (X) axis by first computing the instantaneous helical axis (IHA) [10]. Then, from these IHAs, an optimal direction vector and a point on this vector were calculated [10]. In this method, the vector going from proximal landmark to distal landmark was used to define the coronal plane.

For all methods, the rotation matrix between distal (mobile system) and proximal (fixed system) SCS was computed and joint angles were extracted using an Euler rotation decomposition with X (F-E), Z (A-A), Y (P-S) as rotation sequence.

Result analysis

For this study, only the third metacarpal and the middle finger proximal and middle phalanges were analyzed. To analyze the output joint angles on one DoF, the range of motion (RoM) was computed for each method as the difference between the maximum and the minimum angles obtained for the DoF considered.

3.   RESULTS

Segment Coordinate Systems

Fig. 2A shows F-E axes obtained with the Helical Axis method. For all joints, the IHAs showed some variations in direction. These variations were similar with mean errors of respectively 8.5°, 8.6°and 9.2° for the MCP3, PIP3 and DIP3 joints. Figure 2B shows the SCSs resulting from the three different methods. BLM SCS axes were always less rotated from the Reference SCS than the Helical SCS axes were.

Joint angles

Fig. 3A shows the output PIP3 joint angles of the three different methods corresponding to F-E motions used for the Helical Axis method. And the Table 1 presents the associated RoMs and maximal angles. For the F-E DoF, evolution patterns and RoMs were similar for the three methods. The Reference method presented an offset of approximately 10° with the other methods. On second and third DoFs, the Helical Axis method presented the smallest RoMs and an offset of approximately 10° with the other methods.

Fig. 3B shows the output MCP3 joint angles of the three different methods corresponding to the F-E test motion. The associated maximal angles and RoMs are presented in the Table 2. For the F-E DoF, similar evolution patterns and RoMs were obtained with the three methods. The Reference method resulted in an offset of approximately 10° with the other methods. On second and third DoFs, the Helical Axis method resulted in a smaller RoM only for the A-A joint angle.
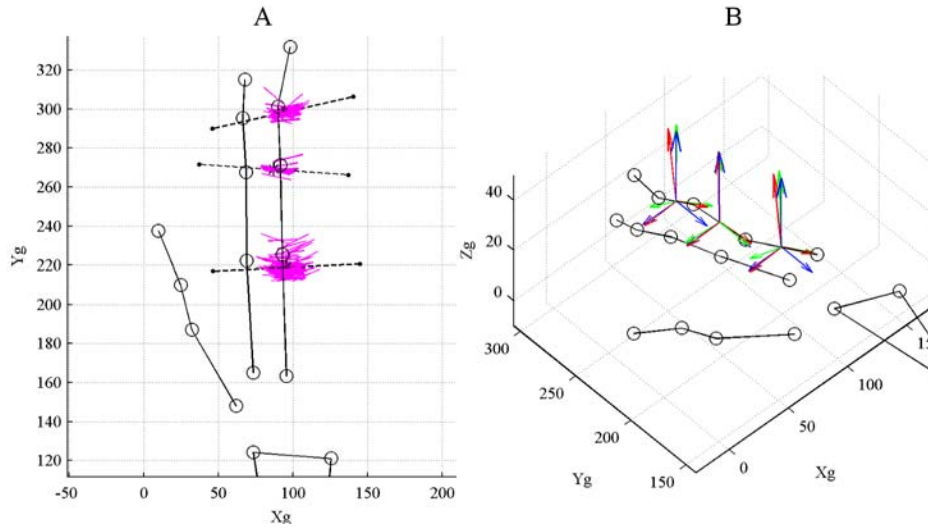
Figure 2. A- The middle finger flexion-extension axes obtained with the Helical Axis method. Magenta solid lines and black dashed lines represent respectively instantaneous helical axes and optimal direction vectors. B- Middle finger SCSs resulting from the three different methods. Blue, red and green vectors correspond to respectively the Reference, Bony-Landmarks and Helical methods. In both graphs, (Xg, Yg, Zg) represent the global coordinates (units: mm) and black circles represent the positions of the palpated bony-landmarks.

4. DISCUSSION

Three methods were compared for the computation of middle finger SCSs. For the Helical Axis method, IHAs presented small variations in orientations. Such variations are hardly avoidable and could be explained by several factors such as skin movement artifacts, sampling inaccuracy as well as the difficulty to execute a pure rotation motion. Compared to other methods, the F-E axes obtained with the Helical Axis method were the closest to the real joint axes of rotation. This can be deduced from the smaller RoMs obtained with this method on A-A and P-S for the PIP3 joint. These angle variations should be small because this joint is assumed to be a single DoF joint in F-E. This also means that when using the BLM or Reference methods, there is risk of observing angle variations which can not be related to the motions in the joint.

Compared to Helical SCSs, the orientations of the BLM SCSs were closer to those of the Reference SCSs. This is not surprising since these both methods are strongly associated to the global coordinate system. Also, the joint angle offsets observed for the Helical Axis method were due to the fact that the estimated F-E axes are not orthogonal to the long axis of the segments in the frontal plane (Fig. 2A).

The Reference method is the easiest and fastest to set-up and can always be used in combination with one of the other options. Nevertheless, this method is strongly depending on the neutral posture whereas some patients can experience difficulties in executing it, like in the case of joint deformities.

Table 1. PIP3 maximal angles and ranges of motion in degrees obtained with three different methods for the F-E calibration motion used for the Helical Axis method.

PIP3	Flexion-Extension angle			Abduction-Adduction angle			Pronation-Supination angle		
	Min.	*Max.*	*RoM*	*Min.*	*Max.*	*RoM*	*Min.*	*Max.*	*RoM*
Reference	-1.7	78.1	79.8	-6.8	1.8	8.6	-8.4	5.2	13.6
BLM	10.4	89.8	79.4	-5.4	4.7	10.1	-9.1	4.1	13.2
Helical	8.3	87.0	78.7	8.9	15.9	7.0	-19.8	-9.0	10.8

Table 2. MCP3 maximal angles and ranges of motion in degrees obtained with three different methods for the test motion.

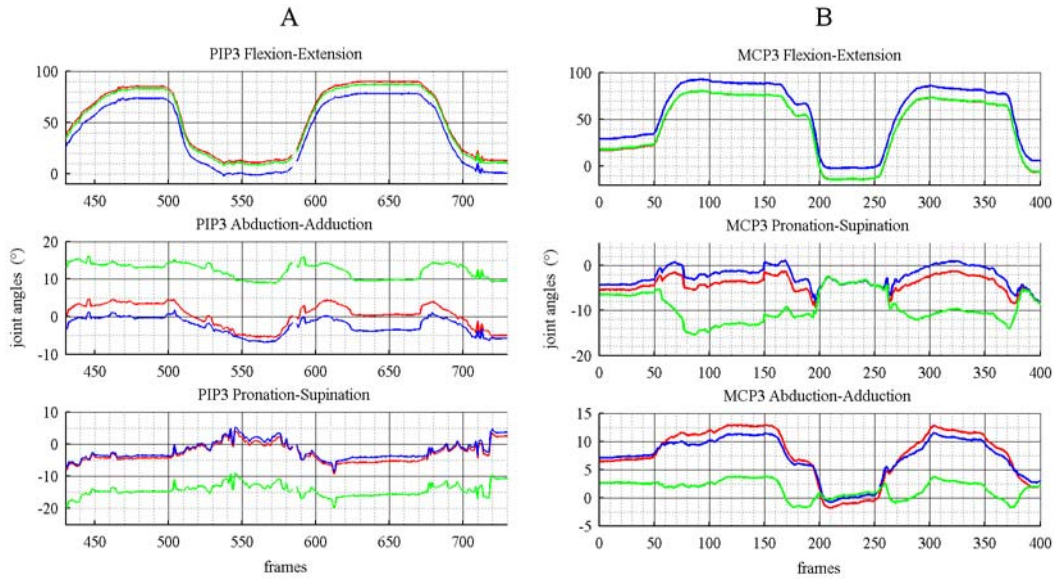| MCP3	Flexion-Extension angle			Abduction-Adduction angle			Pronation-Supination angle		
	Min.	*Max.*	*RoM*	*Min.*	*Max.*	*RoM*	*Min.*	*Max.*	*RoM*
Reference	-2.2	92.5	94.7	-0.8	11.4	12.2	-8.3	1.0	9.3
BLM	-14.0	80.3	94.3	-1.8	12.9	14.7	-9.2	-1.3	7.9
Helical	-14.6	80.8	95.4	-7.2	-1.6	5.6	-6.1	6.8	12.9

Figure 3. A - Time-evolution of the PIP3 joint angles of the three methods corresponding to F-E motions used for the Helical Axis method. B - Time-evolution of MCP3 joint angles corresponding to the test motion. Blue, red and green lines represent respectively the Reference, Bony-Landmarks and Helical Axis methods.

Unlike the Reference method, the BLM method takes into account anatomical differences and thus results in more individualized SCSs. But this makes the comparison of motions between subjects harder since the SCS obtained for one phalanx is different for each subject.

The Helical Axis method provides the most accurate results for the secondary and tertiary rotation components in a hinge joint. Several studies on the carrying angle in the elbow, or abduction in the knee showed that these rotations can only be calculated correctly if the main axis is aligned with the kinematic axis [11]. Nevertheless, several pathologies are making the estimation of helical axes hard or impossible.

In conclusion, all three methods provide a good estimation of large amplitude motions for one DoF, but the Helical Axis method is the best choice to study all three joint rotations at the same time.

REFERENCES

[1]   Ellis, B. and Bruton, A., 2002. A study to compare the reliability of composite finger flexion with goniometry for measurement of range of motion in the hand, Clin. Rehabil. 16(5), pp. 562 -570.

[2]   Vigouroux, L., Domalain, M. and Berton, E., 2009. Comparison of tendon tensions estimated from two biomechanical models of the thumb, J. Biomech. 42(11), pp. 1772-1777.

[3]   [Bae, S. and Armstrong, T.J., 2011. A finger motion model for reach and grasp, Int. J. Ind. Ergon. 41(1), pp. 79-89.

[4]   Carpinella, I., Mazzoleni, P., Rabuffetti, M., Thorsen, R. and Ferrarin, M., 2006. Experimental protocol for the kinematic analysis of the hand: Definition and repeatability, Gait Posture 23(4), pp. 445-454.

[5]   Metcalf, C.D., Notley, S.V., Chappell, P.H., Burridge, J.H. and Yule, V.T., 2008. Validation and application of a computational model for wrist and hand movements using surface markers, IEEE Trans. Biomed. Eng. 55(3), pp. 1199-1210.

[6]   Cerveri, P., Lopomo, N., Pedotti, A. and Ferrigno, G., 2005. Derivation of centers and axes of rotation for wrist and fingers in a hand kinematic model: methods and reliability results, Ann. Biomed. Eng. 33(3), pp. 402-412.

[7]   Zhang, X., 2003. Determining finger segmental centers of rotation in flexion–extension based on surface marker measurement, J. Biomech. 36(8), pp. 1097-1102.

[8]   Wu, G., van der Helm, F.C.T., Veeger, H.E.J.D., Makhsous, M., Van Roy, P., Anglin, C., et al., 2005. ISB recommendation on definitions of joint coordinate systems of various joints for the reporting of human joint motion--Part II: shoulder, elbow, wrist and hand, J. Biomech. 38(5), pp. 981-992.

[9]   Cooney, W., Lucca, M., Chao, E. and Linscheid, R., 1981. The kinesiology of the thumb trapeziometacarpal joint, J. Bone Joint Surg. Am. 63(9), pp. 1371-1381.

[10] Veeger, H.E.J., Yu, B., An, K.-N. and Rozendal, R.H., 1997. Parameters for modeling the upper extremity, J. Biomech. 30(6), pp. 647-652.

[11] Piazza, S.J. and Cavanagh, P.R., 2000. Measurement of the screw-home motion of the knee is sensitive to errors in axis alignment, J. Biomech. 33(8), pp. 1029-1034.

Effect of markers attachment on soft tissue artifact and knee kinematics during gait

Barré A. [1], Thiran J.P. [2], Jolles B.M. [3], Theumann N. [4], Aminian K. [1]

[1] Laboratory of Movement Analysis and Measurement (LMAM), EPFL, Lausanne, Switzerland,
arnaud.barre@epfl.ch
[2] Signal Processing Laboratory (LTS5), EPFL, Lausanne, Switzerland
[3] Department of Orthopaedic Surgery and Traumatology, CHUV and UNIL, Lausanne, Switzerland
[4] Department of Radiology, CHUV and UNIL, Lausanne, Switzerland

The aim of this study was to quantify the effect of the soft tissue artifact on knee kinematics during a treadmill walking task using clusters of 4 markers attached directly on the skin or underwrapped by simulated wraps. Both methods were compared to the knee kinematics estimated by a synchronized bi-plane fluoroscopic system. From the results of 15 subjects, the range of the knee angles and translations estimated by each method were significantly different. However, no systematic difference was found between both systems and then cannot tell the system to privilege.

STA, Knee kinematics, Gait, Cluster, STA compensation

1. INTRODUCTION

The effect of the soft tissue artifact is known as the main source of error when analysis human motion during daily activity [1]. Several studies showed the importance of STA effect on the measure of the skin markers as well as on the joint kinematics during various activities using intra-cortical pins as well as external fixator [2-3] and using mono-plane fluoroscopy [4-5].

To reduce the STA effect, some studies proposed to exploit the redundancy of information when using 3 markers or more defined as a cluster [6-7]. Instead of creating a bone embedded frame at each instant (defined geometrically by the coordinates of 3 noncollinear markers), it is proposed to fit a rigid cluster model onto a set of markers. This model can be determined during a static calibration. Cappozzo et al. [7] introduces several design criteria of the cluster to prevent reconstruction error of bone embedded frame. Hence it was concluded that 4 markers attached to a segment (but not on bone prominences) and defining a quasi-planar cluster is minimally required. The study of Manal et al. [8] proposed to compare 11 marker sets on the shank using mainly wraps as attachment method which decrease local deformation between markers. The best attachment method was determined to be the distal lateral shell underwrapped (DLU). This attachment method was then used on the thigh to estimate knee kinematics during gait [9]. However, no known validation for this segment exists nor comparison with a cluster of markers attached directly on the skin.

The difficulty of such validation resides in the reference system. Indeed, the use of intracortical pins or external fixator is extremely invasive and can affect the estimated kinematics [2, 10]. The use of a single plane fluoroscopic system as reference avoids the invasiveness of the intra-cortical pins and does not restrict the skin movement. Using X-ray images, the contours of the object of interest (e.g. bones or prosthesis' components) were extracted and a 3D model of the object was fitted on them iteratively. However, it was argued recently than it could be not enough accurate to analyze the knee joint kinematics [11].

Using radiostereometric analysis (RSA), some studies developed a bi-plane fluoroscopic system to measure motion of prosthesis, bones and inserted beads, during daily tasks [12-13]. Compared to the mono-plane fluoroscope method, the use of an extra plane gives more information to the fitting algorithm. This has the advantage to be less affected by improper registration, but also to be more accurate. However no known study used this system to assess the effect of marker attachment on STA and then on knee kinematic during gait.

The purpose of this study was to assess the STA effect on the knee angles and translations during gait using two kinds of clusters of markers attached directly on the skin. The first one is composed only of 4 markers while the second one is composed of 12-16 markers and 8-10 markers to simulate wraps around the thigh and the shank respectively. It was assumed that tracking a cluster composed of a large number of markers in an area similar than a wrap will estimate the same kinematics. It was also assumed that tracking of prosthesis' components by bi-plane fluoroscopic system provides an accurate and STA free measurement of knee kinematics. Differences between kinematics of the prosthesis and clusters of markers were used to estimate the STA effect during gait cycle.

2. MATERIAL AND METHODS

Acquisition setup

The acquisition system was devised using 2 fluoroscopes (BV Pulsera 300, Philips, NL) and a Vicon system (Vicon Motion Systems, UK) composed of 7 cameras MX3+. The fluoroscopes were configured to acquire 30 images by second, with a beam energy fixed at 60 kV and a current beam of 5.95 mA. The sample frequency for the Vicon system was set to 240 Hz. Both systems were synchronized a posteriori using a modified X-ray detector (Monitor 4EC, S.E. International, Inc., USA) connected on an analog input of the Vicon system and sampled at 2400 Hz. A calibration procedure based on 3 reflective markers and visible in each system was used to compute the transformation between Vicon and the fluoroscopes to express all of the data in the same coordinate system. The global frame of the fluoroscopic system was selected as the reference frame.

A group of 15 subjects with postero-stabilized mobile-bearing knee F.I.R.S.T. arthroplasty (Symbios, CH) participated to this study. Each subject had read and signed a consent form that was previously approved by the local ethical committee. For each subject 80 reflective markers (Ø 4mm) were attached on one lower limb to cover entirely the anterior and lateral side of the thigh and shank. First a static acquisition representing a quite standing posture was performed during 5 seconds. Then a treadmill gait acquisition was realized during 15 seconds. The gait speed was comfortable and determined by each subject during a warm-up period.

Knee kinematics estimation from X-ray images

The data acquired by the fluoroscopes were first used in a semi-automatic segmentation method to extract the contours of the femoral and tibial component of the prosthesis [14]. These contours were then used in the software MB-RSA (Medis Specials, NL) to fit the corresponding 3D models. The poses extracted from MB-RSA were then converted into orientation and positions for each component. Quaternions were used to represent orientations. A time-invariant orientation filter [15] was designed and applied to quaternion components. The components of the position were filtered independently by a recursive digital filter using a smoothing mask (-1/24, 4/24, 18/24, 4/24, -1/24) very popular in signal processing [15]. Then, the signals were upsampled at 240 Hz using a spherical interpolation method for the quaternion [16] and cubic splines for the positions. The knee kinematics of the prosthesis (PT) was expressed as 3D joint angles and translations using the definitions given by Grood and Suntay [17].

Knee kinematics estimation from simulated wraps and cluster of 4 markers

To determine the kinematic of the knee joint, first a static calibration was realized to construct two clusters of markers representing the thigh and the shank for each method of attachment. For each cluster, a technical frame was built using a principal component analysis method. Mainly, the coordinates of the markers were stacked in a matrix ($n \times 3$, where n is the number of markers in the cluster), then a singular value decomposition of this matrix was performed to extract the orientation of the technical frame, while its mean corresponds to the origin of the technical frame. The markers were then registered locally in the corresponding technical frame. Using the X-ray data recorded during the static calibration, the transformations between the technical frames (thigh and shank) and the corresponding prosthesis frames (femoral and tibial) were determined. Second, a point sets fitting method [18] were used to compute the motion of the clusters during the gait acquisition. Coupled with the static calibration, the motion of the prosthesis frames from the skin markers data were then computed and filtered with the same digital filters used with the X-ray data. The skin markers kinematics of the knee were estimated using same definition of joint coordinates than prosthesis kinematics [17].

The simulated wrap for the thigh was placed in the middle of the thigh while the simulated wrap for the shank was placed distally as indicated by Manal et al. [9]. The height of the wrap for the thigh and the shank were respectively around 120 and 90 mm respectively. All the markers in these areas were selected to create the simulated wraps.

The design of the cluster composed of 4 markers followed the recommendation of Cappozzo et al. [7]. These markers were chosen from the markers used in the simulated wraps. The markers used for the thigh were selected anteriorly (mainly over the rectus femoris) and laterally (over the iliotibial band). The markers used for the shank were selected laterally and mainly over the tendon of the tibial anterior muscle.

STA assessment

The assessment of the STA effect on the knee joint kinematics was defined as the difference between the prosthesis kinematics (PT) extracted from the fluoroscopic data and the kinematics estimated by the simulated wraps (SW) or the clusters or 4 markers (CL). The differences between SW and CL corresponded to the effect of the method of attachment on the STA. The kinematics values (angles and translations) were normalized by gait cycle (GC) and averaged by subject. Then, the range of the average value of each angle and translation was extracted for the stance phase (0-60% GC) and the swing phase (60-100% GC). The comparisons of the

values estimated by PT, SW and CL were realized using non-parametric Friedman ANOVA tests with a significance level of $p < 0.05$. If a group effect was discovered, then Wilcoxon matched pairs tests were realized between the three methods (PT, SW, CL).

3. RESULTS

Between 7 and 10 gait cycles were extracted for each subject. The average gait speed for subjects (n=15) was 1.7 km/h with a standard deviation of 0.3 km/h. The knee flexion/extension (FE), adduction/abduction (AA), and internal/external rotation (IE) angles estimated by the three methods are presented in the Fig. 1.

The comparison of the ranges between PT and SW showed significant difference during the stance phase for FE ($p = 0.047$), AA ($p < 0.001$) and IE ($p = 0.015$). During the swing phase, only AA is significantly different ($p = 0.001$). The comparison between PT and CL showed similar significant difference. The comparison between SW and CL showed significant difference only during the stance phase for AA ($p = 0.041$). The differences between PT-SW and PT-CL didn't show systematic difference in favor of one method.

Similar results were found for the translations, with extremely significant difference ($p < 0.001$) between PT and SW as well as PT and CL for each translation (medio-lateral: ML, posterior-anterior: PA and distraction compression: DC) during the stance phase and the swing phase. The comparison between SW and CL showed only a significant difference for the ML translation during the stance phase ($p = 0.027$), however no systematic difference were found between both method of attachments.

4. DISCUSSION

In this study we assessed the effects of the STA global deformations on the estimation of the kinematics of the knee during gait. A bi-plane fluoroscopic system was used as reference system to estimate accurately the rotations and translations of the knee joint, which were compared to the same kinematics estimated by a stereophotogrammetric system using simulated wraps or clusters of 4 skin markers.

To our knowledge, this study provides the first results to assess STA effect during gait activity using a bi-plane fluoroscopic system with the largest group of subject (15 subjects). As the STA is task dependant, we only compared our results to studies assessing STA effects on the knee kinematics during gait. As far as literature is concerned, we found only 3 comparable studies. Cappozzo et al. [3] used external fixator inserted into the femur or the tibia as reference system on 7 subjects and reported maximal errors for the knee angles between 4° and 12° which are greater than the result of this study. However, these errors were not only reported for gait, but also for a bicycle and a hip rotation task. More recently, Akbarshahi et al. [4] reported root mean square (RMS) errors for the knee joint rotations for 4 subjects using as reference a single plane fluoroscope with MRI-based bone models. The RMS computed from the results of the current study is smaller by a factor 2. Only the maximum RMS for AA is similar. In both former studies, they use only 3 markers by clusters to assess the STA effects, which could lead in the increasing of the reconstruction error of the technical frame [7]. Benoit et al. [2] reported absolute STA errors for the heel strike, the mid-stance and the toe-off using intra-cortical pins as reference. Considering our results to compute the absolute STA error for these events gives results in the same range for the orientations but with smaller standard deviation.
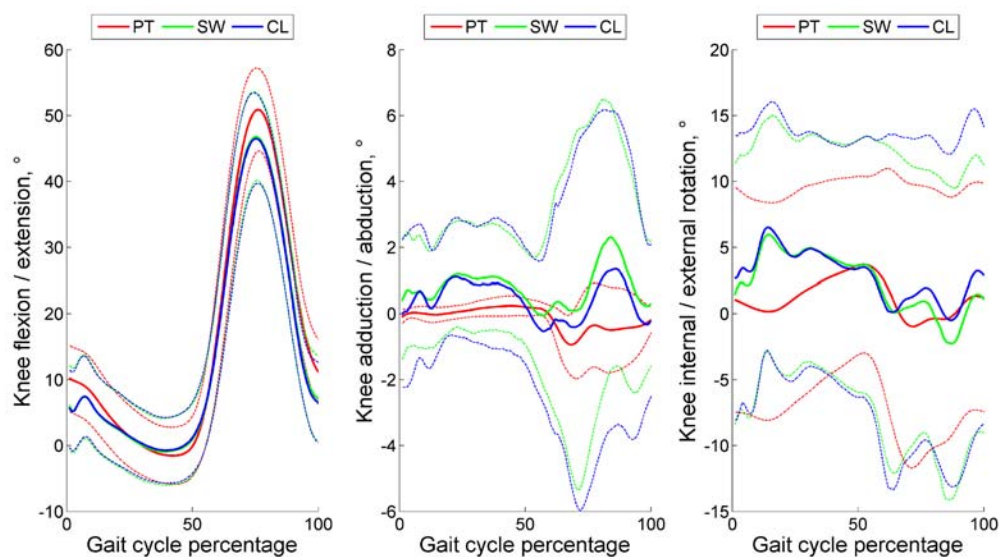

Figure 1. Average (solid line) and standard deviation (dash line) of the knee angles for the subjects (n=15) estimated from PT (red), SW (green) and CL (blue).

For the translation, the STA errors were similar during the three events for the DC translation and during the heel strike for the LM translations. It is worth mentioning that this later study used more than 3 markers by cluster where some of them were mounted on wrap, which can explain the closeness of our results. The reported errors for the angle as well as the PA translations are at least two times greater than in this study. These differences might be a consequence of the use of intra-cortical pins, which can bend during the walking and then increase the variability of the results for the reference system. Another reason could be also the selection of the translation reference points which can reduce the quantity of translation [17]. Another reason for the difference with these studies could be also related to the gait speed as well as the calibration between the technical frame and the bone embedded frame. In this study, the frames of the prosthesis were used as the bone embedded frames, and then avoid the possible bias (cross-talk) introduced by an anatomical calibration.

The kinematics of the prosthesis and both system of attachments showed that STA affects differently the stance phase and the swing phase but with maximum effect at the beginning of each phase. Indeed, stance starts with heel strike generating a shockwave, which propagates along the lower limb during the loading response before to be dissipated and absorbed during the mid stance and the terminal stance. Then, due to the swift lift of the leg at start of swing phase, the STA increases again.

The significant differences between SW and CL can be explained by the location of the markers and the non-homogenous deformation of the soft tissue which may affect CL more importantly. The use of wraps should avoid these deformations but as no systematic difference was found between SW and CL, it is difficult to conclude for the selection of a method. It might be also possible that the simulation of the wrap didn't mimic exactly the mechanical behavior of the true one. However, it is still important to remind that both methods suffer largely of the global motion of the soft tissue relatively to the underlying bone.

In conclusion, STA affects largely the knee kinematics estimated by using clusters of 4 markers attached directly on the skin or underwrapped. Even if more works need to be investigated on the location of the clusters and the wraps, the clinical interpretation of gait kinematics using these methods of attachment should be taken with caution. A method of compensation to reduce the STA effect is still necessary to extract a reliable kinematic, close to the one of the bones.

5. ACKNOWLEDGMENT

6. REFERENCES

[1] A. Leardini, L. Chiari, U. Della Croce, and A. Cappozzo, "Human movement analysis using stereophotogrammetry. Part 3. Soft tissue artifact assessment and compensation," *Gait Posture,* vol. 21, pp. 212-25, Feb 2005.

[2] D. L. Benoit*, et al.*, "Effect of skin movement artifact on knee kinematics during gait and cutting motions measured in vivo," *Gait Posture,* vol. 24, pp. 152-64, Oct 2006.

[3] A. Cappozzo, F. Catani, A. Leardini, M. G. Benedetti, and U. D. Croce, "Position and orientation in space of bones during movement: experimental artefacts," *Clin Biomech (Bristol, Avon),* vol. 11, pp. 90-100, Mar 1996.

[4] M. Akbarshahi*, et al.*, "Non-invasive assessment of soft-tissue artifact and its effect on knee joint kinematics during functional activity," *J Biomech,* vol. 43, pp. 1292-301, May 7 2010.

[5] R. Stagni, S. Fantozzi, A. Cappello, and A. Leardini, "Quantification of soft tissue artefact in motion analysis by combining 3D fluoroscopy and stereophotogrammetry: a study on two subjects," *Clin Biomech (Bristol, Avon),* vol. 20, pp. 320-9, Mar 2005.

[6] A. Cappello, A. Cappozzo, P. F. LaPalombara, L. Lucchetti, and A. Leardini, "Multiple anatomical landmark calibration for optimal bone pose estimation," *Human Movement Science,* vol. 16, pp. 259-274, Apr 1997.

[7] A. Cappozzo, A. Cappello, U. Della Croce, and F. Pensalfini, "Surface-marker cluster design criteria for 3-D bone movement reconstruction," *IEEE Trans Biomed Eng,* vol. 44, pp. 1165-74, Dec 1997.

[8] K. Manal, I. McClay, S. Stanhope, J. Richards, and B. Galinat, "Comparison of surface mounted markers and attachment methods in estimating tibial rotations during walking: an in vivo study," *Gait Posture,* vol. 11, pp. 38-45, Feb 2000.

[9] K. Manal, I. McClay Davis, B. Galinat, and S. Stanhope, "The accuracy of estimating proximal tibial translation during natural cadence walking: bone vs. skin mounted targets," *Clin Biomech (Bristol, Avon),* vol. 18, pp. 126-31, Feb 2003.

[10] D. K. Ramsey, P. F. Wretenberg, D. L. Benoit, M. Lamontagne, and G. Nemeth, "Methodological concerns using intra-cortical pins to measure tibiofemoral kinematics," *Knee Surg Sports Traumatol Arthrosc,* vol. 11, pp. 344-9, Sep 2003.

[11] S. Acker*, et al.*, "Accuracy of single-plane fluoroscopy in determining relative position and orientation of total knee replacement components," *J Biomech,* vol. 44, pp. 784-7, Feb 24 2011.

[12] G. Li, S. K. Van de Velde, and J. T. Bingham, "Validation of a non-invasive fluoroscopic imaging technique for the measurement of dynamic knee joint motion," *J Biomech,* vol. 41, pp. 1616-22, 2008.

[13] S. Tashman, D. Collon, K. Anderson, P. Kolowich, and W. Anderst, "Abnormal rotational knee motion during running after anterior cruciate ligament reconstruction," *Am J Sports Med,* vol. 32, pp. 975-83, Jun 2004.

[14] A. Barré, J. P. Thiran, N. Theumann, B. Jolles, and K. Aminian, "Semi-automatic segmentation method for roentgen fluoroscopic stereophotogrammetric analysis," in *2nd International RSA Meeting*, Leiden, The Netherlands, 2011.

[15] J. Lee and S. Y. Shin, "General construction of time-domain filters for orientation data," *IEEE Transactions on Visualization and Computer Graphics,* vol. 8, pp. 119-128, Apr-Jun 2002.

[16] S. R. Buss and J. P. Fillmore, "Spherical averages and applications to spherical splines and interpolation," *ACM Transactions on Graphics,* vol. 20, pp. 95-126, Apr 2001.

[17] E. S. Grood and W. J. Suntay, "A joint coordinate system for the clinical description of three-dimensional motions: application to the knee," *Journal of Biomechanical Engineering,* vol. 105, pp. 136-44, May 1983.

[18] B. K. P. Horn, "Closed-Form Solution of Absolute Orientation Using Unit Quaternions," *Journal of the Optical Society of America a-Optics Image Science and Vision,* vol. 4, pp. 629-642, Apr 1987.

Improved 3-D Spine & Human Skeleton Model For Posture And Movement Analysis

D'Amico M. [1,2], Roncoletta P. [2], Iodice P. [1], Di Pancrazio L. [1], Bellomo R.G. [1], Saggini R. [1]

[1]S.M.A.R.T. LAB (Skeleton Movement Analysis & Advanced Rehabilitation Technology) - C.U.M.S. (Centro Universitario di Medicina dello Sport) – Università D'Annuzio Chieti;
[2]Bioengineering & Biomedicine Company S.r.l. Via Aterno 154, 66020 S. Giovanni Teatino (CH);

1. INTRODUCTION

Spine and posture disorders cover large interest in both biomechanical research and clinical fields. Quantitative functional evaluation of posture and spine is one of the main concern and at the same time one of the most challenging matter to treat. Unluckily, except for dynamic X-Ray and very recent dynamic MRI, no one of these techniques is able to provide information about the functional state of the rachis and patient's posture. Optoelectronic measurement approach appears to be a potentially significant solution to complete the necessary functional information, complementing other techniques in addressing clinical problems in orthopaedics and rehabilitation. Modern low cost powerful PC workstations allow the implementation of highly sophisticated computing demanding biomechanical models joined to very fast complex 3D image representation. In clinical environment, the optimal trade-off among the minimum as possible number of fitted body landmarks, the high detail level of assessed full skeleton model and measurement trial time length, has to be identified. Nonetheless when Posture and Spine deformities are of interest, a detailed 3D mathematical representation of spine has to be included. Furthermore, results have to be represented in an intuitive and clinical compliant fashion, maintaining a biomechanical strictness but hiding the burden of complex mathematical approach. With all these goals in mind, our group started, years ago, a project to merge into a complete fully 3D parametric biomechanical human skeleton model different segmental biomechanical models presented in literature (upper arms not yet included). The model has been conceived with different level of complexity and its parametric form allows to scale it according to each subject characteristics, by fitting the 3D anthropometric sizes to opto-electronic measurements. Particular care and studies have been devoted to develop a 3D spine model. Thousands of patients in different clinical centres have been already analysed and followed up with this methodology that proved to be useful for various posture and spine related pathologies. Recently the possibility to assess the net internal joint forces and torques at each spine vertebral level and to correlate these latter with all the other model's features has been added. The aim of this paper is to shortly present the methodological aspects, the skeleton model features and their potential applicability in clinical and biomechanical fields for Posture and Locomotor diseases.

2. METHODOLOGY

In order to work at different stages of complexity, depending on the analysis purposes and necessities, the 3D human skeleton model parameterisation can be detailed with different sets of accurate 3D opto-electronic stereo-photogrammetric anthropometric measurements. To this aim various protocols involving different body labelling have been established. The accuracy and precision of this model relies both on anatomical findings (cadaver dissections, in vivo, X-ray and gamma ray measurements, parametric regression equations [1-5]) reported in literature and on the approach and signal processing procedures and optimization methods we largely described [6-9]. To analyse human posture and spinal related pathologies (scoliosis, back pain etc.), a 27 markers protocol has been set and tested extensively in clinical environment [6,7]. The following anatomical landmarks are identified (fig. 1a): zygomatic bones, mentum, acromions, sterno-clavicular joints, xyphoid, ASIS, PSIS, knee joints, heels and spinous processes from C7 down to S3 every second vertebra. Previous studies investigated the reliability and repeatability of both applied protocols and measurements devices including intra-inter operator variability. Such studies established that intrinsic subject postural variability is up to 10 times higher than errors introduced by all measurement process [10,11]. Moreover reliability of 3D spine morphology identification, obtained by opto-electronic measurements and data elaboration processing, has been also validated using x-ray imaging comparison [12]. When a more detailed description of lower limb segmental poses is sought, for instance when gait trials have to be considered, the used number of markers has to be increased [9]. Our proposed solution embrace a 9-link chain model of the human pelvis-lower limbs apparatus, with the pelvis, thigh, shank and foot links joined by ball and socket joints representing the hips, the knees and the ankles respectively. At least three markers per each segment have been used, in particular: Pelvis: as above described, by using ASIS and PSIS bony landmarks; Femur: Great Trocanter middle thigh and Lateral and Medial Femoral epicondyles; Shank: Head of Fibula, middle shank, Lateral and Medial malleoli; Foot: Heel (calcaneous process), 1st and 5th Metatarsal heads, distal big toe end point. In particular this latter

markers set allows to model the foot as subdivided into two different rigid bony segments: fingers-forefoot segment laying on the plane identified by big toe, 1st and 5th Metatarsal heads and rear-mid foot identified by 1st and 5th Metatarsal heads and heel. A cylindrical joint with axis identified by the line joining the 1st and 5th Metatarsal heads is modelled in between such two foot segments. The indirect measurements such as joint centres positions are derived from external markers (for instance, hip joints centres are derived from ASIS and PSIS positions and related pelvis dimension, model and regression function [2,3]). The knee joint centre is taken as the mid-point of the segment linking the femur medial and lateral epicondyles, and the ankle joint centre as the mid-point of the segment joining the two malleoli. In this way the full protocol includes 49 markers (fig. 1b) and it represents the best trade-off among the following challenging needs: 1) the proper identification of each segment pose; 2) the necessity to limit the number of used markers; 3) the requirements of suitable marker clusters configurations to apply mathematical optimisation procedures that minimise the well known soft tissue artefacts and marker misplacement problems [8,13]. To this aim we developed a suitable optimisation procedure named "Double Step GOM" [8]. Our experimental recordings are based on the VICON-Mx[1] and the very brand new G.O.A.L.S.[2] opto-electronic systems; anyway this methodology is a very general one and it can be indifferently applied to any stereo-photogrammetric recording system, provided that this latter would be able to supply all the required landmarks three-dimensional co-ordinates. In addition force platform data, foot pressure maps and surface EMG recordings can be jointly and synchronously measured when a full detailed analysis is sought. Furthermore when particular movements have to be measured, such as forward bending and/or some kind of neck flexion-extension-rotation, which cause face markers to be hidden to TV camera's field of view, a further 3 markers set placed on a head band (being them rigidly related to face markers) is added to the above mentioned protocols [14]. The standard protocol for posture requires at least 5, one second lasting, acquisitions. Given the 100Hz opto-electronic device data acquisition rate, this means that a minimum of 500 measurements are averaged per each static postural stance [6-8]. In order to carry out proper averaging and all the following computations, a subject's local co-ordinate system following SRS recommendations [15] is defined and used to pre-process and re-align measurements. From the 3D reconstruction all the 2D clinical parameters claimed for the correct description and biomechanical characterisation of spinal pathology, related to those usually calculated on the radiographic image, are derived (i.e. Cobb and Kypho-Lordotic angles). Moreover, a set of significant biomechanical variables describing the three-dimensional nature of body posture are obtained, such as frontal and sagittal spinal offsets of each marked vertebrae with respect to the vertical axis passing by S3, frontal and sagittal global offsets of each labelled landmark with respect to the vertical axis passing through the middle point between heels, pelvis frontal and sagittal inclinations, shoulder-to-pelvis, pelvis-to-heels and shoulder-to-heels horizontal rotations, joint forces, joint torques and several more. When the 49 markers set is used the Posture measurements are complemented by the pose of each lower limb chain segment enlightening joint adaptations, anomalies and/or weakness. Our studies as well as our clinical experience led us to identify a set of static attitudes (such as indifferent orthostasis with and/or without an under-foot wedge, self-corrected manoeuvres, sitting posture) and/or movements (lateral and forward bendings head-neck-trunk torsion etc.), that can provide a complete documentation of subject postural balancing, functional and morphological characteristics. As for static Posture, also for Gait the possibility to extract the averaged gait cycle characteristics has been considered and developed. The mathematical details of both optimization procedure as well as mean gait cycle computation are beyond the limits of this paper [8,9]. Briefly after the proper identification of each valid stride a time normalization of each considered numerical variable is performed before the averaging step. The final outcome is the mean gait cycle in which the average time course and associated standard deviation is defined per each variable of interest. Two main advantages can be enumerated with the possibility to extract the mean characteristics of both static posture or cyclic motor task (gait): first, it allows to overcome the single measurements analysis limits by taking into account the ensemble behaviour so improving the statistical reliability of the evaluation; second it permits to obtain information about the repeatability and variability of the performed motor task, thus enlightening the subject's motor control capability. For the graphical representation as well as clinical parameter visualisation, a software package (named ASAP3D[©] and ASAP 3D Skeleton Model[©])[2] based on 3D graphic modelling has been developed.

3. RESULTS AND DISCUSSION

Several studies have been carried out about spine and posture disorders with the described methodology [14,16,17]. Given the length limit of this paper only two paradigmatic examples will be illustrated to fully describe the capability of the approach to produce clinically significant outcomes. In fig. 2 the averaged posture a scoliotic subject is presented both in indifferent orthostasis and in corrected orthostasis using an underfoot wedge. It is evident how the 3D skeleton reconstruction and report allows the clinician to fully and easily
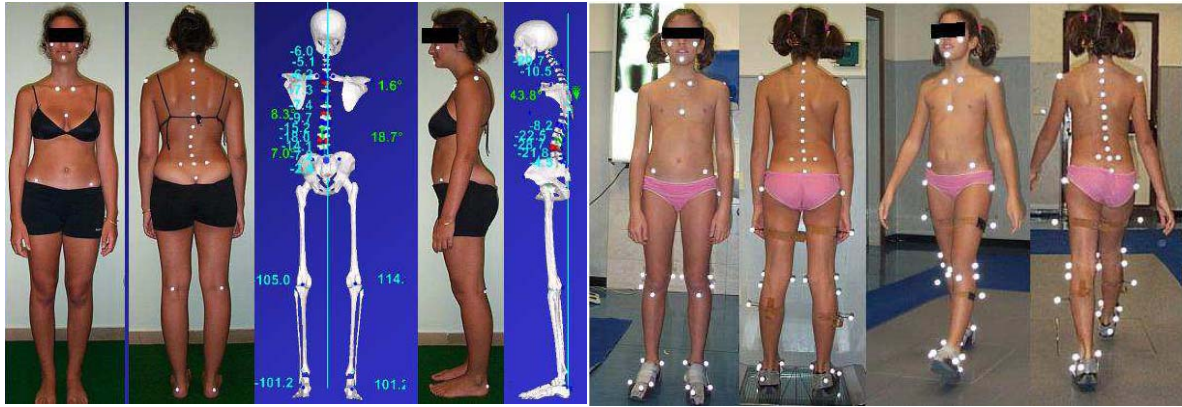
---

[1] O.M.G. UK

[2] *Bioengineering & Biomedicine Company S.r.l. Italy*

evaluate the postural behaviour and the level of spinal deformity of the analyzed subject, in particular the patient's global and trunk unbalancing as well as his pelvic obliquity associated to leg length discrepancy.

Figs.: 1a,b Example of Different markers sets for Posture and Gait Analysis.Full protocol set-up for Posture and Gait analysis;
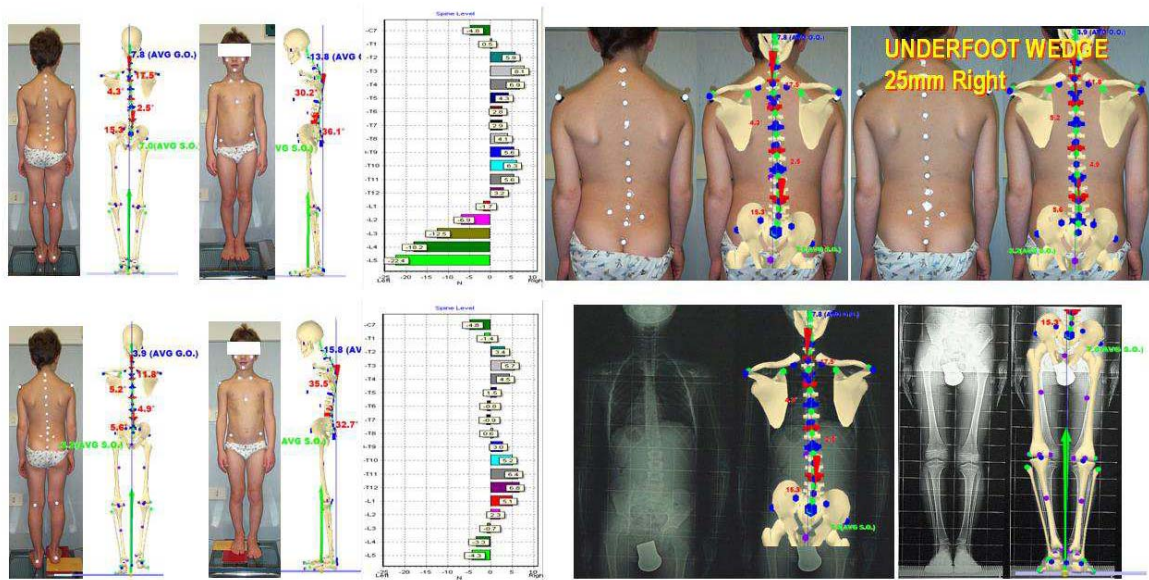

Fig. 2a,b) 3D skeleton representation (27 markers frontal and sagittal view) indifferent orthostasis (upper left panels) compared to corrected orthostasis by the application of a 25mm right underfoot wedge (lower left panels); zoomed spine, pelvis & legs reconstruction compared to X-Ray films (right panels).
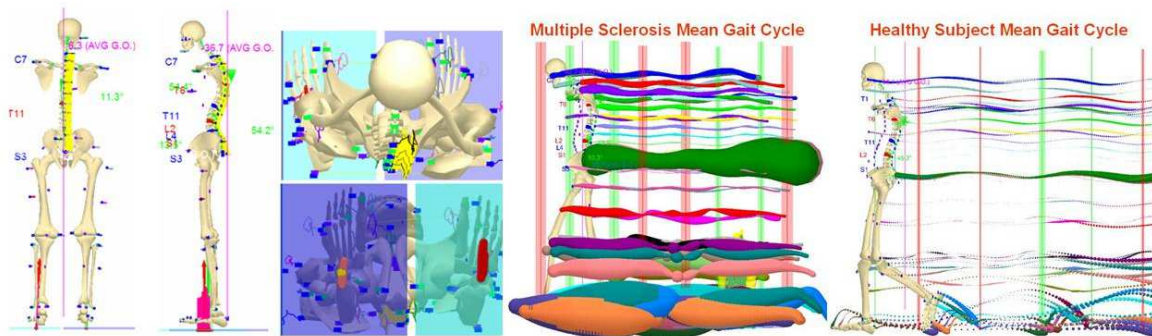

Fig. 3): Multiple Sclerosis: Body Sway in 10 sec. recording showing postural instability and disparities of COPs patterns and underfoot loads (left panels). Mean Gait Cycle vs. Healthy Subject Mean Gait Cycle comparison (right panels) enlightening huge motor control variability/repeatibility differences (each trajectory point is represented by a sphere having center in the computed average and ray size determined by the associated 3D standard deviation $\sigma = \sqrt{\sigma_x^2 + \sigma_y^2 + \sigma_z^2}$)

The peculiarity of the approach is related to its non-ionising nature and its fast response capability. Within a couple of minutes various postural tasks can be analysed and compared getting immediate information about patient's posture function and feedbacks on applied corrections. Applying a series of underfoot wedges of different thicknesses the "optimal" one, which led to the best posture correction, is determined (fig.2). Differences in the assessed vertebral medio-lateral forces in the two conditions are presented showing a significant magnitude reduction and so better balance in wedge corrected posture. Finally the fig. 2 presents the direct comparison in between the stereo-photogrammetric 3D reconstruction and the radiographic frontal projection. It is possible to observe the noticeable pelvis reconstruction as well as the good lower limbs bones assessment despite of the reduced markers number on the legs (only 4) accounted in the 27 markers protocol. Fig 3 shows an example of posture and mean gait cycle extraction by using the 49 markers full protocol. A case of Multiple Sclerosis is represented. Postural balancing, shape characteristics and lower limbs loads asymmetries can be fully exploited during body sway. Mean gait cycle allows to quantify the patient difficulties in managing the locomotion. The high instability and poor repeatability during gait is clearly evident by comparing the extremely larger variability associated to the 3D Mean Gait trajectories with respect to those assessed for an healthy subject.

4. CONCLUSIONS

The easy clinical approach of this procedure suggests its use in routinely clinical evaluation for the study of Posture and Gait. The thousands of analysed patients (in our S.M.A.R.T. biomechanical lab and in different clinical centres) proved the approach to be useful for various posture and spine related pathologies. The developed 3D human skeleton model and software package can be used as stable, accurate, reliable and fast tool for the quantitative identification of human body biomechanical characteristics as well as a guideline to formulate a diagnosis and a therapy plan. The peculiarity to allow the extraction of the averaged behaviour both for static attitude as well as for cyclic motor tasks renders the evaluation of the patient's clinical status statistical robust and reliable based on hundreds of 3D measurements, overcoming the single measurements analysis limits. Information about the repeatability and variability of the performed motor task are used to make both intra-individual and inter-individual comparisons, to monitor the results of therapy along time and/or the evolution of the pathology. Finally, it proved to be well accepted both by clinicians and by patients.

5. REFERENCES

[1] A White. III and M. Panjabi, Clinical Biomechanics of the Spine, Philadelphia, J.B. Lippincott Co., 2nd Ed. 1990, 721

[2] P. De Leva, Joint Center Longitudinal Positions Computed from a Selected Subset of Chandler's data, J. Biomec. 29 (9), 1231-1233, 1996.

[3] G. Seidel et al., Hip Joint Center Location from Palpable Bony Landmarks - A Cadaver Study, J. Biom., 28 (8), 995-998, 1995.

[4] Y.K. Liu J.K. Wickstrom Estimation of the inertial property distribution of the human torso from segmented cadaveric data. In Kenedy R.M. (ed.) Perspectives in Biomedical Engineering 1973, pp. 203-213.

[5] V. Zatsiorsky V. Seluyanov L. Chugunova. In vivo body segment inertial parameters determination using a gamma-scanner method. In Biomechanics of human Movement: Application in Rehabilitation , Sports and Ergonomics (Berme Cappozzo eds.) 1990, pp186-202 Bertec Ohio.

[6] D'Amico M. et al., Algorithm for Estimation, Classification and Graphical Representation of Clinical Parameters in the Measurement of Scoliosis and Spinal Deformities by Means of Non-Ionising Device, in Three Dimensional Analysis of Spinal Deformity (Eds. M. D'Amico et al.) 1995, IOS Press 1995, 33-38.

[7] M. D'Amico, G. D'Amico and P. Roncoletta, A 3-D Parametric Biomechanical Skeleton Model for Posture and Spine Shape Analysis. In Research into Spinal Deformities 3 IOS Press 2002, pp365-369.

[8] M. D'Amico and P.Roncoletta, Bone Position Estimation From Skin Markers measurements using Joint Constrained Multi-link Models and a Double Step Global Optimisation Procedure. "unpublished"

[9] M. D'Amico et al., A 3-D Biomechanical Skeleton Model And Processing Procedure For Posture And Movement Analysis, Eur. Med. Phys. 2007:43 (Suppl. 1)

[10] A. Negrini S. Negrini GC. Santambrogio: Data variability in the analysis of spinal deformity, a study performed by means of the AUSCAN system. In Three Dimensional Analysis of Spinal Deformities (Eds. M. D'Amico et al.), IOS Press; 1995:101-106.

[11] A. Negrini S. Negrini. The three-dimensional easy morphological (3-DEMO) classification of scoliosis, part II: repeatability Scoliosis 1:23 21 December 2006

[12] D'Amico M. and Vallasciani M., Non-Ionising Opto-Electronic Measurement and X-Ray Imaging Two Complementary Techniques for Spinal Deformities Evaluation and Monitoring: Results of one Year Clinical Activity in Research into Spinal Deformities 1, IOS Press,1997, 151-154..

[13] Leardini A, Chiari L, Della Croce U, Cappozzo A. Human movement analysis using stereophotogrammetry. Part 3: soft tissue artifact assessment and compensation. Gait and Posture 21 (2005) 212–225

[14] M. D'Amico et al., A 3-D Skeleton Model & SEMG Approach for Integrated Neck and Low Back Pain Analysis Test Batteries, In Research into Spinal Deformities 6 (ed. P. Dangerfield) IOS Press 2008, pp. 79-84.

[15] Stokes I., Three-Dimensional Terminology of Spinal Deformity: A Report presented to the Scoliosis Research Society by the Scoliosis Research Society Working Group on 3D Terminology of Spinal Deformity, 1994, Spine, 19, 236-248.

[16] D'Amico M., Peharec S. and Rademšic D., The Measurement od the Functional State of Posture and Spine in Low Back Pain Through the 3D Non-Ionising Technique. Kinesiology, 29 (2), 1997, 5-16

[17] M. D'Amico, Scoliosis and Leg Asymmetries: a Reliable Approach to Assess Wedge Solutions Efficacy, Research into Spinal Deformities 3, pp. 285-289, IOS Press Amsterdam 2002.

Thu – July 19th 2012

Chairmen:	**Ugo Della Croce (University of Sassari, Italy)** **Aurelio Cappozzo (Università Foro Italico, Italy)**

Keynote lecture: Herman Woltring Memorial Lecture
8.30 : 9.00   *"Opinions and facts about the reconstruction of functional skeletal movement using stereophotogrammetry"*
        Aurelio Cappozzo

Podium session #3: "Video-based motion tracking - II"
9.00 : 10.30

9.00	A new technique for anatomy-based patellar tracking in navigated total knee arthroplasty: early in-vivo experiences.	Belvedere C., Ensini A., A. Feliciangeli, Dedda V., Cenni F., Giannini S., Leardini A.
9.15	Comparison of the sagittal curvature of the spine measured by skin markers and an open MRI	Zemp R., List R., Gülay T., Lorenzetti S.
9.30	New approach to evaluate dynamic footprint	Samson W., Van Hamme A., Sanchez S., Liu S., Chèze L., Van Sint Jan S., Feipel V.
9.45	Measuring lateral shuffle cut performance	de Melker Worms J.L.A., Whitting J.W., Nigg B.M.
10.00	Motion analysis of front crawl swimming: application of CAST technique for the estimation of 3D joint kinematics	Fantozzi S., Ceccon S., Sawacha Z., Cortesi M., Cobelli C., Gatta G.
10.15	Kinematic comparison of the double and triple Lutz in artistic roller skating	Fantozzi S., Querin L., Di Michele R., Ciacci S., Giovanardi A., Merni F.

!

Herman Woltring Memorial lecture

!

Opinions and facts about the reconstruction of functional skeletal movement using stereophotogrammetry

Aurelio Cappozzo

Department of Human Movement and Sport Sciences, University of Rome "Foro Italico" - Italy

The instantaneous position and orientation of a bone is reconstructed indirectly using the position of a cluster of points defined on the deformable surface of the body segment of interest and associated with the underlying bone (stereophotogrammetry). Then, the morphology of the bone under analysis and of its location relative to the point cluster is added (anatomical calibration). The result is the reconstruction *in silico* of the moving skeleton in the 3-D space and the accomplishment of the starting point for most human or animal movement analysis endeavours.

The state-of-the-art of knowledge allows for the reconstruction of bone pose during activities of daily life, work or sports with resolutions in the order of 10 degrees for orientation and 20 millimetres for position, clearly insufficient to answer many relevant scientific and professional questions. Anatomical calibration suffers from a low resolution and/or precision.

In 1983, a convention, dug from the work of Jeronymus Cardanus, was proposed, from among the many possible, and, since then, has been used to describe the relative movement between adjacent bones. The result is that the three angles that are used for this purpose have no physical meaning, are very sensitive to experimental errors, and are not additive. !

However, in the last decade biomechanics of human movement has gained a clear-cut conceptual framework which is the needed platform for affective leaps toward the development of innovative investigative tools, a new understanding of how and why man moves the way he does, and the generation of knowledge that is both scientifically sound and professionally relevant. These achievements associated with consensus on the relevant metrics, may translate into cost-effective, personalized services to protect and enhance motor function, in an e-Health context.

The establishment of an international consortium rich in scientists, professionals, manufacturers, and public bodies, with the intent of breaking the chains that have held human movement analysis down for too long, is not only timely, but also essential to solve the problems identified above.

A new technique for anatomy-based patellar tracking in navigated total knee arthroplasty: early in-vivo experiences.

Belvedere C. [1], Ensini A. [2], A. Feliciangeli [2], Dedda V. [1], Cenni F. [1], Giannini S. [2], Leardini A. [1]

[1]Movement Analysis Laboratory and [2]Department of Orthopaedic Surgery,
Istituto Ortopedico Rizzoli, Bologna, Italy,
belvedere@ior.it

Patello-Femoral Joint Kinematics; Patellar Anatomical Reference Frame Definition; Patellar Resurfacing, Total Knee Replacement.

1. INTRODUCTION

The thorough comprehension of the natural function of the human knee joint depends on a complete three-dimensional assessment of the motion of all bony segments that articulate within this joint. This is clearly of more value if achieved accurately in-vivo. This analysis would provide valid information that can be used also in a number of associated research fields. For instance, in total knee arthroplasty (TKA) this could result in the improvement of current prosthesis designs and surgical techniques.

In a number of past studies on TKA, both in-vitro and in-vivo, the conventional description for the human knee joint motion generally involved the tibio-femoral joint (TFJ) only, this being based on established anatomical and mechanical conventions [1,2]. Although the patello-femoral joint (PFJ), i.e. the other important articulating complex within the knee, plays an important role in increasing the effectiveness of the extensor apparatus, this has been generally disregarded or superficially considered in the past. However, an in-depth kinematic investigation of this further joint is thought to bring benefits in knee surgical treatments [3]. Particularly, an original methodology has been recently developed also for assessing intra-operatively the PFJ kinematics during TKA [3]. This is based on the decomposition of the pose of the patella with respect to that of the femur into three sequential rotations about and three translations along three anatomical axes, and the efficacy of which has been assessed extensively and successfully only in-vitro until now [3].

Within computer-aided techniques, knee surgical navigation systems (KSNS) have been developed for TKA to optimize femoral and tibial prosthesis component implantation via intra-operative tracking of the femur and the tibia before, i.e. at the original arthritic knee joint, and after trial and final prosthesis components implantation [4,5]. As for the PFJ, the traditional techniques in TKA, even by means of navigated procedures, used to assess patellar motion and to collect patellar morphological data are based only on visual inspections of the patellar articular aspect and manual manoeuvres, and by means of a simple calliper reading to check for patellar thickness. All these actions are ultimately achieved without any computer assistance, this being essential for more accurate measurements and three-dimensional representations [6]. However, even though the inclusion of a procedure for tracking also the PFJ kinematics based on patient-specific bone references seems fundamental in in-vivo navigated TKA, this has been completely disregarded so far within current KSNS.

From a technical point of view, recent KSNSs offer a number of potentialities for tracking PFJ motion during TKA surgery. Enhancement of these current systems plus the possible development of novel ad-hoc algorithms can be derived from related in-vitro experiences reported in the past [3, 6]. Particularly, a novel in-vivo procedure has been developed by these authors, together with dedicated software and surgical instrumentation by a company (Stryker®-Leibinger, Freiburg, Germany), as an extension of a current KSNS. As a result, TKA is enhanced by a navigation procedure, where for the first time both TFJ and PFJ kinematics are tracked simultaneously.

The aim of this study is to report early in-vivo experiences of this novel technique for measuring PFJ kinematics, in addition to standard assessments on the TFJ geometry and motion, in patients undergoing TKA by means of a navigated procedure. Particularly, a custom KSNS was developed and used in parallel to the standard clinical system to monitor the impact of the surgical procedure on PFJ kinematics.

2. MATERIALS AND METHODS

Ten patients affected by primary or inflammatory arthritis underwent primary TKA by means of a navigated technique with a fixed bearing posterior-stabilized prosthesis (NRG, Stryker®-Orthopaedics, Mahwah, NJ-USA) with patellar resurfacing. The novel procedure for patellar tracking was approved by the local ethical

committee; the patients gave informed consent prior the surgery. Particularly, all TKAs were performed using two KSNSs (both, Stryker®-Leibinger, Freiburg, Germany). The novel procedure, in fact, implies the use of a second KSNS for PFJ acquisitions (PFJ-KSNS), with dedicated software for patellar motion data collection and PFJ kinematics data storing and post-operative processing, in addition to the traditional KSNS for TFJ assessments (TFJ-KSNS). Each system is equipped with a localizer compound of three camera sensors. Both systems share the standard femoral and tibial trackers, used for relevant bone tracking and TFJ navigated implant procedures, and a pointer-like tracker used for anatomical landmark digitisations. PFJ-KSNS is further equipped with a specially designed tracker for the acquisitions explicitly dedicated to patellar motion (Figure 1). This tracker is lighter and smaller than the others and fixed by four mono-cortical screws onto patellar anterior aspect. All trackers have three light-emitting diodes embedded at least.

Figure 1. Femoral, tibial and patellar trackers fixed on corresponding bones. All trackers, including the pointer during digitization, are oriented in a way that corresponding active markers can be detected by the localizer (not in the figure).

Femoral and tibial anatomical landmark digitations are used to define anatomical reference frames according to the definitions recommended by the utilized KSNS [3,5]. Particularly, standard TFJ anatomical survey and kinematics data are shared between the two KSNS. As for the patella anatomical survey, the distal apex and the medial and lateral prominences represent the patellar landmarks employed to define the patellar anatomical reference frame. This has the origin in the mid point between the prominences, antero-posterior axis as orthogonal to the plane for these three points, proximo-distal axis along the vector from the apex to the origin, and medio-lateral axis as normal to both these axes. PFJ flex-extension, medial-lateral rotation, tilt and shift are calculated according to a recent proposal [3,7]. The anterior and posterior patellar aspects are also digitized for measuring accurately the patellar thickness.

Before surgery, both navigation systems were initialized and the patellar tracker was assembled with a sterile procedure, by shaping a titanium mesh equipped with three markers to be tracked by PFJ-KSNS only. A resection plane probe and a patella peg hole drilling template were instrumented with standard trackers, and a suitable reference frame was defined on these, by digitization with PFJ-KSNS. Afterwards, the procedures for standard navigation were performed to calculate preoperative joint deformities and TFJ kinematics [1]. The anatomical survey and PFJ kinematics recordings were performed also with PFJ-KSNS. Standard procedures for femoral and tibial component implantation, and TFJ kinematics assessment were then performed by using the corresponding trial components. The procedure for patellar resection followed: once the surgeon had arranged and fixed the patellar resection guide at the desired position, the resection plane probe was inserted into the saw blade slot. At this time, the PFJ-KSNS acquired tracker data to record the planned level and orientation of the patellar bone cut. Then the patella resection was executed, and the level and alignment of this bone cut were recorded by means of the instrumented patella peg hole drilling template. The trial patellar component was positioned, and, with all three trial components in place, TFJ and PFJ kinematics were recorded. Possible adjustments in component positioning could still be performed. Eventually, final components were implanted and cemented, and final TFJ and PFJ kinematics were acquired.

A sterile calliper and pre- and post-implantation lower limb X-rays were used to check for the patellar thickness after resurfacing and for final lower limb alignment. All kinematics variables were compared with reference normality derived using the same methodology [7].

3. RESULTS

During TKA, the procedures for in-vivo acquisition of anatomical patellar survey, definition of patient-based patellar anatomical reference frame and measurement of PFJ kinematics were performed successfully in all cases without complication and resulting only in a 30 min longer operation.

Intra-operatively, at the original arthritic knee, abnormal TFJ kinematics was observed, as expected, and quantified using the standard TFJ-KSNS. By means of the novel technique, altered PFJ kinematics was observed, this being dependent on the patient-specific PFJ state. Particularly, in those patients with a deeply impaired PFJ, this assessment revealed an abnormal tilting. In presence of dysplasia on the patellar side, an abnormal medio-lateral patella translation occurred.
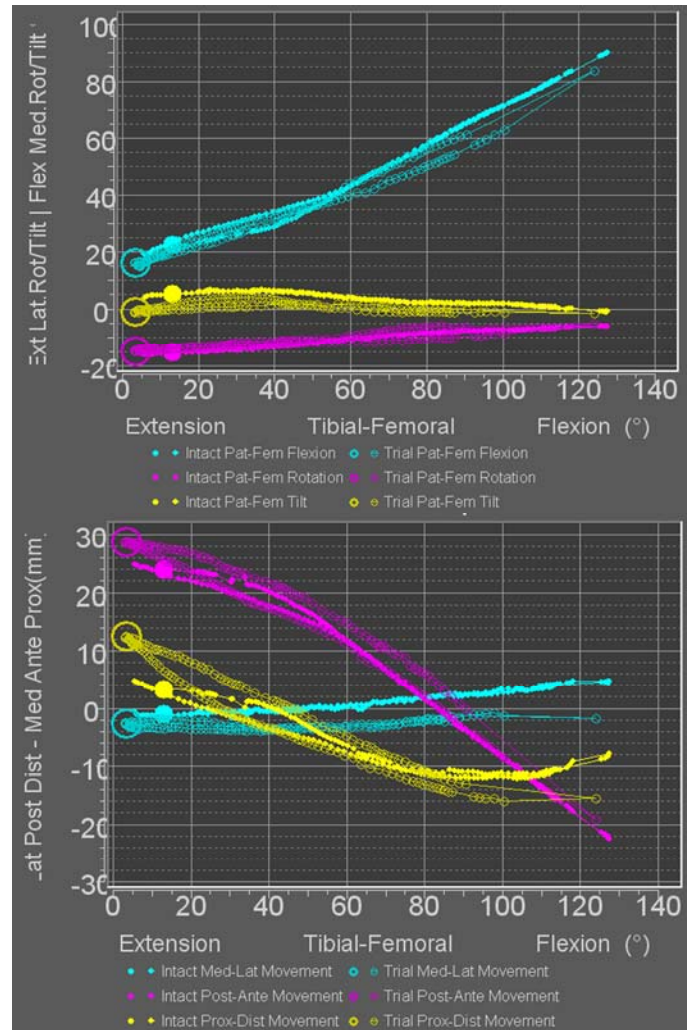

Figure 2. Snapshot of PFJ-SNS screen showing PFJ rotations (top) and translation (bottom) from a well representative TKA case. In order to allow a kinematic comparison between two different situations, data are reported both at the intact knee and after the implantation with the femoral, tibial and patellar trial components.

After the implantation of the three trial components, abnormal paths were observed in a number of patients only for PFJ kinematic variables. In these knees, abnormal lateral tilt, up to 15° more/less than the normality, and a medial translation, up to 10 mm on average more than the normality, were observed. For these patients, abnormal patellar thickness and patellar osteotomy orientation were also observed in a further patellar-dedicated check.

Ultimately, the final results demonstrated restoration of normal TFJ using the standard TFJ-KSNS, whereas the novel technique allowed the surgeon to detect possible abnormalities in PFJ kinematics. For instance, in the patient of figure 2, after TKA the physiological patellar tilt is fully restored, this being within the adopted reference normality [7], whereas the patellar medio-lateral translation is still abnormal.

The goodness of the prosthesis component alignment, this being only on the femoral and tibial side, and final lower limb alignment were observed on post-implantation X-Rays. The need to navigate patellar preparation in

the future was clearly corroborated by observed improper patellar cut execution and discrepancies in thickness of up to 5 mm PFJ-KSNS- and calliper- based measurements, both in the native patella in the arthritic knee and after patellar resurfacing.

4. DISCUSSION

The present results reveal the relevance, feasibility and efficacy of patellar tracking in in-vivo navigated TKA. At the present experimental phase, a second separate PFJ-KSNS was utilised not to affect the standard navigated TKA. These encouraging results may lay ground for the design of a future clinical patella navigation system that the surgeon can use to perform a more comprehensive assessment of the original whole knee anatomy and kinematics, i.e. including also PFJ. Patellar bone preparation would be supported for suitable patellar component positioning in case of resurfacing but, conceptually, also in not resurfacing if patellar anatomy and tracking assessment by KSNS reveals no abnormality. After suitable adjustment and further tests, in the future if this procedure will be routinely applied during navigated TKA, abnormalities at both TFJ and PFJ kinematics can be corrected intra-operatively by more cautious bone cut preparation on the femur, tibia and also patella, in case of resurfacing, and by correct prosthetic component positioning.

5. ACKNOWLEDGMENT

6. REFERENCES

[1] A. Cappozzo, F. Catani, U. Della Croce and A. Leardini. Position and orientation in space of bones during movement: anatomical frame definition and determination. Clin Biomech, 1995, 10: 171-178.

[2] E.S. Grood and W.J. Suntay. 1983. A joint coordinate system for the clinical description of three dimensional motions: application to the knee. J Biomech Eng. , 1983, 105(2):136-44.

[3] C. Belvedere, F. Catani, A. Ensini, J.L. Moctezuma de la Barrera and A Leardini. Patellar tracking during total knee arthroplasty: an in vitro feasibility study. Knee Surg Sports Traumatol Arthrosc., 2007, Aug; 15(8):985-93.

[4] M. Sparmann , B. Wolke, H. Czupalla., D. Banzer and A. Zink. 2003. Positioning of total knee arthroplasty with and without navigation support. A prospective, randomised study. J Bone Joint Surg Br. 2003 Aug;85(6):830-5.

[5] A. Ensini, F. Catani, N. Biasca, C. Belvedere, S. Giannini and A. Leardini. Joint line is well restored when navigation surgery is performed for total knee arthroplasty. Knee Surg Sports Traumatol Arthrosc. 2011 May 28. [Epub ahead of print]

[6] C. Belvedere, A. Leardini, A. Ensini, A. Feliciangeli, F. Catani and S. Giannini. Preliminary patello-femoral joint navigation in computer assisted total knee arthroplasty. An in-vitro study. Proceedings of CAOS-International 2008, 205-208.

[7] C. Belvedere, A. Leardini, A. Ensini, L. Bianchi, F. Catani and S. Giannini. Three-dimensional patellar motion at the natural knee during passive flexion/extension. An in vitro study. J Orthop Res., 2009, Nov;27(11):1426-31.

Comparison of the sagittal curvature of the spine measured by skin markers and an open MRI

Zemp R. [1], List R. [1], Gülay T. [1], Lorenzetti S. [1]

[1] Institute for Biomechanics, ETH Zurich, 8093 Zurich, Switzerland

Skin markers are often used to analyze spine movements. Three sitting positions (upright, flexed and extended) were investigated in an upright MRI to quantify the soft tissue artifacts. Changes of the lumbar and thoracic curvature are assessable with skin marker measurements but the absolute numbers suffer from a large uncertainty of approximately 50%.

Back kinematics; Soft tissue artifacts; Lordosis; Motion capture; In vivo

1. INTRODUCTION

The vertebral column is the central supporting structure of the human body. Back pain is an increasingly common affliction. According to the Swiss Federal Office of Statistics, 47% of women and 39% of man in Switzerland in 2007 had suffered from back pain in the preceding four weeks [1]. The main causes of back pain are abnormal loads and overloading of the spine. External determination of loading conditions requires knowledge of the spine's position and movement. To obtain this knowledge, a marker set for the back was developed at our institute. By using these skin-mounted reflective markers, it is possible to identify global parameters of the spine, such as curvature and back segment rotations [2]. However, it is not known how precise the calculations of these parameters are.

Gait analysis techniques based on motion tracking of skin-mounted reflective markers have increased in popularity and are currently widely used in gait and motion labs. Advantages of skin markers include ease of application, non-invasiveness and the subject's movements being barely affected by the measuring system. However, the main problem of this method involves marker artifacts caused by skin movements with respect to the subjacent bones. Soft tissue deformation during movements occurs in all three directions, and the distributions are non-uniform [3]. Thus, measurements with skin markers are not fully accurate, and an exact analysis of bone position is impossible. Soft tissue artifacts (STAs) cannot be neglected but instead should be quantified to evaluate the quality of the data recorded using skin markers.

Several studies have validated skin markers on different body regions [2-4], but validation studies of back markers are very rare. Hence, the aim of this study is to analyze the soft tissue artifacts and their influence on the determination of global parameters of the spine.

2. MATERIAL AND METHODS

Accuracy of the Open Upright MRI and the image segmentation

The accuracy of the MRI and the data handling were determined using a plate of acrylic glass with five skin markers (represented by MRI-visible paintballs) and two lamb vertebras (Fig. 1). The acrylic glass plate was examined with an Open Upright MRI in a horizontal (0 °), forward tilted (45 °) and vertical position (90 °). The distances between the five markers and the vertebral bodies in the three positions were determined using the MRI pictures and compared with the true values.

Subjects

Seven (3 female and 4 male) healthy subjects gave informed consent to participate in this pilot study which was approved by the local ethics committee. The average age was 29 years (σ=9 y, range: 22-46 y), the mean height was 174 cm (σ=10 cm, range: 160-184 cm), and the average weight was 71 kg (σ=16 kg, range: 55-96 kg).
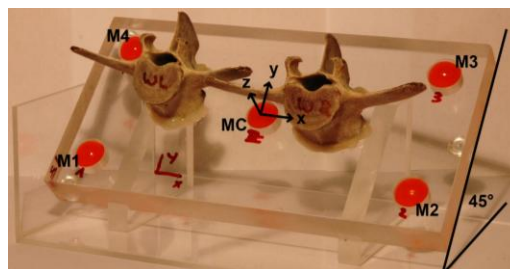

Figure 1. Plate of acrylic glass with five skin markers (orange paintballs: M1, M2, M3, M4, MC) and two lamb vertebras in a forward tilted position (45 °).
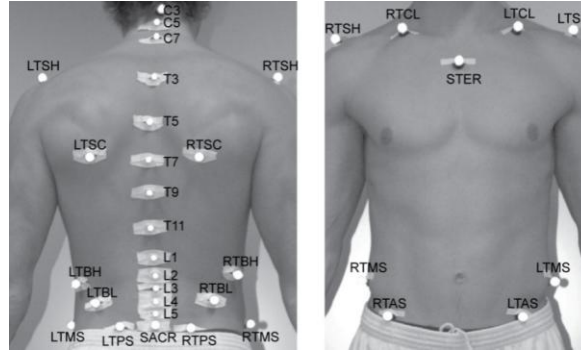
Figure 2. Marker set of the trunk and the pelvis.

Position in the MRI

The subjects' lumbar and thoracic spines were separately examined with their respective markers in an Open Upright MRI in three different seating positions:

- **Upright seating position:** The lower spine had slight contact with the backrest, and the whole upper body was in an upright position.
- **30 °-Flexion of the back:** The upper body was tilted forward (about 30 °) and supported on a bar. The arms were placed on the shanks.
- **10 °-Extension of the back:** The bottom was pushed approximately 20 cm forward and the head was supported by the backrest.

Instrumentation

Measurements were taken in the Upright MRI Center Zürich with the FONAR Upright^{TM} MRI (0.6 Tesla). T2-weighted sagittal images were taken. The resolution was 240x240 in an image plane of 360x360 mm. The layers were ranked without any gaps between the marginal markers. To connect the motion capture system with the MRI measurements, MRI-visible paintballs were used. Their caliber was .68 (diameter of 17.3 mm). The markers were placed on washers and were affixed with a toupee plaster on the skin.

Marker set

The marker set used at our institute consists of 40 skin markers on the lower extremities, 7 on the pelvis and 24 on the trunk. This marker setup is based on the work of Dettwyler [4], List [5] and Unternährer [6] and was used and developed further in Stoop's [7] and Gülay et al.'s works [8]. The upper body marker set [7, 8] includes the 31 markers on the pelvis and the trunk (Fig. 2). In this study, only the markers for the lumbar (L1-L5, RTBL, LTBL) and thoracic (T3-T11, RTBH, LTBH, RTSC, LTSC, STER) segments were used.

Data analysis

The MR images were segmented so that distinct three-dimensional bodies (marker and vertebral bodies) were generated. Spheres were fitted to the markers, and their centers were located. Furthermore, the vertebral body's centers of gravity were determined. Local coordinate systems were created at each investigated vertebral body. Changes in the vectors pointing from the center of mass of the vertebral bodies to the corresponding marker in the local coordinate system describe the STAs in the flexed and extended positions. The marker artifacts were defined as the addition of the direction-related changes calculated with the Gaussian method [9]. The measurements in the upright seating position were considered to be the reference position.

To determine the curvatures c of the lumbar and thoracic spines, the coordinates of the marker and the vertebral bodies were projected into the sagittal plane of the trunk. The curvature was calculated by fitting a circle to the projected center of the markers respective to the vertebral bodies. The fitting was performed using the least squares method of Pratt [10]. The curvature c was calculated as follows:

$$c = 1 / R. \qquad (1)$$

R is the radius of the fitted circle in meters. A kyphosis was defined as a positive ($c > 0$) value, and a lordosis was defined as a negative value ($c < 0$).

To analyze the segment rotation, the lumbar and thoracic segment markers were considered separately. The rotation angles between the upright and flexed or extended positions were calculated for the markers and for the corresponding lumbar and thoracic parts of the spine. The marker cloud calculations were made using the least squares method of Gander and Hrebícek [11]. The rotation matrix or the rotation angle was calculated between the marker cloud in the upright and the flexed or extended positions. As the reference, a 3D regression line was fitted to the gravity center of the vertebral bodies (lumbar: L1-L5, thoracic: T2-T12), and the angles between the lines in the different positions were calculated.

Statistics

All statistics were determined using IBM SPSS Statistics (Version 19, SPSS Inc., Chicago, USA). The statistical significance level was set at $p<0.05$. The lumbar and thoracic measurements were analyzed separately.

The absolute marker artifacts were analyzed with analyses of variances (ANOVA) for the subjects, positions and marker locations. Furthermore, correlations between the curvature values based on the marker and vertebral body coordinates were investigated using linear regression analysis.

3. RESULTS

Accuracy of the Open Upright MRI and the image segmentation

The estimated direction-related measurement accuracy (in standard deviations σ) of the markers and the vertebral bodies are listed in Table 1.

Table 1. Direction-related measurement accuracy (σx, σy, σz [mm]) of the markers and the vertebral bodies expressed in standard deviations.

	σ_x	σ_y	σ_z
Marker	1.0	0.5	0.5
Vertebral body	2.0	1.0	1.0

Marker artifacts due to STA

The mean marker artifacts in the flexed and extended positions were 10.2 ± 6.1 mm (lumbar) / 9.3 ± 4.2 mm (thoracic) and 10.7 ± 4.8 mm (lumbar) / 9.2 ± 4.9 mm (thoracic), respectively. The maximal measured value was 27.4 mm for the marker L5 in the flexed position.

One-factor variance analyses (ANOVAs) indicated significant differences only between subjects (*p*-value<0.001) and not between positions or markers for the individual lumbar and thoracic measurements.

Lumbar and thoracic curvature c

The scatter diagrams (Fig. 3) show the lumbar and thoracic curvature calculated using the markers and the vertebral bodies. The lumbar and thoracic curvature's range of motions (ROM) from the upright to the flexed and extended positions are illustrated in Fig. 4.

Segment rotation

The mean measurement error of the lumbar and thoracic segment rotations calculated using the skin markers were 2.5 ± 2.7 ° (max. 6.6 °) and -1.1 ± 2.9 ° (max. 9.1 °), respectively.

4. DISCUSSION

The marker artifacts of the back are in the same range as they are for other locations in the human body. The observed intra- and interindividual patterns of the STAs of the subjects during flexion and extension of the spine do not allow for determination of a common correction method by which to estimate the behavior of a single marker. In general, the intraindividual differences are larger than the differences within a single subject or the positions. This result is in agreement to results from studies on the knee joint [12].

Besides describing the limitations, this study also opens further possibilities. Based on motion capture data of the marker set used, it is possible to predict the change of the lumbar and thoracic curvature during movement. Furthermore, a rough analysis of the lumbar and thoracic segment rotations is also possible. Our results indicate
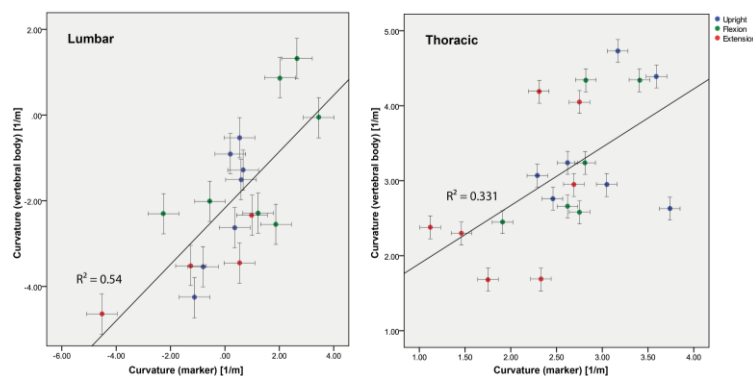

Figure 3. Scatter diagram of the lumbar (left) and thoracic (right) curvature in the upright (blue), flexed (green) and extended positions (red). The x-axis represents the values calculated from the markers, and the y-axis from the vertebral bodies. The crosses show the measurement accuracy of each data point.
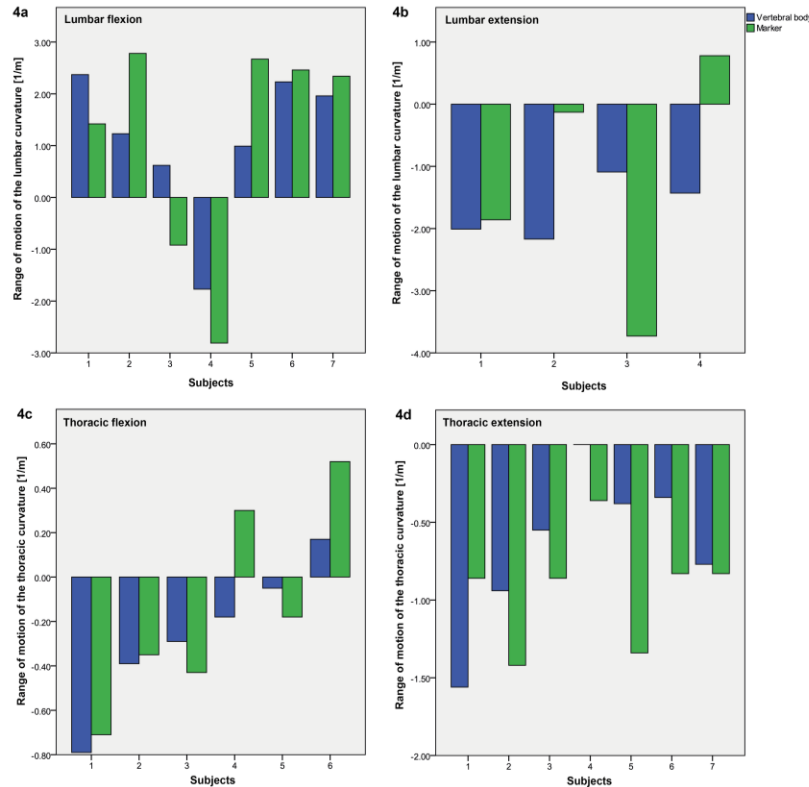
Figure 4. Lumbar (4a/b) and thoracic (3c/d) curvature range of motion (ROM) of the subjects, calculated using the vertebral bodies (blue) and the skin markers (green). The ROM was defined from the upright to the flexed (4a/c) and to the extended positions (4b/d).

that a change of the lordotic/kyphotic shape but not of the absolute amount of curvature can be estimated using skin markers.

In this study, only the movement of the spine in the sagittal plane was assessed. In other planes, the movements are smaller, and it is more difficult to precisely place the skin markers close to the anatomical landmarks with respect to movements. Due to our layer orientation in the open MRI, movement in the frontal and the horizontal plane could only be assessed with reduced accuracy. This fact means that the observed errors are at least of the same magnitude as those in the sagittal plane but are most likely larger. Furthermore, the present study only allowed the quantification of the STAs in a static set up. It must be assumed that in dynamic activities, e.g. during impact situations, STAs are even larger.

In conclusion, this study demonstrates that the used marker set is suitable for measuring the change of the shape of the spine, but measurement of the absolute curvature is not possible with skin markers. A segmental approach is less accurate but could be used to address specific research questions.

5. REFERENCES

[1]   Swiss Federal Office of Statistics (Bundesamt für Statistik): *Swiss Health Survey 2007 (Schweizerische Gesundheitsbefragung)*.
[2]   List, R., T. Gülay, and S. Lorenzetti. *Kinematics of the trunk and the spine during unrestricted and restricted squats - A preliminary analysis*. 28th Conference of the International Society of Biomechanics in Sports. Marquette, Michigan, USA, 2010.
[3]   Gao, B. and N.N. Zheng. *Investigation of soft tissue movement during level walking: translations and rotations of skin markers*. J Biomech, 2008. **41**(15): p. 3189-95.
[4]   Dettwyler, M.T. *Biomechanische Untersuchungen und Modellierungen am menschlichen oberen Sprunggelenk im Hinblick auf Arthroplasiken*. PhD. thesis, ETH Zürich., 2005.
[5]   List, R. *A hybrid marker set: for future basic research and instrumented gait analysis at the Laboratory for biomechanics*. Thesis, ETH Zürich., 2005.
[6]   Unternährer, S. *Entwicklung eines Markersets für Rückfuss und Vorfuss*. Thesis, ETH Zürich., 2005.
[7]   Stoop, M. *Biomechanik der Kniebeuge: Berechnung der Kräfte und Drehmomente am Knie- und Hüftgelelnk in Abhängigkeit der Bewegungsausführung*. Thesis, ETH Zürich., 2009.
[8]   Gülay, T., R. List, and S. Lorenzetti. *Moments in the knee and hip during descent and ascent of squats*. 29th Conference of the International Society of Biomechanics in Sports. Porto, Portugal, 2011.
[9]   Bevington, P.R. *Data reduction and error analysis for the physical sciences*. McGraw-Hill Book Co., New York, 1969.
[10]   Pratt, V. *Direct Least-Squares Fitting of Algebraic Surfaces*. Computer Graphics, 1987. **21**(4): p. 145-152.
[11]   Gander, W. and J. Hrebícek. *Solving Problems in Scientific Computing Using Maple and MATLAB. Chapter 23: Least Squares Fit of Point Clouds*. Springer Verlag, 1997. **3**: p. 339ff.
[12]   Garling, E.H., B.L. Kaptein, B. Mertens, W. Barendregt, H.E. Veeger, R.G. Nelissen, and E.R. Valstar. *Soft-tissue artefact assessment during step-up using fluoroscopy and skin-mounted markers*. J Biomech, 2007. **40 Suppl 1**: p. S18-24.

Motion analysis of front crawl swimming

Application of CAST technique for the estimation of 3D joint kinematics

Fantozzi S. [1,2], Ceccon, S. [3], Sawacha Z. [3], Cortesi M. [2], Cobelli C. [3], Gatta G. [2]

[1] Dept.of Electronics Computer Sciences and Systems, University of Bologna, Bologna, Italy
[2] Faculty of Exercise and Sport Science, University of Bologna, Bologna, Italy
[3] Dept. of Information Engineering, University of Padova, Padova, Italy

Kinematic analysis of swimming is of interest to enhance swimming performances. Although the video recordings of underwater swimmers are widely diffused, the available methodologies are rarely precise enough to adequately estimate the three dimensional (3D) joints kinematics. Thus, a procedure to investigate the right upper limb's 3D kinematics during front crawl swimming is proposed. The method is based upon the Calibrated Anatomical Systems Technique (CAST), a technique widely used in clinics which allows estimation of anatomical landmarks of interest even when they are not directly visible. An automatic tracking technique was adopted. Results showed that the complete 3D kinematics of at least twice as many frames than without CAST can be reconstructed.

front crawl swimming, biomechanics, 3D joint kinematics, calibrated anatomical systems technique

1. INTRODUCTION

In order to define the appropriate performance model of the swimmer it is necessary to analyze the technique of different athletes with different levels of performance [1]. For developing accurate specific athlete coordination patterns and identifying the factors that actually influence the performances, a detailed kinematic analysis of the technique is necessary. This could allow a complete comparison among athletes with different performance levels, anthropometric characteristics, technical skills, and distance specialization, thus helping the coaches to design specific training programs. A limitation with the majority of the studies on kinematic analysis is that little three dimensional (3D) joint quantitative data is provided in order to investigate stroke characteristics. It has been also suggested that the arm trajectory during swimming is mainly described in a mediolateral plane, however the discussion in the literature is concentrated on 2D analysis of swimming, and specifically on the sagittal plane [2; 3]. A 3D analysis of the stroke can also be found in [4] but only in relation to a single segment of the kinematic chain of the upper limb. It should be mentioned that [5] estimated the 3D position of the joint centers during front crawl swimming in sprinters and long distance swimmers. However the markers were drawn on the subject in order to maximize their visibility on the different views and not to accurately obtain the position of standard ALs [6]. Therefore, no standard joint centers and systems of reference were used, thus enabling estimation of joint planar angles but not 3D joint kinematics. In this contest, the authors recently developed a video-based, markerless system for the kinematic analysis of the upper limb during front crawl swimming [7]. 3D coordinates of shoulder, elbow and wrist joints centers of 5 sprint swimmers performing front crawl swimming were determined. To the authors' knowledge, no previous studies estimated 3D joints rotations of the upper limb in terms of both the shoulder and the elbow's rotations during front crawl swimming. The purpose of this paper is to develop a precise and accurate method to investigate 3D joint kinematics of the stroke during the whole underwater phase of crawl swimming. In order to overcome the gaps in the results due to the lack of anatomical features visibility while keeping the markers on the standard ALs, the Calibrated Anatomical Systems Technique (CAST) [8] was adopted. Several technical markers were added to reconstruct all the anatomical features necessary for 3D joint kinematics. Due to the number of markers, the manual tracking of features currently used in the underwater motion analysis system was not adopted. Rather, an automatic tracking of features was developed. This allowed better precision in data reconstruction and reduced elaboration time. In this context, the right upper limb of one swimmer was acquired and analyzed during a front crawl swimming full cycle by means of 6 underwater color analogic cameras.

2. METHODS

Data acquisition

Several front crawl trials were performed by an elite swimmers in a 25 m swimming pool. Six underwater color analogic wide-angle cameras (TS-6021PSC) with 720 x 576 pixel resolution were placed to maximize the field of view for the swimmer's right upper limb in a crawl. Each camera was connected to a computer through an Analog to Digital Video Converter (Canopus ADVC55).. The system was synchronized automatically with an ad-hoc application which routes the triggering signals through a local area network and
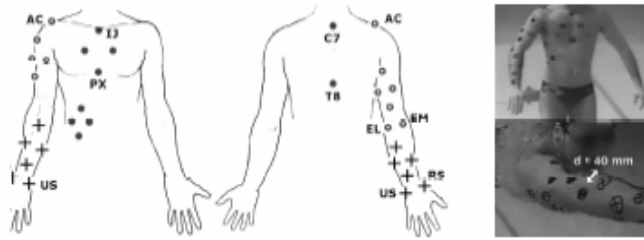
Figure 1. Description of the features for each of the three clusters and the nineanatomical landmarks of interest. A photo showing the actual markers used and their approximate size is also included

stores data in each computer. The synchronization delay was found to be inferior to a frame duration, which in the present study is 20 ms. Calibration of cameras' intrinsic parameters was achieved from a dry acquisition of a checkerboard pattern and corrected for underwater application as suggested by [9]. A correction factor of 1.333 was also applied in order to take into account the different focal length due to the different refractive index of the water. The extrinsic parameters indicating the position and orientation of the cameras in the global reference system were calibrated underwater by means of a steel cage (2070 x 1070 x 1400 mm). The parameter estimation was accomplished using the Camera Calibration Toolbox for Matlab [10].

Protocol

A 3D protocol for upper extremities kinematics based on the CAST technique [8] was adopted. 31 markers were drawn on the body of the swimmer as shown in Figure 1, in relation to 3 segments (trunk, arm, and forearm) of the kinematic chain. The markers, crossed circles with a diameter of about 4 cm, were drawn on the skin with an indelible ink that would not easily come off with water or sweat. The following ALs were chosen in order to perform the 3D kinematics [10]: processus xiphoideus (PX), incisura jugularis (IJ), seventh cervical vertebra (C7), acromion (AC), lateral and medial epicondyles of the humerus (EL and EM, respectively), radial and ulnar styloid process (RS and US, respectively). The following technical clusters formed by several markers were used in order to estimate the ALs of interest: 4 markers on the right abdomen, 1 on the thoracic spinal nerve 8 (T8) and 2 on the upper chest for PX, IJ and C7; 4 markers on the lateral side and 4 on the medial side of the arm for AC, EL and EM; 4 markers on the medial side and 4 on the lateral side of the forearm for US and RS. From a biomechanical viewpoint, the arm was modeled as an open kinematic chain formed by 3 segments (thorax, humerus and forearm), with 5 DOF: 3 of the shoulder and 2 of the elbow. The thorax and the proximal humerus bone embedded reference systems were defined following the ISG recommendations [11]: H1 for the humerus, with the z axis pointing backward. The shoulder girdle was not taken into account in the model in order to avoid possible errors which may affect the accuracy of the reconstruction of the markers position in the current setup. Joint angles were obtained by decomposing the relative orientation of adjacent segments and using appropriate sequences of Euler angles. Further methodological details can be found in [12]. The digitalization of the positions of features from each video sequence, namely tracking, was performed by ad-hoc software. Given an initial guess of the feature position from an experienced operator, the automatic tracker uses the gradient of the spatial intensity to optimally search for the vector that minimizes the difference between the surroundings of the feature in adjacent frames, as proposed by [13] and developed by [14]. The proposed position of the marker in the upcoming frame can then be accepted or corrected on screen by the operator.

Data Analysis

Given the tracked position of the markers from each camera view, the triangulation process was applied to obtain the 3D position of the markers in each frame. The Direct Linear Transformation algorithm [15] was used to perform the triangulation. The results of the manual tracking were compared with those of the automatic tracking. Two procedures were applied and compared to perform the 3D trajectories reconstruction: 1) automatic tracking without applying the CAST technique; 2) automatic tracking together with CAST technique. Root mean square difference values (RMSD) were calculated between trajectories to quantify the agreement between the 2 procedures. A measure of the resolution of the system was obtained by acquiring a moving wand on the volume of interest. Two markers were applied on the wand at a known distance of 10 cm and they were then acquired. The distance between the markers was calculated and compared to the exact distance, obtaining an estimation of the actual error of the acquisition and reconstruction system. The performance of each technique was also evaluated in terms of percentage of the duration of the stroke during which each technique was able to reconstruct the 3D trajectories of the ALs.
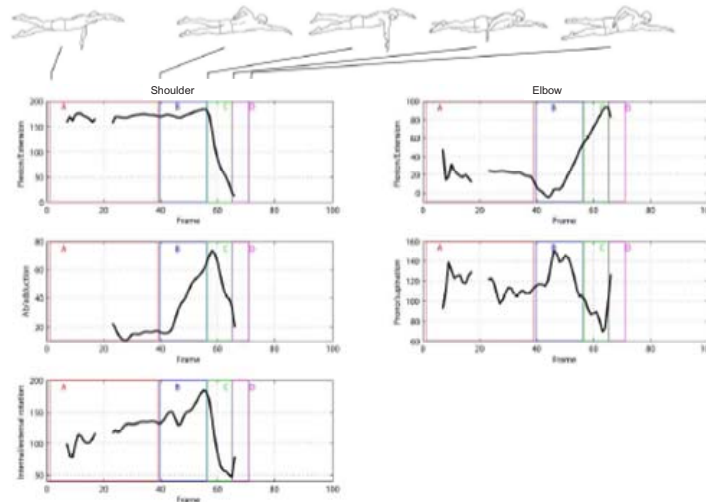
Figure 2. Flexion/Extension, Ab/Adduction and Internal/External rotation of the shoulder joint (left column) and Flexion/Extension and Prono/Supination of the elbow joint (right column). The different phases of the crawl while the arm is underwater are evidenced: A, B, C and D corresponds to the entry and stretch phase, the down sweep phase to catch, the in sweep, and the up sweep respectively

3. RESULTS

From the moving wand acquisition, the accuracy of the set up adopted show a mean error of 0.46 mm with SD of 7.58 mm. 3D joint angles for the shoulder Flexion/Extension, Internal/external rotation and Ab/Adduction and for the elbow Flexion/Extension and Prono/Supination are shown in Figure 2. During the entry and stretch phase, the shoulder joint was flexed (about 170°) and internally rotated (about 130°) the elbow joint was slightly flexed (about 20°) and pronated (about 110°). During the down-sweep phase to catch, the shoulder joint continued its flexed pattern, while abducting (from 15° to 60°) and internally rotating (from 130° to 185°). In the same phase, the elbow joint showed two different trends: the first one displayed an extension (from 10° to -5°) and pronation (from 117° to 150°), while the second shows a flexion (from -5° to 53°) and supination (from 150° to 105°) of the elbow. By considering the joint angles patterns in the frontal plane, in this specific phase, both an "out" and "down" arm motions were identified. During the in-sweep phase, the shoulder joint was extending (from 170° to 10°), adducting (from 70° to 20°) and externally rotating (from 185° to 50°), the elbow joint was flexing (from 53° to 94°) and supinating (from 105° to 70°). Few frames were elaborated for the up-phase. The maximum and minimum values of the internal/external rotation of the shoulder joint clearly identified the different phases of the crawl. Regarding the number of frames in which the 3D kinematics was estimated, there were several gaps in the results without the use of the CAST tecnique. At least twice as many frames can be reconstructed (over the whole underwater front crawl phase) in terms of joints kinematics, compared to manual and automatic tracking. The use of the automatic feature tracker reduced the tracking time of indicatively 25-50% for each 100 frames sequence with 31 markers, although precise estimation of elaboration time was not assessed in this study.

4. DISCUSSION

This study adapted the CAST protocol, an established approach typically used in clinics, to the sport aquatic environment, specifically to front crawl swimming. In this context, the lack of standards and precision, due to the difficult environment and to the complex nature of the movement itself, prevents a full and detailed analysis of the movement, which is instead commonly obtained in clinics. The aim of the present contribution was to develop a precise and accurate method to investigate 3D joint kinematics of the stroke during the whole underwater phase of crawl swimming. Thus, in order to improve precision and to reduce elaboration time, an automatic tracking of features was also developed and used. The developed method was applied on the right upper limb of a swimmer during a front crawl swimming full cycle by means of 6 underwater color analogic cameras.The sensible gaps in terms of frames in which the IJ and AC trajectories can be obtained directly from the tracking were sensibly filled using CAST for both MAN and AUT. Figure 7 clearly illustrates how the use of the CAST technique allows reconstruction of EM, RS, T8, C7 and AC trajectories where by the means of manual tracking was not possible. For the first time, to the authors' knowledge, the availability of a full set of ALs enabled the evaluation of 3D arm's joint angles and the clear identification of the different phases of the movement. Each joint could be analyzed in its typical patterns and in relation to the specific phase of the movement (Figure 2). On the contrary, the planar angles estimated without the use of the CAST technique should not be considered representative of the pattern of motion. Even though they allowed

the collection of more complete results and interesting insights, as in [5], these were estimated by means of interpreting the markers' positions, given the scarce visibility of the conventional anatomical markers during swimming. This prevented the use of repeatable joint centres, and rotation axes to obtain complete results, such as a 3D joint angles description in terms of organization of the DOF of all joints. In the unique previous study [16] which reported the 3D joint kinematics of the upper extremity, the positions of the shoulder, elbow and wrist joints were interpreted, leading to less repeatable results. Regarding the synchronization, it was accomplished without any built-in and highly expensive features and obtained overall acceptable performances for this analysis. The present approach also overcame the shortcomings of the posterior synchronization systems as discussed by [17], particularly those related with an event-based synchronizationj. The correction factor for the water distortion proposed by [9] confirmed in our study its suitability in obtaining precise and faster camera calibration. The present methodology enabled to overcome important limitations of the previous publication [7], in particular the presence of ''phantom volumes'' in the visual hulls reconstructed for some part of the stroke which was exacerbated at shoulder level, which may prevent shoulder joint angles computations. A further limitations of the previous method lied in the requirement that the whole body under investigation should be in view at all times, therefore reconstruction for the initial and final phases of the stroke, when the arm is partially out of water, was not currently possible. In the present study, the application of the CAST technique enables the reconstruction of each stroke phases (see Figure 2). The methodology developed in this paper will be used for comparison and assessment of different characteristics of athletes (e.g. anthropometry, technical skills, performance levels, distance specializations) by analyzing a higher number of subjects. Furthermore, it will be used as a gold standard for the 3D joint kinematic estimation obtained using the markerless technique recently developed by the authors [7].The CAST procedure proposed in this paper shows good agreement and enhanced the efficiency of the 3D joint analysis with respect to a direct measurement of the ALs. The use of the CAST procedure also permitted, for the first time, to assess a repeatable 3D pattern of the angles of the joints during the whole movement action, proving itself as an effective and feasible technique for complete kinematics analysis in these conditions. When combined with an automatic feature tracking technique, more precise and repeatable estimations of the ALs positions can be obtained, in an attempt to solve the high inter- and intra- operator variability affecting the manual tracking.

5. REFERENCES

[1] Consilman, J. E., The science of swimming. Prentice-Hall, Englewood Cliff: New Jersey, 1973.

[2] Chollet, D., Chalies, S., Chatard, J.C., 2000. A new index of coordination for the crawl: description and usefulness. Int J Sports Med 21(1), 54-59.

[3] Seifert, L., Chollet, D., Brady, B.G., 2004. Effect of swimming velocity on arm coordination in the front crawl: a dynamic analysis. J Sport Sci 22, 651-660.

[4] Vezos, N. et al., 2007. Underwater stroke kinematics during breathing and breath-holding front crawl swimming. J Sci Med Sport 6, 58-62.

[5] McCabe, C.B., Psycharakis, S., Sanders, R., 2011. Kinematic differences between front crawl sprint and distance swimmers at sprint pace. J Sports Sci 29, 115-123.

[6] McCabe, C., 2008. Effects of 50m and 400m race paces on three-dimensional kinematics and linear kinetics of sprint and distance front crawl swimmers. PhD Thesis, University of Edinburgh.

[7] Ceseracciu, E., Sawacha, Z., Fantozzi, S., Cortesi, M., Gatta, G., Corazza, S., Cobelli, C. 2011. Markerless analysis of front crawl swimming. J Biomec 44(12), 2236-42.

[8] Cappozzo, A., Catani, F., Della Croce, U., Leardini, A., 1995. Position and orientation in space of bones during movement: anatomical frame definition and determination. Clin Biomech 10(4), 171-178.

[9] Lavest, J.M., Rives, G., Lapresté, J.T., 2003. Dry camera calibration for underwater applications. Mach Vision Appl 13(5), 245-253.

[10] Bouguet, J.Y., 2008. Camera calibration toolbox for Matlab. http://www.vision.caltech.edu/bouguetj/ calib_doc/index. Html

[11] Van der Helm, F.C. et al., 2004. ISB recommendation on definitions of joint coordinate systems of various joints for the reporting of human joint motion—Part II: shoulder, elbow, wrist and hand. J Biomec 38, 981-992.

[12] Garofalo, P. et al., 2009. Inter-operator reliability and prediction bands of a novel protocolto measure the coordinated movements of shoulder-girdle and humerus in clinical settings. Med Biol Eng Comp 47, 475-486.

[13] Lucas, B.D., Kanade, T., 1981. An iterative image registration technique with an application to stereo vision. Intl Joint Conference on Artificial Intelligence 16(3), 674-679.

[14] Tomasi, C., Kanade, T. Detection and tracking of point features. Technical report CMU-CS-91-132, Carnegie Mellon University, Pittsburg, PA, 1991.

[15] Hartley, R., Zisserman, A., 2003. Multiple view geometry in computer vision. Cambridge University Press, Cambridge.

[16] Payton, C.J., Baltzopoulos, V., Bartlett, R., 2002. Contributions of rotations of the trunk and upper extremity to hand velocity during front crawl swimming. J Appl Biomech 18, 243-256.

[17] Pourcelota, P., Audigiéa, F., Degueurcea, C., Geigerb, D., Denoixa, J.M., 2000. A method to synchronise cameras using the direct linear transformation technique. J Biomec 33(12), 1751-1754.

Kinematic comparison of the double and triple Lutz in artistic roller skating

Fantozzi S. [1,2], Querin L. [1], Di Michele R. [1], Ciacci S. [1], Giovanardi, A. [1], Merni F. [1]

[1] Faculty of Exercise and Sport Science, University of Bologna, Bologna, Italy
[2] Dept.of Electronics Computer Sciences and Systems, University of Bologna, Bologna, Italy

The purpose of this study was to compare the double and triple Lutz figure skating jumps and determine their key biomechanical differences in order to provide coaches with helpful information for teaching the triple Lutz. Data were collected from five male world-class roller skaters using a stereophotogrammetric system. The most relevant difference concerned a higher pelvis rotational velocity of the triple with respect to the double Lutz, not only in the flight phase (4.1 vs. 3.3 rev/s, respectively) but also from the toe-pick. Furthermore, a higher vertical velocity at take-off was observed in the triple jump, that can be explained from the greater flexion-extension of the right hip and knee from toe-pick to the take-off. On the contrary, the average horizontal approach speed was lower for the triple compared to the double Lutz.

Keywords: biomechanics, jumping performance, roller skating, stereophotogrammetry.

INTRODUCTION

Elite skaters must be able to perform triple revolutions jumps. The jumps are so quick and complex that coaches have difficulties in discerning what the skaters do while executing double and triple jumps. Knowing the biomechanical key factors of each jump, is therefore fundamental for figure skating coaches in order to more effectively teach triple jumps to their athletes. Biomechanical analysis can assist coaches in this endeavor.

To date, the majority of biomechanical analyses of figure skating jumps have been carried out on ice skating, and they have focused on the Axel jumps. King, Arnold, and Smith [1] in a comparative analysis of single, double and triple Axel in five male skaters, found lower horizontal speed, steepest take-off angles, and higher rotational velocity in triple with respect to double Axel, but no differences in the vertical velocity at take-off and jump height. The rapid evolution of quadruple jumps has motivated research to investigate on this issue. Toe-Loop jump was one of the first quadruple jump performed in competitions. King et al. [2] conducted a detailed biomechanical analysis of triple and quadruple Toe-Loop, focusing on descriptive variables that are decisive in the opinion of coaches. The authors concluded that rotational velocity in the air was higher for quadruple Toe-Loop compared to triples and the greater vertical velocity was gained during the propulsive phase due to the extension of the legs.

While the Axel is an edge jump, and it is fundamentally a different type of jump with respect to the Lutz, the Toe-Loop is a pick jump similar to the Lutz, although the toe pick is performed with the contralateral leg. Since the triple Lutz is necessary for successful performance in figure skating at international level, King [3] examined the segmental contributions of the arms and the free leg and the use of the toe-pick in generating vertical velocity for the triple Lutz. That study showed that during the propulsive phase of the triple Lutz, the relative contribution of the arms and free leg was, on average, only 2.89% of the vertical momentum of the skater. Furthermore, skaters use the toe-pick to generate vertical velocity for the jump through the flexion of the right leg. Notwithstanding the number of studies on ice skating, no biomechanical jump analysis, to the knowledge of the present authors, was performed on roller skating. The purpose of the present study was to compare the double and triple Lutz jumps in roller skating and to determine their key biomechanical differences in order to provide coaches with helpful information for teaching the triple Lutz.

MATERIALS AND METHODS

Five elite male skaters performed a series of double and triple Lutz in an appropriate jump court. Among the several jumps performed by each athlete, one double and one triple Lutz jumps were chosen for the analysis. The jumps were selected if the majority of markers were well reconstructed by the stereophotogrammetic system and if that jump was rated from fair to excellent by two national coaches.

Figure 1 - Photographic sequence representing the Lutz key events.

Ten infrared cameras (Smart-D, BTS, Milan, Italy, 250 Hz) were positioned in two semicircles along the trajectory of the jump. 40 markers were attached on the body of each skater. For the trunk, the upper limbs and the foot segments, the markers were attached directly on specific anatomical landmarks. For the thigh and the shank segments, the Calibrated Anatomical System Technique was exploited, and for each body segment a technical cluster of four markers was used, as described by Cappozzo et al [4]. The reference systems for the lower body segments were defined following the ISB recommendation [5] and appropriate sequences of Euler angles were used. Following data collection, each jump was semi-automatically tracked using the stereo-photogrammetric system software (Smart Tracker, BTS).

In order to analyse the relationship between horizontal and vertical velocity, the resultant velocity angle was also considered: an angle higher than 45° points out that the athlete uses a vertical velocity higher than the horizontal one.

Five key events were identified for each jump (Figure 1): toe-pick (instant the toe-pick was placed into the ground), end of gliding (last contact of the left foot), take-off (last contact of the right foot), maximum height (top of the flight phase), and landing (instant of contact with on the ground).

RESULTS

The hip and the knee were flexed at the toe-pick, whereas the flexion was clearly lower at the take-off (Table 1). On the contrary, the ankle at toe-pick was in the neutral position, and plantarflexed at the take-off, but in a different manner depending on the skater. Other variables as horizontal and vertical velocity of the pelvis and take-off angle were measured during the take-off (Table 2). The skaters' horizontal velocities at take-off for the triple Lutz (mean: 2.69 m/s) were lower than those for the double one (mean: 3.17 m/s). Vertical velocities at take-off showed slightly higher values for the triple compared to the double Lutz. The average resultant velocity angle in the five athletes was 40° in the double and 47° in the triple Lutz, at the take-off. The greatest difference between the double and triple jumps was the rotational velocity during the flight estimated from the rotation of the pelvis segment (Table 3). The pelvis rotation velocity was higher in the triple Lutz already during the toe pick (means D 0.84 rev/s, T 1.75 rev/s). Jumping height and flight time were higher for the triple jump for three skaters.

| Skater | Hip flexion (°) | | | | Knee flexion (°) | | | | Ankle flexion (°) | | | |
| | Toe-pick | | Take-off | | Toe-pick | | Take-off | | Toe-pick | | Take-off | |
	D	T	D	T	D	T	D	T	D	T	D	T
A	28	30	0	0	41	50	15	19	-1	5	-24	-23
B	29	31	10	14	59	64	0	11	-6	-5	-24	-19
C	33	35	4	2	55	57	4	11	0	6	-22	-6
D	37	45	6	5	58	67	3	19	2	9	-7	-8
E	36	38	5	6	55	61	1	18	-1	-3	-1	-35

Table 1 – Double (D) and Triple (T) Lutz toe-pick and take-off parameters for the five skaters.

| Skater | Horizontal velocity (m/s) | | Vertical velocity (m/s) | | Take-off angle (°) | |
	D	T	D	T	D	T
A	2.68	2.07	2.62	2.79	44	53
B	3.35	2.91	2.99	3.13	42	47
C	3.44	3.35	2.90	2.93	40	41
D	3.08	2.66	2.19	2.62	35	45
E	3.32	2.47	2.90	3.01	41	51

Table 2 - Double (D) and Triple (T) Lutz take-off velocity parameters.

Skater	Height (m)		Flight time (s)		Pelvis rotational velocity (rev/s)	
	D	T	D	T	D	T
A	0.34	0.43	0.52	0.58	3.8	4.2
B	0.51	0.52	0.65	0.69	3.3	4.1
C	0.47	0.58	0.64	0.69	3.2	4.1
D	0.33	0.45	0.52	0.61	3.6	4.2
E	0.51	0.52	0.64	0.65	2.4	4.1

Table 3 – Flight variables for double (D) and triple (T) Lutz at the instant of maximum height in the air.

1. DISCUSSION

In order to increase the revolutions of jumps, a figure skater must increase flight time, jumping height, and rotational velocity. During the Lutz, skaters use the phase between the toe-pick and take-off to generate vertical velocity. The higher vertical velocity at take-off results in higher jumps for three skaters, more time in the air available to complete the revolution for the triple jump, and may be due to a more forceful extension of the right hip and knee. Comparing the results with previous studies on ice, the flight time was also longer for the quadruple Toe Loop jumps with respect to the triple: on average, the quadruple jumps had a 0.03 s longer flight time than the triple ones [1]. No difference, as found in the present study for two skaters, in the jumping height was found between quadruple and triple Toe Loop, and also among single, double and triple Axel [2]. The homogeneity in height among jumps with different number of revolutions, for skaters B and E, could be explained with their higher skill level and with the coaches instructions usually received to perform a double jump higher than necessary, as preparatory for the execution of the triple one. The height values in the present study were similar to the ones of the triple Lutz analysed on ice (means 0.48 m) [3]. It is interesting to observe that from toe-pick to take-off, horizontal velocity decreased on average of 36% and vertical velocity increased on average of 81%. Similar percentages, even if with highest values, were observed when analyzing the triple Lutz on ice, too [3]. Regarding the take-off angles, the five skaters showed values between 40° and 45°, which are the best angles for optimizing height and distance. Jumps with angles of projections around 45° will be of medium height and will have the longest arcs. Higher take-off angles of triple with respect to double Axel [1] were also found on ice, with an average of 36° and 43°, for double and triple jumps, respectively. Lastly, the most significant aspect for completing a triple Lutz as compared to a double is being able to have an higher rotational velocity in the flight phase. Similarly, the rotational velocity was 1.0 rev/s larger for the quadruple Toe Loop as compared to triple jumps on ice [2]. There was a lower difference between triple and double Axel considering the rotational velocity because the average in double axel was 4.3 rev/s whereas in triple was 4.9 rev/s.

For the first time a biomechanical comparison between the double and the triple Lutz in roller skating was performed. The main differences observed in the triple jumps with respect to the double ones are: 1) higher rotational pelvis velocity, 2) at the take-off, a lower horizontal velocity and a slightly vertical velocity, 3) greater take-off angle, and 4) a more extended right hip and knee and a more plantarflexed ankle. Some of these findings were already roughly known to coaches and skaters, but only in the present study these and others were characterized and quantified. For instance, the skaters typically believe to have higher horizontal velocity in the triple jump with respect to the double one, but this was not confirmed by the measurements. A major awareness of the biomechanics of the triple and the double Lutz jumps would be useful for coaches to teach more effectively the right executive technique.

REFERENCES

[1] King, D., Arnold, A., and Smith, S. (1994). A kinematic comparison of single, double, and triple axel. *Journal of Applied Biomechanics*, **10**, 51-56.

[2] King, D., Smith, S., Higginson, B., Muncasy, B., and Scheirman, G. (2004). Characteristics of triple and quadruple toe-loops performed during the Salt Lake City 2002 Winter Olympics. *Sports Biomechanics*, **3**, 109-123.

[3] King, D. (2001). Generation of vertical velocity in toe-pick figure skating jumps. *XIX International Symposium on Biomechanics in Sport (ISBS)*, (Pp. 66-69), San Francisco, California.

[4] Cappozzo, A., Catani, F., Croce, U.D., and Leardini A. (1995). Position and orientation in space of bones during movement: anatomical frame definition and determination. *Clinical Biomechanics*, **10**, 171-178.

[5] Wu, G., Siegler S., Allard P., Kirtley C., Leardini A., Rosenbaum D., et al. (2002). ISB Recommendation on defitions of joint coordinate systems of various joints for the reporting of human joint motion-part I: ankle, hip, and spine. International Society of Biomechanics. *Journal of Biomechanics*, 35, 543-548.

Thu – July 19th 2012

Chairman: **Rita Stagni (DEIS, University of Bologna, Italy)**

Keynote lecture: *"*Fusion and visualisation of biomedical data at different temporal
11.00 : 11.30   and dimensional scales for integrative research*"*
                     Marco Viceconti (University of Sheffield, UK)

!

!

Fusion and visualization of biomedical data at different temporal and dimensional scales for integrative research

Marco Viceconti[1] and Debora Testi[2]

[1] University of Shffield, UK

[2] SCS, Italy

The Virtual Physiological Human is a framework of methods and technologies that once established will make biomedical integrative research possible. In particular, it will allow the integration of physiological and pathological processes happening across radically different space-time scale. This implies that, like for any modelling activity data observable at radically different space-time scale have to be collected, visualised, fused, and processed into predictive models. The same applies to the outputs of integrative models, which in general are also defined across widely different space-time scales. This poses an interesting problem: how can we provide interactive visualisation of complex multiscale and heterogeneous data collection, wherever they are observations or predictions of multiscale models? In this paper we present some preliminary results, partially based on the results on an international collaborative project of multiscale visualisation. From these preliminary results we conclude that multiscale interactive visualisation is possible, although it requires additional control elements, and poses considerable additional challenges in the design of the user interface.

Thu – July 19th 2012

Chairmen: **Bart Koning (University of Twente, Enschede, The Netherlands)**
Francesco Cenni (Istituto Ortopedico Rizzoli, Italy)

Poster session #2: *"Motion analysis in health care; Musculo-skeletal and joint modelling;*
14.00 : 15.30 *Industrial design and Other"*

P07	Kinematic analysis of eggbeater kicks with and without fatigue (from male college water polo players)	Toriumi, T., Morishita, A., Watanabe, K.
P20	Mandibular movements and masticatory muscle activity in patients with mild-moderate temporo-mandibular disorders	Mapelli A., Sidequersky F.V., Annoni I., De Menezes M., Musto F., Ferreira C.L.P., De Felicio C.M., Sforza C.
P21	Experimental comparison of functional methods to determine average axis of rotation in polycentric knee	Pastorelli S., Boatti E., Dimanico U., Battezzato A., Caramella M., Gastaldi L.
P22	Kinematics of the lower limbs, pelvis and trunk during asymptomatic cross-slope walking	Villa C., Sauret C., Fodé P., Lavaste F., Pillet H.
P23	Use of 3D analysis of motion to enhance functional assessments of hand activity in patients with rheumatoid arthritis, RA	Tom Armstrong, Kevin Chung, Chuck Woolley, Patricia Burns, Russel Corvese
P25	Measuring total lumbar spine range of motion through two variables: a pilot reliability study	Al Zoubi F., Pakzad M., Li L., Ait El Menceur M., Preuss R.
P26	Effects of minimally invasive percutaneous distal metatarsal osteotomy on gait performance in patients with hallux valgus	Shih K.S., Chang C.F., Li J.D., Lin D., Lu T.W.
P27	A methodological framework based on data mining techniques for movement analysis	Aguilera A., Barbier F.
P28	Biomechanical features of novel stroke rehabilitation programme in acute stroke patients	Skvortsova V.I., Ivanova G.E., Skvortsov D.V., Bulatova M.A., Kovrazhkina E.A., Suvorov A.Y.
P29	Differences in gait parameters between people after right-sided and left-sided stroke	Jurkojć J., Michnik R., Guzik-Kopyto A., Rycerski W.
P30	A cross-sectional biomechanical evaluation of diabetic lower limbs prior to ulceration	O'Brien D., Tyndyk M.
P31	An inertial system for clinical motion analysis and rehabilitation	Skvortsov D.V., Ishutin D.V.
P32	Kinematic comparisons between Mobile-Bearing and Fixed-Bearing designs in Cruciate-Retaining Total Knee Replacements during functional activities	Horng-Chaung Hsu, Cheng-Chung Lin, Tsung-Yuan Tsai, Mei-Ying Kuo and Tung-Wu Lu
P33	Estimating optimal shoulder immobilization postures following simulated surgical rotator cuff tear repairs	Jackson M., Sylvestre É., Bleau J., Allard P., Begon M.
P35	Gender differences in relative motions of tibio-femoral joint articular surfaces and comparison between subject specific and generic knee models	Zou D., Deusinger R.H., Koleini M., Smith K., Hensley G., Machan T.E., Schmitt A., Azevedo S.
P36	A musculoskeletal model for the shoulder complex	Frigo C., Pavan EE.
P37	Can physical activity level affect external mechanical work or energy cost of treadmill walking of healthy adults?	Annoni I., Galvani C., Mapelli A., Sidequersky FV., Ripamonti G., Sforza C.
P38	Markerless analysis of double pooling techniques in cross-country sit-ski athletes during competition	Pastorelli S., Gastaldi L., Frassinelli S.
P39	Kinematic analysis of a volleyball attack	Michnik R., Jurkojć J., Czapla K.

!

Kinematic analysis of eggbeater kicks with and without fatigue

(from male college water polo players)

Toriumi, T. [1], Morishita, A. [1], Watanabe, K. [2]

[1] Institute of Physical Education, Keio University, Yokohama, Japan, bird@z5.keio.jp
[2] Graduate School of System Design and Management, Keio University, Yokohama, Japan

The purpose of this study is to investigate the difference in the lower limb movements between the beginning of eggbeater kicks and the fatigue stage. The lower limb movements during the eggbeater kicks of 13 male college water polo players holding a 15-kg weight are analyzed using a three-dimensional motion analysis.

Keywords-component; water polo; eggbeater kicks; 15-kg weight; duration time; motion analysis

1. Introduction

In water polo, when receiving a pass or hitting a shot, players need to raise their body to a high position above the water surface. The key technique for maintaining such a high position is eggbeater kicks, which essentially produce an upward thrust owing to alternating circular leg movements that include cyclic operation with the knee and the ankle [1]. The duration that a player can perform eggbeater kicks while holding a heavy weight (e.g., 15 kg or 20 kg) correlates positively with the ability to perform these kicks [2]. The ability of a player to perform eggbeater kicks is measured using a three-dimensional (3D) motion analysis of the player's lower limb movements in synchronized swimming [3,4] and in water polo [5,6]. For example, the higher the position of the knee and the ankle, the better are the eggbeater kicks. However, how the efficiency of the lower limb movements during the eggbeater kicks and the ability to perform eggbeater kicks can be measured is still unknown. The purpose of this study is to map the position of the knee during eggbeater kicks with and without fatigue by using a 3D motion analysis and to identify the factors that help players remain at a certain height above water while lifting a heavy weight.

2. Methods

In this study, we selected 13 male college water polo players (age: 20.9 ± 0.6 years; height: 173.7 ± 7.0 cm; body mass: 66.1 ± 6.7 kg; athletic experience: 5.3 ± 1.2 years). Informed consent was obtained from each player before inclusion in the study.

The ability of a player to perform eggbeater kicks was estimated by measuring the duration for which a player could hold a 15-kg weight in a 2-m-deep pool.

For the image analysis of the eggbeater kicks, two video cameras that could take 30 pictures per second with a shutter speed of 1/100 s were used. One camera was set at a depth of 2 m in the pool and a distance of 12 m in front of the player. The other camera was set at a depth of 1 m from the water surface with a horizontal angle of 60° and a distance of 14 m from the player. The two video cameras were synchronized using a frame counter. The digitizing points for each

player were the centers of their hip and knee joints. The players performed eggbeater kicks while holding a 15-kg weight.

The 3D coordinates were obtained by a 3D direct linear transformation (DLT). The 3D DLT control object was a rectangular parallelepiped (1.8 × 1.8 × 2.0 m) structure with 12 control object points. The specific points selected for the analysis were the relative heights of the knees; the greater trochanter was selected as the beginning point (zero) for the measurements.

3. Results and discussion

The duration of performing eggbeater kicks while holding the 15-kg weight for the 13 players ranged from 16.1 to 41.4 s.

From the results of the 3D motion analysis of the hip and knee joints, we determined the distances from the greater trochanter to the knee joints. The number of cyclic operations of the knee ranged from 32 to 77. The time length of one cyclic operation of the knee ranged from 0.45 to 0.60 s. Figure 1 shows the relationship between the duration of the eggbeater kicks while holding the 15-kg weight, which implies the ability of a player to perform the eggbeater kicks in water polo, and the time length of one cyclic operation of the knee as obtained from the 3D motion analysis. This duration correlates positively with the time length of one cyclic operation (R^2 = 0.40).
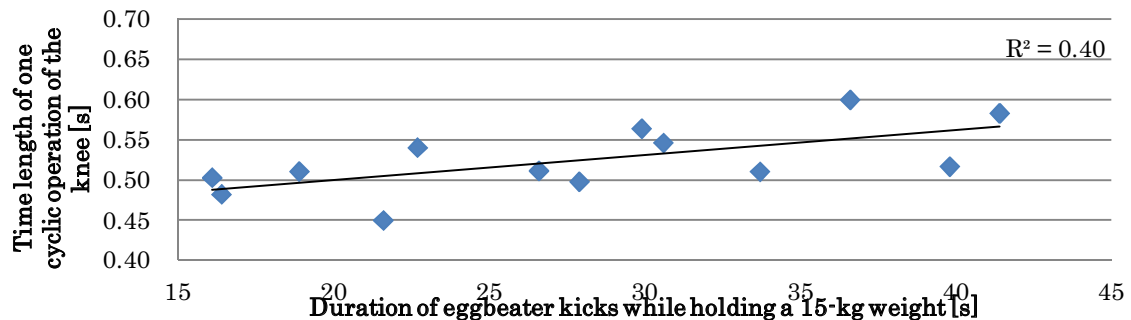

Figure 1. Relationship between the duration of eggbeater kicks while holding a 15-kg weight, which implies the ability of a player to perform eggbeater kicks in water polo, and the time length of one cyclic operation of the knee as obtained from the 3D motion analysis.

4. Conclusions

The characteristic results for eggbeater kicks in the case of 13 college water polo players were as follows: the duration of performing eggbeater kicks while holding a 15-kg weight ranged from 16.1 to 41.4 s, the number of cyclic operations with the knee ranged from 32 to 77, and the time length of one cyclic operation with the knee was 0.45 to 0.60 s/cycle. This duration correlated positively with the time length of one cyclic operation.

5. References

[1] Sanders, R. H. Analysis of the Eggbeater Kick Used to Maintain Height in Water Polo. *Journal of Applied Biomechanics*, **15**: 284-291, 1999.

[2] Enomoto, I. Nautical Chart for Water Polo – International Trend and Athlete Development Program in Japan –. *Suiei Suichu Undo Kagaku*, **1**: 15-19, 2005.

[3] Homma, M. and Homma, M. Coaching Points for the Technique of the Eggbeater Kick in Synchronized Swimming Based on Three-Dimensional Motion Analysis. *Sports Biomechanics*, **4**: 73-88, 2005.

[4] Sanders, R. H. Strength, Flexibility and Timing in the Eggbeater Kick. www.coachesinfo.com/, 2008.

[5] Alexander, M. and Taylor, C. The Technique of the Eggbeater Kick. www.coachesinfo.com/, 2008.

[6] Toriumi, T. and Morishita, A. Kinematic Analysis of Eggbeater Kicks of Junior Water Polo Players. *Proceedings of the 12th International Scientific Conference of Sport Kinetics*, **12**: 121-122, 2011.

Mandibular movements and masticatory muscle activity in patients with mild-moderate temporomandibular disorders

Mapelli A. [1], Sidequersky F.V. [1], Annoni I. [1], De Menezes M. [1], Musto F. [1], Ferreira C.L.P. [2], De Felicio C.M. [2], Sforza C. [1]

[1]Dip. Morfologia Umana e Scienze Biomediche "Città Studi", Università degli Studi di Milano, Milano, Italy
chiarella.sforza@unimi.it
[2]Dep. Oftalmologia, Otorrinolaringologia e Cirurgia de Cabeça e Pescoço, Faculdade de Medicina de Ribeirão Preto, Universidade de São Paulo, Ribeirão Preto, Brasil

Human temporomandibular joint; 3D motion analysis; electromyography; disease

1. INTRODUCTION

Temporomandibular disorders (TMD) consist of a number of clinical problems that involve the masticatory muscles, the temporomandibular joint (TMJ) and associated structures, or both. Approximately 7–15% of the adult population is affected, with higher prevalence in women at reproductive ages. The most frequent complaints reported by subjects with TMD are pain in the TMJ and/or masticatory muscles, TMJ sound and difficulty to chew [1].

Most of the TMD studies rely on self-assessed masticatory function obtained from questionnaires, whereas only a limited number of studies has measured the masticatory performance objectively.

The aim of the current study was to quantitatively compare the three-dimensional jaw kinematics and electromyographic parameters of patients with mild-moderate TMD.

2. MATERIAL AND METHODS

Subjects and data collection

Twenty patients with mild-moderate TMD (5 men and 15 women, 22–56 years of age), and 19 volunteer healthy subjects (9 men and 10 women, 21–49 years of age) were analyzed in this study. To be recruited in the pathologic group, patients had to present TMD according to the Research Diagnostic Criteria for TMD (RDC/TMD) [2], short lasting (at most 6-month duration) mild-moderate severity, according to ProTMDmulti protocol [3], and they should not have been seeking treatment. The inclusion criteria to be recruited in the control group (CTRL) were: a sound, complete, permanent dentition with bilateral canine and molar Angle Class I jaw relationships; anterior teeth with vertical and horizontal overlap between 0 and 3 mm; maxillary and mandibular interincisal lines without lateral deviations larger than 2 mm; no cast restorations or cuspal coverages, no anterior or lateral reverse occlusion; no previous history of craniofacial trauma or congenital anomalies; no TMJ or craniocervical disorders, based on the RDC/TMD and ProTMDmulti questionnaire.

Mandibular kinematics was recorded using an optoelectronic three-dimensional motion analyzer (SMART-E system, BTS S.p.a, Garbagnate Milanese, Italy), with a 60 Hz sampling rate. Six passive markers (diameter 6 mm) were used: three head passive markers were positioned by means of biadhesive tape on the nasion and the left and right frontotemporale landmarks, defining a cranial reference plane. These three markers were insensitive to skin motion artefacts during jaw movement. Other three passive markers were positioned on the three corners of an equilateral triangular stainless steel extra oral device (side 40 mm; weight 2 g); this tool was fixed on the mandibular anterior gingiva just out of dental contact using a surgical adhesive (Stomahesive; Convetec Inc, Deeside, United Kingdom), and provided a mandibular reference system. In a single reference frame, a further passive mandibular marker (diameter: 3 mm) was located on the midline incisor edge (inter-incisor point, IP); it identified a dental (occlusal) landmark, relative to the extraoral system [4]. Similarly, two condylar reference points (CRPs) were firstly individuated by palpation and secondly detected by means of a marked pointer while the subject was keeping his/ her mouth closed in intercuspal position. Surface electromyographic (sEMG) activity was recorded using a wireless device (BTS FREEEMG system, BTS S.p.a, Garbagnate Milanese, Italy). To reduce skin impedance, facial epidermis was carefully cleaned with alcohol prior to the 10 mm-electrodes placement (Kendall Arbo; Tyco Healthcare, Neustadt, Germany). The left and right masseter and temporalis anterior muscles were examined, positioning four probes on their muscular bellies parallel to muscular fibres.

At first, two 10 mm-thick cotton rolls were positioned on the mandibular second premolar/first molars of each subject, and a 5 s-maximum voluntary contraction (MVC) was recorded (COT). Then, the subject was invited

to clench as hard as possible with the maxillary and mandibular teeth in maximum contact (intercuspal position, ICP), and to maintain the same level of contraction for 5 s (CLENCH). All sEMG potentials obtained during CLENCH were standardized as percentages of the potentials obtained during COT [5, 6]. Muscular symmetry (right/ left side), torque (right/ left laterodeviating couple), and activity (masseter/ temporalis activation) were calculated, as well as the total standardized muscular activity.

Mandibular movements and sEMG activity were further recorded during unilateral, left and right, chewing of sugarless gum [7]. The sEMG potentials obtained in the first 15 s of each mastication trial were recorded (about 20 chewing cycles were detected for each trial). For gum chewing, frequency, 3D amplitude of motion and shape of the masticatory cycles (projected on the frontal plane) [8] were obtained, together with assessments of the coordination between masseter and temporalis activities [7].

Mandibular kinematics was also recorded during the performance of maximum mandibular border movements (Posselt diagram: mouth open, close, right and left laterotrusions, protrusion). For border movements, mandibular motion was described by the 3 Cardan angles and the 3D pathways of IP and CRPs.

Statistical analysis

Descriptive statistics of subjects' age, mandibular dimensions, kinematic and electromyographic parameters were calculated separately for CTRL and TMD groups. The normal distribution of data was checked with the Kolmogorov-Smirnov test. All the parameters were compared between CTRL and TMD groups by means of Student's t-test for independent samples. The Fisher's exact test and the Chi-squared test were used, respectively, to test the homogeneity of sex and chewing pattern distributions in the two groups. The significance level was set at 5% for all statistical analyses ($p < 0.05$).

3. RESULTS

Patients and healthy subjects had similar age and mandibular dimensions. The sex distribution was not significantly different in the two analyzed groups (Fisher's exact test: $p = 0.19$).

During MCV, in TMD patients sEMG activities were less symmetric and had a larger torque component than in healthy subjects. The TMD group had an overall standardized activity (STD. IMPACT) nearly identical to that measured in the control group (Table 1).

During the performance of mandibular border movements, there were no inter-group differences in IP and CRP ranges of motions (Fig. 1 and 2, t-test: $p > 0.05$).

Table 1. sEMG indices in maximum voluntary contraction (MVC).

Measure	Healthy		TMD		t-test
	Mean	*SD*	*Mean*	*SD*	*p-value*
ASYMMETRY (abs.) [%]	4.4	4.2	10.4	9.1	0.013
TORQUE (abs.) [%]	4.4	4.0	9.8	10.9	0.047
ACTIVITY [%]	-6.4	12.3	-5.1	21.5	NS
STD. IMPACT [%]	109	35	108	39	NS

abs.   absolute value.

NS   not significant, $p > 0.05$.

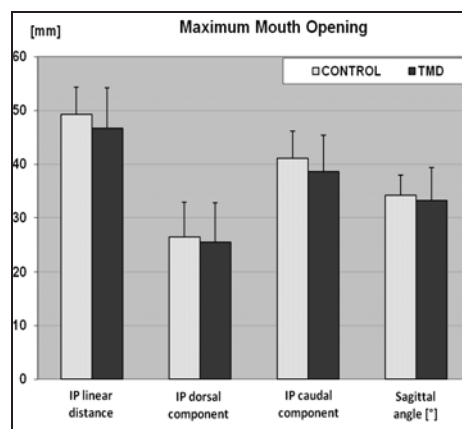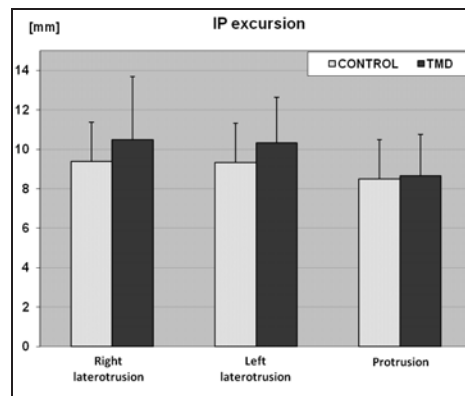Figure 1. IP displacement and sagittal angle at maximum mouth opening (MMO), mean+SD. t-test: $p > 0.05$.

Figure 2. IP maximum lateral and anterior displacements, mean+SD. t-test: p > 0.05.

During mastication, the kinematic characteristics obtained in patients were well comparable to those of healthy individuals (no statistically significant differences, p > 0.05 for all variables). Chewing cycle morphology was more anomalous in patients (74.9% of anomalous chewing patterns) than in control subjects (52.5% of anomalous chewing patterns) (Fig. 3, Chi-squared test: p = 0.000).
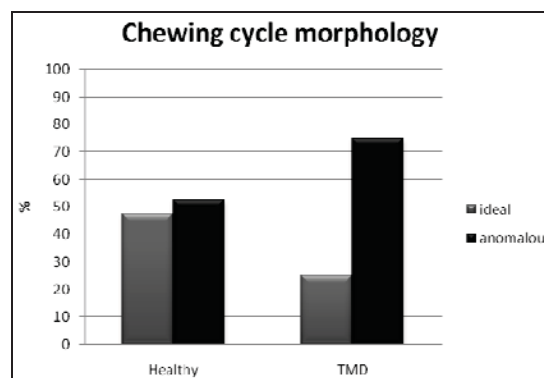

Figure 3. Chewing cycle morphology in healthy subjects and TMD patients.

During chewing, all subjects of the control group had a good coordination between masseter and temporalis activities, with the centres of the Lissajous's ellipses describing unilateral chewing located within the first (right-side chewing prevalence of right masseter and temporalis muscles) and third (left-side chewing prevalence of left masseter and temporalis muscles) quadrants of the Cartesian coordinate system, thus indicating a prevalent activity of the working-side muscles. Among TMD patients, instead, 9 subjects had at least one of their unilateral chewing cycles with the centre of the ellipse positioned outside the correct quadrant. Surface EMG activity of TMD patients was less coordinated than that of control subjects, with a larger variability between chewing cycles (Hotelling's ellipse area: CTRL, 1010±845%; TMD, 2275±2734%, p = 0.061).

4.   DISCUSSION

In the present study, TMD signs and symptoms were classified according to the RDC/TMD criteria [2], the reliability of which has been demonstrated in a multicentre international study [9]. Only patients with mild or moderate impairments were analysed to avoid the effect of pain and major disabilities.
TMD patients showed more asymmetry between the standardized activity of muscle pairs and larger unbalanced contractile activities of controlateral masseter and temporal muscles (TORQUE). Both findings are in accord with the data previously collected on patients with moderate to severe TMD [10]. Asymmetry of muscle activities have already been reported also in long lasting [6, 11] and acute TMD patients [5].
The patients performed significantly more anomalous unilateral chewing patterns than the control subjects, according to both sEMG and morphological outcomes. In general, in healthy subjects the most frequent chewing pattern is a smooth, uncrossed, teardrop-shaped pattern [12]; TMD anomalous cycle shapes were three times more frequent than ideal ones, whereas in the control group there was an almost balanced distribution.
From all these findings, it could be hypothesised that in cases of mild-moderate TMD, the change in muscle recruitment may be a compensatory mechanism for pain relief, and asymmetrical muscle recruitment may precede the muscle pain symptoms [13].

The outcomes suggest that the proposed method could be a useful tool to evaluate the neuromuscular coordination during the performance of static and dynamic masticatory activities, and to detect functionally altered stomatognathic conditions.

5.   REFERENCES

[1] Michelotti, A, Iodice, G., 2010. The role of orthodontics in temporomandibular disorders. J Oral Rehabil 37, 411-429.

[2] Dworkin, S.F., LeResche, L., 1992. Research diagnostic criteria for temporomandibular disorders: review, criteria, examinations and specifications, critique. J Craniomand Dis Facial Oral Pain 6, 301-355.

[3] De Felicio, C.M., Melchior, M.O., Da Silva, M.A., 2009. Clinical validity of the protocol for multi-professional centers for the determination of signs and syntomps of temporomandibular disorders. Part II. Cranio 27, 62-67.

[4] Ferrario, V.F., Sforza, C., Lovecchio, N., Mian, F., 2008. Quantification of translational and gliding components in human temporomandibular joint during mouth opening. Arch Oral Biol 50, 507-515, 2005.

[5] Tartaglia, G.M., Moreira Rodrigues da Silva, M.A., Bottini, S., Sforza, C., Ferrario, V.F. Masticatory muscle activity during maximum voluntary clench in different research diagnostic criteria for temporomandibular disorders (RDC/TMD) groups. Man Ther 13, 434-440.

[6] Tartaglia, G.M., Lodetti, G., Paiva, G., De Felicio, C.M., Sforza, C., 2011. Surface electromyographic assessment of patients with long lasting temporomandibular joint disorder pain. J Electromyogr Kinesiol 21, 659-664.

[7] Ferrario, V.F., Sforza, C., 1996. Coordinated electromyographic activity of the human masseter and temporalis anterior muscles during mastication. Eur J Oral Sci 104, 511-517.

[8] Takeda, H., Nakamura, Y., 2009. Examination of masticatory movement and rhyhm before and after surgical orthodontics in skeletal class III patients with unilateral posterior cross-bite. The J Oral Maxillofac Surg, 67, 1844-1849.

[9] John, M.T., Dworkin, S.F., Mancl, L.A., 2005. Reliability of clinical temporomandibular disorder diagnoses. Pain, 118, 61-69.

[10] Ferrario, V.F., Tartaglia, G.M., Luraghi, F.E., Sforza, C., 2007. The use of electromyography as a tool in differentiating temporomandibular disorders from neck disorders. Man Ther, 12, 372-9.

[11] Santana-Mora, U., Cudeiro, J., Mora-Bermúdez, M.J., Rilo-Pousa, B., Ferreira-Pinho, J.C., Otero-Cepeda, J.L., Santana-Penín, U., 2009. Changes in EMG activity during clenching in chronic pain patients with unilateral temporomandibular disorders. J Electromyogr Kinesiol, 19(6), e543-e549.

[12] Yamashita, S., Hatch, J.P., Rugh, J.D., 1999. Does chewing performance depend upon a specific masticatory pattern? Review. J Oral Rehabil, 26, 547-553.

[13] Lobbezoo, F., van Selms, M.K., Naeije, M., 2006. Masticatory muscle pain and disordered jaw motor behaviour: Literature review over the past decade. Arch Oral Biol, 51, 713-720.

Experimental comparison of functional methods to determine average axis of rotation in polycentric knee

Pastorelli S.[1], Boatti E.[1], Dimanico U.[2], Battezzato A.[1], Caramella M.[2], Gastaldi L.[1]

[1] Dept. of Mechanics, Politecnico di Torino, Torino, Italy, stefano.pastorelli@polito.it
[2] Dept. of Neurorehabilitation, ASL CN1, Fossano Hospital, Italy, ugo.dimanico@aslcn1.it

In gait analysis functional methods to determine axes of rotation represent a valid alternative respect to the standard clinical practice. The current study experimentally compares two functional methods using a mechanical analog of the leg with a polycentric knee. Tests had been performed for two RoMs and for different number of markers on the moving segment. Experimental outcomes show good performances of both tested methods; some results are influenced by RoMs and/or by the number of markers, so the identification of an absolute best performing method is not possible.

Keywords: axis of rotation, polycentric knee, functional analysis, gait analysis.

1. INTRODUCTION

In clinical gait analysis detection of the anatomical joint centers or axes of rotation (AoRs) is crucial, also considering that usually subjects are affected by functional movement deficit and present non-normal anatomy. Traditional techniques, that reconstruct human gait from skin markers, employ predictive methods based on regression equations [1-4]. They are simple and immediate, however they may lack of accuracy, especially when dealing with nonstandard cases. Errors primarily arise from marker placement on anatomic landmarks, anthropometric measurements and regression equations [5]. On the contrary functional methods do not require the placement of markers with respect to anatomic landmarks, following specific clinical protocols. Several functional strategies have been introduced: they can be classified into fitting approaches and transformation techniques. The first ones assume that each marker just rotates around the same joint axis or center with a separate arc [6,7]; hence, each segment is not required to be a rigid body, with a proper optimization of markers position and motion through error functions. On the other side, the second ones consider each body as a rigid one: the axis or the center of rotation is considered as stationary and it is possible to define rigid body transformations, i.e. rotation matrices and translation vectors [8-11].
In comparing in vivo the different functional methods, the main drawback is that the evaluation of their precision, influenced by soft tissue artefacts, can be managed only comparing their results with standard methodologies, that present their own sources of inaccuracy [12]. Some authors [11-13], proposed a preliminary validation of functional methods using a virtual model or a mechanical analog.
Furthermore, some joints, as the knee one, present a more complex pattern of motion that varies according to the relative position between the adjacent segments; hence the identification of the best mean fixed AoR is required for gait analysis porpoises, also to reduce cross-talk effects of the knee. To the best of authors' knowledge, up to now no comparison of different methods applied to a systems with mobile AoRs had been performed. The present work deals with the comparison of two functional methods to identify the axis of rotation in a polycentric knee: the first algorithm is a fitting approach and comes from Halvorsen (H method) [6]. The other method is a transformation technique: it derives from Spoor–Veldpaus (SV method) [9,14]; an helical motion of the leg with respect to the thigh is assumed. In order to investigate and properly compare these different methodologies, a dummy leg articulated with a polycentric knee had been used. The two methods have been implemented with data obtained by laboratory trials, considering two different flexion/extension range of motion (RoM) and different number and positions of markers.

2. MATERIAL AND METHODS

As a mechanical analog, a dummy of the lower limb with a pair of orthopedic polycentric hinges at the knee level were used for testing. During the tests the thigh segment was fixed and a swing movement had been imposed to the shank segment. In Fig. 1A a picture of the dummy is shown, while in Fig. 1B is reported a scheme of the knee hinge. The segments of the brace end with a pair of gears coupled by means of a plate with two pivots. Due to the tests set-up the tight pivot was fixed (fixed axis), while the axis of the shank pivot (mobile axis) swing. The instantaneous axis of rotation of the shank with respect to the thigh coincide with the gears pitch point, thus it moves on a circle centered in the fixed axis.
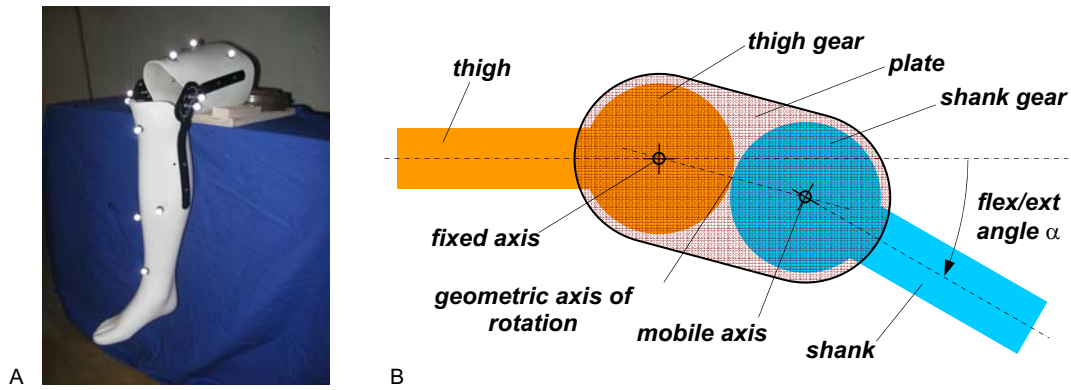
Figure 1. Dummy leg with polycentric knee. A: photo of the dummy with the polycentric knee and reflective markers for experimental testing, B: schematic section of the polycentric hinge

The mechanical analog allowed movement in the sagittal plane, from completely extended leg (0° degree) to a flexion of 120°; movements in the coronal and transverse plane were not allowed. Knee flexion/extension angle is indicated with α.

To perform motion analysis, reflective markers were screwed on the termini of the hinges to identify the fix and mobile axes. A set of 5 markers was placed on the shank (lateral and medial malleolus, one frontal, one medial-frontal and one lateral), and a set of 3 markers were arbitrary positioned on the thigh to check the lack of movement of this segment. The diameter of the markers was 14 mm and their positions were directly acquired using a infrared measurement Vicon 512 motion capture system with 6 cameras at 100 Hz (Oxford Metrics, Oxford, UK). The markers' coordinates with respect to the lab reference frame provided by the Vicon software were then post-processed with functional methods algorithms, implemented by the authors in Matlab, in order to identify an average axis of rotation of the dummy knee.

Two different functional methodologies, already presented in literature, were considered and compared. In the first one the AoR is estimated as the line which best fit the instantaneous rotational axis of the markers in a pair of frames, in accordance to Halvorsen's approach. Instead, the second method considers the distances of the markers on each limb constant (rigid body assumption) to identify a transformation matrix, and thus of the axis of rotation, between a pair of frames. For this approach the Spoor-Veldpaus's algorithm was implemented. For both methods arbitrary initial and final frames are required.

Tests were carried out making the shank to swing with a RoM of about 90° @ 0.3 Hz. Data relative to 10 sessions, with 6 cycles of knee flexion-extension each, were collected. To implement the algorithms, 60 clips concerning single flexion swings were extracted from the acquired data sets, covering two different intervals of the flexion/extension angle: from 40° to 95° (RoM 55°) and from 80° to 95° (RoM 15°). Being n the number of frames for each extracted swing record and m the number of the shank markers, markers positions of the former $n/2$ frames were then merged to generate a virtual "initial" frame containing $m \times n/2$ points. Analogously a virtual "final" frame had been generated considering the latter $n/2$ frames. Concerning the m markers, besides the whole 5 shank markers set, different subsets of 3 and 4 markers out of the 5 were considered.

The two algorithms applied to the virtual pairs of frames yield to determine both the direction of the estimated AoRs and their spatial locations.

3.   RESULTS

Results obtained with the different RoMs and number of markers are summarized in Table 1, while Fig. 2 shows results expressed relative to $m=4$ markers on the shank.

To interpreter and compare results it is necessary to introduce some definitions. The geometric fixed and mobile hinge axes were aligned with the direction between the relative hinge-termini markers; thus the instantaneous geometric AoR of the shank with respect to the thigh was computed according to Fig. 1B. The geometric fixed axis center (GCfa) was assumed as the midpoint between the hinge-termini markers; the knee sagittal plane was defined as the plane perpendicular to the geometric fixed axis containing the GCfa. Instantaneous geometric center of rotation (GCoR) was calculated as the intersection between the geometric AoR and the knee sagittal plane. Analogously the geometric mobile axis center (GCma) was computed as the intersection of the mobile axis with the knee sagittal plane. Finally, once the estimated AoRs are carried out with functional methods, the estimated center of the knee (ECoR) is the intersection point of the estimated AoR and the knee sagittal plane.
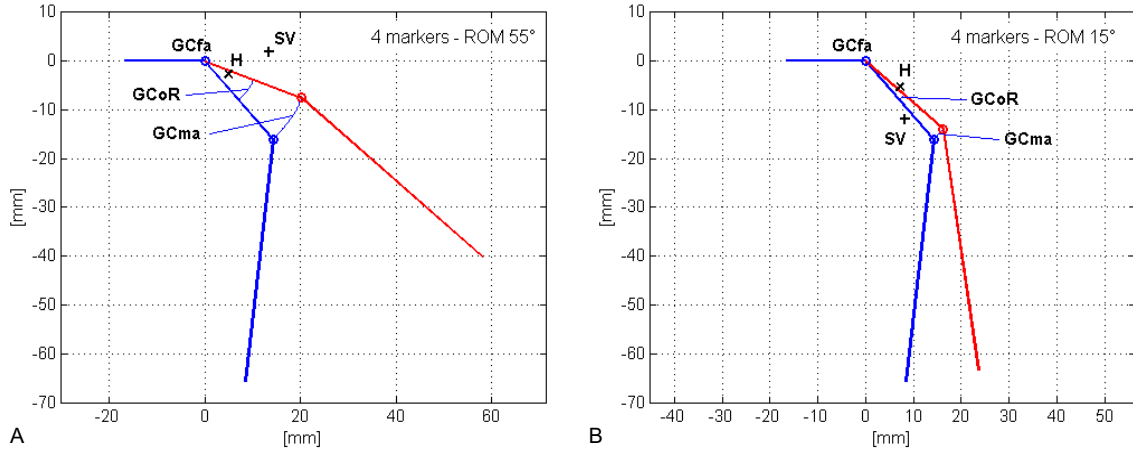
Figure 2. Position in the sagittal plane of the mean ECoR evaluated with H method (H) and with SV method (SV) respect to GCoR trajectory. Results refer to *m*=4 markers on the shank and RoMs of: A. 55° and B. 15°.

Fig. 2 shows, for each RoM, the limb positions corresponding to the extreme swing bounds in the sagittal plane, circular paths of GCma and GCoR. Point H and SV are the mean ECoRs evaluated with Halvorsen's and Spoor-Veldpaus's methods respectively. The mean ECoR is the barycenter of the distribution of the knee centers obtained processing the 60 clips.

In table 1 the mean misalignment between the geometrical AoR and the estimated one, and mean distance between GCoRs and the mean ECoR (H or SV) are reported for the vary analyzed cases.

In relation to the 3 and 4 marker subset elements variability, no appreciable difference could be noticed, hence in the table results relative to only one subset configuration are reported.

4. DISCUSSION

In this study two different functional methods to identify knee AoR for gait analysis purpose had been experimentally compared. Taking into account human knee physiology, the study was conducted on a lower limb mechanical analog with a polycentric hinge and hence with a mobile AoR.

Halvorsen's and Spoor-Veldpaus's algorithms, already tested by other authors [12,13] with fixed hinge systems, had been implemented. It is obvious that, in the specific case of a polycentric knee hinge, the estimated AoR is a unique fixed average axis estimation of the geometrical AoR between shank and thigh. Furthermore the estimated AoR depends on the RoM, besides the flexion/extension angle mean value.

Errors of misalignment and position between the estimated AoR and the geometric one cannot be directly compared with literature results, due to the different hinge type; however values carried out in this study are of the same order of magnitude than the one reported in [11-13], to confirm that the methods implementations are theoretically sound.

Results presented in Table 1 highlight position errors of the ECoR lower for the smaller RoM with both functional methods. As a matter of fact large range of the flexion/extension angle entails wider displacement of the geometric AoR and hence a greater approximation; this behavior is intrinsic in functional methods that

Table 1. Summary of all tests results (mean ± standard deviation): absolute directional error of the estimated AoR with respect to the geometric AoR and mean distance between ECoR and GCoR.

	Range of Motion 15°		Range of Motion 55°	
	H method	SV method	H method	SV method
m = 3 markers				
misalignment [°]	1.34 ± 0.32	1.33 ± 0.41	0.73 ± 0.04	1.35 ± 0.10
mean distance [mm]	1.4 ± 0.08	3.9 ± 0.27	5.3 ± 0.12	7.5 ± 1.69
m = 4 markers				
misalignment [°]	1.13 ± 0.94	0.92 ± 0.24	0.72 ± 0.06	1.08 ± 0.08
mean distance [mm]	2.3 ± 0.24	4.3 ± 0.26	5.3 ± 0.18	8.9 ± 1.71
m = 5 markers				
misalignment [°]	1.12 ± 0.92	0.62 ± 0.23	0.74 ± 0.08	0.70 ± 0.03
mean distance [mm]	5.6 ± 0.19	4.7 ± 0.26	5.7 ± 0.19	10.0 ± 1.71

estimate an average AoR. Vice versa misalignment errors decrease with the larger RoM for the H method, while basically they are constant for the SV method, consistently with [12,13]. This behavior is expected considering that also with the polycentric hinge the geometric AoR maintains a constant direction, unless for not meaningful variation due to geometric and assembling tolerances of the dummy.

As concerning the number m of markers taken into account on the shank, the results show that the misalignment is largely independent of m with H method, while a sensible improvement with m is produced by SV method. Vice versa the location error increases with number m for both methods. This second trend was unexpected and thus more in-depth examinations are necessary.

In the study presented in this paper Vicon markers coordinates were not filtered or compensated and no optimization techniques have been implemented to pair up time frames for the solution; instead more frames were merged to create unique virtual initial and final frames.

This study demonstrates that considering a rigid body, both functional methods perform well, giving reliable assessments of the AoR alignment and location in a polycentric knee. So far, influence of markers misplacements associated with local shifting or deformation of the limb skin, which usually are the main causes of artefacts in human gait analysis [15,16], have not been applied in the mechanical analog.

Follow-up works to this study are under design; they involves a modified polycentric dummy leg with an artificial skin to generate uncontrolled markers movements similar to those found in clinical trials.

5. ACKNOWLEDGMENT

6. REFERENCES

[1] M.P. Kadaba, H.K. Ramakrishnan, and M.E. Wootten, 1990. Measurement of lower extremity kinematics during level walking. Journal of Orthopaedic Research, pp. 8383-392.

[2] A.L. Bell, D.R. Pedersen, and R.A. Brand, 1990. A comparison of the accuracy of several hip center location prediction methods. J. Biomechanics 23(6), pp. 617-621.

[3] I. Davis, S. Ounpuu, D. Tyburski, and J.R. Gage, 1991. A gait analysis data collection and reduction technique. Human Movement Science 10(5), pp. 575-587.

[4] G.K. Seidel, D.M. Marchinda, M. Dijkers, and R.W. Soutas-Little, 1995. Hip joint center location from palpable bony landmarks—A cadaver study. J. Biomechanics 28(8), pp. 995-998.

[5] U. Della Croce, A. Leardini, L Chiari, and A. Cappozzo, 2005. Human movement analysis using stereophotogrammetry. Part 4. Assessment of anatomical landmark misplacement and its effects on joint kinematics. Gait & Posture 21(2), pp. 226–237.

[6] K. Halvorsen, M. Lesser, and A. Lundberg, 1999. A new method for estimating the axis of rotation and the center of rotation. J. Biomechanics 32, pp. 1221-1227.

[7] S.S.H.U. Gamage, J. Lasenby, 2002. New least squares solutions for estimating the average centre of rotation and the axis of rotation. J. Biomechanics 35, pp. 87–93.

[8] H.J. Woltring, R. Huiskes, A. de Lange, and F.E. Veldpaus, 1985. Finite centroid and helical axis estimation from noisy landmark measurements in the study of human joint kinematics. J. Biomechanics 18(5), pp. 379-389.

[9] C.W. Spoor, F.E. Veldpaus, 1980. Rigid body motion calculated from spatial coordinates of markers. J. Biomechanics 13, pp. 391-393.

[10] V. Camomilla, A. Cereatti, G. Vannozzi, and A. Cappozzo, 2006. An optimized protocol for hip joint centre determination using the functional method. Journal of Biomechanics 39 (6), 1096–1106.

[11] M.H. Schwartz and A. Rozumalski, 2005. A new method for estimating joint parameters from motion data. J. Biomechanics 38, pp.107–116.

[12] B.A. MacWilliams, 2008. A comparison of four functional methods to determine centers and axes of rotations. Gait & Posture 28, pp. 673–679.

[13] R.M. Ehrigb, W.R. Taylora, G.N. Dudaa and M.O. Hellera, 2007 A survey of formal methods for determining functional joint axes. J.Biomechanics 40, pp. 2150-2157.

[14] I. Söderkvist and P.A. Wedin, 1993. Determining the movements of the skeleton using well-configures markers. J. Biomechanics 26(12), pp. 1473–1477.

[15] A. Leardini, L. Chiari, L., U.D. Croce and A. Cappozzo, 2005. Human movement analysis using stereophotogrammetry, Part 3. Soft tissue artifact assessment and compensation. Gait and Posture 21, pp.212–225

[16] R. Stagni, S. Fantozzi, A. Cappello and A. Leardini, 2005. Quantification of soft tissue artefact in motion analysis by combining 3D fluoroscopy and stereophotogrammetry: a study on two subjects. Clinical Biomechanics 20, pp. 320–329.

Kinematics of the lower limbs, pelvis and trunk during asymptomatic cross-slope walking

Villa C. [1], Sauret C. [2], Fodé P. [2], Lavaste F. [1,2], Pillet H. [1]
[1] LBM, Arts et Metiers ParisTech, Paris, France
[2] Centre d'Etude et de Recherche sur l'Appareillage des Handicapés, INI, Woippy, France.

Cross-slopes locomotion; gait analysis; pelvis inclination; ankle inversion.

1. INTRODUCTION

Locomotion on cross-slopes is a common situation in urban environment. Indeed many streets and pavements are tilted from less than a degree to few degrees to allow water drainage and can be inclined of 6-10° for garage exit. Though barely studied in the literature [1,2,3], this situation can be a barrier for safe locomotion for elderly or disabled people such as amputee people. In fact, cross-slope walking requires different lower limb kinematics compared to level walking, especially in the frontal plane [1,2,3]. Reference [1] showed that to adapt to cross-slope walking (as a comparison to level walking) ten young healthy males modified the functional lengths of their lower limbs (the up-slope limb was shortened and the down-slope limb was lengthened) by altering ankle and hip kinematics in the coronal plane.

Particularly, the up-slope ankle showed a decreased inversion and the down-slope ankle an increased inversion compared to ankle inversion during level walking. This result showed the importance of setting up a suitable protocol to measure accurate inversion of the ankle when studying cross-slope locomotion. In addition, [1] observed kinematics and kinetics asymmetry between both lower limbs during cross-slope walking. They hypothesized that this asymmetry could be explained by upper-body compensations but did not investigated the motion of the trunk in their protocol.

Thus, the purpose of the present study was to investigate lower limbs kinematics and possible upper-body compensations while walking on a cross-slope. We assumed that a population of asymptomatic subjects would adapt to cross-slope by altering lower limb kinematics in the frontal plane (especially ankle inversion) in order to limit the frontal motions of the trunk and the pelvis.

2. MATERIAL AND METHODS

Seven subjects participated in the study. The mean characteristics of the subject are described in table 1.

Subjects were equipped with 54 markers to record the kinematics of the whole body with a motion analysis optoelectronic system (Vicon V8i, UK). Four markers were placed on the foot as shown in Fig. 1 to compute the anatomical frame of the foot and the angle of motion of the foot in the three directions.

Gender	Age (years)	Size (cm)	Weight (kg)
6 males/ 1female	27	176	71

Table 1: Subjects characteristics

Figure 1: Markers location during the experiments

Figure 2: Cross-slope device instrumented with four force platforms

First, a static trial was performed in order to define a static reference position. Two photographs were taken during this static trial in order to compute inertial parameters of the body of the subjects as described in [4]. Then, subjects were asked to walk five times at a comfortable speed on a flat pathway instrumented with two force platforms (AMTI, 100Hz). Finally, subjects were asked to walk back and forth on a cross-slope inclined of 6° (represented in Fig. 2) instrumented with four force platforms (AMTI, 100Hz)at a comfortable speed. Gait parameters such as gait speed, step width and length, percentage of the stance phase were calculated. Anatomical frames, segmental and articular kinematics and dynamics of the lower limbs (ankle, knee, and hip), the pelvis and the trunk were computed according to [4].

3. RESULTS

Gait parameters:
No significant difference between level walking and cross slope walking was observed in terms of gait speed, step width and length and percentage of the stance phase.

Lower limb kinematics:
In the sagittal plane, no difference was observed among level walking, up-slope and down-slope conditions for the flexion angles of the ankle, the knee and the hip. Regarding the frontal plane, no significant adaptations of the knee and the hip were noticed. On the contrary, as expected, relevant adaptation of the ankle in the frontal plane was observed. Indeed, the inversion angle of the right ankle is increased when downstream and is decreased when upstream on the cross-slope compared to level walking values (see Fig. 3). The difference is of about 6° which corresponds to the incline of the on slopes device.

Upper-limb compensations:
The inclination of the pelvis appeared not being altered by the three tested conditions as shown in Fig. 4. During level and cross-slope walking, healthy subjects' pelvis inclination followed the same pattern and amplitudes: during the double stance phase, the pelvis was slightly tilted towards the limb starting swing phase and showed no inclination during single support phase. Similarly, the trunk inclination in the frontal plane does not vary among the three conditions (see Fig. 5). It can also be noticed from Fig. 4 and Fig. 5 that pelvis and trunk maximum inclinations were both observed at 15% and 65% of gait cycle i.e. during double stance phase.
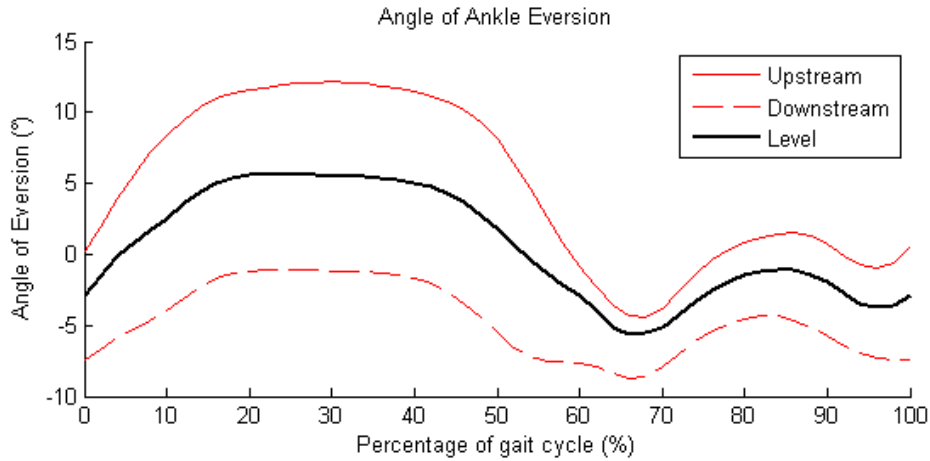
Figure 3 : Mean inversion angle of the right ankle for all subjects in a level walking condition (black line), upstream condition (plain red line), downstream condition (dashed red line).
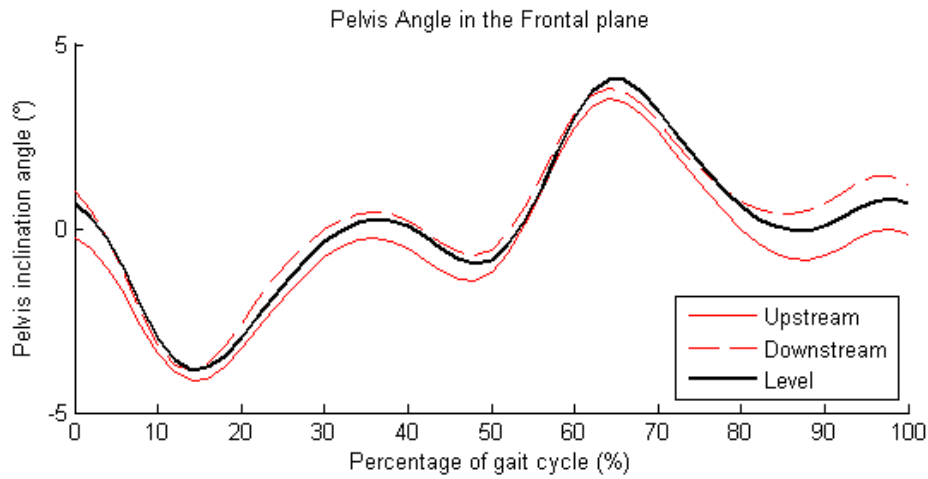

Figure 4 : Mean inclination angle of the pelvis in the frontal plane for all subjects in a level walking condition (black line), upstream condition (plain red line), downstream condition (dashed red line).
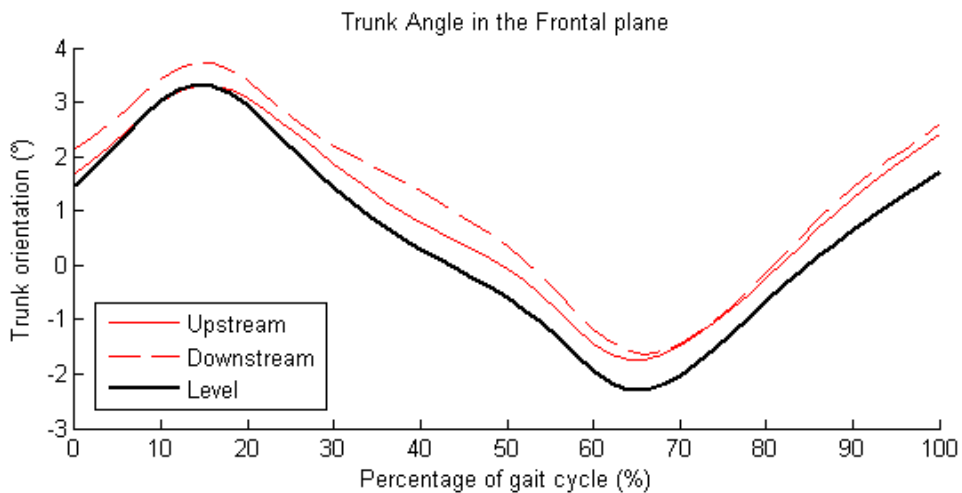

Figure 5 : Mean orientation angle of the trunk in the frontal plane for all subjects in a level walking condition (black line), upstream condition (plain red line), downstream condition (dashed red line).

3DAHM2012

4. DISCUSSION

The aim of the study was to investigate lower limbs kinematics and possible upper-body compensations while walking on a cross-slope. As hypothesized the adaptation to the cross slope is mainly realized by the inversion of the ankle which is the most modified motion compared to level walking. On the contrary, the kinematics of the upper body while walking on cross-slopes is the same as the one during level walking. We can suppose that people use this strategy in order to maintain a stable position of the head whatever the cross slope.

The results are consistent with [1] which observed ankle adaptation in the frontal plane. Yet, nobody studied the kinematics of trunk and pelvis during cross-slopes walking. However the observed inclinations of the trunk and pelvis in the frontal plane are consistent with the literature during level walking [5,6].

Finally, the protocol which was set up for the study allowed to measure 3D kinematics of the ankle. This protocol will be used for any further study on cross-slopes walking as ankle inversion appeared to be the main adaptation to the situation.

The study was conducted with healthy dynamics subjects on a cross-slopes device with small inclination. A larger angle could make appear other compensations for that population. Prospects of that study would be to collect data on a population of amputee which would have more difficulties to adapt to the inclination as their gait might be widely impaired by the slope.

5. ACKNOWLEDGMENT

6. REFERENCES

[1] Dixon, P. C., Pearsall, D. J., 2010. Gait Dynamics on a Cross-Slope Walking Surface. J. of Applied Biomechanics 26, 17-25.

[2] Damavandi, M., Dixon, P. C., Pearsall, D. J., 2010. Kinematic adaptations of the hindfoot, forefoot, and hallux during cross-slope walking. Gait and Posture 32, 411-415.

[3] Dixon, P. C., Tisseyre, M., Damavandi, M., Pearsall, D. J., 2011. Inter-segment foot kinematics during cross-slope running. Gait and Posture 33, 640-644.

[4] Pillet, H., Bonnet, X., Lavaste F., Skalli W., 2010. Evaluation of force plate-less estimation of the trajectory of the center of pressure during gait. Comparison of two anthropometric models. Gait and Posture 31, 147-152.

[5] Viel,E., Plat, F., Blanc, Y., 1979. La marche humaine. Paris, Masson.

[6] Perry, J., 1992. Gait analysis : Normal and pathological function.

Use of 3D Analysis of Motion to Enhance Functional Assessments of Hand Activity in Patients with Rheumatoid Arthritis, RA

Armstrong, T.[1], Chung, K.[2], Woolley, C.[1], Burns, P.[2], Corvese, R.[1]

1 The University of Michigan, Center for Ergonomics, Ann Arbor, MI 48109;
2 the Section of Plastic Surgery, Department of
Surgery, University of Michigan Medical Center, Ann Arbor, MI

Keywords: Motion tracking, functional assessment, rheumatoid arthritis

1. INTRODUCTION

Many musculoskeletal diseases and injuries affect how we move and our ability to grasp and manipulate objects that we use for activities of daily living, work and recreation. Rheumatoid arthritis is one such example. Tools such as the Michigan Hand Questionnaire and the Jebsen-Taylor test [1, 2] provide important information about pain and the ability to perform basic tasks, activities of work, daily living and leisure. Some investigators have expressed concern because the Jebsen-Taylor test is scored based on only the time to complete the task and is not sensitive to the ways that patients may alter their behavior as a result of an underlying pathology. Although such subjects may achieve normal scores for the Jebsen-Taylor test, their motions are not normal and they may have trouble completing many normal daily tasks. [3] We believe that motion tracking provides useful quantitative information about how diseases and injuries affect hand movements and the ability of patients to perform specific tasks. The goal of this study was to determine if motion studies of RA patients supports further development of a functional assessment tools based on motion tracking.

2. METHODS

Hand motions were compared for a control group of subjects with no known hand impairments with those of a RA, group as they performed the Jebsen-Taylor test. The University of Michigan Institutional Review Board approved the study protocol and all subjects provided signed consent to participate. The control subjects were five females between 18 and 23 years of age with no known hand impairments who were recruited from the university community. The patients were recruited from the University of Michigan Department of Surgery Section of Plastic Surgery and included four females who were diagnosed with advanced RA and were potential candidates for MCP joint replacements, but had not yet been treated surgically. The Jebsen-Taylor test consists of a series of transfer tasks in which the size and the weight of the objects being transferred are systematically increased. In this paper we describe the results for "flipping cards." In this task, five cards are arranged all face down or up 10 cm apart near the edge of the table. Subjects were instructed to simply turn the cards from one face to the other. The test was scored as the time required from when the subject reached for the first card until they completed the last card. Five control subjects and four RA patients completed three repetitions of the test with both their right and left hands.

MaxTRAQ -tracking software by Innovision Systems, Inc. was used to track the motion of the shoulder, elbow, wrist and MCP joint of the third digit of the right and left hands [4]. Reflective markers were attached to the dorsum of the metacarpal-phalangeal joint of the long finger, on the center of the dorsum of the wrists, on the lateral epicondyles and on the acromion processes. Four video cameras were positioned so as to record the markers as the subjects completed all of the tasks. A calibration fixture with eight reflective markers located at known locations is shown in Figure 1 and was recorded for subsequent calibration of the system. Video recordings were then obtained as the subjects completed each step of the Jebsen-Taylor test. Video processing was performed later and entailed the following steps: Formatting the video recordings for processing and then manually identifying and labeling the markers on the first video frames. Next the MaxTRAQ system tracks points in the next frames based on detecting pixels that exceed a given level of illumination within a predetermined distance of the point in the previous video frame. If a point cannot be automatically identified from one frame to the next due to blockages or stray light, then it must be identified manually. Finally the MaxTRAQ software was used to produce an array of x, y and z values for each marker and each frame of data. Approximately 2 hours was required for the initial data reduction for all 24 tests; an additional four hours was required to prepare the 3D outputs of all 24 tests. The time to

create the 3d output is directly related to the length of the video that the video clip is taken from. The final analysis using MATLAB can be completed in less than five minutes.

Figure 1: Fixture used to calibrate the MaxTRAK system. (Approximately 200 x 100 x 150 mm)

3 RESULTS

Figure 2 shows representative hand motions for control subjects and RA patients flipping the cards. It is apparent that the RA patient uses a much greater range of hand motion than the control subject. Figure 3 shows the motions for the hand, wrist elbow and shoulder. It can be seen that a greater range of wrist, elbow and shoulder motion is used by the rheumatoid patient than by the control subject.
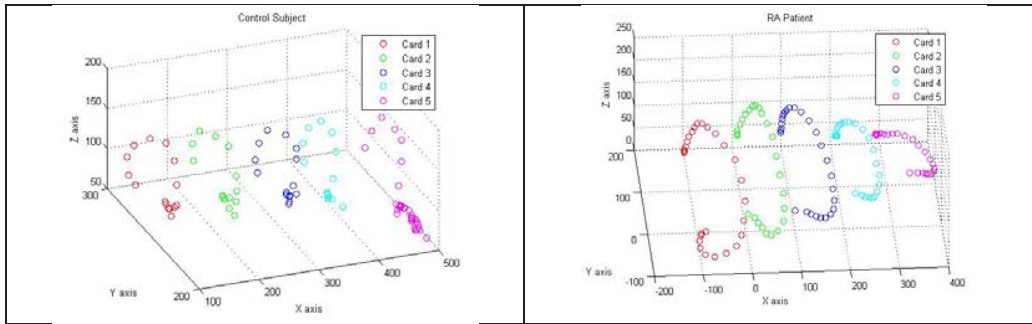
Figure 2: Representative MCP marker movements for a control subject and a RA patient to flip five cards (x, side-to-side; y, fore-aft; and z, up-down, with respect the edge of the table).
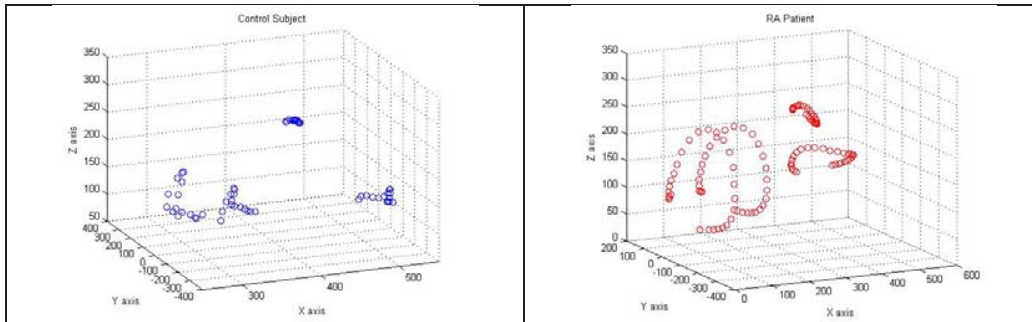

Figure 3: Representative MCP, elbow and shoulder marker movements for a control subject and a RA patient to flip the third card.

The range of motions Δx, Δy and Δz with respect to the edge of the work surface was computed for each condition and subject using Equations 1. The overall range of motion was computed as the magnitude of the vector sum of Δx, Δy and Δz (Equation 2). Descriptive statistics of the displacements are shown in Table 1. The differences between the control and patients subjects were statistically significant ($p < 0.05$). The average range of motions are consistently two to three times greater for the RA patients than the control subjects.

$$\Delta x = x_{max} - x_{min} \qquad [1a]$$
$$\Delta y = y_{max} - y_{min} \qquad [1b]$$
$$\Delta z = z_{max} - z_{min} \qquad [1c]$$

$$R = (\Delta x^2 + \Delta y^2 + \Delta z^2)^{1/2} \qquad [2]$$

Table 1: Means and standard deviations for x (side-to-side), y (fore-aft), and z (up-down) motions in mm with respect the edge of the table and corresponding times. Averaged across four 3 trials for five control subjects and two trials for four patients and 5 cards per trial.

Body Part		(Left hand)		(Right Hand)	
		Control	RA	Control	RA
MCP	Δx	36±12	73±28	34±14	65±30
	Δy	61±32	189±33	52±27	167±27
	Δz	73±19	153±21	71±20	141±25
	R	105±30	256±35	98±26	231±34
Elbow	Δx	44±16	63±24	34±16	92±55
	Δy	34±26	131±48	38±22	89±49
	Δz	25±16	85±31	26±18	73±44
	R	63±29	172±48	60±28	164±47
Shoulder	Δx	18±11	27±15	16±9.2	38±16
	Δy	18±12	37±23	16±13	34±24
	Δz	6.8±3.5	15±6.8	7.7±3.8	15±8.2
	R	28±13	50±24	26±14	48±24
Time, s		0.59±0.25	0.81±0.26	0.50±0.23	0.77±0.29

Included angles for the wrist and elbow were computed from vectors representing the hand, wrist, forearm and arm (Equations 3 and 4) to investigate which joints were contributing to the increased range of motion. Descriptive statistics for each condition are shown in Table 2. It an be seen that the range of motion is

Hand: $\quad V_{12} = (x_2-x_1)i + (y_2-y_1)j + (z_2-z_1)k$ [3a]
Forearm: $\quad V_{23} = (x_3-x_2)i + (y_3-y_2)j + (z_3-z_2)k$ [3b]
Arm: $\quad V_{34} = (x_4-x_3)i + (y_4-y_3)j + (z_4-z_3)k$ [3c]

Wrist: $\quad \cos^{-1}\theta_{wrist} = V_{12} \bullet V_{23} / |V_{12}||V_{23}|$ [4a]
Elbow: $\quad \cos^{-1}\theta_{elbow} = V_{23} \bullet V_{34} / |V_{23}||V_{34}|$ [4b]

Table 2: Range of included wrist and elbow motions ($\theta_{max}-\theta_{min}$) for right and left hands of control subjects and RA patients flipping five cards. It can be seen that the average range of motion for the Elbow is approximately three times greater for the RA patients than for the control subjects and for the wrist is 50 to 70% greater for the rheumatoid patients.

Joint	Control Left	RA Left	Control Right	RA Right
Elbow	9.2±3.6°	26±7.9°	7.5±2.8°	25±13°
Wrist	14±6.1°	24±11°	15±13°	23±13°

4 DISCUSSION

Although average times are different for the normal control subjects than for the RA patients, it does not provide insights into the cause of that time difference. Also, time does not provide insights into the kinds of problems RA patients might have performing activities of daily living, work or leisure other than the need for more time. The motion tracking data show clear differences in motion pattern – most notably increased ranges of motion. These data suggest that what the normal control subjects can do with finger manipulation, the RA patients move use there entire arm. Based on this, we anticipate that RA patients will have more difficulty grasping small objects and will need more room. Tasks such as reaching into a pocket, pocket book, drawer or other confined space would be difficult.

To be clear, the different motion patterns are conspicuous by observation – especially by a trained physician. But, observations are subjective and may vary greatly from one observe to another. Observations cannot measure the range of motion with a high degree of accuracy and precision.

The time required to reduce and analyze the hand motion data – approximately 6 hours per test –makes this protocol unacceptable for most clinical applications. There are alternative motion tracking systems that utilize active markers that can substantially reduce this time [5]. Such a system could be configured and programed to provide measurements in a time frame suitable for many clinical applications. Such a system can track additional markers and compute joint angles and other important motion parameters that provide insight into underlying pathologies and can be used to evaluate alternative treatments.

This pilot study only investigated card flipping. Motion data for larger and especially heavier objects used the Jebsen-Taylor test and for specific work samples can provide important insights into patients' ability to grasp and manipulate objects and to perform activities of daily living, work and leisure. Motion measurements can be compared with normal subjects to as a diagnostic tool and compared with baseline measurements to track interventions.

5 CONCLUSIONS

Motion tracking is a promising clinical tool for diagnosing and managing illnesses and injuries that affect patients' ability to grasp and manipulate objects. Equipment is available that can be used to configure motion tracking systems suitable for clinical applications. This work supports further studies to determine normal ranges of motion for manipulating a range of object sizes and weights and studying the relationship between motion parameters and disability.

6. ACKNOWLEDGEMENT

7   REFERENCES

[1] Chung, K. C., Burns, P. B., Wilgis, E., Burke, F. D., Regan, M., Kim, H. M., & Fox, D. A. (2009). A multicenter clinical trial in rheumatoid arthritis comparing silicone metacarpophalangeal joint arthroplasty with medical treatment. *The Journal of hand surgery*, *34*(5), 815–823.

[2] Kotsis, S. V., & Chung, K. C. (2005). Responsiveness of the Michigan Hand Outcomes Questionnaire and the Disabilities of the Arm, Shoulder and Hand questionnaire in carpal tunnel surgery. *The Journal of Hand Surgery*, *30*(1), 81-86. doi:10.1016/j.jhsa.2004.10.006

[3] Kobus, R. J., & Turner, R. H. (1990). Wrist arthrodesis for treatment of rheumatoid arthritis. *The Journal of Hand Surgery*, *15*(4), 541-546. doi:10.1016/S0363-5023(09)90012-0

[4] MaxTRAQ. (n.d.). Retrieved January 27, 2012, from http://www.innovision-systems.com/Products/MaxTraq.html

[5] Optotrak Certus Motion Capture System - Research-Grade Motion Capture System for Life Sciences Applications | NDI. (n.d.). Retrieved January 27, 2012, from http://www.ndigital.com/lifesciences/certus-motioncapturesystem.php

Measuring total lumbar spine range of motion through two variables

a pilot reliability study

Al Zoubi F. [1,2], Pakzad M. [1,2], Li, L. [2], Ait El Menceur M. [2], Preuss R. [1,2]

[1] School of Physical and Occupational Therapy, McGill University, Montreal, Canada.
[2] Constance-Lethbridge Rehabilitation Centre site of the CRIR, Montreal, Canada.

key words: Lumbar spine range of motion, reliability, 3D motion capture

1. INTRODUCTION

Motion capture technology has the potential to provide objective, three-dimensional measures of spine motion for use in clinical research and, potentially, in clinical practice [1]. Previous studies of motor control and coordination suggest that with, repeated movements, individuals will reach a relatively consistent end-position, but that some normal variability must be expected both within and between-subjects [2, 3]. In order to apply motion capture technology to clinical research, therefore, it is essential to determine what constitutes a meaningful change in the recorded movements, as opposed to normal biological variability [4].

Previous studies using electromagnetic tracking systems have found range of motion testing in the lumbar and cervical spine to be highly reliable, often with reliability values (r-values) >0.9 [5,6]. These studies, however, typically report r-values for individual spine motions (e.g. flexion, right side-bending, etc.), with a range of reliabilities covering all measures of interest. Such an approach complicates the design of clinical research, as not all subjects will present with the same movement impairments, and may therefore respond differently on each individual measure following an intervention.

The objective of this study was to develop a quantitative, reliable and easily interpretable outcome measure representing total available lumbar spine range of motion (ROM), based on two variables.

2. MATERIAL AND METHODS

2.1. PROPOSED MEASURE

While the human lumbar spine, in theory, has as many as 30 degrees of freedom [7], the functional coordination of inter-joint movement requires that these be coupled at both a mechanical and neuromuscular level [8]. As such, for most practical purposes, it is reasonable to treat the lumbar spine as a single functional unit. The orientation of the facet joints also dictates that the vertebrae will follow patterns of coupled rotations, rather than simple rotations in a Cartesian coordinate system, for all but the simplest of movements. The exact nature of this coupling, however, appears to differ from subject to subject [9, 10]. As such, it is more practical to use a measure of ROM based on relative vertebral position rather than orientation - i.e. the actual position attained, rather than the orientation of the joints produced to attain this position.

The proposed measure of lumbar spine ROM, therefore, is based on the quantitative analysis of the position of the first lumbar vertebra (L1) relative to the first sacral vertebra (S1). The measure itself is determined from the point of maximum relative excursion that occurs during eight (8) individual motions of the lumbar spine, to the end of range, at 45° intervals about the full circle (Fig. 1). Two shapes will then be fit to these 8 values: an ellipse, using a least square approach [11], and a form based on a cubic spline interpolation in 2- dimensions. For each of these shapes, two variables will be used to provide a general measure of the total motion available at the lumbar spine: the area and the position of the centre. Fig. 1 provides an example of the ellipse-fitting approach using simulated data points. The area of each ellipse provides an overall measure of the total available ROM, while the position of the centre of the ellipse describes how that motion is distributed.
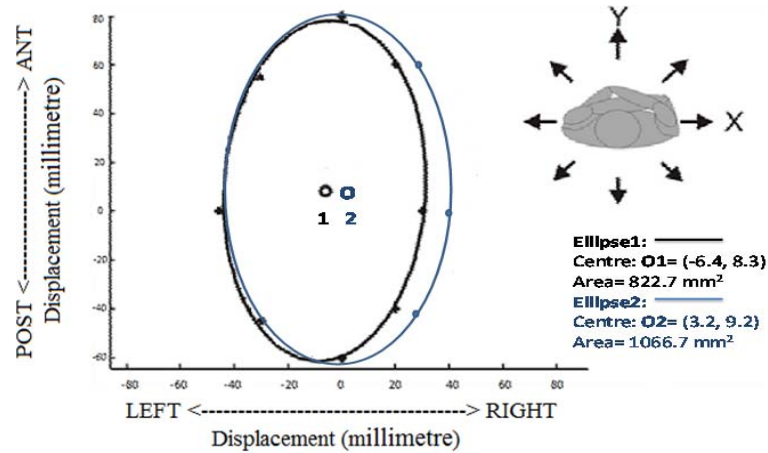
Figure 1. Ellipses fit to two sets of 8 simulated data points. Five of the data points are shared between the two ellipses, while the other 3 have been modified in their right side-bending component. The result is that the second ellipse has a larger area, representing greater overall motion of the spine, and a centre point that is shifted to the right.
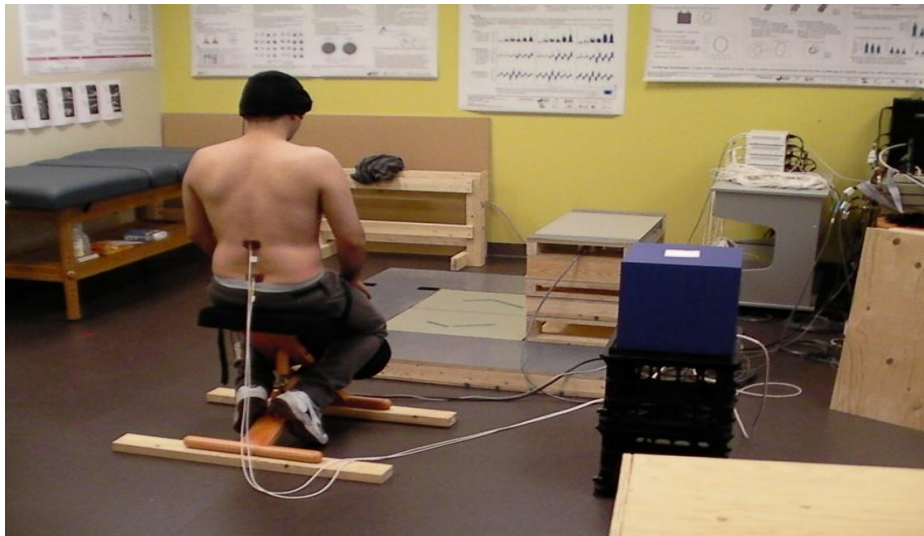

Figure 2. Experimental set-up for data acquisition.

2.2. METHODOLOGY

Eleven (11) participants (age 35.9 ± 8.4 years, 6 male) were recruited for this pilot study. Individuals were eligible to participate if they had a recent (within the last year) history of low back pain (LBP) which at no time presented with symptoms distal to the knee, and which lasted less than 16 days (with either spontaneous resolution of symptoms or resolution following treatment). These inclusion criteria are based on a 5-factor clinical prediction rule for success with a spinal manipulation intervention first described by Flynn et al [12]. Subsequent data from the same research group [13] suggest that the two inclusion criteria selected for the current study alone provide a positive likelihood ratio of 7.2 for success with a spinal manipulation intervention. Individuals were excluded if they presented with current pregnancy, signs consistent with nerve root compression (positive straight-leg raise at <45° and/or diminished lower extremity strength, sensation, or reflexes), a prior lumbar spine surgery, or a history of osteoporosis or spinal fracture. In addition, due to the use of an electromagnetic tracking system, potential subjects were also excluded if they had a cardiac pacemaker or other metal prosthetic device that could not be removed for the duration of the testing.

For data acquisition, participants were positioned in a wooden kneeling chair (Fig. 2). Straps were secured across the hips in order to limit any undesired movement of the lower limbs. For each testing session, participants performed 3 series of 8 randomly-ordered lumbar spine movements (at 45° intervals around the full

circle), through the full pain-free ROM, as described in Section 2.1. Each participant returned for a total of 3 testing sessions within a one-week period.

Lumbar spine kinematics were acquired using a 3-D electromagnetic motion capture system (TrakSTAR, Ascension Tech., Milton, VT, USA), sampled at 100Hz. Sensors (model 800; 8x8x20mm) were mounted over the base of the sacrum (S1) and the spinous process of the first lumbar vertebra (L1) using polyurethane clips and hypoallergenic, double-sided tape. The position of L1 relative to S1, in the transverse plane of S1 (the anterior-posterior and medial-lateral directions) was determined by multiplying the 4x4 rotation-translation matrix for L1 by the inverse of the rotation-translation matrix for S1, using custom software written in Matlab (each rotation matrix having been derived from the position and orientation data of the sensors in the transmitter-embedded reference frame). For each series of 8 movements, the ellipse and spline-fitting approaches described in Section 2.1 were then applied. For each shape, the two principle variables of interest were then determined: area and centre point.

The between-session reliability of the variables of interest (area & centre of the ellipse- and spline-fit shapes), was determined using the intraclass correlation coefficient (ICC) model (3,1) described by Shrout and Fleiss [14]. For the area of each shape, calculation of the ICC was done following standard procedures, as this variable is represented by a single, scalar value. For the centre of each shape, the ICC calculation was modified, as this point is represented by two values (X and Y coordinates). As the ANOVA used to calculate the reliability coefficient is based on the mean-squares difference between data points, it is the magnitude of the distance of any data point from the mean that is important in this calculation (i.e. a single, scalar value), and not the direction in which this difference occurs on the plane. The mean coordinates of a set of data points (Xmean ,Ymean) are simply the mean of the X and Y coordinates of all points within the set. The mean-squared differences required to calculate the reliability coefficient, therefore, are simply the square of the distances of each data point from the mean: $[(X - Xmean)^2 + (Y - Ymean)^2]$.

3. RESULTS

Fig. 3 illustrates data from two different subjects, for a single series of 8 end-range movements, along with the ellipse- and spline-fit shapes for these data. The reliability coefficients for the primary variables of interest, based on the ICC, were moderate. For the centre position of the shapes, the reliability coefficients were 0.57 and 0.64 for the ellipse- and spline-fit shapes, respectively. For the area of these shapes, the reliability coefficients were 0.58 and 0.57 respectively.

4. DISCUSSION

The current study aimed to test the reliability of a proposed measure of total lumbar spine ROM, based on the area and centre-point of a shape fit to a series of 8 end-range movements. The reliability of these variables, for this pilot work, reached only moderate levels. One of the possible reasons for this was that many participants did not perform the 8 movements at the prescribed 45° intervals. This is well illustrated in Fig.3. For the participant data on the right, the movement intervals between the anterior and anterior-diagonal movement directions appear to cover the prescribed 90° range. The remaining movements, for the prescribed lateral, posterior-diagonal and posterior directions, however, are compressed into roughly another 90° range, such that the intervals between these movements are dramatically less than the prescribed 45°. For the participant data on the left, the movements in the lateral and posterior-diagonal directions finish with roughly the same end-point, again illustrating that the participant did not complete the movements as directed.

Future research will focus on improving the reliability of these measures by providing subjects with visual feedback during the movement task. The expectation is that this feedback will help to direct the movements of the participants along the prescribed 45° intervals, and lead to improved reliability of the variables derived from the shape-fitting approaches.
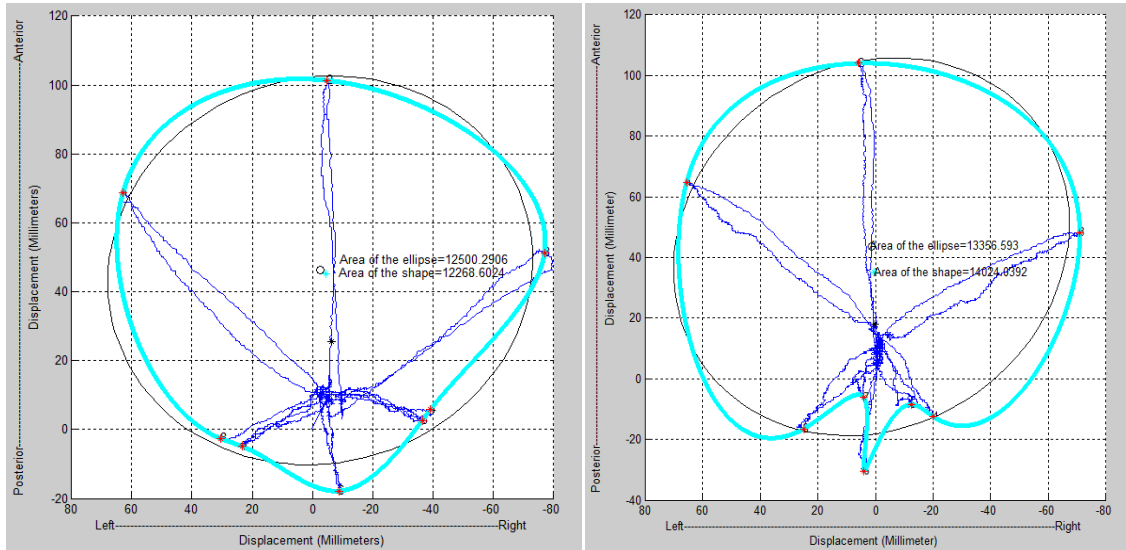
5. ACKNOWLEDGMENTS

Figure 3. Data from two representative subjects, for a single trial of 8 end-range movements, along with the shapes fit to these data using the ellipse- and spline-fitting approaches.

6.   REFERENCES

[1]   R. A. Preuss, and M. R. Popovic, "Three-dimensional spine kinematics during multidirectional, target-directed trunk movement in sitting," J Electromyogr Kinesiol, vol. 20, no. 5, pp. 823-32, Oct, 2010.

[2]   J. P. Scholz, G. Schoner, and M. L. Latash, "Identifying the control structure of multijoint coordination during pistol shooting," Exp Brain Res, vol. 135, no. 3, pp. 382-404, Dec, 2000.

[3]   R. L. Sainburg, C. Ghez, and D. Kalakanis, "Intersegmental dynamics are controlled by sequential anticipatory, error correction, and postural mechanisms," J Neurophysiol, vol. 81, no. 3, pp. 1045-56, Mar, 1999

[4]   S. M. Haley, and M. A. Fragala-Pinkham, "Interpreting change scores of tests and measures used in physical therapy," Phys Ther, vol. 86, no. 5, pp. 735-43, May, 2006.

[5]   C. J. Barrett, K. P. Singer, and R. Day, "Assessment of combined movements of the lumbar spine in asymptomatic and low back pain subjects using a three-dimensional electromagnetic tracking system," Manual Therapy, vol. 4, no. 2, pp. 94-99, 1999.

[6]   K. Jordan, K. L. Haywood, K. Dziedzic et al., "Assessment of the 3-dimensional Fastrak measurement system in measuring range of motion in ankylosing spondylitis," J Rheumatol, vol. 31, no. 11, pp. 2207-15, Nov, 2004.

[7]   I. A. Stokes, and M. Gardner-Morse, "Lumbar spine maximum efforts and muscle recruitment patterns predicted by a model with multijoint muscles and joints with stiffness," J Biomech, vol. 28, no. 2, pp. 173-86, Feb, 1995.

[8]   Hogan, N., (1985). The mechanics of multi-joint posture and movement control. Biol Cybern 52, 315-331.

[9]   P. Russell, M. J. Pearcy, and A. Unsworth, "Measurement of the range and coupled movements observed in the lumbar spine," Br J Rheumatol, vol. 32, no. 6, pp. 490-7, Jun, 1993.

[10] Willems, J., Jull, G., Ng, J., (1996). An in vivo study of the primary and coupled rotations of the thoracic spine. Clin Biomech 11, 311-316.

[11] Fitzgibbon, A., Pilu, M., Fisher, R., (1999). Direct least square fitting of ellipses. IEEE Pattern Anal Machine Intell 21, 476-480.

[12] T. Flynn, J. Fritz, J. Whitman et al., "A clinical prediction rule for classifying patients with low back pain who demonstrate short-term improvement with spinal manipulation," Spine (Phila Pa 1976), vol. 27, no. 24, pp. 2835-43, Dec 15, 2002.

[13] Fritz, J., Childs, J., Flynn, T., (2005). Pragmatic application of a clinical prediction rule in primary care to identify patients with low back pain with a good prognosis following a brief spinal manipulation intervention. BMC Fam Pract 6, 29.

[14] Shrout, P., Fleiss, J., (1979). Intraclass correlations: uses in assessing rater reliability. Psychol Bull 86, 420-428

Effects of Minimally Invasive Percutaneous Distal Metatarsal Osteotomy on Gait Performance in Patients with Hallux Valgus

Kao-Shang Shih [1], Chu-Fen Chang [2, 3, 4], Jia-Da Li [2], David Lin [2], Tung-Wu Lu [2, *]

[1] Orthopaedic Division of Surgical Department, Shin Kong Wu Ho-Su Memorial Hospital, Taipei, Taiwan R.O.C.

[2] Institute of Biomedical Engineering, National Taiwan University, Taipei, Taiwan R.O.C.

[3] Department of Physical Therapy and Assistive Technology, National Yang-Ming University, Taipei, Taiwan R.O.C.

[4] Taipei City Hospital, Taipei, Taiwan R.O.C.

[*] Corresponding author, twlu@ntu.edu.tw

1. INTRODUCTION

Hallux valgus (HV), a common forefoot deformity with a marked female preponderance of about 9:1 [1], has a profound effect on foot biomechanics, as well as the movement of the ankle, knee, and hip joints. Gait disturbance is one of the chief complaints among the patients with HV, and several studies have reported that a rise of plantar pressure of the lateral forefoot correlates closely with the aggravation of the HV deformity [2, 3]. Recently, minimally invasive percutaneous distal metatarsal osteotomy (MIPDMO) has been recommended for the correction of HV with the potential advantages of reduced operating time, decreased surgical exposure and early weight-bearing [4, 5]. After MIPDMO, radiological assessment shows a significant improvement in the hallux valgus angle, first and second intermetatarsal angle, distal metatarsal articular angle (DMA angle) and sesamoid position, and clinical evaluations indicate 91% of the patients were satisfied with the postsurgical results [5]. However, no study reported the effects of MIPDMO on the biomechanics of the lower extremities during gait in patients with HV. Therefore, this study aimed to investigate the biomechanical effects of MIPDMO on the gait performance in patients with bilateral HV through three-dimensional (3D) gait analysis and dynamic foot pressure analysis.

2. MATERIAL AND METHODS

Subjects

Six females with bilateral HV (age: 47.8 ± 8.5 years, body weight: 61.5 ± 5.3 kg, body height: 157.4 ± 4.3 cm, pre/post HV angle: $32.4\pm4.4°/13.8\pm3.2°$) were recruited and classified as either pre-MIPDMO or post-MIPDMO group. The average time between surgery and the study among the post-MIPDMO group was 4.9 months. Six healthy controls were matched with the HV patients according to sex, age, height and body weight (age: 49.2 ± 8.3 years, BW: 58.2 ± 5.5 kg, body height: 160.6 ± 4.9 cm).

Experimental Procedure

Each participant was instructed to walk for 3 times at a self-selected pace while their kinematic data was measured by a 7-camera motion capture system (Vicon 512) at a sampling rate of 120Hz and ground reaction forces (GRF) was captured from two AMTI forceplates at a sampling rate of 1080Hz. Their dynamic plantar pressures during walking were measured simultaneously using a pressure platform (RSscan International).

Data Analysis

Group and surgical effects on the joint angles and moments at the beginning and the end of single leg stance (bSLS, eSLS), and toe-out angle, as well as the peak force (%BW), peak pressure ($\%BW/cm^2$) and the time when the peak force occurred (% of stance phase) at ten foot regions, namely the big toe (T1), 2nd-5th toes (T2), 1st-5th metatarsals (M1-M5), mid-foot (MF), medial and lateral heel (MH & LH) were analyzed by Mann-Whitney U test and Wilcoxon signed ranks test, respectively, with $\alpha = 0.05$.

3.   RESULTS

3D Gait Analysis

Although gait speeds, cadence, and stride length were statistically the same for 2 groups, both pre-MIPDMO and post-MIPDMO groups had significant toe-in angles (p=0.022), Fig. 1. When compared to control group, the pre-MIPDMO group had significantly greater ankle abduction and internal rotation (IR) at bSLS and eSLS, greater vertical GRF at mid-stance, and decreased medial GRF, knee and ankle abductor moments, Figs. 2 and 3. When compared to the pre-MIPDMO group, the post-MIPDMO group had reduced vertical GRF at mid-stance, hip adduction and hip abductor moments at eSLS and increased medial GRF, Figs. 2 and 3.
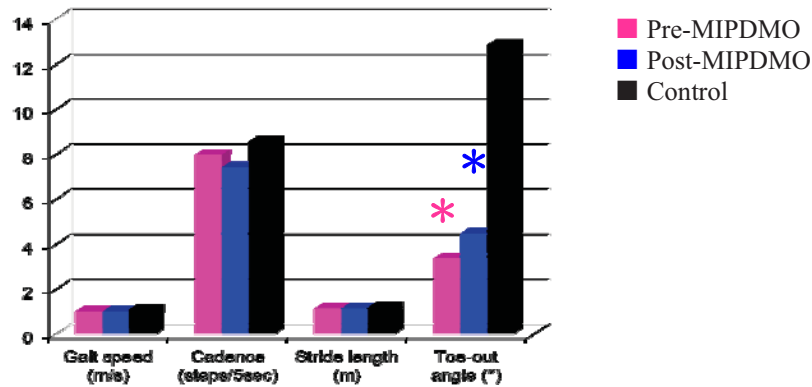

Figure 1. Ensemble-averaged distance-temporal variables (*, *, * : significant differences in Pre-MIPDMO vs Control, Post-MIPDMO vs Control, Pre-MIPDMO vs Post-MIPDMO, respectively)
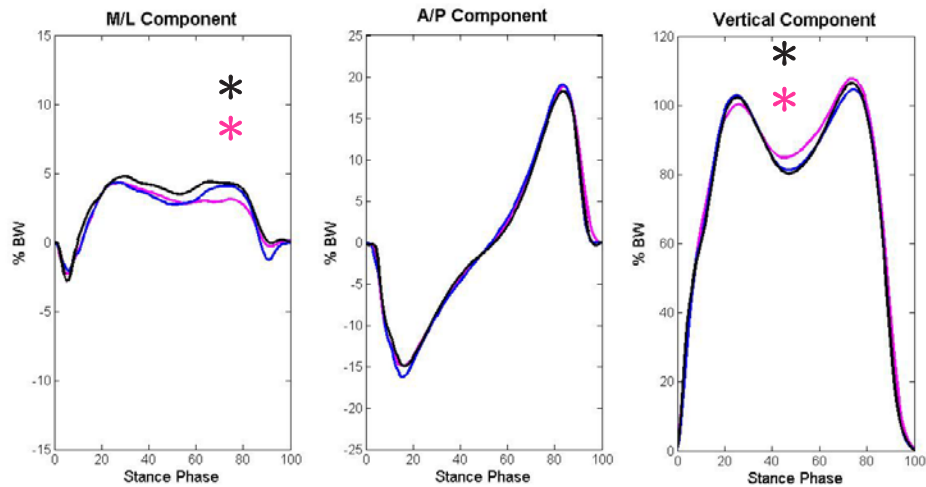

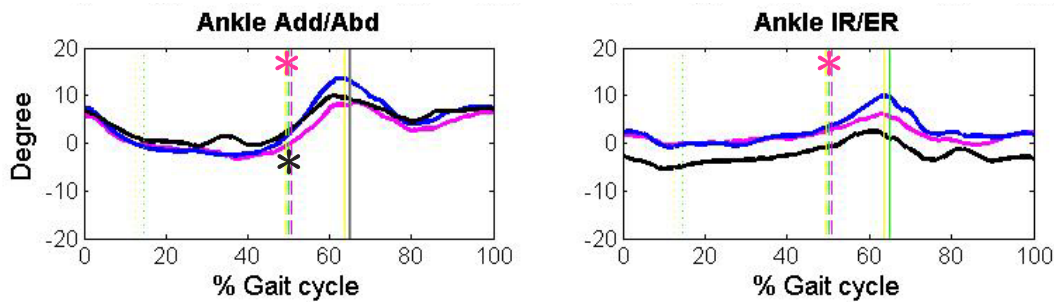Figure 2. Ensemble-averaged GRF of the pre-MIPDMO, post-MIPDMO and Control groups.

Figure 3. Ensemble-averaged ankle angles in frontal and transverse planes of the pre-MIPDMO, post-MIPDMO and Control groups.

Dynamic Plantar Pressures

When compared to the control group, the pre-MIPDMO group had a higher peak force at T2 (p=0.014), greater peak pressures at T1 and T2 (p=0.041 & p=0.001) and decreased peak pressures of M5 and LH (p=0.012 & p=0.013), while the post-MIPDMO group had smaller peak force at T1 (p=0.028) and greater peak force at T2 (p=0.045), Figs. 4 & 5. Comparisons between the pre-MIPDMO and post-MIPDMO groups showed that MIPDMO for bilateral HV led to significantly decreases in the peak force of T2 (p=0.014) and peak pressures of T1 and T2 (p=0.004 & p=0.003), and later occurrences of peak pressure at M2 (p=0.025), M4 (p=0.032) and M5 (p=0.041), Fig. 5.
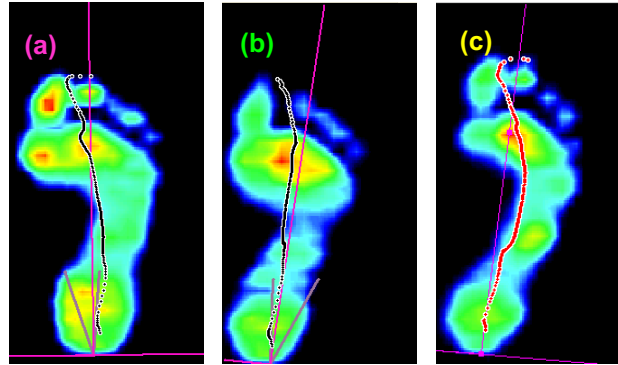

Figure 4. Typical pressure distributions of the HV foot pre-MIPDMO (a) and post-MIPDMO (b), and that of the normal foot (Control).
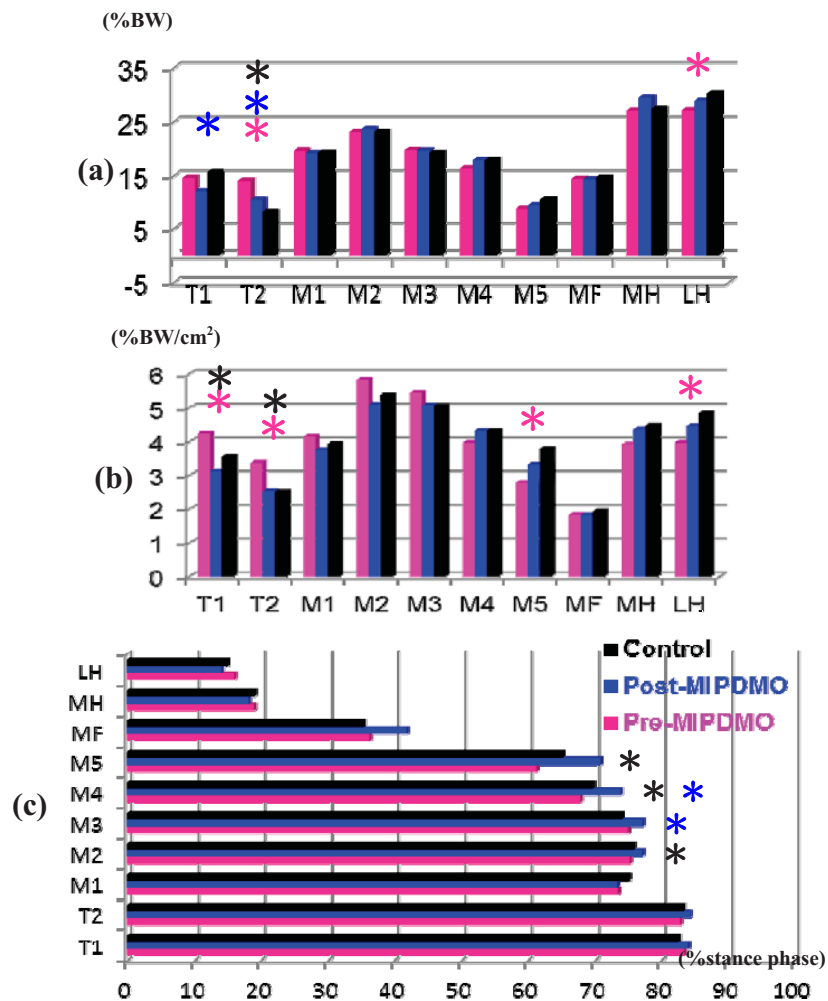

Figure 5. The peak force (a), peak pressure (b) and the time when the peak force occurred (c) in the pre-MIPDMO, post-MIPDMO and Control groups.

4. DISCUSSION

Increased ankle IR and abduction (Fig. 3) were highly related to increased foot pronation and toe-in gait commonly found in feet with HV. Greater toe-in angles have been found to result in smaller medial GRF [6] and decreased knee and ankle abductor moments [7]. Greater toe-in angles might also result in the significantly greater than normal peak pressures under the hallux, and similar trends in the medial metatarsals (M1-M3) that were found in the pre-MIPDMO group (Figs. 4 and 5). Similar findings of the dynamic plantar pressure distribution in the untreated HV patients have been reported in the previous studies [6, 7]. In addition, increased vertical GRF at mid-stance in the pre-MIPDMO group indicated an impaired shock absorption mechanism during walking. Flatfoot with poor compliance of the foot arch had been considered as one of the major causes of HV and would alter the shock absorption mechanism because of exaggerated eversion of the subtalar joint [8, 9].

After MIPDMO, in addition to the satisfactory correction of hallux alignment, HV patients could restore their ability of shock absorption by correcting the abnormal alignment of HV and flatfoot. MIPDMO also alleviated the excessive weight-bearing load on lesser toes, and significantly reduced the abnormal elevated peak pressures of T1 and T2. Decreased peak pressure of T2 showed that MIPDMO could effectively improve the abnormal rise of plantar pressure in the lateral forefoot which was commonly observed in the aggravated HV deformity. However, since the decreased hallux loading may be related to the weakness of intrinsic muscles and changed mechanical function of the hallux [8], the strength of these muscles should be monitored after MIPDMO. Furthermore, the post-MIPDMO group still walked with greater foot pronation and toe-in. Walking in such deviated pattern for a long time could still be anticipated to aggravate HV in future and the follow-up in patients after MIPDMO for HV should be noted. Overall, the MIPDMO appeared to be effective in treating HV with good biomechanical outcome.

5. ACKNOWLEDGMENT

6. REFERENCES

[1] Thomas S, Barrington R, 2003. Hallux valgus. Curr. Orthop. 17, 299-307

[2] Blomgren M, Turan I, Agadir M, 1991. Gait analysis in hallux valgus. J. of Foot Surg. 30, 70-71

[3] Waldecker U, 2004. Pedographic analysis of hallux valgus deformity. Foot Ankle Surg. 10, 121-124

[4] Magnan B, Bortolazzi R, Samaila E, Pezze L, Rossi N, Bartolozzi P, 2006. Percutaneous distal metatarsal osteotomy for correction of hallux valgus. Surgical technique. J Bone Joint Surg-Am Vol 88 135-148

[5] Magnan B, Pezze L, Rossi N, Bartolozzi P, 2005. Percutaneous distal metatarsal osteotomy for correction of hallux valgus. J Bone Joint Surg-Am Vol 87, 1191-1199

[6] Simpson KJ, Jiang P, 1999. Foot landing position during gait influences ground reaction forces. Clin. Biomech. 14, 396-402

[7] Guo M, Axe MJ, Manal K, 2007. The influence of foot progression angle on the knee adduction moment during walking and stair climbing in pain free individuals with knee osteoarthritis. Gait Posture 26, 436-441

[8] Catani F, Benedetti MG, Montanari P, Pignotti E, Ceccarelli F, Ghetti M, Giannini S, 1995. Functional evaluation of gait in children with flat foot. Gait Posture 3, 287-287

[9] Catani F, Benedetti MG, Simoncini L, Giannini S, Leardini A, Bertani A, Cappello A, 1997. Flat foot functional evaluation using Ground Reaction Forces. Gait Posture 5, 149-149

A Methodological Framework Based on Data Mining Techniques for Movement Analysis

Aguilera A.[1], Barbier F.[2]

[1] CAMYTD, FACYT, University of Carabobo,Venezuela, aaguilef@uc.edu.ve
[2] LAMIH UMR-CNRS 8201, University of Lille Nord de France, France, franck.barbier@univ-valenciennes.fr

Abstract. A methodological framework is presented for development of an automated predictor module using gait patterns. This module has been programmed and incorporated in an aid decision system. Learned models have been evaluated and integrated in this predictor. Different types of validation were applied on the models and on the system. A variety of mathematical methods was used for quantitative validation and questionnaire to expert for qualitative validation. A real application in pathologic gait analysis was developed. This application includes kinetic, kinematics, EMG analysis.

Keywords- Automated predictor; Gait Classifications; Data mining; Spastic Hemiplegia

1. INTRODUCTION

The aim of instrumented gait analysis is to support clinicians' decision making process concerning diagnosis and treatment strategies [1]. Gait analysis is now recognized as clinically useful and financially reimbursable for some medical conditions. However its clinical use is most hampered by the length of time and costs required for performing a study and interpreting it. A "gait" report is lengthy, its data are not well understood, and it includes a clinical interpretation, all of which do not occur with other clinical tests [2]. Normally, the data evaluation for clinical purposes is often performed by experienced physicians in a qualitative way. However, in recent years, several new approaches to gait data analysis quantitative have been explored and they have showed their potential to strengthen the gait laboratory's analytical arsenal. These quantitative approaches include artificial intelligent techniques like neural networks, fuzzy logic approaches, and others and different statistical techniques.

A review of analytical techniques for gait data includes fuzzy systems, multivariate statistical techniques and fractal dynamics [3]. An analysis system based on adaptive neuro-fuzzy inference system, which combined the neural network capabilities and fuzzy logic qualitative approaches, was also proposed for gait analysis. In this case, a practical clinical problem of pes cavus and pes planus classification was used as an example to explain the principal and process of this system [4]. The use of support vector machines (SVM) have been explored for automated detection and classification of children with CP using two basic temporal-spatial gait parameters (stride length and cadence) as input features [5]. Statistical techniques like ANOVA test was used in gait analysis and surface electromyograms of seven major lower limb muscles were assessed before and 1–5 years after the multilevel surgery. A two-way ANOVA have determined the effect of the factor DIAGNOSIS (levels: diplegia and hemiplegia), the factor TIME for repeated measurements (levels: examination before and after the surgery) and the interaction between these factors for the norm-distance of the spatiotemporal, kinematic, kinetic and EMG parameters [6]. Other works have been focused in the discriminant feature extraction on gait parameters. The principal component analysis (PCA) is the most popular. A hybrid feature reduction method based on the combination of feature ranking with PCA was proposed by [7]. In this case, three feature reduction methods, namely, feature ranking based the value of signal to noise ratio, PCA and the proposed hybrid approach, were examined in two gait analysis problems. One gait analysis problem was to differentiate the patients with neurodegenerative disease from the controls based on the gait data collected by footswitches. The other problem was to discriminate the patients with complex regional pain syndrome from controls based on the gait data collected by an accelerometer. Other work has employed a kernel principal component analysis algorithm to extract gait feature for initiating the training set of SVM via pre-processing, which SVM with better generalization performance recognized gait patterns [8]. The significance of bayesian classifier model have been investigated on 68 normal healthy and 88 with spastic diplegia form of cerebral palsy, different features including the two basic temporal-spatial gait parameters (stride length and cadence) have been experimented in this work [9]. A methodological modular framework for automated assessment of gait patterns using different mathematical methods was proposed by [10]. Their application was based on the clinical problem of Botulinum Toxin A treatment of the spastic equinus foot. A set of 3670 parameters was ranked by relevance for classification of a group of 42 diplegic cerebral palsy patients.

Data mining, the extraction of hidden predictive information from large databases, is a powerful new technology with great potential to help in many domains. Particularly in the medical field, it can be used for analyzing data from different perspectives and summarizing it into useful information. Others utilities include: identification and diagnosis of disease, detection of patients at risk for a specific disease, hospital management and healthcare, resources administration, recommendation for treatments, etc. Many data mining software integrate number of statistical and intelligent tools for analyzing data.

The aim of this paper is to present a methodological framework for development of an automated predictor module using movement patterns.

2. METHODS

The applications of the predictor module are very diverse. It can be used to test of research hypotheses in an academic sense or to be integrated in a computer application in a practical sense. The steps of the framework are resumed in the figure 1. The processing steps are not limited to a specific field of application and are largely independent of case-based clinical expert knowledge.

| Movement problem Identification | → | Gathering and selection of data movements | → | Study of Discriminant data | → | Datamining techniques: Classification task | → | Evaluation/ Interpretation/ Visualization |

Figure 1. Methodological framework

a. Movement problem Identification

This step is to identify the problem to be studied, its context and purpose of study. For example, if it is a medical problem, what is pathology ?, what are the characteristics of pathological subjects ?, is there normal patterns?, what is the purpose of the study?, identify or diagnose diseases, etc.

b. Gathering and selection of data movements

It identifies, collects and selects the data that will serve for analysis. This data will serve to answer the research objective. It is possible that the data are not debugged and cleaned, that is, data has not an appropriate format for the next step. In this case, data have to be prepared and transformed for the next step. For example, typically, gait information comprise a subset of kinematics, kinetics, EMG, oxygen consumption or foot pressure distribution, videos, ray X, etc. in different formats.

c. Study of discriminant data

Sometimes too much information can reduce the effectiveness of data mining. Some of the columns of data attributes assembled for building and testing a model may not contribute meaningful information to the model. Some may actually detract from the quality and accuracy of the model. Irrelevant attributes simply add noise to the data and affect model accuracy. Noise increases the size of the model and the time and system resources needed for model building and scoring. Moreover, data sets with many attributes may contain groups of attributes that are correlated. These attributes may actually be measuring the same underlying feature. Their presence together in the build data can skew the logic of the algorithm and affect the accuracy of the model. To minimize the effects of noise, correlation, and high dimensionality, some form of dimension reduction is sometimes a desirable preprocessing step for data mining. By reducing the dimensionality of the input set correlated information is eliminated at the cost of a loss of accuracy. Dimensionality reduction can be achieved either by eliminating data closely related with other data in the set, or combining data to make a smaller set of features [11].
Feature selection and extraction are two approaches to dimension reduction. The first involve selection of the most relevant attributes, and the last one consists in combining attributes into a new reduced set of features (Factor Analysis and Principal Components Analysis, Correspondence Analysis, Multidimensional Scaling, Partial Least Squares methods, or singular value decomposition, etc). In some cases, it is possible to increasing the amount of attributes using feature extraction techniques, like correlations and derived of new attributes. The aim of that, it is done increase the effectiveness of learned models.

d. Datamining techniques: classification task

Datamining Techniques include a variety of methods and techniques for knowledge extraction. Usually this knowledge is presented as a model or pattern. Different models can be extracted according to their utility. These are predictive or descriptive models. Predictive models seek to estimate future or unknown values of variables of interest. Descriptive models instead identify patterns that explain or summarize the data. The latter serves to explore the properties of the data examined and fails to predict new data. Some data mining

tasks which produce predictive models are classification and regression while descriptive models are clustering, association rules and correlation analysis. Different techniques can be applied to a task and the same technique can be applied to different tasks.

Some techniques include support vector machines, decision trees, neural networks, regression, nonparametric statistical modeling, Bayesian models, etc. The use of one technique or another depends on the research objective. It is important to consider that a good model should be understandable, expressive, precise, efficient, stable, robust, easy to use, etc.. Another aspect to consider in machine learning is the time consuming required for the model construction. For example, decision trees are useful to find structures in high dimensional spaces and with problems that combine categorical and numerical data. Their advantage is that they are understandable and easy to implement and the disadvantage is their sensitivity to the training set. Neural networks have great potential for generalization to nonlinear problems. Its main disadvantage is that they require a lot of data for training and generally they build models less understandable.

e. Evaluation / Interpretation / Visualization

Learning methods can build models from a dataset. In most cases, it is necessary to evaluate the quality of these models as accurate as possible, in order to develop models closer to reality. For this, there exist several methods that evaluate the quality of model from the evidence. For instance, for classification task the validity and accuracy of a model is the degree to that, it classifies what it has to classify. It is the absence of systematic errors [12]. Reliability is the degree of stability achieved when the test is repeated under similar conditions. The measures commonly used to measure the reliability are: the global concordance index, the Kappa concordance index, coefficient of variation and interclass correlation coefficient. . For the validity of a model are the sensitivity measures and specificity. These measures involve combinations of variables like true possitive, true negatives, false positives and false negatives. Also, the positive verisimilitude rate (LR +) and negative verisimilitude rate (LR-) are other measures used for validity. ROC curves (Receiver Operating Characteristic) are a very useful visual tool when comparing two models of classification. They show the comparison between the true positive rate and false positive rate for a model. The perfect accuracy will have an area of 1.0. Others test include cost models based on cost of errors made by the model, distance between estimated values for regression models, complexity of model, and level of compaction of different groups for clustering models, etc.

3. RESULTS

Gait analysis provides a very large data volume coming from kinematic, kinetic, electromyographic (EMG) registers and physical examinations. The analysis and treatment of these data is difficult and time consuming. Though the data mining techniques have been applied on kinematic, kinetic, electromyographic (EMG) registers and physical examinations, the present work has been focused only on the study of EMG registers in children with spastic hemiplegia, for reasons of simplicity and briefly. The methods studied search to predictive model. Different techniques of feature extraction and selection have been also employed and combined with classifications methods. The predictor module has been integrated in an aid decision system.

a. Movement problem Identification

The data corresponding to records used in this work were collected from Gait Laboratory of Orthopedic Children´s Hospital located in Caracas-Venezuela [13]. These data come from Vicon© acquisition system (it was transmitted a twelve bits with a sampling frequency of 1.5 kHz. The signals are converted into an analog signal in the range of ± 10V).

Gage and his team have suggested that SH could be classified into at least four groups: group I, group II, group III and group IV taking into account the kinematic pattern of cerebral palsy patients [14], [15]. This classification for the four Groups of SH and the normal pattern was done in the sagittal plane kinematic patterns. The kinematic classification goes to involve progressively the other joints such as the ankle (group I), knee (group II), hip (group III) and pelvis (group IV).

b. Gathering and selection of data movements

These data correspond to thirty SH patients with 99 EMG signals normalized and delimited to a gait cycle were considered in C3D format. These data contain registers with a diagnosis from medical staff of the laboratory according to the Gage's classification [14]. The distribution of cases is 51 for Group I, 16 for the Group II, 6 for the group III, 23 for the Group IV and 3 without classification.

c. Study of Discriminant data

Twenty-tree indicators have resulted from studying of EMG records using the contribution of Viloria [16]. For this, it has been evaluated the kinematic classification from an electromyographical point of view, based on time and frequency domain. It has resulted 2 indicators of instant energy, 3 obtained by fast Fourier transform (FFT), 16 from the computation of mean power frequency (MPF) and, others resulting from the

energy spectrum of each component derived from the wavelet decomposition of the normalized EMG. The statistic behaviors for each indicator have been determined computing the mean and standard deviation. The orders of magnitude from these indicators in time and frequency domain were obtained using computation of instant energy, significant frequencies and spectrum power [16]. The computed indicators for EMG including the two legs were considered. A total of 277 attributes have been selected and they correspond to 23 indicators x 6 muscle x 2 legs plus 1 for group type.

d.   Datamining techniques: Classification task

Different data mining algorithms for prediction have been used in classification task. The following classifiers were evaluated for tests: a best-first decision tree classifier (BFTree: 78,8732%), DecisionStump (64,7887%), functional trees (FT: 95,7746%), J48 (77,4648%), a grafted (pruned or unpruned) C4.5 decision tree (J48graft: 70,4225%), a multi-class alternating decision tree (LADTree: 80,2817%), LMT (97,1831%), A Naïve Bayes/Decision tree (NBTree: 88,7324%), RandomForest (90,1408%), RandomTree (67,6056%), Fast decision tree learner (REPTree: 73,2394%), SimpleCart (78,8732%). The percentage represents the correctly classified instances.

e.   Evaluation/Interpretation/ Visualization

A group of patients with pathology of SH treated in hospital were selected random way. The two-dimensional videos in two planes (sagittal and frontal) of each one of these patients and their respective EMG were presented to specialist physicians. After, the results issued by each automatic classifier were compared with those diagnoses generated by physicians. 71 instances of the total (99) have been used for training of model. This model has classified 69 instances correctly. From the confusion matrix it is possible to observe that only for group 1 and 4, 1 instance was classified incorrectly in each group. Test mode used was the Cross-Validation with 10 Folds.

4.   REFERENCES

[1]   Loose, T. Mikut, R. Malberg, H. Simon, J., Schablowski, M., Rupp, R., Döderlein, L. A Computer Based Method to Assess Gait Data, n: Proc. IFMBE, 2nd European Medical and Biological Engineering Conference, EMBEC, 2002.

[2]   Simon, S. Quantification of human motion: gait analysis—benefits and limitations to its application to clinical problems, J. Biomechanics, Vol. 37 (12), pp. 1869-1880, 2004.

[3]   Chau, T. A review of analytical techniques for gait data. Part 1: fuzzy, statistical and fractal methods, Gait & Posture, Vol. 13 (1), pp. 49-66, 2001.

[4]   Xu, S., Zhou, X., Sun, Y., A novel gait analysis system based on adaptive neuro-fuzzy inference system. J. Expert Systems with Applications, Vol. 37 (2), pp. 1265-1269, 2010.

[5]   Kamruzzaman, J., Begg, R.K. Support Vector Machines and Other Pattern Recognition Approaches to the Diagnosis of Cerebral Palsy Gait. IEEE Trans. on Biomedical Engineering, Vol. 53 (12), pp. 2479 – 2490, 2006.

[6]   Patikas, D., Wolf, S., Schuster, W., Armbrust, P., Dreher, T., Döderlein, L., Electromyographic patterns in children with cerebral palsy: Do they change after surgery?, Gait & Posture 26, pp. 362–371, 2007.

[7]   Ming-Jing Yang; Hui-Ru Zheng; Hai-Ying Wang; Mcclean, S.; Harris, N., Combining feature ranking with PCA: An application to gait analysis, in Proc of International Conf. on Machine Learning and Cybernetics (ICMLC), pp. 494 – 499, 2010.

[8]   Jianning, W. Kernel-Based Feature Extraction for Automated Gait Classification Using Kinetics Data. In proceeding of ICNC '08. Fourth International Conference on Natural Computation, Vol. 4, pp. 162 – 166, 2008.

[9]   Zhang, B., Zhang, Y., Begg, R., Gait classification in children with cerebral palsy by Bayesian approach, J. Pattern Recognition Vol. 42 (4), pp. 581-586, 2009.

[10]   Wolf, S., Loose, T., Schablowski, M., Döderlein, L., Rupp, R. Jürgen, H., Bretthauer, G., Mikut, R. Automated feature assessment in instrumented gait analysis, Gait & Posture, Vol. 23 (3), pp. 331-338, 2006.

[11]   Addison D., Wermter S., Arevian G. A Comparison of Feature Extraction and Selection Techniques. Proceedings of the International Conference on Artificial Neural Networks, Istanbul, Turkey, pp. 212-215, June 2003, WWW: http://www.his.sunderland.ac.uk/ps/dalicann.pdf

[12]   Bermejo, B. Clinical Epidemiology applied to decision aid in medicine. Epidemiología Clínica aplicada a la toma de decisiones en medicina. 2001 WWW:http://www.cfnavarra.es/salud/ docencia.investigacion/ textos/Monograf_1/Epidemiologia_clinica.pdf

[13]   FHOI, Fundación Hospital Ortopédico Infantil (2006). Caracas Venezuela.   WWW: http://www.ortopedicoinfantil.org

[14]   Winters TF, Gage JR, Hicks R, Gait patterns in spastic hemiplegia in children and young adults. J Bone Joint Surg (Am), Vol. 69, pp. 437-441, 1987.

[15]   Robb, J. The Treatment of Gait Problems in Cerebral Palsy. Clinics in Developmental Medicine No. 164–165, James R. Gage (Ed.), Mac Keith Press, London, Gait & Posture, Volume 24(1), pp. 130-130, 2004.

[16]   Viloria, N. Electromyographic Evaluation of kinematics classification in Spastic Hemiplegic Patients with pathological gait". Msc Thesis in Biomedical Engineering, Simón Bolívar University, Caracas, Venezuela, 2003.

Biomechanical Features of Novel Stroke Rehabilitation Programme in Acute Stroke Patietns

Skvortsova V.I. [1], Ivanova G.E. [1], Skvortsov D.V. [2], Bulatova M.A. [1], Kovrazhkina E.A. [1], Suvorov A.Y. [1]

[1] Institute of Stroke, Moscow, Russia
[2] Moscow Medical University, Moscow, Russia, dskvorts63@mail.ru

Movement impairment is a common outcome of cerebral stroke. This research has main point to find out mechanisms of recovery a movement function during acute stroke by using ontogenetic principles. The study included 10 acute stroke patients with hemiplegia of varying degrees and 10 healthy adult volunteers. The study protocol included neurological and physiotherapy clinical examination and biomechanical assessment of programme exercises by Qualisis motion capture system 8 of OQUS-500 cameras and surface EMG by ME 6000. Several phenomena of movement patterns were disclosed. Any exercise movement cycle shows time symmetry. There are fore-movement and endplay movement phenomena present in all complicate movements. Poor muscle strength is often compensated by substitutional trunk movement. Symmetric movements would boost performance on paretic side, compared to unilateral movements. EMG muscle response demonstrates at least 2 patterns of activation: hyperactivity on the side of lesion, compared to non-paretic side, and reduced EMG activity on the side lesion.

Keywords: clinical motion analysis, acute stroke, biomechanics.

INTRODUCTION

Movement impairment is a common outcome of cerebral stroke. It develops within acute period and could often persist in some form for the rest of life. Even though, there are many concepts in neurorehabilitation, onotogenetic based and others, biomechanical studies could contribute to understanding of key factors of physical activities and movements patterns.

This research has main point to find out mechanisms of recovery a movement function during acute stroke by using ontogenetic principles.

MATERIAL AND METHODS

A novel ontogenetic based rehabilitation programme was investigated for its efficacy in acute stroke patients. The study included 10 acute stroke patients with hemiplegia of varying degrees and 10 healthy adult volunteers. The study protocol included neurological and physiotherapy clinical examination and biomechanical assessment of programme exercises by Qualisis motion capture system 8 of OQUS-500 cameras and surface EMG by ME 6000. Six muscles were monitored on both sides: sternocleidomastoideus, trapezius, biceps, triceps brachii, rectus femoris, adductor magnus. The exercises are performed and monitored in 7 test positions, consequently from lying to standing on the knees.

RESULTS

Several phenomena of movement patterns were disclosed. They are for the normal group. Movement patterns could vary in different exercises for the same joint or muscle. Any exercise movement cycle shows time symmetry. The maximal ROM is reached at 50% of the motion cycle. There are fore-movement and endplay movement phenomena present in all complicate movements. A trigger fore-movement is a specific trigger small amplitude movement in a direction opposite to a targeted movement. Endplay movement is small amplitude overdo of a targeted movement with consequent reverse movement to the target. Any simple movement in shoulder and hip joints would occur in all 3 of 3D planes. There is kinematic asymmetry between right and left side in right-handed individuals. The left side demonstrates greater range and less selectivity in EMG pattern of phase motion. There are different patterns of trunk and extremity muscle activation in different individuals. In some it would activate distal muscles and reach the core, in others it would occur within the core and extend to extremities.

Phenomena founded for group of patients. There is a marked difference in performance of the same test movement, performed in different test positions, in symmetrical and asymmetrical movements for the same joint or muscle. There is a deviation in time of maximal ROM towards the end of the cycle in cyclic movements. Poor muscle strength is often compensated by substitutional trunk movement. Symmetric movements would boost performance on paretic side, compared to unilateral movements. EMG muscle response demonstrates at least 2 patterns of activation: hyperactivity on the side of lesion, compared to non-paretic side, and reduced EMG activity on the side lesion. The hyperactivity pattern demonstrates an increased number of muscles peak activation on the side of lesion.

Patterns of muscle activation varied significantly in patients and in healthy controls. Patterns of muscle activat demonstrated marked difference if done in different starting positions, which could be an influence of gravity fo vector. Head turn in supine showed bilateral high activity of sternocleidomastoideus and trapezius. When done in standing, there was unilateral activity of these muscles. Unilateral arm rising in supine showed activity of triceps brachii, rectus femoris and adductor magnus on the side of the movement. When done in standing, there was also activation of trapezius and biceps of the same side, concurrent with the muscles, active in supine.

DISCUSSION

We have found few publications concerning at this matter [1; 2]. So, it needs more data for an opportunity to compare our results with other studies. However, we could assume that movement control has more complicate nature when was expected.

Phenomena of fore-movement and endplay movement, which are prerequisite for any movement of any body part, and patterns of core and extremity activation desire further research.

There were different patterns of muscle activation in test movements, when done in different test positions. This might relate to a gravity vector change. As there were various patterns of muscle activation registered.

Three pattern of muscle activation could give some keys for understanding, prevention and treatment of spasticity and movement impairment in acute stroke patients.

1. Esparza D.Y. et all (2003) Exp Brain Res. 2003, 148(4):488-97.
2. 2. Grip H. (2008) Ph.D. dissertation, Umea University, Sweden, 2008.

Differences in gait parameters between people after right-sided and left-sided stroke

Jurkojć J.[1], Michnik R.[1], Guzik-Kopyto A.[1], Rycerski W.[2]

[1]Department of Biomechatronics, Silesian University of Technology, Gliwice, Poland, Jacek.Jurkojc@polsl.pl
[2]Upper Silesian Rehabilitation Center "Repty", Tarnowskie Góry, Poland,

Keywords: gait analysis, stroke.

1. INTRODUCTION

Motion problems are the main complications touching people who survived a stroke. Many of these people can't move at all at the beginning of rehabilitation, but even after a long lasting recovery they still have some problems with walking or manual movements. That is why a good and individually-oriented rehabilitation is crucial. There are many research which aim to aid the rehabilitation process and make it possible to assess its progress. Many of them base on kinematic and dynamic analyses of patients' motion [1,2,3,4].

Presented in this paper research and measurements are the part of a project which aims to elaborate a system enabling monitoring of rehabilitation progress of patients after stroke [3]. Presented results concern relationships between gait parameters and stroke side what seems to be very important in personalization of the recovery process.

2. METHODS

All measurements were performed in the Rehabilitation Centre "Repty" in Tarnowskie Gory, Poland and were carried out for patients who are already able to walk. There were nine persons after right-sided stroke and nine after left sided.

Examined person has 17 markers attached to the characteristic points of lower limb and pelvis according to the Davis's system. Execution of gait was recorded by a set of camcorders and ground reactions were measured by means of dynamometric platforms. Then obtained movies were processed with the use of APAS system and computer program prepared by scientists from the Department of Applied Mechanics [5,6].

3. RESULTS

Measurements and calculations enabled determination of mean courses of courses of joint angles (fig. 3 and 8).

On the basis of these courses the following gait parameters were calculated: mean pelvic tilt, mean pelvic rotation, minimal hip flexion, range of hip flexion-extension, knee flexion at the beginning of the stance phase, range of knee flexion-extension, maximal knee flexion, percent of the gait cycle when the maximal knee flexion occurs, gait velocity, gait cadence, stride length, duration of a gait cycle, duration of a stance phase. The exemplary results are presented in figures 1,2,4 – 7,9,10.
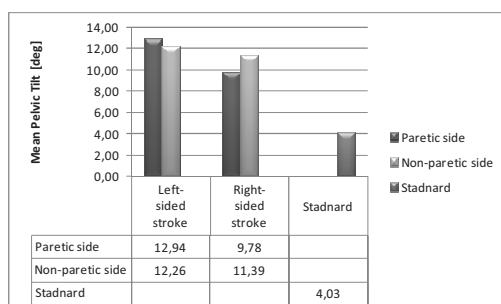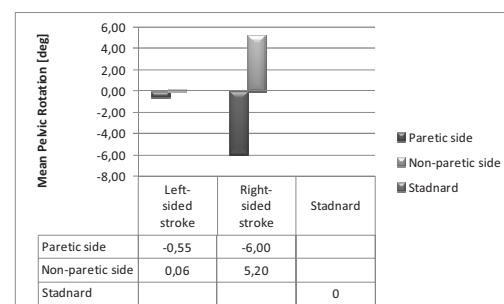

Mean Pelvic Tilt [deg]	Left-sided stroke	Right-sided stroke	Stadnard
Paretic side	12,94	9,78	
Non-paretic side	12,26	11,39	
Stadnard			4,03

Fig. 1 Mean pelvic tilt

Mean Pelvic Rotation [deg]	Left-sided stroke	Right-sided stroke	Stadnard
Paretic side	-0,55	-6,00	
Non-paretic side	0,06	5,20	
Stadnard			0

Fig. 2 Mean pelvic rotation

Fig. 3 Angle courses of pelvic a) obliquity, b) tilt and c) rotation. Dashed line – mean standard value, shaded region – confidence interval of mean standard value, thin line – left sided stroke, paretic side, thick line – right-sided stroke, paretic side
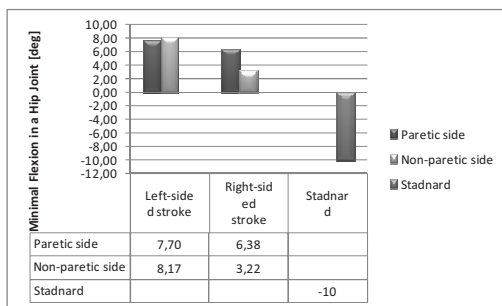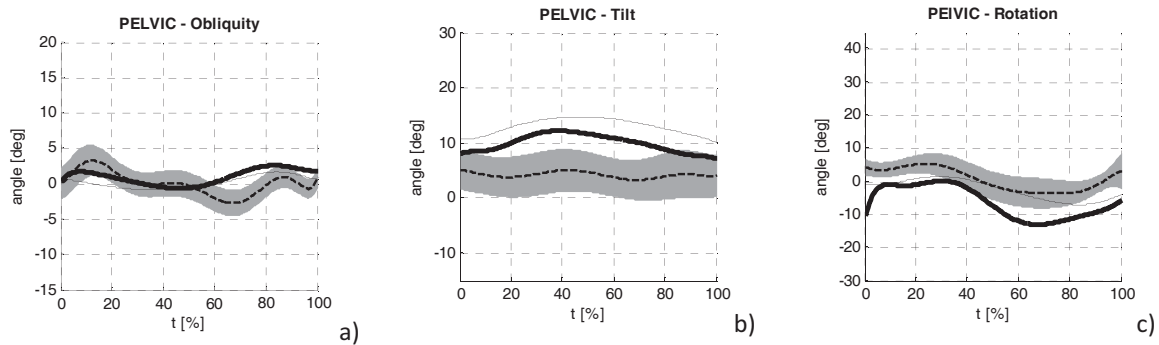

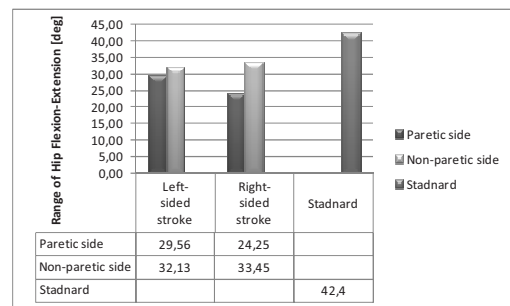Fig. 4 Minimal hip flexion

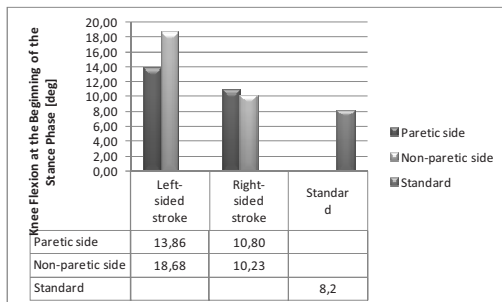Fig. 5 Range of hip flexion-extension

Fig. 6 Knee flexion at the beginning of the stance phase

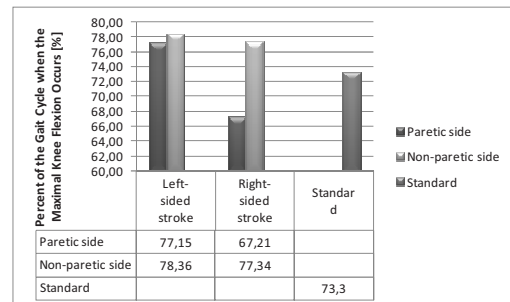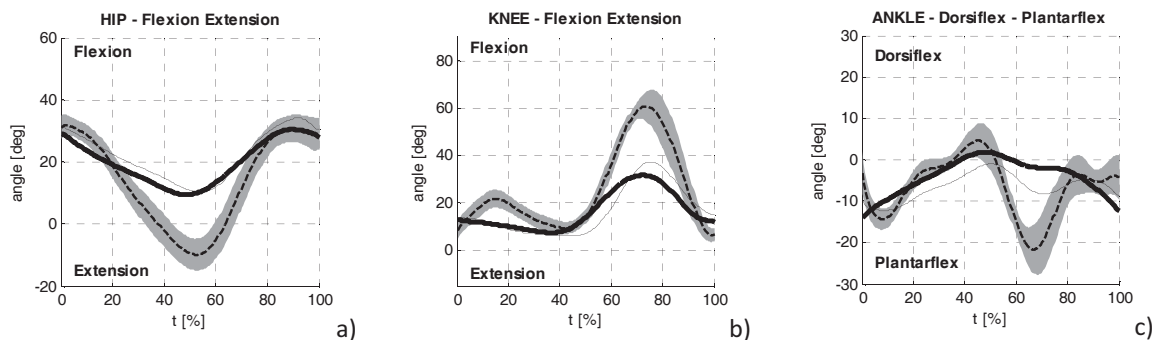Fig. 7 Percent of the gait cycle when the maximal knee flexion occurs

Fig. 8 Angle courses in a) hip, b) knee and c) ankle joints in saggital plane. Dashed line – mean standard value, shaded region – confidence interval of mean standard value, thin line – left-sided stroke, paretic side, thick line – right-sided stroke, paretic side
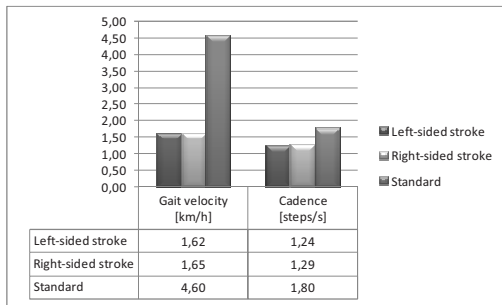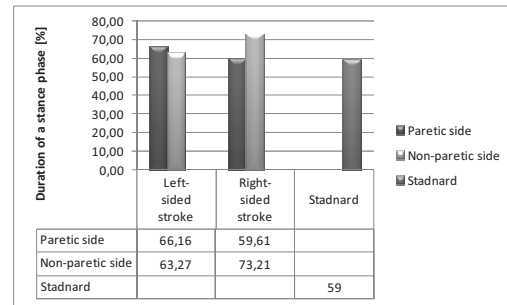
Fig. 9 Gait velocity and cadence

Fig. 10 Duration of a stance phase

Analysis of obtained results

On the basis of obtained results the comparative analysis of gait parameters for left-sided and right sided stroke was carried out. Some parameters were similar for these two types of a stroke, but many of them were significantly different .The detailed analyses are presented in tables 1 - 3.

Table 1. Comparative analysis of quantitative gait parameters for left-sided and right-sided stroke

		Left-sided stroke	**Right-sided stroke**
Pelvis	*Mean Pelvic Tilt (standard 4°)*	Excessive mean Tilt (about 12°)	Excessive mean Tilt (about 10°)
	Mean Pelvic Rotation (standard 0°)	Correct Pelvic rotation	Excessive mean rotation towards the paretic side (about 5.5°)
Hip	*Minimal Hip Flexion (standard -10°)*	Insufficient extension *(+3°to +8°)*	
		Equal for both body sides	Difference between paretic (+6°) and non-paretic (+3°) side
	Range of hip Flexion-Extension (standard 42°)	Reduced range (24° - 33°)	
		Insignificant difference between both body sides	Difference between paretic (24°) and non paretic (33°) side
Knee	*Knee flexion at the beginning of the stance phase (standard 8°)*	Excessive knee flexion and difference between paretic (13°) and non-paretic (18°) side	Insignificant excessive knee flexion (10°)
	Range of knee flexion-extension phase (standard 57°)	Reduced range (31° - 45°)	
		Smaller difference between paretic (38°) and non paretic (45°) side	Greater difference between paretic (31°) and non paretic (41°) side
	Maximal knee flexion (standard 62°)	Reduced maximal flexion and difference between paretic (43°) and non paretic (57°) side	Reduced maximal flexion and difference between paretic (31°) and non paretic (41°) side
	Percent of the gait cycle when the maximal knee flexion occurs (standard 73°)	Maximal flexion occurs too late (63° - 66°)	Maximal flexion occurs too late for the non-paretic (77°) side and too fast for the paretic one (67°)

Table 2. Comparative analysis of time - spatial gait parameters for left-sided and right-sided stroke

	Left-sided stroke	**Right-sided stroke**
Gait velocity	Almost the same velocity and cadence was obtained both for people after left-sided and right-sided stroke.	
Cadence		
Stride length	Slight difference between paretic and non-paretic side.	Almost the same stride length for paretic and non-paretic side
Duration of a gait cycle	There are differences between paretic and non-paretic side	
Duration of a stance phase (standard 59%)	Stance phase a little bit longer than the standard one. Small differences between paretic (66%) and non-paretic (63%) side	Duration obtained for the paretic side equal to the standard value, for non-paretic side significantly longer (73%)

Table 3. Comparative analysis of qualitative gait parameters for left-sided and right-sided stroke

		Left-sided stroke	**Right-sided stroke**
Pelvis	*Tilt*	In both cases pelvis is too bended. Greater value occurs for patients after left-sided stroke.	
	Rotation	Course close to the standard one	Permanent rotation towards the paretic side
	Obliquity	Courses close to the standard one. During the swing phase pelvis bended toward the opposite side	
Hip	*Flexion - Extension*	In both cases (left and right-sided stroke) patients were not able to extend limbs properly.	
Knee	*Flexion - Extension*	Inappropriate angle courses. For the paretic side not enough flexion	Inappropriate angle courses. For both body sides not enough flexion (especially for the paretic side)
Ankle	*Plantarflexion - Dorsiflexion*	For both sides not enough plantar flexion. The worse course shape was obtained for the right-sided stroke.	

4. CONCLUSIONS

Applied methodology enables objective analysis based on kinematic quantities. On the basis of obtained results one can state, that gait of people after right-sided stroke is more disturb than for people after left-sided. The research will be continued in order to make the comparisons on the greater number of people.

5. ACKNOWLEDGMENT

6. REFERENCES

[1] L. Bensoussan, S. Mesure, J. Viton, A. Delarque, "Kinematic and kinetic asymmetries in hemiplegic patients' gait initiation patterns", Journal of Rehabilitation Medicine, 2006, vol. 38, pp. 287-294

[2] A. Ines, Kramers De Quervain, S. Sheldon, S. Leurgans, P. William, David Mcallister, M.D.I, Columbus, Ohio, "Gait Pattern in the Early Recovery Period after Stroke", The Journal of Bone and Joint Surgery, 1996, pp. 1506-1514

[3] J. Jurkojć, R. Michnik, A. Guzik-Kopyto, W. Rycerski and A. Szewczyk Nowak, "Analyses of kinematic quantities of people after stroke during different forms of locomotion" Conference Materials, ISB 2011

[4] C. Kim, J. Eng, „Magnitude and pattern of 3D kinematic and kinetic gait profiles in persons with stroke: relationship to walking speed", Gait and Posture, 2004, vol. 20, pp. 140-146

[5] R. Michnik, J. Jurkojć, A. Guzik, D. Tejszerska, "Analysis of loads of the lower limb during gait, carried out with the use of the mathematical model, made for patients during rehabilitation progress", Eccomas Conference "Multibody Dynamics 2007" Conference Information Booklet & Book of Abstracts, Milano 2007

[6] R. Michnik, J. Jurkojć, P. Jureczko, A. Guzik, D. Tejszerska: Analysis of gait kinematics of patients after total hip or knee replacement, Journal of Vibroengineering, Vilnius 2006, 8, No. 3, pp. 15-18

A cross-sectional biomechanical evaluation of diabetic lower limbs prior to ulceration

(Warning signs for diabetic foot ulceration)

O'Brien D. [1], Tyndyk M. [1]

[1] MEDIC, Dept. of Manufacturing, Biomedical and Facilities Engineering, Cork Institute of Technology, Cork, Ireland, davida.obrien@mycit.ie

Keywords - biomechanics; gait analysis; diabetic foot; diabetic ulcer prevention

1. INTRODUCTION

Over 5% of the Irish population has been diagnosed with diabetes; realistically this number is thought to be about 15% when undiagnosed and pre-diabetes cases are included [1]. Due to undiagnosed and poorly controlled diabetes, patients are needlessly developing foot complications, leading to prolonged hospital stays, increased immobility and more seriously amputation. Diabetic foot complications arise due to peripheral neuropathy, which deprives the patients of the early warning signs of pain and/or pressure.

The epidemiology of lower limb ulceration begins with the onset of peripheral neuropathy which is linked to muscle wastage, gait misalignment and limited joint mobility [2]. These symptoms along with increased body weight contribute to elevated plantar pressures, in turn leading to ulceration and finally the feared result of amputation. To put this in perspective 80% of diabetic amputations are preceded by a plantar ulcer [3].

Previous research has indicated that diabetic foot disease may be reduced by more than 50% with correct foot screening and awareness [1].

Therefore, the objective of this study is to perform an in depth assessment of the lower limb inclusive of (i) lifestyle questionnaire, (ii) biomechanical exam, (iii) 3D gait analysis, (iv) electromyography (EMG) and (v) plantar pressure. It is anticipated comparing the results of low-moderate risk diabetic feet to case matched controls, will highlight biomechanical discrepancies, which will allow for early intervention and a proactive approach to ulcer prevention.

2. RESEARCH DESIGN METHODS

Subjects

Twenty patients with diabetes and a matched control group of healthy counterparts are enrolled for this study. Exclusion criteria involved (i) Aged 18>60 - to avoid multiple co-morbidities, (ii) ability to give informed consent and (iii) no previous foot ulceration or amputation.

In line with the outlined research objective, it was decided to tackle the epidemic of diabetic foot disease prior to active lower limb ulceration, in order to isolate early biomechanical warning signs, which would indicate to susceptible areas within the diabetic foot. Diabetic patients were enrolled post a biomechanical podiatric exam [4]. Only subjects classified within the moderate to low risk category, in accordance with the diabetic foot risk stratification and triage adopted from the Scottish Intercollegiate Guidelines Network (SIGN) were eligible to take part. A low – moderate risk diabetic foot implies that the subject presented with no more than one risk factors i.e. loss of sensation, peripheral vascular disease without callus/ deformity.

Documentation

Ethical approval was attained from Cork Institute of Technology Research Ethics Committee. Prior to commencement of the assessments all subject were informed of the study procedures and the reasoning for this research, informed consent was signed by each participant.

A questionnaire was compiled using influences from previously validated questionnaires [5-7]. The combined questions provided patient feedback in relation to areas such as demographic, physical activity, tobacco and alcohol consumption, diabetic foot care and self opinionated health-related quality of life.

Instrumentation

A comprehensive clinical exam was initially preformed; this encompassed a visual exam of the footwear, socks and plantar surface of the foot. Advancing from this, a goniometer was utilised to record sub-talar joint alignment and range of motion. Pedal pulses were taken to monitor vascular limitations. The dorsalis pedis and tibialis posterior pulses of the foot were recorded as palpable or not. 10g Monofilament screened for lack of sensation in the foot. Ten sites were tested (nine plantar and one dorsal) on both the right and left feet. Results were recorded as present or absent.

Lower body gait analysis was carried out using a 3D motion analysis system (VICON Ltd, UK). Retro-reflective markers were attached to the lower body according to the Vicon Plug in Gait recommendations. A multisegmental biomechanical foot model, the Oxford foot model was used to calculate foot motion (dorsi/planar flexion, adduction/abduction, internal/external rotation). The lower limb muscle activity was recorded simultaneously using wireless EMG sensors (Aurion Ltd, Italy). The Ground Reaction Force (GRF) was measured using four force plates embedded in the gait laboratory ground surface. Patients were encouraged to walk the full length of the fifteen meter gait analysis laboratory. Participants are instructed to naturally build a strike of at least two of the four force plates into their self selected gait speed. Approximately ten trials are recorded with five for inclusion in analysis.

Static and dynamic plantar pressure distributions were thoroughly studied using HR pressure mat (Tekscan Ltd, USA). Five barefoot recordings were attained of the plantar surface of the feet to allow for error omission.

Results are analysed using the VICON software packages of Polygon and Bodybuilder. Also Origin data analysis package is utilised for a more comprehensive method of surveying results and comparing diabetic group and control. Statistical analysis is preformed using Statistical Package for the Social Science (SPSS).

3. RESULTS

The results obtained are to provide understanding of the early biomechanical effects of diabetes on the lower limbs. Though this research, areas prone to ulceration are highlighted, due to normally, visibly undetectable concerns such as incorrect foot alignment and increased plantar pressure.

Preliminary results indicate to common regions susceptible to diabetic foot complications, within this pilot group results are patient specific and of yet no clear correlation has emerged. It is evident, on comparison of assessment groups, that with the onset of diabetes the lower limbs begin to suffer. Analysis of the diabetic participants indicate to diminishing biomechanics of the lower limb such as (i) delayed firing for the Tibilais Anterior _ causing subject to adopt a modified gait pattern (ii) Increased Plantar Pressure_ peak pressure areas point towards the metatarsal heads and heel as shown in Fig.1 (iii) Reduced intersegmental motion_ interaction of the midfoot – hindfoot and hindfoot – tibia have shown to be stiffer then the control groups kinematic results.
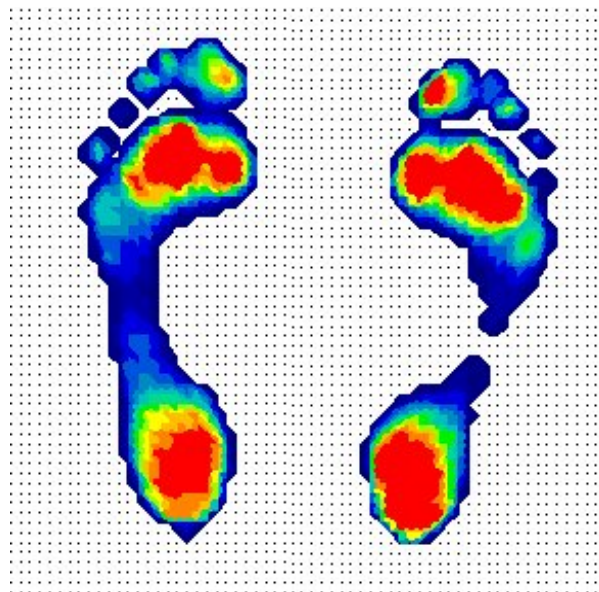

Figure 1. Plantar pressure distribution highlighting the peak pressure at the metatarsal heads and heel.

4. DISCUSSION

The feet are the most vulnerable part of the human body with regard to injury and infection and diabetes makes them more susceptible. To-date, the effect of diabetes on the ankle-foot joint biomechanics has not been well defined. This study offers detailed biomechanical analysis of the complicated diabetic foot. It is hoped that the results of this study can be used to guide future strategies for preventing pressure ulcers associated with diabetes and as such this project will have tremendous impact on the field of podiatric research and orthotic design/development.

5. REFERENCES

[1] http://www.diabetesireland.ie
[2] Payne, C., D. Turner, and K. Miller, *Determinants of plantar pressures in the diabetic foot.* Journal of Diabetes and its Complications, 2002. **16**(4): p. 277-283.
[3] Boulton, A.J.M., *The diabetic foot - An update.* Foot and Ankle Surgery, 2008. **14**(3): p. 120-124.
[4] Health Service Executive, *Diabetic foot screening tool*. North and South Lee Screening Tool. 2009.
[5] World Health Organisation, *The WHO STEPwise approach to chronic disease risk factor surveillance (STEPS)*. WHO STEPS Instrument, 2011. v2.1.
[6] American College of Physicians, *Diabetic foot care questionnaire*. ACP Clinical Skills Module, "Diabetic Foot Ulcers", 2007.
[7] Centers for Disease Control and Prevention, *Behavioral risk factor surveillance system questionnaire*. Module 2-Diabetes, 2009. p. 32-34.

An Inertial System for Clinical Motion Analysi and Rehabilitation

Skvortsov D.V. [1], Ishutin D.V.[2]

[1] Moscow Medical University, Moscow, Russia, dskvorts63@mail.ru
[2] Neurocor Company, Moscow, Russia, www.neurocor.ru

The Clinical Motion Analysis has become an important tool for some medical specialties. Kinematics data are very significant in rehabilitation process. At least they are necessary for biofeedback training and Functional Electrical Stimulation. In this paper we have tried to suggest some way of use of the main features of inertial system for all above medical purpose. This is wireless system. The system is including 3D accelerometers, 3D gyroscopes, 3D magnetometers, central processor unit, Bluetooth or WiFi module, EMG channel, stimulation channel, Li-ion rechargeable battery and a complicate software package. This combined inertial system to cover in one device the most active purpose of medical using. However, this combined system has bigger weight due to need more capacity of battery.

Keywords: clinical motion analysis, rehabilitation, biofeedback training, functional electrical stimulation.

INTRODUCTION

The Clinical Motion Analysis (CMA) has become an important tool for some medical specialties. One of the basic methods of CMA is kinematics investigation. Currently the most popular systems in this field matter are video based. However, recently, due to development of MEMS technology there are active discussions to deliver CMA by an inertial system [2]. The main locomotion used in CMA is gait. So, any CMA system should support collection of kinematic data during level walking. Presently one can find a number of papers where local kinematics from particular joints has been investigated as kinematics of whole body [3; 4].

Right now is known what would be technical parameters preferable for clinical gait analysis [5; 7; 10; 11]. We can briefly assume that quality collection of kinematics data should include: frequency data range from 50 to 100 Hz or higher, accuracy for joint Range of Motion (ROM) close to 1 degree, works using 3D technology, possibly wireless, and etc.

It is very important for a kinematic system to be connected to and synchronized with additional devices like force platform, EMG recorder, footswitches, and video recorder and so on. So, any inertial CMA system should be supplemented with these types of additional devices.

Besides CMA, kinematics data are very important in rehabilitation process. At least they are necessary for biofeedback training and Functional Electrical Stimulation (FES).

The biofeedback training (BT) should be managed by: position of affected extremity or any other part of human body, ROM of involved joint, sensitivity for particular motion and it's representation for patient. The last point is commonly implemented in 3D computer's games. Currently we can see that inertial sensors are used not only as manipulators in computer's games, but also for BT in various cases of pathology [1; 9].

For the FES, capture of kinematics data is basis for synchronization of electrical impulses with a specific motion. The synchronization makes it possible to deliver the electrical impulses to a muscle with high accuracy at the time when muscle should work within its own physiological cycle. Also the most applicable locomotion for the FES are walking and bicycling (this paper describes only non implantable FES systems). In recent years it is a limited investigation found where inertial sensors were used as synchronization tool for FES. Moreover, the main phases of gait can be detected accurately by accelerometers and gyroscopes [6]. It shapes a good perspective for inertial sensors to be used for FES.

Generally, we found that inertial sensors are applicable for CMA, BT and FES. However, in practice they differ by degree of development. The CMA area is the readiest for use. Some clinical findings exist for the BT and very few for FES.

In our work we have tried to work out a system which could be used in all three areas of application. It is some kind of a combined system for diagnostics and rehabilitation intended for a patient with motion disability.

MATERIAL AND METHODS

To work out the system we have created a few criteria. They are: the system should be wireless, with its own power supply, 6 DOF kinematics recording, built in EMG channel, and stimulation channel. For this reason the hardware includes 3D accelerometers, 3D gyroscopes, 3D magnetometers, central processor unit (CPU), Bluetooth or WiFi module, EMG channel, stimulation channel, Li-ion rechargeable battery, battery charge and EMG-stimulation jack and a plastic housing with flat keyboard. One flat surface of the housing is used to fasten these devices on the patient's body by elastic cuff or glued electrodes.

The sampling rate for gyroscopes, accelerometers and magnetometers was set by manufactures and is equal to Hz. It has better than 2 degree pitch and roll angle accuracy. We use LSM3030DH and L3G4200D chips, fundamental technical parameters have been set by the manufacturer.

The EMG channel is built on the ADS1294 chip. It has sampling rate of 1000 Hz for Bluetooth connection and 2000 Hz for WiFi. The input noise level is 1 mkV RMS. Programmable digital filter from 0.1 to 500 Hz. It uses standard variable geometry electrodes with snap connection.

The stimulation channel is current regulated with pulse amplitude range of 0-100 mA, resolution 1 mA and pulses rectangular with constant frequency 80 Hz. The start and duration of pulses is set by software corresponding to necessary tack. Synchronization with motion could be set from any single sensor (accelerometer or gyroscopes) by a number of different algorithms. The FES procedure is supported by two types of hardware: one – directly from the system computer software, second – by the device. So, for the second type the FES is possible to work independently with no wireless connection. For this reason the elected algorithm is loaded on the CPU. After that the wireless link may be disconnected. Due to that it is likely that FES may be made for a number of patients at the same time. Algorithm of synchronization and parameters of pulses are saved in the software and could be simply reloaded to the device or software stimulation package. It makes it easy to repeat the FES procedure for any patient. The standard self adhesive electrodes with different surface with snap connection are used for FES.

Due to that the stimulation channel needs more energy than any other device the battery accounts for the most part of the weight. It it makes possible to work 8 hours at stimulation regime (muscle stimulation by surface electrodes).

The Bluetooth module has the 100-1000 meters work distance. If we use WiFi module it has regular parameters.

The software package consists of four parts: database, diagnostic package, stimulation package and biofeedback package.

The database makes it possible to keep all information about the patient and its investigation or any another procedures.

The diagnostic software is very sophisticated and includes a number of masters: to create method of investigation, model of human body, algorithms to set a cycle, calculate parameters, create a report and save the entire configuration of such data under a unique name. It makes it possible to connect to some additional devices like force platform, footswitches and so on. This software has direct connection to video cameras (numbering from one to four) of different type from web cameras to more complicate construction. All cameras are synchronized with other devices of the system. The final report is generated for the Microsoft Word text processor and could be edited by its own tools.

The stimulation package has been developed to set parameters of the FES. The main part of it is master of viewing and analysis of data (direct or calculated) from single sensors or combines the same. It also includes some tools to set an algorithm of synchronization depending on a specific tack.

The BT software has a specific complicated tool to set parameters of management of computer's game or special virtual environment. The tool has a number of settings. They make it possible to adopt algorithm of management of the game from any part of human body, any clinical condition when motion is limited or abnormal. As in a computer game we use different types of simulator game managed by joystick or self build virtual environment.

Typical system named "Trust-M" includes: 7 devices with charge units, Bluetooth or WiFi antenna, a number of cuffs to install the devices on a body, EMG and stimulation electrodes with an inlet and cables, a computer (IBM compatible) and the whole software package. Often we use second multimedia monitor or virtual glasses for patient. In such case the virtual environment is shown on the second monitor and BT software tools are shown on the first screen. It makes it much easier to manage all BT process.

RESULTS

The general view of a single device is shown in figure 1. At the bottom side it has a Velcro strap glued to the surface of housing. Another variant is a fixation by double side scotch. In this reason the bottom surface of housing remains clear.

Figure 1. Stand-alone device with up and bottom sides shown.

The screenshot of diagnostic software package is shown in figure 2. If it is necessary to use a number of cameras generally recommend to connect the second monitor to the computer.

Figure 2. A screenshot of diagnostic software package.

The BT process is available in simple variant between computer game and a patient and by using different exercise devices (figure 3).

Figure 3. There are two ways how to do BT: a computer game and patient (left) and using exercise device.

The FES method generally is used in some cyclic motion like walking, bicycling and so on (figure 4).

Figure 4. The FES procedure works in walking on a treadmill and bicycling.

By this time the "Trust-M" system was approved at four different hospitals. One of those is a hospital for cereb[...] palsy children and all other ones are clinics for adults with neurological and orthopedic disability.

DISCUSSION

In this paper we have tried to suggest some way of use of the main features of inertial system for medical purpose. Possibly all three areas: diagnostic by CMA, BT and FES do not determinate active possibility of medical inertial system at current time and, of course, for the future. It is in spite of some well known problems with precision of calculated data. Hopefully, the biomechanics investigation should be coming to be common by using inertial system due to less cost and simpler and more convenient for practical aim. But this is not completely true for BT process. For BT inertial devices like "Trust-M" look too complicate and expensive compared to a gaming system on the market. However, it has additional feature – much better accuracy. It makes possible to use it for BT where it is necessary to get more motion ability for a patient. Except that the gaming systems have limited use for medical purposes. It is because they are developed for normal person and normal type of motion. On the other hand, combined system like "Trust-M" suggest important options like EMG channel and combined EMG and inertial (motion) channels to manage the BT process.

The FES area appears relatively new for medical inertial systems. In our opinion, it has a lot of future development by force side – multiple and accruable synchronization. Otherwise, it needs some investigation and working out of new mathematical algorithms to use it for better synchronization.

In this work we have tried to develop some combined inertial system to cover in one device the most active purpose of medical using. By this time we see one relatively negative result of such combined system: little higher weight. The FES method needs more power. So, separate system for CMA or BT could have three of four times less weight. It is price for universal device.

1. Allum JH, Carpenter MG. A speedy solution for balance and gait analysis: angular velocity measured at the centre of body mass. Curr Opin Neurol. 2005 Feb;18(1):15-21.
2. Cloete T., Scheffer C. Benchmarking of a full-body inertial motion capture system for clinical gait analysis. Conf Proc IEEE Eng Med Biol Soc. 2008;2008:4579-82.
3. Catalfamo P., Ghoussayni S., Ewins D. Gait event detection on level ground and incline walking using a rate gyroscope. Sensors (Basel). 2010;10(6):5683-702. Epub 2010 Jun 4.
4. Fong D.T., Chan Y.Y. The Use of Wearable Inertial Motion Sensors in Human Lower Limb Biomechanics Studies: A Systematic Review. Sensors (Basel). 2010;10(12):11556-11565. Epub 2010 Dec 16.
5. Inman V.T., Ralston H.J., Told F. Human Walking.— Baltimore: Williams & Wilkins, 1981.— 154 p.
6. Lau H, Tong K. The reliability of using accelerometer and gyroscope for gait event identification on persons with dropped foot. Gait Posture. 2008 Feb;27(2):248-57. Epub 2007 May 21.
7. Perry J. Gait analysis. Normal and pathological function.— SLACK Incorporated, 1992.— 524 p.
8. Saber-Sheikh K, Bryant EC, Glazzard C, Hamel A, Lee RY. Feasibility of using inertial sensors to assess human movement. Man Ther. 2010 Feb;15(1):122-5. Epub 2009 Jul 25.
9. Saposnik G., Mamdani M., Bayley M., Thorpe K.E., Hall J., Cohen L.G., Teasell R. - Effectiveness of Virtual Reality Exercises in Stroke Rehabilitation (EVREST): Rationale, Design, and Protocol of a Pilot Randomized Clinical Trial Assessing the Wii Gaming System. International Journal of Stroke Vol 5, February 2010, 47–51.
10. Whittle M.W. Gait analysis: an introduction.— Butterworth Heinemann, 1991.— 230 p.
11. Winter D.A. Biomechanics and motor control of Human movement.— N.-Y., Chichster, Toronto, Singapure: John Wiley & Sons, 1990.— 277 p.

Kinematic Comparisons Between Mobile-Bearing and Fixed-Bearing Designs in Cruciate-Retaining Total Knee Replacements During Functional Activities

Horng-Chaung Hsu[1], Cheng-Chung Lin[2], Tsung-Yuan Tsai[2], Mei-Ying Kuo[2,3] and Tung-Wu Lu[2*]

[1] Department of Orthopaedic Surgery, China Medical University Hospital, Taiwan, R.O.C.
[2] Institute of Biomedical Engineering, National Taiwan University, Taiwan, R.O.C.
[3] Department of Physical Therapy, China Medical University, Taiwan, R.O.C.
[*] twlu@ntu.edu.tw

Keywords-Total knee replacement, kinemtics, cruciate-retaining, sit-to-stand

1. INTRODUCTION

Total knee replacement (TKR) has been the main choice of treatment for advanced degenerative osteoarthritis (OA) of the knee over the last few decades. While the primary aim of TKR is restoring the normal function of the knee joint by reconstructing the articular surfaces, the ACL is often sacrificed. With a good long-term survival rate, improvement of functional recovery has received much attention [1, 2]. Therefore, in evaluating TKR designs, it is essential to assess the functional performance of patients during the activities of daily living. Moreover, two main problems in total knee arthroplasty, wear and loosening, are both related to the relative motion and contact kinematics between the femoral and tibial components while under dynamic loading. Altered knee kinematics after TKR may also change the lines of action and lever arms of the tendons of the surrounding muscles, affecting the dynamic function of the joint. Previous kinematic studies of TKR have focused on the comparisons of contact patterns, particularly roll-back phenomena, between cruciate-retaining (CR) and posterior stabilized (PS) type fixed bearing-TKR. From the findings, mobile-bearing deign was developed to improve transverse plane kinematics, namely internal/external rotation. However, few studies focused on investigating the effects of mobile-bearing on kinematics of TKR during functional activities. Recently, model-based 3D fluoroscopy methods were developed to accurately and non-invasively measure the 3D kinematics of the TKR[3]. Therefore, the purposes of the study were to compare the 3D rigid-body and contact kinematics between fixed-bearing and mobile-bearing designs in CR type TKR during non-weight-bearing (isolated active knee flexion/extension (F/E)) and weight-bearing (Sit-to-Stand (STS)) activities using a model-based 3D fluoroscopy method.

2. MATERIALS AND METHODS

Eleven subjects (age: 77.7±6.5 years; mass: 63.4±10.1 kg; height: 151.0±7.0 cm), who had received a posterior cruciate ligament-retaining mobile bearing TKR (MB-CR), and 7 subjects (age: 74.9±10.6 years; mass: 62.4±15.4 kg; height: 155.8±13.5 cm), who had received a posterior cruciate ligament-retaining fix-bearing TKR (FB-CR), volunteered to participate in this study. Each subject gave his/her written informed consent before the experiment, which was approved by the Institutional Human Research Ethics Committee. Computer-aided design (CAD) models of the TKR, including femoral and tibial components, were obtained from the manufacturer for subsequent registration with fluoroscopic images. Each subject was asked to sit with the hips abducted at about 30 degrees on an armless, height-adjustable chair and perform active knee flexion/extension and sit-to-stand at a self-selected speed while kinematic were measured using a fluoroscopy system (Advantx LCA, GE, France). The height of the chair was set at 115% of the knee-heel distance for each subject. The center of the image intensifier was adjusted to the height of the knee.

Prior to data collection, the fluoroscopy system was calibrated for image distortions and for the position of the point source X-ray using a purpose-built calibration object [4]. During the tests, the fluoroscopic images were obtained at 30 Hz using a PCI bus frame grabber (Foresight, USA). The 3D poses of the TKR components were obtained by registering their CAD models to the corresponding 2D fluoroscopy images using the WEMS method [5]. At each image frame, an optimization procedure was used to find the pose of the component whose projected image best matched the fluoroscopic image according to a similarity measure [5]. A projected image of a TKR component was generated by a perspective projection of the component onto the image plane to form an image resembling a radiograph. The registered component pose was described relative to the fluoroscopy coordinate system in terms of its rotation matrix and translation vector. The method was previously evaluated for its accuracy, giving means and standard deviations of errors of -0.08 ± 0.25 mm, 0.01 ± 1.65 mm, and $0.1 \pm 0.33°$ for in-plane translation, out-of-plane translation, and all rotations, respectively [6].

After the registration, the positions and orientations of the femoral and tibial components were obtained. Both the knee components embedded with an orthogonal coordinate system were used to calculate the joint angles for all frames following a z-x-y cardanic rotation sequence, corresponding to flexion/extension (Flex/Ext), adduction/abduction (Add/Abd) and internal/external rotation (IR/ER). The contact points were determined as the lowest point of the femoral component relative to the plane surface of the corresponding tibial components. The contact point displacement was defined as the excursion of the contact points relative to the initial contact points. For comparisons between the results obtained from MB-CR and FB-CR TKR, an independent t-test was used with a significance level of 0.05. SPSS version 10.0 (SPSS Inc., Chicago, USA) was used for all statistical analyses.

3. RESULTS

During non-weight-bearing knee flexion/extension, MB-CR had more internal rotation than FB-CR. Body weight-bearing (STS) reduced the differences in the ROM of IR/ER between FB-CR and MB-CR ($p>0.05$). No difference was found in flexion/extension and abduction/adduction components between FB-CR and MB-CR (Fig.1). Different contact patterns were found between MB-CR and FB-CR. Lateral contact points for FB-CR were more anterior than those in MB-CR during non-weight-bearing activity. Body weight-bearing helped reduce the differences in contact positions since the significant difference were not found between TKR designs (Fig. 2). From the displacements of the contact points, forward sliding was observed for both the MB-CR and FB-CR in the medial compartment. Less forward sliding was observed for MB-CR in lateral compartment during non-weight-bearing activity, but the phenomena were less pronounced during STS (Fig. 3).

4. DISCUSSION AND CONCLUSION

MB-CR TKR was found to produce greater axial rotational angles that were closer to those of the normal knee when compared to the FB-CR TKR. More anterior contact positions were found in the group of the FB-CR TKR in the transverse plane, particularly in the lateral compartment, when compared to MB-CR TKR. The existence of more anteriorly displaced contact positions (forward sliding) during flexion appeared to be responsible for the anteriorly directed lines-of-action and lever arm lengths of the patellar tendon in TKR. This may increase the anterior instability of the TKR and patellofemoral contact forces during extending activity at high flexion angles. Forward displacement of the tibiofemoral contact points during flexion was found more in the FB-CR TKR than in MB-CR TKR. This may attributed to the rotatable insert in the mobile-bearing design. When the knee flexion angles increased, the insert ideally rotated externally, thus decreasing the forward sliding of the lateral compartment of the femoral component in the MB-CR TKR. The anterior sliding of the medial compartment of the femoral component relative to the tibial component which was found in both MB-CR and FB-CR TKR were very different from those in the normal and ACLD knees. Body weight-bearing during closed chain activity (STS) reduced the kinematic differences between MB-CR and FB-CR, suggesting that, with more degrees of freedom as a result of ACL removal, external and muscular forces had greater influence on the TKR kinematics than the surface kinematic design of the prosthesis components. The results of the study may be helpful for the improvement of the design of total knee replacements and rehabilitation following TKR.
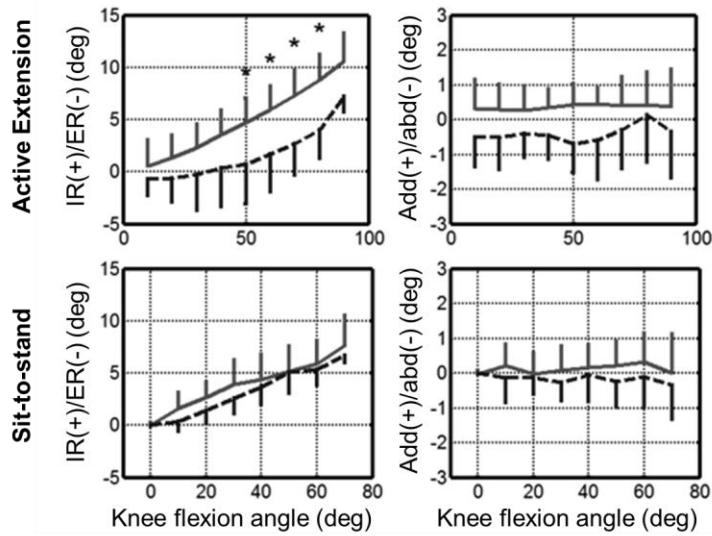
Figure 1. Means and standard deviations of adduction/abduction (Add/Abd) and internal/external rotation (IR/ER) angles of the knee with respect to the knee flexion angles for the MB-CR (gray solid lines) and FB-CR (black dash lines) TKR. Stars mark the significant differences of values obtained from the two measurements; the significance level was set to α = 0.05.
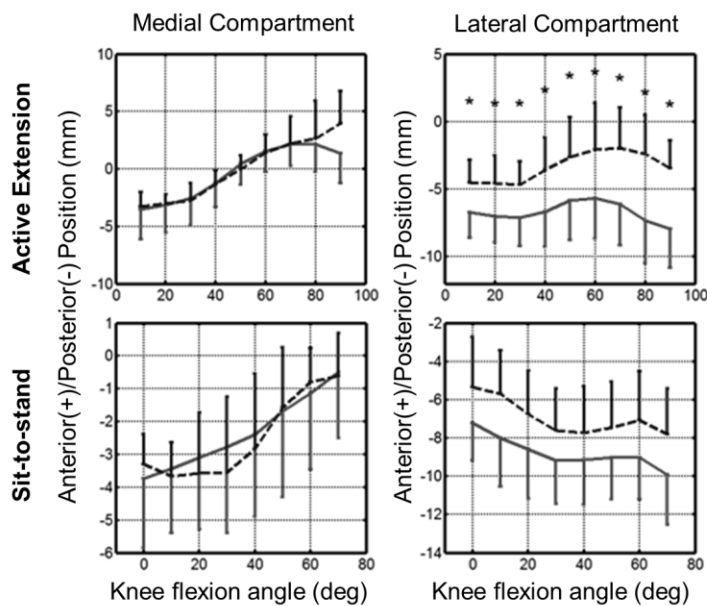

Figure 2. Means and standard deviations of the positions of the conact points in anterior/posterior direction with respect to the knee flexion angles for the MB-CR (gray solid lines) and FB-CR (black dash lines) TKR. Stars mark the significant differences of values obtained from the two measurements; the significance level was set to α = 0.05.
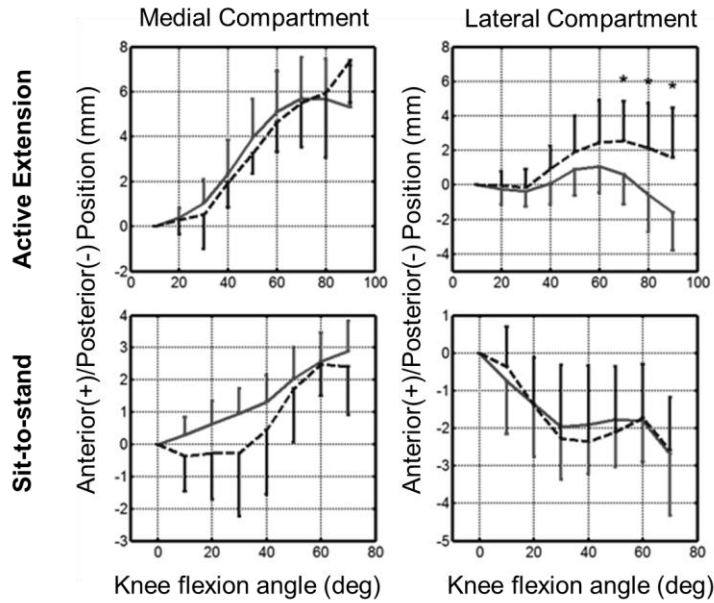
Figure 3. Means and standard deviations of the displacements of the conact points in anterior/posterior direction with respect to the knee flexion angles for the MB-CR (gray solid lines) and FB-CR (black dash lines) TKR. Stars mark the significant differences of values obtained from the two measurements; the significance level was set to α = 0.05.

5. REFERENCES

[1] Andriacchi, T.P., T.S. Stanwyck, and J.O. Galante, Knee biomechanics and total knee replacement. Journal of Arthroplasty, 1986. 1(3): p. 211-219.

[2] Dennis, D.A., et al., Multicenter Determination of in Vivo Kinematics after Total Knee Arthroplasty. Clinical orthopaedics and related research, 2003(416): p. 37-57.

[3] Banks, S.A. and W.A. Hodge, Accurate measurement of three-dimensional knee replacement kinematics using single-plane fluoroscopy. IEEE Transactions on Biomedical Engineering, 1996. 43(6): p. 638-49.

[4] Lu, T.W., et al., In vivo three-dimensional kinematics of the normal knee during active extension under unloaded and loaded conditions using single-plane fluoroscopy. Medical Engineering and Physics, 2008. 30(8): p. 1004-1012.

[5] Tsai, T.Y., et al., A volumetric model-based 2D to 3D registration method for measuring kinematics of natural knees with single-plane fluoroscopy. Medical Physics, 2010. 37(3): p. 1273-1284.

[6] Tsai, T.Y., Development of a 3D Fluoroscopy Method and its Integration with Stereophotogrammetry to Study the Effects of Soft Tissue Artifacts on the Calculated Mechanical Variables of the Knee During Functional Activities, in Institute of Biomedical Engineering2010, National Taiwan University: Taipei.

Estimating optimal shoulder immobilization postures following simulated surgical rotator cuff tear repairs

Jackson M. [1], Sylvestre É. [1], Bleau J. [2], Allard P. [1], Begon M. [1]

[1] Département de Kinésiologie, Université de Montréal, Montréal, Canada
[2] Laboratoire Orthopedique Medicus, Montréal, Canada

Musculoskeletal model, rotator cuff, passive tension, minimax algorithm, shoulder

1. Introduction

Rotator cuff tears are ranked amongst the most common musculoskeletal injuries, afflicting approximately 20% of the population [1]. Surgery is often performed, followed by a period of shoulder immobilization by means of an orthosis. The purpose of the immobilization is to protect the integrity of the repair during the immediate post-operative period.

There is, however, no consensus about the best postures for post-operative shoulder immobilization. Minimizing passive tension in the repaired tendon(s) during the immediate post-operative period could protect the repair and improve the potential for healing. The postural dependence of tension in the supraspinatus following repair has been investigated [2, 3], with arm abduction found to lead to a decrease in passive tension. These studies were limited to isolated supraspinatus injuries; however, supraspinatus tears also occur concomitantly with infraspinatus and/or subscapularis injuries [4]. The dependence of passive tension on shoulder posture is unclear in these complex conditions due to the differing actions of the muscles. The purpose of this study was to develop a method to estimate optimal post-operative shoulder immobilization postures for simulated rotator cuff tears involving more than one muscle, and subsequently apply the method to tears of supraspinatus and infraspinatus.

2. Method

A musculoskeletal model of the shoulder complex (AnyBody Technology A/S, Denmark) was simplified for this study to incorporate just the scapula, humerus and rotator cuff muscles. Six muscle paths were used to represent each of the four rotator cuff muscles, namely supraspinatus (SS), infraspinatus (IF), subscapularis (SB) and teres minor (TM). Each muscle path was represented by a Hill-type muscle-tendon actuator, based on musculoskeletal parameters given in [5].

Tears of varying severity were simulated by reducing the tendon lengths of the repaired tendons by 0 to 20 mm, in 5 mm increments. The reduction in tendon length or gap length represented retraction of the musculotendinous unit as a result of the tear and also tendon removal during surgery. It was assumed that the orthosis compensates for the effect of gravity, and therefore that there was no activation of the rotator cuff during immobilization. As such the tension was assumed to be solely passive tension, due to lengthening of the musculotendinous unit. As the cross-sectional areas of the rotator cuff tendons differ, the passive tension was converted to passive stress to allow comparison between tendons.

An optimal posture, given by three glenohumeral joint angles, namely plane of elevation (θ_{PE}), elevation (θ_E) and rotation (θ_R), was defined as one in which 1) stresses in the repaired tendons are minimized to protect the repair; 2) elevation of the humerus is minimized to ensure the resulting posture is practical; 3) stresses in the uninjured tendons are maintained below an upper limit to ensure integrity of these tendons; and 4) the posture of the humerus is within anatomical limits. The fminimax function (MATLAB, The Mathworks Inc., USA) was used to find the postures that minimized the maximum of the stresses in the repaired tendons and a normalized angle of humerus elevation, subject to constraints on the stress in the uninjured tendons and the glenohumeral joint angles. To allow for better visualization of the results complete upper limb configuration was determined, assuming elbow flexion of 90° and the scapulohumeral rhythm of [6].

3. Results

For tears involving supraspinatus and infraspinatus the optimal post-operative shoulder immobilization postures were with the humerus elevated and externally rotated (Table 1 as illustrated by Fig. 1). Elevation angle increased with gap length from 21° to 45°, while external rotation decreased slightly from 23° to 18°. For short gap lengths of 0-10 mm the plane of elevation was close to the scapular plane (4° - 7° posterior to scapular plane), while for longer gap lengths of 15-20 mm the plane of elevation was substantially posterior to the scapular plane (27° - 30° posterior to scapular plane).
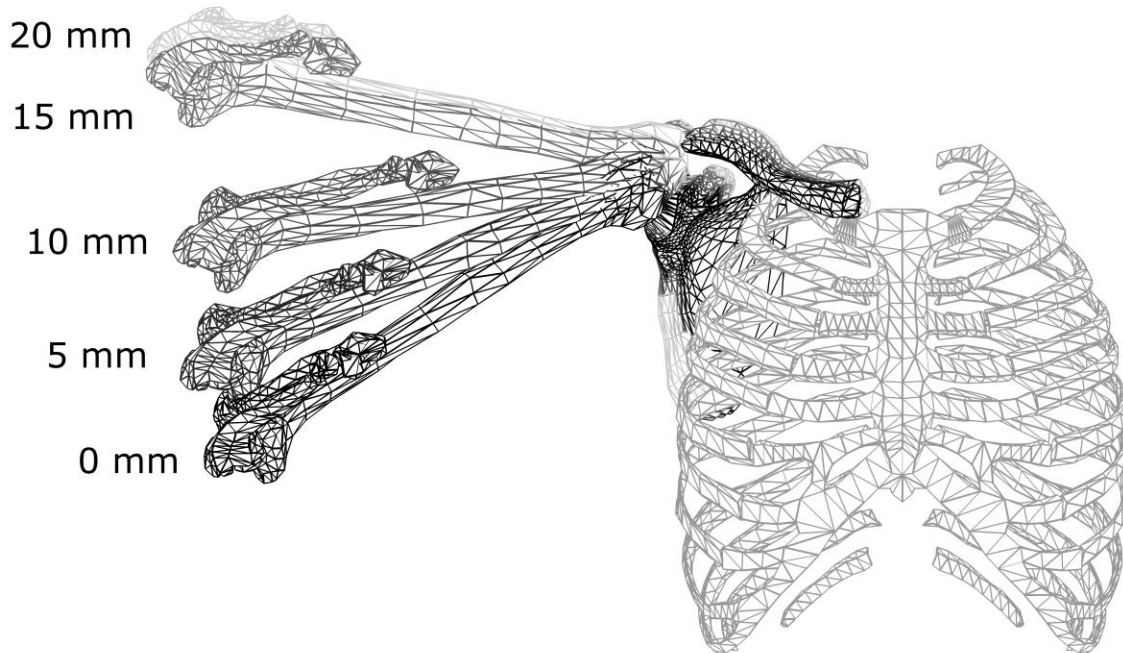

Figure 1. Optimal post-operative immobilization postures for supraspinatus/infraspinatus tears of varying gap length.

Table 1. Optimal post-operative immobilization postures and resulting tendon stress and tension for supraspinatus/infraspinatus tears of varying severity.

Gap length (mm)	Glenohumeral angles (°)			$N\theta_E$ ($°/cm^2$)	Stress (N/cm^2)		Passive Tension (N)	
	θ_{PE}	θ_E	θ_R		IF	SS	IF	SS
0	-7	21	-23	34	7	33	3	16
5	-5	28	-21	45	28	45	14	22
10	-4	37	-18	59	59	59	29	29
15	-27	44	-18	71	98	98	49	49
20	-30	45	-18	72	168	168	83	83

Nomenclature: $N\theta_E$ normalized elevation angle, θ_{PE} plane of elevation, θ_E elevation, θ_R rotation, IF infraspinatus, SS supraspinatus.

4. Discussion

A constrained minimax algorithm was utilized with a musculoskeletal model to estimate optimal shoulder immobilization postures following simulated surgical repair of rotator cuff tears. Within this study the optimal posture was defined as one in which the stresses in the repaired tendons, and the angle of humerus elevation were minimized. Limiting the stresses in the repaired tendons reflects the need to protect the repair, while minimizing the angle of arm elevation ensures the obtained posture is practical for the autonomy of the patient. Use of a minimax algorithm effectively balanced these competing criteria. This advantageous balancing property of minimax algorithms was also identified by [7] when using the algorithm to estimate muscle recruitment.

For supraspinatus/infraspinatus tears the optimal post-operative shoulder immobilization postures were with the humerus elevated and externally rotated. These finding are in line with those of [2] who found passive force in the supraspinatus to decrease with humerus elevation and external rotation. The inclusion of an infraspinatus injury is thought to account for the plane of elevation becoming more posterior to the scapular plane for large gap lengths.

The method led to solutions that did not overstress the repaired tendons. For all gap lengths the tensile forces in the injured tendons were below 83 N, a value that is below reported pull-out forces for suture repairs [8]. Thus integrity of the repair is expected to be preserved in all of the obtained postures.

The solutions obtained also represented feasible immobilization postures. The maximum glenohumeral elevation angle obtained of 45° represents a thoracohumeral elevation angle (elevation of humerus relative to thorax) of 106°, assuming the scapulohumeral rhythm given by [6]. This thoracohumeral elevation angle is similar to that of typical orthoses, for example the Omo Immobil orthosis produced by Ottobock.

In conclusion, the optimization method described in this paper was successfully applied to tears involving supraspinatus and infraspinatus. The method could be used to guide prescription of shoulder immobilization postures for various injuries and therefore represents a step forward in the rehabilitation of rotator cuff injuries.

5. Acknowledgment

6. References

[1] Yamamoto, A., Takagishi, K., Osawa, T., Yanagawa, T., Nakajima, D., Shitara, H., and Kobayashi, T. (2010). Prevalence and risk factors of a rotator cuff tear in the general population. Journal of Shoulder and Elbow Surgery, 19(1):116-120.

[2] Saul, K. R., Hayon, S., Smith, T. L., Tuohy, C. J., and Mannava, S. (2011). Postural dependence of passive tension in the supraspinatus following rotator cuff repair: A simulation analysis. Clinical Biomechanics, 26(8):804-810.

[3] Hatakeyama, Y., Itoi, E., Pradhan, R. L., Urayama, M., and Sato, K. (2001). Effect of arm elevation and rotation on the strain in the repaired rotator cuff tendon. The American Journal of Sports Medicine, 29(6):788-794.

[4] Namdari, S. and Green, A. (2010). Range of motion limitation after rotator cuff repair. Journal of Shoulder and Elbow Surgery, 19(2):290 – 296.

[5] Langenderfer, J., Jerabek, S. A., Thangamani, V. B., Kuhn, J. E., and Hughes, R. E. (2004). Musculoskeletal parameters of muscles crossing the shoulder and elbow and the effect of sarcomere length sample size on estimation of optimal muscle length. Clinical Biomechanics, 19(7):664 – 670.

[6] de Groot, J. H., and Brand, R. (2001). A three-dimensional regression model of the shoulder rhythm. Clinical Biomechanics, 16(9):735-743.

[7] Rasmussen, J., Damsgaard, M., and Voigt, M. (2001). Muscle recruitment by the min/max criterion – a comparative numerical. Journal of Biomechanics, 34(3):409-415.

[8] Ma, C. B., Comerford, L., Wilson, J., and Puttlitz, C. M. (2006). Biomechanical evaluation of arthroscopic rotator cuff repairs: double-row compared with single-row fixation. The Journal of Bone and Joint Surgery, 88(2):403–410.

Gender Differences in Relative Motions of Tibiofemoral Joint Articular Surfaces and Comparison between Subject Specific and Generic Knee Models

Zou D. [1,2], Deusinger RH. [1], Koleini M. [1], Smith K. [2], Hensley G. [1], Machan TE. [1], Schmitt A. [1], Azevedo S. [1]

[1] Program in Physical Therapy, Washington University School of Medicine, St. Louis, USA, zoud@wustl.edu

[2] Mallinckrodt Institute of Radiology, Washington University School of Medicine, St. Louis, USA

Keywords-knee model; tibiofemoral joint; articular surfaces; kinematics

1. INTRODUCTION

Excessive anterior cruciate ligament (ACL) force and distorted joint surface motion (kinematics) are components of tibiofemoral joint mechanics hypothesized as links to ACL injury and osteoarthritis (OA) [1]. Several studies have investigated ACL injury mechanisms and gender differences by examining in vivo kinematics of anterior tibial translation and tibiofemoral joint surface rolling and sliding using a 2D geometric computational tibiofemoral joint model during weight bearing and non-weight bearing activities in healthy and ACL injured knees [2]. The geometry of the tibiofemoral joint is complex and asymmetric within individuals and may also differ between genders [3]. In the current study, relative motions of the tibiofemoral joint articular surfaces were analyzed by quantifying rolling and sliding of the femur condyles relative to the tibia condyles using both a generic model (GM) and a subject specific model (SSM). The characteristic rolling and sliding of the femoral condyles relative to tibial condyles were compared between the GM and SSM and between male and female subjects.

2. METHODS

Eighteen healthy adults, 9 men and 9 women, participated in this study (age 27.5±6.5; height 171±9 cm; body mass 78.7±19.3 kg). Before testing, all subjects signed informed-consent forms approved by the Washington University Human Studies Committee. A computed tomography (CT) scan of the right knee of each subject was obtained and analyzed according to an IRB approved research protocol. Conversion of tibiofemoral joint CT image data to triangulated surface models was performed using Materialize Mimics software version 13.1 (Materialize Inc., Belgium). The data were filtered using a median filter with a radius of 1 to reduce nonstructured image noise and the femur and tibia were segmented (isolated from surrounding soft tissues) using morphological and connected components segmentation. The segmented masks were converted to triangulated surface models and then were loaded into Geomagic Studio software version 12 (Geomagic, Inc., USA) for landmark identification. Subjects' femur geometric dimensions were determined from 6 skeletal landmark locations identified on CT scans of the lateral femoral condyle (LC) and medial femoral condyle (MC) using methodology developed in earlier research [3]. The skeletal landmarks were used to define 2 planes that bisect the LC and MC, respectively (Fig. 1a). The defined surfaces of both the lateral and medial condyles were used to derive the necessary measurements to individualize the curvature geometry for each subject. For the SSM, femoral curvature geometry was represented by continuous curves for the LC and MC, respectively, as measured from CT derived volumetric images of the femur. Proportions (percent) of rolling and sliding were used to describe the relative motion of the articular surfaces of the tibiofemoral joint in this study. Analysis was performed in the sagittal plane by projecting the 3D continuous curves of LC and MC onto the sagittal planes. A 2D knee model [2], using a 2-cm radius and 4-cm radius circular arcs connected with an elliptical curve, served as the GM (Fig. 1b) for comparison to the SSM which consisted of a LC and a MC.

Kinematic data for sit to stand was collected using a Vicon motion capture system (Vicon Motion Systems, Oxford, UK). Subjects were recorded during sit to stand from a chair without using their arms. Each trial was analyzed for knee joint excursion from sitting through full standing by using both the SSM and the GM. The arc length (S_f) between two successive contact points on the femoral condyle convex surface is given by:

$$S_f = \int_{\theta}^{\theta+\Delta\theta} R \cdot d\theta \, ,$$

where R is the radius of curvature and θ is the knee flexion angle. The amount of relative displacement (S_t) between the femoral condyle and the proximal tibial, which is calculated as the arc length between two successive contact points on the tibial surface, is given by:

$$S_t = \int_{\theta}^{\theta+\Delta\theta} (R - r_{icr}) \cdot d\theta \, ,$$

where r_{icr} is the distance from the instantaneous center of rotation location to the femoral contact point. The percentage of rolling was determined by the formula:

$$\%rolling = \frac{S_f}{S_f + (S_f - S_t)} \cdot 100\% \cdot$$

The SSM calculates percent of rolling and sliding of the articular surfaces for both LC and MC based on measured curvature geometry for individual subjects. The 2-cm radius and 4-cm radius circular arcs connected with an elliptical curve (Fig. 1b) were used for all subjects in the GM in calculating percent of rolling and sliding of the articular surfaces.
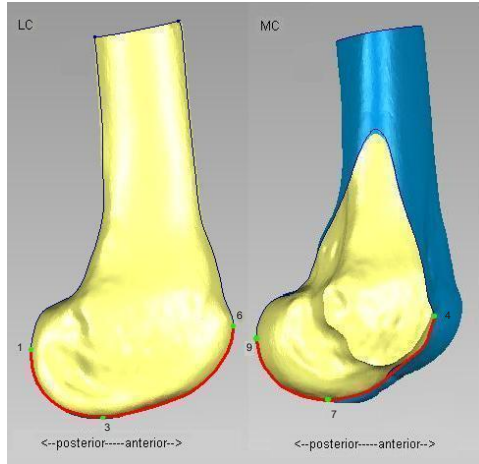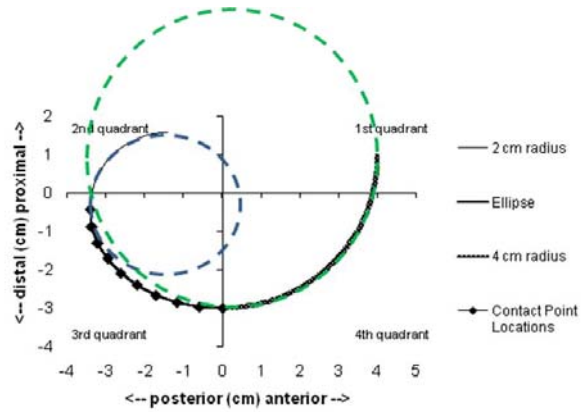
a. Subject specific knee model   b. Generic knee model

Figure 1. Femoral curvature geometry of knee models

3.   RESULTS AND DISCUSSION

All trials were processed individually and data were normalized as percent of activity. ANOVA was used for the analysis of differences of peak percent rolling, timing of peak percent rolling, and mean percent rolling from start to end of trial between genders and models. For both models, percent rolling reached peak values earlier for females than males (Tab. 1 and Fig. 2). The mean percent rolling for males are significantly higher ($p < 0.05$) than females for both the SSM (LC and MC) and GM (Tab. 2). As expected, both models demonstrated wide variations among subjects of both genders, especially in the first half of the sit to stand movement. The GM and SSM differed significantly for both peak and mean % rolling. Males and females had significantly different results for time of % rolling peak, % rolling peak and mean % rolling. No significant interaction effect was found (Tab. 3). We believe further study with a larger sample size is merited to increase the power of the statistical analysis. The small sample size in this study may have limited the strength of the statistical results.

Table 1. Mean values of peak of %Rolling and timing (% of trial) during sit to stand of SSM and GM

Gender	GM		LC SSM		MC SSM	
	% of trial	%Roll	% of Trial	%Roll	% of Trial	%Roll
Male	46.68 ± 10.45	83.63 ± 12.18	45.44 ± 10.52	67.01 ± 10.91	52.54 ± 9.81	80.54 ± 11.09
Female	37.02 ± 10.17	77.66 ± 16.67	39.79 ± 9.90	54.10 ± 17.69	40.69 ± 8.59	68.03 ± 17.33

Table 2. Mean %Rolling of sit to stand for male and female subjects from start to end of trial

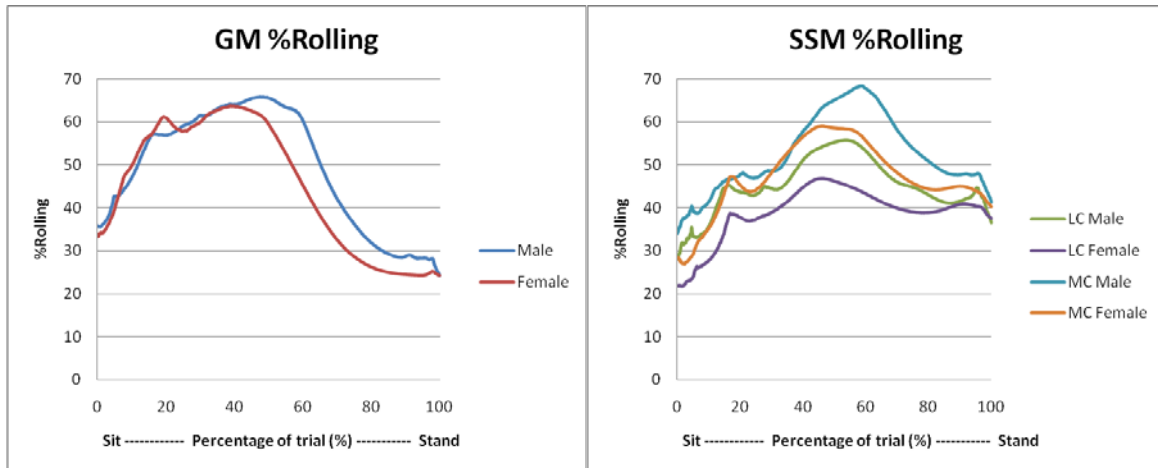| Gender	GM	SSM	
		LC	MC
Male	48.19 ± 2.82	46.54 ± 3.62	55.18 ± 3.55
Female	43.68 ± 5.78	39.37 ± 7.26	49.28 ± 6.71

Figure 2. Comparison of percent rolling during sit to stand for the GM and for the SSM LC and MC of female and male subjects

Table 3. P-values for ANOVA Comparing GM and SSM and Gender

Source	% of Trial at Peak	Peak %Roll	Mean %Roll
Model	0.308	0.000*	0.000*
Gender	0.001*	0.006*	0.000*
Model*Gender	0.638	0.687	0.702

* Significant values

4. CONCLUSIONS

The subject specific knee model was able to quantify rolling and sliding of both the LC and MC relative to the tibia. Further study is needed to investigate and explain the factors that contribute to the gender differences in knee kinematics and its relations to ACL injury and OA

5. ACKNOWLEDGMENT

6. REFERENCES

[1] D.R. Wilson, E.J. McWalter, and J.D. Johnston, "The measurement of joint mechanics and their role in osteoarthritis genesis," Rheum. Dis. Clin. N. Am., 34, pp. 605-622, 2008.

[2] J.H. Hollman, et al, "Tibiofemoral joint-surface motions in weight-bearing and non-weight-bearing movement," J. Sport Rehabil.vol. 12, pp. 143-161, 2003.

[3] D. Zou, R.H. Deusinger, K.E. Smith, M. Koleini, "Reliability and gender differences of internal skeletal dimensions using volumetric quantitative computed tomography," Proceedings of IEEE/ICME CME 2011, pp. 148-153, May 2011.

A musculoskeletal model for the shoulder complex

(Dynamic simulation of different Scapulo-Humeral Rhythms)

Frigo C. [1], Pavan EE. [1]

[1] Dept. of Bioengineering, Politecnico di Milano, Milan, Italy

A musculoskeletal model is presented that allows to estimate motion of different shoulder components based on joint constrains and actuators. The effect of shoulder muscle weakness was simulated dynamically by an hypothesis of reduced shoulder abduction moment. It has been shown that clavicle movement can partially compensate and help recovering the scapulohumeral rhythm. This confirms the need of a sophisticate neuromotor control of the shoulder complex.

Keywords-musculoskeletal models; dynamic simulation; shoulder; scapolohumeral rhythm

1. Introduction

Scapulohumeral rhythm (SHR) is defined as an automatic relationship between the glenohumeral (GH) motion and the scapular (Sc) abduction. The study of this relationship can provide insight into to neuromuscular control of movement [1,2].
Usually it is considered that humeral motion predominates at lower levels of arm elevation and scapular motion predominates at higher levels. A reasonable explanation is the need to enhance the range of motion of the arm with respect to the limits imposed by the GH joint. However the intimate mechanism of this phenomenon is not yet well understood. To analyze the relationship between arm elevation, Sc abduction and Clavicle (Cl) movements, an anthropomorphic musculoskeletal model has been implemented which allows us to dynamically simulate different situations.

2. Method

Model development

Our biomechanical musculoskeletal model was developed on the basis of consolidated knowledge about shoulder functional anatomy [3]. Five functional joints are usually identified, namely: the glenohumeral, the scapulothoracic, the acromioclavicular, the sternoclavicular, the sub-deltoideus joint. Actually, the scapulothoracic and the sub-deltoideus joints are not really joints in a anatomical sense, but rather anatomical structures, muscles and ligaments, aimed at constraining the relative movement of scapula in relation to trunk and humerus in relation to shoulder girdle respectively. To simulate the scapulothoracic constrain, the back surface of the rib cage was modeled as a portion of a torus, vertically oriented, that was obtained by a two bar linkage: one bar was attached to the thorax, in a forward position, and was allowed to rotate around a horizontal axis; the second bar was attached at the free extremity of the first one and was allowed to rotate horizontally. The free extremity of this second bar thus describe a torus surface, having the major radius as the sum of the length of the two bars, and as a minor radius the length of the second bar. The scapula was attached to the extremity of the second bar and was allowed to rotate around an axis that was perpendicular to its own laying plane. A further hinge was applied to allow the Sc to bend in relation to the tangent plane of the torus. In this way the acromion can be

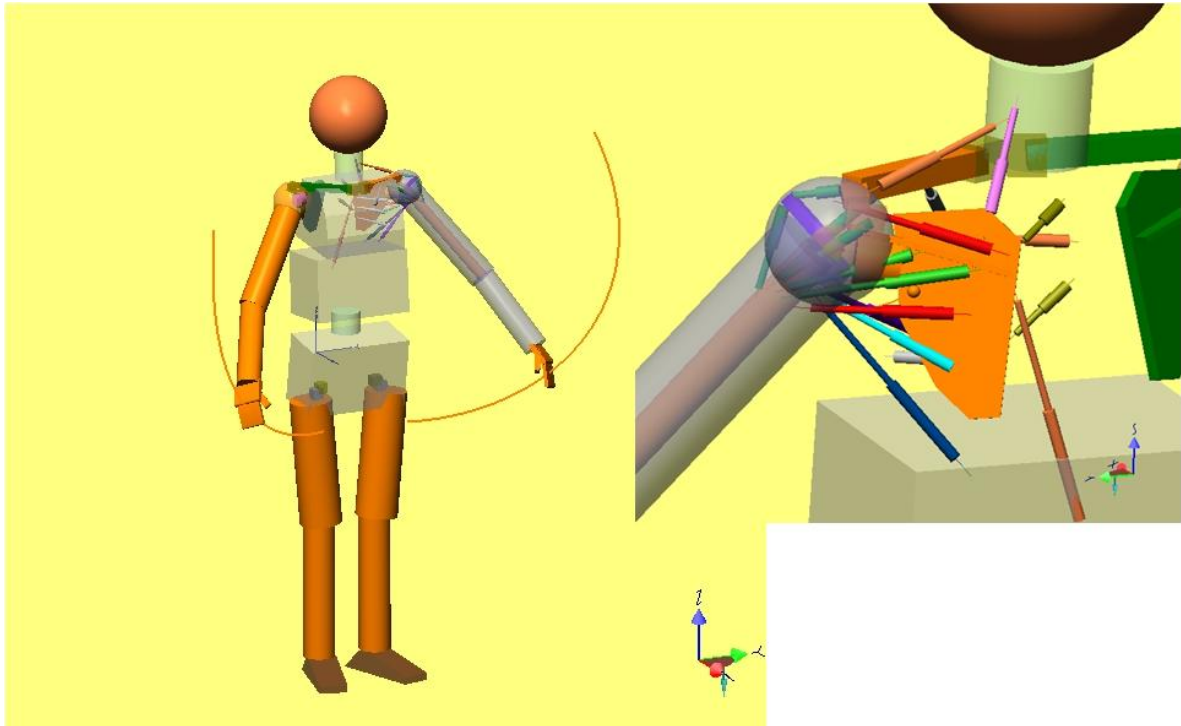attached to the clavicle (acromio-clavicular AC joint) while preserving the Sc constrains (Fig.1).

Figure 1. The biomechanical model. Left: whole body. Right: details of the left shoulder.

The sub-deltoideus joint was not specifically modeled, as the resulting constraint was implicit in the definition of the glenohumeral joint. This joint, that can be functionally approximated to a spherical joint, was created by linking three mutually orthogonal hinges: one representing the elevation plane orientation, around the vertical axis, the second representing the elevation movement angle (horizontal axis), and the third representing the internal/external rotation of the humerus along its longitudinal axis. The Cl was connected to the sternum through two single axis hinges: one oriented vertically, to allow protraction/retraction, and the second oriented horizontally, to allow elevation/depression. The AC joint was modeled as a simple 3 degrees of freedom spherical joint. The rest of the upper limb was composed by the elbow, forearm, wrist and hand. It is not described here because it is out of the objectives of the present study.

Muscles of the shoulder girdle that have a relevant role for the upper limb function are numerous and difficult to schematize. In our model the widest ones have been splitted into the more representative components and represented as a linear element joining the origin and insertion points (see Fig.1). For example the trapezius was splitted into upper, middle and lower portion; serratus was splitted into upper, middle, and lower portion; deltoid into clavicle, acromion, and spinal portion. A via-point was implemented to keep the line of action of the acromion component of the deltoid muscle on the lateral side of the glenohumeral joint. Other muscles were just considered as single elements: superspinatus, infraspinatus, infrascapular, teres minor. Each of these linear elements could be looked at as a meter, able to provide the distance between origin and insertion points, the muscle length.

Animation of the model

All the joints represented in the model can be activated by a motor that controls either the joint angle or the joint torque. To simulate a free hinge the motor torque is set to zero; to simulate a rigid joint the angular velocity is set to zero. In all other situations the control law can vary.

The movement analyzed in the present study was just the arm elevation where the GH joint moved at an angular velocity of 90°/s. The Sc abduction was instead realized by applying an abduction moment to the scapula. The Cl was moved at different elevation angle velocities to see the effect of the clavicle movement on the SHR [4].
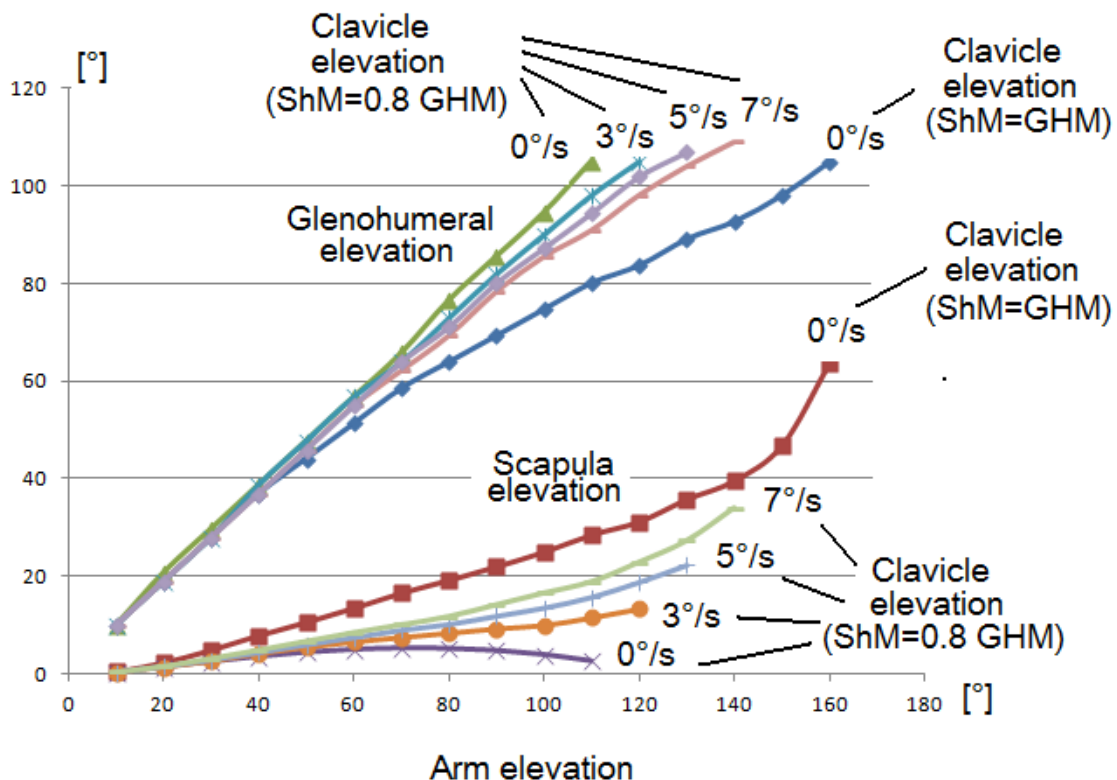

Figure 2. Upper curves: elevation of the glenohumeral joint as a function of the arm elevation. Lower curves: elevation of the scapula (scapula abduction angle) as a function of the arm elevation. Different curves correspond to clavicle still (0°/s) and clavicle elevation at 3, 5, 7 °/s. The rotation moment applied to the shoulder was respectively equal to the glenohumeral moment (ShM=GHM) and 0.8 of the glenohumeral moment (ShM=0.8 GHM).

3. Results

Figure 2 shows the main results of our dynamic simulation. When the abduction moment was equal to the GH moment (ShM=GHM) a realistic SHR was obtained even if the Cl was still. The arm elevation achieved 160°. When the abduction moment was reduced to 80% of the GH moment (ShM= 0.8 GHM) the SHR was disrupted, and the GH joint achieved it limit (approximately 105°) with an arm elevation of less than 120°. We then applied progressively higher elevation velocities to the clavicle, and observed a recovery of the SHR, which in turn allowed to achieve 130°, 137°, 145° of arm elevation, with respectively 3°/s, 5°/s, 7°/s of Cl elevation velocity.

4. Discussion

In accordance with previous studies, our work has shown that a tight relationship exists between motion of GH joint, Sc, and Cl. The SHR can be easily disrupted if the Sc stabilizer muscles are not able to apply the required abduction moment. The Cl movement can, to some extent, help overcoming the muscle deficit. This requires that at list the Cl elevator muscles are relatively efficient. However the coordination of all these three active components is fundamental for proper functioning. Musculoskeletal modeling seems to be an adequate tool to go deep in these complicated mechanisms, allowing to better understand not only the biomechanical aspects of shoulder function but also the neurological implications.

5. References

[1] Kon , Y, Nishinaka N, Gamada K, Tsutsui H, Banks SA, The influence of handheld weight on the scapulohumeral rhythm, J Shoulder Elbow Surg 2008;17:943-946.C.T.M., 2007.

[2] Murray IA, Johnson GR, A study of the external forces and moments at the shoulder and

 elbow while performing everyday tasks, Clinical Biomechanics, 19 (2004): 586–594

[3] Kapandji JA, Fisiologia Articolare (Tronco e Rachide), Monduzzi (Ed)

[4] Wu G, van der Helm FCT, Veeger HEJ, Makhsous M, Van Roy P, Anglin C, Nagels J, Karduna AR, McQuade K, Wang X, Werner FW, Buchholz B, ISB recommendation on the definitions of joint coordinate systems of various joints for the reporting of human joint motion- Part II: shoulder, elbow, wrist and hand, J Biomech, 38 (2005): 981- 992

Can physical activity level affect external mechanical work or energy cost of treadmill walking of healthy adults?

Annoni I. [1,2], Galvani C. [2], Mapelli A. [1], Sidequersky FV. [1], Ripamonti G. [3], Sforza C. [1]

[1] Dipartimento di Morfologia Umana e Scienze Biomediche "Città Studi", Università degli Studi di Milano, Milano, Italy

[2] Laboratorio di Fisiologia Sperimentale, Università Cattolica del Sacro Cuore, Milano, Italy

[3] Corso di Laurea in Scienze Motorie, Università Cattolica del Sacro Cuore, Milano, Italy

Keywords; Energy cost; external mechanical work; physical activity level; treadmill walking

1. INTRODUCTION

Many subjective factors can affect energy cost (V'O$_2$max, [7]; maximal strength and flexibility, [3]) and mechanical work (stride frequency, [6]) of walking. To our knowledge, no studies have been conducted to investigate if the level of daily physical activity (PAL) can affect external mechanical work (W$_{EXT}$) and net energy cost (NetEC) of treadmill walking. The aim of the study was to analyse the relation between NetEC and W$_{EXT}$ with PAL.

2. MATERIALS AND METHODS

20 healthy adults were recruited in the study and were classified as inactive (INACT) and active (ACT) according to the amount of daily moderate and vigorous physical activity (MVPA). Main characteristics are summarized in Table 1.

Table 1. Descriptive statistics of the analysed subjects expressed as mean ± standard deviation.

	ACT (n=10)	INACT (n=10)	TOT (n=20)
Age (yr)	27.3±5.1	27.0±2.9	27.2±4
BMI (kg/m^2)	22.0±1.7	22.8±2.1	22.4±1.9
RMR (kcal/day)	1830±323	1687±168	1758±261
V'O$_2$max (mLO$_2$/kg/min)	43.6±4.9	40.3±7.2	42±6.2
MVPA (min/day)	109±42	40±14	74±46

NetEC (obtained from GrossEC– Standing metabolic rate) was analysed with indirect calorimetry (K4b^2, Cosmed, Italy) and simultaneously, a kinematic analysis was performed with an optoelectronic system (SMART-E, BTS, Italy) to calculate W$_{EXT}$ during 3 bouts of treadmill walking of 10 min each at 0.97/1.25/1.53 m/s. To assess PAL, subjects wore an activity monitor (Actiheart, CamNtech, UK) for a whole week, inferring time spent in sedentary (SED, <1.5 METs), or moderate to vigorous (MVPA, >3 METs) physical activity.

Statistical Analysis: One-way ANOVA was performed to evaluate differences between ACT and INACT. A repeated measure ANOVA (2x3) was used to determine differences between velocities. An ANCOVA analysis was made to find out associations between NetEC and W$_{EXT}$ with PAL. The correlation analysis was performed to investigate relationships between variables. Significance was set at $p<0.05$.

3. RESULTS

When compared with INACT, ACT had a significantly higher amount of MVPA (P<0,0001). No group differences were observed for SED behaviour (Table 2).

Table 2. Differences between groups

Physical activity parameters	ACT	INACT	*p*-Value
SED (min/day)	626±74	680±96	N.S.
MVPA (min/day)	108.5±41.6	40.4±13.5	<0.0001

NetEC increased significantly at all velocities, except for speed from 0.97 to 1.25 m/s. On the contrary, W_{EXT} decreased significantly when velocities grow up, excluding speed from 1.25 to 1.53 m/s (Fig.1-2).
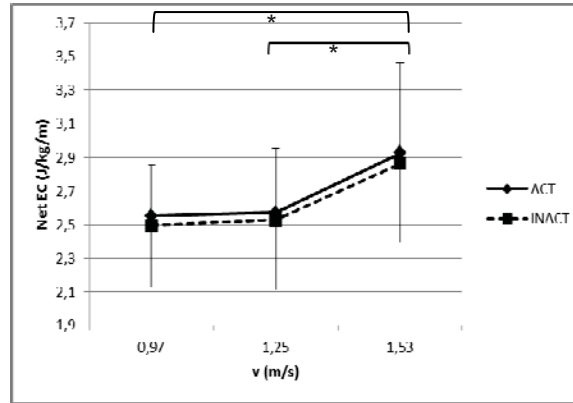
Figure 1. Differences of net energy cost, active versus inactive and between velocities (*p<0.05)
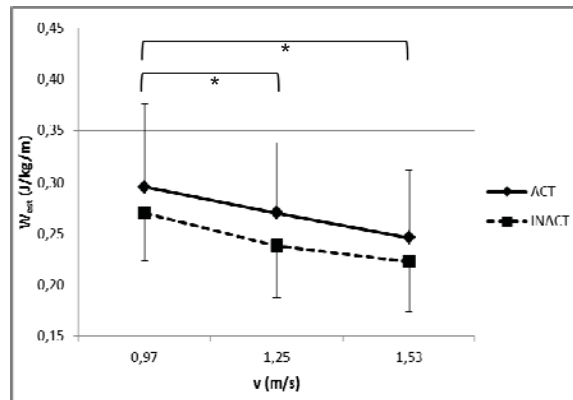
Figure 2. Differences of mechanical external work, active versus inactive and between velocities (*p<0.05)

No significant associations were found between MVPA or SED with neither NetEC nor W_{EXT}. Significant correlations between NetEC or W_{EXT} calculated at the different speeds were found (r>0.583; p<0.01; Table 3).

Table 3-Correlations of net energy cost and mechanical external work

NetEC	*r*	*p-Value*
0.97 vs 1.25 m/s	0.913	<0.001
0.97 vs 1.53 m/s	0.913	<0.001
1.25 vs 1.53 m/s	0.957	<0.001
W_{EXT}	*r*	*p-Value*
0.97 vs 1.25 m/s	0.822	<0.001
0.97 vs 1.53 m/s	0.583	<0.01
1.25 vs 1.53 m/s	0.700	<0.01

4. DISCUSSION

Our data indicate that ACT and INACT adults differ for MVPA but not for SED patterns. For both groups it is extremely important to reduce SED behaviour regardless of performed activities in order to prevent cardiovascular diseases [1]. It is well established that a U-shaped relationship between NetEC and walking speed exists [4]. Our values are substantially in agreement with literature [5;8], even if the U-shaped trend is not visible, probably due to the different number of tested speeds (we have only 3 speeds vs. 4-6 of literature). In addition, different treadmills, metabolic charts and ways to calculate resting metabolic rate may partially explain the variability in the trends. Reference [2] showed that W_{EXT} reaches a minimum at a speed near the preferred walking speed: before and after this threshold, W_{EXT} increases. The absence of significance between 1.25 and 1.53 m/s indicates that our minimum value may be positioned around these speeds. Probably, adding a higher velocity, closer to the preferred walking speed of our subjects, an increase in the values will appear. The absence of associations may be explained by a small sample size and speeds eliciting a $V'O_2$ corresponding to very light/ light activity intensities [1]. Significant correlations between NetEC or W_{EXT} at the three different speeds suggest that subjects motor patterns during walking persist even with increasing speeds.

In conclusion, neither SED nor MVPA seem to influence NetEC and W_{EXT} of light intensity treadmill walking in a healthy adult population.

5. REFERENCES

[1] American College of Sports Medicine, 2011. Quantity and quality of exercise for developing and maintaining cardiorespiratory, musculoskeletal, and neuromotor fitness in apparently healthy adults: guidance for prescribing exercise. Med Sci Sports Exerc, Jul, 43(7), 1334-59.

[2] Cavagna G.A.,Thys H., Zamboni A., 1976. The sources of external work in level walking and running. J Physiol, Nov, 262(3), 639-57.

[3] Hunter G.R., McCarthy J.P., Bryan D.R., Zuckerman P.A., Bamman M.M., Byrne N.M., 2008. Increased strength and decreased flexibility are related to reduced oxygen cost of walking. Eur J Appl Physiol, Nov, 104(5), 895-901.

[4] Margaria R., 1976. Biomechanics and energetics of muscular exercise. Clarendon Press, Oxford, United Kingdom. p.72.

[5] Mian O.S., Thom J.M., Ardigò L.P., Narici M.V., Minetti A.E., 2006. Metabolic cost, mechanical work, and efficiency during walking in young and older men. Acta Physiol (Oxf), Feb, 186(2), 127-39.

[6] Saibene F., Minetti A.E., 2003. Biomechanical and physiological aspects of legged locomotion in humans. Eur J Appl Physiol, Jan, 88(4-5), 297-316.

[7] Sawyer B.J., Blessinger J.R., Irving B.A., Weltman A., Patrie J.T., Gaesser G.A., 2010. Walking and running economy: inverse association with peak oxygen uptake. Med Sci Sports Exerc, Nov, 42(11), 2122-7.

[8] Weyand P.G., Smith B.R., Puyau M.R., Butte N.F., 2010. The mass-specific energy cost of human walking is set by stature. J Exp Biol, Dec 1, 213(Pt 23), 3972-9.

Markerless analysis of double pooling techniques in cross-country sit-ski athletes during competition

Pastorelli S.[1], Gastaldi L.[1], Frassinelli S.[2]

[1] Dept. of Mechanics, Politecnico di Torino, Torino, Italy, stefano.pastorelli@polito.it
[2] Scuola Universitaria Interfacoltà in Scienze Motorie – University of Turin, Torino, Italy

A study of the poling gesture in cross country sit skiers had been implemented based on a markerless stereo-photogrammetric analysis of videos recorded during the Vancouver 2010 Winter Paralympic Games. Comparisons of several athletes underline the different strategies used for propulsion, related to the disability and the residual motor potential. The results let to assess the feasibility of biomechanical studies of the DP gesture of CC disabled sit-skiers during competition.

Keywords: markerless motion analysis, cross-country, sit-skiers, Paralympics.

1. INTRODUCTION

In paralympic cross-country (CC) skiing athletes that cannot compete in a standing position use a sledge mounted on two traditional skis and propulsion is achieved by means of two standard poles, with both arms pushing symmetrically on the poles, similarly to the double poling (DP) technique adopted by standing athletes [1-5] under fast conditions. Several biomechanical studies of double poling in able body subjects have focused on the analysis of cycle characteristics from 2D videos analysis [6-8] and more recently also pole force measurements were performed [2,9-11]. DP is typically considered primarily an upper body exercise; however, in able body skiers legs provide the main energy source [2,9,12,13] as hip, knee and ankle joints co-activation enables the skiers to use body mass to increase the poling force. As a matter of fact, recent research results [14,15] allow to state that it may not be possible to extend results obtained with stand-up athletes to evaluate sit-ski biomechanics, because stand-up athletes activate musculature that the sit-ski athletes with paraplegia or amputation are unable to activate.

To the best of authors' knowledge, no research on sit-skiing double poling technique of disabled athletes had ever been performed. The specific aim of the present study was to perform a biomechanical analysis of the double poling technique developed by Paralympic cross-country sit-skiers during the contests of the 2010 Winter Paralympic Games in Vancouver.

For able body athletes traditionally a functional evaluation in laboratory is preferred to a field test; this choice is strongly reinforced due to the climatic and environment contest in which CC usually is performed (i.e. cold temperatures, inclinations, and snow conditions). This explains the few in the field and during competitions studies [11,16]. Considering that there are no biomechanical studies on sit-skiers and that the push gesture is strongly influenced by the technical capabilities of the skiers' and by snow conditions the authors considered important to start from a kinematic analysis of elite disabled athletes during field competitions. Although this choice limits the variables that can be measured, it will allow a transfer of the analysis to the laboratory in the future, where more kinematics, kinetics and physiological variables can be measured, checking the specificity of the gesture that can be only detected in the field. Furthermore, the choice of an important international competition context makes things more complicated, but on the other hand allows observing a good number of elite athletes at the best of their performances.

In this paper the feasibility of a marker-less kinematic analysis based on videos captured during competitions is demonstrated and results on a kinematic analysis during sprint competition are discussed.

2. MATERIAL AND METHODS

This research was accomplished during the 2010 Paralympic Games in Vancouver, with the approval and support of the International Paralympic Committee (IPC). To capture the pushing gesture kinematics, researchers setup on the competition trails a marker-less stereo-photogrammetric acquisition system based on synchronized digital cameras with a frame rate of 90 fps. In this paper performances obtained during 1 km sprint race will be discussed. Due to logistic reasons in this case only one camera was placed on a rectilinear segment with a slope of 2% and it was located perpendicular to the traces. Due to the international competition contest no markers were placed on the athletes' snow suits nor on their equipments. Subjects were filmed in the sagittal plane and later on a 2D kinematic analysis was performed. As a matter of fact, DP motion for sit-skiers, similarly to what happen for standing athletes [12], is basically a 2D gesture that takes

place mainly in the sagittal plane, hence significant information can be in any case withdrawn from a kinematic analysis in that plane.

Subjects

Athletes were filmed during the sprint race (qualification, semi-final and final laps) at the 2010 Paralympic Games in Vancouver. CC sit-skiers athletes are divided into classes, based on different ranges of disability related to trunk control. They can vary from the LW12 class (athletes eligible for this class have normal trunk muscles, near to normal hip flexion and normal buttock sensibility), to the LW10 one (athletes eligible for this class have no functional abdominals or extensors and no buttock sensibility) with other three intermediate classes: LW10.5, LW11, LW11.5 [17]. All the cross country sit-skiers were considered eligible to be filmed.

Kinematics

Biomechanical model consisted of seven anatomical points, corresponding to the head temple, shoulder, elbow, wrist, hip, knee and ankle left joints; besides technical additional points were added: three to identify pole and one for the sledge. All the points were projected on the sagittal plane for the 2D analysis.

Elbow angle was defined as the relative angle between arm and forearm (0° when forearm is bended on upper arm), shoulder angle was measured between trunk and arm (0° when limb is aligned with trunk), while trunk and pole angles were measured with respect to the ground vertical axis.

Data analysis

Reference points were semi-automatically tracked frame-by-frame on video images and their coordinates in a world reference frame were evaluated. Besides the coordinates of the single markers, the following additional variables were calculated: sledge velocity, trunk, shoulder and elbow angles and pole inclination.

For semi-finalist and finalist athletes more than one push gesture was recorded, one for each bout. They had been compared, but no average value can be calculated, as snow and weather conditions changed from one bout to the other. Kinematics coordinates were smoothed using a moving average filter with radius 2 frames.

3. RESULTS

Analyzed video sequences were referred to 50 subjects: 35 men (aged 36.9 ± 8.9 years), and 15 women (aged 34.3 ± 8.6 years); among them all the medalists were present.

Two types of results are hereafter reported. The former is related to the time progression of the DP gesture and an example of the performed analysis is reported in Fig. 1. In particular Fig. 1a shows the stick diagram of a DP cycle in the sagittal plane for a LW10 athlete. The lower dots are the positions in sequence of the sledge technical point. Stick models have been drawn one out of six frames. Axes actually represent the world reference frame. X axis origin has been assumed coincident with the position of the sledge reference point at the maximum wrist vertical ground elevation. Figs. 1b-g show graphs of main dependent variables changes during the push cycle. The variables are: sledge velocity, elbow, shoulder and trunk angles, wrist y and pole angle. Wrist y represents the vertical ground elevation of the wrist reference point with respect to the local snow level. The variable pole angle is represented with a solid line when the pole is planted into the snow and with a dotted line when it is not. Time $t = 0$ s has been assumed at the maximum wrist vertical elevation. Another type of results (Fig. 2) shows the biomechanics of the DP gesture with respect to a reference frame set in motion with the sledge. Wrist, elbow and shoulder trajectories are reported in Fig. 2a for the same previous athlete in blue, green and red respectively; markers superimposed to the trajectory refer to the DP cycle phases. Fig. 2b-d refer to athletes belonging respectively to LW11, LW12 (bilateral amputee) and LW12 (monolateral amputee) classes.

4. DISCUSSION

The DP gestures of several athletes, typical of different classes can be compared. Athletes have a variety of residual motor functions, sitting postures and sledge fastening devices that influence the push gesture which is the result of a complex interaction of trunk flexion, shoulder and elbow swings. The wide range of residual functions of the athletes, of their training and equipment, together with the few subjects belonging to each single class, did not enabled a significant statistical data processing.

Based on the observations of the DP kinematics for different sit-skiers authors suggest a definition of the poling cycle separated into three phases: poling phase (PP), transition phase (TP) and recovery phase (RP).

These phases are slightly different from the ones proposed in [9]. Referring as an example to the DP cycle reported in Fig. 1, the three phases are hereafter defined. The PP starts with the maximum body and arm extension, assumed at the maximum wrist ground elevation instant (Fig. 1d $t = 0$ s). The end of the PP is identified with the maximum velocity achieved by the sledge (Fig. 1b $t = 0.3$ s).

A decrease of the elbow angle in the first part of the PP, before the pole plant, and afterwards an elbow extension during pole plant can be observed (Fig. 1c). The TP starts with the conclusion of the PP and it ends
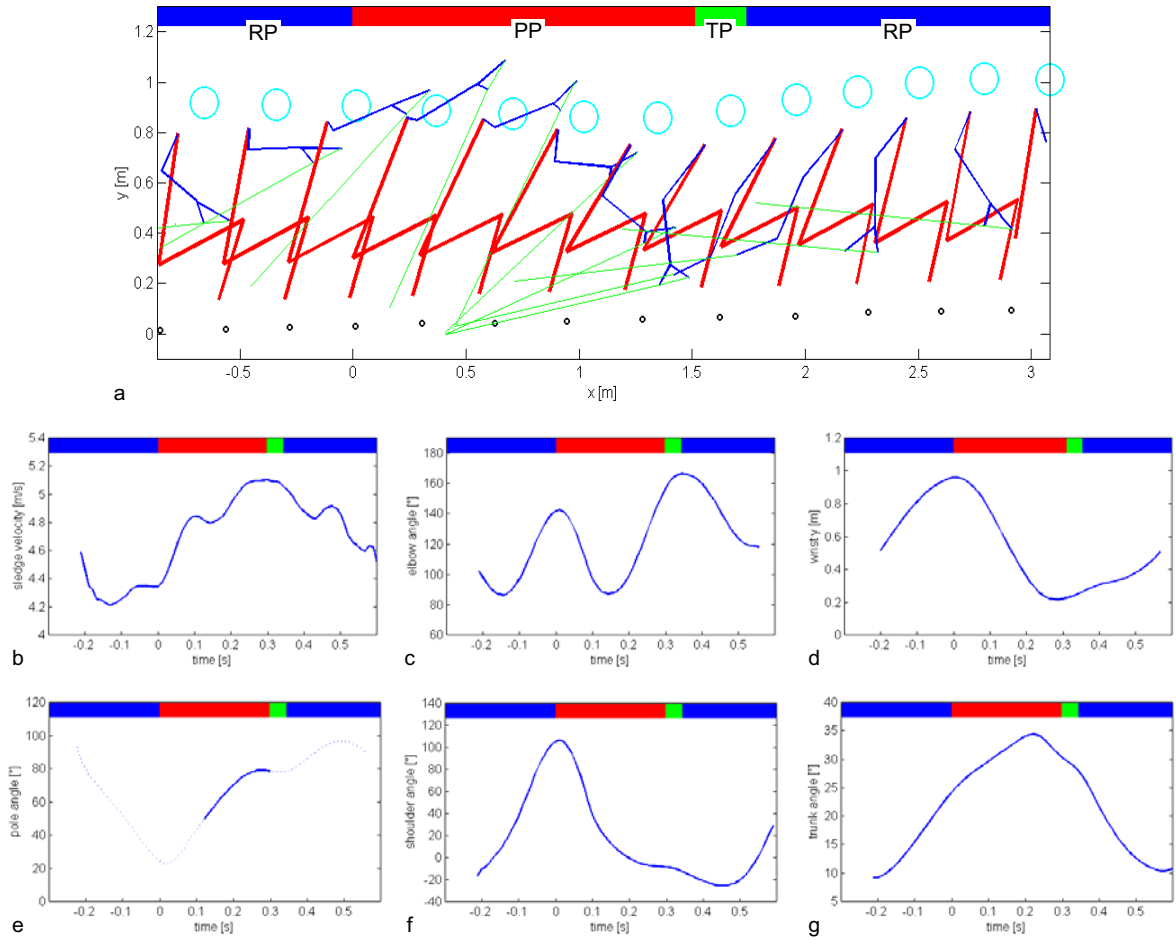
Figure 1. DP cycle of a CC sit-skier: a) stick diagram with respect to ground reference frame; b) sledge velocity; c) elbow angle; d) wrist vertical ground elevation e) pole angle; f) shoulder angle; g) trunk angle.

with maximum elbow extension (Fig. 1c t = 0.35 s). In this phase the pole tip is not anymore in contact with the snow and an antero-posterior arm swing is performed (Fig. 1f). Finally the RP starts with the conclusion of the TP and it ends with the beginning of the PP of the following DP cycle. At the beginning an antero-posterior rotation of the shoulder (Fig. 1f t = 0.35÷0.46 s) with an elbow flexion (Fig. 1c t = 0.35÷0.46 s) can be pointed out, afterwards an upper anterior extension of the arm is present (Fig. 1c and 3f). During the DP cycle, besides an arm movement, a trunk oscillation can be observed (Fig. 1g), with a maximum almost at the end of the PP and a minimum value approximately in the middle of the RP.

Biomechanics of the LW10 athlete DP cycle is summarized in Fig. 2a where cyclic motion trajectories of shoulder, elbow and wrist with respect to the sledge reference system are traced. PP onset, symbolized by circular markers, is at the maximum wrist ground elevation. Squared and triangular markers stand for the end of the PP and the beginning of the RP respectively. Analysis of biomechanics of the DP gesture for athletes belonging to different classes is inferred from the comparison of Fig. 2a-d.
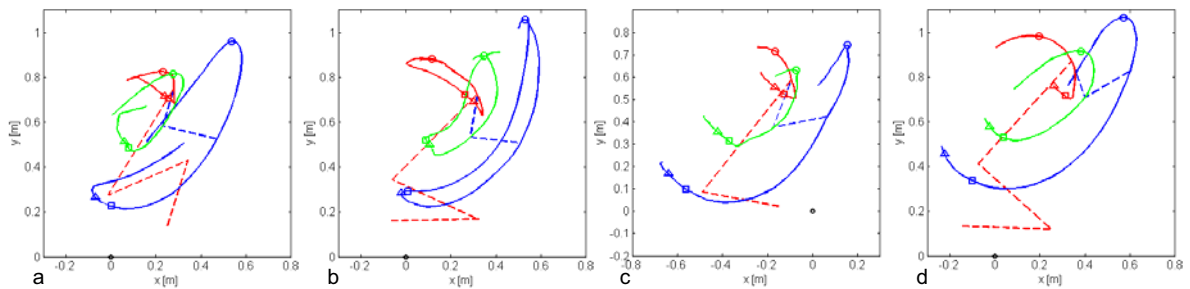

Figure 2. Wrist (blue), elbow (green) and shoulder (red) trajectories during the push gesture with respect to a reference frame set in motion with the sledge of: a) LW10, b) LW11; c) LW12 (bilateral amputee); d) LW12 (monolateral amputee) athletes.

The trunk Range of Motion (RoM) for athletes LW11 and LW12 with mono-lateral amputation (Fig 2b and d) is larger than the RoM for athletes LW10 and LW12 with bilateral amputation (Fig. 2a and c); as a matter of fact the latter have functional limitations due to muscular lacks and unbalance on the sledges. Moreover it is noticeable that athletes of lower classes (LW10, LW11) at the end of the PP and during the TP (i.e. closed to the squared and triangular markers) reach a back extension of the wrist with respect to the hip smaller than athletes classified in the highest classes. Trunk flexion is important to allow shoulder and elbow not to work in an extreme position and hence to generate a greater force and to limit fatigue. Furthermore the trunk motion contributes also to the effectiveness of the push allowing a better control of the poles inclination. As a matter of fact pole forces are transmitted through each pole, but only the horizontal component is helpful to the propulsion. The most effective pushing position is achieved when the pole is inclined towards the horizontal; to get into such positioning trunk flexion combined with shoulder and elbow extension are required.

The presence of abdominal muscles is effective for force generation and represents a big difference between athletes that have no functional abdominals or extensors (in general paraplegics with high lesion) with respect to the ones for which this function is only partially absent or is totally integer. For athletes lacking of these functions trunk flexion is obtained thanks to the gravity force, while extension is obtained by compensation mechanisms that exploit head, arms and upper trunk inertia. Besides, the absence of abdominal and extensor muscles influences also the sledge shape and the seat posture: straps and curled-up legs limit the trunk flexion. In conclusion, the results and the analyses inferred let to assess the feasibility of biomechanical studies of the DP gesture of CC disabled sit-skiers in the field. The knowledge of the gesture specificity acquired during competitions enables the validation of lab analyses, where the study can be integrated with kinetic evaluations and physiological measurements. Furthermore these data allow coaches to have scientific evidence useful to set up customized technical work and athletic training directed to improve the performance of the athletes.

5. ACKNOWLEDGMENT

6. REFERENCES

[1] I.E. Faria, E.W. Faria and D. Parker, 1996. Metabolic and ventilatory response to cross-country skiing classical and double arm poling exercise. J Sports Med Phys Fitness 36, pp. 1-6.

[2] H. Holmberg, S. Lindinger, T. Stoggl, E. Eitzlmair and E. Muller, 2005 Biomechanical analysis of double poling in elite cross country skiers. Med Sci Sports Exerc 37, pp. 807-818.

[3] S. Leirdal, L. Saetran, K. Roeleveld, B. Vereijken, S. Bråten; S. Løset et al., 2006. Effects of body position on slide boarding performance by cross-country skiers. Med Sci Sports Exerc. 38, pp.1462-1469.

[4] G.A. Smith, 1992. Biomechanical analysis of cross-country skiing technique. Med Sci Sports Exerc. 24, pp. 1015-1022.

[5] M.D. Hoffman and P.S. Clifford, 1992. Physiological aspects of competitive cross country skiing. J Sports Sci. 10, pp. 3-27.

[6] J. Nilsson, P. Tveit and O. Eikrehagen, 2004 Effects of speed on temporal patterns in classical style and freestyle crosscountry skiing. Sports Biomech. 3, 85–107.

[7] T. Stöggl T,E. Müller, M. Ainegren and H. Holmberg, 2011. General strength and kinetics: fundamental to sprinting faster in cross country skiing?. Scand J Med Sci Sports 21(6), pp. 791-803.

[8] E.A. Hansen and T. Losnegard, 2010. Pole length affects cross-country skiers' performance in an 80-m double poling trial performed on snow from standing start. Sports Eng. 12, pp. 171–178.

[9] H.C. Holmberg, S. Lindinger, T. Stöggl, G. Björklund and E. Müller, 2006. Contribution of the legs to double-poling performance in elite cross-country skiers. Med Sci Sports Exerc. 38(10), 1853–1860.

[10] S.J. Lindinger, T. Stöggl, E. Müller and H.C. Holmeberg, 2009. Control of speed during the double poling technique performed by elite cross-country skiers. Med Sci Sports Exerc. 41(1), pp. 210–220.

[11] G.A. Smith, J.B. Fewster and S.M. Braudt, 1996. Double poling kinematics and performance in cross-country skiing. J Appl Biomech. 12, pp. 88–103.

[12] T. Stöggl and H.C. Holmberg, 2011. Force interaction and 3D pole movement in double poling. Scand J Med Sci Sports 21(6), pp. e393-404.

[13] G. Van Hall, M. Jensen-Urstad, H. Rosdahl, H.C. Holmberg, B. Saltin and J.A. Calbet, 2003. Leg and arm lactate and substrate kinetics during exercise. Am J Physiol End and Metab. 284(1), pp. E193-E205.

[14] J.L. Tervo, P.B. Watts and R.L. Jensen. Electromyographical Analysis of Double Pole Ergometry: Standing vs. Sitting. In Proc.eedings of the XXVIII Congress of the International Society of Biomechanics in Sports; July 2010.

[15] S.K. Leissring, L.J. Randall, J.L. Tervo and P.B. Watts, 2011. Onset and offset of rectus femoris activation during double poling ergometry in two positions: standing vs. sitting, Rev Port Cien Desp. 11 (suppl. 2), pp. 747-750.

[16] R. Zory, F. Schena and A. Rouard, 2005. Kinematics of sprint cross-country skiing. Acta Bioeng Biomech. 7(2), pp. 89-96.

[17] International Paralympic Committee Nordic Skiing Classification Handbook, March 2011. www.ipc-nordicskiing.org/Classification.

Kinematic analysis of a volleyball attack

Michnik R.[1], Jurkojć J.[1], Czapla K. [2]

[1] Department of Biomechatronics, Silesian University of Technology, Gliwice, Poland,
Robert.Michnik@polsl.pl, Jacek.Jurkojc@polsl.pl
[2] Sports Centre, Silesian University of Technology, Gliwice, Poland

Keywords: motion analysis, volleyball

1. INTRODUCTION

Evaluation of motoric features of professional players, correctness of their movement and technical abilities is a very important part of a training. Present biomechanics and anthropometric measuring methods enable an objective qualitative and quantitative assessment of a human motion system. A methodology of a volleyball attack evaluation and preliminary results obtained for 5 professional players are presented in the paper

2. METHODOLOGY

All measurements of a volleyball attack were carried out in the Silesian University of Technology Sport Centre. There were five professional players who took part in the research – 3 women and 2 men. All participants' data are presented in the table 1.

Table 1 Participants' data

Symbol	K1	K2	K3	M1	M2
Sex	K	K	K	M	M
Body height [cm]	183	180	178	196	195
Body mass [kg]	80	78	61	80	88

Players motion was recorded by means of a set of four Basler camcorders with a frequency of 200Hz. There were 25 reflective markers located on a player (Fig. 1) .

Fig. 1 Markers placement

All recorded movies were processed with the use of the VirtualDub computer program and the optoelectronic system APAS to determine displacements of individual markers (Fig. 2). Then the computer program KinemVoleyball, prepared by the authors of this article in MATLAB environment, was used to calculate positions of upper and lower limbs and angles of body segments with respect to each other and to the global coordinate system.
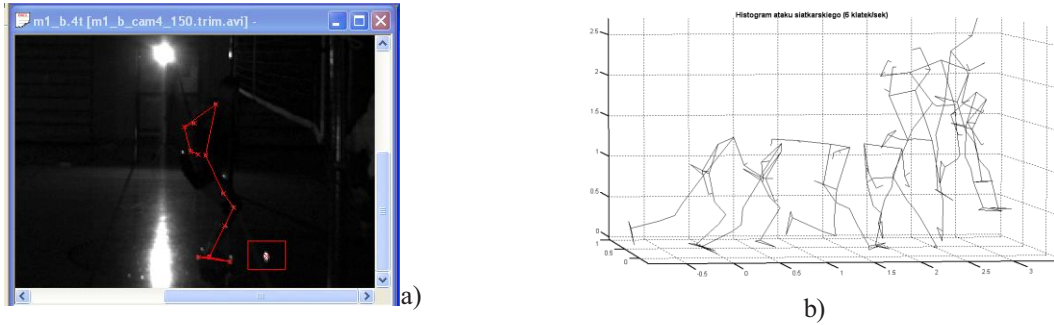
Fig. 2 Measurements (a) and the following positions of markers (b)

The kinematic analysis of a volleyball attack was carried out on the basis of chosen kinematic parameters which are of the great importance to attack correctness and effectiveness, which can be used to describe individual phases of the attack. The following parameters were used in the evaluation:

- run up parameters: lengths of run up steps
- jump parameters: height and length of a jump, range of the attack, duration of the flying phase
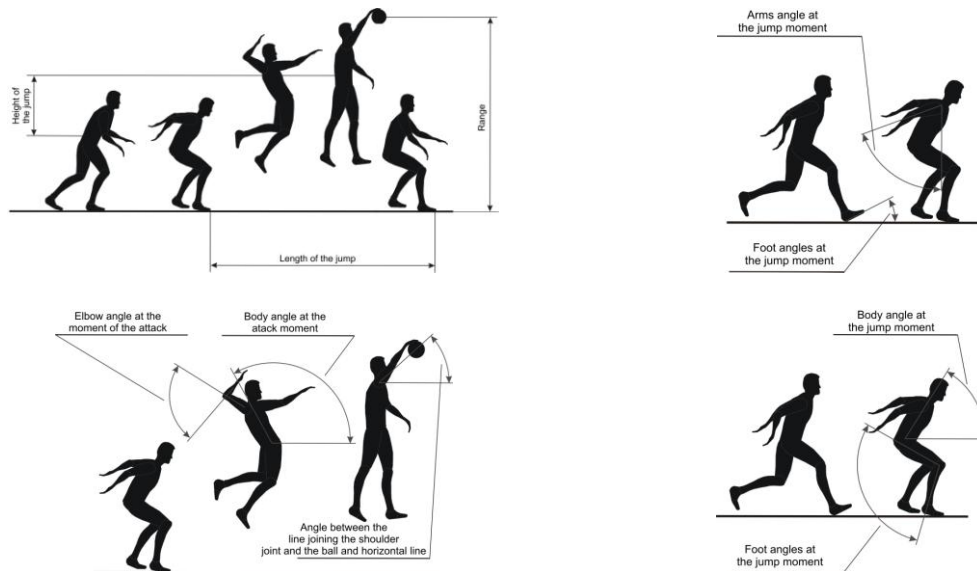- body segments angles in the individual phases of the attack

Fig. 3 Analyzed parameters

3. RESULTS

Values describing players' run up are presented in the table 2. Length of the second step was considerably longer than length of the first one in each case. The first step length is about 41% of the second step length in the men group (M1 - 41.2%, M2 - 42.8%) and about 52% in case of K1 and K2 (K1 - 51%, K2 - 53%) whereas in case of K3 it is 70%. This rate of steps shows that all run ups were performed properly.

Table 2 Steps lengths and run up length

	K1	K2	K3	M1	M2
Length of the first step [m]	0.73	0.73	1.1	0.7	0.68
Length of the second step [m]	1.43	1.37	1.59	1.7	1.59
Length of the run up [m]	2.65	2.48	3	2.54	2.61

Quantities describing players' jumps are the next group of analyzed parameters. Table 3 presets time-spatial parameters. Parameters concerning body segments angles are placed in the table 4. The foot angle at the moment of contact with ground was in the range of 30º to 38º. Analyzing knee angles one can states that this angle was smaller for the leg making jump than for the second one. This difference was about 22º for K1, K2,

K3 and M2 players whereas for the M1 it was 61º. The body angle was about 46º±2,74º. The arms angle at the jump moment was between 86º to 120º and was more or less the same for both upper limbs of each player. The only exception was the K2 player where the angles difference between the right and left upper limb was 50º.

Table 3 Jump parameters

	K1	K2	K3	M1	M2
Jump duration [s]	-	0.59	0.61	0.71	0.71
Height of the jump [m]	0.51	0.59	0.52	0.79	0.75
Length of the jump [m]	-	0.56	0.38	0.63	0.3
Range [m]	2.49	2.47	2.29	2.75	2.76
Distance between the jump position and attack position [m]	0.6	0.67	0.2	0.4	0.63

Table 4. Body segments angles at the moment of the jump

	K1	K2	K3	M1	M2
Foot angle at the jump moment [º]	30	38	36	35	33
Knee angle of the leading leg [º]	103	103.1	99.8	102	105.4
Knee angle of the second leg [º]	128.6	124.5	118.1	163	130.1
Body angle at the jump moment [º]	49.4	43.7	46.1	43.1	48.2
Arms angle at the jump moment [º]	97	86 P 36 L	120	98	104

Angles of body segments at the moment of the attack are the last of analyzing quantities. All results are presented in the table 5.

At the moment of the attack the angle between the line joining the shoulder joint and the ball and the horizontal line was equal 60-68° in case of K1, M1, M2. For players K2 and K3 the angle was equal 82-85° what is incorrect because in that case a ball is almost above a player what makes the correct attack impossible. It can be also harmful for a shoulder joint.

Table 5 Body segments angles at the moment of the attack

	K1	K2	K3	M1	M2
Angle between the line joining the shoulder joint and the ball and the horizontal line [°]	58	82	85	68	62
Elbow angle at the moment of the attack [°]	85	59	75	58	81
Body angle at the moment of the attack [°]	108.7	94.3	102.7	106.7	107.6
Ball velocity [m/s]	11.1	24	22.1	23.8	24.3

4. CONCLUSIONS

The methodology of measurements and kinematic parameters analyses of quantities enabling evaluation of volleyball atack was elaborated within the frame of performed research. Preliminary measurements were carried out on a group of 5 professional players. The motion analysis system APAS and the computer program

prepared by article's authors were used to determine kinematic parameters. Motion of body segments was analyzed

5. ACKNOWLEDGMENT

6. REFERENCES

[1] Buśko K.: Analiza wpływu programów treningu o różnej strukturze intensywności na siłę i moc maksymalną mięśni kończyn dolnych człowieka, Studia i Monografie nr 109, Wydawnictwo AWF Warszawa, Warszawa 2006

[2] Chenfu Huang, Lin-Huan Hu: Kinematic analysis of volleyball jump topspin and float serve,XXV ISBS Symposium 2007, Ouro Preto - Brazil

[3] Grządziel G. Ljach W. J.: Piłka siatkowa, Centralny Ośrodek Sportu, Warszawa 2000

[4] Klocek T., Szczepanik M.: Ocena taktyki ataku w piłce siatkowej mężczyzn – analiza skuteczności gry drużyn uczestniczących w rozgrywkach Ligi Światowej '2001, 2002, 2003 oraz Mistrzostw świata 2002, Obserwacja i ocena działań zawodników w zespołowych grach sportowych, praca zbiorowa pod redakcją Józef Bergier; Paweł Przybylsk, Wydawnictwo: Międzynarodowe Towarzystwo Naukowe Gier Sportowych, Wrocław 2004

[5] Klocek T., Szczepanik M.: Siatkówka na lekcji wychowania fizycznego, Centralny Ośrodek Sportu, Warszawa 2003

[6] Klocek T., Żak S.: Kompensacja cech ujętych w modelu mistrza w piłce siatkowej, Sport Wyczynowy nr 9-10, 1999

[7] Kosmol M., Kosmol A., Kuder A., Kosmol M.: Skuteczność i efektywność ataku w grze w piłkę siatkową, Sport Wyczynowy, nr 7-9, 2007

[8] Król H.: Poziom przygotowania siłowo-szybkościowego skoczków narciarskich, Biomechanika ruchu. Wybrane zagadnienia, praca zbiorowa pod redakcją Czesława Urbanika, Wydawnictwo AWF Warszawa, Warszawa 2007

[9] Kuhlmann C., Roemer K., Milani T.L.: Aspects of a three dimensional motion analysis of the volleyball spike in high level competition, XXV ISBS Symposium 2007, Ouro Preto – Brazil

[10] Li-Fang Liu, Gin-Chang Liu, Chiao-Wen Sue, Chen-fu Huang: The application of range of motion (rom) and coordination on volleyball spike, ISBS Conference 2008, July 14-18, 2008, Seoul, Korea

[11] Lin-Huan Hu, Yug-Hslang Chen, Chenfu Huang, A 3D analysis ot the volleyball spike, ISBS 2005, Beijing, China

[12] Mastalerz A.: Reakcja układu mięśniowego na wysiłki o maksymalnej intensywności, Studia i Monografie nr 124, Wydawnictwo AWF Warszawa, Warszawa 2008

[13] Naglak Z.: Zespołowa gra sportowa, Wydawnictwo AWF Wrocław, Warszawa 1994

[14] Tabor P., Iwańska D., Ostrowski M.: Wpływ pozycji ciała na skuteczność odbicia sposobem oburącz dolnym w piłce siatkowej, Wybrane zagadnienia biomechaniki ruchu człowieka (pod redakcją Urbanik Cz.), Akademia Wychowania Fizycznego w Warszawie, 2007

[15] Tabor P., Mastalerz A., Iwańska D.: Biomechaniczne kryteria skuteczności techniki ataku w siatkówce, Sport Wyczynowy, nr 1-2, 2004

[16] Trzaskoma Z.: Maksymalna siła mięśniowa i moc maksymalna kobiet i mężczyzn uprawiających sport wyczynowo, Studia i Monografie nr 94, Wydawnictwo AWF Warszawa, Warszawa 2003

[17] Wnorowski K.: Analiza ilościowo-jakościowa gry reprezentacji Polski w piłce siatkowej w Igrzyskach Olimpijskich w Atenach w 2004 roku

Thu – July 19th 2012

Chairmen: **Anat Mirelman (Sourasky Medical Center, Israel)**
Claudio Belvedere (Istituto Ortopedico Rizzoli, Italy)

Keynote lecture: "Virtual reality for rehabilitation and treatments"
16.00 : 16.30 *Anat Mirelman*

Podium session #4: "Motion analysis in health care"
16.30 : 18.00

16.30	Three dimensional rotation offset correction	Koning B.H.W., Van der Krogt M.M., Baten C.T.M., Koopman H.F.J.M.
16.45	A combined gait and fluoroscopic analysis: functional performance of replaced ankles	Cenni F., Pieri M., Berti L., Belvedere C., Romagnoli M., Giannini S., Leardini A.
17.00	Reliability of the MMAAS in patients with multiple sclerosis	Murgia A., Alders G., Kerkhofs L., Truyens V., Feys P., Savelberg H., Meijer K.
17.15	Assessment of the mechanical power produced by a manual wheelchair user during ambulation in the field	Sauret C., Vaslin P., Dumas R., Bascou J., Pillet H., Chèze L., Cid M., Lavaste F.
17.30	Evaluating equipment constraints in surgery	Yu D., Sackllah, M., Woolley C., Kasten S., Armstrong T.
17.45	Changes in shoulder kinematics of trans-radial amputees following the use of multi-grip prosthetic hands: a case study	Parel I, Cutti AG, Verni G.

Keynote lecture

!

Virtual reality for rehabilitation and treatments

Anat Mirelman

Sourasky Medical Center, Israel

Virtual Reality (VR) is defined in general as a "high-end-computer interface that involves real time simulation and interactions through multiple sensorial channels". VR, at least theoretically, is an ideal tool for intervention in rehabilitation. The impetus for using VR is that the technology can provide a powerful tool with which to provide individualized repetitive practice of motor function, graded in accordance to the needs and level of ability of the person while engaging and stimulating cognitive processes. At the same time, VR provides feedback about performance to assist with leaning new motor strategies of movement. The realism of the virtual environments allows individuals the opportunity to safely explore their environments independently, increasing their sense of autonomy and independence in directing their own therapeutic experience. These training sessions are typically quite enjoyable and motivating for patients with different disorders and motor impairments, allowing for higher intensity of training in short duration protocols with relatively low patient burden. The use of VR in the literature varies widely and includes the use of different systems for evaluation of cognition, treatment of upper extremity, improvement in activities of daily living and gait in a wide range of patients. In this talk different applications of VR for rehabilitation will be described, the clinical needs that could warrant using this technology will be discussed, and how current and possible future technology can respond to these needs and enhance the field of rehabilitation.

Three dimensional rotation offset correction

(Identification of and correcting for three dimensional anatomical calibration differences when comparing human joint kinematics)

Koning B.H.W. [1,2], Van der Krogt M.M. [1,3], Baten C.T.M. [2], Koopman H.F.J.M. [1]

[1] Laboratory of Biomechanical Engineering, University of Twente, Enschede, The Netherlands
[2] Roessingh Research and Development, Enschede, The Netherlands
[3] Dept. of Rehabilitation Medicine, Research Institute MOVE, VU University Medical Center, Amsterdam, The Netherlands

Segment calibration; offset; quaternions; comparison; joint kinematics

1. INTRODUCTION

Current methods to compare joint kinematics of two measurements, either to validate two different measurement systems or during a follow-up study, are often limited because the non-vectorial behavior of rotations [1] is neglected. As discussed by Pierrynowsky [2] averaging the geometrically dependent (clinical) Euler angles is fundamentally flawed and therefore they do not reflect the real three dimensional systematic error. When comparing joint kinematics, differences are likely to occur due to different segment axes definitions (i.e. offsets) when one or more segments are hard to calibrate accurately. Due to joint cross-talk, these differences are not easy to identify as a systematic error (especially when Euler angles are compared) and have been stated as a major cause of inaccuracies in human movement [3].

From this we believe there is a necessity to define a three-dimensional measure to evaluate differences in joint kinematics; for which we propose the *difference quaternion*. We show how it can be used to identify and correct for systematic offsets in one of the segment frames and illustrate the pitfall of a priori choosing the segment frame in which the kinematics are defined. We also show how simultaneous offsets in the proximal and distal segment frames could be identified using through optimization of parameters that define the three dimensional offset in both segment frames.

2. METHODS

Mathematical Background

Quaternions (1) are commonly used to describe rotations. They consist of four parameters, where $\boldsymbol{u}$ defines the axis of rotation (direction cosines) and α the angle of rotation around this axis (helical angle) [4]. The superscript in (1) denotes that this quaternion describes the orientation of reference frame Ψ_2 in Ψ_1.

$$^{\Psi_1\Psi_2}\boldsymbol{q} = [q_w\ q_x\ q_y\ q_z] = q_w + \boldsymbol{i}q_x + \boldsymbol{j}q_y + \boldsymbol{k}q_z = \cos(\alpha/2) + \boldsymbol{u}\sin(\alpha/2) \tag{1}$$

Using quaternions, joint kinematics can be described in the proximal (2) or distal (3) segment frame using a quaternion division of both segment orientations in the global frame[1], where $\otimes$ is a quaternion multiplication and $\mathbf{q}^* = [q_w\ -q_x\ -q_y\ -q_z]$ the quaternion inverse.

$$^{p1d1}\boldsymbol{q}_{j1} = {}^{Gd1}\boldsymbol{q}\ /{}^{Gp1}\boldsymbol{q}\ = {}^{Gp1}\boldsymbol{q}^* \otimes {}^{Gd1}\boldsymbol{q} \tag{2}$$

and

$$^{d1p1}\boldsymbol{q}_{j1} = {}^{Gd1}\boldsymbol{q}^*\ {}^{Gp1}\boldsymbol{q}\ = \left({}^{Gp1}\boldsymbol{q}^* \otimes {}^{Gd1}\boldsymbol{q}\ \right)^* = {}^{p1d1}\boldsymbol{q}_{j1}^* \tag{3}$$

The three-dimensional difference between two time series of joint kinematics can be defined using the joint quaternions of the proximal (4) or distal (5) segment frame,

$$\boldsymbol{q}_{diff\_P} = {}^{p1p2}\boldsymbol{q}_{diff\_P} = {}^{d2p2}\boldsymbol{q}_{j2}/{}^{d1p1}\boldsymbol{q}_{j1} = {}^{d1p1}\boldsymbol{q}_{j1}^* \otimes {}^{d2p2}\boldsymbol{q}_{j2} = {}^{p1d1}\boldsymbol{q}_{j1} \otimes {}^{p2d2}\boldsymbol{q}_{j2}^* \tag{4}$$

$$\boldsymbol{q}_{diff\_D} = {}^{d1d2}\boldsymbol{q}_{diff\_D} = {}^{p2d2}\boldsymbol{q}_{j2}/{}^{p1d1}\boldsymbol{q}_{j1} = {}^{p1d1}\boldsymbol{q}_{j1}^* \otimes {}^{p2d2}\boldsymbol{q}_{j2} \tag{5}$$

The *distal difference quaternion* (5) can be geometrically interpreted as the orientation difference of both distal segments defined in the first distal segment frame, assuming both proximal segments are perfectly aligned. A similar interpretation is true for the *proximal difference quaternion* (4). Because the helical angle

---

[1] Although we use quaternions, the same method can be applied to define a difference rotation matrix, by replacing the quaternion multiplication $\otimes$ with an ordinary matrix multiplication and using the matrix inverse.

($\alpha = 2\cos^{-1}(q_0)$) of both difference quaternions are equal (6) they can both be used as straightforward measure of the magnitude of the difference in joint kinematics.

$$\boldsymbol{q}_{diff\_P} = \boldsymbol{q}^*_{diff\_D} \Rightarrow q_{w\_diff\_P} = q_{w\_diff\_D} \Rightarrow \alpha_{w\_diff\_P} = \alpha_{w\_diff\_D} \tag{6}$$

Proximal and distal segment offset

Segment orientation offsets can be defined in the proximal (7) and distal (8) segment frame by quaternion multiplication, so a theoretical second time series containing the same joint kinematics, but with segment orientation offsets, can be constructed (9).

$$^{Gp2}\boldsymbol{q} = {}^{Gp1}\boldsymbol{q} \otimes {}^{p1p2}\boldsymbol{q}_{po} \tag{7}$$

$$^{Gd2}\boldsymbol{q} = {}^{Gd1}\boldsymbol{q} \otimes {}^{d1d2}\boldsymbol{q}_{do} \tag{8}$$

$$^{p2d2}\boldsymbol{q}_{j2} = {}^{p1p2}\boldsymbol{q}^*_{po} \otimes {}^{p1d1}\boldsymbol{q}_{j1} \otimes {}^{d1d2}\boldsymbol{q}_{do} \tag{9}$$

Offset identification and correction

When an offset is limited to one of the segments (e.g. ${}^{p1p2}\boldsymbol{q}_{po} \approx \boldsymbol{I}$), it can be identified analytically (10).

$$\boldsymbol{q}_{diff\_D} = {}^{p1d1}\boldsymbol{q}^*_{j1} \otimes {}^{p2d2}\boldsymbol{q}_{j2} \approx {}^{p1d1}\boldsymbol{q}^*_{j1} \otimes \boldsymbol{I} \otimes {}^{p1d1}\boldsymbol{q}_{j1} \otimes {}^{d1d2}\boldsymbol{q}_{do} = {}^{d1d2}\boldsymbol{q}_{do}. \tag{10}$$

However, if this is not the case, offsets can be identified (and corrected for) through optimization of estimated offsets in the proximal (${}^{p1p2}\widehat{\boldsymbol{q}}_{po}$) and distal (${}^{d1d2}\widehat{\boldsymbol{q}}_{do}$) segment frame. The objective is to minimize the average difference between the kinematics of time series one and corrected kinematics of time series two (11).

$$OBJ = \sum_{time}\left\|{}^{p1d1}\boldsymbol{q}_{j1} - {}^{p1p2}\widehat{\boldsymbol{q}}_{po} \otimes {}^{p2d2}\boldsymbol{q}_{j2} \otimes {}^{d1d2}\widehat{\boldsymbol{q}}^*_{do}\right\|/N \tag{11}$$

To reduce the overdetermined number of 8 parameters, the elements of both offset quaternion estimates are converted to attitude 'vectors' [1], which each have only three degrees-of-freedom.

$$\widehat{\boldsymbol{q}}_{offset} \Rightarrow \widehat{A}\boldsymbol{V}_{offset} = \alpha_{offset}\boldsymbol{u}_{offset} \tag{12}$$

The number of parameters can further be minimized by including only those parameters that define an offset which is expected. The example used for the simulations in this abstract assumes a rotation offset around the vertical axis (Z) of both segment frames. This results in six ways to identify and/or correct for a systematic offset in one or both segment frames (Table 1), when comparing two sets of joint kinematics.

Simulation study

Simulations were performed using five cycles of right hip joint kinematics of a subject using a slideboard, which is a land training setup for speed skating. These kinematics were chosen as a typical example of a motion with a relatively large range of motion in all directions, which in combination with a realistic rotation offset in the distal thigh segment frame up to ten degrees [5] leads to considerable cross-talk. The kinematics of time series one were obtained with inertial and magnetic measurement units (IMMUs [6]) using functional segment calibration routines similar to Cutti et al. [7]. An artificial offset was added two create a second time series using (9). Next, the offsets were identified according to the methods of Table 1, which were then used to calculate corrected kinematics. The joint kinematics of time series one and the (un)corrected joint kinematics of time series two are compared using the helical angle of the difference quaternion and the difference in (clinical) Euler angles.

Table 1 Different methods to identify and correct for calibration offsets and the estimated offsets and segment axis definition.

Method		Parameters	
Comment	*Abbr.*	*Proximal offset (Pelvis)*	*Distal offset (Right Thigh)*
Correction by subtracting the mean YXZ-Euler angle differences, where Euler angles can be based on the proximal (pEA) or distal (dEA) joint quaternions.	pEA	a	a
	dEA	a	a
Pre- or post multiply the joint kinematics with proximal (pDQ) or distal (dDQ) difference quaternion (converted to attitude vector elements).	pDQ	X, Y, Z	
	dDQ		X, Y, Z
Pre- and post multiply the joint kinematics with the optimized offset quaternion estimates, using all six parameters in the optimization (fO) or only the parameters that define a rotation offset around the segment long axis (pO).	fO	X, Y, Z	X, Y, Z
	pO	Z	Z
Segment axes definitions: X: posterior-anterior, Y:lateral-medial, Z: inferior-superior.			

a. Not a real systematic offset due to the nature of Euler angles.

3. RESULTS

Figure 1A shows YXZ-Euler angles of the first (Q1) and second time series (Q2, which is equal to Q1 but including a distal offset of ten degrees evenly distributed along all three axes). Although there seemed to be a constant offset in all three Euler angles, this was not true, as illustrated by Figure 1B to E. These figures show the difference in joint kinematics between the first time series and the (un)corrected second time series; Figure 1B shows the helical angle of the difference quaternion in (4), whereas Figure 1C tot D show the difference in Euler angles. Both methods using the differences in Euler angles, showed a near zero-mean for the Euler angle differences, but a variable error remained. Corrections using the distal difference quaternion as well as optimization using all six parameters completely removed the systematic offset. The worst results were obtained using the proximal difference quaternion and optimization of only rotation offsets.

Figure 2 shows the mean root mean square values of the difference quaternion helical angles for simulations with four different distal offsets; a rotation of ten degrees around each axis and the simulation of Figure 1B. The method of Euler subtraction for Euler angles defined in the proximal segment frame completely removed the offset around the Z-axis, whilst for Euler angles defined in the distal frame the offset around the Y-axis was removed. The distal difference quaternion and optimization using all parameters removed the offset in all simulations. When only both Z parameters were used, the offset rotation around the Z-axis was completely removed, whereas there was no correction at all for offset around the Y-axis ($^{p1p2}\widehat{AV}_{po} = [0 \quad 0 \quad -0.88]$ and $^{d1d2}\widehat{AV}_{do} = [0 \quad 0 \quad -0.28]$ in degrees). The only method that was not able to remove the complete offset in any of the simulations is the proximal difference quaternion.

4. DISCUSSION

We introduced the proximal (4) and distal (5) difference quaternions, which can be used to define the magnitude of the difference in joint kinematics over time, by means of the helical angle. The distal difference quaternion can be geometrically interpreted as the orientation difference of both distal segments defined in the first distal segment frame, assuming both proximal segments are perfectly aligned, and vice versa. This property can be used to evaluate the direction of the difference.
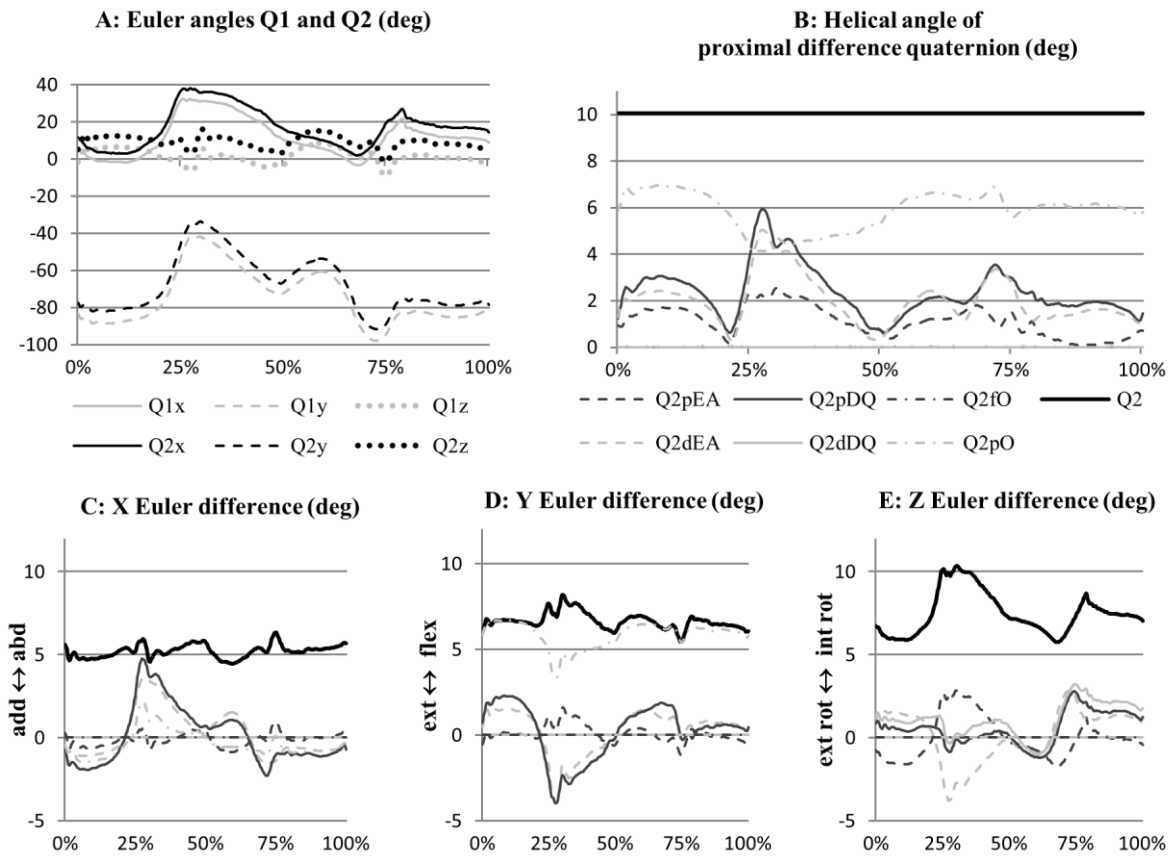

Figure 1 Original and corrected hip joint kinematics for the first of five complete cycles used for analysis in this paper. A: YZX-Euler angles of time series 1 (Q1) and 2 (Q2, which is equal to Q1 except for a systematic orientation offset in the distal segment frame (thigh) of $^{d1d2}_{\square}AV_{do}^{\square} = [5.8 \quad 5.8 \quad 5.8]$). B: Remaining difference expressed using the helical angle after applied corrections of Table 1. C/D/E: Remaining difference in the X, Y and Z components of the (clinical) Euler angles (order 'YXZ').

When comparing joint kinematics, part of the difference is systematic due to differences in the anatomical segment calibration. This abstract focused on an offset in the distal segment, which was completely removed if the correct difference quaternion was chosen (Figure 1 and Figure 2). As opposed to subtracting Euler angles, where the validity depended not only on the segment in which the Euler angles were defined, but were related to the Euler angle order of rotation and the direction of the offset as well (Figure 2). So, subtracting Euler angles only correctly estimates and corrects for the actual systematic offset when the offset Euler angle can be determined independently of other Euler angles, which was true only for the two special cases illustrated in Figure 2.
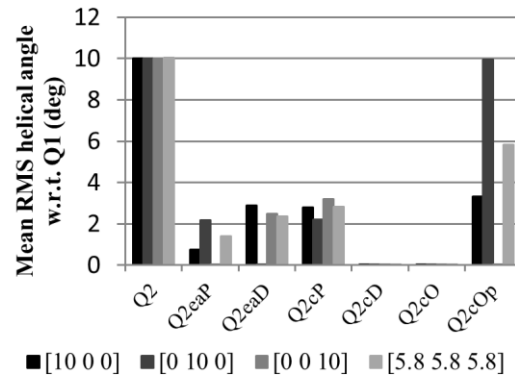

Figure 2 Mean root mean squares of the helical angles of the difference quaternion between the kinematics of the first and second time series with and without the corrections of Table 1.

Though this abstract focused on an offset in a single segment, we also provided a method for offset correction in both segments simultaneously through optimization. When all six offset parameters were included, it completely removed all simulated offsets. However, when just the parameters that defined a rotation offset around the segment long axis were included in the optimization, the offset was only removed completely if this assumption was true. When the offset was only around the Y-axis there was no relevant correction at all. So, when in a follow-up study a clinical difference is expected around the Y-axis (flexion), these offset parameters can correct for offsets around the Z-axis (segment long axis), whilst leaving the clinically relevant difference unaffected.

In conclusion, we proposed a method to define the three dimensional systematic difference between two time series of joint kinematics by defining the *difference quaternion*. When both time series are supposed to be equal by definition (i.e. validation of two different motion capturing systems by simultaneous measurement of joint kinematics) or expected to be similar (i.e. follow-up measurement on the same subject), the difference quaternion and/or optimization of offset parameters can be used to identify and correct for systematic rotation offsets due to differences in anatomical segment calibration. Future study will focus on the robustness of these methods under conditions with additional proximal offsets, low-pass and/or band-pass noise (i.e. noise the frequency band of the motion itself) applied to each segment, and how optimization using a limited amount of offset parameters enables correction of segment long axis rotation offsets, without interfering with the flexion angles. Additionally, including multiple joints, segments and segment offsets in the optimization can improve the offset estimates.

5. ACKNOWLEDGMENTS

6. REFERENCES

[1]   H. J. Woltring, 1994. 3-D attitude representation of human joints: A standardization proposal. Journal of Biomechanics, vol. 27, pp. 1399-1414.

[2]   M. R. Pierrynowski and K. A. Ball, 2009. Oppugning the assumptions of spatial averaging of segment and joint orientations. Journal of Biomechanics, vol. 42, p. 375.

[3]   U. Della Croce, A. Leardini, L. Chiari, and A. Cappozzo, 2005. Human movement analysis using stereophotogrammetry: Part 4: assessment of anatomical landmark misplacement and its effects on joint kinematics. Gait & Posture, vol. 21, p. 226.

[4]   J. B. Kuipers, 2002. Quaternions and rotation sequences: a primer with applications to orbits, aerospace, and virtual reality: Princeton University Press.

[5]   S. J. Piazza and P. R. Cavanagh, 2000. Measurement of the screw-home motion of the knee is sensitive to errors in axis alignment. Journal of Biomechanics, vol. 33, pp. 1029-1034.

[6]   D. Roetenberg, 2006. "Inertial and magnetic sensing of human motion", PhD Thesis, University of Twente, Enschede.

[7]   A. Cutti, A. Ferrari, P. Garofalo, M. Raggi, A. Cappello, and A. Ferrari, 2010. 'Outwalk': a protocol for clinical gait analysis based on inertial and magnetic sensors. Medical and Biological Engineering and Computing, vol. 48, pp. 17-25.

A combined gait and fluoroscopic analysis: functional performance of replaced ankles

Cenni F. [1], Pieri M. [1], Berti L. [1], Belvedere C. [1], Romagnoli M. [2], Giannini S. [1,2], Leardini A. [1]

[1]Movement Analysis Laboratory and [2]Department of Orthopaedic Surgery,
Istituto Ortopedico Rizzoli, Bologna, Italy,
francesco.cenni@ior.it

Total ankle replacement; gait analysis; fluroscopic analysis

1. INTRODUCTION

In recent years, there has been a remarkable advancement in total joint replacement. Part of this is accounted for the progresses in the comprehension of the natural joint kinematics, which has been elucidated also by means of planar linkages or spatial mechanisms. According to these total joint prostheses have been designed, claiming the ability to reproduce physiological joint motion and at the same time to guarantee full congruity between the prosthetic surfaces, with the hope to achieve a better overall functional performance of the lower limb during activities of the daily living. This was achieved time ago for total hip and knee replacements, and only more recently total ankle replacement (TAR), within the current generations. TAR has been becoming a popular treatment for severe erosions of the articular surfaces at this joint, though arthrodesis is still considered the treatment of choice for patients at the end-stage of ankle arthritis [1]. This gap for the ankle joint can be accounted for also to the lack of studies assessing the final efficacy in-vivo of patients implanted with TAR. Therefore, in addition to the pre-implant biomechanical studies and the many post-implant clinical and radiological studies [2], quantitative assessments of the real performance in ankles with TAR should be carried out by means of careful 3D instrumental analyses.

Currently, there are a small number of studies in TAR ankle patients performed by standard gait analysis (GA), and a few tracking the prosthesis components by videofluoroscopy and relevant 2D-to-3D matching techniques, i.e. fluoroscopic analysis (FA). All these studies reported satisfactory results, though this evidence was not clearly supported by corresponding convincing measurements. These studies were performed either by GA or by FA; it is expected that considerable improvements can be obtained through a combination of these two types of measurement techniques in TAR, as obtained in total knee replacement [3,4]. A complete kinematics, kinetics and electromyographic analysis over a number of segments and joints and within a large field of measurement can be performed by the former; a very accurate kinematics measure of the replaced ankle can be performed with the latter. Furthermore, all previous functional studies on TAR were performed during level walking and not a single during stair climbing and descending. The latter activity is expected to be even more revealing, because it is more demanding and therefore it can differentiate functional characteristics among different TAR designs and patients.

A thorough functional assessment after TAR is therefore relevant, particularly for those designs which claim explicitly enhanced restorations of normal joint kinematics. A novel such design was developed [5,6] with the original aim of re-establishing the natural compatibility between the articulating surfaces and the retained ligaments. This was achieved with a special shape of a conforming meniscal bearing free to move between the tibial and talar components. The bearing was designed to move forwards and backwards on both these metal components during dorsi- and plantar- flexion, respectively. Preliminary results in patients are supporting these claims [5,6].

The aim of the present study was to test the ability of a thorough analysis which combines GA and FA measurements to provide a complete and valuable evidence of the replaced overall function after TAR with this novel design. This assessment was performed during a demanding activity of daily living, i.e. stair climbing and descending.

2. MATERIAL AND METHODS

From all patients operated upon in this institute with the BOX Ankle TAR (Finsbury Orthopaedics, Leatherhead-Surrey, UK), a group of the first twenty who provided informed consent according to the relevant procedure of the local Ethics Committee was analyzed. The BOX consists of metal tibial and talar components and a polyethylene meniscal bearing instrumented with three tantalum beads in known positions.

A senior orthopaedic surgeon performed all these TARs. Ten patients were treated on the left side and 10 on the right side; 13 patients were men and 7 women; the average age at the time of surgery was 57.8 years (range 44-67). Patients were analyzed at 12 months after surgery during stair climbing and descending by standard GA and, on the same day and using the same staircase, by FA. GA data were collected (see Figure 1) during the entire gait cycle of both legs using a stereophotogrammetric system with eight M2-cameras (Vicon 612, Vicon Motion Capture, Oxford, UK), two dynamometric platforms (Kistler Instruments, Einterthur, Switzerland) and an electromyographic system (Zero Wire, Aurion, Milan, Italy) for the detection of activation of the following muscles: rectus femoris, biceps femoris, tibialis anterior and gastrocnemius. An established protocol for lower limb joint kinematics and kinetics was used [7]. Joint rotations and moments were calculated according to this protocol for each joint of both legs in the three anatomical planes.

Figure 1. Picture taken at the GA laboratory during data collection of level walking; the patient is instrumented with the reflective markers and the surface EMG electrodes.

FA was performed for replaced ankles only during a part of the stance phase of the gait cycle at the staircase, i.e from flat-foot to heel-off, by means of a standard fluoroscope (digital remote-controlled diagnostic Alpha90SX16, CAT Medical System, Rome, Italy) at 10Hz and an established technique [8]. Tibial and talar component reference frames were defined onto relevant CAD models according to the three anatomical directions, that of the insert was defined by using the 3D coordinates of the tantalum beads. Position and orientation of the three components were obtained by a semi-automatic 2D-to-3D procedure which achieves a best 3D estimation (0.5 mm/1.0° accuracy) between the projection of the 3D CAD of the component and the silhouette of this component in the fluoroscopic image [8]. Dorsi/plantar flexion, inversion/eversion and internal/external rotation, in the sagittal, frontal and transverse planes respectively, with respect to the tibia, as well as antero/posterior translation of the meniscal and talar components, were all expressed according to a standard joint convention [9].
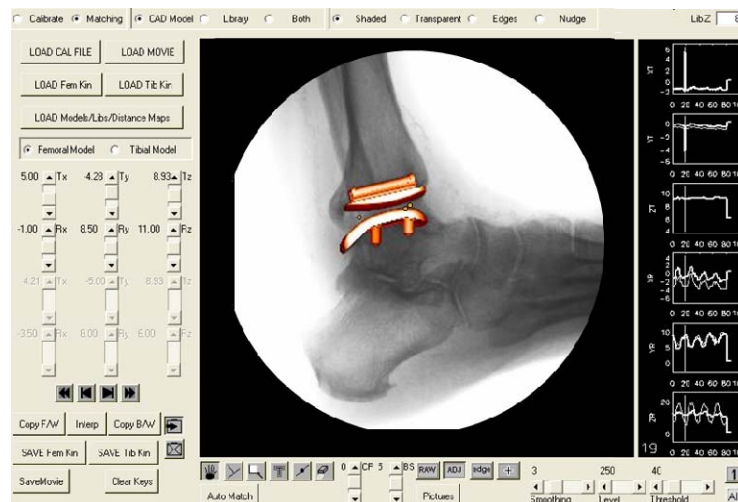

Figure 2. Screenshot from FA, during flexion against gravity. The single radiogram is analyzed together with the projections of the CAD models of the prosthesis components, and the cluster of tantulum beads; on the right hand side the time-history of the six degrees-of-freedom during that motion are shown.

3. RESULTS

In all patients, a very similar measurement of ankle flexion in the stance phase was found from the two techniques; in particular, ankle complex rotation in the sagittal plane from GA and tibiotalar flexion as observed between the two metal components from FA showed nearly the same pattern and a similar range, though with a bias difference (Figure 1). Flexion from GA was found more dorsiflexed than that from FA, likely because of the different reference frames and of the initial positions of the components into the corresponding bones.

From GA, nearly physiological ankle kinematic and kinetic patterns were observed in the contralateral side in both motor activities, whereas in the operated side these patterns were observed only during stair climbing (Table 1). A statistically significant difference between the operated and contralateral sides was found only in the hip and ankle range of flexion, and in dorsi/plantar flexion at foot strike ($p<0.05$). A better restoration of the alternate activity of tibialis anterior and of gastrocnemius was observed in stair climbing than in stair descending. From FA, the mean ranges of tibiotalar rotations at the replaced joint were 4.1° and 7.7° in flexion, 1.2° and 2.2° in inversion/eversion, and 1.5° and 2.1° in internal/external rotation, respectively during stair climbing and descending. The corresponding antero/posterior translation of the meniscal bearing with respect to the tibia was 2.1 and 3.1 mm, with statistically significant correlation with tibiotalar flexion ($p<0.05$).

In both motor activities, a statistically significant correlation was observed between the range of ankle flexion from GA and tibiotalar, i.e. between the two metal components, flexion from FA ($R<0.50$, $p<0.04$). In addition, a statistically larger range of ankle flexion from GA was found also in those replaced ankles with larger meniscal-motion ($R<0.45$, $p<0.05$). In stair descending, also the relationship between maximum ankle plantarflexion moment and the corresponding meniscal-motion was found to be statistically significant ($R=0.56$, $p=0.01$).
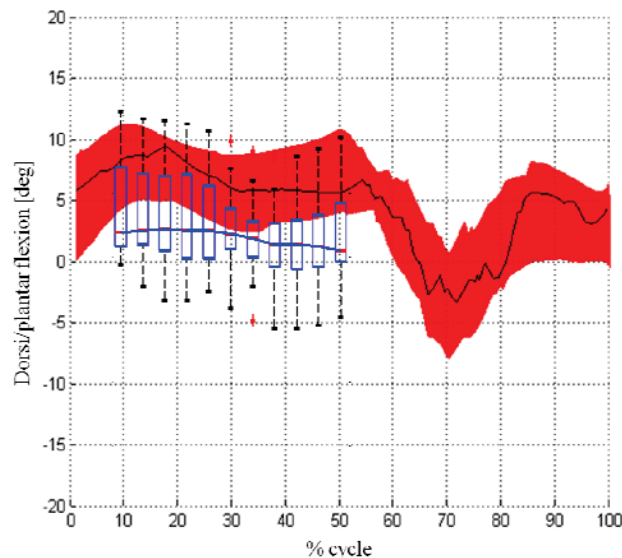

Figure 3. Patterns of dorsi/plantar flexion over all patients during stair climbing, from GA (in red; median ± 25-75% percentile) and FA (blu; box-plot with outliers).

Table 1. The main Gait Analysis parameters of the lower limb; mean ± st.dev.

	Unit	Stair climbing		Stair descending	
		operated side	*contralateral side*	*operated side*	*contralateral side*
Hip range of flex- extension	[Deg]	57.3±4.0	50.4±7.8	24.6±5.3	17.2±4.5
Max hip flexion moment	[% BW*h]	7.5±1.3	6.2±1.1	3.6±1.3	6.9±6.4
Knee range of flexion	[Deg]	55.7±6.3	56.1±4.2	79.7±7.7	76.5±5.5
Max knee extension moment	[% BW*h]	1.6±1.1	5.2±1.8	5.2±1.8	7.4±2.2
Ankle range of flexion	[Deg]	13.8±5.5	39.4±6.5	16.5±5.7	56.1±11.2
Ankle dorsi/plantar flexion at foot strike	[Deg]	5.0±4.9	12.0±5.2	-6.4±6.7	-25.4±9.2
Max ankle plantarflexion moment	[% BW*h]	6.2±1.4	7.8±1.4	6.5±1.4	8.0±1.5

4. DISCUSSION

In the present study we search for the potential additional value of assessing TAR performance in-vivo by using a combination of standard overall GA and accurate joint-specific FA measurements. This was assessment in a cohort of patients operated with a novel TAR design during stair climbing and descending. The results revealed first of all the feasibility of such a combined approach also for TAR, here reported for the first time. During the stance phase from both systems, similar patterns and range of motion were observed for the same measurements, though with an offset probably due to the different reference frames. From this proved connection between the two techniques, the other measurements can be taken as synergic observations of the same phenomenon; in particular overall lower limb functional performances from GA, together with very accurate kinematics at the replaced joint from FA.

Despite the demanding motor activities analyzed, the instrumental findings were satisfactory. Nearly normal kinematics and kinetics patterns were observed at the main joints from the comparison between operated and contralateral sides. This is true in both motor activities, though more physiological motion was found during stair climbing. Particularly from FA, nearly normal function was found restored also at the replaced ankle, with large coupled motion in the three anatomical planes. The considerable antero/posterior meniscal motion and its coupling with flexion, revealed natural motion is restored and maintained at the replaced joint according to the original claims of this TAR designers. A more physiological lower limb functional performance was found in replaced ankles from GA, combined with large meniscal motion from FA.

In conclusion, this combined measuring approach which merges two main measurement techniques provides information largely beyond to what obtained usually by either technique alone [3]. In fact, GA reports full body kinematics and kinetics but it is limited by measurement accuracy due to artifacts associated with skin interposition, and motion of the polyethylene insert cannot be tracked; on the other hand, even this small component can be tracked directly and with a sufficient accuracy by FA, though it is confined within a single joint. Therefore this combination allowed overcoming of the limitations implied in both systems, by providing an accurate and a complete 3D assessment of patients operated for TAR or other total joint replacements.

5. REFERENCES

[1] Park J.S. and Mroczek K.J., 2011. Total ankle arthroplasty. Bulletin of the NYU Hospital for Joint Diseases 69(1):27-35.

[2] Stengel D., Bauwens K., Ekkernkamp A., Cramer J.,2005. Efficacy of total ankle replacement with meniscal-bearing devices: a systematic review and meta-analysis. Arch Orthop Trauma Surg. 125:109–119.

[3] Fantozzi S., Benedetti M.G., Leardini A., et al., 2003. Fluoroscopic and gait analysis of the functional performance in stair ascent of two total knee replacement designs. Gait Posture, 17:225-34.

[4] Catani F., Ensini A., Belvedere C., et al., 2009. In-vivo kinematics and kinetics of a bi-cruciate substituting total knee arthroplasty: a combined fluoroscopic and gait analysis study. J Orthop Res, 27(12):1569-75.

[5] Leardini A., O'Connor J.J., Catani F., Giannini S., 2004. Mobility of the human ankle and the design of total ankle replacement. Clin Orthop Relat Res. 424:39–410 46.

[6] Giannini S., Romagnoli M.,O'Connor J.J., Malerba F.,Leardini A., 2010. Total ankle replacement compatible with ligament function produces mobility, good clinical scores, and low complication rates. Clin Orthop Relat Res. 468:2746-53.

[7] Leardini A., Sawacha Z., Paolini G., et al., .G., 2007. A new anatomically based protocol for gait analysis in children. Gait Posture, 26(4):560-71.

[8] Banks S.A. and Hodge, W.A., 1996. Accurate measurement of three-dimensional knee replacement kinematics using single-plane fluoroscopy. IEEE Trans Biomed Eng. 43:638–649.

[9] Grood E.S. and Suntay W.J. 1983. A joint coordinate system for the clinical description of three dimensional motions: application to the knee. J Biomech Eng. 105(2):136-44.

Reliability of the MMAAS in patients with multiple sclerosis

Murgia A. [1], Alders G. [2], Kerkhofs L. [3], Truyens V. [3], Feys P. [2], Savelberg H. [1], Meijer K. [1]

[1] Department of Human Movement Sciences, Maastricht University Medical Centre + (MUMC+), Maastricht, The Netherlands, alessio.murgia@maastrichtuniversity.nl

[2] BIOMED (Hasselt University) and REVAL (PHL), Hasselt, Belgium, peter.feys@uhasselt.be

[3] Revalidatie & MS Centrum Overpelt, Overpelt, Belgium

Keywords - multiple sclerosis; robot mediated rehabilitation; upper limb kinematics

1. INTRODUCTION

In the management of multiple sclerosis (MS) moderate exercise has been shown to improve the patients' physical fitness [1], walking [2] as well as quality of life [3], particularly through a combination of resistance and endurance training [1]. Alternative forms of exercise training both for upper and lower limbs include the use of robot-mediated therapy, which has gained support, mainly in stroke rehabilitation, as an established method to provide treatment of the same quality as that provided by a trained therapist for the improvement of motor function [4]. However in the management of MS there is still limited evidence on the benefits of this treatment. MS patients who used a robot-controlled manipulandum have been shown to adapt to haptic force fields [5], and additional evidence indicates that upper limb motor coordination also improved mainly in patients with ataxia who performed reaching tasks using, again, a robotic manipulandum [6]. Several research groups have begun to investigate the effect of upper limb training in MS using virtual reality and robot-based exercise programmes for wheelchair-bound patients who presented muscle weakness [7].

In the course of the Interreg IV project we developed a robot-mediated virtual learning environment, named I-TRAVLE (Individualized Technology and Robot-Assisted Virtual Learning Environment) that can provide upper limb therapy to subjects recovering from neurological conditions [8]. However in order to assess the effect of robot therapy on the quality of a patient's arm movements, clinically interpretable outcome measures should become available. In addition to the dynamic measurements recorded by the robot [9], kinematic measurements of compensation, muscle and joint activity provide the most objective methods to monitor and quantify clinical progresses. In order to obtain more objective measurements a portable motion capture system (Motion and Muscle Ambulatory Activity System or MMAAS) was developed to enable wireless monitoring of upper limb function in clinical settings [10]. A system's reliability is one of the pre-requisites in the clinic. In this study we present a reliability analysis on the measurements carried out using the MMAAS on a group of MS patients who received upper limb robot therapy. The aim of this study is to evaluate whether the test-retest reliability of the MMAAS is sufficient to use it as a clinical assessment tool. We discuss the significance of the results and their implication for remote monitoring of MS subjects receiving therapeutic treatment.

2. METHODS

Subjects

Six MS subjects participated in the study, 4 subjects presented muscle weakness on the left arm and 2 subjects on the right arm (age 55 ys ± 3.8 ys; EDSS score 7.3 ± 1.6; MI tested side 55.8 ± 24.5). Ethical approval was obtained for the study (Adres Ethical Committee, Overpelt, Belgium). Subjects were asked to wear a jacket where 4 MMAAS sensors (inertial and magnetic) were embedded. The sensors were located on the thorax, the cranial edge of the scapular spine, the middle of the arm facing the lateral side and on the dorsal side of the distal end of the forearm. A fifth sensor was attached to a grounded support parallel to the thorax. The arm and forearm sensors were secured with additional straps to limit their movement relatively to the skin. The setup is illustrated in Fig. 1. The axes of the different body segments were oriented according to the ISB recommendations [11]. The joint angles were calculated in the MMAAS software from the sensor data according to the procedure described in [12].

Measurement Protocol

The participants were instructed to perform a series of activities from a standardized protocol. Subjects were instructed to perform the task using the affected arm, while measurements with the MMAAS were carried out by the same investigator. In order to evaluate test-retest reliability each subject performed the protocol twice, with the jacket being removed and put back on between the two occasions. The protocol consisted of daily activities. Each activity was performed by starting and ending at the same point, indicated to the subject, while
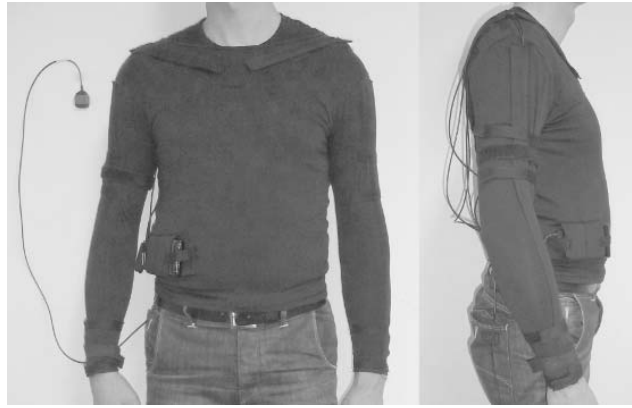
Figure 1. Front and side view of the MMAAS jackets and sensors.

4 repetitions were completed according to a set of instructions explained beforehand. Several activities from the protocol were analyzed for reliability, as described in Table 1.

Data Analysis

The parameters considered in this study were: active range of motion (*AROM*) during the task, maximum angular value, and minimum angular value. The movements considered were chest flexion, shoulder abduction, rotation and flexion, elbow flexion and elbow rotation. The values used in the reliability analysis were the means across the 4 repetitions of these parameters. The intraclass correlation coefficient (*ICC*) was used to quantify test-retest reliability: *ICC* for consistency in the two-way mixed effect model was used. The standard error of the measurement (*SEM*) was also calculated to quantify the reliability within individual subjects. The *SEM* was calculated as the square root of the error mean square term in the repeated measures ANOVA [13].

3. RESULTS

The results of the reliability analysis are reported in Table 1. Although the number of subjects was limited statistically significant results were found on a number of activity/parameter combinations. The values for the *ICC* found in this study were comparable with those found in reliability studies on 3D gait measurements using optoelectronic motion capture systems [14]. The *SEM* values were generally higher than the 2-5º error range reported in the literature for 3D gait studies [14]. *ICCs* ranging between 0.7 and 0.9 are considered acceptable in measurements with human subjects and indicate moderate to good reliability respectively [15]. However the results should be interpreted in the contexts of subject variability as explained below.

A decrease in *AROM* was observed in some subjects during the third and fourth repetition of activities involving reaching. The subjects also remarked on feeling fatigued while performing the tasks where decreasing *AROM* was observed. The movement pattern is illustrated in Fig. 2 left. This movement pattern is expected from participants affected by MS. As part of the protocol, an activity consisting solely of shoulder internal/external rotation was also analyzed for reliability but was not reported in Table 1 as the result was not significant. It was observed that the *AROM* during this activity was very small as the participants found difficult to accomplish shoulder external rotation.

4. DISCUSSION

The aim of this study was to evaluate whether the test-retest reliability of the MMAAS was sufficient to use it as a clinical assessment tool. The relative large values found for the *ICCs* indicate a good reliability (*ICC* 0.8-0.9) for most of the tasks considered. The interpretation of the *ICC* should however be carried out while considering the amount of between-subject variability [13], which in this study can be attributed to the heterogeneous movement abilities of the MS group also indicated by the variability in the MI score. Particular attention should be paid to the *SEM* to discern whether large between-subject variability is not masking poor subject consistency [13]. Based on the results showed in Table 1 it can be observed that elbow and thorax *AROM* were the movements with the highest consistency between trials, while shoulder flexion and elbow rotation *AROM* were the less consistent ones. Thus although reliability of the system is comparable to that found in 3D gait studies, subject consistency can still be reduced. In particular further research should be concentrated on assessing the influence of factors such as sensor placement, skin movement artifacts and muscle fatigue. An additional reliability study of the MMAAS has been carried out exclusively on healthy subjects using the same movement protocol described here [16]. The *ICCs* found ranged between 0.7-0.9 and are comparable with those found in this study, while the *SEM* values ranged between 2-6º and are lower, but not considerably. However, in that study statistical significance was also found for shoulder rotation.
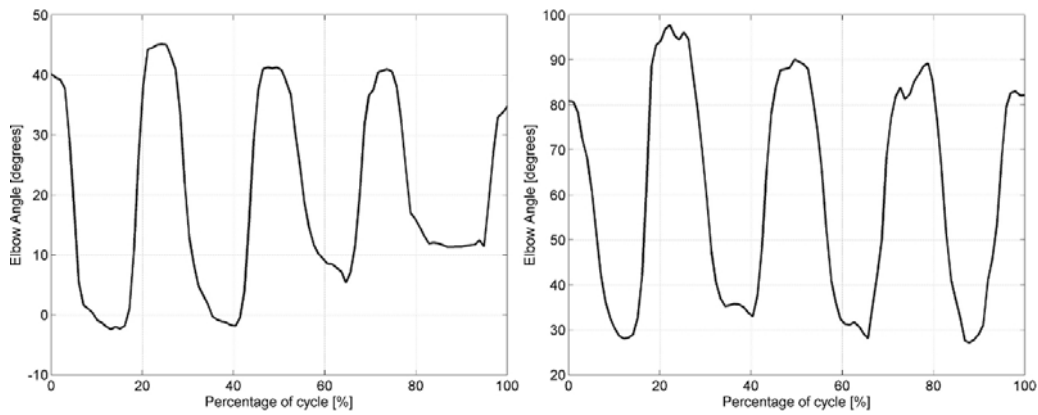
Figure 2. Elbow flexion (+) / extension (-) angle for a subject reporting fatigue during the 3rd and 4th repetition (left) and for a subject who reported no susceptibility to fatigue (right). The task considered was Reaching to the contralateral side and is described in Table 1.

Limits of the present study were the restriction in the number of subjects and the number of measurement occasions. These should be both addressed in further investigations on the clinical value of the system. In this study the test group consisted of MS subjects rather than of individuals with no impairment. This choice was made to understand the statistical consistency of the clinical measurements done using the MMAAS. In conclusion the results are comparable to those found in 3D gait using optoelectronic systems as far as the *ICC* is concerned, but should be kept in perspective by taking into account the *SEM* for specific movements. A system with reliability and validity comparable to that of an optoelectronic motion capture equipment would facilitate the assessment of patients outside laboratory setting and make home monitoring more robust. Future developments will be focused on a validity study and on extending the clinical reliability study to a group of subjects suffering from stroke.

Table 1. Test-retest reliability results during selected activities.

Activity	*Parameter*	*ICC*	*SEM (degrees)*
Sitting with arm and hand in the anatomical position, abduct the arm up to 120º and return to the initial position	Shoulder Abduction/Adduction *AROM* (between thorax and arm)	0.866 *(p<0.01)*	7.7
"	Max Shoulder Abduction	0.918 *(p<0.01)*	7.8
Sitting with arm and hand in the sagittal plane, flex the arm up to 120º and return to the initial position	Shoulder Flexion/Extension *AROM* (between thorax and arm)	0.808 *(p<0.05)*	11.0
"	Max Shoulder Flexion	0.812 *(p<0.05)*	7.9
Sitting with elbow flexed at 90º, execute full supination-pronation	Elbow Pronation/Supination *AROM*	0.764 *(p<0.05)*	10.9
Sitting with elbow flexed at 90º, reach from middle to contralateral side at arm length and return to the initial position. Target was at shoulder height and one shoulder width	Throax Flexion/Extension (relative to grounded support)	0.795 *(p<0.05)*	2.5
"	Shoulder Flexion/Extension *AROM*	0.782 *(p<0.05)*	5.7
"	Elbow Flexion/Extension *AROM*	0.916 *(p<0.01)*	4.1
"	Max Elbow Flexion	0.809 *(p<0.05)*	7.1
Sitting with elbow flexed at 90º, reach from middle to mouth and return to the initial position	Elbow Flexion/Extension *AROM*	0.690 *(p<0.05)*	4.9
"	Max Elbow Flexion	0.737 *(p<0.05)*	6.1

5. ACKNOWLEDGMENT

6. REFERENCES

[1] Dalgas, U., Stenager, E., Ingemann-Hansen, T., 2008. Multiple sclerosis and physical exercise: recommendations for the application of resistance-, endurance- and combined training. Multiple Sclerosis 14, 35-53..

[2] Snook, E.M., Motl, R.W., 2009. Effect of exercise training on walking mobility in multiple sclerosis: a meta-analysis. Neurorehabilitation and Neural Repair 23, 108-116.

[3] Motl, R.W., Gosney, J.L., 2008. Effect of exercise training on quality of life in multiple sclerosis: a meta-analysis. Multiple Sclerosis 14, 129-135.

[4] Lo, A.C., et al., 2010. Robot-Assisted therapy for long-term upper-limb impairment after stroke. New England Journal of Medicine 362, 1772-1783.

[5] Casadio, M., Sanguineti, V., Solaro, C., Morasso, P.G., 2007. A haptic robot reveals the adaptation capability of individuals with multiple sclerosis. The International Journal of Robotics Research 26, 1225-1233.

[6] Carpinella, I., Cattaneo, D., Abuarqub, S., Ferrarin, M., 2009. Robot-based rehabilitation of the upper limbs in multiple sclerosis: feasibility and preliminary results. Journal of Rehabilitation Medicine 41, 966-970.

[7] Gijbels, D., et al., 2011. The Armeo Spring as training tool to improve upper limb functionality in multiple sclerosis: a pilot study. Journal of NeuroEngineering and Rehabilitation 8:5.

[8] Notelaers, S., et al., 2010. Data Management for Multimodal Rehabilitation Games. In 2010 Workshop on Database and Expert Systems Applications, Bilbao, Spain, pp. 137-141.

[9] Harwin, W.S., Murgia, A., Stokes, E.K., 2011. Assessing the effectiveness of robot facilitated neurorehabilitation for relearning motor skills following a stroke. Medical & Biological Engineering & Computing 49, 1093-1102.

[10] Murgia, A., Kerkhofs, V., Savelberg, H., Meijer, K. 2010. A portable device for the clinical assessment of upper limb motion and muscle synergies. In 32nd Annual International Conference of the IEEE EMBS, Buenos Aires, Argentina, pp. 931-934.

[11] Wu, G., et al., 2005. ISB recommendation on definitions of joint coordinate systems of various joints for the reporting of human joint motion - Part II: shoulder, elbow, wrist and hand. Journal of Biomechanics 38, 981-992.

[12] Roetenberg, D., Luinge, H.J., Baten, C.T.M., Veltink, P.H., 2005. Compensation of magnetic disturbances improves inertial and magnetic sensing of human body segment orientation. IEEE Transactions on Neural Systems and Rehabilitation Engineering 13, 395-405.

[13] Weir, J.P., 2005. Quantifying test-retest reliability using the intraclass correlation coefficient and the SEM. Journal of Strength and Conditioning Research 19, 231-240.

[14] McGinley, J.L., Baker, R., Wolfe, R., Morris, M.E., 2009. The reliability of three-dimensional kinematic gait measurements: A systematic review. Gait and Posture 29, 360-369.

[15] Batterham, A.M., George, K.P., 2003. Reliability in evidence-based clinical practice: a primer for allied health professionals. Physical Therapy in Sport 4, 122-128.

[16] Murgia, A., Jaspers, E., Savelberg, H., Desloovere, K., Meijer, K., 2011. Reliability of the MMAAS: A wearable system for monitoring motion and muscle synergies in clinical settings. In XXIIIrd Conference of the International Society of Biomechanics, Brussels, Belgium.

Assessment of the mechanical power developed by a manual wheelchair user during ambulation in the field

Sauret C. [1,2], Vaslin P. [2], Dumas R. [3], Bascou J. [1,4], Pillet H. [4],
Chèze L. [3], Cid M. [5], Lavaste F. [1,4]

[1] CERAH, Institution Nationale des Invalides, Woippy, France
[2] LIMOS, Université Blaise Pascal, Clermont-Ferrand, France
[3] LBMC, Université Claude Bernard Lyon 1 - IFSTTAR, Lyon, France
[4] LBM, Arts et Métiers ParisTech, Paris, France
[5] LMP, Université Bordeaux 1, Bordeaux, France

Keywords: manual wheelchair, mechanical power, energy transfert, rehabilitation

1. INTRODUCTION

Assessing the mechanical power developed by the user of a manual wheelchair (MWC) during daily ambulation is an important issue for both scientists and clinicians as it highlights the user's difficulties when he moves in his environment. On laboratory ergometers, this power was initially computed from the opposite of the rolling resistance during propulsion at a supposed "constant" speed [1]. Currently, this power is assessed by the power of the handrim (HR) propelling torque measured with one instrumented wheel mounted on one side of a MWC [1]. Although this latter method takes into account the obvious propulsive actions of the user on the instrumented HR, three assumptions are made: 1) the power computed on one side is assumed to be half of the total power produced by the user; 2) the powers of the user's actions on the seat, backrest and footrest are neglected; and 3) the kinetic power due to user's movements is also neglected.

The aim of this paper is to present a new method, which relies on classical mechanical principles, for assessing the total mechanical power developed by the user during MWC ambulation in the field.

2. APPLICATION OF MECHANICAL PRINCIPLES

In order to assess the mechanical power developed by any mechanical system, it is useful to isolate this system and to list all the external mechanical actions exerted on this system. Using this approach for the {user} system during actual MWC ambulation, the external actions applied on the {user} are his weight ($\overline{w}$), the reaction wrenches of both HRs and those of the seat, the backrest and the footrest. The air drag can be neglected with respect to the velocity reached during daily ambulation [2].

On the other hand, according to classical mechanics, the {user} kinetic power (P_{kin}) is the time differentiation of the {user} kinetic energy and it is equal to the sum of the powers of all the external actions (P_{ext}) and of all the internal actions (P_{int}):

$$P_{kin} = P_{ext} + P_{int} \qquad (1)$$

where P_{int} is the resulting power of all the mechanical actions produced by the user's musculo-skeletal system. Thus, P_{int} corresponds to the mechanical power developed by a MWC user and can be calculated from the following equation:

$$P_{int} = P_{kin} - P_{ext} \qquad (2)$$

In this expression, P_{ext} represents the sum of the power of the user's weight ($P_{(\overline{w})}$) and the resulting power of all the reaction wrenches exerted by the MWC on the {user} on both HRs, the seat, the backrest and the footrest ($n_D = 5$), which is the opposite of the power put by the user in the MWC (Pl) [3]. The resulting power Pl is calculated by the sum of the n_D co-moments between the wrenches of mechanical actions {T_A} exerted by the user on the MWC and the respective kinematics wrenches {T_C}:

$$PI = \sum_{k=1}^{n_D} \left\{ T_{C_k} \right\} \otimes \left\{ T_{A_k\,User \rightarrow MWC} \right\} \qquad (3)$$

So, P_{ext} is given by equation 4:

$$P_{ext} = P(\vec{w}) - PI \qquad (4)$$

Besides, the user's kinetic power (P_{kin}) is calculated from the time differentiation of the half sum of the n_S co-moments between the respective kinetics $\{T_K\}$ and kinematics $\{T_C\}$ wrenches of the n_S {user} segments:

$$P_{kin} = \frac{1}{2\,dt} \sum_{i=1}^{n_S} \left\{ T_{K_i} \right\} \otimes \left\{ T_{C_i} \right\} \quad (5)$$

Then, the power of all the internal actions produced by the user can be calculated from the following expression:

$$P_{int} = \frac{1}{2\,dt} \sum_{i=1}^{n_S} \left\{ T_{K_i} \right\} \otimes \left\{ T_{C_i} \right\} - P(\vec{w}) + \sum_{k=1}^{n_D} \left\{ T_{C_k} \right\} \otimes \left\{ T_{A_k\,User \rightarrow MWC} \right\} \quad (6)$$

3. MATERIALS AND METHODS

In order to assess P_{int} during actual propulsion on a horizontal floor, the mechanical actions (i.e. forces and torques) applied by the user on both HRs and on the {seat + backrest + footrest} system of an instrumented MWC (FRET-1) [4] were measured with three six-component dynamometers (TSR-mesures, France). Kinematics of both rear wheels and of the frame was computed from the measurements of two angular potentiometers (Spectrol 601-1045, Vishay, USA) fixed on rear wheels axles, while assuming the MWC rolled without slipping. All sensors data were synchronized and sampled at 500 Hz using a 16-bit A/D conversion card (DAQCard-6036E, National Instruments, USA) plugged into an embedded mini-computer (TC1100, Hewlett-Packard, USA). The data were transmitted in real time to a remote computer (M5200N, ASUS, Taiwan) using IEEE 802.11b and TCP/IP wireless transfer protocols, where they were recorded.

The {user} was segmented into 16 segments (2 feet, 2 legs, 2 thighs, 1 pelvis, 1 trunk segmented in two parts: abdomen and thorax, 1 head & neck, 2 arms, 2 fore-arms, 2 hands). The body segment inertial parameters were assessed from [5-6] in segment reference frames recommended by the International Society of Biomechanics [7-9]. Kinematics of user's segments was determined from the measurement of the 3D positions of 54 reflective markers placed on the user's skin, recorded by a motion capture system (Motion Analysis, USA) composed of 6 digital cameras recording at a video rate of 100 Hz.

Synchronization between the measurements of the instrumented MWC and those of the motion capture system was processed *a posteriori* from signals resulting from a little stroke on the left instrumented HR with a sledge-hammer equipped with a reflective marker.

Kinematic data provided by the motion capture system were used to compute the kinetic and kinematic wrenches of the user's segments (n_S = 16), and then P_{kin} *according to equation (1)*. These data were also used to compute the vertical velocity of the user's center of mass, and then $P(\vec{w})$. Dynamic and kinematic data provided by the instrumented MWC were used to compute the wrenches of mechanical actions applied by the user on the {seat + footrest + backrest} system and on both HRs (n_D = 3), and the associated kinematic wrenches. These wrenches were then used for computing PI according to equation (3). Finally, the resultant mechanical power produced by the user (P_{int}) could be calculated from equation (6).

The outcomes of this method are illustrated by the results obtained by one able-bodied subject familiar with MWC locomotion (26 y.o., 1.75 m, 63.0 kg) who performed 8 trials of a 7-m long straightforward displacement on a level floor covered with a short-pile carpet. During each displacement, the subject crossed the calibrated volume of the motion capture system allowing the measurement of the subject's kinematics during one complete propulsion cycle. Each trial was performed at a self-selected comfortable velocity, and it began at least two pushes before the MWC went into the calibrated volume, and finished one or two pushes after it was out of this volume.

4. RESULTS

Results of the 8 trials showed a cycle mean velocity of 1.21 m/s. The cycle time was 1.14 s (±0.04 s) in which push and free-wheeling phases represented 46 and 54 % of the cycle time (±3 %), respectively. However, the time course of the kinetic power (P_{kin}) varied so much that it would not have had any sense to present the results of a mean cycle. Consequently, the following analysis is only focused on one trial (the first one) without any *a priori* on the results obtained in this trial.

Within the propulsion cycle, the internal power (P_{int}) showed wide variations with values ranging from 3 to 104 W during the push phase and from -13 to 46 W during the free-wheeling phase (Fig. 1, left). P_{int} strongly increased during the first three quarters of the push phase before suddenly decreasing during the last quarter, though remaining positive. During the free-wheeling phase, P_{int} continued to decrease and became negative during a few instants before it became positive again until the end of the cycle. In average, P_{int} was 51 W during the push phase, 12 W during the free-wheeling phase and 31 W for the whole cycle.
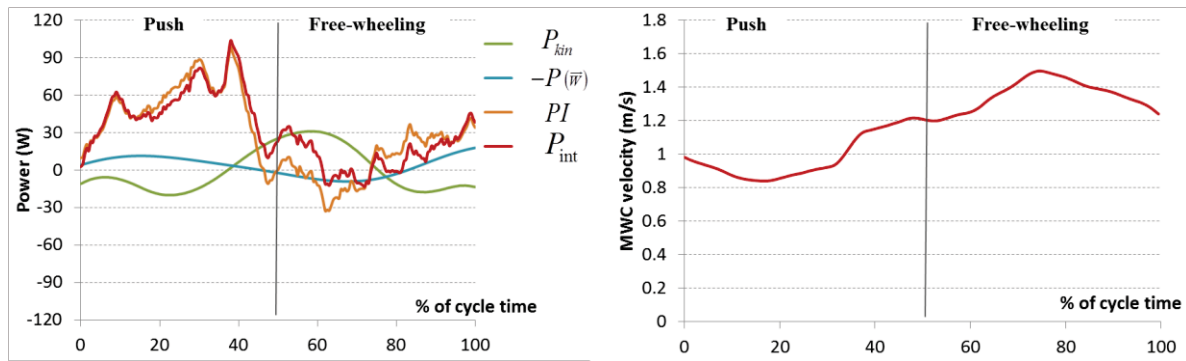

Figure 1. Normalized time course of the {user} internal power and its components (left), and of the MWC linear velocity (right).

When detailing the components of P_{int} expressed in equation 6, it can be shown that during the push phase, P_{int} was principally communicated to the MWC. Indeed, during the push phase, P_{int} almost followed PI, which is the sum of the power put by the user into the HRs, the seat, the backrest and the footrest. However, PI was slightly higher than P_{int} during the first three quarters of the push phase and slightly lower during the last quarter. During the same period, P_{kin} reached negative values (-20 W) during the first three quarters and positive values (24 W) during the last quarter. During all the push phase, the power required to raise up the {user} center of mass ($-P_{(\overline{W})}$) exibited positive values while it became negative at the beginning of the free-wheeling phase before reaching again positive values at the end of this phase.

Finally, the {user} internal power induced visible effects on the MWC linear velocity (Fig. 1, right), which slightly decreased during the first third of the push phase, reaching 0.84 m/s. Then, it increased until the first half of the free-wheeling phase, reaching 1.50 m/s, before decreasing until the end of the cycle. At the end of the propulsion cycle, the MWC velocity was about 0.2 m/s higher than at the beginning.

5. DISCUSSION

Despite the propulsion cycle analyzed in this paper cannot be generalized to the other trials of this study, the obtained results are original in comparison to those related in the literature. Indeed, the method has shown that the user did not only produce mechanical power ($P_{int} > 0$) during the push phase but also during the free-wheeling phase, which can no longer be considered as a recovery phase or a resting time. In addition, during a short period of the free-wheeling phase, the subject himself dissipated ($P_{int} < 0$) a small part of the energy he had produced before.

The analysis of the components of P_{int} reveals that the energy put by the user into the MWC (PI) was partly due to a transfer of the {user} kinetic energy ($P_{kin} < 0$) and inversely. Finally, both at the beginning and at the end of the propulsion cycle, the MWC slowed down whereas PI was positive and almost equal to P_{int}, which indicates that the power produced by the user is not sufficient to compensate the energy lost in the rolling resistance.

The main difficulty of this study was to obtain a reproducible cycle when propelling a MWC on the floor, which is expressed by the variable time courses of P_{kin} between trials. One explanation could be that the analyzed cycles were not performed at a steady state but at a transient rhythm. This hypothesis is supported by the difference noted between the MWC velocity at the beginning and at the end of the propulsion cycle of trial 1. This problem could be solved by increasing the distance before the MWC crossed the motion capture calibrated volume, but that was not possible in the room where these trials were recorded.

6. CONCLUSION

The method presented in this paper demonstrated that the strict application of the classical mechanical principles to the {user} system allows to better understand MWC propulsion than previous methods related in the specific literature [1]. For instance, this method enlightens on the energy transfers between the user and his MWC.

However, since this method implies to determine the {user} kinetic power, its accuracy depends on 1) the refinements of user's segmentation model, 2) the body segment inertial parameters, and 3) the markers movements (skin movements and numerical filtering method).

7. REFERENCES

[1] van der Woude, LHV, Veeger, HEJ, Dallmeijer, AJ, Janssen, TWJ, Rozendaal, LA. 2001, Biomechanics and physiology in active manual wheelchair propulsion. Med Eng Phys. 23, pp. 713-733.

[2] Hofstad, M, Patterson, PE. 1994, Modelling the propulsion characteristics of a standard wheelchair. J Rehabil Res Dev. 31(2), pp. 129-137.

[3] Sauret, C, Bascou, J, Pillet, H, Lavaste, F, Vaslin, P. (submitted) "Asseessing "power input" of the manual wheelchair user during real life ambulation". 18th ESB congress, 1-4 July 2012, Lisbon.

[4] Dabonneville, M, Vaslin, P, Kauffmann, P, de Saint Rémy, N, Couétard, Y, Cid, M. 2005. A self-contained wireless wheelchair ergometer designed for biomechanical measures in real life conditions. Technology and Disability. 17(2), pp. 63-76.

[5] Dumas, R, Chèze, L, Verriest, JP. 2007. Adjustments to McConville et al. and Young et al. body segment inertial parameters. J Biomechanics. 40(3), pp. 543-553.

[6] Dumas, R. 2007. Complements to "Adjustments to McConville et al. and Young et al. body segment inertial parameters. [J Biomech. 40(3) 543-553]". Not published.

[7] Wu, G, Cavanagh, PR. 1995. ISB recommandations for standardization in the reporting of kinematic data. J Biomechanics. 28(10), pp 1257-1261.

[8] Wu, G, Siegler, S, Allard, P, Kirtley, C, Leardini, A, Rosenbaum, D, Whittle, M, D'Lima, DD, Cristofolini, L, Witte, H, Schmid, O, Stokes, I. 2002. ISB recommandation on definitions of joint coordinate system of various joints for the reporting of human joint motion – Part I: ankle, hip and spine. J Biomechanics. 35(4), pp. 543-548.

[9] Wu, G, van der Helm, FCT, Veeger, HEJ, Makhsous, M, van Roy, P, Anglin, C, Nagels, J, Karduna, AR, McQuade, K, Wang, X, Werner, FW, Buchholz, B. 2005. ISB recommandation on definitions of joint coordinate system of various joints for the reporting of human joint motion – Part II: shoulder, elbow, wrist and hand. J Biomechanics., 38(5), pp. 981-992.

Evaluating equipment constraints in surgery

Motion analysis of microsurgeon posture and joint loads

Yu D. [1], Sackllah, M. [1], Woolley C. [1], Kasten S. [2], Armstrong T. [1]

[1] Dept. of Industrial and Operations Engineering, University of Michigan, Ann Arbor, USA
[2] Dept. of Surgery, University of Michigan, Ann Arbor, USA

The long-term aim of this work is to minimize postural stress and fatigue in surgeons through the design of equipment and procedures. A pilot laboratory study was conducted to evaluate the use of motion tracking for collecting posture data for simulated surgical tasks and developing a biomechanical model that can be used to interpret and apply motion-tracking data. Sixteen subjects participated in the study and performed surgical tasks on a microscope and a flat-panel display. Motion tracking analysis found average neck postures for both visual displays to be close to neutral. The standard deviation of angles is higher in flat-panel displays, which may indicate less postural constraints. The less postural constraints from the flat-panel displays may allow more movement and minimize discomfort.

Keywords- motion analysis in healthcare; surgery; posture; biomechanical modeling; visual displays;

1. INTRODUCTION

Motion tracking is an important tool for understanding and controlling stressful work postures that can adversely affect work performance. Constrained postures are a major cause of localized fatigue and discomfort in many occupations [1, 2, 3]. Health care and in particular microvascular surgery stand out. The constraints imposed by surgical equipment necessary to complete the surgery limit the degree of freedoms especially in their head, neck, back, and upper extremities [4]. The arrows on Figure 1 show some key examples of posture constrains in the operating rooms. For example, due to the small work area of the surgery, the patient's body imposes constraints on where surgeons can place their hands. The presence of the operating table constrains surgeons' hips and lower body. The last arrow illustrates a critical continuous constraint imposed by microscope equipment where movement of the neck and upper body prevents access to the visual information on the work area. Previous investigators [5, 6] have proposed a simple model that shows how the muscle forces are required to support the head and neck increase with increasing neck angle. These models can be used to interpret and apply motion-tracking data for design of work equipment and procedures.
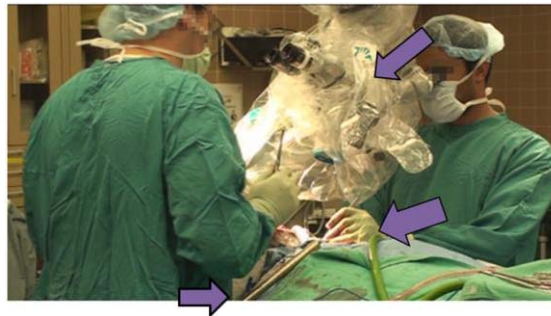

Figure 1. Operating room view of surgeons performing microsurgery. Purple arrows illustrates some key areas of postural constraints.

Several studies have used motion analysis to investigate ergonomic problems in healthcare. Van Veelen et al. [7, 8] used motion analysis to investigate optimal placements of operating table and monitors and found improved postures with flat-screen monitors and operating tables at 0.8 of the surgeon's elbow height. Galleano et al. [9] used motion studies to support their recommendation of armrests to improve surgeon comfort. This study will focus on how different magnifying visual equipment used in surgery affects postures.

The long-term aim of this work is the design of equipment and procedures that will minimize postural stress and fatigue for surgeons. But there are reasons that make studying surgeons difficult: Surgery is a demanding task, distractions can have profound consequences, and surgeon availability is very limited. For these reasons, it is important that study protocols be well developed before they are introduced into an operating room. Towards this end we first conducted a pilot study in laboratory to evaluate the use of motion tracking for collecting posture data for simulated surgical tasks and developing a biomechanical model that can be used to interpret and apply motion-tracking data.

2. METHODS

Study Population

Eight male and eight female subjects were recruited with no prior surgical experience. The study was approved by the University of Michigan Human Subjects Review Board and written informed consent was obtained from each subject. The mean age of the participants was 21.8 years old ± 2 years. The mean height was 170 cm ± 10.15 cm. All subjects were right-handed. Sixty-three percent of subjects wore corrective lenses and eighty-one percent of subjects had previous experience with microscopes.

Test Procedures

In this study, four treatments were studied: stereoscopic microscope, monocular microscope, 2-dimensional flat-panel display, and 3-dimensional (3D) flat-panel display. For the purposes of demonstrating how motion tracking can be used to evaluate equipment and postural stresses, treatment comparisons will be limited to the stereoscopic microscope and the 3D flat-panel display. A 4x4 latin square design with four replications was used to minimize order effects. Each subject performed two tasks on each treatment for a total time of 144 minutes. First task was a pegboard transfer task where subjects transfer 1-2mm silicon tubes from one side of a pegboard to the other side. The second task is a threading task where subjects the silicon tubes into a 0.29mm diameter thread.

Equipment

For the microscope treatment, a binocular lab-scope (Sciencescope) with 5x magnification was used. For the 3D flat-panel treatment, a 101.6 cm 3D flat-panel display (Samsung, Model: UN40C7000WF) was used. Real-time video was streamed and interlaced from two synchronized microscope cameras. Subjects wore 3D active-shutter glasses to view the 3D video.

Posture and motion data was gathered using Northern Digital Inc. (NDI) Optotrak Certus tracking system with two position sensors. Thirty-one markers were affixed to each subject on his/her wrists, elbows, arms, shoulders, neck, head, back, hips, and knees. Three-dimensional marker locations were sampled at one hundred hertz using NDI First Principles software (v1.2.2).

Data Analysis

Posture angles and locations were analyzed using MATLAB software (MathWorks Inc.). Biomechanical modeling and strength prediction was created using 3D Static Strength Prediction Program (3DSSPP) [10].

3. RESULTS

The following figures and tables show results from the motion analysis of subjects while performing the experimental tasks. Comparisons between microscope and the flat-panel displays will be made to show how motion tracking can be used to evaluate surgical equipment.

Time Plot Analysis

A representative time plot for the Neck Flexion for one subject is shown in Figure 1. Overall, the flat-panel display shows higher variations around neutral than the traditional microscope display. The subject begins the task in flexion for both displays; however, the subject extends and flexes his neck more frequently in the flat-panel than the microscope.
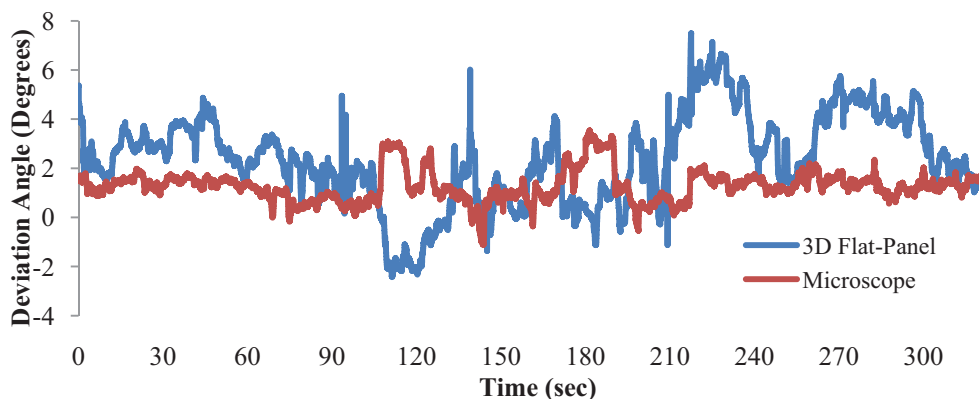

Figure 1: Time plot for Neck Flexion for one subject. Positive angles represent flexion and negative angles represent extension.

Histogram Analysis

The results from ten subjects are averaged and shown in Figure 2. Although histograms are centered around 1.5 degrees, the histogram for the flat-panel display is much wider than the microscope. The standard deviation is higher for the flat panel visualization method than the microscope.
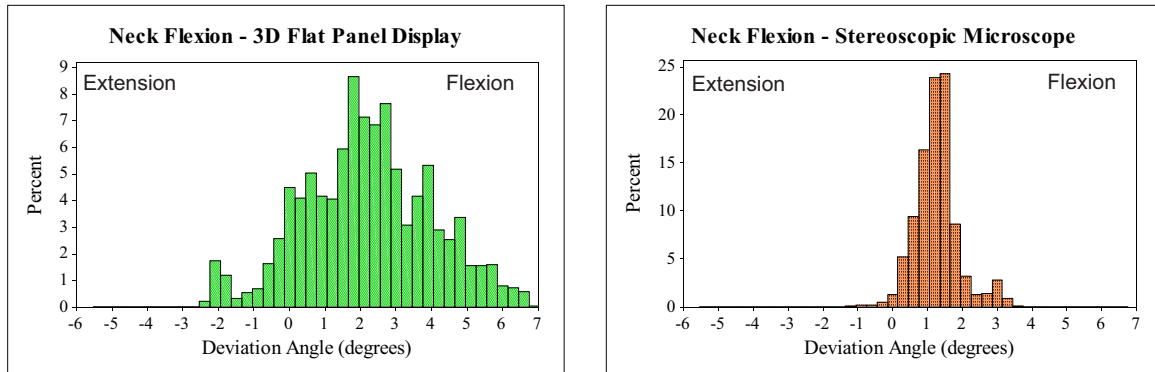

Figure 2: Histograms for average neck flexion for ten subjects. Positive angles represent flexion and negative angles represent extension.

The descriptive statistics from motion analysis are shown in Table 1. The average angles from all subjects show that 3D visualization method has the highest flexion angle at 2.19 degrees. The average neck angle for subjects using the microscope is 1.28 degrees which is lower than the alternative display.

Table 1. Mean Flexion Angles. Flexion is positive and extension is negative.

	Visualization Methods	
	3D Display (°)	Stereoscopic Microscope (°)
Neck	2.19 ± 1.82	1.28 ± 0.63

By using the angles obtained through motion analysis, biomechanics can be used to model how the differences in angles can influence the stresses experienced in the joints. Figure 3 is a 3DSSPP model that illustrates how the different angles affect neck joint loads.
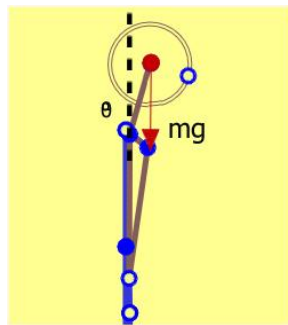

Figure 3. Biomechanic model from 3DSSPP software showing how angle affect joint loads

Using equation (1, 2) and assuming constant mass of the head and fixed head-neck length (r), the calculations reveal that the average moment the neck joint experiences on the flat-panel is 1.71 times the moment on the microscope when using the average angles subjects assumed while working with each display.

$$\text{Moment} = \text{Mass}_{head} * \text{gravity} * r * \sin(\theta_{Microscope}) \qquad (1)$$

$$\text{Moment} = \text{Mass}_{head} * \text{gravity} * r * \sin(\theta_{Flat\text{-}Panel}) \qquad (2)$$

4. DISCUSSION

In a similar study [11], motion analysis using MaxTraq software (Innovision Systems Inc) found that average neck flexion angles in the microscope is 36° and a flat panel display is 16°, creating neck moments that are two times higher in the microscope than the flat-panel display. Although this study also found differences in

average neck moments, the relatively neutral neck postures during both treatments may not be as clinically significant. However, this methodology can be used to study extreme neck angles and other body segments. Although this pilot study resulted in different neck postures and neck joint moments, the trend in the range of motion is consistent in both studies. Subjects were observed assuming a wider range of neck angles in the flat-panel display than in the microscope. This observation supports that the flat panel displays imposes less postural constraints than using the microscopes, which may reduce fatigue by allowing more posture changes [3]. Whether the increase degrees of freedom from flat-panel displays are associated with lower discomfort and fatigue can be a topic for future research.

This pilot study showed how motion analysis tools can study equipment used in healthcare. Motion tracking was able to show that flat-panel displays allow subjects much more freedom to move while performing the task. Additionally, this study showed how motion tracking can be used in conjunction with biomechanics modeling to investigate postural stresses from surgical equipment. Motion and angle data can be applied to modeling software like 3DSSPP to estimate joint loads and worker capabilities.

Some limitations of this study include the use of surgical skill tasks and the study's controlled laboratory environment. A major difference between this study and a previous study [11] are the differences in tasks which resulted in differences in postures. Postures which subjects assume may varies while performing these different tasks, indicating that future studies may need to focus on surgical procedures to obtain more representative data of surgeon postures. However, due to high demands of surgery, costly consequences of distractions and surgeon availability procedures and data collection must be developed in a laboratory setting. Several steps are needed before this system can be applied in the operating room. Obstructions from motion tracking markers must be minimized and alternatives to microscope equipment (like 3D flat-panels) must be improved so surgeon performance does not diminish while using alternative displays.

5.   ACKNOWLEDGMENT

6.   REFERENCES

[1]   Berguer, R., G. T. Rab, H. Abu-Ghaida, A. Alarcon, & J. Chung (1997). "A comparison of surgeons' posture during laparoscopic and open surgical procedures." Surgical endoscopy **11**(2): 139-142.

[2]   Park, A., G. Lee, F. Seagull, N. Meenaghan, & D. Dexter (2010). "Patients benefit while surgeons suffer: an impending epidemic." Journal of the American College of Surgeons **210**(3): 306-313.

[3]   Bernard, B.P. Musculoskeletal disorders and workplace factors: a critical review of epidemiologic evidence for work-related musculoskeletal disorders of the neck, upper extremity, and low back, Department of Health and Human Services, National Institute for Occupational Safety and Health, Cincinnati, OH (1997).

[4]   Yu, D., M. Sackllah, et al. "Alternative 2D and 3D Visualization Methods for Microsurgery." Proceedings of the Human Factors and Ergonomics Society Annual Meeting **55**(1): 715-719.

[5]   Harms-Ringdahl, K., J. Ekholm, K. Schuldt, G. Nemeth, & U. Arborelius (1986). "Load moments and myoelectric activity when the cervical spine is held in full flexion and extension." Ergonomics **29**(12): 1539.

[6]   Armstrong, T. J., M. O. Bengt Jonsson, et al. (1993). "A conceptual model for work-related neck and upper-limb musculoskeletal disorders." Scand J Work Environ Health **19**: 73-84.

[7]   Galleano, R., F. Carter, S. Brown, T. Frank, & A. Cuschieri (2006). "Can armrests improve comfort and task performance in laparoscopic surgery?" Annals of surgery **243**(3): 329.

[8]   Veelen van, M. A., Jakimovicz, J. J., Goossens, R., Meijer, D. W., & Bussmann, B. J. (2002). Evaluation of the usability of two types of image display systems during laparoscopy. *Surg Endosc* , 674-678.

[9]   Veelen van, M. A., Kazemier, G., Koopman, J., Goossens, R., & Meijer, D. W. (2002). Assessment of the Ergonomically Optimal Operating Surface Height for Laparoscopic Surgery. *Journal of Laparoendoscopic and advanced surgical techniques* , 47-52.

[10] Chaffin, D.B.; "Biomedical Modeling for Simulation of 3D Static Human Exertions;" Chapter in Computer Applications in Ergonomics, Occupational Safety and Health; Elsevier Publishers, B.V., 1992.

[11] Yu, D., Sackllah, M., Wooley, C., Kasten, S. J., & Armstrong, T. J. (2012). Quantitative Posture Analysis of 2D, 3D and Optical Microscope Visualization Methods for Microsurgery Tasks. 18th World Congress on Ergonomics. Recife, Brazil Feb. 2012,

Changes in shoulder kinematics of transradial amputees following the use of multi-grip prosthetic hands: a case study

Parel I [1,2], Cutti AG[1], Verni G. [1]

[1] Centro Protesi INAIL, Vigorso di Budrio, Bologna, Italy
[2] DI3, University of Trieste, Trieste, Italy

Keywords-component; Prosthetic hand, scapula kinematics, ADL

1. INTRODUCTION

In most daily activities upper limb and trunk have the goal to position and orient the hand in such a way that the hand can effectively and efficiently reach/grasp a desired object and transport it to the aimed target. When a prosthetic joint with intrinsic motor or sensorial limitations replaces either the end-effector or one of the joints in the upper-limb chain, compensatory movements take place in the remaining joints. Commonly, transradial amputees using a myoelectric prosthesis need to compensate the loss of the wrist flexion-extension movement and the availability of a single "tri-digital" pinch, resulting in non-physiological movements of elbow, shoulder, trunk and neck [1]. It is questioned to which extent the availability of more gripping patterns in the prosthetic hand can restore a more physiological shoulder kinematics during the execution of common activities.

2. MATERIALS AND METHODS

A case study was conducted assessing the upper limb kinematics of a transradial amputee fitted with both a standard Otto-Bock Digital Twin hand (DT) and the novel Otto-Bock prosthetic hand named "Michelangelo" (M). The Michelangelo hand features are the wrist flexion-extension kinematics through a passive frictioned joint and three gripping patterns (i.e. lateral, tri-digital and pinch grip).

A 50-year-old male transradial amputee (GS) participated in this experiment after giving his informed consent. He has been using a myoelectric prosthesis for more than 15 years, for about 8 hours a day.

His affected side scapulo-thoracic, girdle-thoracic, humero-thoracic, elbow and wrist kinematics was measured in two sessions through an optoelectronic system (Vicon Motion Systems, UK): the first session with DT and the second session with M, after 3 months of exclusive use. Twenty-six reflective markers were positioned over the upper limb segments (head, thorax, humerus, forearm and hand) [2] and the scapula kinematics was assessed by means of an acromion cluster [3] (Fig. 1). During each session he performed standardized ADL tasks sitting on a chair in front of a table in a predefined position (knee flexed of 90°, wrist hold on the edges of the table with the elbow flexed of 90°). Among the ADLs, the subject performed a1) Jar transfer activity and 2) a Carton pouring task based on the SHAP scale [4]; 3) a task named Disk task, which consists in moving back and forth 3 times a Minnesota test disk over the table, from an area in front of the prosthetic hand to an area in front of the controlateral side. In order to have a reference for the kinematics, the sound side was collected too, in a third session.

Figure 1 Marker-set for the motion analysis based on an optoelectronic system

3. RESULTS

Regarding the Jar task, scapula and humerus kinematic patterns are reported in Fig. 2. The whole movement was divided into 6 phases, which were time normalized: 1) reaching, 2) holding and transport, 3) back to starting position, 4) reaching, 5) holding and transport, and 6) back to starting position. The percentages of movements were based on the sound side timing. The most noticeable differences are that with the DT hand the patient approaches the object in adduction and with a relevant posterior tilting. On the contrary, with the sound and the M hand, the patient approaches the object in abduction and without almost relying on scapula tilting. Regarding the overall time taken to perform the activity, with the sound side the mean duration was 7s, while it was about 15s with both DT and M hands.
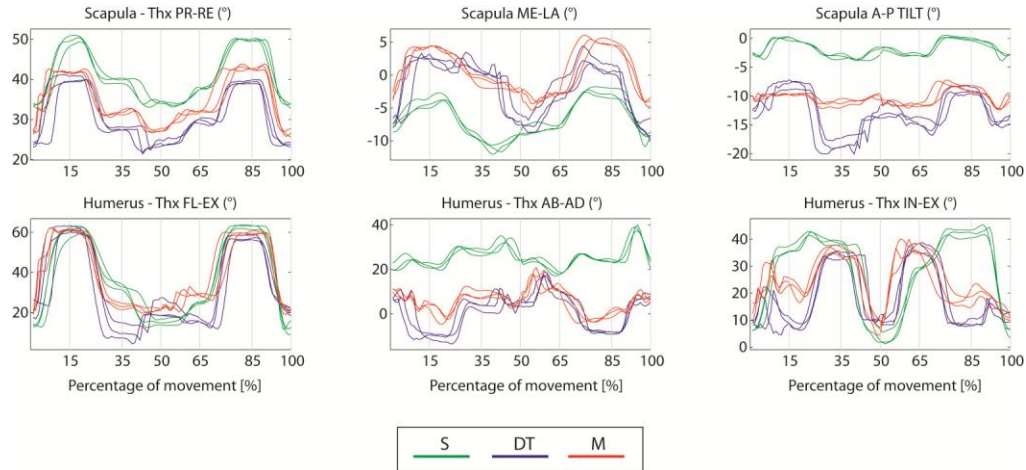

Figure 2 Kinematic pattern for the Jar task

Regarding the Carton pouring task, Fig. 3 reports the scapula and humerus kinematics, with the movement divided into 4 phases, namely: 1) reaching the carton, 2) pouring the water, 3) bringing back the carton to its original position, and 4) returning to the starting position. Percentages of movements were based on the sound side timing. Due to the lack of the active wrist prono-supination, the patient is forced to complete the pouring activity relying on increased scapula lateral rotation and humerus internal-external rotation, both with the M and DT hand compared to the sound side. However, with the M hand the amputee is able to reach the carton in abduction, similarity to the sound side, as seen with the Jar task. For what concerns the timing, the activity required about 11s for the sound side and about 20s with the prosthetic side.
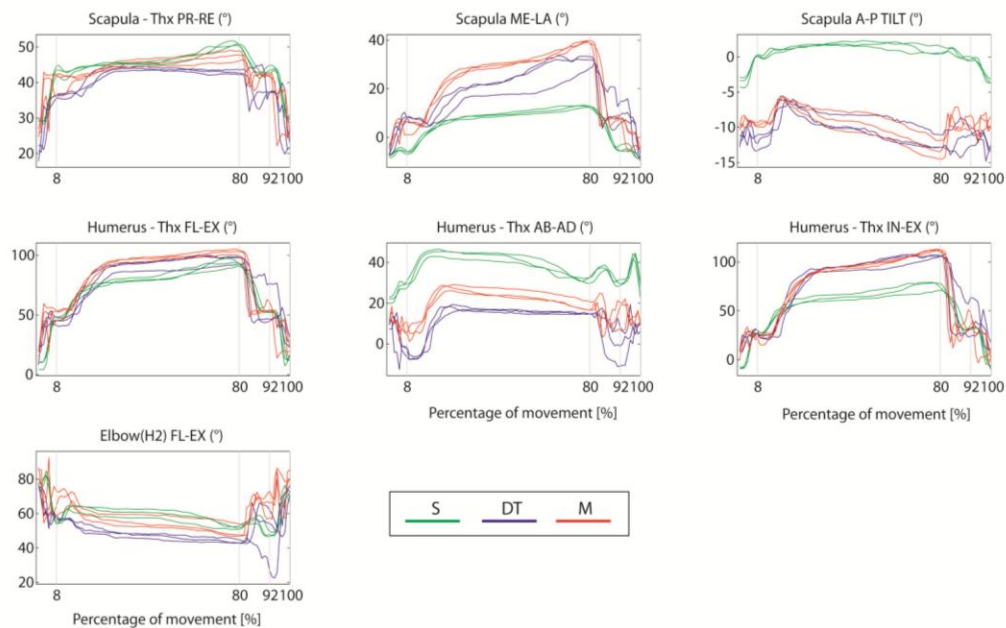

Figure 3 Kinematic for the Carton pouring task

Finally, Fig. 4 reports the kinematics for scapula and humerus for the Disk task. The movement was divided into 6 phases, namely: 1) reaching the disk in position 1, 2) grasping and moving the disk to position 3, 3) returning to the starting position, 4) reaching the disk in position 3, 5) grasping and moving the disk to position 1, 6) returning to the starting position. Percentages of movements were based on the sound side timing. For this task, the patient used the lateral grasping with the M hand. Due to this reason, major difference can be observed compared to the movement while using the DT hand. With this latter, the amputee is forced to perform the movement relaying on humerus flexion, abduction, internal rotation, scapula lateral rotation. With the M hand and the sound side, the amputee avoids the subacromial impingement position. Timing is equally informative of the change between DT and M hands. With the DT hand the whole movement takes 11s on average, while it takes 7s with both the M hand and the sound side.
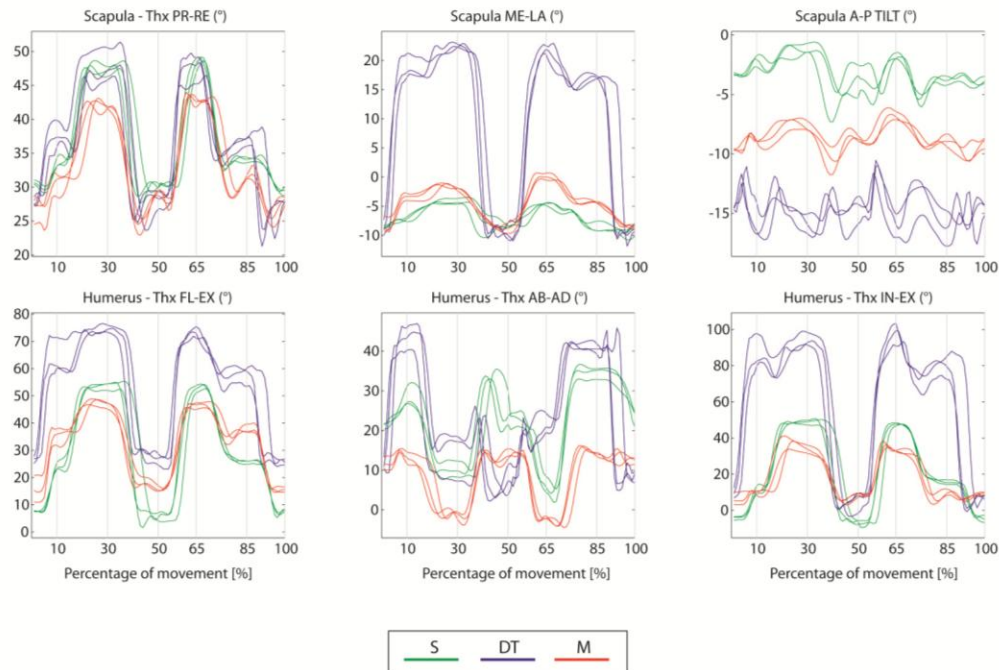
Figure 4 Kinematic pattern for the Disk task

4. DISCUSSION

The biomechanical analysis brought in evidence differences between the upper-limb motion strategies while the patient uses DT, M and the sound side. Firstly, the Pouring task highlighted differences between the prosthetic side and the sound side, with advantages for M hand in the more natural approach to the object, as also highlighted by the Jar task. The Jar task also showed that M hand allows the amputee the reduce the scapula tilting motion, with the scapula working in a more physiological way. The Disk showed the most relevant improvements of M hand over DT hand in comparison with the sound side. The Disk task reproduces a very common working-place activity. M hand can thus lead to a major advantage over DT hand in terms of preservation of the shoulder joint by avoiding subacromial impingement positions.

Great changes are occurring in the upper-arm prosthetic field: innovative solutions are coming out from the laboratories to be used by patients in everyday life. In order to offer successful solutions to patients and justify higher costs, it is necessary to intensify the activities of technology assessment, based on scientific evidences, which is possible only through the planning and execution of appropriate clinical trials. Further activities will be focused toward an extensive application of the protocol to gain further insight about its completeness and applicability.

5. REFERENCES

[1] S.L. Carey, M.J. Highsmith, M.E. Maitland and R.V. Dubey, "Compensatory movements of transradial prosthesis users during common tasks" Clin Biomech, 2008 vol. 23, pp. 1128-1135.

[2] P. Garofalo, A.G. Cutti, M.V. Filippi, S. Cavazza, A. Ferrari, A. Cappello and A. Davalli, "Inter-operator reliability and prediction bands of a novel protocol to measure the coordinated movements of shoulder-girdle and humerus in clinical settings" Med Biol Eng Comput 2009, vol. 47, pp. 475-486.

[3] A. Kontaxis, A.G. Cutti, G.R. Johnson and H.E.J. Veeger, "A framework for the definition of standardized protocols for measuring upper-extremity kinematics" Clin Biomech 2009, vol 24, pp. 246-253.

[4] C. M. Light, P. H. Chappell and P. J. Kyberd, "Establishing a standardized clinical assessment tool of pathologic and prosthetic hand function: Normative data, reliability, and validity" Arch Phys Med Rehabil 2002, vol 83, pp. 776-783.

Fri – July 20th 2012

Chairmen: **Vincenzo Parenti Castelli (DIEM, University of Bologna, Italy)**
J.J. Trey Crisco (Brown University, USA)

Keynote lecture: *"Tracking skeletal motion in the upper extremity -*
8.30 : 9.00 static CT imaging to high-speed bi-plane videoradiography*"*
J.J. Trey Crisco

Podium session #5: "Industrial design, ergonomics and other applications"
9.00 : 10.30

9.00	3-D joint torques in car egress motions	Robert T., Causse J., Wang X.
9.15	Emergence of visomotor coordination with training in bimanual movements	Srinivasan D., Martin B. J.
9.30	A new method for internal-external rotation measurement in a prosthetic knee	Arami A., Aminian K.
9.45	Phase analysis of multi-segmental spine kinematics at two gait speeds	Pakzad M., Al Zoubi F., Preuss R.
10.00	Introducing a soft tissue artifact model in multi-body optimization: a feasibility study	Richard V., Camomilla V., Chèze L., Cappozzo A., Dumas R.
10.15	Low-Cost markerless motion-capture system for kinematic assessment of postural tests	Ieluzzi R., Fioretti S.

!

Tracking Skeletal Motion in the Upper Extremity - Static CT Imaging to High-Speed Bi-plane Videoradiography

J.J. Trey Crisco

The Warren Alpert Medical School of Brown University and Rhode Island Hospital, Providence, Rhode Island, USA

Tracking the skeletal motion of the hand, wrist and forearm is challenging from numerous perspectives. Firstly, these segments possess over 70 kinematic degrees of freedom. Unlike gait and running, cyclic functional tasks for the upper extremity remain ill-defined. Lastly, the numerous bones per body segment severely limit the applications of skin-based motion capture systems. One aim of our lab has been to determine the function of the carpus, the eight small irregularly shaped bones of the wrist. Given these stated challenges and our focus on *in vivo* studies, we developed a computed tomography (CT) based technique to measure the *in vivo* skeletal motion. Our approach utilizes markerless bone registration of sequential CT volume images to track the complete 3-D kinematics of each individual carpal bone. This technique has permitted new understandings of normal carpal bone function, demonstrating that kinematic patterns are unique with each direction of wrist motion. These patterns are highly consistent across healthy wrists, and vary with numerous pathologies. We have also identified that the most functional axes of the wrist is oblique to the classically defined anatomical axes. We are currently using this technique to examine the *in vivo* motion of the thumb's carpometacarpal (CMC) joint during functional tasks, as well as the changes associated with early stages of osteoarthritis. While yielding new insights into carpal bone function, this technique is limited to static data acquisition because it is CT-based. To address this limitation we have designed, fabricated and validated a bi-plane videoradiography system (referred to as XROMM for x-ray reconstruction of moving morphology) that is capable of tracking skeletal motion up to 1000 Hz. I will present our validation approach and conclude with our early findings in tracking the dynamic skeletal motion of the hand, wrist and forearm during functional tasks.

3-D Joint Torques in Car Egress Motions

Robert T. [1], Causse J. [1,2], Wang X. [1]

[1] LBMC, Université de Lyon, IFSTTAR – UCBL, F-69675 Bron
[2] PSA Peugeot-Citroën, Vélizy-Villacoublay, France

This study presents the first analysis of 3-D joint torques developed during car egress motion. Influence of the car geometry (an in particular the seat height) and subjects' stature on these torques is also analyzed. It showed that, on overall, the shorter the subjects and the larger the cars (or the higher the seat), the smaller joint torques.

Keywords-Joint torques; car egress; Ergonomics

1. INTRODUCTION

Getting in and out of a car represents a challenging task. Indeed ingress and egress are complex 3-D motions, preformed in a cluttered environment, dealing with equilibrium constraints and involving relatively large efforts. However, the ease to get in and out of the car is both an economical and social challenge. For car manufacturers, it represents a major ergonomic issue as car ingress-egress represents the first-last physical contact with the car. Moreover, considering the general ageing of the population, it is essential to propose designs that facilitate the access to the car, even for elderly or disable persons.

Therefore, it is not surprising that car ingress-egress motions have attracted a lot of research attention. First researches analyzed the difficulty inherent to these motions, in particular the link with car design parameters [1, 2]. More recently, detailed description of the 3-D kinematics have been proposed, notably by [3] and [4] who described the different kinematic strategies used by volunteer subjects. Regarding the dynamics, a preliminary analysis of the left hip abduction for one subject can be found in [5]. Causse et al. [6] have recently proposed an analysis of the contact loads between the subject and its environment, and demonstrated the feasibility of the joint loads estimation for these motions. However a complete 3-D analysis of the joint loads acting of car ingress-egress motions is still missing.

In order to fill this gap, we propose in this study: 1/ to describe the joint torques developed during egress motions 2/ to analyze the influence of the car geometry and subject anthropometry on the torques developed. This analysis focused on egress motions, as they gathered most of the difficulties [7] and involved larger torques during the raising up of the Center of Mass (CoM).

2. MATERIALS AND METHODS

Experiments

Data of 15 young volunteers, out of the 26 who participated in this experiment, were analyzed in this study. They were free from any disorder and routinely driving cars. Subjects were spread in three groups of five according to their anthropometry (see Table 1).

An adjustable mock-up was used to represent the car (see Figure 1). It consists of a seat, a steering wheel, pedals, a door frame and a door (kept open at 70°). The main dimensions were varied so that they corresponded to three types of car: a small car, a medium-sized car and a minivan (see Table 2). These three configurations are mainly differentiated by their seat height. The longitudinal position of the seat relative to the pedals and the longitudinal and vertical position of the steering wheel were adjusted by the subjects once at the beginning of the experiment. In addition, roof height and sill width were also adjusted. In this study, only retained were the data sets with the medium sill width and the medium roof height (the middle between the first uncomfortable and the lowest acceptable roof heights identified by subjects prior to experiment [8]). Note that this last parameter affects almost solely the cervical joints [8, 9].

The mock-up was equipped with four 6-D forces sensors: two Bertec force plates embedded in the car floor under the steering wheel and in the ground next to the doorframe, a specific force plate located under the seat and a load sensor (Denton) behind the steering wheel. In addition, subjects were equipped with 44 reflective markers, whose trajectories were recorded using a 10 cameras optoelectronic system (Vicon MX).

The task consisted in getting out of a car, from an initial driving posture, and to move away from the door frame without using the door. Detailed experimental protocol can be found in [8].

Table 1. The three groups of subjects

Group	Stature (m)	Weight (kg)	Sex
Short	1.59 (1.57 – 1.61)	51.0 (41.6 – 56.8)	5 F
Medium	1.68 (1.63 – 1.75)	63.8 (53.7 – 80.3)	2F – 3 M
Tall	1.85 (1.81 – 1.87)	74.2 (66.2 – 82.0)	5 M

Table 2. Main dimensions of the three car configuration (mm)

	V1	V2	V3
Seat height above ground	470	550	700
Sill height above ground	360	360	420
Sill height above floor	130	100	70
Doorway width	900	850	850
Roof width from SW	220	220	250
Sill width from SW	470	460	450

Figure 1. the car mock-up used in this study

Data Processing

Egress motions were defined between the instant when the left foot leaves the floor and the instant when the right foot touches the ground (see Figure 2).

Joint angles were estimated from marker trajectories using a global optimization procedure and a 16 rigid bodies - 33 degrees of freedom kinematic model adjusted to subjects' anthropometry (Wang SAE 2005). Rotation conventions were adapted to ISB's standard (REF Wu). An example of reconstructed motion is displayed in Figure 2.

An inverse dynamics procedure was used to compute the net joint torques developed during these motions. 3-D Body Segment Inertial Parameters were estimated from regressions [10]. The procedure is based on a Newton-Euler recursive approach using a homogeneous (4x4) matrices formalism [11, 12]. The Net Joint Torques were then projected orthogonally onto the mobility axes (axes of the non-orthogonal Joint Coordinate Systems – see [13]), made unitless [14] and time normalized over 101 frames (0 to 100 % of the motion). Influence of subject's anthropometry and car configuration was evaluated at particular points of the joint torques curves (see section Results) using an ANOVA with factors *Stature* ("Short", "Medium", "Tall") and *Configuration* ("V1", "V2", "V3").

3. RESULTS

An example of egress reconstructed motion is shown in Figure 2. Figure 3 displays the principal joint torques developed by subject from the "medium" group in the V2 configuration ("medium-sized car"). Results of the ANOVAs are summarized in the Table 3. Significant effects were found for both factors, without any significant interaction.

4. DISCUSSION

From the joint torque analyses, egress motions can be spread into two main phases. The beginning of the motion is characterized by: 1) flexion torque in the left hip to transport of the left foot above the sill; 2) right ankle abduction, right hip internal rotation and abduction torques, corresponding to the body rotation and transfer to the left by the right leg. The second phase is characterized by high extension peaks: left ankle plantarflexion, and extension of the left and right knee left hip and lumbar joint, used to rise elevate the Center of Mass. They are similar to those observed in Sit-to-Stand motions [15]. The extension torques in the right knee tends to transfer the body to the left and facilitate the exit. One can also observe that, during this phase, the left knee axial rotation is opposed to the general body rotation to the left. The left leg was not sufficiently rotated during the transport phase, leading the knee to its joint limit in axial rotation during the extension phase.
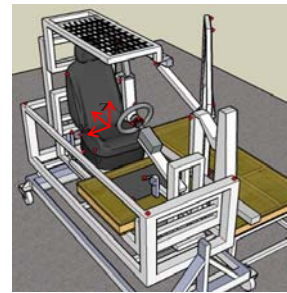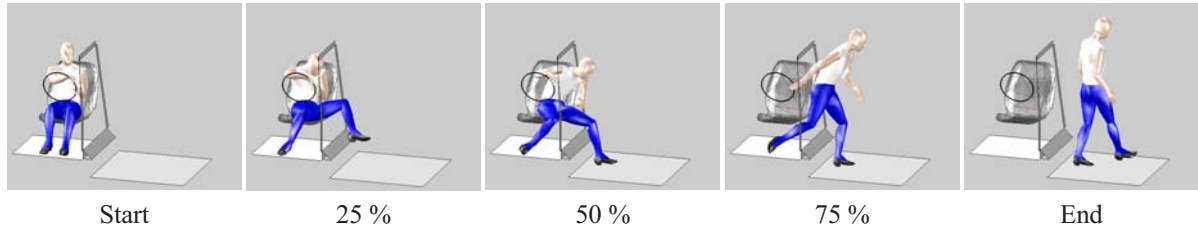
Figure 2. Exemple of reconstruction for a typical egress motion (medium subject and medium-sized car
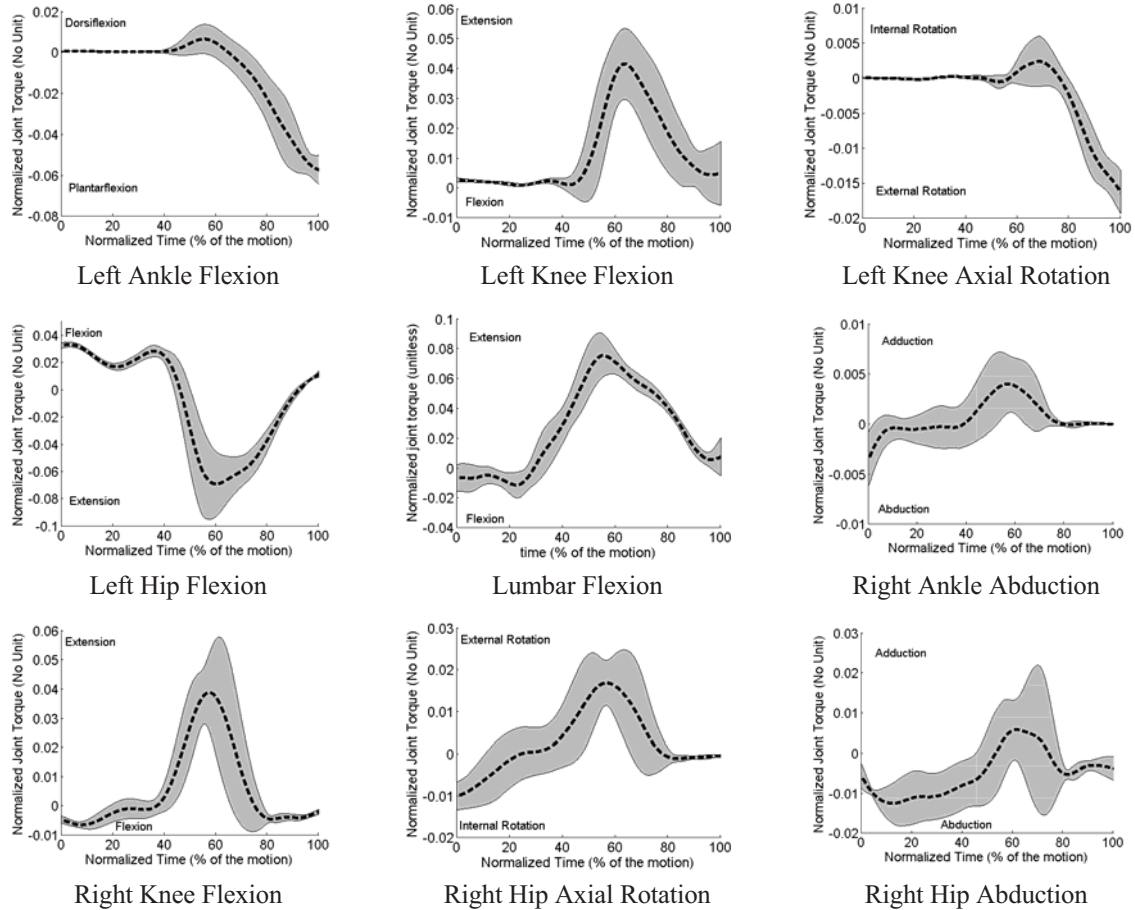

Figure 3. Net joint torques profiles (from proximal to distal segment) projected on mobility axes (axes of the JCS) for egress motions of the medium group of subjects and the V2 vehicle configuration ("medium-sized car") averaged (thick line) ± one standard deviation (shaded area) across subjects. Torques are unitless.

Table 3. Results of the ANOVAs on peak joint torques

Joint	Peak torque considered	Significant para. ($p<0.05$)	Significant groups from post-hoc tests
Left Ankle	Dorsiflexion	Configuration	V3 < (V1,V2)
Left Knee	Extension	Configuration	V3 < V2 < V1
		Stature	Short < (Medium, Tall)
	Internal rotation	Stature	Tall < (Short, Medium)
Left Hip	Extension	Configuration	V3 < V1
		Stature	Short < Tall
Lumbar	Extension	Configuration	V3 < (V1,V2)
		Stature	Short < Medium < Tall
Right Ankle	Adduction	Configuration	V3 < V1
Right Knee	Extension	Configuration	V3 < (V1,V2)
Right Hip	External Rotation	Configuration	V3 < (V1,V2)
		Stature	(Short, Medium) < Tall

Effects of car geometry had systematically the same effect on joint torques: the V3 configuration induced lower torques than V2 and V1. Decrease of extension torques can be directly linked to the increase of the seat height, as already observed in Sit-to-Stand motions for example [16]. The dorsiflexion peak on the left ankle for the lower seat configuration (V1 and V2) is explained by the fact that subjects hit the ground with the toes instead of the heel as in the V3 configuration. Decreased adduction in the right ankle and extension in the right hip can be explained by the combined facts that the right foot-ground contact force decreases with the seat height and that these degrees of freedom primarily transfer this loads toward the pelvis. The fact that larger car configurations with a higher seat induce lower joint torques matches ergonomics evaluations of car ingress-egress discomfort (e.g. [8]), pointing the ease to get in and out of minivans compared to smaller cars.

Due to torque normalization, stature effects can not be reasonably explained by differences in body mass or segment lengths between groups of subject. They rather highlight differences in the ingress-egress kinematics between groups (e.g. [9]) resulting from the interaction between the non-adjusted dimensions of the car configurations and subjects of different anthropometry. Results showed that smaller subjects, whose motions were less restricted by the car geometry, developed lower joint torques. The left knee external rotation is an exception: taller subjects were advantaged to exit their left leg and correctly positioned it (rotate it) before loaded it.

5. REFERENCES

[1]   Giacomin J, Quattrocolo S. An analysis of human comfort when entering and exiting the rear seat of an automobile. Appl Ergon. 1997, 28:397–406.

[2]   Petzäll J. The design of entrances of taxis for elderly and disabled passengers: an experimental study. Appl Ergon. 1995, 26:343–352.

[3]   Chateauroux E, Wang X. Car egress analysis of younger and older drivers for motion simulation. Appl Ergon. 2010, 42:169 – 177.

[4]   Aït El Menceur MO, Pudlo P, Gorce P, Thevenon A, Lepoutre FX. Alternative movement identification in the automobile ingress and egress for young and elderly population with or without prostheses. Int J Ind Ergon. 2008, 39:1078–1087.

[5]   Debril JF, Pudlo P, Ait El Menceur M, Gorce P, Lepoutre F. Human Articulation Efforts Estimation in the Automobile Vehicle Accessibility Movement - A Pilot Study. In: Duffy V, editor. Digital Human Modeling. vol. 4561 of Lecture Notes in Computer Science. Springer Berlin / Heidelberg; 2007. p. 23–32.

[6]   Causse J, Chateauroux E, Monnier G, Wang X, Denninger L. Dynamic Analysis of Car Ingress/Egress Movement: an Experimental Protocol and Preliminary Results. SAE International Journal of Passenger Cars-Mechanical Systems. 2009, 2:1633–1640.

[7]   Institute for Consumer Ergonomics. Problems experienced by disabled and elderly people entering and leaving cars. Edited at the Transport and Road Research Laboratory from the original reports by the Institute for Consumer Ergonomics, Loughborough, 1985.

[8]   Causse J. Analyse cinématique et dynamique du mouvement d'accessibilité à une automobile (Kinematic and dynamic analysis of car accessibility movements). Ph.D. thesis, University Claude Bernard Lyon1, 2011.

[9]   Causse J, Wang X, Denninger L. An experimental investigation on the requirement of roof height and sill width for car ingress and egress. Ergonomics. Unpublished.

[10]   Dumas R, Cheze L, Verriest JP. Adjustments to McConville et al. and Young et al. body segment inertial parameters. J Biomech. 2007, 40:543–553.

[11]   Doriot N, Chèze L. A three-dimensional kinematic and dynamic study of the lower limb during the stance phase of gait using an homogeneous matrix approach. IEEE Trans Biomed Eng. 2004, 51:21–27.

[12]   Robert T, Cheze L, Dumas R, Verriest JP. Validation of net joint loads calculated by inverse dynamics in case of complex movements: application to balance recovery movements. J Biomech. 2007, 40:2450–2456.

[13]   Desroches G, Cheze L, Dumas R. Expression of Joint Moment in the Joint Coordinate System. J Biomech Eng. 2010, 132:114503.

[14]   Hof AL. Scaling gait data to body size. Gait Posture. 1996, 4:222 – 223.

[15]   Bahrami F, Riener R, Jabedar-Maralani P, Schmidt G. Biomechanical analysis of sit-to-stand transfer in healthy and paraplegic subjects. Clin Biomech. 2000, 15:123 – 133.

[16]   Su FC, Lai KA, Hong WH. Rising from chair after total knee arthroplasty. Clin Biomech. 1998, 13:176–181.

Emmergence of Visomotor Coordination with Trainnig in Bimanual Movements

Srinivasan D. [1,2], Martin B. J.[2]

[1] Centre for Musculo-Skeletal Research, University of Gavle, Gavle, Sweden
[2] Dept. of Industrial and Operations Engineering, University of Michigan, Ann Arbor, U.S.A.

Keywords-Eye-hand coordination, bimanual movements; learning; gaze strategy; left-right asymmetry

1. INTRODUCTION

It has been suggested that practice leads to the evolution and stabilization of newly learned motor patterns in bimanual movements. For example, in discrete bimanual movements, spatial interference in the performance of drawing tasks [4] decreases with training [13]. These studies suggest that the mechanisms underlying bimanual coordination might be plastic, and modifiable to some extent through training. In this context, the importance of sensorimotor and attentional processes in bimanual skill acquisition and in overcoming the inherent manual asymmetries of the left and right hand sub-systems [1, 2] have received increasing attention [11].

Complex patterns of task-dependent variation in gaze strategies and patterns of movement termination have been revealed [3, 8]. Although an inherent tendency to synchronize bimanual movements may exist [4], such synchrony may break down during the final movement phases. This task-dependent breakdown in temporal synchrony has been associated with an increase in visual demand, and it was suggested that visual constraints are the main determinants of coordination patterns in bimanual goal-directed movements [7, 9]. The present study investigated changes in eye-hand coordination strategies with simple practice.

2. METHODS

Experimental setup and procedure

Six right-handed young adults, with normal vision and free from disorders participated in this experiment. The Institutional Review Board of the University of Michigan approved the experiment and all participants signed an informed consent form. Each hand transferred identical objects from initial positions to target locations symmetric relative to the sagittal plane. Object size, target tolerance and inter-target distance were the task variables. Two pairs of light weight cylindrical objects (height 120 mm, with ø 8 mm and 44 mm) were used. The target diameter (Td) was defined with respect to the object diameter (Od). Two target tolerances (tol) of 0 and 45 mm were defined for each object, i.e. Td = Od + 0 or 45 mm. The object-to-target distance was set at 400mm for all trials. The inter-target distance (D), defined as the distance between the two targets was set at either 30 or 200 mm (Fig 1). The initial object and final target locations were displayed on a horizontal 52" flat-screen TV adjusted at elbow height. An eight-camera Qualisys® motion capture system recorded kinematic data at 60 Hz. Eye movements were recorded simultaneously and in synchrony by an ASL® head mounted eye tracking system. Gaze data was obtained using a two-step calibration procedure [9].
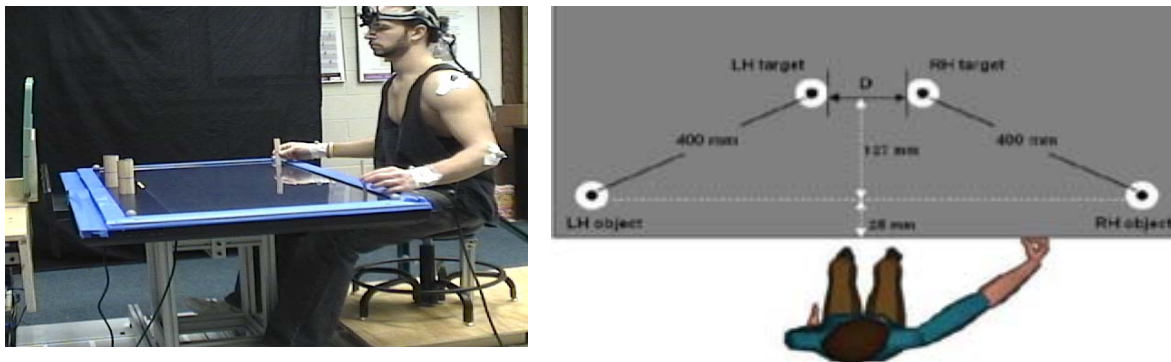

Figure 1. Experimental setup & Schematic. RH, LH = right & left hand, respectively; D = inter-target distance

Each trial started with the objects finger-pinched at marked locations, and the eyes fixating a target in the mid-sagittal plane at eye level. Movement speed was not constrained, and subjects were asked to move at a comfortable pace to complete the task. No other instruction was given. The only constraint imposed on task-

performance was zero error tolerance in the accuracy of positioning. If accuracy constraints were not met, corresponding trials were repeated at the end of the experiment. The participants first performed a set of 100 practice trials including a randomized order of bimanual and unimanual movement trials of both the left and right hands in similar conditions. The practice session was followed by the experimental session in which each bimanual trial condition was repeated thrice in random order with 15 s inter-trial intervals.

Data analysis

3D motion data were low pass filtered at 6Hz (2nd order Butterworth filter). Kinematic data from the markers placed on the wrists were used to calculate the onset and end times of movements using a wrist velocity threshold of 5mm/s and object contact with the LCD screen [9]. In bimanual trials, the hand moving to the target fixated first was defined as the "primary" hand. The absolute differences in movement durations between the left and right hands ($|MT_{L-R}|$) was also computed. Movement termination was defined as 'sequential' if $|MT_{L-R}| > 100$ ms and 'synchronous' if otherwise. The practice session was split into 2 sections for comparison with the experimental trials: The first 30 practice trials (1-30) and the last 30 practice trials (70-100). Within each session, the effect of task condition and gaze strategy on $|MT_{L-R}|$ was analyzed using repeated measures ANOVA. Mean $|MT_{L-R}|$ values were compared between sessions using unpaired Student t tests.

3. RESULTS

The labels low and high were respectively associated with the lowest and highest level of each task factor (object size, target tolerance and inter-target distance) to simplify descriptions hereafter.

Gaze strategies

Four gaze strategies were identified in experimental bimanual trials [9]. 1) **Terminal** strategy: gaze was directed towards one target first, and after completion of the corresponding hand movement gaze shifted to the other target. 2) I**ntermittent** strategy: multiple gaze transitions between the two targets occurred during execution of the bimanual task. 3) **Predictive** strategy: gaze was directed towards one target first, but then re-directed to the other target even before completion of hand movement to the former target. 4) S**elective** strategy: gaze was directed to one of the two targets, and remained there until the completion of the entire bimanual task. These gaze strategies vary with bimanual task conditions.

Initial Practice (practice trials 1-30)

Both hand movements were initiated simultaneously and peak velocities were reached at nearly the same time, irrespective of task condition ($P > 0.5$). The pattern of termination of bimanual movements varied significantly with task condition. The difference in movement durations between the right and left hands ($|MT_{L-R}|$) was significantly longer ($P_{tol} = 0.003$) for low than high target tolerance, and increased with inter-target distance (D) when target tolerance was low ($P_D= 0.006$, $P_{D*tol} = 0.011$). Similarly, $|MT_{L-R}|$ decreased with increasing object size, when target tolerance was low ($P_{Od} = 0.034$, $P_{Od*tol} = 0.022$).

Only 2 gaze strategies – Terminal (in 66% of bimanual trials) and Intermittent (in remaining 34% of bimanual trials) were observed. Although both these strategies were observed in conditions corresponding to low target tolerance, the intermittent strategy was predominantly observed in trials corresponding to high target tolerance. The terminal gaze strategy corresponded to sequential termination of hand movements, while the intermittent gaze strategy corresponded to synchronous termination of hand movements. In addition, neither hand was systematically chosen as the primary hand (61% left, 39% right) in these initial practice trials. Fig 2A shows the distribution of gaze strategies and $|MT_{L-R}|$ according to task conditions.

Comparison between initial practice and experimental sessions

Experimental session results were presented in [9]. When target tolerance was high, $|MT_{L-R}|$ was not significantly different ($P=0.36$) between the initial practice and experimental sessions, although different gaze strategies were used for the same task conditions in the two sessions. When target tolerance was low, although the terminal gaze strategy was used, $|MT_{L-R}|$ was significantly higher in the practice than the experimental session ($P=0.031$).

Final Practice (practice trials 70-100)

Both hand movements were initiated simultaneously and peak velocities were reached at about the same time irrespective of task condition. The pattern of termination of bimanual movements varied significantly with task condition in manners similar to those in initial trials. However, variations of $|MT_{L-R}|$ with task condition are quite complex and are better understood by decoupling the effect of task condition on $|MT_{L-R}|$ into variation of gaze strategy with task condition and variation of $|MT_{L-R}|$ with gaze strategy [9]. Fig 2B shows $|MT_{L-R}|$ and the relationship between gaze strategy and $|MT_{L-R}|$ as a function of task condition.
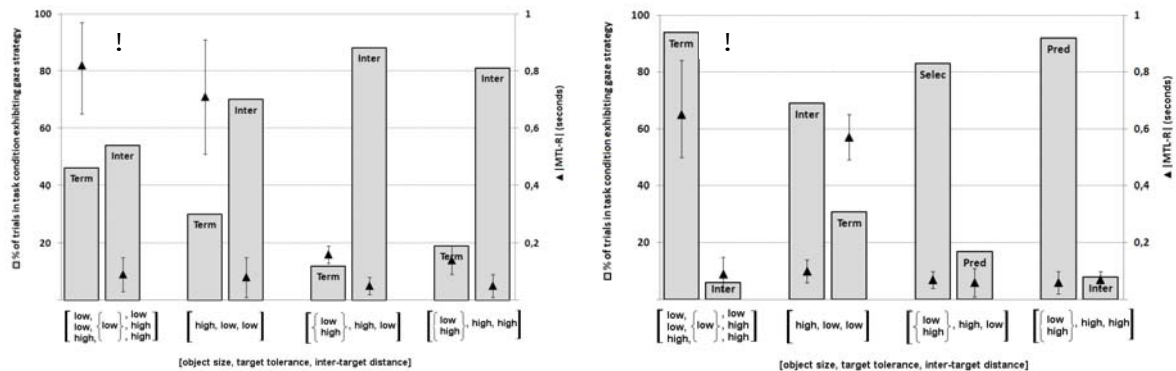
Fig 2. Gaze strategies and terminal coordination patterns in initial (**A**) and final (**B**) practice sessions. Bars = % of trials in each condition in which a particular gaze strategy was observed: Term = Terminal, Inter = Intermittent, Selec = selective, Pred= Predicted; ▲ = |MT$_{L-R}$|

The four gaze strategies were observed in final practice. Sequential movement termination corresponded to the terminal gaze strategy and the left hand target was the first to be foveated. Consequently, the left hand movement was completed first in 95% of bimanual trials. Synchronous movement termination was observed either when the intermittent, predictive or selective gaze strategy was used. Although hand movements were completed simultaneously, the left hand target was the first to be foveated in 91% of corresponding trials. Thus, based on the order of gaze fixation and placement sequence, the left hand was defined as the primary hand (primary task goal in the bimanual task) and the right hand was defined as the secondary hand.

Comparison between final practice and experimental sessions
|MT$_{L-R}$| was not significantly different between final practice trials (70-100) and experimental trials (p >0.5). The choice of gaze strategy also presented similar trends in this comparison.

Comparison of Bimanual Movement Time (MT) Between Practice and Experimental Sessions

Asynchronous termination of hand movements was observed when the terminal gaze strategy was selected, which corresponded to low target tolerance, in initial practice, final practice and experimental test, respectively. Hence MTs associated with this strategy were compared. There were no significant differences in either hand MT between final practice and experimental session when the terminal gaze strategy was used (Fig 4 left 2 columns, P = 0.19, *t*-test). During initial practice, the left hand was not systematically chosen as the primary hand. So the sequentially terminating movements were split into two groups (Fig 4 right 2 columns), based on which hand was used as the primary hand. Irrespective of which hand was the primary hand, the overall bimanual movement time was significantly longer during initial practice than final practice (P = 0.015, *t*-test) or experimental test (P = 0.008, *t*-test). In those trials in which the left hand was used as the primary hand, |MTL-R| was significantly greater in initial practice than in final practice and test trials (P=0.017, P=0.013, *t*-test). Overall bimanual movement times as well as the temporal phase lag between the left and right hand movements (|MTL-R|) were not significantly different for trials using the other gaze strategies between any of the sessions compared.
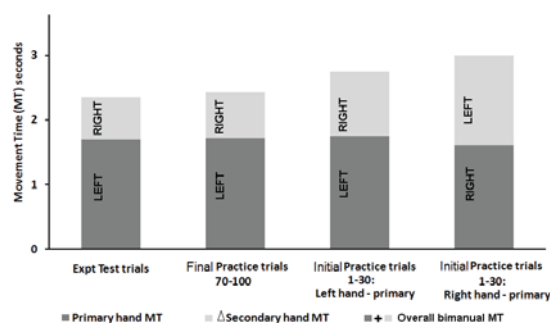

Fig 3. Bimanual MTs in initial & final practice, compared to experimental session. ΔSecondary hand MT = completion time lag of secondary hand. Results correspond to low target tolerance-terminal gaze strategy.

4. DISCUSSION

What is learned and why?
The left hand movement is prioritized in terms of gaze orientation and movement sequencing while the right hand is relegated to becoming secondary (the opposite prioritization observed in some trials before training is

associated with longer bimanual movement times). A preference for left-target fixation in bimanual movements has previously been reported [7] and a consequent reduction in temporal phase lags between the two hand movements has been observed in other studies [10]. This systematic prioritization and a consequent decrease in temporal phase lags between the two hand movements lends to assume an inherent asymmetry in utilizing feedback information between the left and right hands [8]; the right hand may be able to rely on proprioceptive feedback better than the left hand and hence the left hand might benefit from greater visual guidance of its movement [9]. This systematic emergence with practice points out that the CNS adjusts movement control strategies to make the best use of limb control asymmetry.

When target tolerance was high, the intermittent gaze strategy was replaced by predictive and selective gaze strategies with training. This indicates that the intermittent gaze strategy might be the default for extensive visual guidance in a hitherto unknown/new environment, when performing tasks with multiple constraints. Decrease with training in the number of gaze transitions between the two targets required to successfully complete both hand-tasks suggest adaptive learning. In the computational modeling framework, this adaptation is analogous to an adaptation to the internal forward model controlling the hand movement, which predicts the sensory outcome based on an efferent copy of a motor command [12, 14]. This scheme may be extended in the current context to suggest that in bimanual movements to targets of high tolerance, once both movements are initiated, the CNS learns that predictions of the internal forward model become reliable enough to guide the primary hand movement to successful completion. Hence gaze shifts back and forth between the two targets are no longer needed. The use of a predictive gaze strategy in which gaze leaves the primary target before completion of the primary hand movement strongly supports this perspective. This pre-emptive transition of gaze to the secondary hand movement allows both hand movements to be completed synchronously (unlike sequential movement execution in the terminal gaze strategy). These strategies may contribute to a cost reduction to acquire visual information since head movements contribute to even small changes in gaze direction [6].

5. ACKNOWLEDGMENT

6. REFERENCES

[1] Adamo, D. E., Scotland S., Martin B. J. (2012) Asymetry in grasp force matching and sense of effort. Exp. Brain Res, (in press).

[2] Adamo, D. E., Martin B. J. (2009) Position sense asymmetry. Exp Brain Res 192, 87–95.

[3] Bingham, G. P., Hughes, K., & Mon-Williams, M. (2008). The coordination patterns observed when two hands reach-to-grasp separate objects. Exp Brain Res, 184(3), 283-293.

[4] Franz, E. A., Eliassen, J. C., Ivry, R. B., & Gazzaniga, M. S. (1996). Dissociation of spatial and temporal coupling in the bimanual movements of callosotomy patients. Psychol Sci, 7(5), 306-310.

[5] Kelso, J. A. S., Southard, D. L., & Goodman, D. (1979). Coordination of 2-Handed Movements. J Exp Psychol Hum Percept Perform, 5(2), 229-238.

[6] Kim, K. H., Reed, M., Martin, B. J. (2010) A model of head movement contribution to gaze transitions. Ergonomics, 53(4) 447-457.

[7] Riek, S., Tresilian, J. R., Mon-Williams, M., Coppard, V. L., & Carson, R. G. (2003). Bimanual aiming and overt attention: one law for two hands. Exp Brain Res, 153(1), 59-75.

[8] Roy, E. A., & Elliott, D. (1986). Manual asymmetries in visually directed aiming. Can J Psychol, 40(2), 109-121.

[9] Srinivasan, D., & Martin, B. J. (2010). Eye-hand coordination of symmetric bimanual reaching tasks: temporal aspects. Exp Brain Res, 203(2), 391-405.

[10] Swinnen, S. P., Verschueren, S. M. P., & Dounskaia, N. (1996). Is motor pathology associated with setting new CNS priorities or with increased difficulty in overcoming or suppressing preexisting CNS priorities? Behav Brain Sci, 19(1), 87-92.

[11] Temprado, J. J., Monno, A., Zanone, P. G., & Kelso, J. A. S. (2002). Attentional demands reflect learning-induced alterations of bimanual coordination dynamics. Eur J Neurosci, 16(7), 1390-1394.

[12] Tseng, Y. W., Diedrichsen, J., Krakauer, J. W., Shadmehr, R., & Bastian, A. J. (2007). Sensory prediction errors drive cerebellum-dependent adaptation of reaching. J Neurophysiol, 98(1), 54-62.

[13] Wenderoth, N., Puttemans, V., Vangheluwe, S., & Swinnen, S. P. (2003). Bimanual training reduces spatial interference. J Mot Behav, 35(3), 296-308.

[14] Wolpert, D. M., & Kawato, M. (1998). Multiple paired forward and inverse models for motor control. Neural Netw, 11(7-8), 1317-1329.

A new method for internal-external rotation measurement in a prosthetic knee

Arami A., Aminian K.

Laboratory of Movement analysis and Measurement, Ecole polytechnique Federal de Lausanne (EPFL), Switzerland, arash.arami@epfl.ch, kamiar.aminian@epfl.ch

In this work, a magnetic measurement system was designed and tested to estimate the Internal-External rotation between the Tibial and Femural parts of a knee prosthesis. To obtain this, the sensors were inserted in polyethylene part while a permanent magnet was placed below the Tibial plate. The configuration was designed to keep the intrinsic unbiassness to the positive and negative internal-external angles. A linear regression model was used to map magnetic measurements of the sensors to the angles. For validation the prosthesis was placed in a mechanical simulator equipped with reflective markers tracked by optical motion capture system.

Keywords-knee prosthesis, knee internal external rotations

1. INTRODUCTION

There are a few studies on instrumented knee prostheses in the world, and most of these prostheses have been designed for measuring forces and moments applied on the prosthesis [1], [2], [3]. Those systems were implanted on a few subjects for measurements of joint loading in level walking and stair climbing [4], studying the components of joint contact forces during different activities and exercises [5], [6]. More recently, *in-vivo* force measurements in knee prosthesis was designed [7], in which the sensors and electronic components were positioned inside the polyethylene part of the implant offering this way no change in metallic components.

Although these works provided important outcomes for actual measurement of forces and moments, none of them were designed for *in-vivo* kinematic measurements. Indeed, implanted movement sensors can provide the actual kinematics of a prosthetic joint, and avoid the drawbacks of skin-mounted markers or sensors suffering from soft tissue artifact (STA) [8], [9], [10]. For example, the RMS error of the Stereophotogrammetry motion capture (MoCap) due to the STA, based on measurements on several subjects were reported in stance phase of walking between 2 to 5.3 degree for internal external (IE) rotations [10].

Recently we introduced a new concept of instrumented knee prosthesis to measure force and STA-free kinematics [11], however the kinematics was limited to abduction adduction (AA) and flexion extension (FE) rotations [11]. Considering the importance of the IE rotations in evaluation of the mobile-bearing prosthetic knee function, in the current work we focused on the design of a separate sensory system for measuring this rotation.

2. METHOD AND MATERIALS

Sensor Configuration and Angle Estimation Model

The F.I.R.S.T knee prosthesis (Symbios Orthopédie SA, Switzerland) was used, which has three main parts namely Femural part (FP), Tibial part (TP), and a Polyethylene insert (PE) [11]. Based on the conforming interface of FP and PE, we assumed that the IE rotation between FP and TP can be considered as the IE rotation between PE and TP. A magnet was placed below the TP (Fig. 1). This placement converts the IE rotations to the rotations of the magnet around a center of rotation. The magnet rotation causes the variation of magnetic flux, in two biaxial AMR sensors (HMC1512, Honeywell, USA) placed symmetrically to the axis of the magnet in PE and results in resistance change of the AMRs. Considering the signals of each biaxial AMR (i.e. sensor 1: A_1, B_1 and sensor 2: A_2, B_2), a linear regression model of measurements (1) was used to estimate IE rotations ($\hat{\theta}$).

$$\hat{\theta} = \alpha_0 + \alpha_1 A_1 + \alpha_2 B_1 + \alpha_3 A_2 + \alpha_4 B_2 \qquad (1)$$

Where α_i are the coefficients of the linear model were estimated by minimizing sum of squared differences between estimated angle and reference angle measured by a reference system.
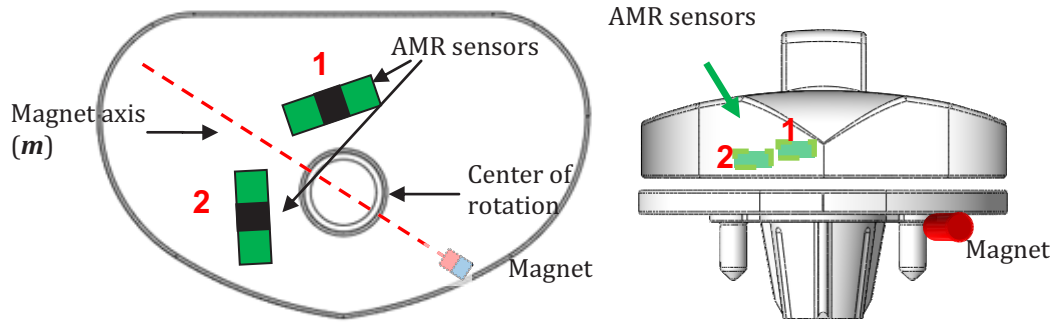
Figure 1. The configuration of sensors and magnet, left a PE cut, right a frontal-verical cut.

Reference System and Validation

The actual IE angle was estimated by the reference motion capture system (MoCap) consisting of five cameras (Vicon, UK) and reflective markers fixed on a mechanical knee simulator which holds all parts of prosthesis, and is capable to rotate the prosthesis in 3D. To validate the system, we performed both static and dynamic measurements of IE rotations while the AMR sensors and the reference MoCap were synchronized. The static measurements included the measurements in 42 different angles, while in dynamic measurements, eight IE rotations were performed in range of $[-11.3^0\ 9.7^0]$. The *Mean* and *Standard Deviation (STD)* of the difference (error) between the actual angle (MoCap) and the estimated angle (AMR) were considered to estimate the accuracy and precision of the IE estimation.

3. RESULTS

An example of estimated angle in dynamic measurement versus the reference measured angle is depicted in Fig. 2. The IE angle estimations' errors for static and dynamic data are illustrated in table 1. An RMS error of less than 0.4º was obtained in both static and dynamics conditions.

4. DISCUSSION AND CONCLUSION

This work showed how the low cost AMR sensors can be used to measure the Internal External rotation in prosthetic knee, while avoiding soft tissue artifact. The proposed configuration, consisting of two sensors and one permanent magnet, provided an unbiased highly accurate and precise estimation of IE angles. The results
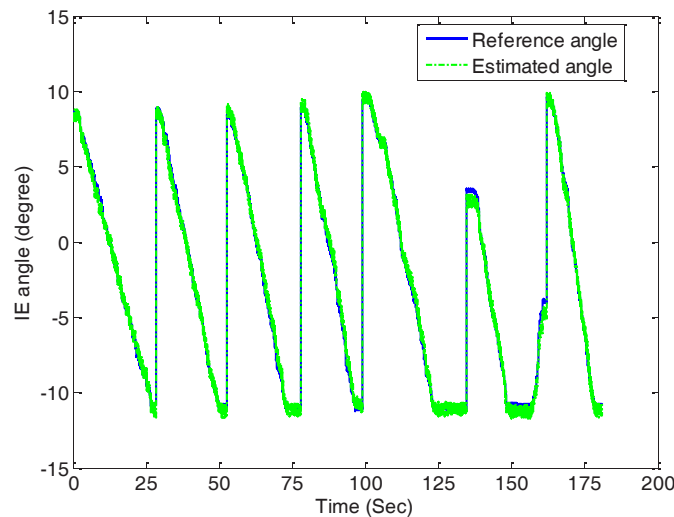

Figure 2. Estimated angle versus reference angle (dynamic measurements).

Table 1. Accuracy (Mean error) and precision (STD error) and RMS error of IE estimation

Movement Type	Accuracy and Precision of estimation		
	Mean error	*STD error*	*RMS error*
Static	0.00°	0.40°	0.40°
Dynamic	0.00°	0.37°	0.37°

depicted in the table 1 also postulate that the quality of estimation will not change because of the dynamicity of the movement. The linear regression model, which only used the crude measurements of channels of the sensors as its inputs, did not face any over-fitting thanks to its simple model.

In next step, the measurement systems for AA and FE rotations need to be combined with the proposed measurement system for IE rotations to provide 3D rotation measurement of the prosthetic knee.

5. ACKNOWLEDGMENT

6. REFERENCES

[1] Heinlein, B., Graichen, F., Bender, A., Rohlmann, A., Bergmann, G., 2007. Design, calibration and pre-clinical testing of an instrumented tibial tray. J. Biomechanics 40, S4-10.

[2] Morris, B.A. D'Lima, D.D., Slamin, J., Kovacevic, N., Arms, S.W., Townsend, C.P., Colwell, J.C.W., 2001. e-knee: Evolution of the electronic knee prosthesis-Telemetry technology development. J. Bone Joint Surg., 83-A, 62–66.

[3] Kirking, B., Krevolin, J., Townsend, C., Colwell, C.W., D'Lima, D.D., 2006. A multiaxial force-sensing implantable tibial prosthesis. J. of Biomechanics 39, 1744-1751.

[4] Heinlein, B. et al., 2009. ESB Clinical Biomechanics Award 2008: Complete data of total knee replacement loading for level walking and stair climbing measured in vivo with a follow-up of 6-10 months. Clin Biomech Bristol Avon 24, 315-326.

[5] Kutzner, I. et al., 2010. Loading of the knee joint during activities of daily living measured in vivo in five subjects. J. of Biomechanics 43, 2164-2173.

[6] D'Lima, D.D., Steklov, N., Patil, S., Colwell, C.W., 2008. The Mark Coventry Award: in vivo knee forces during recreation and exercise after knee arthroplasty. Clinical Orthopaedics and Related Research 466, 2605-2611.

[7] Crescini, D., Sardini, E., Sepelloni, M., 2011. Design and test of an autonomus sensor for force measurements in human knee implants. Sensors and Actuators A 166, 1-8.

[8] Cappozzo, A., Catani, F., Leardini, A., Benedetti M.G., Della Croce, U., 1996. Position and orientation in space of bones during movement: experimental artefacts. Clinical Biomechanics 11, 90-100.

[9] Benoit, D.L., Ramsey, D.K., Lamontagne, M., Xu, L., Wetenberg, P., Reström, P., 2006. Effect of skin movement artifact on knee kinematics during gait and cutting motions measured in vivo. Gait & Posture, 24(2), 152-164.

[10] Leardini, A., Chiari, L., Della Croce, U., Cappozzo, A., 2005. Human movement analysis using stereophotogrammetry Part 3. Soft tissue artifact assessment and compensation. Gait & Posture 21, 212-225.

[11] Arami, A., Simoncini, M., Atasoy, O., Hasenkamp, W., Ali, S., Bertsch, A., Meurville, E., Tanner, S., Dejnabadi, H., Leclercq, V., Renaud, P., Dehollain, C., Farine, P.A., Jolles, B. M., Aminian K., Ryser, P., 2011. Instrumented Prosthesis for Knee Implants Monitoring. In proceeding of the 7th IEEE Conf. on automation science and engineering, Trieste, Italy.

Phase analysis of multi-segmental spine kinematics at two gait speeds

Pakzad M. [1,2], Al Zoubi F. [1,2], Preuss R. [1,2]

[1] School of Physical and Occupational Therapy, McGill University, Montreal, Canada.
[2] Constance-Lethbridge Rehabilitation Centre site of the CRIR, Montreal, Canada.

Keywords: Phase Analysis, Spine, Gait

1. INTRODUCTION

During gait, the range of spinal motions should not be great enough to cause injury [1]. Many individuals, however, develop low back pain (LBP) after a period of walking, while other individuals with LBP report relief of symptoms with walking. As such, the ability to provide a detailed analysis of inter-segmental spine motion during gait may provide insight into those movement patterns that are associated with symptom exacerbation and relief.

Historically, studies of human gait have treated the trunk and spinal column as a single rigid segment between the hips and shoulders. Studies that have assessed trunk motion in relation to the pelvis, however, have found that the limbs, trunk and pelvis all contribute in a coordinated manner to help minimize mechanical energy demands during gait. Furthermore, the manner of this contribution changes as a function of gait speed. In healthy subjects, for example, the phasic relationship between pelvic and thoracic segments in the transverse plane has been shown to change from an in-phase relationship ($\sim25^{o}$ phase difference) at slow gait speeds to an out-of-phase pattern ($\sim120^{o}$ phase difference) at higher speeds [2,3]. Acquiring kinematic data from multiple regions of the spine will allow us to increase our understanding of the inter-segmental spinal motions that occur during walking, and of the potential interactions that exist between the adjacent spinal regions. These data may help to shed light on the possible relationship between spine kinematics during gait and LBP.

The objective of this descriptive case report was to track the kinematic behavior of the spine, at multiple segmental levels, at two gait speeds.

2. MATERIAL AND METHODS

A 29-year old asymptomatic male volunteer, with a history of recurrent low back pain, participated in this study. The subject walked on a split-belt, R-Mill treadmill (ForceLink, Culemborg, The Netherlands) at two speeds: 0.75m/s and 1.50m/s. He was instructed to walk normally on the treadmill and to look straight ahead. Following a period of familiarization [4], 10 consecutive gait cycles were collected for analysis at each gait speed.

Segmental motion during gait was acquired, in three dimensions, using a TrakSTAR electromagnetic motion capture system (Ascension Technology, Milton, VT), sampled at 100Hz. Sensors (model 800; 8x8x20mm) were mounted over the lateral side of the thighs, the base of the sacrum (S1), and the spinous processes of the third lumbar (L3), twelfth thoracic (T12), ninth thoracic (T9), sixth thoracic (T6), third thoracic (T3) and seventh cervical (C7) vertebrae using custom molded urethane clips and double-sided tape. These data were then low-pass filtered, with a cut-off frequency of 10Hz, using a 4th order, zero phase-lag Butterworth filter, and re-sampled at 1000Hz using a cubic spline interpolation. Joint angles for the hips were determined by multiplying the 4x4 rotation-translation matrix for the thigh segments by the inverse of the rotation-translation matrix for the adjacent segment, using custom software written in Matlab (each rotation matrix having been derived from the position and orientation data of the sensors in the transmitter-embedded reference frame).

Gait cycles were separated between successive points of maximum right hip flexion. The data for each gait cycle was then re-sampled to 360 frames using a polyphase implementation (*resample* command in Matlab R2009b). Data from the 10 gait cycles, at each gait speed, were used for the phase analysis.
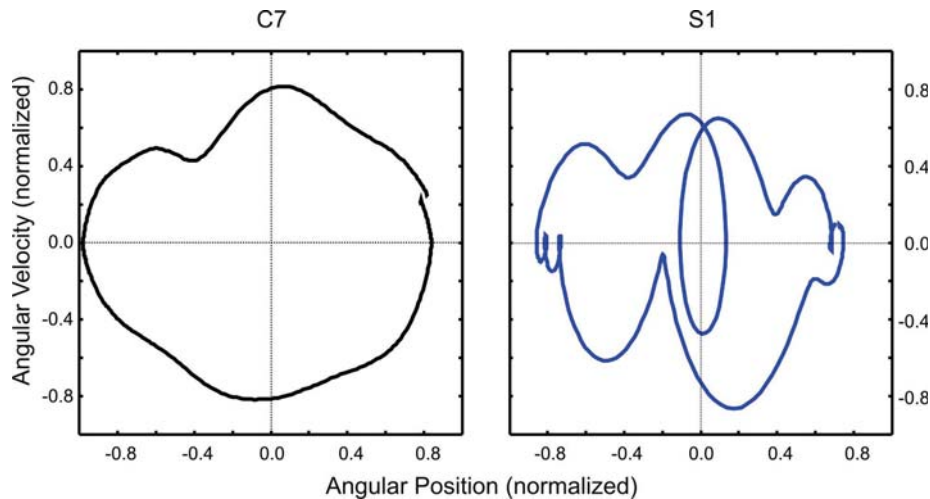
Figure 1. Mean phase plane plots for C7 and S1 at 0.75m/s gait speed

The phase analysis for each segment was conducted using an approach modified from Burgess-Limerick et al. [5], based on the normalized angular velocity of the segment (absolute maximum scaled to an absolute value of one, leaving zero points unaltered) as a function of its normalized angular position (minimum and maximum angular positions scaled to -1 and 1). Each data point is represented as a vector on the resulting phase-plane plot (Fig.1), with the phase offset between two segments at that point in the gait cycle determined from the angle between their respective vectors. Using the law of cosines, this gives values from 0° (perfectly in-phase) to 180° (perfectly out of phase). For each spine segment, the phase offset at both gait speeds was determined relative to the S1 segment.

3. RESULTS

Fig. 2 illustrates the mean spine segment angles across the entire gait cycle, at the 2 gait speeds. Movements in the sagittal plane are biphasic at all spine levels, generally corresponding to the right and left step cycles. Local maxima in flexion occur with each limb loading response, followed by local minima around mid-stance. Frontal plane movements follow a similar bi-phasic pattern, with slightly greater segmental motion amplitudes at the faster speed. Transverse plane movements show the greatest difference between the two gait speeds. At the slower speed, the segmental motion patterns are primarily monophasic. At the faster speed, however, the movement of S1, in particular, transitions to a more bi-phasic pattern, similar to what is seen in the other planes, albeit with a notable asymmetry.

Fig.3 illustrates the mean phase offsets for each spine segment, relative to S1. At the slow gait speed, the spine segments show a general trend toward an incrementally increasing out-of-phase behavior relative to S1, in the caudo-cranial direction. The most notable exception is L3 relative to S1, in the transverse plane. This is likely explained by the slight deviation from the sinusoidal pattern in the motion of S1 and L3 around 270° in the gait cycle (Fig.1 and Fig. 2). At the faster gait speed, the peak out-of-phase behavior in the sagittal plane, relative to S1, occurs at T12, with the more cranial segments becoming progressively more in-phase. In the frontal plane, the phase offsets are similar to the slower speeds, with the most notable exception being T12, which demonstrates a much larger phase offset than at the slower speed. In the transverse plane, the phase offsets are decidedly more out-of-phase ($\geq 90^o$) compared to the slower gait speed, once again showing a general trend toward greater out-of-phase behavior in the caudo-cranial direction.
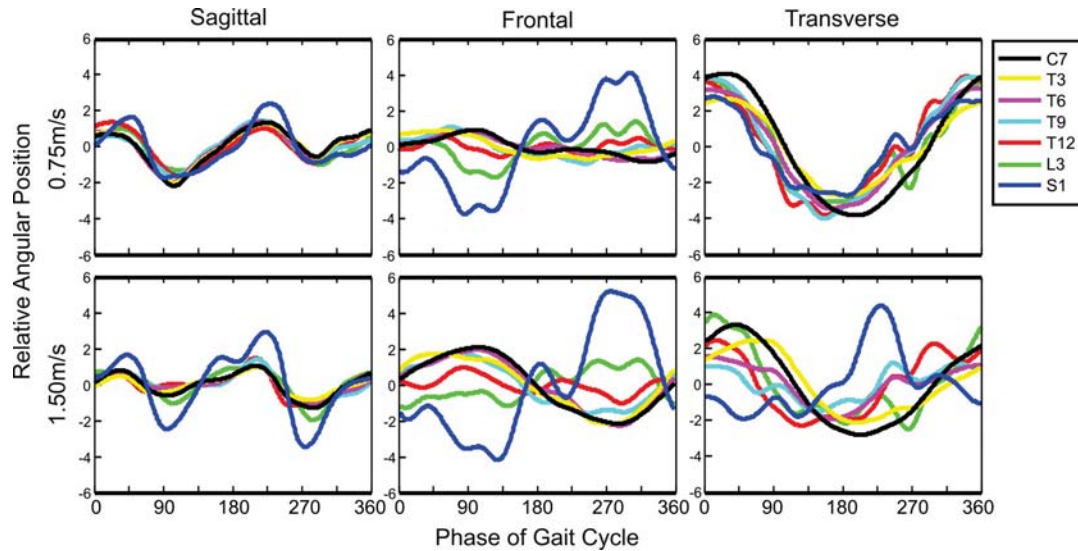
Figure 2. Mean spine segment angles across the gait cycle (zeroed to mean values). Positive values represent flexion (sagittal plane), right side-bending (frontal plane) and left rotation (transverse plane).
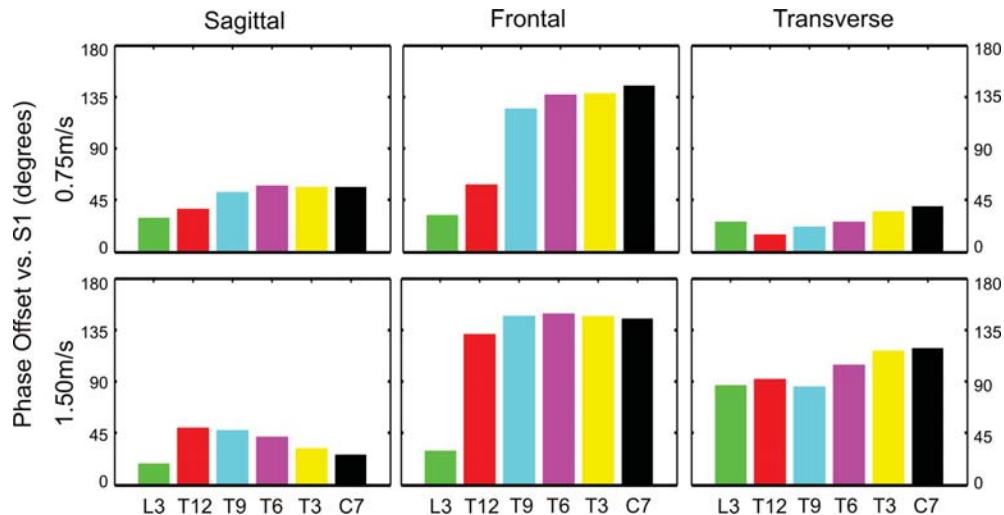

Figure 3. Mean phase offset for each spine segment relative to S1

4.   DISCUSSION

This descriptive case report was intended to illustrate the kinematic behavior of the spine, at multiple segmental levels, at two gait speeds. The results presented above clearly demonstrate measureable inter-segmental motions (Fig.2) and distinctive phase-offsets (Fig.3) during gait, at multiple spine levels.

In general, the findings in this report, with respect to movement amplitudes and phase offsets, are in agreement with previous studies providing a less detailed description of spine motion during gait [2,3,6,7]. For example, different phase-offsets are clearly demonstrated at the slower vs. faster gait speeds (Fig.3).

These findings also demonstrate the potential clinical utility of this type of detailed kinematic analysis of the spine for the identification of pathological movement patterns. In particular, the movement patterns in the transverse plane demonstrated by this subject showed two behaviors of note. First, at the slow gait speed, the caudo-cranial progression of mean phase-offsets was not present at L3 relative to S1 (Fig.3), likely due to a brief deviation in the movement of S1 and L3, from their otherwise sinusoidal trajectories, around 270° in the gait cycle (Fig.1 and Fig. 2). Examination of individual gait cycle kinematics found this deviation to be present in 9 of the 10 gait cycles. Further examination is required to determine if this deviation may be representative of a segmental instability or other pathology. Second, at the faster gait speed, movement in the transverse plane appeared to transition toward a more multi-phasic pattern across the gait cycle, as described in previous studies [3]. This pattern, however, was decidedly asymmetrical. Once again, further investigation is required to determine the precise clinical relevance of this transverse plane asymmetry.

5. ACKNOWLEDGMENTS

6. REFERENCES

[1] Callaghan JP, Patla AE, McGill SM. Low back three-dimensional joint forces, kinematics, and kinetics during walking. Clin Biomech. 1999; 14:203–16

[2] Lamoth CJ, Beek PJ, Meijer OG. Pelvis-thorax coordination in the transverse plane during gait. Gait Posture. 2002; 16(2):101-14

[3] Van Emmerik REA, Wagenaar RC. Effects of walking velocity on relative phase dynamics in the trunk in human. J Biomech 1996; 29:1175–84

[4] Taylor NF, Evans OM, Goldie PA. Angular movements of the lumbar spine and pelvis can be reliably measured after 4 minutes of treadmill walking. Clin Biomech. 1996; 11:484–486

[5] Burgess-Limerick, R., Abernethy, B., Neal, R. Relative phase quantifies interjoint coordination. J Biomech. 1993; 26, 91-94

[6] Crosbie J, Vachalathiti R, Smith R. Patterns of spinal motion during walking. Gait Posture 1997; 5: 6–12

[7] Syczewska M, Oberg T, Karlsson D. Segmental movements of the spine during treadmil walking with normal speed. Clin Biomech. 1999; 14:384–8

Introducing a soft tissue artifact model in multi-body optimization: a feasibility study

Richard V. [1], Camomilla V. [2], Chèze L. [1], Cappozzo A. [2], Dumas R. [1]

[1] Université de Lyon, F-69622 Lyon, France, UMR_T9406, Laboratoire de Biomécanique et Mécanique des Chocs, IFSTTAR, Bron, France, Université Lyon 1, Villeurbanne, France

[2] Department of Human Movement and Sport Sciences, Università degli Studi di Roma "Foro Italico"

Keywords: Soft tissue artifact, Multi-body optimization, Lower limb, Gait analysis

1. INTRODUCTION

While assessing human movement using stereophotogrammetry and skin markers, the inaccuracies engendered by the movement of these markers relative to the underlying bone (soft tissue artifacts: STAs) represent an unsolved problem. Indeed, bone pose and notably joint kinematics estimation are jeopardized by these inaccuracies. In recent years, methods have been proposed with the aim of compensating for STA [10]. Two groups of methods are typically used: single body optimization and constrained multi-body optimization (MO). MO uses a model of a chain of body segments with specific joint constraints and minimizes the distances between measured and model-determined marker positions [11]. Moreover, the modeling of STAs is also a current topic [2, 6] and some models have been embedded in single body optimizations [1].

This study aims at incorporating a STA model, at a cluster level, in the MO. The objective is to investigate the practicability and potentiality of such approach, focusing on the value of the objective function residual, on the amplitude of rotation, translation, homothety and stretch of the cluster of markers, and on the pattern of joint kinematics.

2. MATERIAL AND METHODS

Multi-body optimization methods with soft tissue artifact model

Parameter set

Generalized parameters $\mathbf{Q}_i$ [7] expressed in the inertial coordinate system (ICS) have been used, for each body segment i, consisting in the position vectors of proximal and distal endpoints, P_i and D_i respectively, and two unit orientation vectors $\mathbf{u}_i$ and $\mathbf{w}_i$ (Fig.1):

$$\mathbf{Q}_i = \begin{bmatrix} \mathbf{u}_i & \mathbf{r}_{P_i} & \mathbf{r}_{D_i} & \mathbf{w}_i \end{bmatrix}^T . \qquad (1)$$

Affine STA model

The transformation of the clusters of skin markers from their model-determined shape to a deformed shape (with the positions of the markers in both shapes expressed in the ICS, see Fig.1) is defined for each body segment i by the vector $\mathbf{A}_i$:

$$\mathbf{A}_i = \begin{bmatrix} a_0^x & a_1^x & a_2^x & a_3^x & a_0^y & a_1^y & a_2^y & a_3^y & a_0^z & a_1^z & a_2^z & a_3^z \end{bmatrix}_i^T . \qquad (2)$$

The coefficients a_0^x, a_0^y, a_0^z represent the translation $\mathbf{t}_i$ of the origin of the ICS (considered as fixed with respect to the cluster of markers) [8]:

$$\mathbf{t}_i = \begin{bmatrix} a_0^x & a_0^y & a_0^z \end{bmatrix}_i^T . \qquad (3)$$

The other nine components represent, as a whole, rotation, homothety and stretch [8]:

$$\mathbf{T}_i = \begin{bmatrix} a_1^x & a_2^x & a_3^x \\ a_1^y & a_2^y & a_3^y \\ a_1^z & a_2^z & a_3^z \end{bmatrix}_i . \qquad (4)$$

After a polar decomposition of $\mathbf{T}_i$ the direction cosine matrix, the three coefficients of homothety and the three coefficients of stretch are defined about the XYZ axes of the ICS.

Joint model

Ankle, knee and hip joints are modeled by spherical joints [11].

Objective function

STA parameters $\mathbf{A}_i$ are optimized in the same time as the segment position parameters $\mathbf{Q}_i$.

For the jth marker of segment i M_i^j, we define a set of driving (or motor) constraints (Fig.1):

$$\boldsymbol{\Phi}_{ij}^m = \mathbf{r}_{M_i^j} - \left(\mathbf{T}_i \left(\mathbf{N}_i^{M_i^j} \mathbf{Q}_i \right) - \mathbf{t}_i \right). \quad (5)$$

$\boldsymbol{\Phi}_{ij}^m$ is the difference between the measured marker position $\mathbf{r}_{M_i^j}$ and the corresponding model-determined marker position $\mathbf{N}_i^{M_i^j} \mathbf{Q}_i$ (obtained through an interpolation matrix $\mathbf{N}_i^{M_i^j}$ [7, 9]), further transformed with $\mathbf{T}_i$ and $\mathbf{t}_i$ (noted $\mathbf{r}_{M_i^j}^*$ in Fig.1).

The optimization problem is:

$$\min_{\left|\begin{array}{c}\mathbf{Q}\\\mathbf{A}\end{array}\right.} f = 1/2 \left(\boldsymbol{\Phi}^m \right)^T \boldsymbol{\Phi}^m$$

$$subject\,to \begin{cases} \boldsymbol{\Phi}^k = 0 \\ \boldsymbol{\Phi}^r = 0 \\ \boldsymbol{\Phi}^a = 0 \end{cases} \quad (6)$$

with $\boldsymbol{\Phi}^m$ the vector of driving constraints with all markers of all segments, $\boldsymbol{\Phi}^k$ and $\boldsymbol{\Phi}^r$ the kinematic and rigid-body constraints respectively [9] and $\boldsymbol{\Phi}^a$ the STA model constraints.

Minimization is solved using a Newton-Raphson algorithm [3] in Matlab™, on the following equation:

$$\mathbf{F}\begin{pmatrix}\mathbf{Q}\\\mathbf{A}\\\boldsymbol{\lambda}\end{pmatrix} = \begin{bmatrix} \left(\mathbf{K}^m\right)^T \boldsymbol{\Phi}^m + \begin{bmatrix}\mathbf{K}^k\\\mathbf{K}^r\\\mathbf{K}^a\end{bmatrix}^T \begin{pmatrix}\boldsymbol{\lambda}^k\\\boldsymbol{\lambda}^r\\\boldsymbol{\lambda}^a\end{pmatrix} \\ \boldsymbol{\Phi}^k \\ \boldsymbol{\Phi}^r \\ \boldsymbol{\Phi}^a \end{bmatrix} = \mathbf{0} \quad (7)$$

with $\mathbf{K}^m$ the Jacobian matrix of $\boldsymbol{\Phi}^m$; $\mathbf{K}^k$, $\mathbf{K}^r$ and $\mathbf{K}^a$ the Jacobian matrices of $\boldsymbol{\Phi}^k$, $\boldsymbol{\Phi}^r$ and $\boldsymbol{\Phi}^a$ respectively, and $\boldsymbol{\lambda}^k$, $\boldsymbol{\lambda}^r$, $\boldsymbol{\lambda}^a$ the corresponding Lagrange multipliers.

STA model constraints

Three conditions were tested: 1. affine transformation of the cluster of markers with no constraint on the parameters of the matrix $\mathbf{T}_i$; 2. rigid transformation of the cluster of markers where homothety and stretch are the identity transformation (their coefficients are 1 and 0 respectively), constraining $\mathbf{T}_i$ to be orthogonal (i.e. $\mathbf{T}_i^T \mathbf{T}_i = \mathbf{E}$ with $\mathbf{E}$ the identity matrix); 3. no transformation of the cluster of markers ($\mathbf{T}_i = \mathbf{E}$ and $\mathbf{t}_i = \mathbf{0}$).
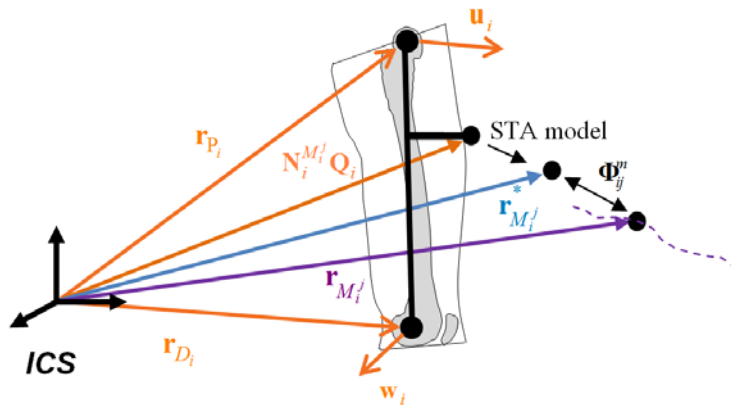

Fig.1: Parameterization of segment i and positions of the marker M_i^j in the ICS.

Data acquisition and processing

Five healthy male subjects (age: 29±5 years; height: 1.74±0.09 m; mass: 76.5±13.5 kg) participated in the study. The trajectories of 32 skin-based markers on the right lower limb (eight markers by segment) were recorded at 100 samples per second during a level walking cycle.

The rotation angle (in degree) of the STA transformation is extracted by projection of the direction cosine matrix onto the helical axis, and we focused on the norm of the displacement of the centroid of the cluster, deduced from $\mathbf{t}_i$. Concerning the homothety and stretch, the average value over the respective coefficients (i.e. about the XYZ axes of the ICS) was computed.

3. RESULTS

For all the subjects, the optimization residual on f was smaller when introducing an affine transformation of the cluster of markers compared to an optimization with no transformation.

STA model on the thigh

Rotation (maximal value over the gait cycle and throughout subjects: 2 degrees with affine transformation and 1.5 degrees with rigid transformation of the cluster of markers) and translation (maximal value over the gait cycle and throughout subjects: 19 mm with affine transformation and 11 mm with rigid transformation of the cluster of markers) parameters resulted to be larger with the affine than with the rigid STA model (Fig.2). Homothety and stretch coefficients were very close to 1 and 0 respectively (Fig.3).

Knee joint kinematics

On the whole, the amplitudes and curve patterns of the knee joint kinematics were similar with the different STA models tested (Fig.4). The choice of the STA model at the cluster level (affine, rigid or no transformation) does not influence significantly the optimized joint kinematics.
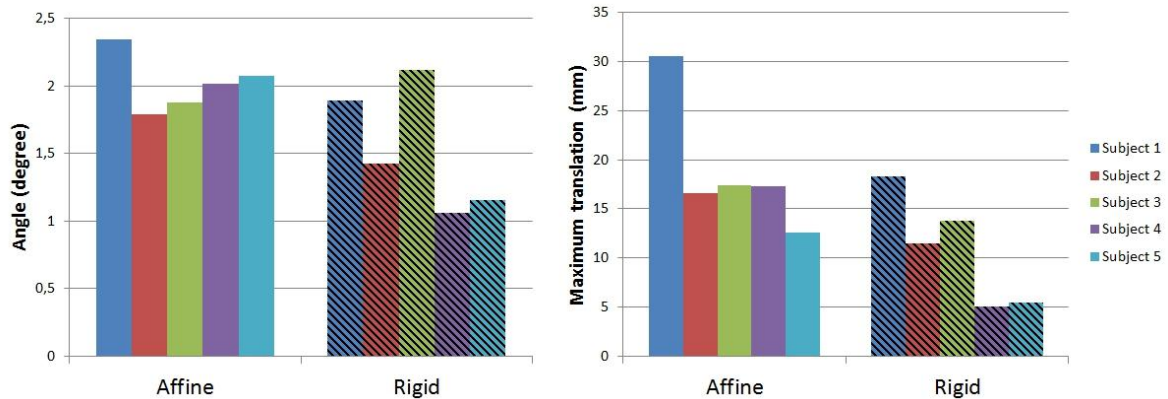

Fig.2 : Maximal angle of rotation (in degree) about helical axis (on the left) and maximal value of the norm of translation (in mm) (on the right) for the right thigh performed over the duration of gait cycle on five subjects with two different STA models, affine (plain) and rigid (striped) transformation.
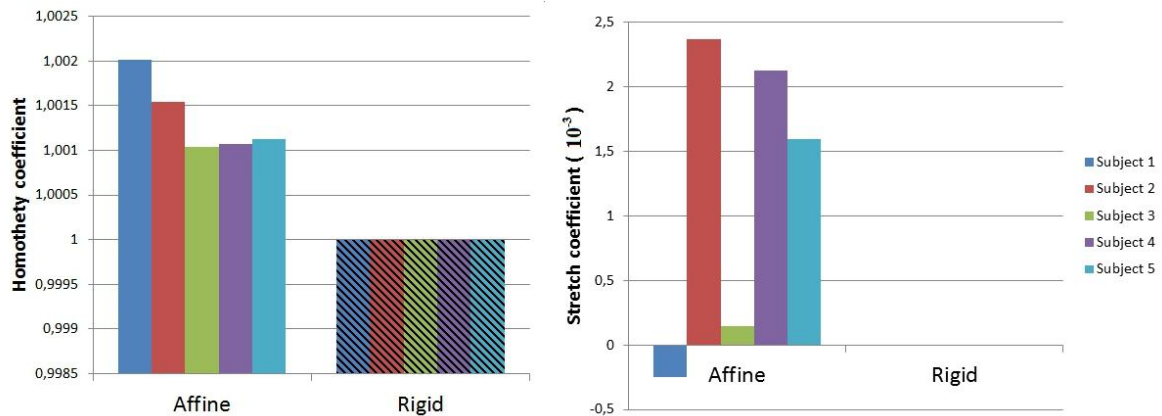

Fig.3 : Maximum, over the duration of gait cycle, of the mean, over the three axes, of homothety (on the left) and stretch (on the right) coefficients, for the right thigh performed on five subjects with two different STA models, affine (plain) and rigid (striped) transformation.
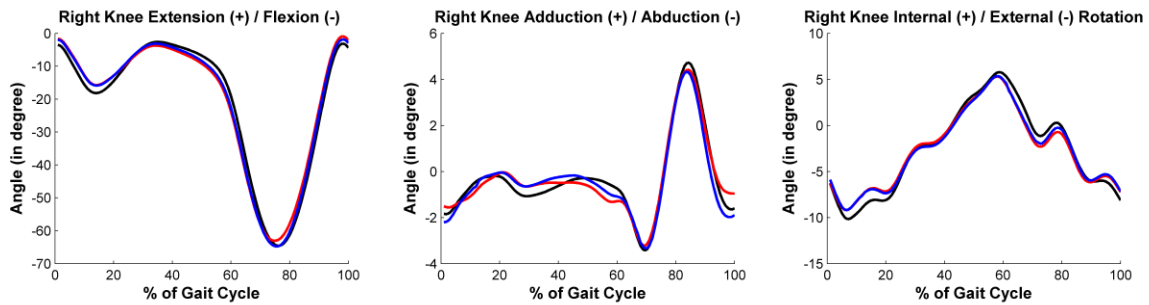
Fig.4: Kinematics of the right knee for a representative subject. Angles (in degree) of Extension/Flexion, Adduction/Abduction and Internal/External Rotation, from the left to the right respectively, are represented with affine (red), rigid (blue) and without (black) STA model.

4. DISCUSSION

In this feasibility study, a new approach for the simultaneous optimization of segment pose and parameters of a STA model was presented by introducing an affine transformation of the cluster of markers in the objective function. The choice of a linear model at a cluster level is comforted by the study of Andersen et al. (2012) [2]. Camomilla et al. (2011) [5], showed a linearity of the relationship between position of a given marker relative to the underlying bone and the closest joint kinematics. The fact that the choice of STA model (affine, rigid or no transformation) has no influence on the optimized joint kinematics, but has an influence on the objective function residual, shows that this method may eventually provide a non-invasive assessment of the deformation of the marker cluster due to STAs. Other approaches have already been proposed for the non-invasive assessment of the soft tissue deformation at the marker level [6]. The present results confirm studies which state that the most important components of skin marker artifact movement are essentially rigid-body translation and rotation of the cluster. The deformation (homothety and stretch) of the cluster is definitely small [2, 4]. However, we can see that a slight variation of the homothety and stretch coefficient influences the rotation and translation values.

To conclude, this new approach may allow estimating the parameters of a defined STA model, but showed some limitations. Actually, this method may provide information about the transformation of marker clusters, but not about the displacement of individual markers relative to the underlying bones. Furthermore, experimental validation data (e.g. with bone pins) would be essential to confirm the results. Next steps would consist in further validating the method and developing the MO method through the use of better joint models [9] and other STA models [5].

5. REFERENCES

[1] E. Alexander and T. Andriacchi, "Correcting for deformation in skin-based marker systems," *Journal of Biomechanics,* vol. 34, pp. 355-361, 2001.

[2] M. Andersen, M. Damsgaard, J. Rasmussen, D. Ramsey and D. Benoit, "A linear soft tissue artefact model for human movement analysis: Proof of concept using in vivo data," *Gait and Posture,* vol. In press, 2012.

[3] M. Andersen, M. Damsgaard and J. Rasmussen, "Kinematic analysis of over-determinate biomechanical systems," *Computer Methods in Biomechanics and Biomedical Engineering,* vol. 12, no. 4, pp. 371-384, 2009.

[4] K. Ball, "Rigid and pliant movement analysis: Use of invasive and external observations to determine tibial and femoral motion during gait," 1998.

[5] V. Camomilla, A. Cereatti, M. Donati and A. Cappozzo, "Functional estimate of the hip joint center location : a soft tissue deformation model for simulation studies," *Proceedings of XXIII ISB Conference,* 2011.

[6] V. Camomilla, M. Donati, R. Stagni and A. Cappozzo, "Non-invasive assessment of superficial soft tissue local displacements during movement: A feasibility study," *Journal of Biomechanics,* vol. 42, pp. 931-937, 2009.

[7] R. Dumas and L. Chèze, "3D inverse dynamics in non-orthonormal segment coordinate system," *Medical and Biological Engineering,* vol. 45, pp. 315-322, 2007b.

[8] R. Dumas and L. Chèze, "Soft tissue artifact compensation by linear 3D interpolation and approximation methods," *Journal of Biomechanics,* vol. 42, no. 13, pp. 2214-2217, 2009a.

[9] S. Duprey, L. Chèze and R. Dumas, "Influence of joint constraints on lower limb kinematics estimation from skin markers using global optimization," *Journal of Biomechanics,* vol. 43, no. 14, pp. 2858-2862, 2010.

[10] A. Leardini, L. Chiari, U. D. Croce and A. Cappozzo, "Human movement analysis using stereophotogrammetry Part 3. Soft tissue artifact assessment and compensation," *Gait and Posture,* vol. 21, pp. 212-225, 2005.

[11] T. Lu and J. O'Connor, "Bone position estimation from skin marker co-ordinates using global optimisation with joint constraints," *Journal of Biomechanics,* vol. 32, pp. 129-134, 1999.

Low-Cost Markerless Motion-Capture System for kinematic assessment of postural tests

Ieluzzi R.[1], Fioretti S.[1]

[1] Department of Information Engineering (DII), Università Politecnica delle Marche, Ancona, Italy

Keywords: Markerless systems, Real-Time, Functional Reach

1. INTRODUCTION

Maintenance of upright posture is a complex task requiring the center of gravity to reside over a small base of support. Sophisticated neuro-muscular mechanisms are necessary to sustain this position. The postural control system deteriorates with age and disease, balance becomes increasingly tenuous resulting in an enhanced susceptibility to falls. Consequently, it is important to be able to assess the subject's ability to maintain balance and to be able to predict the risk of falls. In literature there are many clinical balance tests used to predict falls. An example is provided by the Functional Reach (FR) Test, defined as the maximal distance one can reach forward beyond arm's length while maintaining a fixed base of support in the standing position[1]. The simple clinical measure, extracted from the test, correlates with the risk of recurrent falls in elderly subjects. Nevertheless FR is affected by characteristic flaws of functional evaluation scales, particularly by the ceiling-floor effect, that is a poor sensibility in the middle part of the measurement range. Moreover, as shown in [2], FR cannot be considered as a measure of dynamic balance because it is not able to differentiate healthy elders from individuals with balance impairments. More information can be obtained from this motor task if it can be described looking at the kinematic behavior and at the motor strategies employed. Currently, the kinematic assessment is usually provided in laboratory environment with marker-based stereophotogrammetric systems. Ambulatory systems would require different specifications such as: low-costs, easiness of use and non-intrusive techniques. The Motion-Capture system here described, allows to calculate the biomechanical FR index and the relative flex-extension angle between the torso and the thigh of the subject using only one commercial webcam. The technique does not require any physical contact, it results totally non-invasive, and easy to use. It is suited for a 2D analysis of the FR or similar 2D tasks, giving in real-time the expected results, and allowing the contemporary recording of the video signal. Validation tests have been carried out in an indoor and not structured environment.

2. MATERIALS AND METHODS

A commercial webcam, model Logitech Quick-Cam Pro 9000 (resolution 640x480 pixels, frame-rate 30fps), is located at 1.5 m height from the floor, 3m away from the subject performing the Functional Reach Test. The Zhang's calibration technique [3] is implemented to compute intrinsic and extrinsic camera parameters, from multiple views of a flat planar pattern of control points. Lens distortion parameters are calculated according to Brown [4]. By a preliminary acquisition, the software acquires the background frames and computes, from color intensity values of the image pixels, the background statistical model. So every background pixel is represented by a unimodal Gaussian probability distribution function, described by the mean and variance of the pixel's color intensity. When the FR test acquisition starts, every new pixel of the video sequence is compared with the background statistical model and, if the pixel's color intensity at that time instant does not belong to the correspondent background pixel distribution function, the pixel is then marked as a movement pixel (i.e. as a pixel that probably belongs to the moving subject). Afterwards the software calculates the edge pixels to approximate the external boundary of the moving subject and stores only the longest contour retrieved, so that only pixels physically connected and belonging to the biggest object in the scene are considered. In this way the segmentation procedure becomes less sensitive to salt-and-pepper and shadow noise. Once the external boundary of the subject is calculated, it is discretized into six body sub-parts using the anthropometric stick-figure model shown in Winter [5]. For each body sub-part, the software calculates the least squares ellipse that best-fits the corresponding points cloud. These best-fitted ellipses are used for the motion tracking and to compute the flexion-extension angle between the body parts of interest. The relative angle between the torso and the thigh is defined as the angle between the major semiaxis of the ellipses that approximates the corresponding body parts. The clinical FR measure is estimated as the greatest displacement of the point corresponding to the furthest hand pixel. Through the calibration procedure

the pixel distance calculated for the FR can be converted in a metric distance. Angular values validation has been performed comparing the results obtained by the Motion-Capture system developed and those obtained by an electrogoniometric system (STEP 32, DemItalia); the FR distance estimated has been compared with the direct measure (by a yardstick) of the anterior-posterior displacement of the subject's hand.

3. RESULTS

Fig.1 shows the results of the image processing algorithm implemented for the frame segmentation of the video sequence, once background acquisition has been performed. Fig.2 shows a comparison between the flexion-extension angle measured from the electrogoniometric system, and that estimated by the markerless system. An average error of 0.97 ($\pm$3.99) degrees was obtained. The highest error is located nearby the minimum of the trajectory of the flex-extension angle and ranges between 0 and 4.5 degrees (in absolute value). Fig.3 shows the flat planar pattern used in the calibration procedure with the automatic identification of the internal corners of the chessboard used as control points. The FR has been measured with the markerless system and compared with the measure taken directly with a common yardstick. A further estimate of the FR distance has been computed by means of the anthropometric measures of the subject and by the angular values obtained by the markerless and by the electrogoniometric systems. With respect to the yardstick measure of the FR, the error of the markerless system resulted to be 0.75 ($\pm$1.70); the error in the FR distance estimated by the anthropometric measures of the subjects and by the angular values of body segments obtained by the markerless and by the electrogoniometric systems was 1.23 ($\pm$2.21) cm and is 2.79 ($\pm$5.19) cm, respectively.
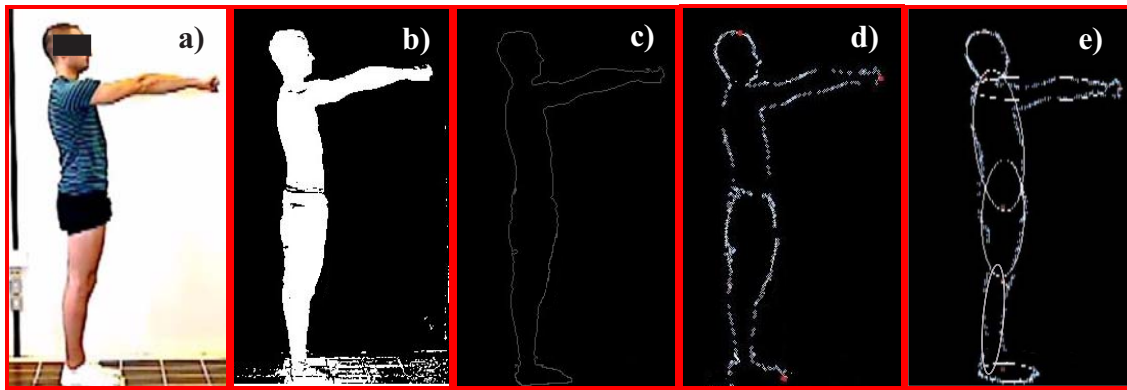

Figure 1.   Results obtained by the Motion Capture System software: a) Original frame, b) segmentation result, c) contours extraction, d) contours discretization e) ellipse approximation
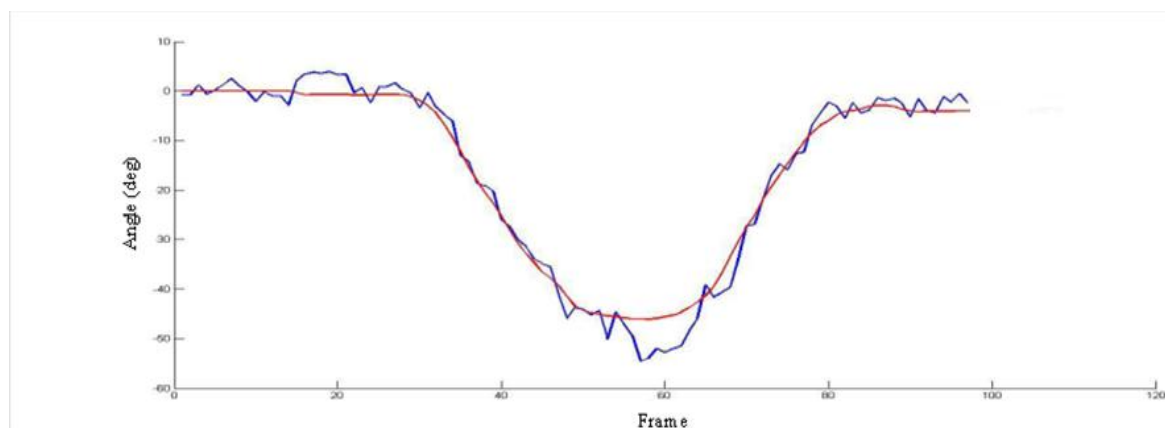

Figure 2. Angle between torso and thigh assessed by the markerless system (blue line), and measured by the electrogoniometric system (red line).

Figure 3. Flat planar pattern used in the calibration procedure; internal corners are detected automatically and colour-marked to show the positive matches resolved by the software.

4. DISCUSSION

Aim of this work was the implementation of a markerless algorithm to estimate the characteristic parameters of a motor task like FR that is significant in the context of functional evaluation of motor disorders and in particular of maintenance of balance. As working hypothesis we assumed: a) the use of a low cost instrumentation, b) unstructured environment, c) user friendliness of the whole tool in the sense that no specific technical skill is required for the end user. All these assumptions have been completely satisfied. The preliminary numerical results show satisfactory level of accuracy in the estimate of both linear and angular displacement data. The system software runs in real-time so that the user can immediately verify the outcome of the test. Moreover the video sequences are not lost but stored for later visualization and use. The software has been meant to be applied also for the analysis of other simple, 2D, yet significant motor tasks as those used in the functional evaluation scales of motor disorders.

5. REFERENCES

[1] P.W. Duncan, D.K. Weiner, J. Chandler and S. Studenski, "Functional reach: a new clinical measure of balance," J. of Gerontology, 1990, vol. 45(6), pp.192-197.

[2] M. Wernick-Robinson, D.E. Krebs, M.M. Giorgetti, "Functional reach: does it really measure dynamic balance?," Arch Phys Med Rehabil, 1999; vol. 80, pp.262-269.

[3] Z. Zhang, "Flexible Camera Calibration by viewing a plane from unknown orientations", IEEE Trans. on Pattern Analysis and MI, 2000, vol. 22(11), pp. 1330-1334.

[4] D.C. Brown, "Decentering Distortion of Lenses", Photometric Engineering, 1966, vol. 32(3), pp. 444-462.

[5] D.A. Winter, "Biomechanics and motor control of human movement", Wiley, 3rd ed. , 2004.

Fri – July 20th 2012

Chairmen: **Paul Allard (Département de Kinésiologie, Université de Montréal, Canada)**

Scott Delp (University of Stanford, USA)

Keynote lecture: ISB Keynote Lecture
11.00 : 11.30 *"*Insights from modeling gait dynamics and disorders*"*
  Scott Delp

Podium session #6: "Musculo-skeletal and joint modelling"
11.30 : 13.00

11.30	Sensitivity and stability analysis of a kinematic model for human joints (an application to human ankle)	Conconi M., Parenti-Castelli V.
11.45	Spherical one-degree-of-freedom models of the knee and ankle joints for lower limb modelling	Sancisi N., Parenti-Castelli V., Belvedere C., Baldisserri B., Leardini A.
12.00	The effect of including accurate pelvis bony landmarks in a nonlinearly scaled musculoskeletal lower extremity model	Andersen M.S., Mellon S., Lund M.E., Grammatopoulos G., Gill H.S.
12.15	Effects of palpation errors on the estimated body segment inertial parameters using an optimization-based method	Hu C.C., Lu T.W., Chiang H., Chen S.C.
12.30	A multi-body optimisation with a knee joint kinematic model including deformable ligament constraints	Gasparutto X., Dumas R., Jacquelin E.
12.45	Introduction of a selection of joint reaction forces in the objective function when solving the muscular redundancy by static optimization	Moissenet F., Chèze L., Dumas R.

!

!

Insights from simulating gait dynamics and disorders

Scott Delp

University of Stanford, USA

The outcomes of treatments performed to correct movement abnormalities are variable. This problem exists, in part, because the biomechanical causes of the abnormal movement patterns are unclear, and the effects of common treatments are not understood. I believe that the design of treatments will improve if computer simulations are developed that complement experimental movement analysis and help explain the causes of movement abnormalities and predict the functional consequences of interventions. This presentation will describe a range of computer simulations that provide insights into the dynamics of human walking and running and the mechanics of common movement abnormalities.

Sensitivity and Stability Analysis of a Kinematic Model for Human Joints

(An Application to Human Ankle)

Conconi M. [1], Parenti Castelli V. [2]

[1] HST-ICIR, University of Bologna, Italy, michele.conconi@unibo.it
[2] DIEM, University of Bologna, Italy, vincenzo.parenti@unibo.it

Biologic tissues tend to arrange themselves in order to achieve the optimal mechanical resistance (functional adaptation). In a previous work, a joint kinematic model has been proposed exploiting this concept. The joint capability to withstand an applied load has been hypothesized to be proportional to a measure of the joint congruence, which indicates how well mating surfaces fit together in a given joint configuration. The envelope of maximum congruence configurations defines a spatial trajectory along which the functional adaptation is satisfied and it is thus called functionally adapted trajectory. In this paper, the sensitivity of the kinematic model to the parameters defining the congruence measure is analyzed, together with the algorithm stability with respect to initial guess variations.

Functional adaptation; joint congruence; joint kinematics; ankle

1. INTRODUCTION

In the last thirty years the literature has documented the impressive capability of animal tissues to modulate their structures and mechanical properties in response to the loads that muscles exert on them. This mechanism, often called "Wolff's low" for bone, was extended to tissues and organs in general by Roux [1] under the name of functional adaptation. Despite these concept dates back to the 19th century, it took up to 1960s for it to became systematically studied. Today, many experimental evidence [2,3] support analytical models [4-8] able to predict the adaptation of different biological tissues. The most studied one is certainly the bone: the mechanisms governing its (re)modeling have been identified, together with the actors involved in it [2,9] and many numerical models exist for the bone adaptation to loads [5,6,10]. Soft tissues are in general more complex: ligaments and tendons behavior is partially understood [11], but their mechanotransduction is still unclear [12,13] and few models are available for predicting their adaptation [4]. The most challenging tissue is anyway the cartilage. Many authors attempted to model it, obtaining good description for its in vitro response to load [14,8]. Still, the dynamics of in vivo behavior is not yet modeled and little is known about its mechanotransduction and on how (and if) it adapts to mechanical requirements [15,16,3]. In order to evaluate the cartilage adaptation, in [17] a measure of joint congruence was exploited that was hypothesized to be proportional to the joint capability to withstand an applied load. A kinematic model for human ankle was build on it. The outcomes of this model were validated against experimental data, obtaining a very good agreement. This was considered an indirect proof of the original assumptions. In this paper, the sensitivity of the kinematic model to the parameters defining the congruence is analyzed, together with the algorithm stability to initial guess variations.

2. JOINT CONGRUENCE

Joint congruence is a common concept in medical literature. It indicates how well mating surfaces fit together, essentially referring to a quality whose evaluation is left to the doctors experiences. From a medical point of view, joint congruence can help to describe the normal physiology of an articulation and may be a good indicator of its functionality: an increase of it corresponds to a better mating between the articular surfaces and it is reasonably associated with an improved capability of distributing and thus withstanding to an applied load. The definition of a measure for the joint congruence is the first step toward a quantitative evaluation of the articulation state. Many congruence measures have been presented, all essentially based on the evaluation of relative curvature of surfaces at or near the contact point (see for instance [18]). This approach does not take into account the relative position and orientation of the bones in the joint (joint configuration) and depends on the surface approximation employed. In [17], a different approach to measure joint congruence was proposed that: i) does not require curvatures computation nor contacts determination, ii) takes into account the joint configuration and iii) is independent from the articular surfaces representation, permitting the use of meshes. Without loss of generality, the measure has been presented for the tibio-talar joint. Let us call S_{tib}, S_{tal}, V_{tib} and V_{tal} the surfaces and the volumes of bone together with the articular cartilage for the distal epiphysis of the tibia and for the talus. The surface of a bone (for instance the tibia) is offsetted of a quantity Δ, defining a surface S_Δ and a corresponding volume V_Δ (Fig. 1.a). The volume trapped between S_Δ

and S_{tib} is called control volume V_c, i.e. $V_c = V_\Delta - V_{tib}$. Joint congruence (CM) at a given configuration is defined as the volume of the intersection between V_c and V_{tal}. In order to obtain a continuous function, more suitable for numerical optimization, copenetration is allowed. Its volume $V_{tib} \cap V_{tal}$, penalized by an experimental term k, is subtracted from the measure. Globally we have:

$$CM = V_c \bigcap V_{tal} - k \cdot (V_{tib} \bigcap V_{tal}) \qquad (1)$$

Clearly, the better the mating between the two articular surfaces will be, the bigger will be the portion of the talus within the control volume. Defining by $\underline{x}$ the six dimensional vector of the coordinates representing the configuration of the tibio-talar joint, it is possible to write the following function f for CM:

$$CM = f(S_{tib}, S_{tal}, \Delta, k, \underline{x}) \qquad (2)$$

3. MATERIALS AND METHODS

Adapted and Passive Motion

In an adapted motion, ligaments should stay isometric. Indeed, they grow in length in order to avoid continuous tensioning and they shorten to compensate relaxation due to creep [11]. In vivo experimental evidences [16] show that articular cartilages thickness decreases of a 5% after few cycles and then it stabilizes, independently from the performed activity. Thus, in a normal adapted motion cartilage may be considered uncompressible. The same ligament and cartilage deformation states [19] may be found in passive motion [20]. Therefore it is possible to take the latter as representative of the former.

Data Acquisition

Tibio-talar relative passive motion was recorded in vitro as a sequence of neutral equilibrium configuration using a Stryker Navigation stereophotogrammetric system (precision: ±0.5 degrees, ±0.5 mm), and represented by means of a sequence-independent joint coordinate system [21]. Using the same instrumentation and a pointer, the articular surfaces were digitalized as clouds of points. The whole procedure and experimental setup are described in [22]. Triangular mesh models for the bone surfaces were found in the VAKHUM database. These models were then manually adapted to fit the experimental data for the articular surfaces.

Trajectory Generation

Functional adaptation requires the optimal use of tissues. Thus, assuming that a given joint is adapted implies it arranges its material in order to achieve the greatest mechanical resistance. The proposed congruence measure is hypothesized to be proportional to the joint capability to withstand an applied load. It follows that, among many physiological trajectories, the adapted one will be the envelope of maximum congruence configurations. The tibio-talar joint may be considered as a single degree of freedom (DOF) joint [19], therefore its motion can be parameterized with one independent scalar parameter. The remaining dependent coordinates can be obtained by congruence maximization. Numerically, congruence is evaluated by means of boolean operation as implemented in the GNU Triangulated Surface Library (GTS). The search for maximum congruence configurations is performed with Nelder-Mead Simplex algorithm as implemented in the GNU Scientific Library (GSL).

4. ALGORITHM SENSITIVITY AND STABILITY

The algorithm may be sensitive to the parameterization of motion, to the bone chosen for the control volume definition, to the offset Δ and to the penalty factor k. Each one of the six components of $\underline{x}$ was taken as independent reference parameter of the talar motion within the control volume built on V_{tib}. In order to evaluate the sensitivity to the V_c definition, a further parameterization for the motion of the tibia within the control volume built on V_{tal} was considered. Δ and k were investigated in the range 1-7 mm and 1-10 respectively, both with steps of 0.5. For every parameterization and for every value of Δ, a value of k_{conv} was found above which the algorithm is almost insensitive to k and converges to a single trajectory, k_{conv} growing with Δ. The algorithm sensitivity to Δ variation was studied for 70 evenly distributed pair of Δ and k values, with $k \geq k_{conv}$. Table 1 shows the mean standard deviation (MSD) of the dependent coordinates for every parameterization considered. The small MSD values indicate a small sensitivity to Δ variation when $k \geq k_{conv}$. The parameterizations based on the dorsi-plantar flexion angle (DPF) show similar MSD, suggesting the algorithm insensitivity to the bone used in V_c definition. The optimal working value for the offset was chosen noticing that the sensitivity to k further decreases when Δ grows. Thus, the upper bound of the investigated range was taken ($\Delta = 7$). The optimal k was chosen as the value leading to a residual copenetration compatible with clinical data: assuming a mean cartilage thickness of 1.3 mm for each articular surface in the ankle joint , and admitting deformations of 5% [16], a 0.13 mm copenetration may be considered physiological. Values of $\Delta = 7$ and k=20 result in an acceptable mean copenetration for all the parameterizations (table 2). Table 2 shows the mean absolute error (MAE) between each coupled coordinates of the mean experimental trajectory
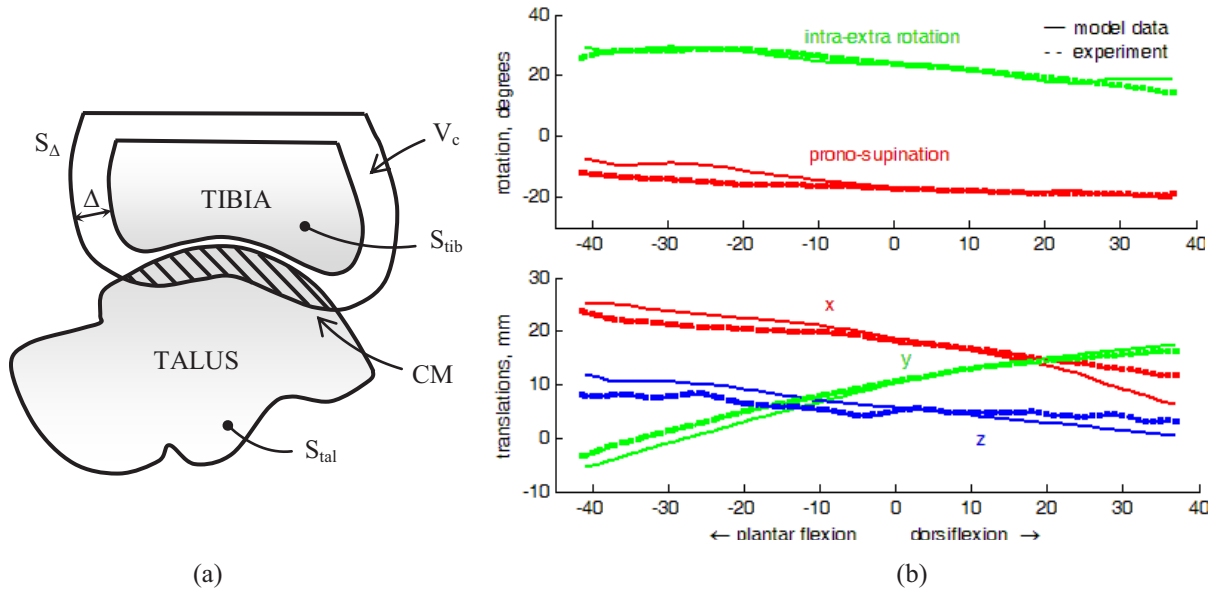
(a)

(b)

Figure 1: a) representation of control volume (V_c) and congruence measure (CM); b) computed (Δ=7, k=20, flexion angle, talus motion) (-) vs mean experimental (- -) trajectory.

Table 1: MSD of the dependent coordinates for every parameterization considered

	DPF (degree)	PS (degree)	IE (degree)	X (mm)	Y (mm)	Z (mm)
MSD - param. DPF	/	0.30	0.66	0.15	0.07	0.14
MSD - param. DPF$_{tib}$	/	0.25	0.52	0.09	0.11	0.24
MSD - param. PS	1.41	/	0.53	0.45	0.50	0.11
MSD - param. IE	1.73	0.34	/	0.52	0.49	0.26
MSD - param. X	0.65	0.26	0.59	/	0.19	0.17
MSD - param. Y	0.67	0.59	1.08	0.29	/	0.47
MSD - param. Z	2.75	0.50	0.94	0.81	1.05	/

Table 2: For each parameterization is reported the MAE between mean experimental trajectory and the computed motion (Δ=7 and k=20), the predictable flexion range and the mean residual copenetration

	PS (degree)	IE (degree)	X (mm)	Y (mm)	Z (mm)	Flexion range	d$_{mean}$
MAE - param. DPF	2.08	1.04	1.83	1.11	1.87	[-41 ÷ 36]	-0.16
MAE - param. DPF$_{tib}$	1.50	1.38	1.98	0.78	1.30	[-41 ÷ 36]	-0.16
MAE - param. PS	0.93	1.77	2.03	0.96	1.34	[-22 ÷ 2]	-0.10
MAE - param. IE	2.33	0.74	1.53	1.18	1.78	[4 ÷ 15]	-0.15
MAE - param. X	2.25	1.26	0.93	0.81	1.89	[-30 ÷ 36]	-0.18
MAE - param. Y	1.89	0.69	0.92	0.69	1.43	[-39 ÷ 29]	-0.15
MAE - param. Z	0.52	1.63	0.40	0.20	0.48	[-28 ÷ 19]	-0.15

Table 3: MSD of the dependent coordinates for DPF parameterization over 1444 different IGs

	DPF (degree)	PS (degree)	IE (degree)	X (mm)	Y (mm)	Z (mm)
MSD - total	/	0.048	0.099	0.015	0.006	0.017

and the motion computed with Δ and k optimal values. Different parameterizations result in similar MAE. DPF parameterizations were chosen as optimal due to their small MSD. Algorithm stability was evaluated by testing its convergence for different initial guesses (IGs) on both the DPF parameterizations. Neighborhoods of radius 5 of the extreme dorsiflexion, extreme plantarflexion and the neutral experimental configurations were taken. Within each of them, 243 evenly spaced IGs were considered, for a total of 1446 IGs. The algorithm converged within three steps on the same trajectory in all the case but two, which clearly result in a smaller minimum. Table 3 reports the MSD after the convergence and neglects these two cases. It is possible to conclude that the maximum found is very stable. Figure 1.b shows the computed trajectory, against the mean experimental trajectory for the passive motion, when the DPF parameterization is used, V_c is defined based on tibia, Δ=7 and k=20. The first plot shows the progression of the prono-supination (PS) and intra-

extra (IE) rotation angles while the second shows the progression of the x, y and z displacements, all plotted versus DPF.

5. CONCLUSION

In this work, sensitivity and stability of a kinematic model of human joint have been assessed. The model shows small sensitivity to all the parameters defining the congruence measure and it is very stable with respect to a wide range of initial perturbations, namely to different IGs. The comparison between experimental and computed trajectories has shown a very good agreement between computed and experimental trajectories for the tibio-talar joint on a range of more than 70 degrees of DPF. It is worth to underline the predictive nature of the model: it does not rely on a measure of the trajectory it aims to match, but it simply need a description of bone and articular surfaces. This makes it possible to generate subject-specific models for the joint kinematics that could possibly result helpful in pre-surgical planning, in the study of the effect of articular surface damages on the overall joint behavior and in the prosthesis design.

6. REFERENCES

[1] W. Roux, "Der Zuchtende Kampf der Teile, oder die Teilauslese im Organismus (Theorie der Funktionellen Anpassung)", W. Engelmann, Ed. Leipzig, 1881.

[2] A. G. Robling, A. B. Castillo, C. H. Turner, "Biomechanical and molecular regulation of bone remodeling," Annu Rev Biomed Eng, vol. 8, pp. 455–498, 2006.

[3] X. L. Lu and V. C. Mow, "Biomechanics of articular cartilage and determination of material properties," Med Sci Sports Exerc, vol. 40, pp. 193–199, Feb 2008.

[4] T. Wren, G. Beaupre, D. Carter, "A model for loading dependent growth, development, and adaptation of tendons and ligaments," J Biomech, vol. 31, pp. 107–114, Feb 1998.

[5] D. Carter, "Mechanical loading history and skeletal biology" J Biomech, vol. 20, pp. 1095–109, 1987.

[6] R. Huiskes, R. Ruimerman, G. H. van Lenthe, J. Janssen, "Effects of mechanical forces on maintenance and adaptation of form in trabecular bone," Nature, vol. 405, pp. 704–706, Jun 2000.

[7] J. H. Heegaard, G. S. Beaupre, D. R. Carter, "Mechanically modulated cartilage growth may regulate joint surface morphogenesis," J. Orthop. Res., vol. 17, pp. 509–517, Jul 1999.

[8] W. M. Lai, J. S. Hou, V. C. Mow, "A triphasic theory for the swelling and deformation behaviors of articular cartilage," J Biomech Eng, vol. 113, pp. 245–258, Aug 1991.

[9] J. Letechipia, A. Alessi, G. Rodriguez, J. Asbun, "Would increased interstitial fluid flow through in situ mechanical stimulation enhance bone remodeling?" Med. Hypotheses, vol. 75, pp. 196–8, Aug 2010.

[10] T. Adachi, Y. Kameo, M. Hojo, "Trabecular bone remodelling simulation considering osteocytic response to fluid-induced shear stress," Philos Trans A Math Phys Eng Sci, vol. 368, pp. 2669–82, 2010.

[11] H. M. Frost, "Skeletal structural adaptations to mechanical usage (SATMU): 4. mechanical influences on intact fibrous tissues," Anat. Rec., vol. 226, pp. 433–439, Apr 1990.

[12] D. Kaneko, Y. Sasazaki, T. Kikuchi, T. Ono, K. Nemoto, H. Matsumoto, Y. Toyama, "Temporal effects of cyclic stretching on distribution and gene expression of integrin and cytoskeleton by ligament fibroblasts in vitro," Connect. Tissue Res., vol. 50, pp. 263–269, 2009.

[13] C. Chen, R. McCabe, A. Grodzinsky, R. Vanderby, "Transient and cyclic responses of strain-generated potential in rabbit patellar tendon are frequency and ph dependent," J Biomech Eng, vol. 122, pp. 465–470, 2000.

[14] V. Mow, S. Kuei, W. Lai, C. Armstrong, "Biphasic creep and stress relaxation of articular cartilage in compression? theory and experiments," J Biomech Eng, vol. 102, pp. 73–84, Feb 1980.

[15] H. M. Frost, "Skeletal structural adaptations to mechanical usage (SATMU): 3. the hyaline cartilage modeling problem," Anat. Rec., vol. 226, pp. 423–432, Apr 1990.

[16] F. Eckstein, M. Hudelmaier, R. Putz, "The effects of exercise on human articular carti-lage," J. Anat., vol. 208, pp. 491–512, Apr 2006.

[17] M. Conconi, V. Parenti Castelli, "Joint kinematics from functional adaptation: an application to human ankle.", XI MTM & Robotics, Clermont-Ferrand, France, June 2012.

[18] K. Connolly, J. Ronsky, L. Westover, J. Kupper, R. Frayne, "Analysis techniques for congruence of the patellofemoral joint," J of Biomec.l Eng., vol. 131, no. 12, pp. 1 – 7, 2009.

[19] A. Leardini, J. O'Connor, F. Catani, S. Giannini, "Kinematics of the human ankle complex in passive flexion; a single degree of freedom system," J. of Biomech, vol. 32, no. 2, pp. 111 – 18, 1999.

[20] D. Wilson, J. O'Connor, "A three-dimensional geometric model of the knee for the study of joint forces in gate," Gait and Posture, vol. 5, pp. 108–115, 1997.

[21] E. Grood, W. Suntay, "A joint coordinate system for the clinical description of three-dimensional motions: Application to the knee," Journal of Biom.echilnlcal Engineering, vol. 135, pp. 136–144, 1983.

[22] R. Franci, V. Parenti-Castelli, "A 5-5 one-degree-of-freedom fully parallel mechanism for the modeling of passive motion at the human ankle joint," in DETC2007, vol. 8 PART A, Las Vegas, NV, United states, pp. 637 – 644, 2007.

Spherical one-degree-of-freedom models of the knee and ankle joints for lower limb modelling

Nicola Sancisi [1], Vincenzo Parenti-Castelli [1], Claudio Belvedere [2], Benedetta Baldisserri [1], Alberto Leardini [2]

[1] Department of Mechanical Engineering-DIEM, University of Bologna, Italy – nicola.sancisi@unibo.it
[2] Movement Analysis Laboratory, Istituto Ortopedico Rizzoli, Bologna, Italy – leardini@ior.it

Keywords: spatial mechanisms; knee joint; ankle joint; spherical wrist; kinematics analysis

1. INTRODUCTION

In virtually unloaded conditions, the human tibiofemoral (knee) and tibiotalar (ankle) joints behave as single degree-of-freedom (1DOF) systems [1]. In these conditions, fibers within the ligaments remain nearly isometric throughout the flexion arc and articular surfaces nearly rigid. Relevant theoretical models are showing that the ligaments and the articular surfaces act together as mechanisms to control the passive joint kinematics [2-4]. In the knee joint, isometric fibers were identified within the anterior cruciate, posterior cruciate and medial collateral ligaments, whereas rigid contacts were associated to the two condylar articular surfaces [2,3]. In the ankle, isometric fibers were identified within the calcaneal-fibular and tibio-calcaneal ligaments, rigid contacts were associated to the articular surfaces between the tibio-fibular mortise and the talus [4]. Kinematic measurements and corresponding model predictions also revealed that the instantaneous screw axes of both the knee and ankle motion all pass near to a single point, hereinafter called the pivot point (Figure 1). This observation proves that a nearly-spherical motion is experienced by these human joints.
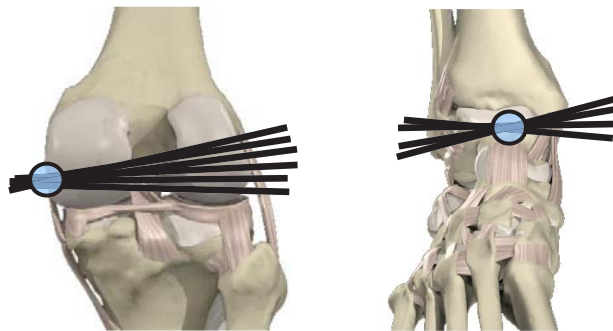

Figure 1. Graphical representation of the instantaneous screw axes of motion at the knee (left) and ankle (right); these axes pass near to a single point, i.e. the pivot point.

Based on this experimental evidence, a first group of mechanisms was proposed by these authors for the kinematic modeling of the knee and ankle joints [3,4]. These models feature two members (i.e. the rigid bones including cartilages) in mutual contact at the articular surfaces and interconnected by rigid links (i.e. the ligaments' isometric fibers). Different models were defined by increasing the quality of articular surface representation; in particular, the model that features a spherical approximation for each of the anatomical articulating surfaces (hereinafter called ESM2, for consistency with previous studies [3]) revealed to be very accurate. These mechanisms replicated well the natural kinematics of these joints by direct representations of the anatomical structures that guide the passive motion. However, these mechanisms are limited by high computational costs and overall mechanical complexity; they show also numerical instability of the relevant mathematical models, that is source of singularity problems, of high sensitivity to geometrical parameter variations and of oscillations of the simulated motion. All these aspects can be a problem when simpler analyses are necessary as in musculo-skeletal modeling of the lower limb, or when simple and stable prostheses and orthoses have to be designed. Thus, still novel mechanisms are necessary to drastically simplify the

geometry of the models and to improve their numerical stability. Spherical Parallel Mechanisms (SPM) are being analyzed [5-7], based both on anatomy and kinematics of human joints: two isometric ligaments (the cruciates for the knee and the calcaneal-fibular and tibio-calcaneal ligaments for the ankle) are modeled as binary links of constant length, and the bones are also connected by a spherical pair centered at the pivot point, in order to approximate the nearly spherical motion observed for the knee and ankle joints (Figure 2). The model is still a 1DOF equivalent spatial mechanism.
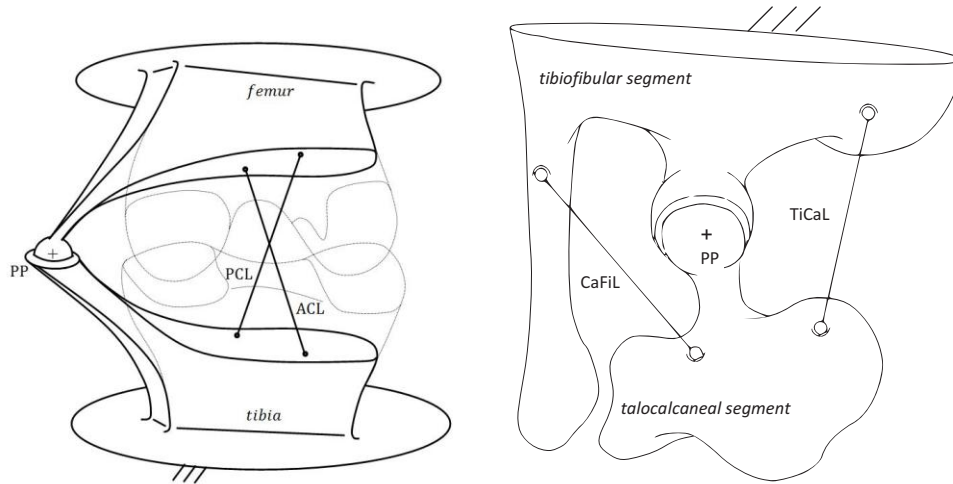

Figure 2. SPM models of the knee (left) and ankle (right) joints, with diagrammatic representation of the relevant ligaments, and the pivot point.

The present study is aimed at defining and testing original SPM models for the kinematics analysis of the human knee and ankle joints. For this purpose, anatomical and kinematics measurements were taken from in-vitro experiments, from which the models were defined. Model predictions were compared with original measurements, and with those from the previous equivalent mechanism ESM2. Advantages and disadvantages of these new models are discussed.

2. MATERIALS AND METHODS

Experimental measurements

Geometrical data and reference motion for the definition of SPM and ESM2 mechanisms were obtained from experiments in fresh frozen amputated lower limbs, 4 knees and 5 ankles, free from anatomical defects. Passive flexion-extension cycles were performed and relevant bone motion was recorded by a standard stereo-photogrammetric device. Anatomical landmarks, articular surfaces and ligament origins and insertions were also digitized. Anatomical reference frames were defined and the relative displacements and rotations of the joints were obtained [8]. Isometric fiber attachment points were determined in the ligament attachment areas. The articular surfaces required by ESM2 models were obtained by means of spherical approximation of the digitized point clouds. The pivot point required by SPM models was obtained by searching the point with the least mean squared distance from the instantaneous screw axes of passive motion.

Kinematics analysis

The closure equations of the SPM and ESM2 models were solved to obtain the simulated motion of the joints, in order to compare it with the experimental one. For each model, a bounded optimization procedure was performed to find the optimal geometric parameters which allow the different models to best-fit the corresponding experimental motion. The bounds on geometric parameters were chosen in order to keep the optimal parameters close to their first estimate based on anatomy. The mean squared and weighted error (err) between the calculated and experimental joint motion was used as an index to compare the accuracy of the models. In other words, the square root of err is the rms value of the per cent difference between the calculated and experimental motion parameters, with respect to the corresponding range.

3. RESULTS

Mechanical complexity of the new spherical mechanism SPM is lower than the previous models. The number of links and kinematic pairs is indeed lower, and only 16 independent geometrical parameters are required to define SPM, against the 35 parameters required by ESM2. This aspect does affect the computational costs, in particular during the optimization procedure: each SPM geometry was approximately optimized in 10 minutes on a personal computer with a 2.8 GHz processor and 6 GB of RAM; the ESM2 model required from 2 to 11 hours on the same platform. The lower computational time was a consequence also of the higher numerical stability of SPM: almost no singularity problems were found during the optimization of SPM, contrarily to ESM2 (Table 1); moreover, a preliminary analysis [9] proved that the sensitivity to geometrical parameter variations of SPM is lower than ESM2. The SPM model replicated passive motion with a comparable though lower precision with respect to ESM2 (Figure 3). In particular, for the knee mechanisms (Table 1), the values of accuracy index err for SPM are nearly twice those for ESM2. These results prove that the passive motion of the knee and ankle joints can be approximated well also by a 1DOF spherical motion.
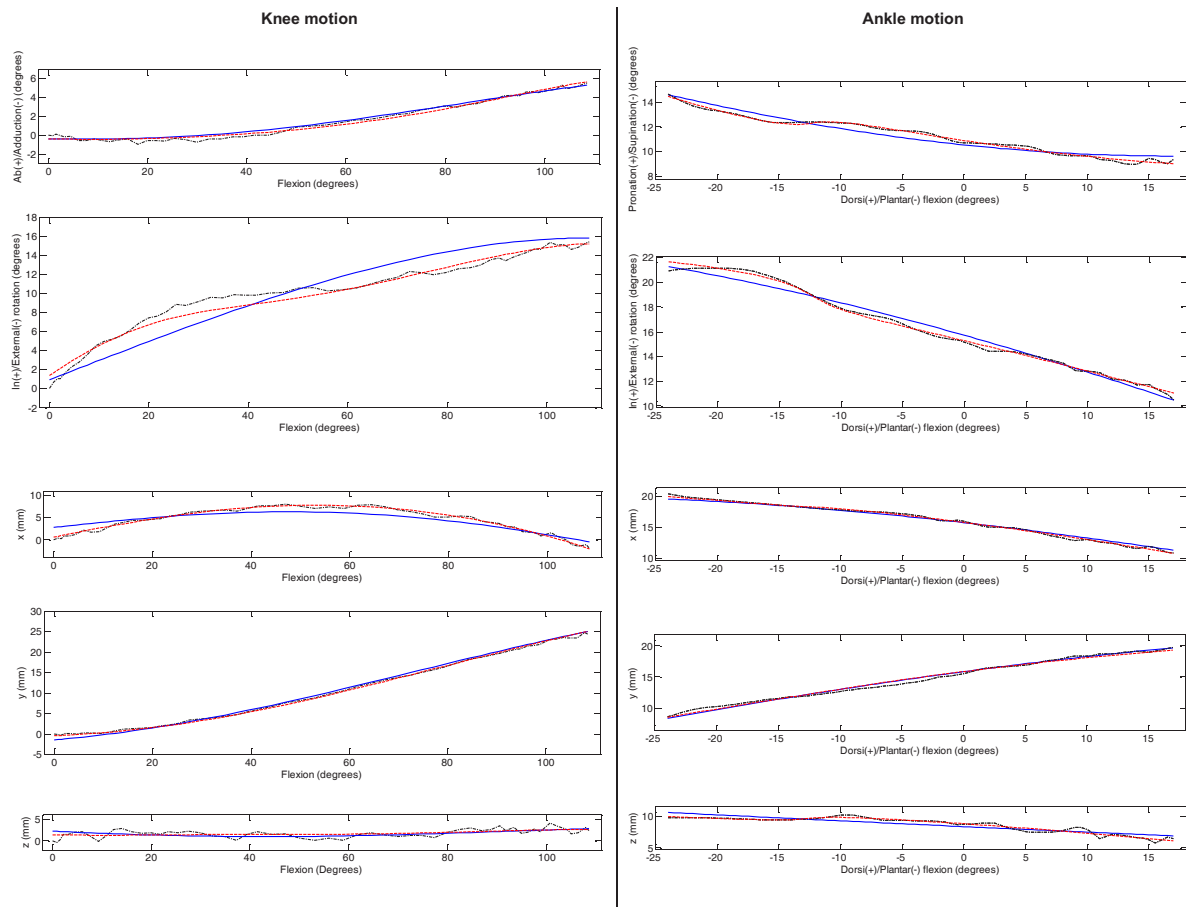

Figure 3. Rotations (top two) and translations (bottom three) patterns from a typical knee (left) and ankle (right) specimen: superimposition of the experimental (black point-dashed), and corresponding ESM2 (red dashed) and SPM (blue solid) motion. Similar results were obtained for the other knee and ankle specimens.

Table 1. Accuracy index *err* and number of singularity problems for the ESM2 and SPM models over the four knee specimens. Similar results were obtained for the ankle mechanisms.

Parameters:		Specimen 1	Specimen 2	Specimen 3	Specimen 4
err	ESM2	0.0033	0.0072	0.0039	0.0028
	SPM	0.0087	0.0132	0.0058	0.0066
Number of singularity problems	ESM2	172	2430	12235	8557
	SPM	0	0	854	0

4. CONCLUSIONS

Any 1DOF spatial mechanism is an important means for more physiological mechanical models of both the knee and ankle joints. In addition to the very good performance of the previous mechanisms in replicating natural joint kinematics, also spherical mechanisms seem to represent joint motion with a similar good accuracy, despite their much simpler structure. With respect to the previous more complex mechanisms, the slightly less satisfactory results in terms of replication of natural motion were observed in fact to be counterbalanced by a reduction of computational costs, by an improvement of numerical stability of the mathematical models and by a reduction of the overall mechanical complexity of the mechanisms.

All these aspects are very important for lower limb kinematics modeling [10], dynamic analysis, design of prostheses and orthoses for these joints [11], and also for musculo-skeletal modeling of the lower limb [12-15].

5. ACKNOWLEDGMENT

6. REFERENCES

[1] O'Connor JJ, Lu TW, Wilson DR, Feikes J, Leardini A. Review: Diarthrodial Joints-Kinematic Pairs, Mechanisms or Flexible Structures? Comput Methods Biomech Biomed Engin. 1(2):123-150, 1998.

[2] Wilson DR, Feikes JD, O'Connor JJ. Ligaments and articular contact guide passive knee flexion. J Biomech. 31(12):1127-36, 1998.

[3] Ottoboni A, Parenti-Castelli V, Sancisi N, Belvedere C, Leardini A. Articular surface approximation in equivalent spatial parallel mechanism models of the human knee joint: an experiment-based assessment. Proc Inst Mech Eng H. 224(9):1121-1132, 2010.

[4] Franci R, Parenti-Castelli V, Belvedere C, Leardini A. A new one-DOF fully parallel mechanism for modelling passive motion at the human tibiotalar joint. J Biomech. 42(10):1403-1408, 2009.

[5] Sancisi N, Parenti-Castelli V. A 1-Dof parallel spherical wrist for the modelling of the knee passive motion. Mech Mach Theory. 45(4): 658-665, 2009.

[6] Sancisi N, Zannoli D, Parenti-Castelli V, Belvedere C, Leardini A. A one-degree-of-freedom spherical mechanism for human knee joint modelling. Proc Inst Mech Eng H. 2011 Aug;225(8):725-35.

[7] Franci R, Parenti-Castelli V. A one-degree-of-freedom spherical wrist for the modelling of passive motion of the human ankle joint. IAK 2008, Lima, 9-11 January 2008, 1-13.

[8] Grood ES, Suntay WJ. A joint coordinate system for the clinical description of three-dimensional motions: application to the knee. J Biom Eng. 105:136-144, 1983.

[9] Sancisi N, Zannoli D, Parenti-Castelli V, Leardini A. Numerical stability of two classes of mechanisms for the kinematic modelling of the knee. Proceedings of ICABB, Venezia, Italy, 2010.

[10] Sholukha V, Leardini A, Salvia P, Rooze M, Van Sint Jan S. Double-step registration of in vivo stereophotogrammetry with both in vitro 6-DOFs electrogoniometry and CT medical imaging. J Biomech. 2006,39(11),2087-95.

[11] Kent J, Franklyn-Miller A. Biomechanical models in the study of lower limb amputee kinematics: a review. Prosthet Orthot Int. 2011 Jun;35(2):124-39.

[12] Delp SL, Loan JP, Hoy MG, Zajac FE, Topp EL, Rosen JM. An interactive graphics-based model of the lower extremity to study orthopaedic surgical procedures. IEEE Trans. Biomed. Eng 1990;37(8):757–767

[13] Arnold EM, Ward SR, Lieber RL, Delp SL. A model of the lower limb for analysis of human movement. Ann Biomed Eng. 2010 Feb, 38(2), 269-79.

[14] Seth A, Sherman M, Eastman P, Delp S. Minimal formulation of joint motion for biomechanisms. Nonlinear Dyn. 2010 Oct 1; 62(1):291-303.

[15] Pandy MG, Andriacchi TP. Muscle and joint function in human locomotion. Annu Rev Biomed Eng. 2010 Aug 15; 12:401-33.

The effect of including accurate pelvis bony landmarks in a nonlinearly scaled musculoskeletal lower extremity model

Andersen M. S. [1], Mellon S. [2], Lund M. E. [1], Grammatopoulos G. [2], Gill H. S. [2]

[1] M-Tech, Aalborg University, Aalborg, Denmark, msa@m-tech.aau.dk
[2] NDORMS, University of Oxford, Oxford, United Kingdom

In this study, we computed the hip compressive forces for 12 Metal-on-Metal Hip Resurfacing Arthoplasty (MoMHRA) patients using a newly developed musculoskeletal modeling approach. This two-stage modeling approach first 1) builds a patient-specific stick-figure model based on a standing reference trial and 2) nonlinearly morphs a cadaver-based musculoskeletal model to fit the stick-figure model and identified bony landmarks. For each patient, two models were built: one where the photometric markers were assumed to represent the bony landmarks on pelvis and the hip joint centers estimated using the regression equation of Davis et al. For the second model, a Computerized Tomography (CT) scan of the pelvis region was used to obtain accurate information of the bony landmarks and the hip joint centers. The results showed significantly different results between the two models in terms of average, standard deviation and peak compressive force at the hip for sit to stand whereas no differences were found during gait and stair descent. The computed hip compressive forces obtained from the model with the patient-specific bony landmarks tended to be lower.

Keywords-component; Musculoskeletal model; Nonlinear scaling

1. INTRODUCTION

Patient-based musculoskeletal models are commonly constructed by scaling a cadaver-based model to the size of the patient using simple linear scaling laws [1]. As a result, variations in the joint axis orientations between patients are not captured by the model. Secondly, when a model is driven by motion capture data, the assumed positions of the markers on the model are based on the qualified guess made by the modeler. Thus, the results obtained from the same set of experimental and cadaver data will be different, depending on the modeler.

To address these issues, we recently developed a new modeling approach to ensure that the obtained results are independent of the modeler and also, among others, capture the differences in bony geometry, including joint axis, and muscle insertion sites specific to the patient. As this method relies on joint center and bony landmark information of the patient, we studied the difference between including detailed information as derived from a Computerized Tomography (CT) scan or using surface marker locations as indicators of the underlying bony landmarks.

In this study, we apply this new musculoskeletal modeling approach to compute the hip compressive force on the affected leg for 12 Metal-on-Metal Hip Resurfacing Arthoplasty (MoMHRA) patients. MoMHRA is an alternative treatment option for younger and more active patients with endstage osteoarthritis of the hip [2].

2. METHODS

Musculoskeletal models of 12 MoMHRA patients were constructed (6 females, 6 males, height 1.71 ± 0.09 m, weight 75 ± 12 kg). The study was approved by the local ethics committee and all patients gave informed consent. Ten patients had MoMHRA unilateral whereas two had a Total Hip Replacement (THR) on the contralateral limb.

A Plug-in-Gait marker protocol with additional photometric markers on the first and fifth metatarsal was used. The trajectories of the markers in a global laboratory-fixed reference frame was recorded by a 12 camera Vicon Nexus MX system (Vicon, Oxford, UK) and the ground reaction forces measured by three AMTI force plates (AMTI, MA, USA). Data were obtained for gait, sit to stand, and stair descent among others. A standing reference trial with additional markers on the medial side of the knee and ankle was also recorded.
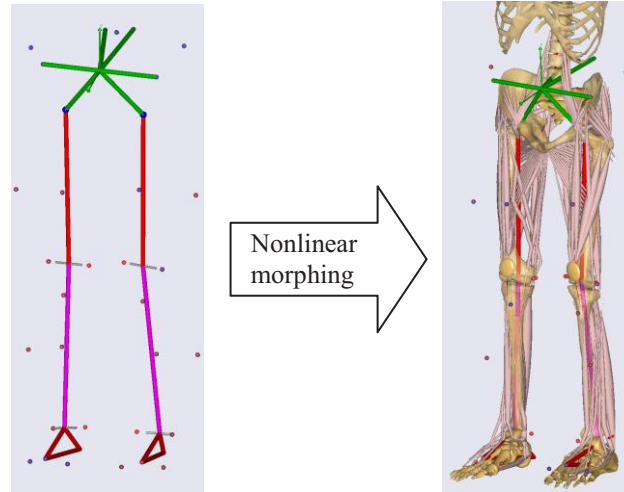
Figure 1: Morphed musculoskeletal model based on the patient-specific information derived from a standing reference trial.
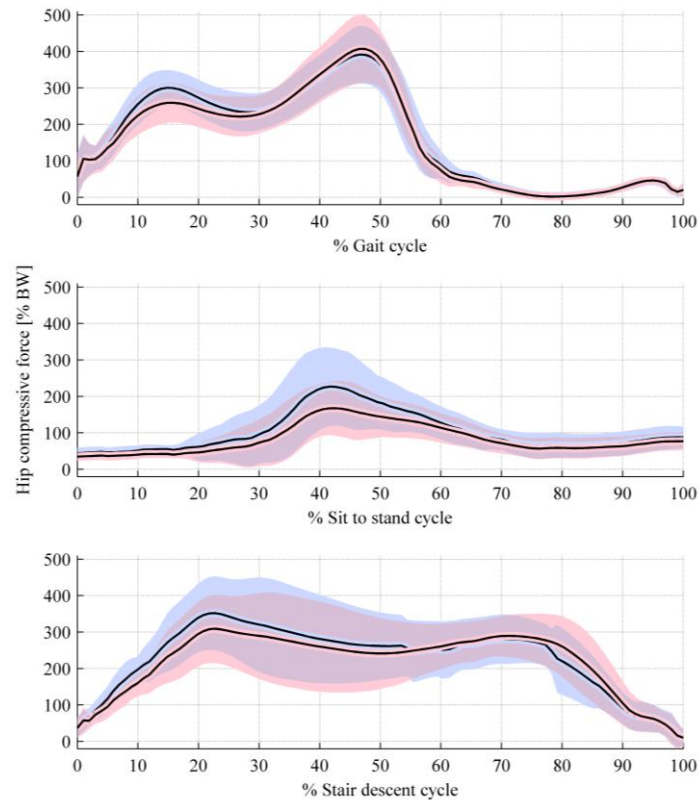

Figure 2: Computed hip compressive force during gait (top), sit to stand (middle) and stair descent (bottom). The blue curve shows the results for the model scaled only based on the markers and the Davis et al. [3] HJC regression equation. The pink curve shows the results for the model with patient-specific bony landmarks on pelvis as well as HJCs. The shaded areas indicate one standard deviation over the subjects. Gait cycle: from heel strike to heel strike. Sit to stand cycle: from a sitting position to full extension of hips and knees. Stair descent cycle: from foot strike to toe off.

After the motion capture session, the photometric markers on pelvis were replaced with Computerized Tomography (CT) visible markers and a CT scan of the pelvis was obtained to estimate the location of the Hip Joint Centers (HJCs) and the left and right ASIS and the left and right PSIS bony landmarks.

Two musculoskeletal models for each patient were built in the AnyBody Modeling System v. 5.0 (AnyBody Technology A/S, Denmark) based on the Twente Lower Extremity Model (TLEM) [4]. For the first model, a kinematic stick-figure model was built from a standing reference trial, and the regression equation of Davis et al. [3] was used to estimate HJCs. The photometric markers were used to represent the underlying bony

landmarks with some additional offset. The TLEM model was then morphed using Radial Basis Functions (RBF) to match the assumed bony landmarks and the mechanism of the stick-figure model. The second model was constructed with the same procedure, but the available CT data were used to estimate the location of the pelvis bony landmarks and HJCs. For the native and THR hips, a sphere was fitted to the femoral head and the HJC obtained as the center of the sphere. For MoMHRA hips, the HJC was estimated by selecting six points from the CT scan on the edge of the acetabular component and fitting a plane to the open face of the component. The average centre of three circles fitted through the six points was projected out from the acetabular component to a distance determined by each patients component size and component coverage angle. This point was taken as the HJC. Thus, the second model represents the patient with inaccuracies of marker placement on the pelvis and HJCs estimation eliminated. From both models, the muscle and joint reaction forces were computed through an inverse dynamic analysis with a quadratic muscle recruitment criterion. The model is illustrated in Fig. 1.

Paired two-tailed Student's t-tests were performed on the average, standard deviation and peak compressive hip forces to test for significant difference between the two models. Significant differences are reported for $p < 0.05$.

3. RESULTS

In Fig. 2, the average and standard deviation over the subjects of the computed hip compressive force for the three activities and two models are shown. Root-Mean-Square (RMS) differences of 29±23 % BW, 30±23 % BW and 47±43 % BW between the two models were seen for gait, sit to stand, and stair descent, respectively. The sit to stand trial showed significantly different results between the two models in average (p=0.0006), standard deviation (p=0.007) and peak compressive forces (p=0.002). No significant differences were observed in the gait and stair descent trials in any of the three tested variables. However, the compressive forces obtained from the model using the patient-specific bony landmarks tended to be lower.

4. DISCUSSION

Musculoskeletal models are known to generally over-predict joint reaction forces. Compared to the in vivo measured forces of Bergmann et al. [5], both the gait and stair descent trials show larger compressive forces than measured in vivo. Our results for sit to stand with the patient-specific bony landmarks are within the ranges of forces measured in vivo. The computed compressive forces show similar trends in terms of the number of the peaks and their locations compared to the measured forces.

Although the computed joint compressive forces are still slightly higher than those measured in vivo, our proposed musculoskeletal modeling methodology has several advantages over the traditional, linearly scaled models: 1) the model is constructed as an extension to the stick-figure model already used in most motion capture systems. Hence, the joint moments generated by the muscles are consistent with those traditionally reported in gait analysis reports. 2) It captures the differences in joint axis orientations between patients. 3) It allows easy batch processing of multiple trials and subjects.

5. REFERENCES

[1] Rasmussen, J., de Zee, M., Damsgaard, M., Christensen, S. T., Marek, C., Siebertz, K., 2005. A general method for scaling musculoskeletal models. In Proceedings of the International Symposium on Computer Simulation in Biomechanics, Cleveland, Ohio, USA.

[2] Mabilleau, G., Kwon, Y., Pandit, H., Murray, D. W., Sabokbar, A., 2008. Metal-on-metal hip resurfacing arthroplasty: A review of periprosthetic biological reactions. Acta Orthop. 79, 734-747.

[3] Davis III, R. B., Õunpuu, S., Tyburski, D., Gage, J. R., 1991. A gait analysis data collection and reduction technique. Hum. Mov. Sci. 10, 575-587.

[4] Klein Horsman, M. D., Koopman, H. F. J. M., van der Helm, F. C. T., Prosé, L. P., Veeger, H. E. J., 2007. Morphological muscle and joint parameters for musculoskeletal modeling of the lower extremity. Clin. Biomech.. 22, 239-247.

[5] Bergmann et al., 2001. Hip contact forces and gait patterns from routine activities. J. Biomech., 34(7), 859-871.

Effects of Palpation Errors on the Estimated Body Segment Inertial Parameters Using an Optimization-Based Method

Chih-Chung Hu[1,2], Tung-Wu Lu[2]*, Hao Chiang[2] and Sheng-Chang Chen[2]

[1] Department of Mechanical Engineering, Ming Chi University of Technology, Taipei, Taiwan, ROC,
cchu@mail.mcut.edu.tw

[2] Institute of Biomedical Engineering, National Taiwan University, Taipei, Taiwan, ROC, twlu@ntu.edu.tw

Keywords- Motion Analysis, Optimization, Inertial parameters

1. INTRODUCTION

In human motion analysis, mechanical variables such as joint forces, moments and energy are calculated using mathematical models with experimental measurements [1]. Body segment inertial parameters (BSIPs) and other anthropometric data are necessary for model customization in individual subjects. Several methods for estimating subject-specific BSIPs have been proposed, including cadaver-based prediction equations [2], medical imaging methods [3] and mathematical modeling methods [4]. However, these methods are subject to one or more limitations, such as population specificity, high cost and radiation dose.

To address the limitations of the existing methods, a new method, referred to as the optimization-based method (OM), has been proposed for noninvasive, radiation-free estimation of subject-specific BSIPs [5]. The OM is capable of producing subject-specific BSIPs with better accuracy than other predictive methods. The OM works with standard equipment in a motion laboratory, namely a motion capture system and two forceplates, and requires only input from the forceplates and skin markers placed in a specific position of the segments. Since palpation error remains one of the major sources of error in human motion analysis [6], the purpose of the current study was to investigate the effect of palpation errors on the performance of the OM using computer simulations.

2. METHODS

A healthy young subject was recruited for the current study. The subject wore 54 retroreflective markers placed by a well-trained physical therapist at positions used by Huang et al. [7], and at the mandibular condylar processes, sternal notch, C7, radial styloid processes, and the second and fifth metacarpal heads. The proximal and distal circumference lengths for each segment were measured with a measuring tape. The subject stood on a forceplate (AMTI, USA) in 10 different static postures, each for 5s, including abduction and flexion of the shoulder; flexion, extension and abduction of the hip; flexion of the knee; flexion and extension of the trunk; and their combinations. These postures displaced the relevant body segments horizontally as far as possible from their anatomical positions, while being stabilized by a metal frame fixed to a second forceplate with two height-adjustable plates to support vertically the extremities. The marker coordinates were measured using a 7-camera motion capture system (VICON, Oxford, UK).

A 3D, 16-rigid-segment model of the body was developed, wherein the head modeled as a spheroid, the neck, upper arms, forearms, thighs and shanks as frustums, and the trunk, pelvis, hands and feet as ellipsoids. Marker and circumference length data were used to customize the model to individual subjects. The method (OM) used the density of each segment and the COM coordinates of the trunk as the design variables. The objective function was to minimize the sum of the distances between the center of pressure (COP) and the vertical projection of center of mass (VCOM) for all static postures. After this optimization problem was solved, the BSIPs could be determined.

To investigate the effect of palpation errors on the estimated BSIPs using OM, a computer simulation was performed. The OM was first used to estimate the BSIPs for the subject from the experimental data. The calculated BSIPs were then used to calculate the COP. Together, with the other parameters, these data were used as the gold standard.
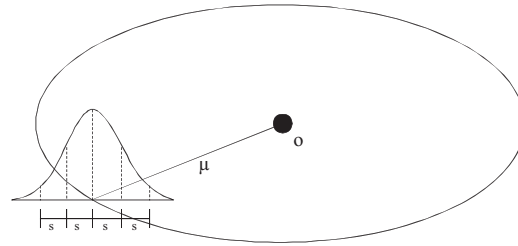
Figure 1. Error model for each marker coordinate. O is the original coordinate of the marker, is the mean of the palpation error and is the standard deviation of the palpation error. The error randomly added lies between +2 and -2 .

An error model was created to generate a series of simulated trials in which marker positions were added with palpation errors. The simulation included intra-rater palpation errors and inter-rater palpation errors. We created 20 simulated trials with intra-rater palpation errors and another 20 with inter-rater palpation errors. Based on the method for determining means and standard deviations of intra-rater and inter-rater palpation errors presented by Moriguchi et al. [8], the errors we added to each marker coordinates in a randomized nature so that the magnitude of the error would lie between the mean error plus two standard deviations and the mean minus two standard deviations (Fig. 1).

For each set of simulated trials, the BSIPs, including the mass, COM and moments of inertia were estimated by the OM, for every segment and the COP of the body. The errors in the calculated BSIPs were defined as the differences from the gold standard. Apart from the BSIPs, the distances between the calculated and measured COP were also calculated and referred to as COP errors.

3. RESULTS AND DISCUSSION

The intra-rater and inter-rater errors in the calculated COM positions were less than 0.1 mm for most segments (Table 1). The intra-rater errors in the body's COM were about 2 mm, and the inter-rater errors were about 3 mm (Table 1). The intra-rater errors in the calculated COP were about 0.1 mm, and about 0.3 mm for inter-rater errors (Table 1). The intra-rater errors in segmental mass values were less than 5% for all segments, and less than 7% for inter-rater errors (Table 2). Both intra-rater and inter-rater errors in the calculated segmental moments of inertia were less than 1% (Table 3).

While the intra-rater and inter-rater errors in the BSIPs of most body segments were very small, those for the pelvis were a bit bigger. This may be owing to the greater intra-rater and inter-rater palpation errors of the ASISs. Therefore, improving the palpation accuracy for the ASISs may be necessary to improve the reliability of the estimation of the BSIPs for the pelvis segment. Alternatively, another definition of the pelisse using different markers may be considered. Overall, the performance of the OM in estimating segmental BSIP's appeared to be quite reliable given errors during palpation within and among examiners.

4. CONCLUSION

From the current simulation study, the intra-rater and inter-rater palpation errors in the BSIPs estimated by the OM were found to be quite small. The estimated BSIPs did not appear to be affected significantly by the palpation errors that may be present in the daily motion analysis sessions. The results suggest that the OM can be considered to be of excellent reliability and will be useful for subject-specific motion analysis.

Table 1.Intra-rater and inter-rater errors in the calculated segmental COM positions, body's COM positions and COP error.

	Intra-rater		Inter-rater			Intra-rater		Inter-rater	
	Mean (mm)	STD (mm)	Mean (mm)	STD (mm)		Mean (mm)	STD (mm)	Mean (mm)	STD (mm)
Head	0.02	0.01	0.02	0.01	L thigh	0.08	0.03	0.12	0.07
Neck	0.04	0.02	0.07	0.03	L shank	0.0	0.0	0.0	0.0
Trunk	0.08	0.02	0.10	0.05	L foot	0.02	0.01	0.03	0.01
L upper arm	0.01	0.01	0.01	0.01	R thigh	0.08	0.03	0.14	0.06
L forearm	0.0	0.0	0.0	0.0	R shank	0.0	0.0	0.01	0.01
L hand	0.02	0.01	0.03	0.01	R foot	0.03	0.01	0.04	0.01
R upper arm	0.01	0.01	0.01	0.0	Pelvis	0.06	0.02	0.09	0.05
R forearm	0.0	0.0	0.0	0.0	Whole body	1.88	1.07	2.86	1.78
R hand	0.02	0.01	0.03	0.01	COP error	0.07	0.16	0.30	0.24

R: The segment at right side. L: The segment at left side.

Table 2. Intra-rater and inter-rater errors in the calculated segmental mass as percentages of the gold standard values.

	Intra-rater		Inter-rater			Intra-rater		Inter-rater	
	Mean (%)	STD (%)	Mean (%)	STD (%)		Mean (%)	STD (%)	Mean (%)	STD (%)
Head	1.04	3.13	0.77	3.58	R hand	-0.45	2.60	-0.74	2.37
Neck	-0.15	0.48	-0.35	0.51	L thigh	-1.16	0.85	-1.41	1.91
Trunk	0.22	1.72	0.92	2.98	L shank	0.61	0.58	1.21	1.42
L upper arm	0.19	1.20	-0.93	2.25	L foot	0.85	2.65	0.15	3.00
L forearm	-1.57	1.53	-1.10	1.92	R thigh	-1.17	1.62	-1.83	3.37
L hand	0.43	3.09	0.12	2.53	R shank	0.73	1.20	1.51	2.16
R upper arm	-0.33	1.34	0.04	1.43	R foot	0.30	2.00	0.52	3.08
R forearm	-0.75	1.11	-1.53	1.52	Pelvis	1.10	4.61	0.12	6.50

R: The segment at right side. L: The segment at left side.

Table 3. Intra-rater and inter-rater errors in the calculated segmental moments of inertia as percentages of the gold standard values.

	Intra-rater		Inter-rater			Intra-rater		Inter-rater	
	Mean (%)	*STD (%)*	*Mean (%)*	*STD (%)*		*Mean (%)*	*STD (%)*	*Mean (%)*	*STD (%)*
Head	-0.01	0.03	-0.01	0.03	*L hand*	0.07	0.41	0.41	0.48
Neck	0.0	0.0	0.0	0.0	*R hand*	0.07	0.39	0.27	0.45
Trunk	0.19	0.76	0.22	1.33	*L thigh*	0.10	0.24	0.18	0.53
Pelvis	-0.84	4.13	0.05	5.84	*R thigh*	0.05	0.47	0.04	0.78
L upper arm	0.09	0.28	0.31	0.42	*L shank*	0.01	0.24	0.03	0.54
R upper arm	0.09	0.32	0.15	0.31	*R shank*	0.06	0.46	0.10	0.63
L forearm	0.22	0.29	0.36	0.34	*L foot*	-0.03	0.48	0.26	0.59
R forearm	0.11	0.30	0.24	0.27	*R foot*	0.11	0.42	-0.05	0.59

R: The segment at right side. L: The segment at left side.

5. REFERENCES

[1] Elftman H. Forces and energy changes in the leg during walking. Am J Physiol 1939;125(2):339–56.

[2] Dempster WT. Space requirement of the seated operator. Ohio: Aerospace Medical Research Laboratories; 1955.

[3] Jensen RK. Estimation of the biomechanical properties of three body types using a photogrammetric method. J Biomech 1978;11(8–9):349–58.

[4] Hatze H. A new method for the simultaneous measurement of the movement of inertia, the damping coefficient and the location of the centre of mass of a body segment in situ. Eur J Appl Physiol Occup Physiol 1975;34(4):217–26.

[5] Chen, S.C., Hsieh, H. J., Lu, T. W. and Tseng, C. H. A method for estimating subject-specific body segment inertial parameters in human movement analysis. Gait and Posture, 2011. 33(4): p. 695-700.

[6] Andriacchi, T.P. and E.J. Alexander, Studies of human locomotion: Past, present and future. Journal of Biomechanics, 2000. 33(10): p. 1217-1224.

[7] Huang SC, Lu TW, Chen HL, Wang TM, Chou LS. Age and height effects on the center of mass and center of pressure inclination angles during obstaclecrossing. Med Eng Phys 2008;30(8):968–75.

[8] Moriguchi, C.S., Carnaz, L., Silva, L. C. C. B., Salasar, L. E. B., Carregaro, R. L. , Sato, T. d O. and Coury, H. J. C. G. Reliability of intra- and inter-rater palpation discrepancy and estimation of its effects on joint angle measurements. Manual Therapy, 2009. 14(3): p. 299-305.

A multi-body optimisation with a knee joint kinematic model including deformable ligament constraints

Gasparutto X. [1], Dumas R. [1], Jacquelin E. [1]

[1] Université de Lyon, F-69622 Lyon, France, UMR_T9406, Laboratoire de Biomécanique et Mécanique des Chocs, IFSTTAR, Bron, France, Université Lyon 1, Villeurbanne, France
xavier.gasparutto@univ-lyon1.fr

In order to obtain an accurate skeleton kinematics of the lower limb from skin-based markers, the soft tissue artifact has to be compensated. Multi-body optimisation method, based on predefined joint kinematic models, is used in that way. The aim of this study is to introduce four deformable ligaments in a kinematic model of the knee. This implies to manage the ligament constraints with a weighted penalty-based method. This model was compared to the constraints of a parallel mechanism model with three isometric ligaments.

The results showed that the knee kinematics of both model is close to the reference, even if the knee external rotation seems overestimated for the deformable ligament model. Penalty-based method "loosen" the constraints, consequently inter-subject variability appears with the deformable method conversely to the results with the isometric method.

To conclude, by introducing deformable ligaments in the kinematic constraint, this model is a new step in the way of more physiological kinematic models. Next steps would consist in further validating the method and completing the ligament geometry with the different anterior and posterior bundles.

Keywords : Soft tissue artefact, kinematic model, multibody optimisation, ligament

1. INTRODUCTION

Motion capture systems based on skin markers have a great accuracy in the position of markers. But those markers have a relative motion with the underlying bones due to the soft tissue. Those soft tissue artifacts (STA) are one of the major issues in biomechanics [1]. They introduce large errors in joint kinematics calculation. Several methods can be used to compensate those artifacts such as the multi-body optimization (MO) [2]. Duprey et al. [3] have developed a versatile MO method with generalised coordinate (GC) that allows to easily switch from one kinematic model to another. It allows the utilisation of one degree of freedom (DoF) parallel mechanisms developed by Feikes et al. [4] and Di Gregorio et al. [5].

One of the limitations of the parallel mechanism used to model the knee joint [4] is that only three isometric ligaments are considered. The principle of using non-isometric ligaments in a MO has been recently proposed in the literature [6] but its implementation and evaluation is still to be done.

The aim of this study is to introduce in the MO a more detailed model with four ligaments bundles at the knee. This implies to manage the ligament constraints with a weighted penalty-based method.

2. MATERIAL & METHOD

The method was tested during gait on five healthy male subjects (age: 28.8±4.8 years; height: 1.74±0.09 m; mass: 76.5±13.5 kg). The trajectories of 32 skin-based markers on the right lower limb (eight markers by segment) were recorded at 100 samples per second during a level walking cycle.

Knee kinematic model

The knee was modeled by two sphere-on-plane contacts from the model of Feikes et al. [4] adapted with an affine transformation to fit with the coordinates of four deformable ligaments taken from Shelburne [7]: anterior bundle of anterior cruciate ligament (ACL), anterior bundle of posterior cruciate ligament (PCL), anterior bundle of medial collateral ligament (MCL) and lateral collateral ligament (LCL).

Optimisation method

This present method consists in considering the knee ligament constraint with a penalty-based method. The four ligament constraint are solved 'as well as possible' and not exactly fulfilled, conversely to the three

ligament constraints with Lagrange multiplier method as in Duprey et al. [3]. Both optimisations (denoted deformable and isometric) will be compared. The new optimisation problem can be written as:

$$\min_{Q} \ f = \begin{pmatrix} \mathbf{\Phi}^m \\ \mathbf{\Phi}^{k_1} \end{pmatrix}^T \begin{bmatrix} \mathbf{W}^m \\ \mathbf{W}^{k_1} \end{bmatrix} \begin{pmatrix} \mathbf{\Phi}^m \\ \mathbf{\Phi}^{k_1} \end{pmatrix}$$

$$subject\ to \begin{pmatrix} \mathbf{\Phi}^{k_2} \\ \mathbf{\Phi}^r \end{pmatrix} = 0$$

$\mathbf{\Phi}^m$ is the vector of 'motor' constraints (i.e. the distance between the measured and model predicted marker position), $\mathbf{\Phi}^{k1}$ the knee ligament constraints (i.e. the difference between the reference and calculated norm of the ligament), $\mathbf{\Phi}^{k2}$ the other kinematic constraints (as in Duprey et al.), $\mathbf{\Phi}^r$ he rigid body constraint and $\begin{bmatrix} \mathbf{W}^m \\ \mathbf{W}^{k1} \end{bmatrix}$ a weight matrix.

The Lagrange formulation of the minimisation under constraints of f is equivalent to the following zero search problem solved by a Newton-Raphson algorithm [8]:

$$\mathbf{F}\begin{pmatrix} \mathbf{Q} \\ \lambda \end{pmatrix} = \begin{pmatrix} \begin{bmatrix} \mathbf{K}^m \\ \mathbf{K}^{k_1} \end{bmatrix}^T \begin{bmatrix} \mathbf{W}^m \\ \mathbf{W}^{k_1} \end{bmatrix} \begin{pmatrix} \mathbf{\Phi}^m \\ \mathbf{\Phi}^{k_1} \end{pmatrix} + \begin{bmatrix} \mathbf{K}^{k_2} \\ \mathbf{K}^r \end{bmatrix}^T \begin{pmatrix} \lambda^{k_2} \\ \lambda^r \end{pmatrix} \\ \mathbf{\Phi}^{k_2} \\ \mathbf{\Phi}^r \\ \end{pmatrix} = \mathbf{0}$$

The $\mathbf{K}$ matrices are the jacobian of the corresponding constraint: m (motor), k_1 (knee ligament), k_2 (kinematic constraint), r (rigid body). The λ vectors are the Lagrange multipliers associated with the absolute constraint.

Initial guess

The initial guess is the non-optimized GC obtained directly from the skin-based markers [9].

Defining weight of ligament and markers

The weights of ligament W^{k1} (table 1.) were chosen to be consistent with the maximal lengthening found in literature ([6], [10], [11])in the knee range of motion during gait (0-60 degree of flexion). A ligament with a small lengthening will have a bigger weight than one with greater lengthening.

Table 1. Ligament weight

Ligament	aACL	aPCL	aMCL	LCL
Weight	1,000	10,000	10	1

3. RESULT

Knee joint kinematics

Extension-flexion (EF), adduction-abduction (AA) and anterior/posterior displacement pattern and amplitude computed with both optimisations (deformable and isometric) are very similar and in agreement with knee reference kinematics [12]. The main difference is for the internal/external rotation, shifted towards external with the deformable method. Lateral/medial and proximal/distal displacement are in reasonable boundaries. The results obtained with the deformable method have an inter-subject variability contrary to those obtained with isometric method.
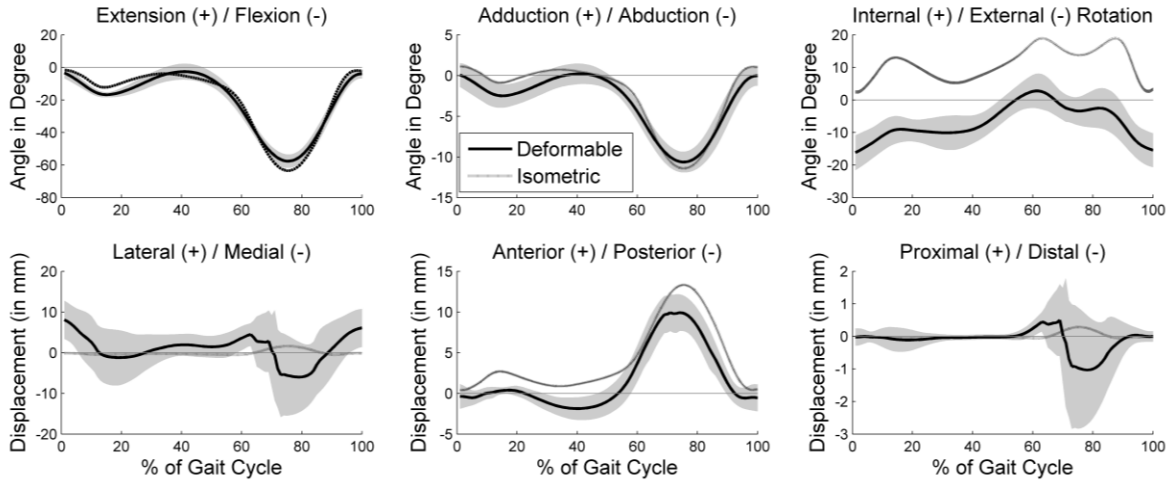
Figure 1: Knee Kinematics: deformable ligament model VS isometric ligament model. (Curves represent the mean ± 1S.D of the parameters on the 5 subjects of the study)

Ligament lengthening

ACL, PCL and MCL are in a range of ±10% of length variation which is consistent with the literature. LCL lengthening seems overestimated as it shortens of 50% during knee flexion. This ligament lengthening varies linearly with the knee EF angles.
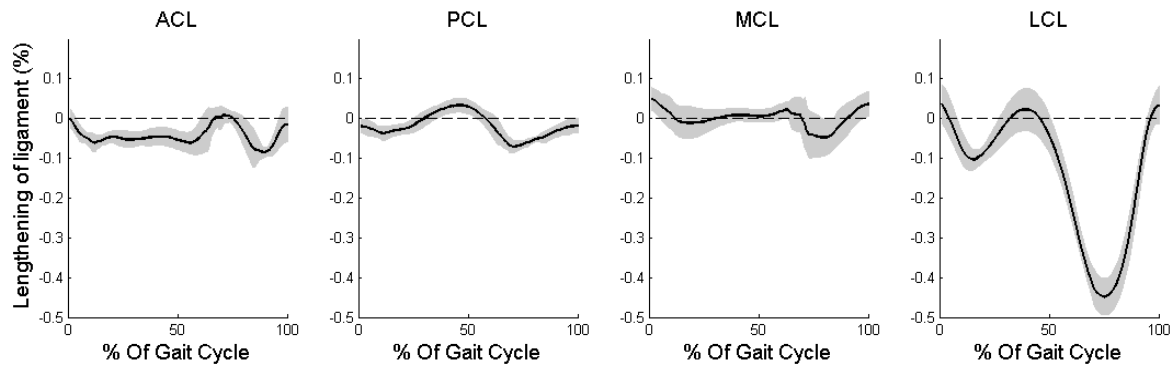

Figure 2: Ligament lengthening (in % of reference length) during Gait Cycle

4. DISCUSSION & CONCLUSION

In this study, we tested a new type of kinematic constraints in MO. A weighted penalty-based method have been use to introduce deformable knee ligaments in the kinematic model.

The model with four deformable ligaments keeps the coupling between the DoFs but without prescribing a strict 1-DoF model as with the parallel mechanism [4].

However, the internal/external rotation presents an offset. The ACL seems to be responsible for this effect. As it direction in the frontal plane is medio-lateral, a shortening of this ligament could implies an external rotation of the knee. The geometry of the LCL insertion and a small weight assigned in the optimization seems to be responsible for it high shortening. The weight of ligaments is one of the major issues of the penalty-based method. A two-level optimisation [13] could be used to find these weights. Another solution would be to prescribe lengthening of ligament at each joint position [6].

This method "loosen" the constraints, consequently inter-subject variability appears with the deformable method conversely to the results with the isometric method. It's a positive effect; the computed kinematics may not only reflect the model kinematics, but also the subject knee joint kinematics. Experimental validation data (e.g. with bone pins) would be essential to confirm the results.

To conclude, this method, by introducing deformable ligaments in the kinematic constraint, is a new step in the way of more physiological kinematic models. Next steps would consist in further validating the method and completing the ligament geometry with the different anterior and posterior bundles.

5. REFERENCES

[1] A. Leardini, L. Chiari, U. D. Croce and A. Cappozzo, "Human movement analysis using stereophotogrammetry Part 3. Soft tissue artifact assessment and compensation," *Gait and Posture,* vol. 21, pp. 212-225, 2005.

[2] T. Lu and J. O'Connor, "Bone position estimation from skin marker co-ordinates using global optimisation with joint constraints," *Journal of Biomechanics,* vol. 32, pp. 129-134, 1999.

[3] S. Duprey, L. Cheze and R. Dumas, "Influence of joint constraints on lower limb kinematics estimation from skin markers using global optimization," *Journal of Biomechanics,* vol. 43, pp. 2858-2862, 2010.

[4] J. Feikes, J. O'Connor and A. Zavatsky, "A constraint-based approach to modelling the mobility of the human knee joint," *Journal of Biomechanics,* vol. 36, pp. 125-129, 2003.

[5] R. DiGregorio, V. Parenti-Castelli, J. O'Connor and A. Leardini, "Mathematical models of passive motion at the human ankle joint by equivalent spatial parallel mechanisms," *Medical \& Biological Engineering \& Computing,* vol. 45, pp. 305-313, 2007.

[6] E. Bergamini, H. Pillet, J. Hausselle, P. Thoreux, S. Guerard, V. Camomilla, A. Cappozzo and W. Skalli, "Tibio-femoral joint constraints for bone pose estimation during movement using multi-body optimization," *Gait \& Posture,* vol. 33, pp. 706-711, 2011.

[7] K. Shelburne and M. Pandy, "A musculoskeletal model of the knee for evaluating ligament forces during isometric contractions," *Journal of Biomechanics,* Vols. 30, issue 2, pp. 163-176, 1997.

[8] M. Andersen, M. Damsgaard and J. Rasmussen, "Kinematic analysis of over-determinate biomechanical systems," *Computer Methods in Biomechanics and Biomedical Engineering,* Vols. 12, No 4, pp. 371-384, 2009.

[9] R. Dumas and L. Chèze, "3D inverse dynamics in non-orthonormal segment coordinate system," *Medical \& Biological Engineering \& Computing,* vol. 45, pp. 315-322, 2007.

[10] J. Rovick, J. Reuben, R. Schrager and P. Walker, "Relation between knee motion and ligament length patterns," *Clinical Biomechanics,* vol. 6, pp. 213-220, 1991.

[11] P. Walker, J. Rovick and D. Robertson, "The effects of knee brace hinge design and placement on joint mechanics," *Journal of Biomechanics,* vol. 11, pp. 965-974, 1988.

[12] M. Lafortune, P. Cavanagh, H. Sommer and A. Kalenak, "Three-dimensional kinematics of the human knee during walking," *Journal of Biomechanics,* vol. 25, pp. 347-357, 1992.

[13] J. Reinbolt, J. Schutteb, B. Fregly, B. Kohc, R. Haftka, A. Georgec and K. Mitchell, "Determination of patient-specific multi-joint kinematic models through two-level optimization," *Journal of Biomechanics,* vol. 38, pp. 621-626, 2005.

Introduction of a selection of joint reaction forces in the objective function when solving the muscular redundancy by static optimization

Moissenet F. [1], Chèze L. [2], Dumas R. [2]

[1] Laboratoire d'Analyse du Mouvement et de la Posture, Rehazenter – Centre National de Rééducation Fonctionnelle et de Réadaptation, L-2674 Luxembourg, Luxembourg, florent.moissenet@mailoo.org

[2] Université de Lyon, F-69622 Lyon, France, UMR_T9406, Laboratoire de Biomécanique et Mécanique des Chocs, IFSTTAR, Bron, France, Université Lyon 1, Villeurbanne, France

Musculo-tendon forces and joint reaction forces are typically predicted using a two-step method, computing first the musculo-tendon forces by a static optimization procedure and then deducing the joint reaction forces from the force equilibrium. However, this method does not allow studying the interactions between musculo-tendon forces and joint reaction forces in establishing this equilibrium and the joint reaction forces are usually overestimated. In this study, a one-step method is described allowing the introduction of a selection of joint reaction forces in the objective function of the static optimization procedure. This new method produced reliable joint reaction forces, lower than those obtained using the typical two-step method. Nevertheless, the results also demonstrated that the idea of introducing joint contact forces in the objective function is questionable since it remains difficult to define an objective function that provides in the same time physiological musculo-tendon forces and valid joint contact forces.

Keywords: Musculo-tendon forces · Joint contact forces · Partial parameter reduction · Static optimization · Musculo-skeletal modeling

1. INTRODUCTION

Instrumented prostheses [5,17], by measuring joint contact forces during a movement, give nowadays a unique opportunity to validate the ability of musculo-skeletal models in predicting internal forces. To perform this validation, an efficient musculo-skeletal model and a method computing both musculo-tendon and joint reaction forces (i.e., joint contact and ligament forces) are needed. In the case of lower limb forces prediction during gait, different models and methods have been proposed, but failed in replicating the interaction between musculo-tendon and joint reaction forces (i.e., using the typical two-step method : computing first the musculo-tendon forces and then deducing the joint reaction forces) [9], or in reproducing the musculo-skeletal anatomy in terms of joint modeling [2,13]. In this study, a one-step optimization method is described allowing the introduction of a selection of joint reaction forces in the objective function. This can be done using a recent versatile 3D lower limb musculo-skeletal model [15] giving a direct access to the musculo-tendon forces, joint contact forces and ligament forces. The model and the method are then tested using the experimental data of the "2nd Grand Challenge Competition to Predict in Vivo Knee Loads" [11], combining synchronized kinematics, kinetics, EMG and knee contact force data during gait.

2. MATERIAL AND METHODS

Versatile 3D lower limb musculo-skeletal model

A previously described [7,15] versatile 3D lower limb musculo-skeletal model, consisting of pelvis, thigh, shank and foot segments and 43 muscular lines of action, was used to perform this study. Hip was modeled using a spherical joint [1,16]. Knee and ankle were modeled using parallel mechanisms made respectively of 2 sphere-on-plane contacts with 3 isometric ligaments [10] and a spherical joint with 2 isometric ligaments [4]. Then, in order to introduce the muscular geometry, a widely-used generic musculo-skeletal geometric model [3] was adapted to our model.

Computation framework

The originality of this model is to use generalized coordinates in a full dynamic equation of the lower limb with Lagrange multipliers, giving a direct access to the musculo-tendon forces and to detailed joint reaction forces [15]. First, each segment position is defined using generalized coordinates [6]. Second, the kinematic

constraints and the associated Jacobian matrix are defined for each joint [8]. Third, a constrained global optimization [8,15] is performed in order to obtain consistent segment positions, velocities and accelerations. Fourth, the full dynamic equation of the lower limb is written, introducing the musculo-tendon forces and the Lagrange multipliers [7,15]:

$$\mathbf{G\ddot{Q}} + \mathbf{K}^T\boldsymbol{\lambda} = \mathbf{E} + \mathbf{Lf} \qquad (1)$$

where $\mathbf{G}$ is the generalized mass matrix, $\mathbf{\ddot{Q}}$ the consistent generalized accelerations, $\mathbf{K}$ the Jacobian matrix of both joint kinematic and rigid body constraints, $\boldsymbol{\lambda}$ the Lagrange multipliers, $\mathbf{E}$ the external forces, including both weight and ground reaction forces and moments, $\mathbf{L}$ the generalized muscle moment arms and $\mathbf{f}$ the musculo-tendon forces. Fifth, (1) gives a direct access to the musculo-tendon forces and the Lagrange multipliers that are the only unknowns of this system. A previous study [15] has shown that some of these Lagrange multipliers directly represent the corresponding joint reaction forces.

Partial parameter reduction and one-step optimization

The following linear system can be obtained from (1):

$$\begin{bmatrix} \mathbf{L} & -\mathbf{K}_1^{\,T} & -\mathbf{K}_2^{\,T} \end{bmatrix} \begin{bmatrix} \mathbf{f} \\ \boldsymbol{\lambda}_1 \\ \boldsymbol{\lambda}_2 \end{bmatrix} = \mathbf{G\ddot{Q}} - \mathbf{E} \qquad (2)$$

where $\boldsymbol{\lambda}_1$ and $\boldsymbol{\lambda}_2$ are respectively the Lagrange multipliers corresponding to the selection of joint reaction forces that should be introduced in the objective function and all the other ones, and $\mathbf{K}_1$ and $\mathbf{K}_2$ the Jacobian matrices of the constraints associated with these Lagrange multipliers. The second group of Lagrange multipliers can be cancelled from (2) by projecting the system on the kernel of $\mathbf{K}_2$, using the projection matrix $\mathbf{Z}_{\mathbf{K}_2}$:

$$\mathbf{Z}_{\mathbf{K}_2}^{\,T}\mathbf{Lf} - \mathbf{Z}_{\mathbf{K}_2}^{\,T}\mathbf{K}_1^{\,T}\boldsymbol{\lambda}_1 - \mathbf{Z}_{\mathbf{K}_2}^{\,T}\mathbf{K}_2^{\,T}\boldsymbol{\lambda}_2 = \mathbf{Z}_{\mathbf{K}_2}^{\,T}\left(\mathbf{G\ddot{Q}} - \mathbf{E}\right)$$

$$\Leftrightarrow \mathbf{Z}_{\mathbf{K}_2}^{\,T}\begin{bmatrix} \mathbf{L} & -\mathbf{K}_1^{\,T} \end{bmatrix}\begin{bmatrix} \mathbf{f} \\ \boldsymbol{\lambda}_1 \end{bmatrix} = \mathbf{Z}_{\mathbf{K}_2}^{\,T}\left(\mathbf{G\ddot{Q}} - \mathbf{E}\right) \qquad (3)$$

where $\mathbf{Z}_{\mathbf{K}_2}$ is a matrix composed of the eigenvectors of the square matrix $\mathbf{K}_2^{\,T}\mathbf{K}_2$ corresponding to the null eigenvalues. The unknowns $\begin{bmatrix} \mathbf{f} & \boldsymbol{\lambda}_1 \end{bmatrix}^T$, corresponding respectively to the musculo-tendon and the selected joint reaction forces, are then introduced in a typical static optimization procedure in order to solve the muscular redundancy problem [7,15].

Experimental data and simulations

In order to evaluate this method, simulations were performed based on the experimental data from the "Second Grand Challenge Competition to Predict in Vivo Knee Loads" [11]. We present here the results obtained using one gait trial recordings of a male subject (67kg, 172cm). These recordings combine synchronized kinematics, kinetics, EMG and knee contact force data.

The following results are obtained for two different simulations. The first simulation (i.e., Simu1) corresponds to the minimization of the musculo-tendon forces only (i.e., using the typical two-step method) and the second one (i.e., Simu2) corresponds to the minimization of both the musculo-tendon forces and the knee contact force.

Data analysis

The predicted musculo-tendon forces of each simulation are qualitatively compared to the envelopes of the measured EMG signals (EMG signals amplitudes are fitted to the Simu1 predicted forces amplitudes). Then, the predicted knee contact force of each simulation is quantitatively compared to the measured contact force (i.e., Reference) by computing the root mean square error (i.e., RMSE) and the correlation coefficient (i.e., R).

3. RESULTS

Musculo-tendon forces

On the whole, the amplitudes and patterns of the musculo-tendon forces predicted by minimizing the musculo-tendon forces only (i.e., Simu1) are mostly in accordance with the envelopes of the measured EMG signals (Fig. 1). Conversely, the amplitudes and patterns of the musculo-tendon forces predicted by minimizing both the musculo-tendon forces and the knee contact force (i.e., Simu2) are mostly dissimilar (Fig. 1). From a simulation to another one, the differences in terms of amplitudes and patterns show a higher or lower recruitment but also an important redistribution of the musculo-tendon forces.

Joint reaction forces

When comparing predicted to measured knee contact force (Fig. 2), the minimization of the musculo-tendon forces gives a similar pattern but a higher amplitude (Simu1 vs. Reference: R = 0.9370, RMSE = 1.0304 BW). Conversely, the minimization of both the musculo-tendon forces and the knee contact force (Fig. 2) gives both similar pattern and amplitude (Simu2 vs. Reference: R = 0.9579, RMSE = 0.3535 BW).
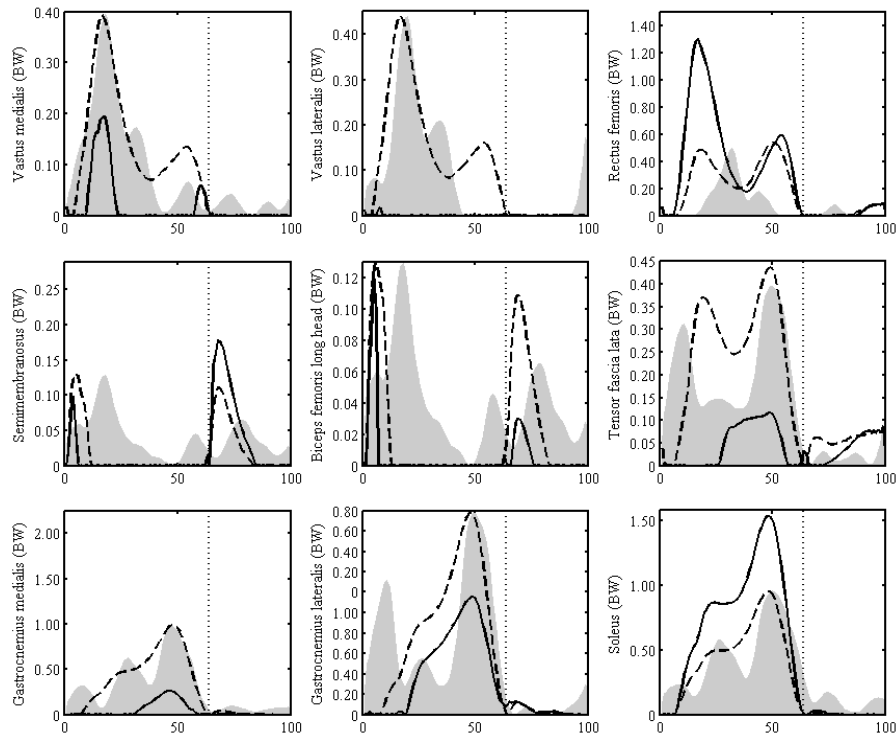

Figure 1. Predicted musculo-tendon forces (i.e., Simu1 – dashed black lines and Simu2 – plain black lines) and EMG signals (i.e., grey areas) during a gait cycle (%) (toe-off is indicated by a vertical dotted line).
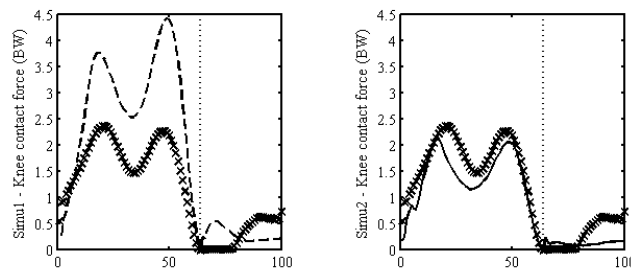

Figure 2. Predicted knee contact force (i.e., Simu1 – dashed black lines and Simu2 – plain black lines) and measured knee contact force (black crosses) during a gait cycle (%) (toe-off is indicated by a vertical dotted line).

4. DISCUSSION

In this study, a new approach for the simultaneous prediction of musculo-tendon forces and joint reaction forces was presented by introducing a selection of joint reaction forces in the objective function through a partial parameter reduction and solving the muscular redundancy with a traditional static optimization procedure.

The musculo-tendon forces predicted by minimizing the musculo-tendon forces only are qualitatively similar to the measured EMG. But when the knee contact force is introduced in the objective function, some unphysiological results arise, such as the partial extinction of the vastus and gastrocnemius during the stance phase. Such results were also reported on the gastrocnemius when testing different objective functions during a vertical jumping simulation [2]. Similarly, when comparing, for gait and stair climbing, the minimization of the musculo-tendon forces using different powers in the objective function [14], a unitary power provided unphysiological musculo-tendon forces compared to EMG signals, but hip contact force was in better agreements with in vivo measurements. All these results highlight an important limit of the current musculo-skeletal models and methods since it remains difficult to define an objective function that provides in the same time physiological musculo-tendon forces and valid joint contact forces.

To conclude, this new approach was able to give a reliable prediction of knee contact force during gait when compared to the measured one [11], but showed some limitations. A next step could be to complete the current musculo-skeletal model with other joint structures such as menisci or cartilages in order to introduce dissipation and thus reduce the joint contact forces.

5. REFERENCES

[1] M.S. Andersen, M. Damsgaard, and J. Rasmussen. Kinematic analysis of over-determinate biomechanical systems. *Computer Methods in Biomechanics and Biomedical Engineering*, 12(4):371–384, 2009.

[2] D.J. Cleather and A.M.J. Bull. An optimization-based simultaneous approach to the determination of muscular, ligamentous, and joint contact forces provides insight into musculoligamentous interaction. *Annals of Biomedical Engineering*, 39(7):1925–1934, 2011.

[3] S.L. Delp, J.P. Loan, M.G. Hoy, F.E. Zajac, E.L. Topp, and J.M. Rosen. An interactive graphics-based model of the lower extremity to study orthopaedic surgical procedures. *IEEE Transactions on Biomedical Engineering*, 37(8):757–767, 1990.

[4] R. Di Gregorio, V. Parenti-Castelli, J. O'Connor, and A. Leardini. Mathematical models of passive motion at the human ankle joint by equivalent spatial parallel mechanisms. *Medical and Biological Engineering and Computing*, 45(3):305–313, 2007.

[5] D.D. D'Lima, S. Patil, N. Steklov, J.E. Slamin, and C.W. Colwell. Tibial forces measured in vivo after total knee arthroplasty. *The Journal of Arthroplasty*, 21(2):255–262, 2006.

[6] R. Dumas and L. Cheze. 3d inverse dynamics in non-orthonormal segment coordinate system. *Medical & Biological Engineering & Computing*, 45(3):315–322, 2007.

[7] R. Dumas, F. Moissenet, X. Gasparutto, and L. Cheze. Influence of the joint models on the lower limb musculo-tendon and contact forces during gait. *Proceedings of the Institution of Mechanical Engineers, Part H, Journal of Engineering in Medicine*, 226(2):146–160, 2012.

[8] S. Duprey, L. Cheze, and R. Dumas. Influence of joint constraints on lower limb kinematics estimation from skin markers using global optimization. *Journal of Biomechanics*, 43(14):2858–2862, 2010.

[9] A. Erdemir, S. McLean, W. Herzog, and A.J. van den Bogert. Model-based estimation of muscle forces exerted during movements. *Clinical Biomechanics*, 22:131–154, 2007.

[10] J. Feikes, J. O'Connor, and A. Zavatsky. A constraint-based approach to modelling the mobility of the human knee joint. *Journal of Biomechanics*, 36(1):125–129, 2003.

[11] B.J. Fregly, T.F. Besier, D.G. Lloyd, S.L. Delp, S.A. Banks, M.G. Pandy, , and D.D. D'Lima. Grand challenge competition to predict in vivo knee loads. *Journal of Orthopaedic Research*, doi: 10.1002/jor.22023, 2011.

[12] J. Garcia de Jalon and E. Bayo. *Kinematic and dynamic simulation of multibody systems. The real-time challenge*. Springer-Verlag, New-York, 1994.

[13] Y.C. Lin, J.P. Walter, S.A. Banks, M.G. Pandy, and B.J. Fregly. Simultaneous prediction of muscle and contact forces in the knee during gait. *Journal of Biomechanics*, 22:945–952, 2010.

[14] L. Modenese, A.T.M. Phillips, and A.M.J. Bull. An open source lower limb model: Hip joint validation. *Journal of Biomechanics*, 44:2185–2193, 2011.

[15] F. Moissenet, L. Cheze, and R. Dumas. Anatomical kinematic constraints: consequences on muscular forces and joint reactions. *Multibody System Dynamics*, doi: 10.1007/s11044-011-9286-3, 2012.

[16] J.A. Reinbolt, J.F. Schutte, B.J. Fregly, B.I. Koh, R.T. Haftka, A.D. George, and K.H. Mitchell. Determination of patient-specific multi-joint kinematic models through two-level optimization. *Journal of Biomechanics*, 38(3):621–626, 2005.

[17] B.W. Stansfield, A.C. Nicol, J.P. Paul, I.G. Kelly, F. Graichen, and G. Bergmann. Direct comparison of calculated hip joint contact forces with those measured using instrumented implants. an evaluation of a three-dimensional mathematical model of the lower limb. *Journal of Biomechanics*, 36(7):929–936, 2003.

3DAHM 2012
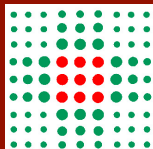
SERVIZIO SANITARIO REGIONALE
EMILIA - ROMAGNA
Istituto Ortopedico Rizzoli di Bologna
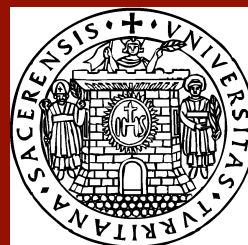Istituto di Ricovero e Cura a Carattere Scientifico

INAIL
Centro Protesi

DEIS
DEPARTMENT OF ELECTRONICS, COMPUTER SCIENCES
AND SYSTEMS

DIEM
DEPARTMENT OF MECHANICAL, NUCLEAR, AVIATION
AND METALLURGICAL ENGINEERING

Università
degli Studi
di Sassari